





**Organized by the  
International Atomic Energy Agency**

**Hosted by  
the Principality of Monaco**

The material in this book has been supplied by the authors and has not been edited. The views expressed remain the responsibility of the named authors and do not necessarily reflect those of the government of the designating Member State(s). The IAEA cannot be held responsible for any material reproduced in this book.

ISOTOPES IN HYDROLOGY,  
MARINE ECOSYSTEMS AND  
CLIMATE CHANGE STUDIES

VOLUME 2

The following States are Members of the International Atomic Energy Agency:

AFGHANISTAN	GUATEMALA	PANAMA
ALBANIA	HAITI	PAPUA NEW GUINEA
ALGERIA	HOLY SEE	PARAGUAY
ANGOLA	HONDURAS	PERU
ARGENTINA	HUNGARY	PHILIPPINES
ARMENIA	ICELAND	POLAND
AUSTRALIA	INDIA	PORTUGAL
AUSTRIA	INDONESIA	QATAR
AZERBAIJAN	IRAN, ISLAMIC REPUBLIC OF	REPUBLIC OF MOLDOVA
BAHRAIN	IRAQ	ROMANIA
BANGLADESH	IRELAND	RUSSIAN FEDERATION
BELARUS	ISRAEL	RWANDA
BELGIUM	ITALY	SAUDI ARABIA
BELIZE	JAMAICA	SENEGAL
BENIN	JAPAN	SERBIA
BOLIVIA	JORDAN	SEYCHELLES
BOSNIA AND HERZEGOVINA	KAZAKHSTAN	SIERRA LEONE
BOTSWANA	KENYA	SINGAPORE
BRAZIL	KOREA, REPUBLIC OF	SLOVAKIA
BULGARIA	KUWAIT	SLOVENIA
BURKINA FASO	KYRGYZSTAN	SOUTH AFRICA
BURUNDI	LAO PEOPLE'S DEMOCRATIC REPUBLIC	SPAIN
CAMBODIA	LATVIA	SRI LANKA
CAMEROON	LEBANON	SUDAN
CANADA	LESOTHO	SWAZILAND
CENTRAL AFRICAN REPUBLIC	LIBERIA	SWEDEN
CHAD	LIBYA	SWITZERLAND
CHILE	LIECHTENSTEIN	SYRIAN ARAB REPUBLIC
CHINA	LITHUANIA	TAJIKISTAN
COLOMBIA	LUXEMBOURG	THAILAND
CONGO	MADAGASCAR	THE FORMER YUGOSLAV REPUBLIC OF MACEDONIA
COSTA RICA	MALAWI	TOGO
CÔTE D'IVOIRE	MALAYSIA	TRINIDAD AND TOBAGO
CROATIA	MALI	TUNISIA
CUBA	MALTA	TURKEY
CYPRUS	MARSHALL ISLANDS	UGANDA
CZECH REPUBLIC	MAURITANIA	UKRAINE
DEMOCRATIC REPUBLIC OF THE CONGO	MAURITIUS	UNITED ARAB EMIRATES
DENMARK	MEXICO	UNITED KINGDOM OF GREAT BRITAIN AND NORTHERN IRELAND
DOMINICA	MONACO	UNITED REPUBLIC OF TANZANIA
DOMINICAN REPUBLIC	MONGOLIA	UNITED STATES OF AMERICA
ECUADOR	MONTENEGRO	URUGUAY
EGYPT	MOROCCO	UZBEKISTAN
EL SALVADOR	MOZAMBIQUE	VENEZUELA
ERITREA	MYANMAR	VIETNAM
ESTONIA	NAMIBIA	YEMEN
ETHIOPIA	NEPAL	ZAMBIA
FIJI	NETHERLANDS	ZIMBABWE
FINLAND	NEW ZEALAND	
FRANCE	NICARAGUA	
GABON	NIGER	
GEORGIA	NIGERIA	
GERMANY	NORWAY	
GHANA	OMAN	
GREECE	PAKISTAN	
	PALAU	

The Agency's Statute was approved on 23 October 1956 by the Conference on the Statute of the IAEA held at United Nations Headquarters, New York; it entered into force on 29 July 1957. The Headquarters of the Agency are situated in Vienna. Its principal objective is "to accelerate and enlarge the contribution of atomic energy to peace, health and prosperity throughout the world".

PROCEEDINGS SERIES

ISOTOPES IN HYDROLOGY,  
MARINE ECOSYSTEMS  
AND CLIMATE CHANGE STUDIES

PROCEEDINGS OF THE INTERNATIONAL SYMPOSIUM  
HELD IN MONACO,  
27 MARCH–1 APRIL 2011

*In two volumes*

VOLUME 2

INTERNATIONAL ATOMIC ENERGY AGENCY  
VIENNA, 2013

## COPYRIGHT NOTICE

All IAEA scientific and technical publications are protected by the terms of the Universal Copyright Convention as adopted in 1952 (Berne) and as revised in 1972 (Paris). The copyright has since been extended by the World Intellectual Property Organization (Geneva) to include electronic and virtual intellectual property. Permission to use whole or parts of texts contained in IAEA publications in printed or electronic form must be obtained and is usually subject to royalty agreements. Proposals for non-commercial reproductions and translations are welcomed and considered on a case-by-case basis. Enquiries should be addressed to the IAEA Publishing Section at:

Marketing and Sales Unit, Publishing Section  
International Atomic Energy Agency  
Vienna International Centre  
PO Box 100  
1400 Vienna, Austria  
fax: +43 1 2600 29302  
tel.: +43 1 2600 22417  
email: [sales.publications@iaea.org](mailto:sales.publications@iaea.org)  
<http://www.iaea.org/books>

© IAEA, 2013

Printed by the IAEA in Austria

July 2013

STI/PUB/1580

### **IAEA Library Cataloguing in Publication Data**

Isotopes in hydrology, marine ecosystems and climate change studies : proceedings of the International Symposium held in Monaco, 27 March–1 April 2011 : in two volumes. — Vienna : International Atomic Energy Agency, 2013.

p. ; 24 cm. — (Proceedings series, ISSN 0074–1884)

STI/PUB/1580

ISBN 978–92–0–135610–9

Includes bibliographical references.

1. Radioisotopes in hydrology — Congresses. 2. Groundwater flow. 3. Climatic changes — Research. I. International Atomic Energy Agency. II. Series: Proceedings series (International Atomic Energy Agency).

IAEAL

13–00820

## FOREWORD

Humanity is facing many water related challenges, including access to safe water, pollution of continental and coastal waters and ocean acidification, as well as the growing impact of climate change on the hydrological cycle. Many countries are confronted by increasingly stressed water resources due to rapidly growing populations, increasing agricultural and energy production demands, industrial development, and pollution. The greatest issues of the 21st century, including competition for resources and possible related conflicts, may well focus on the role of water in food and energy security.

For more than 50 years, the IAEA has played a key role in advancing and promoting the development and use of isotope techniques to address global environmental issues, such as water resources assessment and management, the study of marine ecosystems, and more recently the impact of climate change. This symposium was jointly organized by the Water Resources Programme and IAEA Environment Laboratories to commemorate the 50th anniversary of the establishment of the IAEA laboratory in the Principality of Monaco, and represented the 13th edition of the quadrennial symposium on isotope hydrology and water resources management, which has been regularly organized by the IAEA since 1963.

The main objectives of the symposium were to review the state of the art in isotope hydrology, the use of isotopes in the study of climatic systems and in marine ecosystems and to outline recent developments in the application of isotope techniques, as well as to identify future trends and developments for research and applications. The contributions submitted by the authors are included in two volumes of proceedings with editorial corrections. These proceedings are intended to serve as an aid for those using isotopes for applied problems in hydrology as well as for the research community.

The IAEA officers responsible for this publication were H. Nies of the IAEA Environment Laboratories and B. Newman and L. Araguas of the Department of Nuclear Sciences and Applications.

## EDITORIAL NOTE

*The papers in these Proceedings (including the figures, tables and references) have undergone only the minimum copy editing considered necessary for the reader's assistance. The views expressed remain, however, the responsibility of the named authors or participants. In addition, the views are not necessarily those of the governments of the nominating Member States or of the nominating organizations.*

*Although great care has been taken to maintain the accuracy of information contained in this publication, neither the IAEA nor its Member States assume any responsibility for consequences which may arise from its use.*

*The use of particular designations of countries or territories does not imply any judgement by the publisher, the IAEA, as to the legal status of such countries or territories, of their authorities and institutions or of the delimitation of their boundaries.*

*The mention of names of specific companies or products (whether or not indicated as registered) does not imply any intention to infringe proprietary rights, nor should it be construed as an endorsement or recommendation on the part of the IAEA.*

*The authors are responsible for having obtained the necessary permission for the IAEA to reproduce, translate or use material from sources already protected by copyrights.*

*This publication has been prepared from the original material as submitted by the authors. The views expressed do not necessarily reflect those of the IAEA, the governments of the nominating Member States or the nominating organizations.*

*The IAEA has no responsibility for the persistence or accuracy of URLs for external or third party Internet web sites referred to in this book and does not guarantee that any content on such web sites is, or will remain, accurate or appropriate.*

# CONTENTS

## ISOTOPE HYDROLOGY 2: GENERAL GROUNDWATER STUDIES, AND FLOW AND TRANSPORT MODELLING

Chalk catchment transit time: unresolved issues . . . . .	3
<i>W.G. Darling, J.A. Barker, D.C. Gooddy, M. Robinson</i>	
Isotope investigations of groundwater movement in a coarse gravel unsaturated zone . . . . .	11
<i>N. Mali, J. Kožar-Logar, A. Leis</i>	
Changes in isotopic composition of bottled natural waters due to different storage conditions . . . . .	19
<i>T. Ferjan, M. Brenčič, P. Vreča</i>	
Investigating natural analogues for CO <sub>2</sub> sequestration in ultramafic rocks: a reactive transport modelling approach . . . . .	27
<i>F. Gherardi</i>	
Dissolved inert gases in three karstic systems in Europe (France and Greece) . . . .	35
<i>G. Magro, R. Cioni, M. Guidi, F. Gherardi</i>	
Groundwater flow computed with MODFLOW and isotopic age tracer data in the Continental Intercalaire (Sahara) . . . . .	45
<i>J.O. Petersen, J. Goncalves, P. Deschamps, B. Hamelin, K. Zouari, A. Guendouz, J.-L. Michelot</i>	
Hydrogeochemical and isotopic characteristics of tufa precipitating waters: a case study of the river Krka (Slovenia) . . . . .	53
<i>S. Zavadlav, S. Lojen</i>	
Isotopic and geochemical signatures of Melgaço CO <sub>2</sub> rich cold mineral waters, NW Portugal . . . . .	63
<i>P.M. Carreira, J.M. Marques, M.R. Carvalho, D. Nunes, M. Antunes da Silva</i>	
A case study from southwest Germany — shifting of groundwater age during one year pumping test and comparison of isotope methods . . . . .	73
<i>G.D. Lorenz, L. Eichinger, E. Funk, M. Heidinger, J. Schneider</i>	

Changes in chemical and isotopic composition of groundwater during a long term pumping test in Brestovica karst aquifer . . . . .	83
<i>K. Mezga, J. Urbanc</i>	
Use of isotopes in assessing the response of groundwater to cross-catchments water diversion in the Tarim Basin . . . . .	91
<i>Z. Pang, T. Huang, Y. Kong</i>	
Origin and evolution of reactive and noble gases dissolved in matrix pore water . .	99
<i>F. Eichinger, H.N. Waber, J.A.T. Smellie</i>	
Multiple tracer ( $^4\text{He}$ , $^{14}\text{C}$ , $^{39}\text{Ar}$ , $^3\text{H}/^3\text{He}$ , $^{85}\text{Kr}$ ) depth profile in an extensively exploited multilevel aquifer system in the Venetian plain, Italy . . . . .	109
<i>A. Mayer, R. Purtschert, J. Sültenfuß, C. Claude, Y. Travi</i>	
Unexpected $\delta^{18}\text{O}$ and $\delta^2\text{H}$ variability of groundwater in the eastern Paris Basin . .	117
<i>L. Gourcy, E. Petelet-Giraud</i>	
Use of isotopic techniques for the assessment of hydrological interactions between ground and surface waters — Rio Man, Ciénaga Colombia . . . . .	125
<i>P. Palacio, C. Dapeña, T. Betancur</i>	
Application of environmental isotopes in hydrological studies along the River Nile Valley, Egypt . . . . .	137
<i>A.A. Nada</i>	
Isotope investigations at an alpine karst aquifer by means of on-site measurements with high time resolution and near real-time data availability . . . . .	145
<i>A. Leis, R. Schmitt, A. Van Pelt, M. Plietschnegger, T. Harum, W. Zerobin, H. Stadler</i>	
Recharge rates to deep aquifer layers estimated with $^{39}\text{Ar}$ , $^{85}\text{Kr}$ and $^{14}\text{C}$ data: A case study in Odense (Denmark) . . . . .	153
<i>R. Purtschert, T.K. Bjerre, J. Linderberg, K. Hinsby</i>	
Using isotope methods to assess groundwater recharge in some hydraulic atchments in a semiarid region in central Tunisia . . . . .	161
<i>K. Zouari, R. Trabelsi, A. Kacem</i>	
Isotopic composition and age of surface water as indicators of groundwater sustainability in a semiarid area: Case of the Souss basin (Morocco). . . . .	169
<i>L. Bouchaou, T. Tagma, W. Nathaniel, J.L. Michelot, S. Boutaleb, Y. Hsissou, M. Massault, A. Vengosh, M. Elfaskaoui</i>	

Isotopes tracing the water cycle in the Pampeano aquifer at the southeast of Buenos Aires province, Argentina . . . . .	177
<i>D.E. Martínez, O.M. Quiroz Londoño, E. Bocanegra, H.E. Massone, C. Dapeña</i>	
Isotopic and hydrogeochemical techniques for the sustainable management of water resources in an arid watershed of northern Chile . . . . .	185
<i>R. Oyarzún, J.F. Muñoz, E. Aguirre, J. Oyarzún, C. Ortiz, S. Marín, H. Maturana, N. Kretschmer, E. Jofré.</i>	
Contribution of isotopic tools to the numerical simulation of the Mar del Plata coastal aquifer, Argentina . . . . .	195
<i>E. Bocanegra, M. Pool, J. Carrera, D.E. Martínez</i>	
Hydrochemical and isotopic investigation of groundwater in the Hammamet-Nabeul aquifer system, north-eastern Tunisia . . . . .	203
<i>A. Ben Moussa, K. Zouari, T. Kurttas</i>	
Hydrogeochemical and isotopic studies of groundwater in the central region of Ghana . . . . .	215
<i>S.Y. Ganyaglo, S. Osae, J.R. Fianko, A. Gibrilla, E. Bam</i>	
Uranium isotopes as a tracer of groundwater evolution in the Complexe Terminal aquifer of southern Tunisia. . . . .	225
<i>F. Hadj Ammar, P. Deschamps, N. Chkir, B. Hamelin, K. Zouari</i>	
Insight into groundwater flow within a crystalline aquifer: Case study of the Ursuya Mount, northern Basque Country (France). . . . .	235
<i>J. Jaunat, F. Huneau, A. Dupuy, H. Celle-Jeanton, M. Franceschi, P. Le Coustumer</i>	
Hydrogeochemical and isotopic characterization of the hydrogeological model of the Parrita aquifer, Central Pacific of Costa Rica. . . . .	245
<i>R. Matamoros-Arguedas</i>	
Determining MRT of groundwater by modelling the distribution of environmental (hydrogen and oxygen) isotopes . . . . .	255
<i>E. Anovska-Jovcheva, Z. Jovchev, T. Anovski, V. Popov</i>	
Understanding the hydrogeology of Raya valley basin, Northern Ethiopia using stable isotopes of water . . . . .	263
<i>M. Gebre Egziabher, T. Ayenew, S. Kebede</i>	

Groundwater ages and hydrochemical evolution along a flow-path in the Northeastern sector of the Guarani Aquifer System (GAS) derived from structural geology, isotopes and hydrochemical data . . . . .	271
<i>D. Gastmans, H.K. Chang, P.K. Aggarwal, N. Sturchio, L. Araguás Araguás</i>	
Role of isotopes in the development of a general hydrogeological conceptual model of the Guarani Aquifer System (GAS) . . . . .	281
<i>H.K. Chang, R. Aravena, D. Gastmans, R. Hirata, M. Manzano, L. Vives, L. Rodrigues, P.K. Aggarwal, L. Araguás Araguás</i>	
Application of isotopic tools for the integrated management of the Santa Elena coastal aquifer, Ecuador . . . . .	291
<i>P. Carrión, S. Jiménez, P. Romero</i>	
The use of multiple environmental tracers in age interpretation of the Mount Amba Aquifer, Kinshasa, Democratic Republic of Congo . . . . .	299
<i>L.J. Ndembo, N. Plummer, Y. Ravi, T. Vitvar</i>	
Quantification of submarine groundwater discharge in southeastern Brazil using natural and conservative tracers . . . . .	309
<i>T.A. Souza, J.M. Godoy, M.L.D.P. Godoy, I. Moreira, Z.L. Carvalho</i>	
Geostatistical analysis of spatial isotope ( $\delta^{18}\text{O}$ , $\delta^2\text{H}$ and $^3\text{H}$ ) variability of groundwater across Morocco . . . . .	319
<i>H. Marah, N. Zine, M. Qurtobi, B. Ouda, F. Taous, F. Raibi</i>	
Using isotope techniques $^{34}\text{S}/^{32}\text{S}$ ( $\delta^{34}\text{S}$ ) to determine the origin of dissolved sulphate in Thuan My mineral water . . . . .	327
<i>Vo Thi Tuong Hanh</i>	
Feasibility of chemometrics assisted exploration and management of geothermal resources in the Kenya Rift System utilizing stable isotope and related measurements . . . . .	335
<i>K.H. Angeyo, P.O. Ogwari</i>	
Detection of water leaks in the Beni-Haroun dam (Algeria) . . . . .	343
<i>N. Hocini, M. Mami</i>	
Application of isotope and dye tracing methods in hydrology (Case study: Havassan Dam Construction) . . . . .	351
<i>Y. Khalaj Amirhosseini</i>	

## ANALYTICAL METHODS AND INSTRUMENTATION

- New hydrological age-dating techniques using cosmogenic radionuclides  
beryllium-7 and sodium-22 ..... 361  
*S. Frey, C. Külls, C. Schlosser*
- Advances in radiocarbon measurement of water samples ..... 369  
*R. Janovics, M. Molnár, I. Světlík, I. Major, L. Wacker*
- Three new offset  $\delta^{11}\text{B}$  isotope reference materials for environmental boron  
isotope studies ..... 377  
*M. Rosner, J. Vogl*
- ISOBORDAT: an online database on boron isotopes ..... 381  
*M. Pennisi, A. Adorni-Braccesi, D. Andreani, L. Gori, P.F. Sciuto,  
R. Gonfiantini*
- Normalization methods and selection strategies for reference materials in stable  
isotope analyses – review ..... 389  
*G. Skrzypek, R. Sadler, D. Paul, I. Fórizs*
- IAEA reference materials for quality assurance: A study in the quality  
control of marine radioactivity ..... 395  
*Pham Mai Khanh, J. Bartocci, E. Chamizo, J. Gastaud,  
J.-M. Gómez-Guzmán, H. Nies, E. Vasileva, M. Betti*
- Optimization of plastic scintillator thicknesses for online beta detection  
in mixed fields ..... 403  
*K. Pourtangestani, R. Machrafi*
- Determination of Pu, Am and Cm in environmental samples ..... 411  
*G. Lujanienė*
- Analysis of a single hot particle by a combination of non-destructive  
analytical methods ..... 419  
*E. Hrnccek, L. Aldave de las Heras, M. Bielewski, R. Carlos, M. Betti*
- Uranium series radionuclides in the water column of the northeast  
Atlantic Ocean ..... 427  
*F.P. Carvalho*
- Traditions and new perspectives for marine radioecology in Romania ..... 443  
*V. Pătraşcu, A.S. Bologna*

## ISOTOPES AND RADIONUCLIDES IN THE MARINE ENVIRONMENT

Applications of radium isotopes to Ocean studies . . . . .	453
<i>W.S. Moore</i>	
Iodine-129 in the European environment . . . . .	467
<i>R. Michel, A. Daraoui, M. Gorny, D. Jakob, R. Sachse, L. Tosch V. Alfimov, H.-A. Synal, H. Nies, J. Herrmann, I. Goroncy</i>	
Supported lead in Pb-210 chronology. . . . .	477
<i>D. Pittauerová, B. Hettwig, H.W. Fischer</i>	
Use of stable carbon and nitrogen isotopes for trophic level evaluation and food webs reconstruction in the Bay of Biscay: Case study . . . . .	485
<i>T. Chauvelon, J. Spitz, F. Caurant, P. Méndez Fernandez, P. Bustamante</i>	
Global distributions of $^{137}\text{Cs}$ , $^{239,240}\text{Pu}$ and the ratio of $^{239,240}\text{Pu}/^{137}\text{Cs}$ in an ocean general circulation model. . . . .	493
<i>D. Tsumune, M. Aoyama, K. Hirose, T. Tsubono, K. Misumi, Y. Yoshida</i>	
Origin of organic matter in sediments of the Campos Basin (SE Brazilian Continental margin) by means of stable isotopes and molecular markers. . .	501
<i>A.L.R. Wagener, R.S. Carreira, C.O. Farias, C.E. Rezende, L.G.M.S. Cordeiro, D.R. Oliveira, M. Almeida, A. Baeta, A.L. Scofield</i>	
Application of natural radioisotopes as tracers of particulate organic carbon transport, export and burial processes in Chukchi Sea, Arctic Ocean . . . . .	509
<i>Wen Yu, Jianhua He</i>	
$^{137}\text{Cs}$ Distribution in the northern Adriatic Sea (2006–2010) . . . . .	519
<i>D. Pavičić-Hamer, D. Barišić</i>	
Sources of $\text{CO}_2$ in the Gulf of Trieste (N. Adriatic): Stable carbon isotope evidence. . . . .	527
<i>N. Ogrinc, D. Turk, S. Zavadlav, J. Faganeli</i>	
Radiotracers in the Black Sea: a tool for marine environmental assessments . . . .	535
<i>S.B. Gulin, V.N. Egorov, G.G. Polikarpov, I. Osvath, N.A. Stokozov, N.Y. Mirzoeva, N.N. Tereshenko, L.V. Gulina, V.Y. Proskurnin</i>	
Cs-137 in marine sediments of the Eastern Mediterranean from the pre-Chernobyl age to the present . . . . .	545
<i>H. Florou, N. Evangeliou, P. Kritidis</i>	

Caesium and plutonium isotopes as tracers of various events in sediment records in the Bay of Toulon (northwestern Mediterranean Sea) . . . . .	553
<i>C. Duffa, M. Arnaud, S. Charmasson, H. Thébault</i>	
Temporal assessment of natural radionuclide bioaccumulation by the cubera snapper fish ( <i>Lutjanus cyanopterus</i> , Cuvier, 1828) from the Brazilian coast . . . . .	563
<i>W.S. Pereira, A. Kelecom, D.A. Py Jr</i>	
Inter and intra basin scale transport of <sup>137</sup> Cs in the Pacific Ocean . . . . .	571
<i>M. Aoyama, M. Fukasawa, Y. Hamajima, K. Hirose, T. Kawano, H. Nakano, P.P. Povinec, J.A. Sanchez-Cabeza, D. Tsumune</i>	
<b>CHAIRPERSONS OF SESSIONS . . . . .</b>	<b>579</b>
<b>ADVISORY COMMITTEE . . . . .</b>	<b>580</b>
<b>SECRETARIAT OF SYMPOSIUM . . . . .</b>	<b>581</b>
<b>SCIENTIFIC ORGANISING COMMITTEE . . . . .</b>	<b>581</b>
<b>LIST OF PARTICIPANTS . . . . .</b>	<b>583</b>
<b>AUTHOR INDEX . . . . .</b>	<b>631</b>



ISOTOPE HYDROLOGY 2:  
GENERAL GROUNDWATER STUDIES, AND FLOW  
AND TRANSPORT MODELLING



# CHALK CATCHMENT TRANSIT TIME: UNRESOLVED ISSUES

W.G. DARLING<sup>a</sup>, J.A. BARKER<sup>b</sup>, D.C. GOODDY<sup>a</sup>, M. ROBINSON<sup>c</sup>

<sup>a</sup> British Geological Survey,  
Crowmarsh Gifford, Wallingford,  
Oxfordshire, United Kingdom

<sup>b</sup> School of Civil Engineering and the Environment,  
University of Southampton,  
Southampton, United Kingdom

<sup>c</sup> Centre for Ecology and Hydrology,  
Crowmarsh Gifford, Wallingford,  
Oxfordshire, United Kingdom

## Abstract

The mean transit time (MTT) of a catchment is the average residence time of water from rainfall to river outflow at the foot of the catchment. As such, MTT has important water quality as well as resource implications. Many catchments worldwide have been measured for MTT using environmental isotopes, yet the Chalk, an important aquifer in NW Europe, has received little attention in this regard. The catchment of the River Lambourn in southern England has been intermittently studied since the 1960s using isotopic methods. A tritium peak measured in the river during the 1970s indicates an apparent MTT of ~15 years, but the thick unsaturated zone (average ~50 m) of the catchment suggests that the MTT should be much greater because of the average downward movement through the Chalk of ~1 m/a consistently indicated by tritium and other tracers. Recent work in the catchment using SF<sub>6</sub> as a residence time indicator has given groundwater ages in the narrow range 11–18 yrs, apparently supporting the river tritium data but in conflict with the unsaturated zone data even allowing for a moderate proportion of rapid bypass flow. The MTT of the catchment remains unresolved for the time being.

## 1. INTRODUCTION

The mean transit time (MTT) of a catchment is the average residence time of water from rainfall to river outflow at the foot of the catchment. MTT includes runoff and baseflow and is therefore a function of storage and flow pathways. As such, it has important water resource and quality implications, for example, regarding the large expansion of fertilizer use over the past half-century and its implication

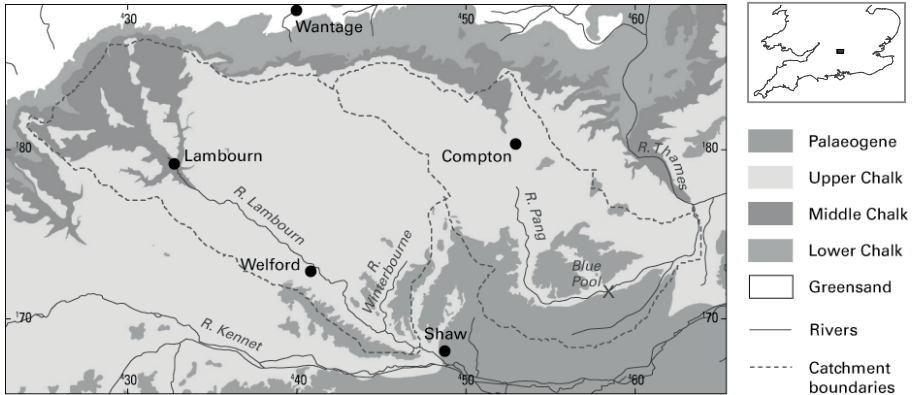


FIG. 1. Map of the Lambourn and adjoining Pang Chalk catchments, showing basic geology and surface catchment boundaries. 10 km grid tick marks shown. Inset: the location in southern England.

for the future. Clearly, reliable forecasting of the water quality status of streams and rivers over the decades to come requires a good understanding of how catchments function. The Chalk catchments of NW Europe, however, have barely been studied in terms of MTT.

The Chalk is a multi-porosity limestone aquifer, with a microporous matrix. Typical matrix pores are of the order of 0.1–1  $\mu\text{m}$  in diameter. Larger voids are defined by the fracture porosity. Fracture apertures range from a few  $\mu\text{m}$  to about 1 mm for primary, or undeveloped, fractures, and reach a few hundreds of mm for secondary fractures where there has been local karstic development of the fracture. This means that the movement of water through the Chalk can occur in complex ways [1], making the prediction of MTT far from straightforward.

The present study is based on the catchment of the River Lambourn in Berkshire, UK (Fig. 1). The area of this mesoscale catchment is 235  $\text{km}^2$ . Interfluvial areas rarely rise above 200 m asl (above sea level), whereas river elevation at the foot of the catchment is  $\sim 50$  m asl. Mean annual precipitation (1968–1997) is 731 mm [2]. The thickness of the Chalk unsaturated zone is seasonally variable to some extent, but reaches a maximum thickness of over 100 m at the water divide at the top of the escarpment on the northern flank of the catchment. While much of the water movement through the saturated zone of the aquifer is likely to occur relatively rapidly through the fracture network, in the unsaturated zone it is more likely to occur via lengthy spells as slow or even immobile porewater, interrupted periodically by fracture flow when matric potentials rise sufficiently [1].

With a baseflow index (BFI) of 0.95 [3], surface flow can be more or less discounted as a factor in the MTT of the Lambourn catchment. This means that for

practical purposes the MTT should be the sum of mean residence times in the unsaturated and saturated zones.

## 2. CALCULATION OF THE MEAN TRANSIT TIME OF THE LAMBOURN CATCHMENT

### 2.1. Mean residence time in the unsaturated zone

The mean unsaturated (vadose) zone thickness of the Lambourn has been calculated to be 53 m. In a borehole in the central part of the catchment, porewater tritium ( $^3\text{H}$ ) from the Chalk showed that the downward movement of the bulk of infiltration was  $<1$  m/a, but that there was also an estimated bypass flow of  $\sim 15\%$  with an indeterminate but much shorter residence time [4]. With an average unsaturated zone thickness of 53 m in the Lambourn catchment, this implies a mean residence time (MRT) of  $\sim 60$  yrs for the Lambourn unsaturated zone.

### 2.2. Mean residence time in the saturated zone

$\text{SF}_6$  has been increasing in the atmosphere, and therefore in recharge, over the past 50 yrs, so it can be used to date young groundwaters [5]. Groundwater ages based on the  $\text{SF}_6$  input curve are nearly all in the range 11–18 yrs for springs and boreholes in the Lambourn catchment (Fig. 2). This homogeneity appears to be due to the water sampled in each of the different springs or boreholes being the product of a range of flowlines. The range may not be the same in each case, but the relative amounts of water from individual flowlines result in similar MRTs as predicted

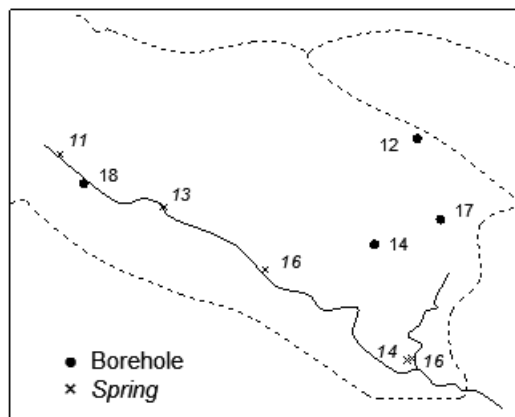


FIG. 2. Residence times in years for groundwater from springs and boreholes in the Lambourn Chalk catchment, based on  $\text{SF}_6$  concentrations. Piston flow model assumed.

by the sectional model of Ref. [6] and also considered in Ref. [7]. On account of the largely open system conditions believed to prevail in the unsaturated zone, it is considered that the SF<sub>6</sub> ‘clock’ starts effectively at the water table [8, 9]. This implies that the SF<sub>6</sub> ages very largely relate to saturated zone residence only.

### 2.3. Combining MRTs to determine the MTT of the Lambourn catchment

The combination of an MRT of ~60 yrs for the unsaturated zone with an MRT of ~15 yrs for the saturated zone yields an MTT of ~75 yrs on the assumption of a baseflow index of 95% (see above). This can be compared to the modelled MTT of the Lambourn system of ~100 yrs [10].

## 3. DIRECT EVIDENCE FOR THE MEAN TRANSIT TIME OF THE LAMBOURN CATCHMENT

One way of estimating the MTT of a catchment has been to make use of the thermonuclear tritium peak of the 1960s [11]. Tritium data from the River Lambourn at Welford (location: Fig. 1) show elevated <sup>3</sup>H activities only commencing in a sustained manner from early 1975, compared to the start of the main UK precipitation <sup>3</sup>H peak in the early 1960s (Fig. 3). It is clear from the figure that there is a delay of ~15 yrs before the river peak appears, apparently equivalent to the MTT.

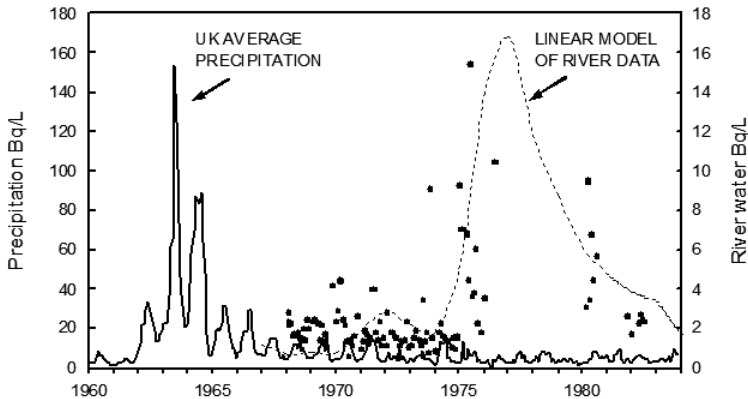


FIG. 3. Tritium measurements (Bq/L) on samples from the River Lambourn at Welford, superimposed on the UK monthly mean for precipitation. A simple linear model has been fitted to the data, and indicates a delay of ~15 a before the precipitation peak appears in the river. Note the ten-fold expansion in scale of the river water axis.

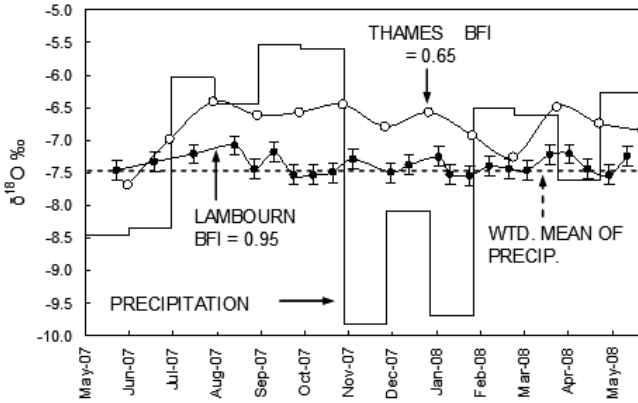


FIG. 4. Confirmation of the very high baseflow index (BFI) of the River Lambourn is provided by the highly damped response of the river to major variations in the  $\delta^{18}\text{O}$  record of precipitation as measured at the nearby Wallingford GNIP station. In contrast, the neighbouring River Thames with a lower BFI shows more variation. Measurement precision is shown for the Lambourn samples only.

#### 4. DISCUSSION

Even 15 years is a long MTT for a mesoscale catchment [11], let alone the 75 years based on unsaturated and saturated zone residence time measurements. But assuming that the MTT lies somewhere in the range 15–75 years, what could explain the disparity between the ‘direct’ and ‘indirect’ estimates? Four possibilities may be considered.

Firstly, that there is a big disparity between surface and groundwater catchments: if the groundwater catchment was very much smaller than the surface catchment, the imbalance might give a greater role to short residence surface runoff. It is likely that the groundwater catchment is smaller than the surface catchment owing to the valley of the larger River Thames lying to the north of the Lambourn and acting as a regional ‘drain’ because of its lower elevation. However, the difference in area is considered to be relatively small [2] and therefore insufficient to affect MTT significantly.

Secondly, that the baseflow index of the river is incorrect: for example, a significantly lower BFI would mean a greater input of surface runoff with much shorter MRT. However, Chalk catchments typically have high BFIs, and the hydrograph separation technique used to measure them is robust [3]. Additional support for a very high BFI for the Lambourn comes from the almost complete damping of stable isotope composition in the river water (Fig. 4).

Thirdly, that rapid bypass flow is greater than commonly accepted: if fast flow predominated through the unsaturated zone, residence time within the saturated

zone would become the main determinant of MTT. However, there is little evidence for this. The frequently quoted figure of 15% bypass flow in the Chalk is based on the study in Ref. [4] carried out within the Lambourn catchment itself, so unlikely to be grossly incorrect for the catchment as a whole. Also, studies in other Chalk catchments using a variety of applied or environmental tracers generally concur with this level of bypass flow.

Fourthly, that the tritium peak measured in the river simply represents bypass flow: if fast bypass flow transited the unsaturated zone in  $\leq 1$  a, then resided in the saturated zone for the  $\sim 15$  a suggested by  $\text{SF}_6$  dates, the water emerging in the river would provide the  $^3\text{H}$  peak observed in the mid-1970s. The difficulty with this interpretation is that river  $^3\text{H}$  activity is about 25% of the precipitation peak, and 40% of the porewater peak, after correction for radioactive decay, implying a proportion of bypass flow much greater than 15% which, as mentioned above, is not supported by available evidence from the Chalk.

## 5. CONCLUSIONS

The mean transit time (MTT) of the Lambourn Chalk catchment is an important parameter in consideration of future water quality evolution, yet remains poorly understood, not least because of the Chalk's unique multi-porosity. The apparent mean residence of recharge in the unsaturated zone for several decades, followed by a decade or more in the saturated zone, implies a very long MTT. However, the appearance of a river tritium peak  $\sim 15$  yrs after the thermonuclear precipitation maximum appears to contradict this. Either the river peak is the consequence of a moderately large proportion of fast 'bypass' flow through the unsaturated zone, which is not supported by studies of the Chalk elsewhere, or the unsaturated zone of the Chalk behaves very differently from the currently accepted model. There is a lack of similar tritium based studies in other Chalk catchments with which the present findings can be compared.

## ACKNOWLEDGEMENTS

The assistance of our colleagues with sample collection and discussion of results is gratefully acknowledged. D.B. Smith is thanked for providing the river tritium data.

## REFERENCES

- [1] PRICE, M., LOW, R.G., McCANN, C., Mechanisms of water storage and flow in the unsaturated zone of the Chalk aquifer, *J. Hydrol.* **233** (2000) 54–71.
- [2] WHEATER, H.S., PEACH, D.W., BINLEY, A., Characterising groundwater-dominated lowland catchments: The UK Lowland Catchment Research Programme (LOCAR), *Hydrol. Earth System Sci.* **11** (2007) 108–124.
- [3] GUSTARD, A., BULLOCK, A., DIXON, J.M., Low flow estimation in the United Kingdom, Report 108, Institute of Hydrology, Wallingford, UK (1992).
- [4] SMITH, D.B., WEARN, P.L., RICHARDS, H.J., ROWE, P.C., “Water movement in the unsaturated zone of high and low permeability strata by measuring natural tritium”, *Isotope Hydrology*, 1970, Proc. Symp., International Atomic Energy Agency, Vienna (1970).
- [5] BUSENBERG, E., PLUMMER, L.N., Dating young groundwater with sulphur hexafluoride: Natural and anthropogenic sources of sulphur hexafluoride, *Water Resour. Res.* **36** (2000) 3011.
- [6] VOGEL, J.C., “Investigation of groundwater flow with radiocarbon”, *Isotopes in Hydrology*, Proceedings Series, IAEA, Vienna (1967) 255.
- [7] SOLOMON, D.K., COOK, P.G., PLUMMER, L.N., “Models of groundwater ages and residence times”, *Use of Chlorofluorocarbons in Hydrology: A Guidebook*, IAEA, Vienna (2006) 73–88.
- [8] DARLING, W.G., MORRIS, B.L., STUART, M.E., GOODDY, D.C., Groundwater age indicators from public supplies tapping the Chalk aquifer of Southern England, *Water Environ. J.* **19** (2005) 30–40.
- [9] GOODDY, D.C., DARLING, W.G., ABESSER, C., LAPWORTH, D.J., Using chlorofluorocarbons (CFCs) and sulphur hexafluoride (SF<sub>6</sub>) to characterise groundwater movement and residence time in a lowland Chalk catchment, *J. Hydrol.* **330** (2006) 44–52.
- [10] JACKSON, B.M., et al., Catchment-scale modelling of flow and nutrient transport in the Chalk unsaturated zone, *Ecological Modelling* **209** (2007) 41–52.
- [11] McGUIRE, K.J., McDONNELL, J.J., A review and evaluation of catchment residence time modelling, *J. Hydrol.* **330** (2006) 543–563.



# ISOTOPE INVESTIGATIONS OF GROUNDWATER MOVEMENT IN A COARSE GRAVEL UNSATURATED ZONE

N. MALI

Geological Survey of Slovenia,  
Department of Hydrogeology,  
Ljubljana, Slovenia

J. KOŽAR-LOGAR

Jožef Stefan Institute,  
Ljubljana, Slovenia

A. LEIS

Institute of Water Resources Management,  
Hydrogeology and Geophysics,  
Joanneum Research Forschungsgesellschaft mbH,  
Graz, Austria

## Abstract

The unsaturated zone above an aquifer serves as a water reservoir which discharges water and possible pollution to the saturated zone. This paper presents the application of oxygen-18 and tritium isotope methods in the study of groundwater transport processes in the unsaturated zone of Selniška Dobrava coarse gravel aquifer. The Selniška Dobrava gravel aquifer is an important water resource for Maribor and its surroundings, therefore the determination of transport processes in the unsaturated zone is important regarding its protection. Groundwater flow characteristics were estimated using isotopes and based on experimental work in a lysimeter. Tritium investigation results were compared with the results of long term oxygen-18 isotope investigation. In this paper the analytical approach, results and interpretation of  $\delta^{18}\text{O}$  and tritium measurements in the unsaturated zone are presented.

## 1. INTRODUCTION

The processes in the coarse gravel unsaturated zone develop quite differently from those in aquifers with finer unsaturated zone granulation. To define hydrogeological properties in a high permeability coarse gravel aquifer, the lysimeter in Selniška Dobrava was constructed. Since 2001, several isotope investigations have been performed. In the first research period, two tracing experiments have been performed using different tracers and deuterated water as a conservative tracer [1].

The long term isotope investigations with oxygen-18 have been realized to define characteristic behaviours of the unsaturated zone processes which cannot be determined in one hydrogeological period or with single sampling. Previous results show that the environmental isotope oxygen-18 is a suitable tool for the quantification of recharge water movement in the unsaturated zone [2]. Based on the  $\delta^{18}\text{O}$  signal, tracing water movement in the lysimeter is possible. The oxygen-18 isotope composition signal of the precipitation can be traced in the lysimeter samples with some retardation with time and with diminishing amplitudes with depth. The mean residence time of the water in unsaturated zone was estimated by using lumped parameter models [2–4]. We also tried to determinate the processes in the unsaturated zone with tritium investigations. The research is in progress and some results are presented in this paper.

## 2. AREA DESCRIPTION

Selniška Dobrava is situated in the northeast of Slovenia near Maribor, the capital of the region. The coarse gravel aquifer lies on the north bank of the Drava River (Fig. 1). The aquifer is recharged by the Drava, by infiltration and seepage from the upper terrace aquifer. The thickest coarse gravel deposit is 50 m thick. The groundwater table is found at an average depth of 25 to 37 m, thus the thickness of the saturated layer along the aquifer axis is 7–14 m, possibly even more in the deepest sections. The hydraulic conductivity of the principal aquifer has been reported as  $5 \times 10^{-3}$  m/s [5]. The research area belongs to the moderate continental climate

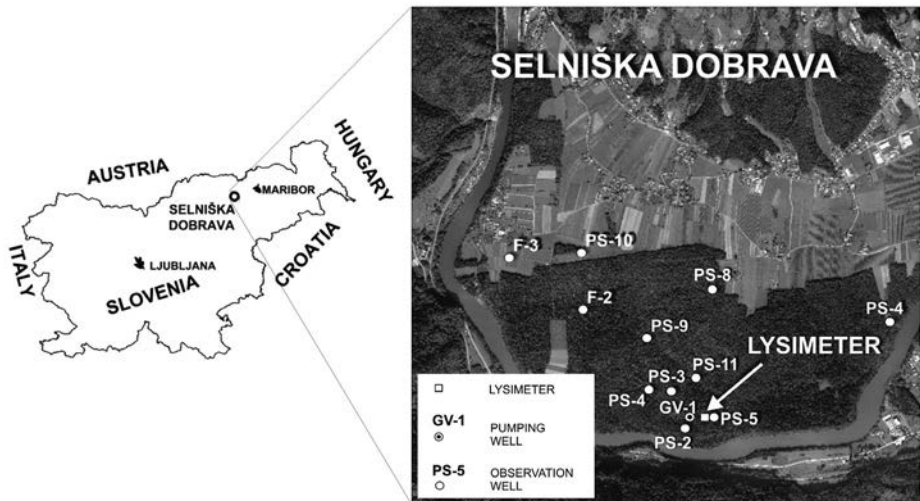


FIG. 1. Study area — location of lysimeter.

of central Slovenia with a typical continental precipitation regime and an average yearly precipitation between 1200 and 1300 mm. The average yearly air temperature lies between 8 and 12° C. In the conceptual model, the lysimeter area is defined as a homogeneous coarse gravel aquifer.

### 3. METHODS

#### 3.1. Experimental set-up

The lysimeter was designed as a concrete box, dimensions 2 × 2 m, 5 m deep, with 0.2 m thick walls. There are 10 sampling and measuring points (JV-1 to JV-10) positioned according to a randomized design by lysimeter width but at approximately equal distances by depth. Drainage samplers were installed for groundwater sampling in the unsaturated zone. The drains are stainless steel profiles 10 cm × 10 cm, 1.7 m long, with inverse inner perforated profiles and with a water collection system on the end. The closed system was made up of one 400 mL glass bottle and collecting containers. Drains, bottles and collectors were linked with silicone tubes. The precipitation collecting station was used for precipitation sampling at the location. A detailed description of the lysimeter can be found in Refs [1, 2].

#### 3.2. Sampling

Since 2001, over several research (project) periods, samples of groundwater in the unsaturated zone were collected monthly in containers at all ten sampling points (JV-1 to JV-10) at different depths in the lysimeter to determine oxygen-18 isotope composition and, since November 2007, also tritium composition. The water was sampled in plastic bottles of 120 mL volume to determine  $\delta^{18}\text{O}$  values and in 1 L volume for tritium analysis. Precipitation was also sampled at monthly intervals.

#### 3.3. Measurements

All stable isotope analyses were performed in the laboratory of the JOANNEUM RESEARCH Institute of Water Resources Management, Hydrogeology and Geophysics in Graz, Austria.

Oxygen-18 was measured with a fully automated device for the classic  $\text{CO}_2$  equilibration technique coupled to a Finnigan DELTA plus light stable isotope ratio mass spectrometer working in dual inlet mode [6].

Tritium analyses were performed in the Laboratory for Liquid Scintillation Spectrometry of the Department for Low and Medium Energy Physics of the Jozef Stefan Institute in Ljubljana, Slovenia.

The method of electrolytic enrichment was used for sample preparation. Sodium peroxide ( $\text{Na}_2\text{O}_2$ ) was added to the sample's distillate with proper pH and conductivity. Electrolytic enrichment ran in the system with 500 mL electrodes (Faculty of Physics and Applied Computer Science, AGH University of Science and Technology, Krakow, Poland). After a second distillation with  $\text{PbCl}_2$ , the measurements were prepared with 12 mL of scintillation cocktail — Hi Safe 3 or Ultima Gold uLLT, and 8 mL of distilled sample. The samples were stored in Qunatulus 1220 at  $18^\circ\text{C}$  at least 12 hours before measurement. Each sample is counted at least  $3 \times 100$  min to ensure satisfactory low statistic uncertainty. QC samples are measured in the same queue as well.

#### 4. RESULTS AND DISCUSSION

Samples for tritium analyses of the unsaturated zone groundwater and precipitation were collected in the period from October 2007 to February 2010. For a detailed observation of groundwater movement in the unsaturated zone, the sampling point JV-8 at 3.4 m below the surface was chosen. The characteristics of the tritium data series was compared with the results of  $\delta^{18}\text{O}$ . Table 1 shows the statistics of monthly measurements of tritium and oxygen-18 in JV-8 and in local precipitation. In both cases the ranges of tritium and  $\delta^{18}\text{O}$  values are higher in precipitation. Higher tritium content and  $\delta^{18}\text{O}$  values in precipitation occur in summer time.

The diagrams in Fig. 2 and Fig. 3 show the time series of  $\delta^{18}\text{O}$  and T compositions of both precipitation and unsaturated groundwater for the sampling point JV-8. Being more complete, the data set of precipitation measurements for Ljubljana was taken for the tritium diagram. Seasonal effects were recognized in both isotope compositions in precipitation. In summertime, the highest tritium content and  $\delta^{18}\text{O}$  values are detected, and in wintertime, the lowest. The same effect could be traced also in samples from JV-8. The diagrams for both parameters show stronger oscillations in precipitation than in groundwater in the unsaturated zone.

TABLE 1. STATISTICS OF TRITIUM CONTENTS AND  $\delta^{18}\text{O}$  VALUES

	JV-8 A(TU)	Precipitation A(TU)	JV-8 $\delta^{18}\text{O}(\text{‰})$	Precipitation $\delta^{18}\text{O}(\text{‰})$
<i>n</i>	22	14	18	24
Mean	9.49	8.10	-8.83	-10.15
Max	10.83	12.90	-7.87	-6.09
Min	7.63	5.16	-10.28	-17.97
Range	3.20	7.74	2.41	11.88

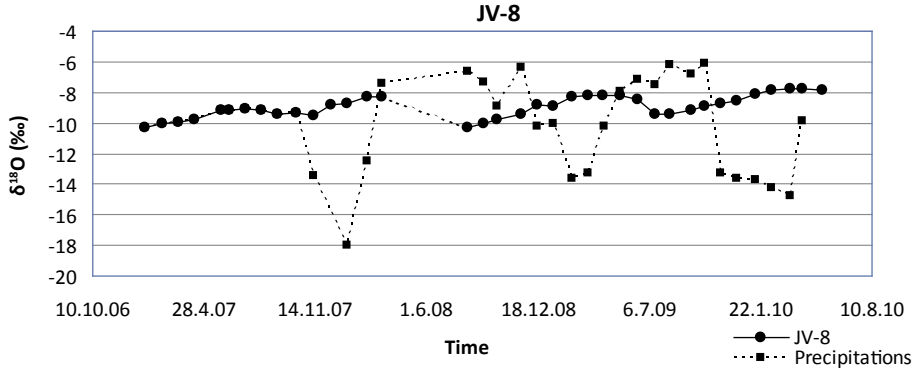


FIG. 2.  $\delta^{18}O$  isotope composition plots of monthly sampled water.

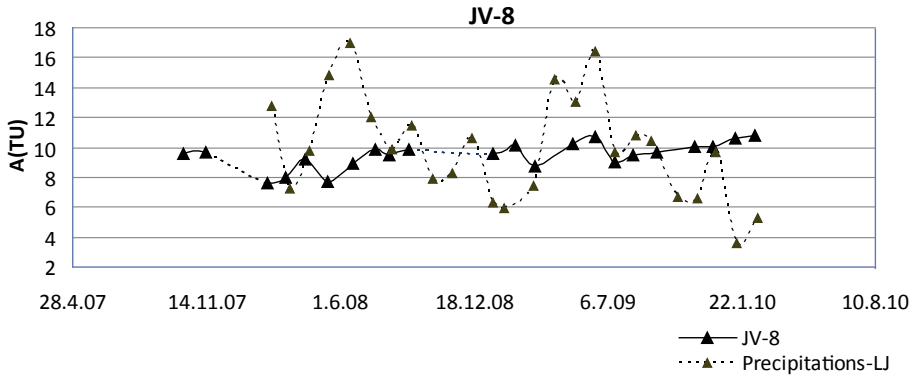


FIG. 3. Tritium content plots of monthly sampled water.

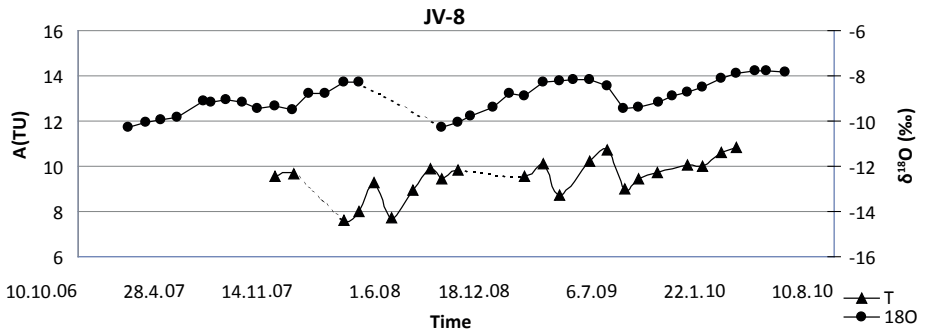


FIG. 4. Tritium and  $\delta^{18}O$  isotope composition for JV-8.

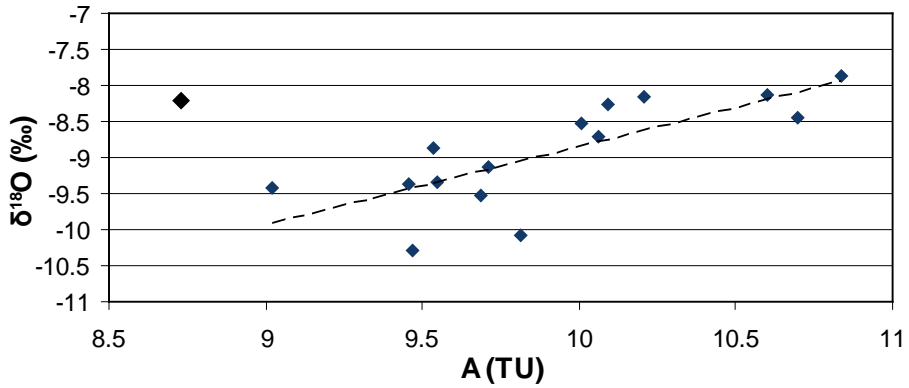


FIG. 5. Relationship between tritium and  $\delta^{18}\text{O}$  contents.

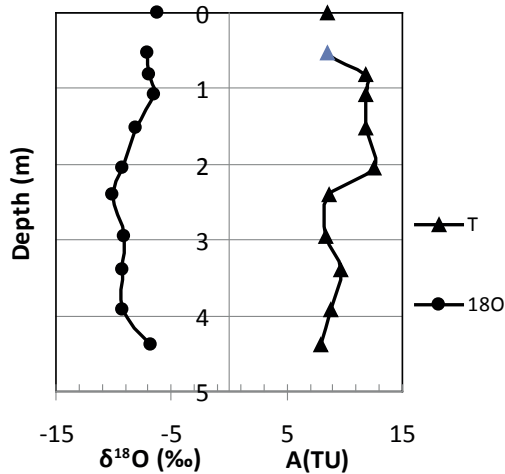


FIG. 6. Depth profile of  $\delta^{18}\text{O}$  and tritium contents.

Previous oxygen-18 investigations of groundwater movement and the unsaturated zone indicate that peak precipitation values (summer or winter signal) were detected in unsaturated zone sampling point measurements in reduced amplitude with depth. Peak values were also observed to be retarded with depth. Peak (winter) precipitation signal of the  $\delta^{18}\text{O}$  values in the observed dataset was detected at the observation point JV-8 over 5–6 months. The peak in the precipitation data series is not so significant in the tritium dataset. In Fig. 4, the comparison of both isotope values is presented in a diagram at the same time scale. The diagram of tritium values is not so smooth and clearly formed. The diagram in Fig. 5 shows the dependency of tritium and  $\delta^{18}\text{O}$  measurements. A correlation between both isotope values is recognizable and a similar behaviour can be assumed.

For a detailed observation of water movement through the unsaturated zone, based on tritium measurements, samples from all observation points were analysed on the 16th of September 2009. The profile of tritium values by the depth on the chosen date is shown in Fig. 6. In the same diagram the  $\delta^{18}\text{O}$  composition profile on the same date is compared. Both diagrams show that, based on tritium and  $\delta^{18}\text{O}$  signals, the tracing of water movement in the coarse gravel unsaturated zone is possible. The signal of the positive values (summer) was recognized in sampling points lying in the upper part of the lysimeter, down to 1–2 m depth. In the following part of the profile (2–3 m depth) more negative values were observed. The isotope characteristics of the water in the deepest part of the lysimeter showed more homogenised water.

## 5. CONCLUSIONS

The aim of this study was to describe transport processes in a coarse gravel unsaturated zone by means of the isotope tritium. Isotope oxygen-18 has already proven a suitable tool for the quantification of recharge water movement in the unsaturated zone, and was therefore chosen for comparison. Results show that based on both signals, the tracing of water movement in the unsaturated zone is possible. Isotope composition signal can be traced in the lysimeter water samples with some time retardation and with diminishing amplitude with depth. The groundwater dynamics in the unsaturated zone are highly dependent on the precipitation rate. Each hydrogeological year has its own characteristics in groundwater dynamics in the unsaturated zone, necessitating more analytical data and hence the need to continue with tritium isotope research. It is difficult to afford an equal number of analyses for the oxygen-18 and tritium isotopes. Based on the existing set of samples from the lysimeter, more tritium analyses for different observation points will be performed and all the results will be evaluated once more. A more complete and longer dataset of tritium analyses will also be used to estimate the mean residence time with lumped parameter models. The results will be compared with the findings of previous studies of processes in a coarse gravel unsaturated zone at the same lysimeter.

## ACKNOWLEDGEMENTS

The study presented in the paper was carried out within the research programmes Groundwater and Geochemistry (P-1-0020-0215) and Structure of hadronic systems (P-1-0102-0106) financed by the Ministry of Higher Education, Science and Technology of Republic Slovenia.

## REFERENCES

- [1] MALI, N., URBANC, J., LEIS, A., Tracing of water movement through the unsaturated zone of a coarse gravel aquifer by means of dye and deuterated water, *Environ. Geol.* **51** (2007) 1401–1412.
- [2] MALI, N., URBANC, J., Isotope oxygen-18 as natural tracer of water movement in a coarse gravel unsaturated zone, *Water Air Soil Pollut.* **203** 1–4 (2009) 291–303.
- [3] MALOSZEWSKI, P., ZUBER, A., “Lumped parameter models for interpretation of environmental tracer data”, *Manual on Mathematical Models in Isotope Hydrogeology*, IAEA-TECDOC-910, IAEA, Vienna (1996) 9–58.
- [4] OZYURT, N.N., BAYARI, C.S., LUMPED: A Visual Basic code of lumped-parameter models for mean residence time analyses of groundwater systems, *Computers & Geosciences* **29** (2003) 79–90.
- [5] MALI, N., JANŽA, M., Ocena možnosti zajema podzemne vode z uporabo MIKE SHE programskega orodja za hidrogeološko modeliranje — primer Selniška Dobrava (Evaluation of water resource exploitation options using the MIKE SHE integrated hydrogeological modelling package — case study Selniška Dobrava), *Geologija* **48** 2 (2005) 281–294.
- [6] AVAK, H., BRAND, W.A., The Finning MAT HDO-Equilibration — A fully automated  $\text{H}_2\text{O}/\text{gas}$  phase equilibration system for hydrogen and oxygen isotope analyses, *Thermo Electronic Corporation, Application News* **11** (1995) 1–13.

# CHANGES IN ISOTOPIC COMPOSITION OF BOTTLED NATURAL WATERS DUE TO DIFFERENT STORAGE CONDITIONS

T. FERJAN<sup>a</sup>, M. BRENČIČ<sup>b,a</sup>, P. VREČA<sup>c</sup>

<sup>a</sup> Geological Survey of Slovenia,  
Department of Hydrogeology,  
Ljubljana, Slovenia

<sup>b</sup> Faculty of Natural Sciences and Engineering,  
Department of Geology,  
Ljubljana, Slovenia

<sup>c</sup> Jožef Stefan Institute,  
Department of Environmental Sciences,  
Ljubljana, Slovenia

## Abstract

To establish the influence of environmental conditions on processes affecting the stable isotopic composition of bottled water during storage, various brands of bottled water were exposed for 2 years in different conditions. Selected low mineralized natural mineral water of one particular brand stored in polyethylene terephthalate (PET) bottles was placed at three different locations with different physical conditions (temperature, relative humidity, air pressure, exposure to sunlight). For comparison, bottles of three other low mineralized natural mineral water brands, each from a different aquifer source, were placed in parallel at one of the locations. Each location was characterized by temperature, relative humidity and air pressure measurements. pH, conductivity and stable isotopic composition of oxygen, hydrogen and carbon in dissolved inorganic carbon ( $\delta^{18}\text{O}$ ,  $\delta^2\text{H}$ ,  $\delta^{13}\text{C}_{\text{DIC}}$ ) were measured in regular intervals for nearly two years. Preliminary results from each location show noticeable changes in isotopic composition as well as the physical parameters of water with time of storage.

## 1. INTRODUCTION

Bottled water first became a sizeable, mainstream commercial beverage category in Western Europe, where consumption of it has long been part of many residents' daily routine. It is now a truly global beverage [1]. The quality of bottled water is regulated by state laws but these regulations control the quality of bottled water only to the point of its filling. What happens to water in the bottle after that is

rarely the point of interest. The original water at the filling plant fulfils the legislative regulations for chemical composition and physical parameters. What are the consequences of storing water in PET bottles for a longer period of time? In the last years many investigations have confirmed the effects of food packaging on the quality of packaged goods. The same can be observed in bottled water. Results reported in the literature focus mostly on the leaching and migration of genotoxic compounds from PET bottles into water and microbiological quality [2–4]. Some work focussed on the determination of stable isotope ratios of oxygen, hydrogen and carbon in dissolved inorganic carbon in bottled water for the need of identification of sources and production processes of bottled waters [5–7]. The majority of investigations of bottled waters consider bottled water only as a result of processes which took place in the aquifer. Our research focuses on bottled waters from another aspect. We are interested in bottled water from the point when it arrives from the filling plant to the storehouse, markets and finally to the consumer. The different environments during its life cycle and the changing conditions to which the bottled water is exposed all affect its characteristics. Conditions at a certain stage of life cycle of bottled waters are best described with stable isotopes, as they represent ideal tracers for processes and environments that water could be exposed to. Variations of  $^2\text{H}$  and  $^{18}\text{O}$  content in waters are closely related to isotopic fractionation occurring during evaporation and condensation of water [8]. Isotopic fractionation in bottled waters can also be entailed by water sorption and the diffusive transfer of water molecules through organic polymeric material [9]. Isotopic fractionation during evaporation as well as diffusivity of water in PET membranes are both strongly dependent on the temperature and relative humidity in the environment of the reaction [10]. The aim of the present study is to gradually determine possible changes in isotopic composition of natural mineral waters stored in PET bottles in different environmental conditions from filling to consumption and to find out the rate to which described changes mask the primary natural mineral water characteristics. For this purpose an experimental setup with low mineralized natural mineral waters from different sources, packed in PET bottles and stored under different environmental conditions was established.

## 2. METHODS

Packages of low mineralized natural mineral water of one particular brand were collected at the filling plant just after the end of production process, to obtain a representative state and chemical composition of water. For the comparison three other brands were purchased in one of the supermarkets in Ljubljana. All waters were filled in transparent, uncoloured PET bottles with 1.5 L water content. Three storage sites were appointed for bottled water storage. These sites were chosen with the intention to assure a variety of environmental conditions that bottled waters could be exposed to during storage in storehouses or markets. The first group of samples was located



FIG. 1. Location 1.



FIG. 2. Location 2.



FIG. 3. Location 3.

TABLE 1. PHYSICAL CONDITIONS AT STORAGE LOCATIONS

Storage site	Temperature (°C)			Relative humidity (%)			Air pressure (hPa)		
	Min	Max	Average	Min	Max	Average	Min	Max	Average
Location 1*	20.8	33.2	26	13	59	38	943	994	977
Location 2	7	22.9	15	23	83	61	943	995	976
Location 3*	-9.6	36	14	13	100	67	945.7	993.2	975

\* samples exposed to sunlight

in the laboratory (location 1), where the bottles were stored at room temperature and exposed to sunlight. The second location was in the closed room (location 2). Bottles on this location were stored in the dark at quite constant temperature but with seasonal fluctuations. The last storage location is outdoor, where the bottles are exposed to daily changes of weather conditions and sunlight (location 3). On each of the locations physical parameters (temperature, relative humidity, air pressure) were registered hourly. Location sites are presented in Figs 1–3. A description of physical conditions on each of location during storage period is given in Table 1.

## 2.1. Sampling

All the bottles were marked with labels according to the storage location. 90 bottles of natural mineral water were placed in each of the locations. The earlier mentioned comparative brands were located at location 1. The original labels of the bottles were not removed. Before sampling, the serial numbers of bottles which were to be sampled were chosen by lot. Firstly, the on set sampling was performed only at location 1. During first sampling five samples from five bottles of one particular brand were taken. In the following samplings only four samples were taken for the main brand at each of the locations and one sample from the comparative brands. Duplicate samples of  $\delta^{18}\text{O}$ ,  $\delta^2\text{H}$  and  $\delta^{13}\text{C}$  were taken from the same bottle during each

sampling. For the analysis of  $\delta^{18}\text{O}$  and  $\delta^2\text{H}$  the water was filled in 100 mL brown glass bottles, which were rinsed three times before filling. The bottles were filled to the top and closed with PET screw-caps. All the bottles were additionally sealed with paraffin wax tape. 100%  $\text{H}_2\text{PO}_4$  was added into 12 mL glass extainers which were purged with pure He. Samples for  $\delta^{13}\text{C}_{\text{DIC}}$  (5 mL) were injected immediately into glass extainers. All samples for  $\delta^{13}\text{C}_{\text{DIC}}$  analyses were collected in duplicates. Water characteristics (pH, temperature, electroconductivity) were measured for each sample taken. During the first two months of our two year sampling period, sampling was carried out every 14 days and later on after every two months. All bottled waters on every location were randomly mixed every 14 days to assure the same exposure to the outer conditions. Samples for  $\delta^{18}\text{O}$  and  $\delta^2\text{H}$  analyses were sent to the laboratories in random order, identified only by numbers so that their identities were unknown to the analyst at the time of the analysis.

## 2.2. $\delta^{18}\text{O}$ , $\delta^2\text{H}$ and $\delta^{13}\text{C}_{\text{DIC}}$ analyses

Hydrogen and oxygen isotope analyses of the water samples were performed at the Joanneum Research Institute of Water Resources Management in Graz, Austria. The isotopic composition of hydrogen ( $\delta^2\text{H}$ ) was measured in  $\text{H}_2$  generated by reduction of water over hot chromium at  $1050^\circ\text{C}$  on a continuous flow Finnigan DELTA<sup>plus</sup> XP (Thermo Electron Corporation, Bremen, Germany) stable isotope mass spectrometer with HEKAtech hightemperature oven. Isotopic composition of oxygen ( $\delta^{18}\text{O}$ ) was determined by means of the water- $\text{CO}_2$  equilibration technique on a dual inlet Finnigan DELTA<sup>plus</sup> (Thermo Electron Corporation) stable isotope mass spectrometer with fully automated capabilities. Isotopic composition of dissolved inorganic carbon ( $\delta^{13}\text{C}_{\text{DIC}}$ ) was determined on  $\text{CO}_2$  collected after the reaction with 100%  $\text{H}_3\text{PO}_4$  on a continuous flow Europa 20-20 ANCA-TG stable isotope mass spectrometer in isotopic laboratory at the Jožef Stefan Institute in Ljubljana. Results are expressed in standard delta notation ( $\delta$ ) as per mille (‰) deviation from the standard V-SMOW for  $\delta^2\text{H}$  and  $\delta^{18}\text{O}$  and for  $\delta^{13}\text{C}_{\text{DIC}}$  from the standard V-PDB as:

$$\delta^Y X (\text{‰}) = \left( \frac{R_{\text{sample}}}{R_{\text{std}}} - 1 \right) \times 1000$$

Where  $^Y X$  is  $^{18}\text{O}$  or  $^2\text{H}$ ,  $R_{\text{sample}}$  and  $R_{\text{std}}$  are  $^{18}\text{O}/^{16}\text{O}$ ,  $^2\text{H}/^1\text{H}$  or  $^{13}\text{C}/^{12}\text{C}$  ratios of the sample and standard, respectively. All measurements were carried out against laboratory standards that were periodically calibrated against international standards recommended by the IAEA. Measurement reproducibility was better than  $\pm 0.1\text{‰}$  for  $\delta^{18}\text{O}$ ,  $\pm 1\text{‰}$  for  $\delta^2\text{H}$  and  $\pm 0.2\text{‰}$  for  $\delta^{13}\text{C}_{\text{DIC}}$ .

### 3. RESULTS AND DISCUSSION

Results show very distinctive influences on the bottled water isotopic composition. Changes in isotopic composition of  $\delta^2\text{H}$  and  $\delta^{18}\text{O}$  at storage locations 1–3 are presented in Fig. 4–6.

In all three cases gradual enrichment in heavy isotopes is noticed. This trend is especially well defined in oxygen isotopic composition, where the biggest enrichment is detected in location 1. In the other two locations values are quite similar. As for oxygen isotopic composition, and also for hydrogen isotopic composition, the biggest enrichment was detected at location 1, followed by location 2 and the smallest difference from initial isotopic composition was detected at location 3. The isotopic composition of  $\delta^{13}\text{C}_{\text{DIC}}$  in the experimental storage location is given in Fig. 7. Also in the  $\delta^{13}\text{C}_{\text{DIC}}$  composition, gradual enrichment with periodical fluctuations is observed. Rate of changes for  $\delta^{13}\text{C}_{\text{DIC}}$  composition is similar at locations 1 and 2, followed by location 3. Descriptive statistics for the isotopic composition of the studied low mineralized natural mineral water are given in Table 2.

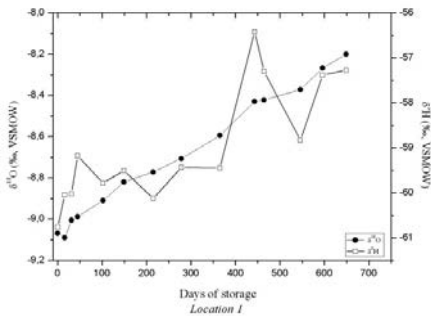


FIG. 4.  $\delta^2\text{H}$  and  $\delta^{18}\text{O}$  composition versus time of storage at location 1.

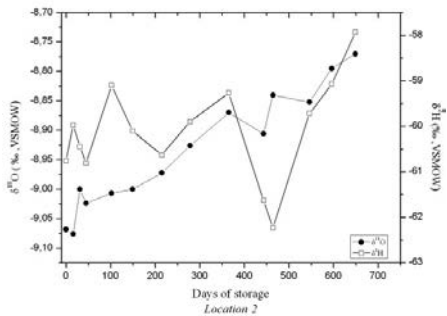


FIG. 5.  $\delta^2\text{H}$  and  $\delta^{18}\text{O}$  composition versus time of storage at location 2.

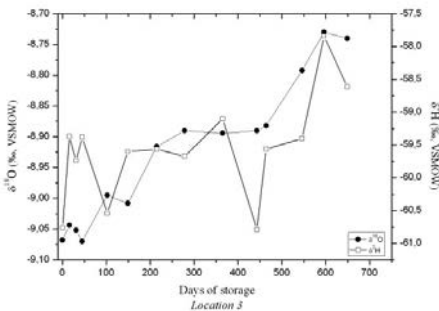


FIG. 6.  $\delta^2\text{H}$  and  $\delta^{18}\text{O}$  composition versus time of storage at location 3.

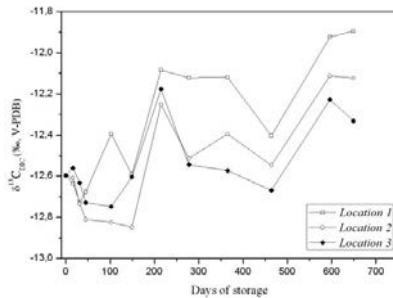


FIG. 7. Isotopic composition of  $\delta^{13}\text{C}_{\text{DIC}}$  at all three storage locations.

TABLE 2. DESCRIPTIVE STATISTICS OF  $\delta^2\text{H}$ ,  $\delta^{18}\text{O}$  AND  $\delta^{13}\text{C}_{\text{DIC}}$  AT STORAGE LOCATIONS

	Average	Median	Min	Max	Range	N
$\delta^2\text{H}$ (‰)						
Location 1	-59.03	-59.34	-62.52	-56.20	6.32	55
Location 2	-60.15	-60.13	-62.53	-57.58	4.95	51
Location 3	-59.57	-59.54	-61.52	-57.04	4.48	49
$\delta^{18}\text{O}$ (‰)						
Location 1	-8.69	-8.74	-9.10	-8.20	0.90	55
Location 2	-8.94	-8.95	-9.11	-8.74	0.37	51
Location 3	-8.93	-8.92	-9.10	-8.69	0.41	49
$\delta^{13}\text{C}_{\text{DIC}}$ (‰)						
Location 1	-12.36	-12.42	-12.98	-11.68	1.31	55
Location 2	-12.53	-12.54	-13.30	-11.94	1.36	52
Location 3	-12.55	-12.61	-12.94	-11.90	1.04	52

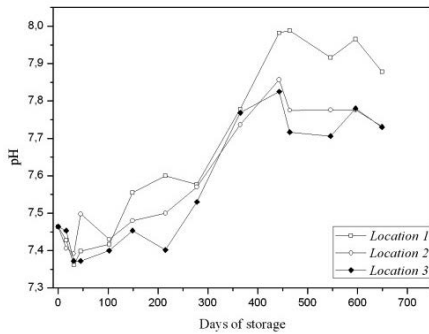


FIG. 8. pH versus time at storage locations 1–3; average values are presented

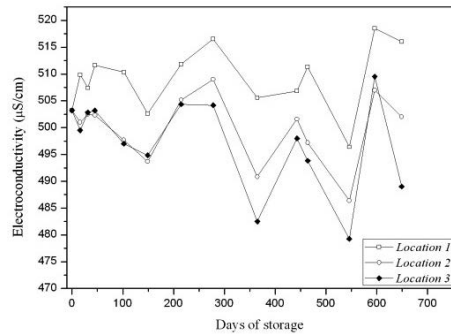


FIG. 9. Electroconductivity versus time at storage locations 1–3; average values are presented.

Changes in physical parameters (pH and electroconductivity) at storage locations are presented in Figs 8 and 9.

In the pH versus time diagram, the increase in pH values is noticed at all three locations. The biggest changes are noticed at location 1, where the highest value of pH (8) is determined. Values of electroconductivity in all three locations have quite

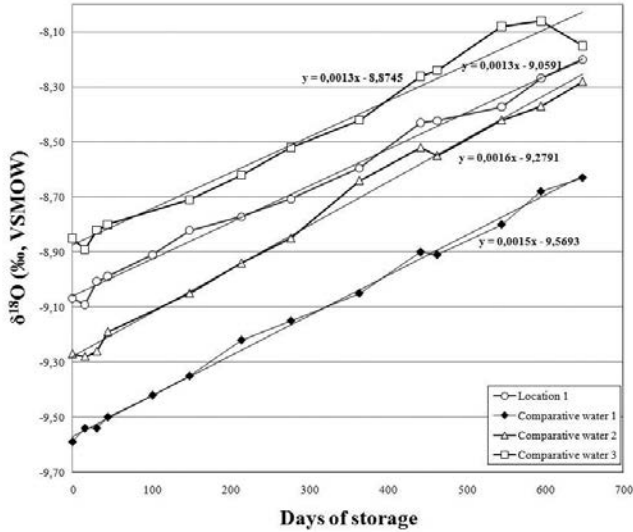


FIG. 10. Oxygen isotope composition versus time in studied and comparative bottled waters at location 1.

similar trends, while the biggest changes in bottled water electroconductivity are detected at location 3.

An interesting fact was noticed in the analysis of oxygen isotope composition of comparative brands at location 1. In Fig. 10, the oxygen isotopic composition of all waters is presented. From the diagram, the resemblance in rate of oxygen isotopic composition change is noticed in all waters. Equations presented show that slope values are quite similar for all waters even if their sources are different, which leads to an important fact concerning the verification of bottled water.

#### 4. CONCLUSION

The analysis of isotopic composition is a useful tool in determining changes in bottled waters during storage. These changes start to occur right after the bottling and the rate of changes is additionally connected with physical conditions in the storage location. Together with changes in isotopic composition, changes in physical parameters also occur. Since our experiment is still in progress, only preliminary results of the experiment are given. In the future, additional research work will be focused in determining the processes accountable for changes in bottled water characteristics and the rate of its dependence upon different storage conditions.

## ACKNOWLEDGEMENT

The results were obtained through the research programs 'Groundwater and geochemistry' of the Geological Survey of Slovenia and 'Cycling of substances in the environment, mass balances, modelling of environmental processes and risk assessment' of the Jožef Stefan Institute, financially supported by the Slovene Research Agency, ARRS.

## REFERENCES

- [1] INTERNATIONAL BOTTLED WATER ASSOCIATION, Challenging Circumstances Persist: Future Growth Anticipated (2009), <http://www.bottledwater.org/files/2009BWstats.pdf>
- [2] KERESZTES, S., et al., Leaching of antimony from polyethylene terephthalate (PET) bottles into mineral water, *Sci. Total Environ.* **407** (2009) 4731–4735.
- [3] LEIVADARA, S.V., et al., Determination of organic compounds in bottled waters, *Food Chemistry* **108** (2008) 277–286.
- [4] REIMANN, C., et al., Bottled drinking water: Water contamination from bottle materials (glass, hard PET, soft PET), the influence of colour and acidification, *Appl. Geochem.* **25** (2010) 1030–1046.
- [5] BOWEN, G.J., et al., Stable hydrogen and oxygen isotope ratios of bottled waters of the world, *Rapid Commun. Mass Spectrom.* **19** (2005) 3442–3450.
- [6] BRENČIČ, M., VREČA, P., Identification of sources and production processes of bottled water by stable hydrogen and oxygen isotope ratios, *Rapid Commun. Mass Spectrom.* **20** (2006) 3205–3212.
- [7] BRENČIČ, M., VREČA, P., Isotopic composition of dissolved inorganic carbon in bottled waters on the Slovene market, *Food Chemistry* **101** (2007) 1516–1525.
- [8] ARAGUÁS-ARAGUÁS, L., et al., Deuterium and oxygen-18 isotope composition of precipitation and atmosphere moisture, *Hydrol. Process.* **14** (2000) 1341–1355.
- [9] SPANGENBERG, J.E., VENNEMANN, T.W., The stable hydrogen and oxygen isotope variation of water stored in polyethylene terephthalate (PET) bottles, *Rapid Commun. Mass Spectrom.* **22** (2008) 672–676.
- [10] CLARK, I., FRITZ, P., *Environmental Isotopes in Hydrogeology*, Lewis Publishers, New York (1997).

# INVESTIGATING NATURAL ANALOGUES FOR CO<sub>2</sub> SEQUESTRATION IN ULTRAMAFIC ROCKS: A REACTIVE TRANSPORT MODELLING APPROACH

F. GHERARDI

Istituto di Geoscienze e Georisorse,  
Consiglio Nazionale delle Ricerche,  
Pisa, Italy

## Abstract

Serpentinites of Ligurian ophiolites are studied as natural analogues for CO<sub>2</sub> mineral sequestration in Italy. Mineralogical and geochemical observations indicate that silicification and carbonation are typical alteration processes induced by the interaction of CO<sub>2</sub> charged fluids with pristine ultramafic rocks. Multicomponent reactive transport models have been applied to reproduce natural patterns and investigate carbon sequestration efficiency under high P<sub>CO<sub>2</sub></sub> conditions. Temporal changes in porosity and permeability are predicted to affect the spatial and temporal occurrence of secondary minerals. The feedback between mineralogical transformations and transport properties of the geological media emerges as a key factor controlling the mineral carbonation potential of the investigated ultramafic rocks.

## 1. INTRODUCTION

The universal concern about anthropogenically induced climate change is resulting in the development of strategies aimed at reducing or, at least, slowing down, the increase of greenhouse gas concentrations in the atmosphere. Sequestration of CO<sub>2</sub> in deep geological reservoirs is one of the most effective disposal options currently taken into consideration [1]. The carbonation of silicate minerals has the highest capacity and longest storage time of CO<sub>2</sub> of any the storage options currently known [2]. The precipitation of carbonate minerals is especially effective because it would fix gaseous CO<sub>2</sub> at depth in a permanent manner. Despite the fact that the conversion of CO<sub>2</sub> to a thermodynamically stable and immobile form has been investigated since the early 1990s [3–5], making this process work industrially still represents a difficult task [6]. The most comprehensively studied process for industrial carbonation is the aqueous carbonation process, because of its potential for achieving needed carbonation rates in a relatively simple chemical process [7]. The same type of process is expected to occur upon injection of CO<sub>2</sub> into deep geological media, when large amounts of Ca- or Mg-bearing silicates are available. Suitable materials include ultramafic intrusive or extrusive rocks, i.e. peridotites, dunites, hornblendites,

pyroxenites and komatiites, and their metamorphic varieties, i.e. serpentinites, talc and asbestos rocks [5, 8, 9].

Despite this potential, mineral sequestration in ultramafic geological media could be problematic in perspective, because, due to the intrinsic low primary effective porosity and permeability of these rocks, difficulties are expected in the achievement and maintenance of adequate injectivity to sustain injection at commercial rates over extended periods.

Recently, serpentinites of Ligurian ophiolites have been studied from a geochemical point of view as natural analogues for CO<sub>2</sub> mineral sequestration in Italy [10], on the basis of available data on mineralogy [11] and porewater chemistry [12]. In this paper, reactive transport modelling techniques have been applied to explore key factors controlling the ‘geochemical feasibility’ of carbon sequestration under transport controlled, multiphase, high-P<sub>CO<sub>2</sub></sub> conditions. Numerical simulations do not account for geomechanical aspects likely related to the mineralogical re-organization of the primary assemblage. These aspects, together with a detailed description of geological and tectonic features of the area, depth and nature of the pressure confinement, spatial variability of hydraulic, petrophysical and geochemical rock properties, should be taken into account to evaluate if the target formation could be a good candidate for CO<sub>2</sub> storage.

## 2. MODEL SETUP

### 2.1. Conceptual model

Much specific and detailed information is required to assess the feasibility of disposing of CO<sub>2</sub> in a geological formation at any particular site. Before moving into site specific investigations, general features relating to the target geological formation for CO<sub>2</sub> injection should be explored. In the present work, this has been performed for an idealized ultramafic formation. Mineralogical and fluid geochemistry data, specific to a well known hydrogeological system in northern Italy [10], have been used to constrain the numerical model. The focus is on a fractured portion of the aquifer, where relatively high values of porosity and permeability allow for an hypothetical injection of CO<sub>2</sub> at depth.

### 2.2. Modelling approach

The modelling work has been built in stages of increasing complexity. Firstly, zero dimensional models (‘Phase A’) have been used to simulate water–rock interactions occurring under variable P<sub>CO<sub>2</sub></sub> conditions within the deep aquifers hosted in the serpentinites of Ligurian ophiolites. The thermodynamic consistency of numerical results has been checked against the chemical composition of present day porewaters.

The best-fitting geochemical conditions obtained by such a procedure have then been used to initialize the second set of simulations ('Phase B'), aimed at predicting the geochemical evolution of the deep aquifer if high pressure CO<sub>2</sub> gas is present. Numerical results from 'Phase B' simulations are addressed in this paper in some detail compared to those of 'Phase A'.

### 2.3. Geometry and boundary conditions

A simplified, one-dimensional conceptual model has been implemented to simulate the flow between the ends of a fractured zone within the deep aquifer ('Phase B simulations'). Due to the lack of specific information on the hydraulic properties of the investigated lithology, the fractured volume has been arbitrarily modelled as a homogeneous porous domain with moderate effective porosity (0.20) and permeability ( $10^{-15}$  m<sup>2</sup>). The model mesh consists of 50 grid cells, covering an overall extent of 50 m, with a transversal section of  $0.1 \times 0.1$  m. Multiphase advection is the predominant process controlling mass transport of both gas and aqueous phases along the fracture. The 1-D domain is modelled as an isolated system with Dirichlet-type boundary conditions at the ends of the fracture domain. By applying specified pressure conditions on the two opposite sides of the domain, a constant, unidirectional flow of gas, water and solute mass is forced along the fracture. Isothermal conditions at 15°C were maintained during a simulation time of 100 years.

### 2.4. Initial conditions

The primary assemblage is composed of 4 minerals (antigorite, magnetite, talc, diopside), with antigorite and magnetite accounting for more than 90% by vol. of the total solid volume. Numerical calculations account for possible precipitation/dissolution reactions of 25 additional minerals. The chemical composition of the deep-seated, Ca-OH primary fluid is characterized by high pH values in the range 10.7–11.2, and very low log P<sub>CO<sub>2</sub></sub> values (< -8). CO<sub>2</sub> charged waters flowing through the fracture have quite acidic pH values in the range 5.2–5.5, and log P<sub>CO<sub>2</sub></sub> values between 0.1–1.3.

### 2.5. Numerical simulator, thermodynamic and kinetic data

All the simulations have been performed with the TOUGHREACT numerical simulator [13]. Dissolution and precipitation processes are integrated in this code with a feedback on porosity and permeability changes. Mineral dissolution/precipitation can take place subject to either local equilibrium or kinetic controls. Thermodynamic data have been taken from the EQ3/6 data0.ymp.R2.dat dataset [14]. Minerals are allowed to dissolve and/or precipitate according to a TST type kinetic

reaction mechanism [15]. Kinetic parameters, e.g. reaction rates and reactive surface areas, have been taken from the literature [16], and references therein.

### 3. RESULTS AND DISCUSSION

The overall reactivity of the modelled system can be conveniently traced by inspecting temporal and spatial variations of pH and gas saturation ( $S_g$ ). The pH evolution (Fig. 1A) is driven by the advancement of a gaseous front (Fig. 1B) through the fracture domain. The early onset of a free,  $\text{CO}_2$  rich gas phase, causes pH to

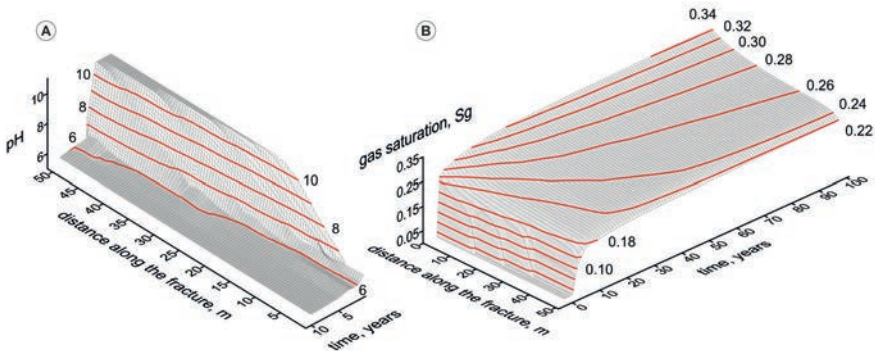


FIG. 1. pH and gas saturation ( $S_g$ ) surface diagram showing the time and space variation of these parameters all along the fracture domain over a time span of 100 years. Features refer to a ‘low flow conditions’ run, with gas advective velocity equal to 2 m/a.

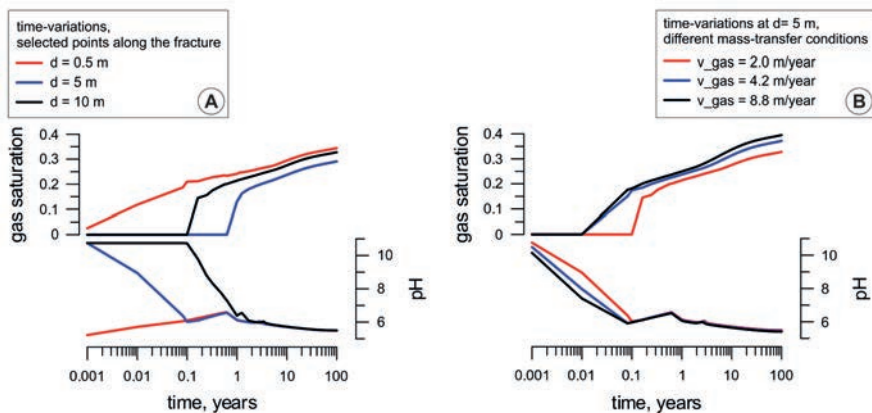


FIG. 2. Scatter diagrams showing the temporal variation of pH and gas saturation ( $S_g$ ) at different points along the fracture domain under ‘low flow conditions’ ( $v_{\text{gas}} = 2$  m/a; box A), and at a fixed distance of 5 m from the inlet point, under different fluid flow conditions (box B).

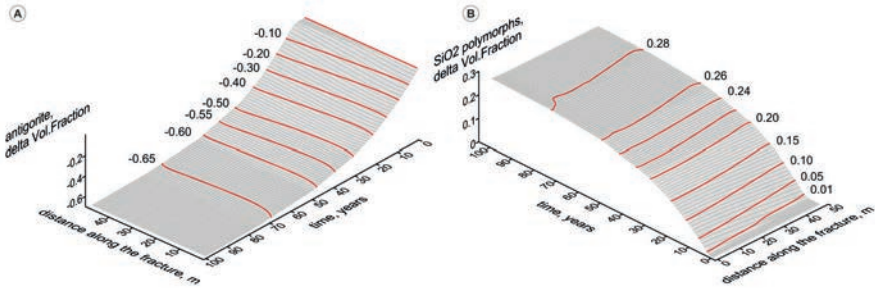


FIG. 3. Surface diagrams showing time and space variation of antigorite (box A) and silica polymorphs (box B) volume fractions along the fracture domain over a time span of 100 years.

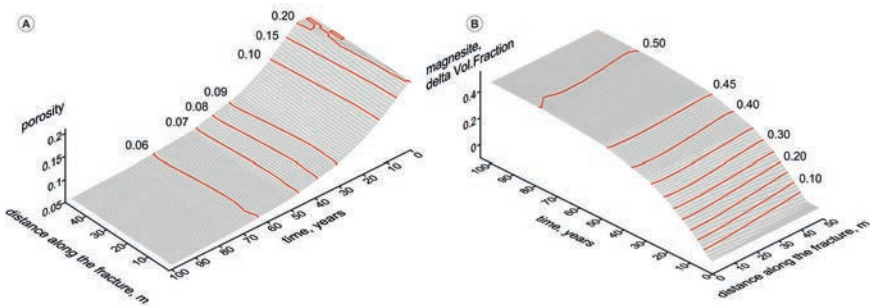


FIG. 4. Surface diagrams showing time and space variation of porosity (box A) and magnetite volume fraction (box B) along the fracture domain over a time span of 100 years.

decrease, overwhelming the buffer capacity of the primary mineralogical assemblage. The onset of variable flow conditions (i.e. pressure gradients at the ends of the fracture domain arbitrarily set between 2 and 20 bar in our model), has a negligible effect in terms of both gas and pH acid front propagation (Fig. 2A and 2B), and in all the investigated cases, pH quickly stabilizes at 5.4–5.8 throughout the fracture, after 10 years simulation time.

The advancement of the two phase,  $\text{CO}_2$  rich, acidic front along the fracture induces significant mineralogical transformations. Both the predicted alteration of primary rock minerals and the development of a secondary mineral assemblage are generally consistent with field observations in ultramafic formations interacting with  $\text{CO}_2$ -charged fluids (e.g. [10], and references therein). In detail, the main mineralogical transformations predicted over the reference simulation time of 100 years are:

(i) antigorite (Fig. 3A) steadily dissolves until almost complete disappearance all along the fracture domain (volume fraction  $<0.01$ ); (ii) magnetite and diopside show a monotonic pattern of dissolution and a moderate decrease in concentration; (iii) a relevant precipitation of silica polymorphs (chalcedony or cristobalite- $\beta$ , depending on the thermodynamic proxy used in the calculations; Fig. 3B) is predicted

all over the fracture; (iv) magnesite (or hydromagnesite, depending on model initial conditions; Fig. 4B) is the main secondary by-product of antigorite dissolution, and the most abundant mineral at the end of the simulations; (v) talc always precipitates, up to a maximum volume fraction of 0.04; (vi) the phyllosilicate fraction is virtually absent, with minor, transitory precipitation episodes involving Ca and Mg smectites and montmorillonites; (vii) chlorites are not predicted to form; (viii) carbonate minerals, such as siderite and proto-dolomite (a thermodynamic proxy for disordered-dolomite in the numerical model), are predicted to precipitate in very minor amounts (less than 1% by vol. of the solid volume fraction), whereas ankerite and dawsonite do not precipitate; (ix) sepiolite and nesquehonite are not predicted to form; (x) very minor precipitation of iron hydroxides (volume fraction always  $< 0.001$ ), i.e. goethite or ferrihydrite, may occur, depending on redox conditions; (xi) overall, significant variations in porosity (Fig. 4A) are predicted to occur in all the simulations.

### 3.1. Sensitivity analysis

Adequate porosity, thickness and permeability values are critical parameters for storage capacity and injectivity of CO<sub>2</sub> geological repositories. As porosity–permeability changes directly relate to mineral redistribution in geological media, in this work porosity and permeability have been used as master variables to monitor the efficiency of gas–water–rock interactions. In addition, even if a simple functional porosity–permeability relationship is not realistically attainable because of the complexity of natural geologic media [17], several porosity permeability correlations have been used in the calculations in an attempt to evaluate the effect of the heterogeneous, non-predictable organization of the space in geological media [18] on numerical outputs.

Numerical results indicate that the precipitation or dissolution of minerals in the pore throats results in strongly nonlinear changes of permeability. Depending on initial conditions, namely liquid residual saturation and mass transfer efficiency along the fracture domain, the initial porosity may be significantly reduced (down to complete clogging) as a consequence of the replacement of primary ultramafic minerals with carbonates and silica polymorphs. In addition, an early (few tens of years) severe lowering in absolute permeability is predicted when the tube-in-series model of Ref. [18] is used. This occurs in particular for low values ( $< 0.1$ ) of the so-called ‘critical porosity threshold’, i.e. the porosity value (arbitrarily set) at which initial permeability is almost reduced to zero. Under these conditions, the ultramafic formation is not suitable for CO<sub>2</sub> injection.

Uncertainty related to the intrinsically poor knowledge of kinetic rates, reactive surface areas and spatial variability of hydraulic, petrophysical and geochemical rock properties is an additional first order controlling factor of the mineralogical alteration intensity predicted by the code. Additional sensitivity analyses have then been performed on: (i) thermodynamic and kinetic parameters of carbonate minerals;

(ii) thermodynamic parameters of silica polymorphs. These additional simulations revealed that: (i) the use of hydromagnesite as a thermodynamic proxy for magnesite, leads to a massive precipitation of Mg carbonate, and to enhanced clogging of the initial porosity (residual porosity always below 0.02); (ii) chalcedony or cristobalite- $\beta$  can be used almost interchangeably as thermodynamic proxies of SiO<sub>2</sub> without any significant effect on numerical results.

#### 4. CONCLUSIONS

Reactive transport modelling suggests that the injection of supercritical CO<sub>2</sub> in a idealized, fractured ultramafic rock having the same average mineralogical composition of the serpentinites of the Ligurian Ophiolites, may cause a severe alteration of the primary mineralogical assemblage. The mineralogical transformation of primary ultramafic minerals always leads to a significant reduction in porosity and permeability.

The spatial and temporal occurrence of secondary minerals, and then the mineral carbonation potential of the investigated ultramafic rocks, depend sensitively on temporal changes in porosity and permeability. Depending on the different transport properties and functional porosity–permeability relationships used in the calculations, a complete clogging of pores and/or a lowering in absolute permeability can be predicted in a few decades.

As the alteration advance distance is largely constrained by transport parameters related to advection, and the overall reactivity depends upon the ratio of transport to reaction rate, a reactive transport modelling approach is needed to properly assess the geochemical feasibility of CO<sub>2</sub> injection and storage in the investigated lithology. Sensitivity analysis on different functional laws describing the feedback between mineralogical transformations and transport properties of the geological media is also highly recommended.

#### REFERENCES

- [1] INTERGOVERNMENTAL PANEL ON CLIMATE CHANGE, Carbon Dioxide Capture and Storage, Intergovernmental Panel on Climate Change, Cambridge University Press, Cambridge (2005).
- [2] LACKNER, K.S., A guide to CO<sub>2</sub> sequestration, *Science* **300** (2003) 1677–1678.
- [3] SEIFRITZ, W., CO<sub>2</sub> disposal by means of silicates, *Nature* **345** (1990) 486.
- [4] LACKNER, K.S., WENDT, C.H., BUTT, D.P., JOYCE, E.L., Jr., SHARP, D.H., Carbon dioxide disposal in carbonate minerals, *Energy* **20** (1995) 1153–1170.
- [5] GOFF, F., LACKNER, K.S., Carbon dioxide sequestering using ultramafic rocks, *Environ. Geosci.* **5** 3 (1998) 89–101.

- [6] TEIR, S., KUUSIK, R., FOGELHOLM, C.-J., ZEVENHOVEN, R., Production of magnesium carbonates from serpentinite for long term storage of CO<sub>2</sub>, *International Journal Miner. Process.* **85** (2007) 1–15.
- [7] O'CONNOR, W.K., DAHLIN, D.C., TURNER, P.C., WALTERS, R., Carbon Dioxide Sequestration by Ex-situ Mineral Carbonation, Proc. 2nd Dixy Lee Ray Memorial Symposium, Albany Research Center, Washington DC (1999).
- [8] LACKNER, K.S., WENDT, C.H., BUTT, D.P., JOYCE, E.L., Jr., SHARP, D.H., Carbon dioxide disposal in carbonate minerals, *Energy* **20** (1995) 1153–1170.
- [9] WU, J.C.-S., SHEEN, J.-D., CHEN, S.-Y., FAN, Y.-C., Feasibility of CO<sub>2</sub> fixation via artificial rock weathering, *Ind. Eng. Chem. Res.* **40** (2001) 3902–3905.
- [10] CIPOLLI, F., GAMBARDELLA, B., MARINI, L., OTTONELLO, G., VETUSCHI ZUCCOLINI, M., Geochemistry of high-pH waters from serpentinites of the Gruppo di Volpi, *Appl. Geochem.* **19** (2004) 787–802.
- [11] CORTESOGNO, L., MAZZUCOTELLI, A., VANNUCCI, R., Alcuni esempi di pedogenesi su rocce ultrafemiche in clima mediterraneo, *Ofioliti* **4** (1979) 295–312 (in italian).
- [12] BRUNI, J., et al., Irreversible water–rock mass transfer accompanying the generation of the neutral, Mg–HCO<sub>3</sub> and high-pH, Ca–OH spring waters of the Genova province, Italy, *Appl. Geochem.* **17** (2002) 455–474.
- [13] XU, T., SONNENTHAL, E.L., SPYCHER, N., PRUESS, K., TOUGHREACT – A simulation program for non-isothermal multiphase reactive geochemical transport in variably saturated geologic media: Applications to geothermal injectivity and CO<sub>2</sub> geological sequestration, *Computer & Geosciences* **32** (2006) 145–165.
- [14] WOLERY, T.J., JOVE-COLON, C.F., Qualification of thermodynamic data for geochemical modelling of mineral-water interactions in dilute systems, ANL-WIS-GS-000003 REV00, United States Department of Energy Report, Las Vegas, NV (2004).
- [15] LASAGA, A.C., SOLER, J.M., GANOR, J., BURCH, T.E., NAGY, K.L., Chemical weathering rates and global geochemical cycles, *Geochim. Cosmochim. Acta* **58** (1994) 2361–2386.
- [16] PALANDRI, J.L., KHARAKA, Y.K., A Compilation of Rate Parameters of Water–Mineral Interaction Kinetics for Application to Geochemical Modelling, Open File Report 2004-1068, U.S. Geological Survey, Mnlo Park, CA (2004).
- [17] RAFFENSPERGER, J.P., “Numerical simulation of sedimentary basin-scale hydrochemical processes”, *Advances in Porous Media* (CORAPCIOGLU, Y.C., Ed.), Elsevier Science, Amsterdam, The Netherlands (1996) 185–305.
- [18] VERMA, A., PRUESS, K., Thermohydrological conditions and silica redistribution near high-level nuclear wastes emplaced in saturated geological formations, *J. Geophys. Res.* **93** (1988) 1159–1173.

# DISSOLVED INERT GASES IN THREE KARSTIC SYSTEMS IN EUROPE (FRANCE AND GREECE)

G. MAGRO, R. CIONI, M. GUIDI, F. GHERARDI  
CNR-Istituto di Geoscienze e Georisorse,  
Pisa, Italy

## Abstract

Dissolved noble gases (He, Ne, and Ar) and  $N_2$  were measured in spring waters from three karstic systems in Europe: Baget and Larzac in France, and Drama in Greece. The content of dissolved gases was higher than those expected for water equilibrated to air at the spring's temperature range (0–15°C) and was related to both the presence of air and He excess. The He isotopic composition reveals: a dominant air and air saturated water origin for the Baget samples, a slight mantle derived He excess for Larzac and a clear crustal He excess for Drama. Although the recording time was limited, the influence of deepest waters enriched in He was more evident during the dry season. Karstic waters are therefore the result of a complex hydrologic circulation of several reservoirs characterized by different water residence times exchanging water mainly during floods.

## 1. INTRODUCTION

Karstic regions are characterized by an underground drainage system made up of cracks, caverns and channels. A series of well connected channels allows the fast transport of rainwater during floods. The development of a drainage system by dissolution by meteoric waters flowing inside an initial fissure network is now understood, due to numerical simulations (e.g. Refs [1, 2] and references therein). However, these models failed to produce annex drainage systems (ADS) that are characterized by long water residence times [3]. Different mechanisms are proposed to be involved, i.e. the presence of allogenic waters drained from non-karstic rocks into soluble limestones, the upwelling of warm fluids and/or any source of acid component such as deep production of  $CO_2$  or  $H_2S$ , or the interaction with acid bearing silicates in deep sedimentary basins that causes the change of solubility of calcite in water with temperature (e.g. [4, 5] and references therein).

The concentration of noble gases and  $N_2$  have been usefully used for the determination of recharge temperature (e.g. Refs [6, 7] and references therein) the ground-water age (e.g. Refs [8, 9] and references therein) and more generally to trace fluid origin and circulation in the crust (e.g. Refs [10, 11] and references therein). To add more information on karst system dynamics we present here measures of He and its isotopic composition, along with Ne,  $N_2$  and Ar in waters flowing from springs of

three European karstic systems: Baget and the nearby Larzac in France, and Drama in Macedonia (Greece). The main goal is to trace with inert gases the mixing of waters with different origins and residence times, as occurs in ADS.

## 2. GEOLOGICAL SETTINGS

### 2.1. The Baget Karst system (France)

The Baget karst system (Fig. 1) is located in the French Pyrenees. The system is composed of carbonate rocks from Jurassic and Cretaceous ages (up to 70% of the area) and impervious rocks as flysch, shales and marls. The system has a typical karstic structure with hierarchised drainage from upstream to the outlet. Three annex-to-drain (ADS) systems (La Peyrere. La Hillère. Ste Catherine) are well known and the existence of a few others has been reported (e.g. Refs [12, 13] and references therein). The main perennial springs are at Las Hountas, that represents the 70% of the average total discharge and three overflows named Moulo de Jaur La Hillere and La Peyrère (Fig. 1a).

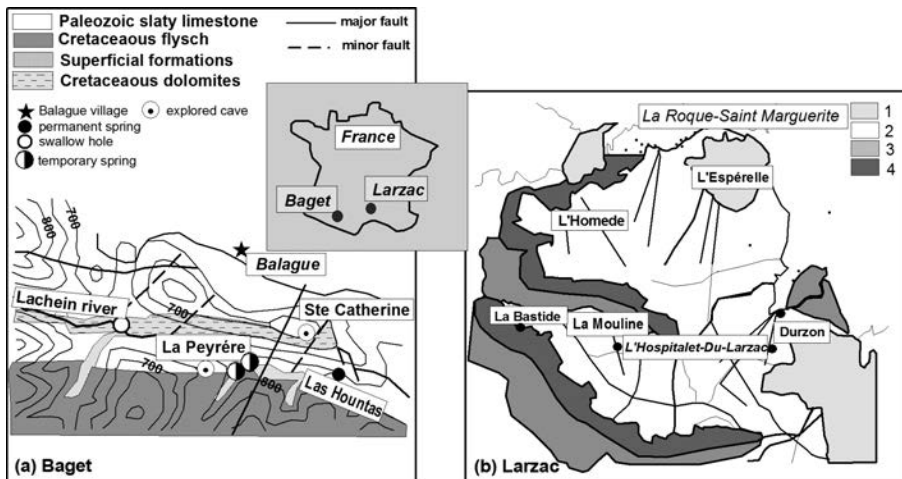


FIG. 1. Location of the two karstic areas in France: (a) geological sketch of the lower Baget watershed showing the boundary between calcareous rocks and flysch, temporary springs, the Las Hountas permanent spring and La Peyrère cave (modified after Ref. [5]); (b) hydrogeological map of Larzac karstic system: (1) Upper Jurassic dolomite; (2) middle Jurassic limestones; (3) lower and middle Liassic limestones and dolomite; (4) upper Liassic marls (modified after Ref. [14]).

## 2.2. The Larzac system (France)

Causse du Larzac is the southernmost and the widest unit of typical karst region of the Grands Causses, in southern France, shown in Fig. 1b. The limestones and dolomites of the Lias and middle Jurassic ages of the Grands Causses area are surrounded by a hard rock base that feeds important rivers; the fractured carbonate units form an aquifer overlying an impermeable base [14]. Three major springs, Durzon, Espérelle and L'Homede (Fig. 1b), carry about 70% of the total karst groundwater that discharges from northern Larzac. All these springs, hydrodynamically and chemically monitored during several hydrological cycles, drain aquifers having undeniably karstic characteristics. Nevertheless, groundwater flow seems to be neither very well organized nor concentrated along an integrated conduit network. Karst does not seem as well developed as in other parts of the Grands Causses [14].

## 2.3. The Drama karst system (Greece)

The Aggitis karst system, also known as Mara, developed in the marbles of the Rhodope massif in Eastern Macedonia, Greece (Fig. 2). The springs discharge from the calcareous Falakro massif. The karstic system developed during the uplift of the Falakro massif in the Miocene and is an original example of conditions of karstification in an active tectonic context [15]. The development of its karstic drainage network is intensely developed in the western part of the Falakro mountain. Despite the extension of the cave system and of the conduits, the functioning appears

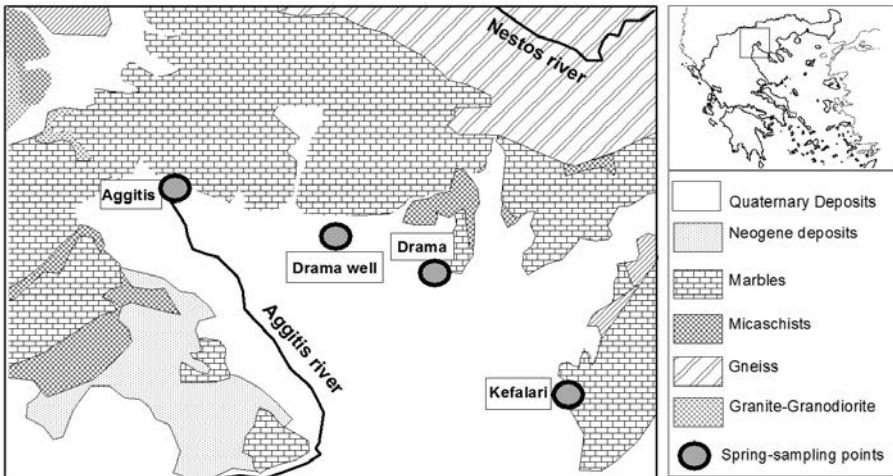


FIG. 2. Location of the study area and geological situation of the Aggitis spring (modified after [15]).

complex, with a significant storage, and slow infiltration as well as easy drainage. The karst aquifer has also an allogenic recharge by surface rivers from a large catchment area, geologically very different, localised at the north of the Falakro massif, flowing into swallow holes of a wide polje and most likely through the thick and porous alluvium filling the polje. The Drama karst system (Fig. 2), characterized by a low variability in its hydrological and geochemical characteristics, does not show any karst functioning [15].

### 3. METHODS

More than 50 samples of waters were taken from February 1996 to April 1997 in the Baget, Larzac and Drama karst systems within the framework of an European project. In the Baget system two permanent springs (Las Hountas and Moulo de Jaur) and four non permanent springs (Bernech, Gers, Moulo La Peyrere and St. Barbe) were sampled for dissolved gas analyses (Fig. 1a). Out of the total of 33 samples, 17 analyses for N<sub>2</sub> and Ar concentrations in water, 10 analyses for He and Ne and 3 for He isotopic concentration were performed. In the Larzac system three permanent springs (Le Durzon, L'Esperelle and L'Homede; Fig. 1b) were sampled and 8 analyses for N<sub>2</sub> and Ar concentrations in water, 10 analyses for He and Ne and 3 for He isotopic concentration were performed. In the Drama system three permanent springs (Mara, Drama and Kefalari; Fig. 2) were sampled along with the nearby thermal spring of Loutras-Eleftherion.

The dissolved gases were extracted from sampled water by means of the space head method [16], and the measured noble gases and N<sub>2</sub> concentrations were recalculated to spring water conditions by Henry's law. The concentration of N<sub>2</sub> and Ar were measured in 38 samples by gas chromatography. The abundances of He and Ne were measured in 34 samples by a quadrupole mass spectrometer after separation in a suitable all metal high vacuum line [17]. The He isotopic composition (expressed as  $R/R_a = ({}^3\text{He}/{}^4\text{He})_{\text{sample}}/({}^3\text{He}/{}^4\text{He})_{\text{air}}$ ) was obtained by means of a magnetic mass spectrometer for rare gases (MAP 215–50). The air reproducibility is better than 10% for  $R/R_a$  ratios and better than 5% for He/Ne ratios over the analysis period.

### 4. RESULTS AND DISCUSSION

The N<sub>2</sub>/Ar (Fig. 3a) and He/Ne (Fig. 3b) ratios, measured on dissolved gases in water samples from the three karstic systems, are plotted against spring temperature. Noble gases concentrations and N<sub>2</sub> for ASW were calculated with solubility equations assuming the air component to be adequately represented by a single value corresponding to the composition of an average dry atmosphere at 0.1 MPa and 20°C [18].

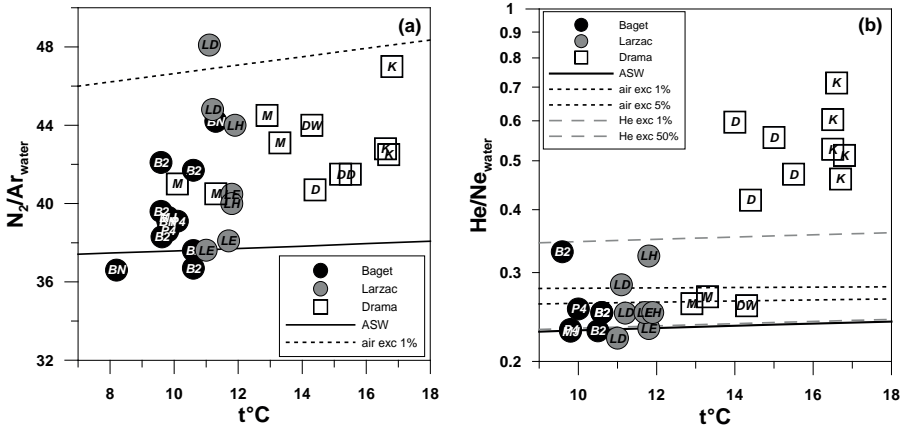


FIG. 3.  $\text{N}_2/\text{Ar}$  (a) and  $\text{He}/\text{Ne}$  (b) ratios of dissolved gases vs. temperature of springs of the three karstic are; mixing lines with air (from 1% to 5%) and He excesses (from 1% to 100%) are reported.

Most of the spring water samples show  $\text{N}_2/\text{Ar}$  and  $\text{He}/\text{Ne}$  ratios higher than those expected for water equilibrated to air (ASW curve in Figs 3a and 3b) in the temperature interval of cold spring ( $0^{\circ}$  to  $15^{\circ}\text{C}$ ), and higher than those expected for air and/or He excess plotted in the figures as a set of theoretical curves representative of variable air (Figs 3a and 3b) and He excesses (Fig. 3b). The presence of excess of air in water is a common event mainly due to small bubbles of air entrapped by recharge water at the undersaturated–saturated interface that later could be dissolved in groundwater for hydrostatic pressure increase in the saturated zone [19, 20].

For all the samples the shift of  $\text{N}_2/\text{Ar}$  from theoretical values is well explained by mixing with air excess close to the 1% dilution curve. However, the presence of  $\text{N}_2$  excess derived from sources different from air cannot be excluded. The presence of air excess alone can not explain the shift of  $\text{He}/\text{Ne}$  ratios from theoretical values both in a few Larzac and Baget samples and in most of the Drama samples which plot close to the 50% He excess representative curve, while all the remaining samples exhibit He excesses larger than 100%.

#### 4.2. Origin of excess of He

The deep origin of He in excess can be well traced by the He isotopic composition ( $R/R_a$ ). In Fig. 4 the He isotopic composition of dissolved gases is plotted versus the  $\text{He}/\text{Ne}$  ratios in water together with mixing curves and the  $R/R_a$  and  $\text{He}/\text{Ne}$  ratios measured in free gases issuing as bubbles in the thermal water close to the Larzac and Drama karst system area.

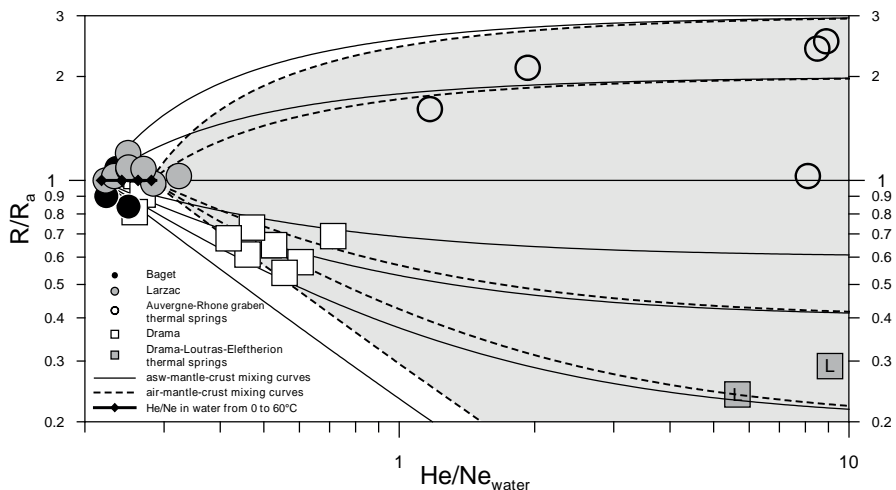


FIG. 4.  $R/R_a$  vs.  $He/Ne$  ratio in karstic waters and free gases of nearby thermal waters at the Larzac and Drama karstic systems.

The waters of the Baget karst system are characterized by a narrow  $R/R_a$  interval of  $1 \pm 0.1$  with  $He/Ne$  ratios from  $0.25 \pm 0.03$ . Even if the  $He/Ne$  ratio range of Larzac is the same of Baget, the  $R/R_a$  is slightly higher than 1 in the range  $1 \pm 0.2$ , higher than the expected error value.

A slight  $^3He$  excess is then envisaged in the Larzac waters. For the Larzac system the closest thermal water are those issuing in the Auvergne and the Rhone graben area in France [21]. The Larzac samples are the results of the mixing of a dominant air/ASW endmembers and a deeper  $^3He$  enriched endmember that could be the same of fluids issuing in the nearby thermal spring of the Auvergne and Rhone Graben, marked by  $R/R_a$  up to 2.5 [21].

The Drama system shows a higher variability: a quite constant  $R/R_a$  value close to 1 with  $He/Ne$  ratio close to 0.26 for the karst springs of Mara-Aggetis. The  $R/R_a$  ratio decrease in Kefalari and Drama spring waters, being in the range 0.58–0.81 with increasing He excess as shown by  $He/Ne$  ratio from 0.42 to 0.71. The thermal waters, as expected, are marked by the highest  $He/Ne$  ratio (close to 10) and the lowest  $R/R_a$  ratio of 0.2. They are the results of the mixing of the air/ASW endmember with  $^4He$  enriched fluids derived from the crust endmember. The mixing between the two endmembers can be estimated to vary from an atmospheric fraction close to 90% for the Drama well and the Aggitis spring, and between 50 to 30% for the Drama and Kefalari springs. The deep endmember is dominant in the free gases of thermal springs, having  $R/R_a$  values up to 0.2 [22].

Different seasonal samplings revealed that a slight increase of  $N_2/Ar$ ,  $He/Ne$  ratios were evident in all three karstic areas during the dry season, approximately

from July to September. Synchronously the He isotopic composition deviates from air/ASW typical one ( $R/R_a = 1$ ) towards higher values for Larzac and lower values for Drama.

The recorded increase of all the ratios seems to be compatible with the exchanging of waters from several reservoirs, which mainly occurs during floods, as largely proved on the basis of the water chemical composition (major ionic species,  $^{13}\text{C}$  and  $^{18}\text{O}$ ) (e.g. Ref. [23] and references therein).

## 5. CONCLUSION

Noble gas isotopic composition emerges as a very useful tool to trace mixing processes during underground water circulation in karst systems and to identify the presence of both air excess and deep He excess in the spring waters of all the three studied areas.

He sources different from air and/or ASW were clearly recognized both in Larzac and Drama karstic springs. The dissolved noble gases concentration and He isotopic composition not only confirm the presence of warm upwelling fluids but they add further information on the origin of these warm fluids. A prevalent crustal origin for the Drama karstic system and thermal waters and, more in general, in all the thermal springs issuing within the Strimon basin, with variations in the  $^3\text{He}/^4\text{He}$  and He/Ne ratios, reflect the different efficiency by which radiogenic He is extracted from the deep seated granites [22]

A dominant air/ASW origin with mantle derived fluids can be envisaged in samples from Larzac where the presence of  $^3\text{He}$  enriched fluids seems to be related to the same source feeding the thermal springs and spas of the Auvergne and Rhone Graben area.

As shown by different seasonal sampling, the presence of these fluids is more evident after the flood when the contribution of dissolved atmospheric components from meteoric water entering in the system decreases.

## REFERENCES

- [1] LIEDL, R., SAUTER, M., HÜCKINGHAUS, D., CLEMENS, T., TEUSCH, G., Simulation of the development of karst aquifers using a coupled continuum pipe flow model, *Water Resour. Res.* **39** 3 (2003) 1057.
- [2] KAUFMANN, G., BRAUN, J., Karst aquifer evolution in fractured rocks, *Water Resour. Res.* **35** (1999) 3223–3238.
- [3] BAKALOWICZ, M., MANGIN, A., L'aquifère karstique: Sa définition, ses caractéristiques et son identification, *Mém. H. Série Soc. Géol. France* **11** (1980) 71–79.

- [4] BAKALOWICZ, M.J., FORD, D.C., MILLER, T.E., PALMER, A.N., PALMER, M.V., Thermal genesis of solution caves in the Black Hills, South Dakota, *Bull. Geol. Soc. Am.* **99** (1987) 729–738.
- [5] GENTHON, P., SCHOTT, J., DANDURAND, J.-L., Carbonate diagenesis during thermoconvection: Application to secondary porosity generation in clastic reservoirs, *Chem. Geol.* **142** (1997) 41–61.
- [6] MAZOR, E., *Applied Chemical and Isotopic Groundwater Hydrology*, Halsted Press of John Wiley & Sons, New York, NY (1991).
- [7] KIPFER, R., AESCHBACH-HERTIG, W., PEETERS, F., Noble gases in lakes and ground waters, *Rev. Mineral. Geochem.* **47** 1 (2002) 615–700.
- [8] ANDREWS, J.N., LEE, D.J., Inert gases in groundwater from the Bunter Sandstone of England as indicators of age and palaeoclimatic trends, *J. Hydrol.* **41** (1979) 233–252.
- [9] SCHLOSSER, P., WINCKLER, G., Noble gases in ocean waters and sediments, *Rev. Mineral. Geochem.* **47** 1 (2002) 701–730.
- [10] BALLENTINE, C.J., BURGESS, R., MARTY, B., Tracing fluid origin, transport and interaction in the crust, *Rev. Mineral. Geochem.* **47** 1 (2002) 539–614.
- [11] BALLENTINE, C.J., BURNARD, P.G., Production, release and transport of noble gases in the continental crust, *Rev. Mineral. Geochem.* **47** 1 (2002) 481–538.
- [12] LABAT, D., MANGIN, A., ABABOU, R., Rainfall–runoff relations for karstic springs: Multifractal analyses, *J. Hydrol.* **256** 3–4 (2002) 176–195
- [13] BAKALOWICZ, M., “Water geochemistry: water quality and dynamics”, *Groundwater ecology* (GIBERT, J., DANIELOPOL, D., STANFORD, J., Eds), Academic Press (1994) 97–127.
- [14] PLAGNES, V., BAKALOWICZ, M., The protection of karst water resources: the example of the Larzac karst plateau (south of France), *Environ. Geol.* **40** 3 (2001) 349–358.
- [15] NOVEL, J.P., DIMADI, A., ZERVOPOULOU, A., BAKALOWICZ, M., The Aggitis karst system, Eastern Macedonia, Greece: Hydrologic functioning and development of the karst structure, *J. Hydrol.* **334** (2005) 477–492.
- [16] GIGGENBACH, W.F., GOGUEL, R.L., Methods for the collection and analysis of geothermal and volcanic water and gas samples, *Professional Paper CD 2387*, Department of Science and Industrial Research, Petone, New Zealand (1988) 53.
- [17] MAGRO, G., PENNISI, M., Noble gases and nitrogen: Mixing and temporal evolution in the fumarolic fluids of Vulcano, Italy, *J. Volcan. Geothermal Res.* **47** (1991) 237–247.
- [18] SMITH, S.P., KENNEDY, B.M., The solubility of noble gases in water and NaCl brine, *Geochim. Cosmochim. Acta* **47** (1983) 503–515.
- [19] HEATON, T.H.E., VOGEL, J.C., “Excess air” in groundwater, *J. Hydrol.* **50** (1981) 201–216.
- [20] HERZBERG, O., MAZOR, E., Hydrological applications of noble gases and temperature measurements in underground water systems: Examples from Israel, *J. Hydrol.* **41** (1979) 217–231.
- [21] MARTY, B., O’NIONS, R.K., OXBURGH, E.R., MARTEL, D., LOMBARDI, S., Helium isotopes in Alpine regions, *Tectonophysics* **206** 1–2 (1992) 71–78.

- [22] MAGRO, G., GHERARDI, F., BELLANI, S., “Noble gases in karstic and thermal waters of Strimon basin (Greece-Bulgaria)”, *Water-Rock Interaction* (BIRKLE, TORRES-ALVARADO, Eds), (2010) 345–348.
- [23] BAKALOWICZ, M., Karst groundwater: a challenge for new resources, *Hydrogeol. J.* **13** (2005) 148–160



# GROUNDWATER FLOW COMPUTED WITH MODFLOW AND ISOTOPIC AGE TRACER DATA IN THE CONTINENTAL INTERCALAIRE (SAHARA)

J.O. PETERSEN, J. GONCALVES, P. DESCHAMPS, B. HAMELIN  
Centre Européen de Recherche et d'Enseignement  
de Géosciences de l'Environnement,  
Aix-en-Provence, France

K. ZOUARI  
Laboratoire de Radio-Analyses et Environnement,  
Sfax, Tunisia

A. GUENDOOUZ  
University of Blida, Science Engineering Faculty,  
Soummaa Blida, Algeria

J.-L. MICHELOT  
Interactions et Dynamique des Environnements de Surface,  
Université Paris-Sud,  
Orsay, France

## Abstract

In one of the largest confined aquifers of the world, the Continental Intercalaire (Sahara), which is located in an arid region (57 mm/y of mean of precipitation), groundwater flow patterns are rather complex. Coupling measurements of isotopic composition of water and age mass calculations obtained by numerical simulations can allow, to a greater extent than a simple comparison, to constrain and validate the recharge scenario, transport and age of groundwater. First, the multiple tracers  $^{14}\text{C}$ ,  $^{36}\text{Cl}$ , or  $^{234}\text{U}/^{238}\text{U}$  used in this study including noble gases such as  $^4\text{He}$ , allow investigation of a large range of groundwater ages. Then a MODFLOW simulation is built using (i) the distribution of hydrological parameters, (ii) geometrical limits and (iii) the concept of age mass of water, accounting for the tracers data. This approach improves the understanding of the hydrodynamics of this system. In particular, the mixing of old and young waters should be better constrained and the interpretation of paleohydrological conditions is permitted.

## 1. INTRODUCTION

Deep aquifers of semiarid and arid regions of Africa, such as the North-Western Sahara Aquifer System (NWSAS), are some of the largest freshwater reserves in

the world. These groundwaters are mainly inherited from past and more humid periods and modern recharge seems in most cases very limited. Quantifying the modern recharge of these aquifers is pivotal to assess the renewability of these groundwater resources, extensively exploited nowadays. Knowledge of past recharge is also critical since piezometric evolution observed in large groundwater bodies may be partly controlled by transient effect between more humid periods that occurred in the past and present day drier conditions. All this information is essential for developing a reliable aquifer model and implementing sustainable water resource management plans, especially within the context of climate change.

Identifying and quantifying recharge and paleorecharge remain challenging, however. Geochemical or hydrodynamic approaches provide invaluable information on residence time and/or the recharge period, but may lead in many cases to inconsistent results. The concept of ‘groundwater age’ faces several theoretical difficulties [1], that can be resolved by using the age mass variable [2]. It provides a simple but complete treatment of dispersion and mixing compared with most hydrodynamics models, where only advection is considered.

Conversely, groundwaters can be used as paleoclimatic archives that enable reconstitutions of past climatic and hydrological changes, to be determined especially in desertic and semi-desertic area where other archives remain scarce [3].

The aim of this study is to further our understanding of the present day and past hydrogeological behaviour of NWSAS that extends over  $10^6$  km<sup>2</sup>, from the Algerian Atlas mountains to the Tassili mountains of the Hoggar (north–south direction) and from the Guir-Saoura valley to the Libyan Desert (west–east direction, see Fig. 1). NWSAS is vital in that arid region (57 mm/y mean precipitation [4]), where groundwater is the main, if not the only, resource for water supply. This multi-layer aquifer contains sedimentary deposits, which, from bottom to top, contain two main aquifers, the Continental Intercalaire (CI) and the Complex Terminal (CT). Due to the increasing demand for irrigation development, water withdrawal has increased from 14 L/s in 1950 to 75 L/s in 2000 [5], leading to a general drawdown of the piezometric level.

This study focuses mainly on the CI aquifer. Comparable in scale to the Australian Great Artesian Basin, the CI is one of the largest confined aquifers in the world. Its recharge areas are mainly located in the Algerian Atlas and in the Grand Erg Occidental area, on the western border ([4, 6] see Fig. 1). The question of the modern recharge of the CI aquifer is still debated. Estimates of the modern recharge derived from numerical simulations range between 4 and 8 m<sup>3</sup>/s (see Ref. [4] and references therein). <sup>36</sup>Cl measurements allow the derivation of chemical water ages of up to one million years in the central Algerian part of the CI [7, 9].

However, no comparisons between these geochemical ages and those computed by numerical model are available so far since such calculations were not implemented for the NWSAS. To launch a first comparative study, we use the age-mass concept, defined as  $T$  (kg·s) =  $\rho V\tau$  ( $\rho$  is fluid density,  $V$  is elementary volume,  $\tau$  is groundwater age), following the approach primarily introduced in Ref. [2] and then discussed

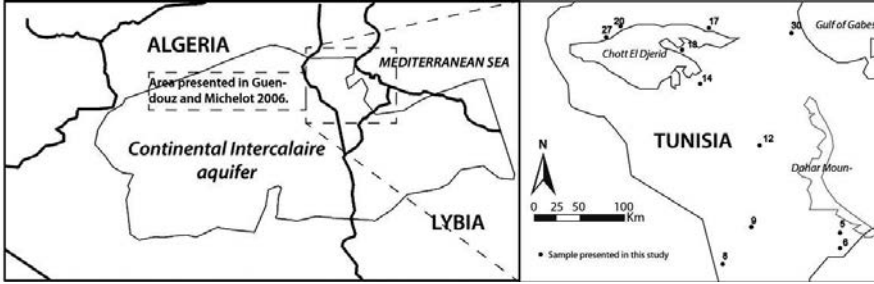


FIG. 1. CI aquifer limit after Ref. [4] and location of the studied area Ref. [7]. Inset: location of the samples collected in Tunisia in November 2010

in Ref. [9, 10].  $T$  is thus considered as an extensive and additive quantity following classical transport laws (advection, dispersion) and mixing between different water bodies, like a conservative solute.

The general objectives of this study are (i) to augment the  $^{36}\text{Cl}$  data base by extending the sampling to the Tunisian part of the CI and (ii) to combine the geochemical approaches ( $^{36}\text{Cl}$ ) with direct simulated ages in order to improve the knowledge of the age distribution in the CI aquifer. We present here new  $^{36}\text{Cl}$  measurements obtained on samples collected in the southern part of Tunisia in 2010 (see Fig. 1). We also provide a first simulation of age mass transport [2, 9, 10] in order to improve our understanding of the NWSAS dynamics.

## 2. GEOLOGICAL AND HYDROGEOLOGICAL SETTINGS

Geological studies [11,12] lead to consider the CI aquifer as a succession of several units (lower Cretaceous) of sandstone including clay rich strata. In the central part of the basin, the facies are continental and, towards the east, lacustrine facies are progressively replaced by marine facies [13]. From south to north, the aquifer depth increases.

The aquifer is considered hydraulically continuous over the whole basin in agreement with major ions and most trace element distributions which indicate continuous water–rock interaction, except near the Tunisian Chotts where the uniform evolution is disturbed by converging groundwater flow lines [13]. Three main flow-paths are identified: W–E (from the Saharan Atlas and the M'Zab dorsal in Algeria), SW–NE (from southern Algeria, see Fig. 2) and S–N (from the Dahar region of Tunisia). They converge towards the Chotts region and Gulf of Gabès (main discharge areas). Chloride concentrations increase from 200 to 800 mg/L along the main

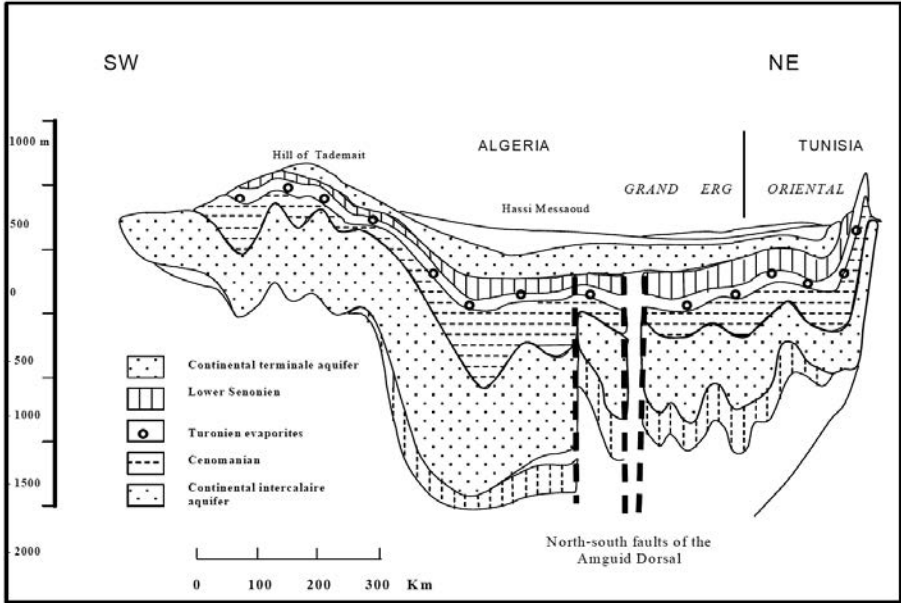


FIG. 2. Schematic cross-section of the Continental Intercalaire aquifer in Algeria and Tunisia, showing the main aquifer horizons (after Refs [13, 7]).

flow path in Algeria, and the Br/Cl ratios confirm the dissolution of non-marine evaporites or interstitial waters as the main source of salinity [13].

Concerning geochemical age,  $^{14}\text{C}$  contents are close to the detection limit [14]. Using  $^{36}\text{Cl}$ , (301 kyr half-life) and Michelot [7, 8] estimated the residence time from 16 to 500 ka for the minimum ages, and from 25 to 1200 ka for the maximum ages (depending on the choice of initial  $^{36}\text{Cl}/\text{Cl}$  atmospheric ratio and equilibrium ratio between radioactive decay and deep production of  $^{36}\text{Cl}$  by neutron activation of  $^{35}\text{Cl}$ ).

### 3. PRELIMINARY RESULTS

#### 3.1. First $^{36}\text{Cl}$ data in the Tunisian part of the CI aquifer

Thirty-three samples of CI groundwater were collected in November 2010 in the southern part of Tunisia (Fig. 1). The  $^{36}\text{Cl}/\text{Cl}$  ratios were measured for ten of these samples on the French AMS National Facility, ASTER, located at CEREGE<sup>a</sup>. Cl concentrations were measured by ion liquid chromatography at the Laboratory of Radio-Analysis and Environment of the National School of Engineers of Sfax. Our new  $^{36}\text{Cl}$  and  $^{36}\text{Cl}/\text{Cl}$  data are consistent with data obtained in the Algerian part of the CI by Guendouz and Michelot [7] (see Fig. 3). The  $^{36}\text{Cl}/\text{Cl}$  ratio range from 5.4 to

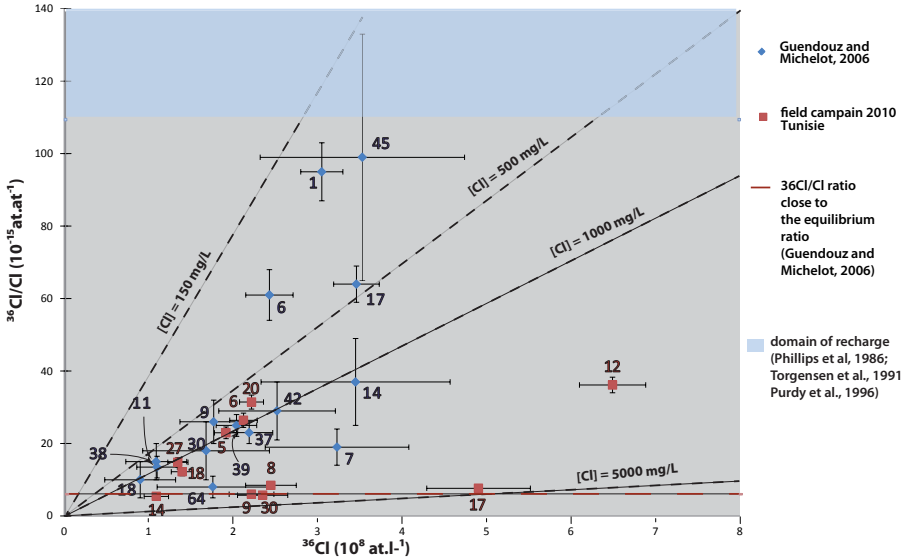


FIG. 3.  $^{36}\text{Cl}$  data from the Algerian [7] and Tunisian part of the CI (this study).

$36.2 \times 10^{-15}$  and  $^{36}\text{Cl}$  contents from  $1.1$  to  $6.5 \times 10^{-8} \text{ at}\cdot\text{L}$ . As for recharge ratio, higher values, from  $110$  to  $200 \times 10^{-8} \text{ at}\cdot\text{L}$  are available in the literature [15–17] (see Fig. 3).

### 3.2. Numerical simulations of the CI aquifer

First, we constructed a simplified model of the aquifer based on (i) the topography obtained from a digital elevation model (<http://eros.usgs.gov>); (ii) the structural and hydrological parameters from previous models [4, 5], with the top of the layer from  $-1500$  to  $600 \text{ m}$ , the thickness from  $0$  to  $1000 \text{ m}$ ,  $10^{-4} \text{ m/s}$  for the horizontal hydraulic conductivity,  $10^{-4}$  for the storage coefficient and  $0.1$  for the porosity.

A preliminary hydraulic head distribution as close as possible to the reference hydraulic head map of 1950 [5] was computed at steady state. Although globally consistent with the reference map, this distribution remains poorly constrained in large areas (especially in the eastern part) as shown in Fig. 4a. A visualisation of the subtraction of the reference from our model is proposed in Fig. 4b, given in metres. The difference does not exceed  $200 \text{ m}$  especially in the central part and the northern and southern borders of the SASS. In the eastern part, the results are more inconsistent.

Because the main flow paths are globally reproduced, we used this first simulation to carry out a preliminary transient simulation. Age mass calculations were implemented using the mass transport model MT3DMS using a sink–source term to account for the age increase of groundwaters through time. The common use of this

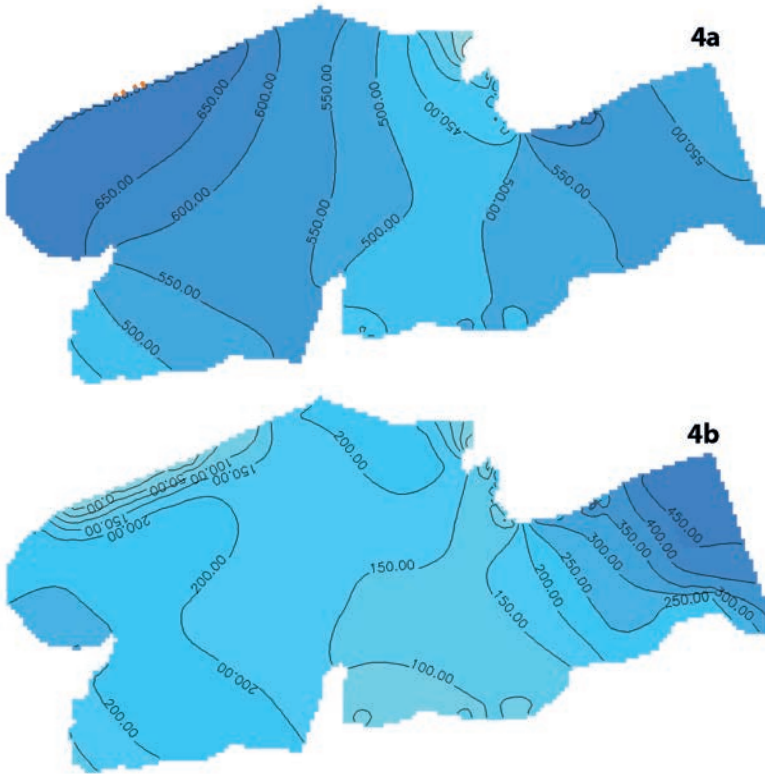


FIG. 4. (a) Hydraulic heads calculated by our model and (b) the same minus the reference field of 1950 [5].

code is solute transport but the age mass approach allows transporting age as a conservative solute.

This first transient simulation was conducted by maintaining the same boundary conditions during 1 Ma (constant hydraulic heads spatial distribution through time), and only convective transport, i.e. water ages are shown in Fig. 5.

#### 4. PRELIMINARY CONCLUSIONS AND PROSPECTS

Our preliminary results confirm that coupling numerical flow model with isotopic tracers seems a promising approach to validate more realistic scenarios of the CI aquifer dynamics. The next steps of our project will involve introducing the spatial heterogeneity of the parameters (e.g. hydraulic conductivity, storativity) using relationships between these parameters and depth, although the available measurements to calibrate such relations are scarce. This will allow the improvement of

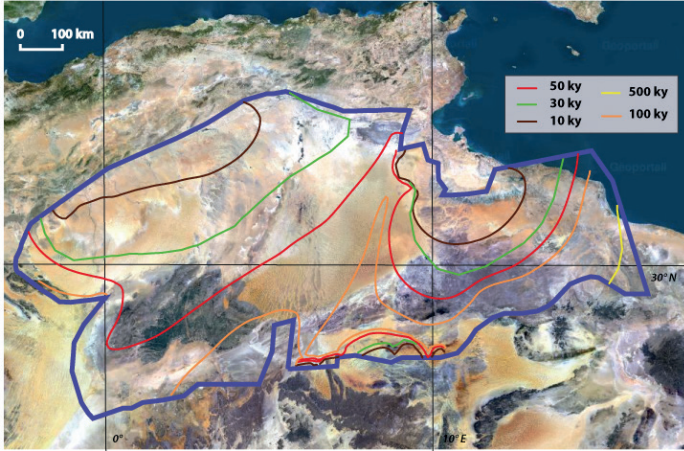


FIG. 5. Isolines of age (10; 30; 50; 100; 500 ky) computed for the CI aquifer.

the steady state calculation. Then age mass transient calculations will be based on this first round of calibrated parameter fields. Dispersion will be introduced and more realistic boundary conditions will be implemented.

$^{14}\text{C}$  and  $^4\text{He}$  measurements are in progress and will be also compared to  $^{36}\text{Cl}$  ages and simulated ages mass.

## REFERENCES

- [1] CASTRO, M.C., GOBLET, P., Calibration of regional groundwater flow models: Working toward a better understanding of site-specific systems, *Water Resour. Res.* **39** 6 (2003) 1172.
- [2] GOODE, D.J., Direct simulation of groundwater age, *Water Resour. Res.* **32** 2 (1996) 289–296.
- [3] EDMUNDS, W.M., et al., “Groundwater as an archive of climatic and environmental change, The PEP-III traverse”, *Past Climate Variability through Europe and Africa* (BATTARBEE, R.W., GASSE, F., STICKLEY, C.E., Eds), *Developments in Palaeo-environmental Research Series*, Kluwer, Dordrecht, The Netherlands (2004) 279–306.
- [4] BABA SY, M.O., Recharge et paléorecharge du Système Aquifère du Sahara Septentrional, Doctoral Thesis, Université Tunis El Manar (2005) 261.
- [5] OBSERVATOIRE DU SAHARA ET DU SAHEL, Système Aquifère du Sahara Septentrional, Vol. 2: Hydrogéologie, Projet SASS, Internal Report, Tunis, Tunisie (2003) 275.
- [6] OBSERVATOIRE DU SAHARA ET DU SAHEL, Etude des Ressources en Eau du Sahara Septentrional, Final report, Tunis, Tunisia (1972).

- [7] GUENDOOUZ, A., MICHELOT, J.-L., Chlorine-36 dating of deep groundwater from northern Sahara, *J. Hydrol.* **328** 3–4 (2006) 572–580.
- [8] GUENDOOUZ, A., Contribution à l'étude hydrochimique et isotopique des nappes profondes du Sahara Septentrional, Algérie, PhD thesis, Univ. Paris XI, Orsay (1985).
- [9] BETHKE, C.M., JOHNSON, T.M., Paradox of groundwater age, *Geology* **30** (2002) 385–388.
- [10] BETHKE, C.M., JOHNSON, T.M., Groundwater age and groundwater age dating. *Annu. Rev. Earth Planet. Sci.* **36** (2008) 121–152.
- [11] CORNET A., Introduction à l'hydrogéologie saharienne, *Rev. de géogr. phys. et de géol. dyn.* (2), vol. VI, fasc.1 (1964) 5–72.
- [12] CASTANY, G., Bassin sédimentaire du Sahara septentrional (Algérie-Tunisie), Aquifères du Continental Intercalaire et du Complexe Terminal, *Bull. BRGM* **2 III** 2 (1982) 127–147.
- [13] EDMUNDS, W.M., et al., Groundwater evolution in the Continental Intercalaire aquifer of southern Algeria and Tunisia: Trace element and isotopic indicators, *Appl. Geochem.* **18** 6 (2003) 805–822.
- [14] GONFIANTINI, R., CONRAD, G., FONTES, J.C., SAUZAY, G., PAYNE, B.R., “Etude isotopique de la nappe du Continental Intercalaire et de ses relations avec les autres nappes du Sahara septentrional (Isotopic investigation of the Continental Intercalaire aquifer and its relationship with other aquifers in the northern Sahara”, *Isotope Techniques in Groundwater Hydrology (Proc. Symp)*, Vol. 1, Proceedings Series, IAEA, Vienna (1974) 227–241.
- [15] PHILLIPS, F., BENTLEY, H., DAVIS, S., ELMORE, D., SWANICK, G., Chlorine 36 dating of very old groundwater: 2. Milk River Aquifer, Alberta, Canada, *Water Resour. Res.* **22** 13 (1986) 2003–2016.
- [16] TORGERSEN, T., et al., Chlorine 36 dating of very old groundwater: 3. Further studies in the Great Artesian Basin, Australia, *Water Resour. Res.* **27** (1991) 3201–3213.
- [17] PURDY, C., et al., Aquia aquifer dissolved Cl<sup>-</sup> and <sup>36</sup>Cl/Cl: Implications for flow velocities, *Water Resour. Res.* **32** 5 (1996) 1163–1171.

# HYDROGEOCHEMICAL AND ISOTOPIC CHARACTERISTICS OF TUFA PRECIPITATING WATERS: A CASE STUDY OF THE RIVER KRKA (SLOVENIA)

S. ZAVADLAV, S. LOJEN  
Jožef Stefan Institute,  
Department of Environmental Sciences,  
Ljubljana, Slovenia

## Abstract

The geochemical and stable isotope composition of tufa precipitating water in the River Krka in the Slovenian karst area were studied. Surface water chemistry in the River Krka is controlled by groundwater interactions with carbonate rocks, soil CO<sub>2</sub> and meteoric water in the aquifer. Major element chemistry of water is controlled by dissolution of dolomite and calcite. The aquifer is the main source of cations, since concentrations of Mg<sup>2+</sup>, Sr<sup>2+</sup> and Ba<sup>2+</sup> in water are highest at the spring. Ca<sup>2+</sup> concentrations are slightly increasing due to the additional mixing of surface and groundwater downstream. Oxygen isotope composition of water indicates homogenization of meteoric water in the aquifer, while δ<sup>13</sup>C values of dissolved inorganic carbon in water are affected by biological activity in the soil. δ<sup>18</sup>O and δ<sup>13</sup>C of bulk tufa show that deposition of tufa precipitates in the River Krka is kinetically controlled resulting in enrichment with heavier isotopes. Calculated equilibrium temperature of tufa precipitation based on the oxygen isotope composition of water and tufa fit with measured water temperature when average δ<sup>18</sup>O values of water and tufa are considered.

## 1. INTRODUCTION

Tufa depositing waters represent a unique freshwater carbonate system, thus offering an opportunity to study mechanisms by which waters establish equilibrium with conditions in the atmosphere. Over the past several decades these environments were intensively studied. Geochemical studies of water and tufa precipitates provide knowledge of freshwater carbonate systems and controls associated with calcite precipitation, e.g. kinetic processes [1] and deposition rates [2]. The distribution of Mg, Sr and Ba, and the stable oxygen isotope (δ<sup>18</sup>O) composition of tufa reflect temperature dependant fractionation at the water–solid interface [3–5]. Whereas δ<sup>18</sup>O shows simple temperature dependence, the stable carbon isotope (δ<sup>13</sup>C) of tufas results from interactions of potential carbon sources such as carbonate bedrock, atmosphere and soil air, and the degree of CO<sub>2</sub> degassing by water [5–7]. Morphological variability of tufas was a motive for the determination of physicochemical and biological

influence on tufa growth and diagenesis [8, 9]. Laminas in tufas reflect seasonal changes in climate and depositional processes on an annual scale [10]. However, the potential of tufas as environmental archives is conditioned with the equilibrium state of  $\text{CaCO}_3$  precipitation, which is an important assumption regarding palaeoclimatic interpretations of tufa formation environment. In general, equilibrium conditions of precipitation are typical for water systems fed by meteoric waters, with a constant and low discharge rate and small seasonal temperature changes [4]. In contrast, in large karst areas with groundwater recharge and turbulent water flow, tufas often precipitate in non-equilibrium conditions due to high discharge rates and greater climate deviations [11].

Several studies proposed (e.g. [5, 12]) that only contemporary research of tufa precipitation and its parent water chemistry lead to reliable conclusions either on tufa precipitation mechanisms or tufa as being a proper object reflecting environmental conditions during its deposition. Therefore, the purposes of this study were to constrain processes influencing water chemistry and associated tufa precipitation in the River Krka system.

## 2. STUDY SITE

The tufa bearing River Krka rises in a broad valley, at the interface of the Jurassic limestone and Triassic dolomite formations on the karst Dinaric plateau in SE part of Slovenia. The River Krka catchment covers an area of 2238 km<sup>2</sup> with predominant carbonate bedrock and typically very few surface tributaries, thus water recharges from numerous underground karst springs on the river banks. The river has an altitude drop of 129 m and runs for 94 km towards the confluence into the larger Sava river. Tufa precipitation begins a few kilometres from the main spring and forms characteristic barrages and underwater bands in the upper reaches, while in the middle reaches underwater bands prevail.

## 3. METHODS

Surface water samples were collected seasonally during the end of 2007 and 2010 at 19 sampling points, selected for tufa occurrences and geomorphological conditions. Carbonate samples were collected on the 16 largest tufa barrages. Rainwater was collected monthly. The temperature, pH and electrical conductivity of water were measured on site at each sampling point, where several aliquots of water were first filtered through 0.45  $\mu\text{m}$  membrane filters for alkalinity and cation determination and through 0.20  $\mu\text{m}$  filters for carbon and oxygen stable isotope analysis. Alkalinity was measured by acid–base titration, while concentrations of dissolved inorganic carbon were determined using the coulometric method. Samples for cation analyses were

first acidified with ultrapure nitric acid and measured by ICP–OES. Samples for stable isotope composition of dissolved inorganic carbon ( $\delta^{13}\text{C}_{\text{DIC}}$ ) were prepared by injecting water samples into evacuated septum tubes with phosphoric acid. Released  $\text{CO}_2$  gas was then analysed with continuous flow isotope ratio mass spectrometer (Europa 20–20 with ANCA TG trace gas separation module).  $\delta^{18}\text{O}$  of water was determined by the  $\text{CO}_2$  equilibration technique with IsoPrime MultiFlow IRMS. Carbonates for  $\delta^{13}\text{C}$  and  $\delta^{18}\text{O}$  analysis were prepared by digestion in 100% phosphoric acid at 25 °C for 24 h.  $\text{CO}_2$  released during acid treatment was analysed using Varian MAT 250 IRMS.  $\delta^{13}\text{C}$  and  $\delta^{18}\text{O}$  values of water and carbonate are expressed as ‰ vs. VSMOW and VPDB, respectively. For carbon analysis, reproducibility is better than  $\pm 0.2\%$  for water,  $\pm 0.1\%$  for carbonates and for oxygen better than  $\pm 0.05\%$  for water and carbonate samples. The partial pressure of  $\text{CO}_2$  ( $p\text{CO}_2$ ) and mineral saturation state of calcite were calculated using the PHREEQC speciation program [13].

## 4. RESULTS AND DISCUSSION

### 4.1. Water chemistry

The water temperature of the River Krka varies in a range between 3.4–21.8°C and reflects seasonal air temperature. The pH of water is typical for karst water and varies between 7.26–8.68 with an average value of 7.99. The highest pH was always measured in the section with the most intensive tufa precipitation, which also fits with the calculated saturation index for calcite (SIc) and  $\text{CO}_2$  partial pressures.

Total alkalinity shows a weak seasonal pattern, in general low in spring and high in autumn and late winter. A significantly large range between 2.96 mM and 5.7 mM indicates high variability of water chemistry. Alkalinity generally decreases downstream, however, the amplitude of alkalinity variations is normally large in summer and winter, in the upper stream distinctly so. The water chemistry of the River Krka is controlled by groundwater interactions with carbonate bedrock, soil  $\text{CO}_2$  and meteoric water, since neither intensive rainfall nor flow rate affect alkalinity.

Concentrations of dissolved inorganic carbon (DIC) vary similar as alkalinity, but in a narrower range between 3.61–5.94 mM. The highest concentrations of dissolved carbon are a response to the larger addition of soil carbon in autumn, whereas the lowest concentrations were measured in spring. DIC concentrations normally decrease downstream and have smaller amplitudes than those of alkalinity. As expected DIC correlates well with alkalinity (Fig. 1a), especially in autumn ( $R^2 = 0.91$ ) and summer ( $R^2=0.65$ ). Thus, total alkalinity can be ascribed to carbonate alkalinity [14].

The major element chemistry in the River Krka is controlled by the dissolution of carbonate minerals (Fig. 1b). The  $\text{Mg}^{2+}/\text{Ca}^{2+}$  molar ratio (Mg/Ca) of the carbonate dominated catchments indicates the relative proportions of calcite and/or dolomite

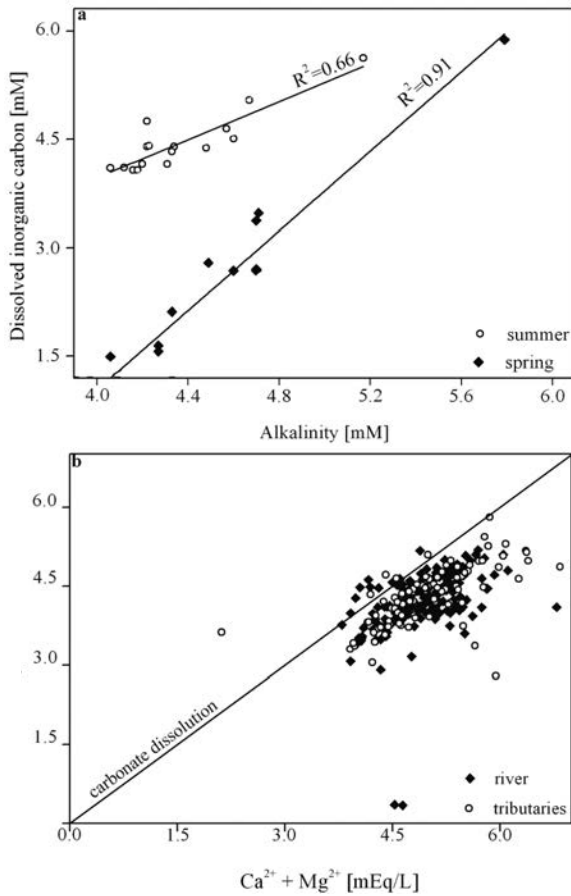


FIG. 1. Positive correlation between dissolved inorganic carbon and alkalinity (a). Plot (b) shows carbonate dissolution of rocks in the river Krka aquifer.

weathering [15]. The highest Mg/Ca ratios in the River Krka water are at the spring, indicating the dissolution of Mg rich carbonates in the aquifer. A weak trend of Mg rich carbonate weathering in the upper reaches and calcite weathering in the lower reaches of the River Krka can be observed (Fig. 2d), though it is not possible to distinguish whether calcite or dolomite dissolution prevails.  $\text{Sr}^{2+}/\text{Ca}^{2+}$  and  $\text{Ba}^{2+}/\text{Ca}^{2+}$  molar ratios in water show similar behaviour as the  $\text{Mg}^{2+}/\text{Ca}^{2+}$  ratio. They both decrease downstream and are highest in the spring, and especially in summer and autumn.  $\text{Mg}^{2+}$  concentrations in the water are decreasing downstream, implying that the aquifer is the only source of magnesium.

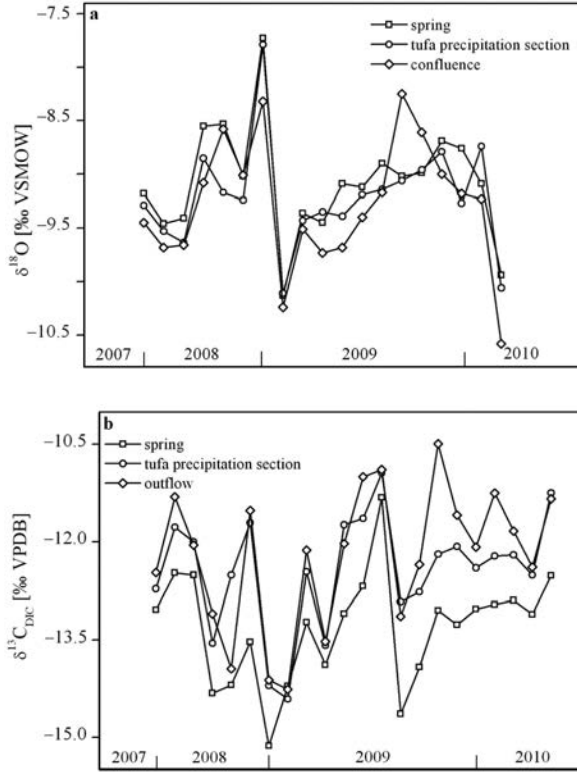


FIG. 2. Seasonal and downstream variability of water  $\delta^{18}\text{O}$  and  $\delta^{13}\text{C}_{\text{DIC}}$  values.

#### 4.2. Isotope composition of water

Oxygen isotopic composition ( $\delta^{18}\text{O}$ ) of the River Krka varies between  $-11.00\%$  and  $-7.73\%$ . The highest  $\delta^{18}\text{O}$  values of water were measured in summer and autumn, whereas most negative  $\delta^{18}\text{O}$  values were noticed in spring, likely due to snowmelt (Fig. 2a). Larger variations are found in  $\delta^{18}\text{O}$  values of meteoric water, ranging from  $-17.02\%$  (January 2009) to  $-5.77\%$  (July 2009). Tufa depositing water is essentially karst groundwater which is fed by recharging meteoric water [6] whose isotope composition is moderated during residence time in the aquifer. Nevertheless, groundwater is often close to the long term mean of local rainfall [14, 16] which is the case in the Krka river system, where the mean annual  $\delta^{18}\text{O}$  of water ( $-9.22\%$ ) and of meteoric water ( $-9.84\%$ ) are similar. Another indication of water homogenization within the aquifer is the non-synchronized response of water discharge to rainfall events. The oxygen composition of water  $\delta^{18}\text{O}$  is slightly increasing downstream (between 0.25 and 0.59‰), thus excluding evaporation effects and implying the additional mixing of surface water with groundwater downstream.

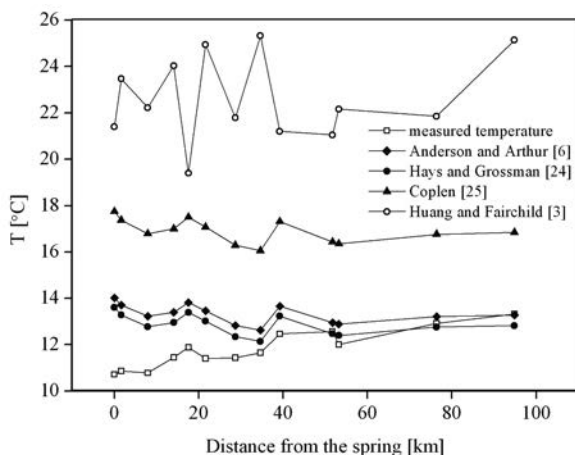


FIG. 3. Differences between measured and calculated water temperatures using oxygen isotope and Mg/Ca ratio as temperature proxies.

The isotope composition of dissolved inorganic carbon ( $\delta^{13}\text{C}_{\text{DIC}}$ ) of the River Krka varies between  $-15.13\text{‰}$  and  $-10.49\text{‰}$  (average  $-12.65\text{‰}$ ). In contrast to the  $\delta^{18}\text{O}$  values of water,  $\delta^{13}\text{C}_{\text{DIC}}$  values show no distinct seasonal change, only a slight decrease in late autumn. The  $\delta^{13}\text{C}_{\text{DIC}}$  values generally increase downstream (Fig. 2b). This probably results from the preferential loss of  $^{12}\text{C}$  due to degassing of  $\text{CO}_2$  [17]. The largest decrease of around 2.5‰ in  $\delta^{13}\text{C}_{\text{DIC}}$  from the spring to the outflow was observed in autumn (October 2008 and 2009). In a carbonate aquifer system, the main carbon source is the dissolution of carbonate minerals. The isotope composition of dissolved carbon in carbonate groundwater is therefore expected to fit closely to the isotopic signature of host rocks (0‰). Other sources of dissolved carbon are atmospheric ( $-7\text{‰}$ ) and soil  $\text{CO}_2$ . The source of DIC, which provides additional carbon, was determined by calculating the isotopic composition of added DIC [18]. The  $\delta^{13}\text{C}$  value of added DIC was estimated to be  $-11.9\text{‰}$ . Carbon isotope separation between gaseous  $\text{CO}_2$  and DIC was estimated at  $-8.62\text{‰}$  as the sum of weighted enrichment factors for each carbon species using equations from [19–21]. Final  $\delta^{13}\text{C}_{\text{DIC}}$  would then be  $-20.52\text{‰}$ , which fits with stable isotopic composition of biogenic soil  $\text{CO}_2$  in the Slovenian karst area ( $-21.40 \pm 3.4\text{‰}$  [22]).

### 4.3. Tufa deposition and its potential as environmental proxy

Deposition of tufa in the River Krka results from changes in water chemistry. The sequence of key reactions ( $\text{CO}_2$  out gassing, increasing SiC and final calcite precipitation) in the River Krka fits with the established model of tufa deposition in fluvial river systems [23]. Simultaneous precipitation of carbonate occurs when

oversaturation of 4–10 times is reached [1]. According to Merz–Preiß and Riding [8], carbonate precipitation in freshwater systems occurs at a much lower oversaturation of 0.6, respectively, however, precipitation of carbonate in flowing freshwater settings is promoted by the presence of biofilms [9]. Calculations of saturation of Krka riverwater with respect to calcite (SIc) show that the water is constantly oversaturated (0.01–1.24), except in very cold winter. Highest SIc values over 0.6 were obtained in summer and autumn. The minimum oversaturation required for spontaneous tufa precipitation was reached a few kilometres further from the spring, where natural barriers and microbial films are present.

The  $\delta^{18}\text{O}$  and  $\delta^{13}\text{C}$  values of bulk tufa range between  $-9.16$  and  $-8.33\text{‰}$  (average  $-8.88\text{‰}$ ) and between  $-10.97$  and  $-9.47\text{‰}$  (average  $-10.41\text{‰}$ ). A good correlation between  $\delta^{13}\text{C}$  and  $\delta^{18}\text{O}$  of tufa indicates kinetic controls on tufa precipitation. The smallest differences between the average  $\delta^{18}\text{O}$  values of water and tufa are observed in summer and autumn (0.01 to 0.04‰ enrichment in tufa). The temperature of carbonate precipitation was estimated presuming  $^{18}\text{O}$  oscillations in tufa, mainly reflecting variations in water temperature using equations developed in Refs [24, 25] and Anderson and Arthur [6]. Measured and calculated water temperatures are best fitted when the average  $\delta^{18}\text{O}$  of water and tufa are considered (Fig. 3). The tufa samples are enriched with  $^{13}\text{C}$  for 2.09–2.49‰ in comparison to  $\delta^{13}\text{C}_{\text{DIC}}$ . This is due to preferential loss of  $^{12}\text{C}$  during rapid  $\text{CO}_2$  degassing [17] and photosynthetic microbial activities [26] during  $\text{CaCO}_3$  precipitation.

In some natural environments the Mg/Ca ratio in carbonate precipitates is useful for inferring water temperature [3, 4]. Use of Mg/Ca ratio as a temperature proxy depends on its stability and correlation with the temperature in waters. The Mg/Ca ratio in Krka riverwater is unstable, however, it correlates well with the water temperature measured in autumn, especially in the upper stream ( $R^2=0.74$ ). Despite such good agreement the calculated water temperatures are much higher than the measured ones (Fig. 3).

## 5. CONCLUSIONS

The surface water chemistry of the River Krka is controlled by groundwater interactions with carbonate bedrock in the aquifer. The carbonate aquifer is the main source of cations, since their concentrations are constantly decreasing downstream. The isotopic composition of oxygen and carbon in the water results from the homogenization processes of water within the aquifer, since  $\delta^{18}\text{O}$  and  $\delta^{13}\text{C}_{\text{DIC}}$  show no response to rainfall amount or water flow rates. Total alkalinity and concentrations of dissolved inorganic carbon show similar seasonal and downstream variability. They both increase in autumn when soil erosion from river banks and carbonate dissolution are most intensive.

Deposition of tufa in the River Krka is influenced by physicochemical and biological processes. In comparison to  $\delta^{13}\text{C}_{\text{DIC}}$ , the  $\delta^{13}\text{C}$  values of tufa are enriched due to loss of light carbon during photosynthetic processes and rapid  $\text{CO}_2$  degassing involved in tufa precipitation. Oxygen isotope composition of water and tufa are very similar, implying little or no fractionation. Estimations of carbonate precipitation temperature yield similar results to measured water temperature. However, this is true only when average water and tufa  $\delta^{18}\text{O}$  values are considered and the water temperature equations developed by Anderson and Arthur [6] and Hays and Grossman [24] are used. The Mg/Ca ratio of the water varies across a large range, therefore the Mg/Ca ratio of tufa cannot be used as a geothermometer in the River Krka.

### ACKNOWLEDGEMENTS

We thank Mr. Stojan Žigon for technical assistance and the Slovenian Research Agency for providing financial support (research projects PR-02497 and J1-9498).

### REFERENCES

- [1] HERMAN, J.S., LORAH, M.M., Calcite precipitation rates in the field: Measurement and prediction for the travertine depositing stream, *Geochim. Cosmochim. Acta* **52** (1988) 2347–2355.
- [2] DIETZEL, M., et al., Oxygen isotopic fractionation during inorganic calcite precipitation — Effects of temperature, precipitation rate and pH, *Chem. Geol.* **268** (2009) 107–115.
- [3] HUANG, Y., FAIRCHILD, I.J., Partitioning of  $\text{Mg}^{2+}$  and  $\text{Sr}^{2+}$  into calcite under karst-analogue experimental conditions, *Geochim. Cosmochim. Acta* **65** 1 (2001) 47–62.
- [4] IHLENFELD, C., et al., Climatic significance of seasonal trace element and stable isotope variations in modern freshwater tufa, *Geochim. Cosmochim. Acta* **67** 13 (2003) 2341–2357.
- [5] KAWAI, T., et al., Seasonal variation in water chemistry and depositional processes in a tufa-bearing stream in SW-Japan, based on 5 years of monthly observations, *Chem. Geol.* **232** (2006) 33–53.
- [6] ANDREWS, J.E., Palaeoclimatic records from stable isotopes in riverine tufas; Synthesis and review, *Earth Sci. Rev.* **75** (2006) 85–104.
- [7] HORI, M., et al., Seasonal patterns of carbon chemistry and isotopes in tufa depositing groundwaters of southwestern Japan, *Geochim. Cosmochim. Acta* **72** (2008) 480–492.
- [8] MERZ-PREIß, M., RIDING, R., Cyanobacterial tufa calcification in two freshwater streams: Ambient environment, chemical thresholds and biological processes, *Sed. Geol.* **126** (1999) 103–124.
- [9] ROGERSON, M., et al., New insights into biological influence on the geochemistry of freshwater carbonate deposits, *Geochim. Cosmochim. Acta* **72** (2008) 4976–4987.

- [10] KANO, A., et al., Origin of annual laminations in tufa deposits, southwest Japan, *Palaeogeogr. Palaeoclimatol. Palaeoecol.* **191** (2003) 243–262.
- [11] LOJEN, S., et al., C and O stable isotope variability in recent freshwater carbonates (River Krka, Croatia), *Sedimentology* **51** (2004) 361–375.
- [12] LOJEN, S., et al., Continuous 60-year stable isotopic and earth-alkali element records in a modern laminated tufa (Jaruga, river Krka, Croatia): Implications for climate reconstruction, *Chem. Geol.* **258** (2009) 242–250.
- [13] PARKHURST, D.L., APPELO, C.A.J., User's guide to PHREEQC (version 2) — A computer program for speciation, batch-reaction, one-dimensional transport, and inverse geochemical calculations, Water–Resources Investigations Report 99–4259, Denver, CO (1999).
- [14] CLARK, I., FRITZ, P., *Environmental Isotopes in Hydrogeology*, Lewis, New York (1997).
- [15] SZRAMEK, K., et al., Relative weathering intensity of calcite versus dolomite in carbonate-bearing temperate zone watersheds: Carbonate geochemistry and fluxes from catchments within the St. Lawrence and Danube river basins, *Geochem. Geophys. Geosys.* **8** (2007) 26.
- [16] DARLING, W.G., Hydrological factors in the interpretation of stable isotopic proxy data present and past: A European perspective, *Quatern. Sci. Rev.* **23** (2004) 743–770.
- [17] USDOWSKI, E., et al., Relationship between  $^{13}\text{C}$  and  $^{18}\text{O}$  fractionation and changes in major element composition in a recent calcite-depositing spring – A model of chemical variations with inorganic  $\text{CaCO}_3$  precipitation, *Earth Planet. Sci. Lett.* **42** (1979) 267–276.
- [18] SAYLES, F.L., CURRY, W.B.,  $\delta^{13}\text{C}$ ,  $\text{TCO}_2$ , and the metabolism of organic carbon in deep sea sediments, *Geochim. Cosmochim. Acta* **52** (1988) 2963–2978.
- [19] VOGEL, J.C., et al., Isotope fractionation between gaseous and dissolved carbon dioxide, *Z. Phys.* **230** (1970) 225–238.
- [20] MOOK, W.G., et al., Carbon isotope fractionation between dissolved bicarbonate and gaseous carbon dioxide, *Earth Planet. Sci. Lett.* **22** (1974) 169–176.
- [21] DEINES, P., et al., Stable carbon isotope ratios and the existence of a gas phase in the evolution of carbonate ground waters, *Geochim. Cosmochim. Acta* **38** (1974) 1147–1164.
- [22] ELER, K., et al., Soil respiration of dry calcareous grassland with woody plant encroachment (in preparation).
- [23] PEDLEY, H.M., Classification and environmental models of cool freshwater tufas, *Sediment. Geol.* **68** (1990) 143–154.
- [24] HAYS, P.D., GROSSMAN, E.L., Oxygen isotopes in meteoric calcite cements as indicators of continental palaeoclimate, *Geol.* **19** (1991) 441–444.
- [25] COPLEN, T.B., Calibration of the calcite–water oxygen-isotope geothermometer at Devils Hole, Nevada, a natural laboratory, *Geochim. Cosmochim. Acta* **71** (2007) 3948–3957.
- [26] ARP, G., et al., Fluvial tufa formation in a hard-water creek (Deinschwanger Bach, Franconian Alb, Germany), *Facies* **44** (2001) 1–22.



# ISOTOPIC AND GEOCHEMICAL SIGNATURES OF MELGAÇO CO<sub>2</sub> RICH COLD MINERAL WATERS, NW PORTUGAL

P.M. CARREIRA<sup>a</sup>, J.M. MARQUES<sup>b</sup>, M.R. CARVALHO<sup>c</sup>, D. NUNES<sup>a</sup>,  
M. ANTUNES DA SILVA<sup>d</sup>

<sup>a</sup> Instituto Tecnológico e Nuclear,  
Unidade de Ciências Químicas e Radiofarmacêuticas,  
Sacavém, Portugal

<sup>b</sup> Instituto Superior Técnico, Universidade Técnica de Lisboa,  
Lisbon, Portugal

<sup>c</sup> Universidade de Lisboa, Faculdade de Ciências,  
Departamento de Geologia,  
Lisbon, Portugal

<sup>d</sup> UNICER Bebidas, S.A.,  
S. Mamede de Infesta, Portugal

## Abstract

The isotopic and chemical compositions of CO<sub>2</sub> rich mineral waters found in the NW of Portugal were investigated. These mineral waters are mainly related to granitic and granodioritic rocks. Based on their chemical composition, two water types are distinguished (Ca-HCO<sub>3</sub> and Ca-Na-HCO<sub>3</sub>), indicating different underground flow paths. Through comparison with local shallow groundwaters, water chemistry indicates that the Melgaço mineral waters evolved through water–rock interaction with the hosted rocks. Stable isotope data indicates the meteoric origin of these CO<sub>2</sub> rich mineral waters, being recharged from about 480 up to 730 m a.s.l. Considering the  $\delta^{18}\text{O}$ ,  $\delta^2\text{H}$  and the hydrochemical data, no indication of mixing seems to occur between the shallow and deep groundwater systems. The  $\delta^{13}\text{C}$  determinations carried out on TDIC of the CO<sub>2</sub> rich mineral waters point to the hypothesis of methanogenesis (upper mantle CH<sub>4</sub> source) within the system, leading to <sup>13</sup>C enrichment. The negligible <sup>14</sup>C content ( $\approx 2$  pMC) also indicates a mantle derived carbon source for the groundwater system.

## 1. INTRODUCTION

A number of springs containing mineral waters are found in the Portuguese mainland part of the Iberian Massif and in its western and southern Meso-Cenozoic

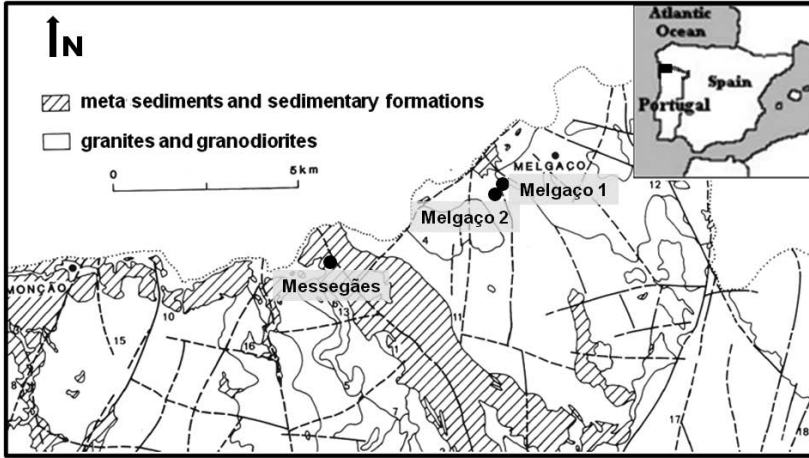


FIG. 1. Simplified geological map of the region. Location of the mineral boreholes. Adapted from Ref. [4].

Borders. On the western Meso-Cenozoic Border, mineral springs occur near faults forming valleys in areas of gypso-saline diapirism. On the southern Meso-Cenozoic Border, occurrence of mineral waters is related to magmatic (e.g. nefeline syenites) and sedimentary (e.g. limestone) rocks [1]. In the present case study, the  $\text{CO}_2$  rich mineral groundwater systems are located in the Iberian Massif at the NW part of the Portuguese mainland, where the geological environment is basically composed by Variscan granites and granodiorites [2–3] (Fig. 1). In this region, the natural conditions of the shallow dilute and deep mineral groundwater resources had not been seriously degraded by human intervention. Groundwater resources have been utilized locally at lower flow rates, and the exploitation was generally compensated by natural regeneration. Nevertheless, over the last decades, local groundwater resources have become progressively more endangered, both in quality and quantity, by accelerated modification of their natural conditions due to industrial (mineral bottled waters) and/or agricultural activities. In order to update our knowledge of the Melgaço  $\text{CO}_2$  rich mineral groundwater system, emphasis was set on the definition of the recharge areas, underground flow paths and identification of possible mixing between shallow and deep groundwaters, based on geochemical and isotopic fingerprints.

## 2. HYDROGEOLOGICAL SETUP

Several authors have described in detailed the geology of the region [4–5]. Locally, three types of granitic rocks can be distinguished based on their structural relationships and internal deformations. The igneous rocks in the region can be

divided into: (a) sin-tectonic granites with minute flakes of muscovite and biotite, usually presenting metamorphic minerals, and strongly correlated with migmatitic rocks; (b) tardi-tectonic granites (frequently associated with granodiorites) with a large presence of biotite (muscovite as secondary mineral); (c) post-tectonic granites: usually characterized by the presence of mega-crystals of K-feldspar and biotite [6] (Fig. 1).

The main fracture systems in the region are represented by structural lineaments (strike-slip faults), with the directions ENE-WSW, WNW-ESE, NNE-SSW and NNW-SSE, of late Hercynian age, and still active during the Meso-Cenozoic [7]. The geological studies carried out in the Monção region have indicated that the ENE-WSW fracture system (left strike-slip fault) is responsible for the morphology of the Minho River valley. Melgaço and Messegães mineral borehole waters emerge along NNW-SSE structures where appropriate conditions are found.

### 3. SAMPLING AND METHODS

Three fieldwork campaigns were carried out (February 2002, February and July 2006). Groundwater samples were collected from boreholes (mineral system) and from springs (located at different altitudes within the surrounding of the research area) representing the shallow dilute groundwater systems. Major and minor elements in waters were determined at IST (CEPGIST), Portugal, using the following methods: atomic absorption spectrometry for Ca and Mg; emission spectrometry for Na and K; colorimetric methods for SiO<sub>2</sub>, Fe<sub>total</sub>, F and Al; ion chromatography for SO<sub>4</sub>, NO<sub>3</sub> and Cl; potentiometry for alkalinity. The  $\delta^2\text{H}$  and  $\delta^{18}\text{O}$  measurements (vs V-SMOW) were performed by mass spectrometry (SIRA 10-VG ISOGAS) at ITN – Portugal following the analytical methods of Refs [8–9], with an accuracy of  $\pm 1\text{‰}$  for  $\delta^2\text{H}$  and  $\pm 0.1\text{‰}$  for  $\delta^{18}\text{O}$ . The  $^3\text{H}$  water content (reported in Tritium Units, TU) was also determined at ITN, using electrolytic enrichment followed by liquid scintillation counting (standard deviation varies between  $\pm 0.5$  and  $\pm 0.6$  TU). The  $\delta^{13}\text{C}$  and  $^{14}\text{C}$  determinations were performed at the Geochron Laboratories, USA, by AMS. The  $\delta^{13}\text{C}$  values are reported in  $\text{‰}$  vs. V-PDB, with an accuracy of  $\pm 0.1\text{‰}$ ; the  $^{14}\text{C}$  contents are given in pMC.

### 3. WATER GEOCHEMISTRY

The mean temperature of the Melgaço CO<sub>2</sub> rich mineral waters (at the wellhead) varies between 15–20°C, while the shallow groundwater systems presently display temperatures of around 14°C (from 12–16°C). An enormous gap in mineralization is observed between these two groundwater systems. Melgaço CO<sub>2</sub> rich mineral waters are characterized by a TDS from 365 to 1515 mg/L, while the shallow aquifers show

that TDS varies from 24 to 120 mg/L. The geochemical *facies* of the mineral and shallow groundwater systems is also rather different. Melgaço and Messegães CO<sub>2</sub> rich mineral waters are Ca-HCO<sub>3</sub> and Na-Ca-HCO<sub>3</sub>, respectively. The shallow groundwater system is characterized by Na-HCO<sub>3</sub>-type waters. High CO<sub>2</sub> gas content found in the mineral waters is responsible for the increase in water–rock interaction processes. In fact, Ca and Na in natural waters are usually derived from feldspar hydrolysis in granitic environments, as indicated by the Na-HCO<sub>3</sub> nature of the waters. However, the presence of Ca-HCO<sub>3</sub> type waters suggests different underground flow paths (fracture environments), by the amount of the dissolved Ca in these waters, probably due to Ca rich plagioclases hydrolysis occurring in the granodioritic terrains [4, 2].

The geochemical signatures of the shallow groundwater systems show large variability, probably related to the location of different springs downhill, frequently in areas of intensive agricultural activities. The human impact in the area results in the increase in the concentrations of NO<sub>3</sub><sup>-</sup>, Cl<sup>-</sup> and SO<sub>4</sub><sup>2-</sup>. The heterogeneity of the CO<sub>2</sub> rich mineral water samples reveals water–rock interaction processes with different lithologies, depending on calcium availability, associated with different underground flow paths. From the chemical point of view, no mixing between the deep CO<sub>2</sub> rich mineral water systems and local shallow dilute groundwater systems seems to occur.

#### 4. ISOTOPE FINGERPRINTS IN THE MELGAÇO GROUNDWATER SYSTEMS

##### 4.1. Oxygen-18 and deuterium assessment

The δ<sup>18</sup>O and δ<sup>2</sup>H diagram (Fig. 2A) indicates that Melgaço CO<sub>2</sub> rich mineral waters are derived from the local meteoric waters. Using the isotopic composition of the shallow groundwater samples, the equation of the Local Meteoric Water Line (Local MWL) obtained is (Fig. 2A): δ<sup>2</sup>H = 7.85 δ<sup>18</sup>O + 9.42. In this study, the ‘altitude effect’ has been successfully used for the identification of the recharge areas and in the investigation of the origin and interconnections of different groundwater bodies. Data from the literature indicates values of the isotopic gradient ranging from -0.15 to -0.50‰ δ<sup>18</sup>O/100m, with an average rate of depletion of about -0.26‰ [10–12]. In the Melgaço area the isotopic gradient obtained for δ<sup>18</sup>O is -0.15‰ per 100m of altitude (Fig. 2B), which is in conformity with the data presented above. This mean isotopic gradient was obtained using the discharge altitude of the spring waters (shallow groundwater systems) instead of the infiltration altitude, as these spring waters are representative of very local circulation systems. Based on the isotopic gradient of the region (Fig. 2B) and using the mean isotopic signatures (δ<sup>18</sup>O) of the mineral waters samples Melgaço 1, Melgaço 2 and Messegães) the recharge altitude of the CO<sub>2</sub> rich mineral water systems was calculated. The obtained values range from 480 m a.s.l (Melgaço 1) to 730 m a.s.l. (Messegães). These elevations are

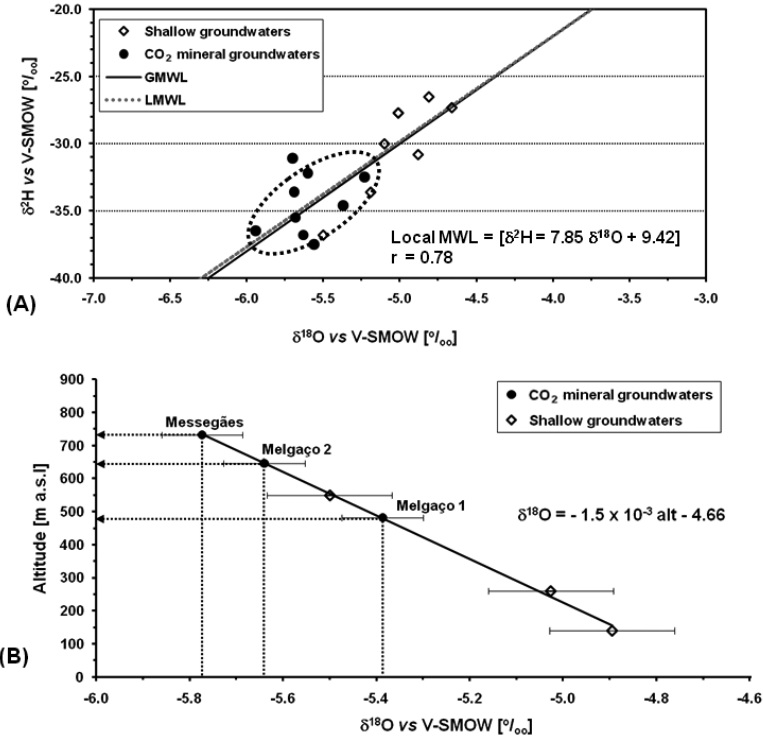


FIG. 2. (A)  $\delta^2\text{H}$  versus  $\delta^{18}\text{O}$  from the Melgaço area, the GMWL and the Local Meteoric Water Line are plotted. (B) Estimation of the recharge altitude of the mineral system;  $\delta^{18}\text{O}$  values as a function of the altitude of the sampling sites.

pointing out to a recharge area located south of the Minho River towards the Peneda Mountain.

#### 4.2. Tritium and carbon-14 signatures

During the different fieldwork campaigns carried out in the study area, groundwater samples were always collected for  $^3\text{H}$  determination. In the shallow groundwater systems,  $^3\text{H}$  contents ranged from  $5.2 \pm 0.6$  TU (October 1999 [13]) to  $2.1 \pm 0.6$  TU (February 2003). The  $\text{CO}_2$  rich mineral waters from Melgaço 1, Melgaço 2 and Messegães boreholes show the lowest  $^3\text{H}$  concentrations from 0 up to  $2.2 \pm 0.5$  TU.

Plotting the  $^3\text{H}$  content as a function of the oxygen-18 and electrical conductivity the lowest  $^3\text{H}$  values are found in the groundwater samples with the highest mineralization, pointing to a longer circulation path and higher water-rock interaction (Fig. 3B,C). The oxygen-18 pattern seems to be related to different recharge altitudes

(Fig. 3A). From the diagrams in figure 4C, it is possible to observe that Messegães CO<sub>2</sub> rich borehole waters, with the higher recharge altitude (higher than 730 m), presents the lowest tritium content, indicating a longer residence time, promoting high water–rock interaction. This trend (increase in mineralization and lowest <sup>3</sup>H content) can be also found in Melgaço 1 and Melgaço 2 CO<sub>2</sub> rich mineral waters. It should be stated that Melgaço 1 CO<sub>2</sub> rich mineral waters present lower mineralization, higher

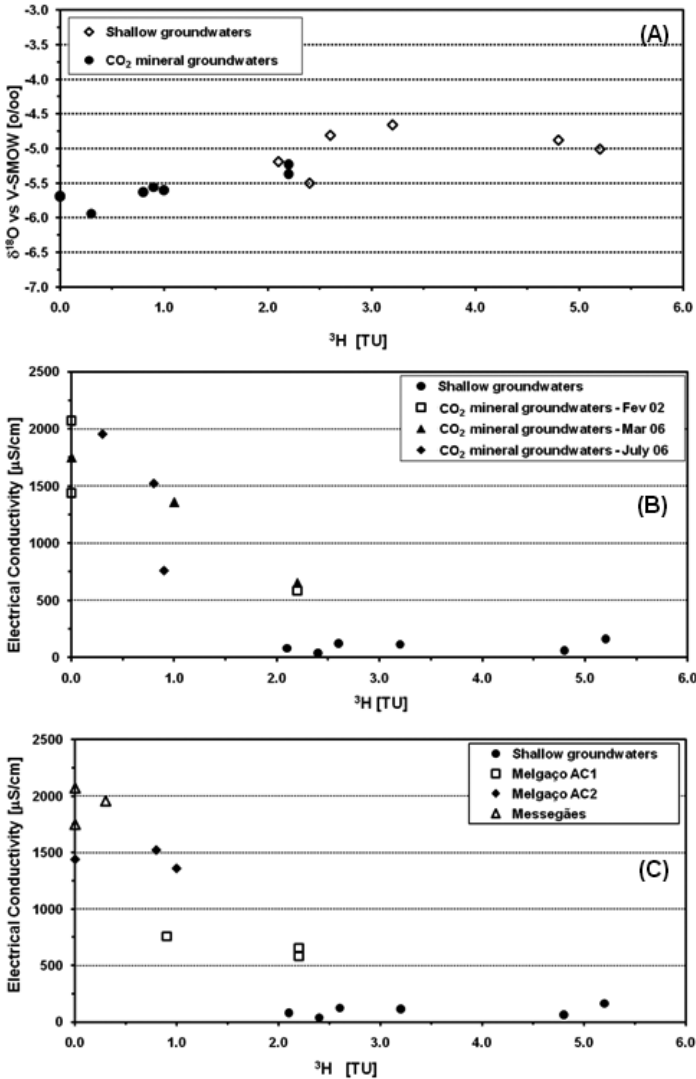


FIG. 3.(A)  $\delta^{18}O$  versus  $^3H$ ; (B) Electrical conductivity versus  $^3H$  evolution across the 3 fieldwork campaigns and (C) Electrical conductivity versus  $^3H$  with the boreholes separated in the Melgaço area.

$^3\text{H}$  content and low recharge altitude, when compared with Melgaço 2, indicating a shorter underground flow path.

If one considers a tritium input of the same order of magnitude as found for the Porto meteorological station (4.5 TU – mean arithmetic weight value [14]), and taking into account the range of  $^3\text{H}$  data obtained in the  $\text{CO}_2$  rich mineral borehole waters studied, a minimum residence time of 40 years should be indicated.

Carbon-14 determinations by AMS were carried out in the Total Dissolved Inorganic Carbon (TDIC) of the Melgaço 1 and Melgaço 2 borehole waters, and simultaneously  $\delta^{13}\text{C}$  determinations were carried out. The values obtained were:

$$^{14}\text{C} = 2.33 \pm 0.07 \text{ pMC} \text{ and } \delta^{13}\text{C} = 4.7\text{‰} \quad \text{— Melgaço 1}$$

$$^{14}\text{C} = 1.01 \pm 0.04 \text{ pMC} \text{ and } \delta^{13}\text{C} = 4.7\text{‰} \quad \text{— Melgaço 2}$$

The radiometric age of these groundwaters is that of the dissolved carbon, which may not be that of the water. In addition to carbon-14 dating, the  $\delta^{13}\text{C}$  value of a groundwater is also dependent upon many factors such as dissolution of carbonate minerals, introducing relatively heavy carbon to the water system; oxidation of organic matter, with the input of relatively light carbon; transport of  $\text{CO}_2$  in soil gas with light carbon; and methanogenesis (redox reactions involving methane). According to Ref. [15], methane is a common trace constituent of groundwaters, sometimes reaching concentration values greater than 20% of the total carbon. Reference [15] states that where methane bearing groundwaters discharge into aerobic environments microbial methane oxidation can occur, leading to progressive enrichment in  $^{13}\text{C}$  in the residual methane.

The fractionation between  $\text{CO}_2$  and  $\text{CH}_4$  is large at about 75‰, producing methane with depleted  $\delta^{13}\text{C}$  values and the  $\text{CO}_2$  being isotopically more enriched with  $\delta^{13}\text{C}$  values between  $-20$  and  $+10\text{‰}$ . Nevertheless, Ref. [16] calls attention to the fact that in areas with  $\text{CO}_2$  abundance in the gas phase (as for example in complex crystalline basements or in areas with younger volcanic activity),  $\text{CO}_2$  with isotopic compositions of  $\delta^{13}\text{C}$  values lesser than  $-10\text{‰}$  is often found. In many cases, such values are interpreted as biogenic/organic  $\text{CO}_2$  or mixtures between magmatic and biogenic  $\text{CO}_2$  (mantle and crustal endmembers, respectively) or could be also explained by gas fractionation with the  $\text{HCO}_3$  formed.

Works carried out in the NE of Portuguese mainland at Vidago-Pedras Salgadas  $\text{CO}_2$  rich mineral water systems, also within granitic rocks, have found occurrences of methane, reported within the groundwater systems in the free gas phase, with a mean value of 583 mg/L of  $\text{CH}_4$  (varying between 41–1021 mg/L at Vidago AC18 and Vidago Areal 3, respectively) [17]. Taking into consideration all these data, the hypothesis that the heavy isotopic signatures found in the  $\delta^{13}\text{C}$  of Melgaço  $\text{CO}_2$  rich mineral waters could be related to deep seated (upper mantle) methanogenesis should not be excluded. Regarding the radiocarbon content obtained in these two boreholes, the negligible  $^{14}\text{C}$  content ( $\approx 2$  pMC) most probably also indicates a mantle derived carbon source to the groundwater system.

## 5. FINAL CONSIDERATIONS

The regional geomorphology seems to favour a conceptual circulation model, suggesting that the recharge area of the CO<sub>2</sub> rich mineral water system at the south of Melgaço up hill between 480 and 730 m a.s.l based on the isotopic composition ( $\delta^{18}\text{O}$  values). The flow paths should be associated with the fault systems from which these waters emerge, when appropriate conditions are found. The recharge altitudes are in agreement with a longer circulation path for Messegães CO<sub>2</sub> rich mineral waters and a shorter circulation path associated to Melgaço 1 CO<sub>2</sub> rich mineral waters. The  $\delta^{13}\text{C}$  determinations carried out on TDIC of the CO<sub>2</sub> rich mineral waters are pointing to the hypothesis of methanogenesis within the system leading to <sup>13</sup>C enrichment and the mantle derived carbon source to the groundwater system to a decrease in the radiocarbon content to negligible values. During future investigations on the CO<sub>2</sub> rich mineral waters located in the N of the Portuguese mainland, a special emphasis will be placed on the  $\delta^{13}\text{C}$  determinations of the CH<sub>4</sub>, in order to enhance the identification of the processes responsible for the enriched  $\delta^{13}\text{C}$  values found in Melgaço CO<sub>2</sub> rich mineral waters.

## ACKNOWLEDGEMENTS

The authors would like to express their thanks to UNICER Bebidas. This research was developed under the scope of the POCTI/CTA/45159/2002 R&D Project DISGAS – Dissolved gases in subsurface hydrology – CO<sub>2</sub> rich thermomineral waters (N-Portugal), funded by the Portuguese Foundation for Science and Technology (FCT) and FEDER EU Programme.

## REFERENCES

- [1] AIRES-BARROS, L., Comments about the geochemistry of the Portuguese mineral waters, Bol. Museu Lab. Min. Geol. Fac. Ciências de Lisboa **16** (1979) 123–135 (in Portuguese).
- [2] FARÍAS, P., et al., Aportaciones al conocimiento de la litoestratigrafía y estructura de Galicia Central, Mem. Mus. Lab. Min. Geol. Fac. Ciênc. Univ. Porto **1** (1987) 411–431.
- [3] RIBEIRO, A., et al., “Geodynamic evolution of the Iberian Massif”, Pre-Mesozoic Geology of Iberia (DALLMEYER, R.D., et al., Eds), Springer Verlag, Berlin (1990) 397–410.
- [4] RIBEIRO, M.L., MOREIRA, A., Geological map of Portugal, Sheet No. 1B, 1:50 000, Monção, Portuguese Geological Survey, Lisbon (1986) (in Portuguese).
- [5] MOREIRA, A., SIMÕES, M., Geological map of Portugal, Sheet No. 1D, 1:50 000, (Arcos de Valdevez), Portuguese Geological Survey, Lisbon (1988) (in Portuguese).

- [6] FERREIRA, N., et al., “Granites from the Center-Iberia Zone and their geodynamic features”, *Geología de los granitóides y rocas asociadas del Macizo Hespérico*, Libro de Homenaje a L. C. García de Figuerola (BEA, F., et al., Eds), Editorial Rueda, Madrid (1987) 37–51.
- [7] SOARES DE CARVALHO, G., “Quaternary and Cenozoic deposits”, Report on the Geological Map of Portugal, Sheet No. 1, 1:200 000 (PEREIRA, E., Ed.), Portuguese Geological Survey, Lisbon (1992) 47–50 (in Portuguese).
- [8] EPSTEIN, S., MAYEDA, T., Variation of  $^{18}\text{O}$  content of waters from natural sources, *Geochim. Cosmochim. Acta* **4** (1953) 213–224.
- [9] FRIEDMAN, I., Deuterium content of natural waters and other substances, *Geochim. Cosmochim. Acta* **4** (1953) 89–103.
- [10] YURTSEVER, Y., GAT, J.R., “Atmospheric waters”, *Stable Isotope Hydrology: Deuterium and Oxygen-18 in the Water Cycle*, Technical Report Series, IAEA **210** (1981) 103–142.
- [11] ARAGUÁS-ARAGUÁS, L., et al., Deuterium and oxygen-18 isotope composition of precipitation and atmospheric moisture, *Hydrol. Process.* **14** (2000) 1341–1355.
- [12] GONFIANTINI, R., et al., The altitude effect on the isotopic composition of tropical rains, *Chem. Geol.* **181** (2001) 147–167.
- [13] NASCIMENTO, I.B., Contribution to the Knowledge of the Groundwaters from Monção Region, MSc. Thesis, Instituto Superior Técnico, Technical University of Lisbon (2000) (in Portuguese).
- [14] CARREIRA, P.M., et al., “Temporal and seasonal variation of stable isotopes and tritium in precipitation over Portugal”, *Isotopes in Environmental Studies (Proc. Intern. Conf. Monaco, 2004)*, IAEA, Vienna (2005) 370–373.
- [15] BARKER, J.F., FRITZ, P., Carbon isotope fractionation during microbial methane oxidation, *Nature* **293** (1981) 289–291.
- [16] WEINLICH, F.H., Isotopically light carbon dioxide in nitrogen rich gases: The gas distribution pattern in the French Massif Central, the Eifel and western Eger Rift, *Annals Geoph.* **48** (2005) 19–31.
- [17] CARREIRA, P.M., et al., Mantle-derived carbon in Hercynian granites. Stable isotopes signatures and C/He associations in the thermomineral waters, N-Portugal. *J. Volcanol. Geoth. Res.* **189** (2010) 49–56
- [18] CLARK, I., FRITZ, P., *Environmental Isotopes in Hydrogeology*, Lewis, New York (1997).



# A CASE STUDY FROM SOUTHWEST GERMANY — SHIFTING OF GROUNDWATER AGE DURING ONE YEAR PUMPING TEST AND COMPARISON OF ISOTOPE METHODS

G.D. LORENZ<sup>a</sup>, L. EICHINGER<sup>a</sup>, E. FUNK<sup>b</sup>, M. HEIDINGER<sup>a</sup>,  
J. SCHNEIDER<sup>a</sup>

<sup>a</sup> Hydroisotop GmbH,  
Schweitenkirchen, Germany

<sup>b</sup> Buero fuer Hydrogeologie,  
Staufen, Germany

## Abstract

A two in one well in southwest Germany, separately tapping aquifers in the formations of Muschelkalk and Keuper, was tested in a one year pumping test. The waters were continuously analysed for chemical and isotopic composition (major ions, <sup>3</sup>H, <sup>18</sup>O, <sup>2</sup>H, <sup>13</sup>C, <sup>14</sup>C, <sup>85</sup>Kr) and trace gases (CFC, SF<sub>6</sub>). The analytical results of <sup>3</sup>H and <sup>85</sup>Kr showed a shift in the composition of 25% young, <sup>3</sup>H-bearing water to a proportion of 50% young water after half a year of pumping. The residence time of the young water of about 10 to 20 years remained the same. The shift is also visible in the increasing contents of nitrate and chloride. Though the analytical results of SF<sub>6</sub> showed the same shift, SF<sub>6</sub> — most probably influenced by crystalline gravel — indicates a residence time of the young water of less than one year. The CFCs, on the other hand, point to lower proportions of young water as they are influenced by degradation processes and/or adsorption. Though both aquifers are effectively separated from each other, the same shifting of age structure can be observed.

## 1. INTRODUCTION

For groundwater management, the top priority is to quantify the origin of resources, the flow paths and the availability. Besides classic hydrological methods, the use of environmental tracers provides important additional information about flow dynamics, leakage, recharge areas and mixing portions of different water components [1]. Consequently, a two in one well, tapping two aquifers separately, was analysed for potential mixing components, not only once, but frequently during a short multiple level and a one year one level pumping test. Multi-tracer investigations are required to obtain a sound characterization of the groundwater system. In this study tritium (<sup>3</sup>H), stable isotopes of the water molecule (<sup>18</sup>O, <sup>2</sup>H), krypton-85 (<sup>85</sup>Kr),

carbon isotopes ( $^{13}\text{C}$ ,  $^{14}\text{C}$ ) as well as gas tracers (SF and CFCs) were applied alongside intensive hydrochemical analyses of inorganic and organic components [2]. In this paper we present this case study to highlight the changes in groundwater age structure which can occur during pumping. Additionally, a comparison of different environmental tracers is shown, which provides the basis for the evaluation of different methods.

## 2. SITE DESCRIPTION AND HYDROLOGY

The two in one well is located in southwest Germany. The less productive well 1 (km) was pumped only with 2 L/s, while the more efficient well 2 (mo) was tested for 30 and 20 L/s for one year. Well 1 is tapping groundwater from a confined aquifer in sediments of middle and upper Keuper (km, ku; Upper Triassic), consisting of fissured mudstone, marl and dolomite with gypsum at depths of 20 to 49 m (Fig. 1). Well 2 is tapping groundwater from a confined aquifer in karstified carbonates of lower and middle Muschelkalk (mo, mm; Middle Triassic) at depths of 51 to 130 m. The aquifers are covered with clay rich, low permeable layers of Quaternary and Keuper. Though the intra triassic barrier layer is only 2 m thick, the water levels of both aquifers show a difference of 10 m. Both aquifers were considered hydraulically separated. As the recharge area of the Muschelkalk aquifer also encloses the Quaternary basin and river area (Fig. 1), infiltration of river water was of special interest in the study.

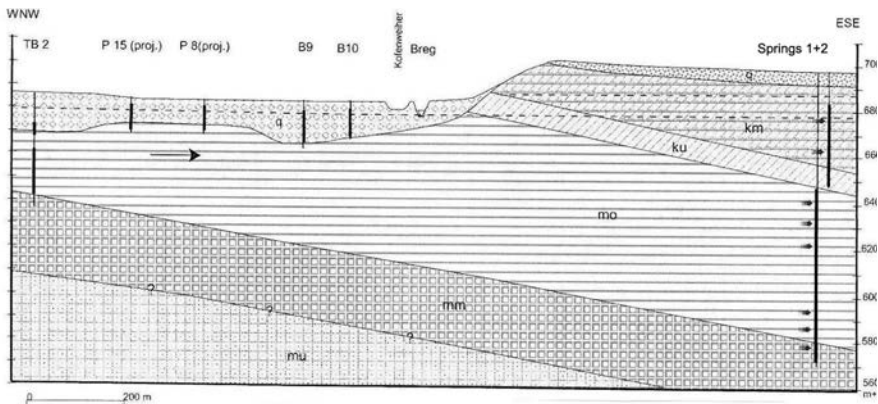


FIG. 1. Geological cross section with well 1 (km) and well 2 (mo).

### 3. CONCEPTUAL APPROACH AND METHODS

First short time tests of the newly installed wells showed the potential of high quality groundwater supply at high quantity. The vulnerability of the karstified aquifers, especially in case of river infiltration, and the thin barrier layer between the two aquifers was the reason for implementing a long time test with regular sampling for hydrochemical, microbial and isotope analyses. Special attention was paid to the possibility of leakage. Due to the shallow screen depths of the extractions wells, locally recharged water will be marked with anthropogenic substances as  $^{85}\text{Kr}$  ( $T_{1/2}$ : 10.76 a),  $^3\text{H}$  ( $T_{1/2}$ : 12.32 a),  $\text{SF}_6$  and CFCs. Previous studies in the area indicate that the groundwater in the confined aquifer of the Keuper formation can be found without these environmental tracers and is therefore older than ~55 years. Mean residence times (MRT) and mixing portions of shallow groundwater were estimated using lumped parameter models [3]. For the  $^{85}\text{Kr}$  input function the mean annual concentrations measured at the station Schauinsland (D) [4] were used. Tritium input concentrations in precipitation were reconstructed from data from the weather station in Steisslingen (D) (time period 1992–2009) and correlated and extended with data from the closest IAEA station Constance (D) [5]. Trace gas input concentrations in the atmosphere of  $\text{SF}_6$  and CFC were adjusted for altitude and mean temperature [6, 7].  $^{85}\text{Kr}$  activities were measured at UEP Bern by low level counting [8–10]. Tritium and  $^{14}\text{C}$  ( $T_{1/2}$ : 5730 a) concentrations were measured at Hydroisotop GmbH by liquid scintillation counting.  $\text{SF}_6$  and CFCs were measured at Spurenstofflabor Oster by gas chromatography.

### 4. ENVIRONMENTAL TRACER RESULTS

#### 4.1. Hydrochemical composition and water dynamics in the karst aquifers

Both groundwaters are dominated by Ca,  $\text{SO}_4$  and  $\text{HCO}_3$ , though the gypsum-bearing Keuper aquifer shows a higher Ca- $\text{SO}_4$  mineralization. The major components in the water from well 1 (km) remained more or less constant during the pumping period, while the water from well 2 (mo) decreased in total mineralization gradually from 780 to 700 mg/L TDS. This hydrochemical evolution proves that no significant leakage effects the deeper aquifer. The decrease of total mineralisation indicates a common effect of a double porosity system with dynamic gypsum leaching.

Possible anthropogenic compounds such as nitrate, but also chloride, are present in both tested groundwaters. In well 2 (mo) the trace components increased during pumping time as well as the dissolved oxygen. Well 1 (km) shows anaerobic conditions in a passive state, but the oxygen content increases to 0.5 mg/L during pumping. The increase of nitrate in well 1 (km) from 0.3 to 3 mg/L and in well 2 (mo) from 4 to 10 mg/L relates to the increase of young groundwater with agricultural

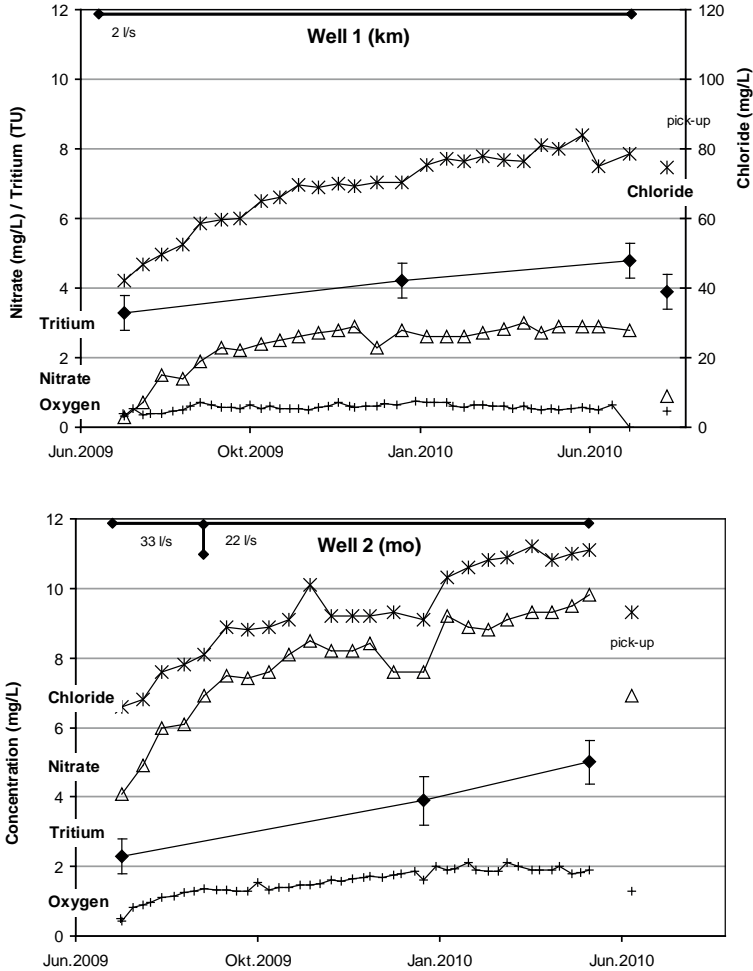


FIG. 2. Time courses of measured concentration of chloride, nitrate, oxygen and tritium.

influence. The increase of chloride in well 1 (km) from 42 to 84 mg/L is untypically high for young groundwater in the area of southwest Germany. Other groundwater components with processes of evaporate leaching are discussed in the detailed analysis of groundwater age. After a recovery period of one month following the pumping, both wells were sampled again. The oxygen, nitrate and chloride concentrations had decreased consequently, but not to the same degree as before the tests.

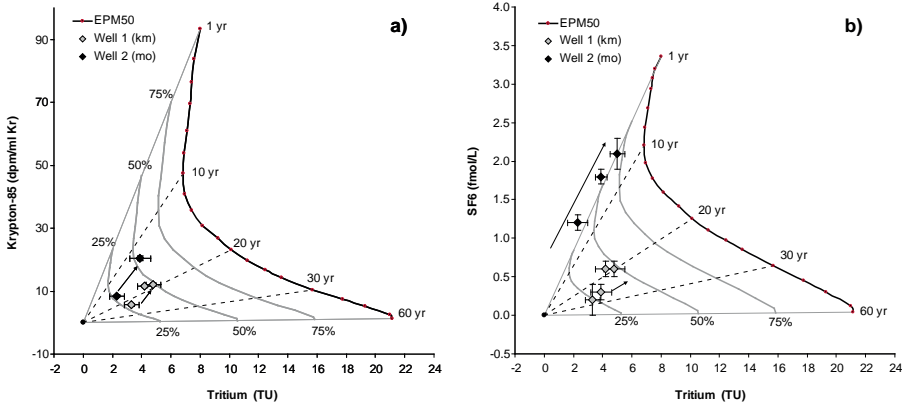


FIG. 3. Measured activities of  $^{85}\text{Kr}$  and  $\text{SF}_6$  versus  $^3\text{H}$  plotted with calculations applying a hydrological model [3]. The model curve is labelled with the MRT and portion of admixed young water and  $^3\text{H}$ ,  $\text{SF}_6$  and  $^{85}\text{Kr}$  free old water components (EPM50). The arrows indicate the shift of the parameters with pumping time.

## 4.2. Age structure and variation during pumping period

The wells were sampled three times during the one year pumping test for  $^3\text{H}$ ,  $^{85}\text{Kr}$ ,  $\text{SF}_6$  and CFCs. Additionally, samples of tritium and the trace gases were taken during short time multiple level tests. In Fig. 3, the measurements of  $\text{SF}_6$ ,  $^{85}\text{Kr}$  and  $^3\text{H}$  are plotted together with the calculated relation using a combined model with 50% exponential and 50% piston flow (EPM50). The box-model was selected according to local hydrogeological information [11, 12]. The admixture of tracer free water is indicated by a shift of the concentration towards lower values. Uncertainties of the tracer input functions and of the model selection result in an uncertainty of around 15% for the young water fractions and the mean residence time. While the values of the groundwater from well 1 (km) indicate the same age structure and shift both for the combination of  $^{85}\text{Kr}$  and  $^3\text{H}$  and of  $\text{SF}_6$  and  $^3\text{H}$  (Fig. 3), the values of the samples from well 2 (mo) present quite a different situation. Well 1 (km) taps an old,  $^3\text{H}$ -free water portion of around 25%, which increases to 50% during pumping time parallel to the increase of nitrate. The young groundwater has a relatively constant MRT of around 20 years. The parameters measured from well 2 (mo) show a young water component of 25%, increasing to 75% with a MRT younger than 5 years for the combination of  $\text{SF}_6$  and  $^3\text{H}$  (Fig. 3b). The combination of  $^{85}\text{Kr}$  and  $^3\text{H}$ , though, is interpreted as an increase of the young water amount from 25% to only 50% with a higher mean residence time of around 10–15 years (Fig. 3a). One reason for the discrepancy could be the influence of crystalline rocks, which can cause geogenic input of  $\text{SF}_6$ . Crystalline rocks can be found exposed in the river basin within the mo aquifer's area (Fig. 1). The fluvialite sediments consist of gravel and debris from the crystalline

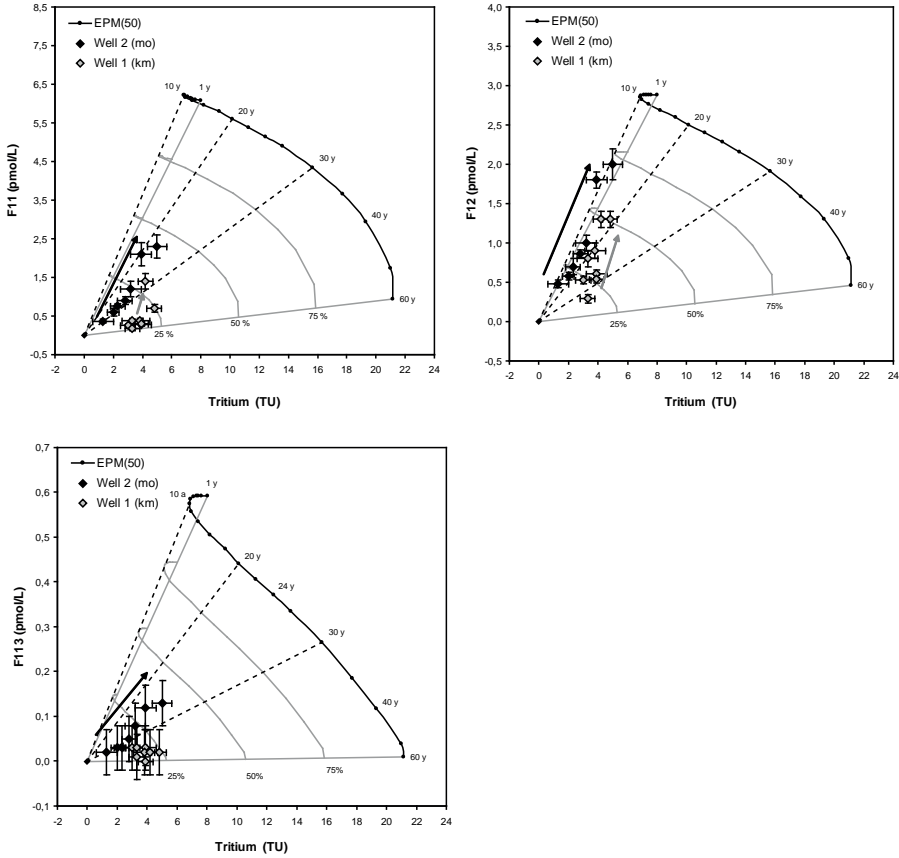


FIG. 4. Measured activities of CFCs and  $^3\text{H}$  plotted with calculations applying EPM50 [11].

rocks of the Black Forest. The lower MRT of young water proportion overall in the mo aquifer is considered as evidence that pumping does not enforce leakage.

To prove this thesis, the results of CFCs and calculations of MRT have been compared as well (Fig. 4). While the results of F11 and F113 indicate a reduction of the tracers in comparison to  $^{85}\text{Kr}$ , the results of F12 show an elevation of concentration both for the samples from well 1 (km) and well 2 (mo). Reduction of CFCs can be caused by microbial degradation or adsorption at clayey material [6]. As other groundwater wells of the area are known for contaminants of CHCs, the elevation of F12 might be due to contamination.

The time series of oxygen-18 only indicates for well 2 (mo) the presence of a young water portion which still indicates the seasonal signatures of the precipitation (Fig. 5a). As all values are alike regarding the analytical uncertainty, the amount of the young water is quite small, however, it is existent. These circumstances do not correspond easily with higher MRT. One possible explanation could be given by

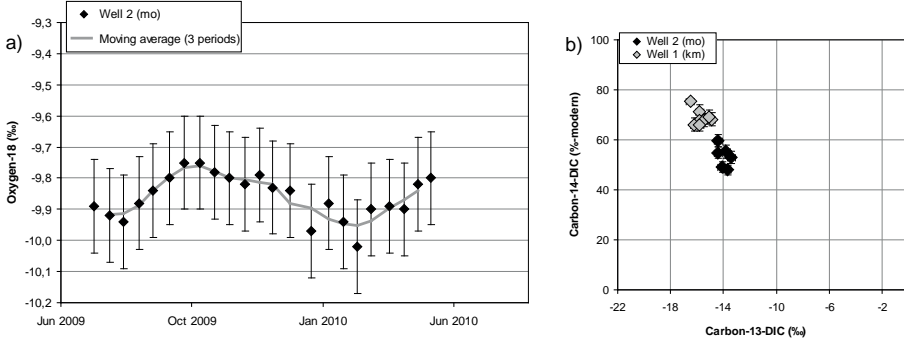


FIG. 5. (a): Time series of oxygen-18. The lines are calculated as the moving average of 3 periods each. (b): Measured carbon isotopes of DIC.

a double porosity system which was already suggested because of the hydrochemical evolution. The stable isotope values of the samples from well 2 (mo) are around 0.3‰ lighter than those of well 1 (km) which represent the different recharge areas to the aquifers.

Depleted stable isotopes can both be attributed to the higher elevated recharge area and cooler climate. Based on  $^{14}\text{C}$  groundwater ages, groundwater recharge during the cooler climatic conditions in the Pleistocene cannot be excluded completely for the mo aquifer. However, portions of Pleistocene groundwater would be very small (Fig. 5b). The modelled  $^{14}\text{C}$  groundwater age of the old,  $^3\text{H}$ -free components in the km aquifer (hundreds to 1500 years old) is slightly smaller than those of the mo aquifer (a few thousand years), though the difference of the  $^{14}\text{C}$ -DIC values are mostly determined by different carbon dissolution and carbon isotope exchange processes. Different initial compositions for the geochemical evolution in the marl and limestone aquifers have to be considered as well [13–15]. The results of the carbon isotopes show no significant shift during pumping time, though the results of the hydrochemical analyses indicate a variation of the dissolution of  $\text{Ca-SO}_4$  and Cl components.

## 5. CONCLUSION

This case study of two aquifers in southwest Germany demonstrates explicitly the shift of groundwater age structure which can occur during long term pumping times. Both wells show a significant increase of the young,  $^3\text{H}$ -bearing groundwater components from 25 to 50% with increasing pumping time. This is accompanied by a decrease of the water quality as the nitrate contents increase. The residence time of both young and old water components remained constant. Though both wells are

effectively technically and hydraulically separated, are quite different productively and have different recharge areas, the particular shift of age structure is characteristic and similar for both. The hydrochemical composition which varies over pumping time as well, corresponds only in a few parameters of anthropogenic influence e.g. nitrate. The investigation of hydrochemical and isotopic parameters could exclude leakage, and give evidence that lateral flow is dominating the mo aquifer.

The case study also compares a series of young groundwater parameters such as  $^{85}\text{Kr}$ ,  $\text{SF}_6$ , CFCs and  $^3\text{H}$ . While all parameters provide reasonable results which give no suspicious hints for secondary influence, the age calculations differ significantly. This single study of a two in one well can therefore show the elevation and reduction of trace gases caused by contaminants, microbial degradation or adsorption and geogenic input. As pumping rates of water supply are often based on discharge rates and response of groundwater withdrawal, these aspects have to be considered in detail.

### ACKNOWLEDGEMENTS

We would like to acknowledge the unhesitant permission of the well's owner to publish the data. We wish to thank Dr. Grimm from Regierungspräsidium Tübingen for initiating and supporting the project. We would also like to acknowledge R. Purtschert from University of Bern for analysing the Kr isotopes and H. Oster for analysing the trace gases.

### REFERENCES

- [1] ALTHAUS, R., et al., "Cross-border groundwater management: The contribution of deep groundwater to quaternary basins deduced from isotope data", *Advances in Isotope Hydrology and its Role in Sustainable Water Resources Management (Proc. Symp. Vienna, 2007)*, Vol. 2, Proceedings Series, IAEA, Vienna (2007) 111–120 .
- [2] COOK, P.G., HERCZEG, A.L. (Eds), *Environmental Tracers in Subsurface Hydrology*, Kluwer Academic, Boston (2000).
- [3] ZUBER, A., "Mathematical models for the interpretation of environmental radioisotopes in groundwater systems", *Handbook of Environmental Geochemistry*, (FRITZ, P., FONTES, J.C., Eds), Elsevier, Amsterdam (1986) 1–59.
- [4] WEISS, W., SARTORIUS, H., STOCKBURGER, H., "Global distribution of atmospheric  $^{85}\text{Kr}$ : A database for the verification of transport and mixing model", *Isotopes of noble gases as tracers in environmental studies*. IAEA, Vienna (1992) 29–62.
- [5] INTERNATIONAL ATOMIC ENERGY AGENCY/WORLD METEOROLOGICAL ORGANIZATION, *The GNIP database (2001)*, <http://www.iaea.org/water>.
- [6] OSTER, H., *Datierung von Grundwasser mittels FCKW: Voraussetzungen, Möglichkeiten und Grenzen*, Dissertation Univ. Heidelberg (1994).

- [7] PLUMMER, L.N., MICHEL, R.L., THURMANN, E.M., GLYNN, P.D., "Environmental tracers for age-dating young ground water", *Regional Ground-Water Quality* (ALLEY, W.M., Ed.), Van Nostrand Reinhold, New York (1993) 255–294.
- [8] LOOSLI, H.H., HEIMANN, M., OESCHGER, H., Low-level gas proportional counting in an underground laboratory, *Radiocarbon* **22** (1980) 461–469.
- [9] LOOSLI, H.H., LEHMANN, B.E., SMETHIE, W.M.J., "Noble gas radioisotopes:  $^{37}\text{Ar}$ ,  $^{85}\text{Kr}$ ,  $^{39}\text{Ar}$ ,  $^{81}\text{Kr}$ ", *Environmental Tracers in Subsurface Hydrology*, (COOK, P.G. HERCZEG, A.L., Eds), Kluwer Academic, Boston (2000) 379–397.
- [10] LOOSLI, H.H., A dating method with  $^{39}\text{Ar}$ , *Earth Plan. Sci. Lett.* **63** (1983) 51–62.
- [11] ARMBRUSTER, V., et al., Verweilzeiten des Grundwassers in oberflaechennahen Grundwasserleitern in Baden-Wuerttemberg, *LGRB-Fachbericht* **01/08** (2008) 31.
- [12] BERTLEFF, B., et al., "Interpretation of hydrochemical and hydroisotopical measurements on palaeogroundwaters in Oberschwaben, south German alpine foreland, with focus on Quaternary geology", *Isotope Techniques in the Study of Past and Current Environmental Changes in the Hydrosphere and the Atmosphere* (Proc. Int. Conf. Vienna, 1993), Proceedings Series, IAEA, Vienna (1993) 337–357.
- [13] GONFIANTINI, R., ZUPPI, G.M., Carbon isotope exchange rate of DIC in karst groundwater, *Chem. Geol.* **197** (2003) 319–336.
- [14] KLOPPMANN, W., DEVER, L., EDMUNDS, W.M., Residence time of Chalk groundwaters in the Paris Basin and the North German Basin: A geochemical approach, *Appl. Geochem.* **13** 5 (1998) 593–606.
- [15] INGERSON, E., PEARSON, F.J., "Estimation of age and rate of motion of groundwater by the  $^{14}\text{C}$ -method", *Recent Researches in the Fields of Hydrosphere, Atmosphere and Nuclear Geochemistry* (MIYAKE, Y., KOYAMA, T., Eds), Univ. of Nagoya (1964) 263



# CHANGES IN CHEMICAL AND ISOTOPIC COMPOSITION OF GROUNDWATER DURING A LONG TERM PUMPING TEST IN BRESTOVICA KARST AQUIFER

K. MEZGA, J. URBANC  
Geological Survey of Slovenia,  
Department of Hydrogeology,  
Ljubljana, Slovenia

## Abstract

A pumping test of the Klariči water supply near Brestovica was performed in August 2008, in order to determine the karst groundwater resource capacity. Groundwater was pumped for a month with a total capacity of 470 L/s. During the experiment, sampling for chemical and isotopic composition of groundwater and surface water was carried out. Intensive pumping in dry meteorological conditions caused a lowering of the water table and changes in the chemical and isotopic composition of pumped water. Local meteoric waters are infiltrated into the aquifer at a lower mean altitude; therefore the  $\delta^{18}\text{O}$  is enriched with the heavy oxygen isotope. The duration of pumping resulted in changes in the isotopic composition of oxygen due to a greater impact of the intergranular Soča River aquifer on the karst aquifer. On the basis of isotope composition it was possible to quantify the impact of the Soča River on the karst aquifer.

## 1. INTRODUCTION

Karst aquifers present a very important source of drinking water supply. Karst areas cover almost half of Slovenia's territory, and more than half of its drinking water comes from karst aquifers [1]. However, the supply of bacteriologically and chemically safe drinking water in sufficient quantities to Karst inhabitants has always been a problem. It was discovered that the water rich Brestovica aquifer could provide much of the needed drinking water to Slovenian Karst and coastal inhabitants [2]. Therefore, the Brestovica karst aquifer has been a constant target of much research from the middle of the 1970s until the early 1990s. Our study took place at the Klariči pumping station, which is located in the vicinity of the village Brestovica near Komen in the southwestern part of Slovenia. The pumping station Klariči, as part of the Karst water supply company Kraški vodovod Sežana, supplies five karst communities with drinking water (Miren-Kostanjevica, Komen, Sežana, Divača and Hrpelje-Kozina), and, during the summer months, also the Slovene coastal region. Usually about 100 L/s are pumped for the Karst area, but when the coastal area is

supplied simultaneously, around 200 L/s are pumped [3]. The main aim of the experimental pumping test, which was carried out for 30 days in the arid summer period in August 2008, was to assess the groundwater resource quantity which could be pumped at the time of the highest water needs for the Slovene coastal and Karst areas. Furthermore, we wanted to test the chemical status of groundwater to assure its suitability for further use and to assess the influence of the Soča River aquifer on this karst aquifer.

## 2. CHARACTERISTICS OF THE RESEARCH AREA

The classical karst aquifer Brestovica is a part of the low dinaric Trieste-Komen Karst, located in the southwestern part of Slovenia, near the Italian border. On the Slovenian side, this aquifer extends from Vremščica in the southeast, to Dutovlje and Komen in the east and Kostanjevica in the north, crossing the Italian border up to Doberdob and Gradišča at the Soča River. The surface of the aquifer has the form of various karst phenomena (barren karstic areas, dolinas, caves...) and low conical hills with gentle elevations reaching on average 250–300 m a.s.l. [4]. The aquifer is quite large with its surface measuring around 560 km<sup>2</sup> [5]. It is built primarily of well permeable carbonate rocks of the Cretaceous and Paleogene age, which are intensively karstified. In the north and northeast of the aquifer, carbonate rocks are in contact with low permeable layers of Paleogene flysch from Vipava Valley to Trstelj Hill. In the flysch sequence sandstone, siltstone, claystone and marl are to be found. In the southwest, near the Italian border, the aquifer is limited with Eocene flysch beds at the Gulf of Trieste and, in the west and southwest, with alluvial deposits of the Soča River [4]. The aquifer is recharged mainly by precipitation with an average yearly precipitation rate of 1480 mm [6], average yearly evapotranspiration 530 mm, and by effective precipitation, which actually recharges the aquifer with 760 mm. These mean values were obtained by Kennessey methodology [5]. The aquifer is also supplied by allogenic water derived from sinking rivers and streams (Raša River, Reka River, Sajevče brook, Senožeče brook and the streams from Brkini hills) [7, 8]. Groundwater flow in the eastern part of the aquifer is oriented to the northwest and in the western part of the aquifer the flow direction changes to the southwest [9]. It has been suggested by numerous authors [10–12] that water from the Soča and Vipava rivers also contributes to this aquifer's groundwater. Urbanc and Kristan [12] confirmed that the aquifer at the pumping station Klariči depends on changing seasonal hydrologic conditions during pumping. During the rainy season, the aquifer is mainly recharged from the Slovene Karst area, but during arid summer periods, when the hydraulic pressure of the karst aquifer decreases, 50–60% of the aquifer is fed by the water from the intergranular Soča River aquifer. Similar observations were also noticed in the hydrogen ( $\delta^2\text{H}$ ) and carbon ( $\delta^{13}\text{C}_{\text{DIC}}$ ) isotopic composition of groundwater at pumping station Klariči [10]. To date, the exact area of the Soča River

inflow into the aquifer is still not clear. Both recharge components are mixed within the aquifer and are discharged at spring Timavo which represents the natural effluent from the aquifer [9].

### 3. METHODS

#### 3.1. Pumping test

During the pumping test the total pumping capacity was 470 L/s from 4 wells. Groundwater was pumped from 3 wells at Klariči (VB-4/79, VB-4/80 and VB-4/81) with a joint capacity of 205 L/s, and from well B-10, 80 m distant, yielding 265 L/s. Water pumped from well B-10 was discharged through a temporary pipeline located in the area outside the zone of the influence of the pumping wells. Water from the exploitation wells in Klariči was discharged via the existing water supply network. Since the amount of precipitation at that time was small and an intensive growth of vegetation additionally reduced the infiltration of meteoric water into the aquifer, the water table was low.

#### 3.2. Groundwater measurement, sampling and analyses

During the intensive pumping test, detailed observations were performed at the same time, where groundwater level, temperature and electrical conductivity were measured in 5 wells (VB-4/79, VB-4/80 and VB-4/81, B-10 and B-9) and 9 piezometers (B-4, Br-1, Br-2, Br-3, Br-4, Br-5, Br-6, Br-7, Br-8), all located within 400 m radius of well B-10. The exact quantity of pumped water from the pumping station Klariči was measured in the reservoir Sela, where water comes from pipes and is further distributed to users. At the pumping station Klariči the amount of precipitation was measured with an electronic ombrograph with data logger. During the experiment, water samples from the wells B-10 and B-9 and from the Soča River were taken every 5 days for hydrochemical and isotopic analysis. Basic hydrochemical parameters (pH, electrical conductivity,  $\text{HCO}_3^-$ ,  $\text{Cl}^-$ ,  $\text{Ca}^{2+}$ ,  $\text{Mg}^{2+}$ ,  $\text{Na}^+$ ,  $\text{K}^+$ ,  $\text{NO}_3^-$  and  $\text{SO}_4^{2-}$ ) were analysed in the laboratory of the public utility Vodovod-Kanalizacija in Ljubljana. The analysis of the stable isotope  $\delta^{18}\text{O}$  in water was performed by Hydroisotop GmbH in Germany. The isotope composition of oxygen ( $\delta^{18}\text{O}$ ) was determined by the  $\text{CO}_2$  equilibration technique using the dual inlet method. Furthermore, samples from well B-10 were taken for drinking water quality analysis, performed at the laboratories of the Institute of Public Health in Koper, Novo Mesto and Nova Gorica.

## 4. RESULTS AND DISCUSSION

Groundwater from the karst aquifer (water samples from wells B-10 and B-9) is of carbonate type with Ca-HCO<sub>3</sub> hydrochemical facies. This water has a high content of HCO<sub>3</sub><sup>-</sup> and a low content of Mg<sup>2+</sup>, which is typical of water with a limestone catchment area. Oxygen-18 content from the karst aquifer suggests that the water originates from meteoric waters with a lower mean altitude. Water from the Soča River on the other hand has a somewhat different hydrochemical facies of Ca-Mg-HCO<sub>3</sub>, while its natural catchment area is the dolomites and dolomitized limestone mountains of the Julian Alps. The Soča River is depleted of oxygen-18, which is a consequence of meteoric waters falling at the higher altitudes of the Julian Alps. The mean values of basic chemical parameters and oxygen-18 in the water from wells B-9 and B-10 and the Soča River, are listed in Table 1 and Table 2.

Although intense pumping caused a decrease in the water table in well B-10 of only 17cm, an influence from the intergranular Soča River aquifer was detected. This has been proven by both the chemical and isotopic composition of groundwater in exploitation wells at Klariči, wells B-10 and B-9, and in surrounding piezometers. Groundwater pumped from well B-10 showed a decrease in electrical conductivity, chemical parameters (HCO<sub>3</sub><sup>-</sup>, Na<sup>+</sup>, Ca<sup>2+</sup>, Cl<sup>-</sup> and SO<sub>4</sub><sup>2-</sup>) and isotope oxygen-18 content in the water. A decrease of the molar ratio (Ca/Mg) was also detected. These observations suggest that during intense pumping the karst groundwater chemical composition was progressively shifted towards the Soča River water composition.

TABLE 1. MEAN VALUES FOR EACH MEASURED PARAMETER IN GROUNDWATER FROM WELLS B-9 AND B-10 AND THE SOČA RIVER

Mean	El. Cond.	Ca <sup>2+</sup>	Mg <sup>2+</sup>	Na <sup>+</sup>	K <sup>+</sup>	HCO <sub>3</sub> <sup>-</sup>	Cl <sup>-</sup>	NO <sub>3</sub> <sup>-</sup>	SO <sub>4</sub> <sup>2-</sup>
	μS/cm	mg/L	mg/L	mg/L	mg/L	mg/L	mg/L	mg/L	mg/L
B-9	432.17	90.00	6.25	4.65	0.50	282.83	6.48	8.43	9.60
B-10	360.50	60.50	9.50	7.75	0.78	213.00	12.33	6.22	9.65
Soča River	264.67	43.17	8.57	1.60	0.49	169.33	1.69	2.89	6.43

TABLE 2. DESCRIPTIVE STATISTICS OF δ<sup>18</sup>O (‰) FOR WATER FROM WELLS B-9 AND B-10 AND THE SOČA RIVER

	Mean	Median	Min	Max	Range	N
B-9	-7.2	-7.24	-7.32	-6.99	0.33	6
B-10	-8.061	-8.07	-8.15	-7.89	0.26	6
Soča River	-8.185	-8.22	-8.26	-8.01	0.25	6

The comparison between oxygen-18 isotope composition in water and its electrical conductivity is presented in Fig. 1. All the samples lie almost on a straight line, which is interpreted as a mixing line between karst recharge and the Soča River aquifer endmembers. With pumping duration, the isotopic composition of  $\delta^{18}\text{O}$  in groundwater from well B-10 changes towards that of the Soča River water. Samples with higher electrical conductivity are also enriched in the heavy oxygen isotope. Assuming the mean  $\delta^{18}\text{O}$  value of the Soča River water to be  $-8.1\text{‰}$  and the mean

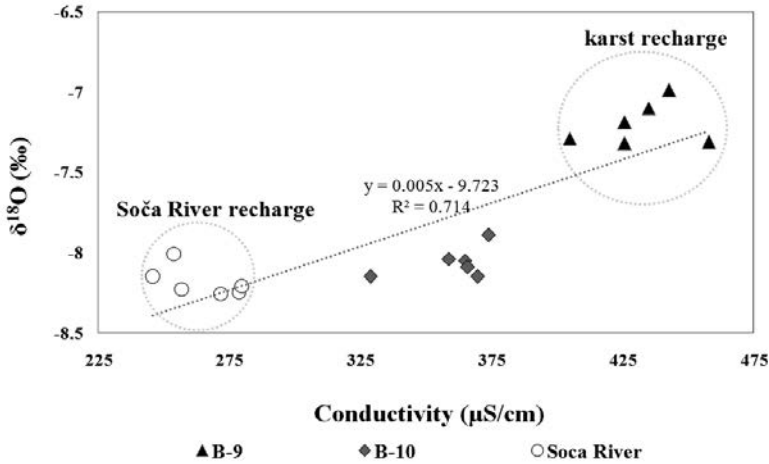


FIG. 1. Conductivity related to oxygen isotope composition in wells B-9 and B-10 and the Soča River.

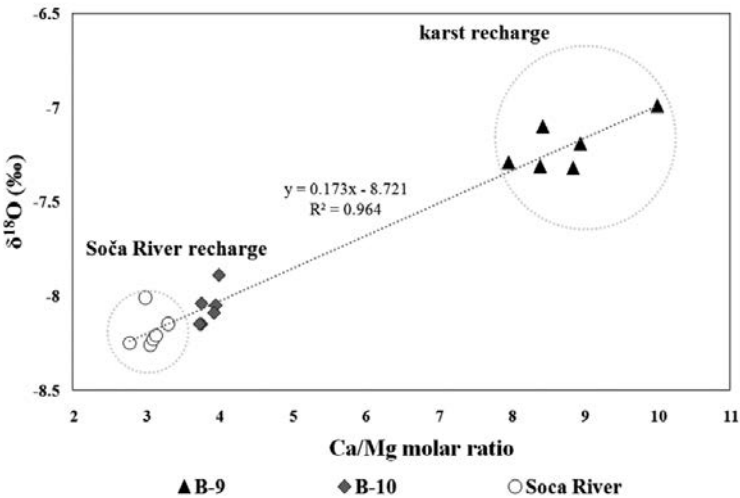


FIG. 2. Water oxygen isotope composition in comparison with Ca/Mg molar ratio.

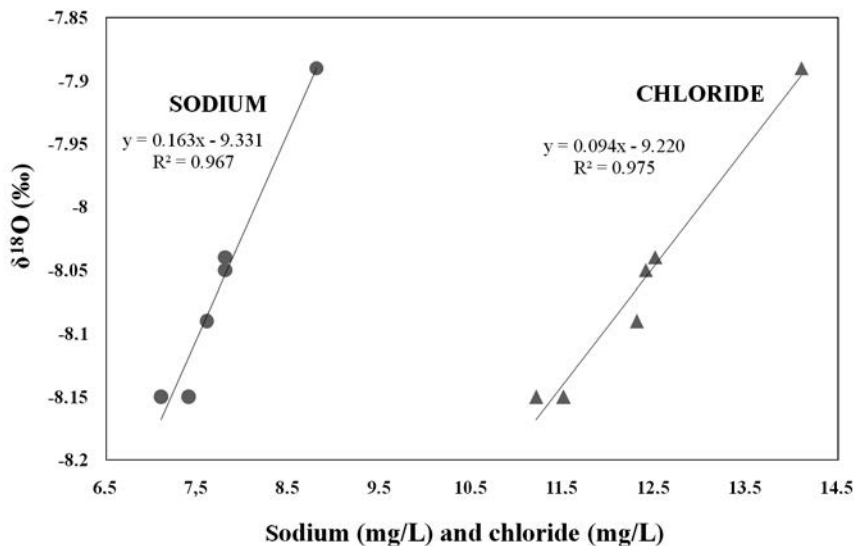


FIG. 3. Oxygen isotope composition of water in comparison with sodium and chloride in the water from the well B-10.

$\delta^{18}\text{O}$  value of the karst aquifer Brestovica (groundwater from well B-9)  $-7.2\text{‰}$ , it can be assessed that groundwater from the Soča River aquifer amounted to approximately 53% during the intense pumping test in well B-10. We assume the water from Soča River does not flow directly to the karst aquifer but from the intergranular Soča River aquifer.

The mixing line between  $\delta^{18}\text{O}$  in the water and its Ca/Mg molar ratio (Fig. 2) is oriented towards the Soča River water composition since it has a larger magnesium content in the water compared to other karst waters. Calcium prevails compared to magnesium in groundwater from the well B-9 and is also enriched in oxygen-18 isotope compared to the Soča River water. During the pumping test the content of magnesium and light oxygen isotope in the groundwater from well B-10 increases due to the Soča River water inflow.

When comparing oxygen-18 isotope with sodium and chloride in the water (Fig. 3), changes during the pumping test were noticed. The heavy isotope O-18 is enriched and sodium and chloride are depleted. The reason why we focused on those two parameters is the proximity of the Adriatic Sea. We assume the higher concentrations of sodium and chloride in the groundwater from the karst aquifer are due to sea spray, but further research needs to be done regarding this matter.

Groundwater samples from the well B-10 show that none of the chemical parameters exceeds the threshold values of the current standards on drinking water [13]. All pesticides are below detection level and the nitrate level is 6.5 mg/L. But the

sample does not meet the quality standards for bacteriological parameters, which is quite usual for karst aquifers.

## 5. CONCLUSION

Intense pumping during dry meteorological conditions in the karst aquifer in 2008 caused increased inflow of water from the intergranular Soča River aquifer into the karst aquifer, which has been detected by chemical and isotopic analysis of groundwater. This also suggests that the karst aquifer has a complementary flow during arid periods. Data obtained suggests that water from the Soča River aquifer is mixed with groundwater from the karst aquifer Brestovica in the broader area of the pumping station Klariči. The chemical quality of groundwater is appropriate for the purpose of drinking water supply. The presence of bacteria in groundwater is typical of karst aquifers and the water needs to be disinfected for further use.

## ACKNOWLEDGEMENTS

We would like to thank the Ministry of the Environmental and Spatial Planning for financial support with the pumping experiment. Further, we would like to thank the water supply company Kraški vodovod Sežana (Slovenia), the Department of Geological, Environmental and Marine Sciences at the University of Trieste (Italy) and the water supply company Azienda Comunale Elettrocità Gas ed Acqua (ACE-GA) of Trieste, Italy, for help in organizing the pumping test, tracer test, and with water sampling during the experiment.

## REFERENCES

- [1] RAVBAR, N., Drinking water supply from Karst water resources (the example of the Kras plateau, SW Slovenia), *Acta Carsologica* **33** 1 (2004) 73–84.
- [2] KRIVIC, P., Letno poročilo: Hidrogeološke raziskave zaledja vodnih virov pri Klaričih (III. faza), Pitne in mineralne vode: Hidrogeološke raziskave vodnih virov v karbonatnih kamninah, Geological Survey of Slovenia, Ljubljana (1988).
- [3] KRISTAN, S., SKRINJAR P., 1948–1998: 50 LET: 1948–1998, Water supply company Kraški vodovod Sežana, Sežana (1998).
- [4] JURKOVŠEK, B., Geological Map of the Northern Part of the Trieste-Komen Plateau 1:25 000 — Explanatory book, Geological Survey of Slovenia, Ljubljana (2010).
- [5] PRESTOR, J., JANŽA, M., Ocena višine infiltracije (po metodi Kennesy) in ranljivost podzemne vode na območju Slovenije, Geological Survey of Slovenia, Ljubljana (2006).

- [6] BAT, M., Vodna bilanca Slovenije 1971–2000 (Water balance of Slovenia 1971–2000), Ministry of Environment and Spatial Planning, Environmental Agency of the Republic of Slovenia, Ljubljana (2008).
- [7] HABIČ, P., Sledenje kraških voda v Sloveniji, *Geografski vestnik* 61 (1990) 3–19.
- [8] KOGOVSĚEK, J., PETRIČ, M., Directions and dynamics of flow and transport of contaminants from the landfill near Sežana (SW Slovenia), *Acta Carsologica* 36 3 (2007) 413–424.
- [9] CIVITĀ, M., et al., The Timavo hydrogeologic system: An important reservoir of supplementary water resources to be reclaimed and protected, *Acta Carsologica* 24 (1995) 169–186.
- [10] DOCTOR, D.H., LOJEN, S., HORVAT, M., A stable isotope investigation of the Classical Karst aquifer: Evaluating karst groundwater components for water quality preservation, *Acta Carsologica* 29 1 (2000) 79–92.
- [11] PEZDIČ, J., DOLENEC, T., KRIVIC, P., URBANC, J., “Environmental isotope studies related to groundwater flow in the central Slovenian karst region, Yugoslavia”, *Proc. 5th International Symp. on Underground Water Tracing, Athens* (1986) 91–100.
- [12] URBANC, J., KRISTAN, S., Isotope investigation of the Brestovica water source during an intensive pumping test, *RMZ – Materials and Geoenvironment* 45 1–2 (1998) 187–191.
- [13] Rules on Drinking Water, Official Journal of the Republic of Slovenia 19/2004, 35/2004, 26/2006, 92/2006, 25/2009.

# USE OF ISOTOPES IN ASSESSING THE RESPONSE OF GROUNDWATER TO CROSS-CATCHMENTS WATER DIVERSION IN THE TARIM BASIN

Z. PANG, T. HUANG, Y. KONG  
Institute of Geology and Geophysics,  
Chinese Academy of Sciences,  
Beijing, China

## Abstract

Since 2000, more than 2 billion m<sup>3</sup> of water has been diverted from the Peacock River to the neighbouring Lower Tarim River in NW China via a 900 km canal for ecosystem rescue by cross-catchment water diversion. Isotope techniques have been used in the riparian groundwater–river interactions along the 350 km long river channel through sampling of monitoring wells and river stream as well as soil profiles. Stable isotopes ( $\delta^2\text{H}$ ,  $\delta^{18}\text{O}$ ) show that groundwater is enriched in heavy isotopes, attributed to evaporation during recharge. Tritium data show that the extent of modern recharge is limited to 600–1500 m from the riverbank in the middle reaches and 200–600 m in the lower reaches. The salinity of groundwater is affected by river recharge, residence time and evapotranspiration. The zone of appropriate water table for arid plants is confined to a narrow scope. The assessment calls for a more favourable water allocation and management scheme catchment wide.

## 1. INTRODUCTION

Although discharge from the headwater streams of Tarim River, Xinjiang Uygur, NW China, a typical inland catchment of its kind, has been relatively stable or even increased to some extent, water discharge to the lower reaches has decreased rapidly as a result of large scale agricultural development and irrational water resource utilization in the upper and middle reaches of the river in recent decades. The runoff ceased to flow into the 350 km long Lower Tarim River when the construction of the Daxihaizi Water Reservoir in 1972, causing severe damages to the riparian forest dominated by *Populus euphratica* [1]. The so-called ‘Green Corridor’ and the national high way along the river bank (Korla to Ruoqiang, part of the National Highway, G218) are endangered by degrading riparian vegetation and desertification.

Since 2000, a water diversion project began to be implemented that transports water, through a 960 km long channel, from the neighbouring Peacock River to supplement flow from the upper Tarim above the Daxi reservoir as the control point for water release to the lower reaches, aiming at alleviating ecological disaster. Up

to now, more than 2.3 billion m<sup>3</sup> of water has been diverted altogether to the lower reaches by the project.

Better understanding the essential groundwater–surface water interaction and water chemistry evolution is of great significance to ecological restoration [2]. Earlier studies had indicated an optimistic impact of the river augmentation based on groundwater depth monitoring that showed rising trends [3]. The aim of this study is to test the usefulness of environmental tracers in assessing the effectiveness of the water diversion.

## 2. THE ECOLOGICAL WATER DIVERSION

The Tarim River Basin is located in the south of Xinjiang, NW China. It has an area of  $1.04 \times 10^6$  km<sup>2</sup> and is flanked by the Tianshan Mountains to the north and by the Kunlun Mountains to the south (Fig. 1). The Taklimakan Desert, the largest desert in China, is located in the centre of the basin, occupying an area of  $3.37 \times 10^5$  km<sup>2</sup> [4]. The Aksu River, the Yarkant River and the Hotan River are three large rivers in the west of the basin, which feed the Tarim River at Aral. Due to river regulation, at present the latter two recharge the Tarim River only during large floods. The Kaidu River flows into Bosten Lake and is then pumped into the Peacock River at the south-west of the lake, and finally reaches Lop Nur. There are two deserts situated on both sides of the lower Tarim River, the Taklimakan Desert on the west and the Kuluk Desert on the east, with moving and semi-moving sand dunes.

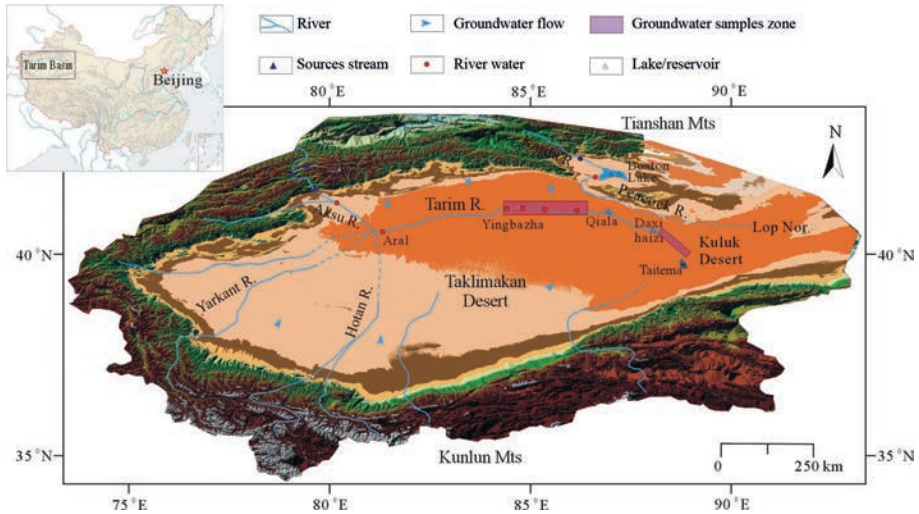


FIG. 1. Sketch map of the Tarim River Basin and water sampling sections in 2007 and 2008 for the assessment.

In order to protect the Green Corridor, the restoration of the riparian vegetation is imperative. Taking advantage of the wet period of the Kaidu River, the Ku-Ta Channel (Yuli to Qiala) was constructed for diverting water from the Peacock River to the lower Tarim River. The source water was all stored in the Daxihaizi Water Reservoir before being released to the lower reaches. Altogether 2.27 billion m<sup>3</sup> of water (1.30 billion m<sup>3</sup> from the Bosten Lake and 0.97 billion m<sup>3</sup> from the Tarim River) had been diverted to the lower Tarim River from the reservoir since year 2000. Water flow reached Taitema Lake, the terminal lake of the Tarim River. The groundwater system has been changed by the water diversions, resulting in redistribution of water salinity, water table and soil moisture content, which will affect the evolution of the ecosystem.

### 3. SAMPLING AND ANALYSES

Groundwater samples were collected from boreholes at varying distances from the riverbed along five groundwater monitoring transects in the middle Tarim River, namely: Shajilike (MA), Shazihe (MB), Wusiman (MC), Aqiye (MD) and Tieyizi (ME) and nine transects in the Lower Tarim River, namely: Akdun (A), Yahopumarhan (B), Yengsu (C), Abudali (D), Karday (E), Tugmailai (F), Aragan (G), Yikanbujima (H), and Kargan (I). Along each transect, monitoring wells with depth of 8–17 m were dug at intervals of 100–200 m. In total, 70 monitoring wells were measured and sampled. The water table and TDS of groundwater have been monitored three times a month during the water diversions and once a month in between the water diversion events.

Surface water including the Aksu River, the Upper Tarim River, the Qiala Water Reservoir, the Daxihaizi Water Reservoir and the neighbouring Kaidu River, Bosten Lake and Peacock River were also sampled. The depth of boreholes, water table, location (GPS), water temperature, pH, TDS and electrical conductivity (EC) were measured at the sites. Stable isotopes and tritium were measured in the Stable Isotopes Laboratory, Institute of Geology and Geophysics, Chinese Academy of Sciences. The analytical precision is  $\pm 0.2\%$  for  $\delta^{18}\text{O}$  and  $\pm 0.3$  TU for  $^3\text{H}$ . The water chemistry was measured using ion chromatography at the Beijing Research Institute of Uranium Geology. The analytical precision is 3% of the respective concentration.

### 4. RESULTS AND DISCUSSION

#### 4.1. Sources of recharge

Isotopic enrichment occurs in the Bosten Lake and the Peacock River as a result of evaporation. However, the Bosten lakewater is not completely mixed with

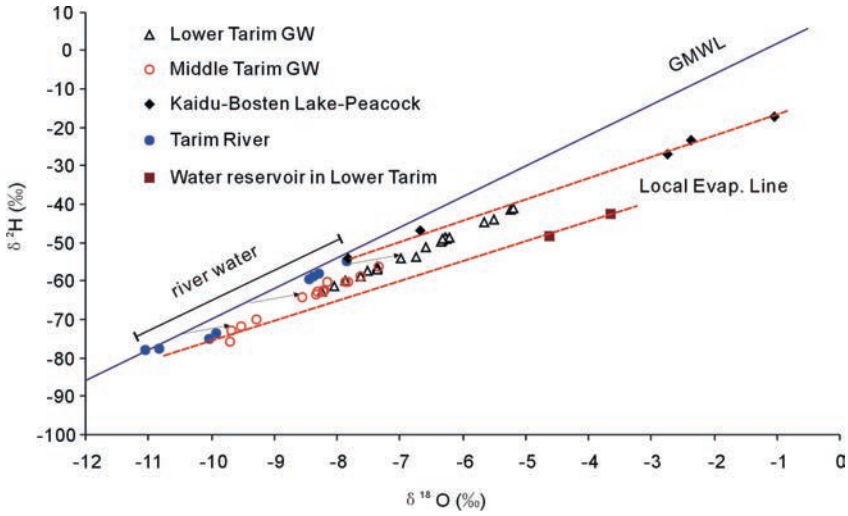


FIG. 2. Stable isotopic composition for surface waters and groundwaters in the middle and lower reaches of the Tarim River and Kaidu-Bosten-Lake-Peacock River-Lake systems as a consequence of water diversion.

the deviation of 0.7‰ in  $\delta^{18}\text{O}$  of the three water samples collected in the south part of the lake (Fig. 2). Those five samples form an evaporation line with a slope of 5.4:

$$\delta^2\text{H} = 5.4\delta^{18}\text{O} - 11.3, R^2 = 0.998, n = 5 \quad (1)$$

This evaporation line points to the source water of the Kaidu-Bosten-Lake-Peacock river-lake system. The isotopic composition is around  $-7.8\text{‰}$  and  $-55\text{‰}$  for  $\delta^{18}\text{O}$  and  $\delta^2\text{H}$ , respectively. The water samples of the Qiala and Daxihaizi Reservoir are enriched in heavy isotopes due to extended evaporation and the source water isotope composition is approximately  $-11\text{‰}$  and  $-80\text{‰}$  for  $\delta^{18}\text{O}$  and  $\delta^2\text{H}$ , respectively. The distinctive stable isotopic compositions of the two catchments may potentially be used to determine the mixing ratio of groundwater from the two water sources in the recipient riparian sectors in the water diversion.

Stable isotopes show that groundwaters from the middle and lower reaches are all enriched in heavy isotopes and are plotted in parallel to the meteoric water line in the  $\delta^{18}\text{O}$ – $\delta^2\text{H}$  plot (Fig. 2). This quasi-linear relationship can be attributed to evaporation during river recharge to the riparian groundwater in a rather uniform manner. In the meantime, riparian groundwater shows recharge from either or both of the sources with varying isotopic compositions between the two source water endmembers.

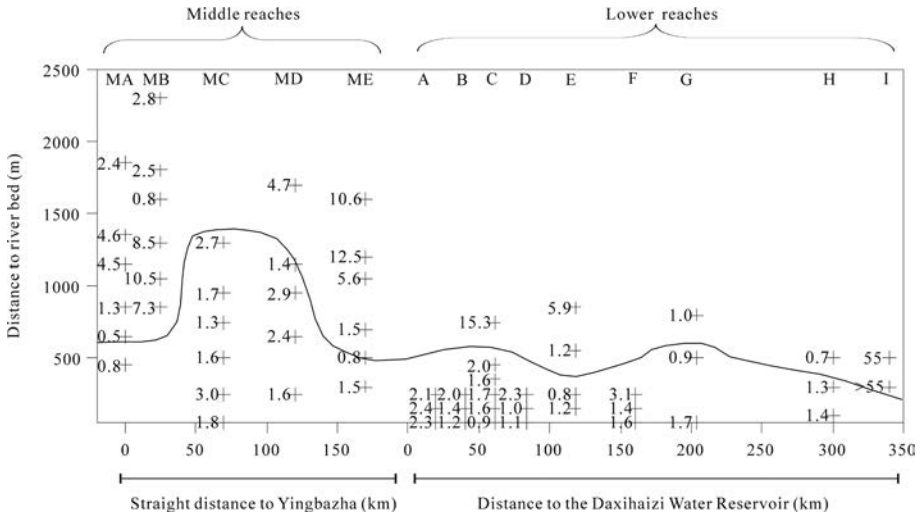


FIG. 3. The modern recharge scope (solid line) and the TDS distribution (g/L).

## 4.2. Modern recharge scope

Tritium is used to distinguish pre-modern recharge from modern recharge in this study. The approximate tritium input sequence of precipitation in the study area is reconstructed jointly from the tritium sequence of the neighbouring Lop Nur area (1952–1996) [5], the Urumqi observation station from GNIP (1986–2001) database [6], river samples collected in 2001 [7] and river samples plus one rainfall sample collected in this study. The reconstructed tritium concentrations show the decayed tritium in precipitation for 2007, which represents tritium concentrations in groundwater that would have infiltrated into groundwater during 1952 to 2007 [8–9].

According to the reconstructed tritium sequence above, if mixing of different waters is not considered, i.e. piston flow condition is assumed, groundwater with a tritium content of less than 10 TU has been recharged before 1960, or in other words, is pre-modern water. The rest is modern water. Groundwater with tritium contents from 40 TU to 110 TU, the highest measured in this study, must have been recharged during the 1961 to 1966 window of bomb tritium peak.

Based on our sample data, the scope of modern recharge has been mapped, which forms a zone within 600 to 1500 m from the riverbank in the middle reaches and this zone is 200 to 600 m from the riverbank in the lower reaches (Fig. 3).

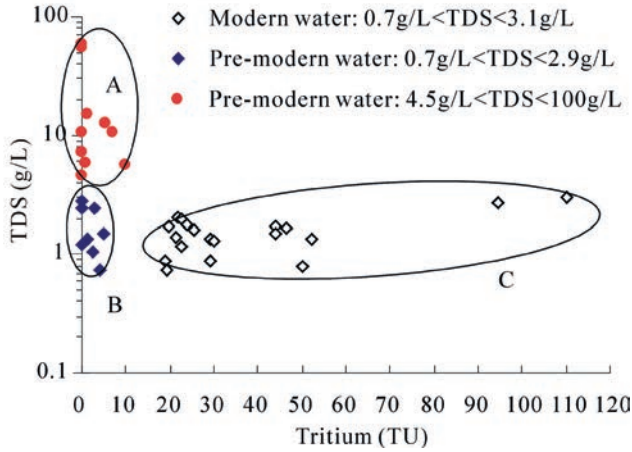


FIG. 4. The relationship between tritium content and TDS in groundwaters.

### 4.3. Groundwater salinity

The relationship between TDS and tritium shows that modern water has a low salinity of less than 3g/L, favourable for plant growing. Pre-modern water can be further divided into two groups, one of which has less than 3 g/L, the other more than 4.5 g/L, unfavourable to plant growing (Fig. 4). Pre-modern groundwaters have a wider range of TDS ranging from 0.7 to more than 55 g/L. Those pre-modern groundwaters are distributed far away from the riverbank. Low salinity pre-modern groundwaters are located about 500 to 1500 m away from the riverbank, with a relatively low TDS of <2.82 g/L. The groundwaters were recharged by the Tarim River in historical periods but have not been subject to strong evaporation afterwards, likely due to their deeper groundwater depth (>5 m) and so are less evaporated. High salinity (4.5–55 g/L) pre-modern groundwaters are also located away from riverbanks, but are subject to strong evapotranspiration due to their relatively long residence time.

### 4.4. Groundwater and riparian vegetation

After water diversion, the observed response of riparian groundwater systems includes a general decrease in salinity and the rise of the water table [3]. While modern recharge is limited to within 600–200 m from the riverbank in the lower reaches, the scope for a greater than 1 m rise in the water table is within 700–300 m from the riverbank, implying that the rise is caused by pressure propagation but the water molecules have not arrived at the same distance.

Where the modern recharge scope in the middle Tarim River is limited to 600–1500 m, the vegetation is distributed in a 10 km wider area. Furthermore,

the embankment built in 2001 along one side of the middle Tarim River appears to have reduced groundwater recharge [8], causing the water table to drop and the ecosystem to degenerate. Since the area of vegetation in the middle reaches (113 000 ha) is in fact nearly 10 times larger than that of the lower reaches (12 000 ha), the potential ecosystem degradation in the middle reaches could aggravate the ecological crisis of the whole basin.

In the lower reaches, the scope of proper groundwater depth (<5 m) favourable for the existing *Populus euphratica* and *Tamarix ramosissima* to grow is restricted to 200 m from the riverbank and narrows downstream, while the vegetation is distributed up to 2000 m, so the situation is far from meeting the demand of the existing vegetation.

## 5. CONCLUSIONS

Environmental tracers including water isotopes and chemistry are effective tools in investigation of riparian groundwater recharge and hydrological processes in arid riparian zones, such as the Tarim River Basin. Stable isotopes helped to identify the source of recharge, and tritium, the modern water scope.

The effectiveness of the current savable and linear water diversion scheme for ecological restoration in the Tarim Basin is limited compared to the demand of widely distributed vegetation.

The embankment built in the middle reaches of the river appears to prevent groundwater from receiving recharge from the river, causing groundwater depth to increase and degradation of riparian vegetation. Correction to this needs to be carried out and a more tangible water diversion scheme needs to be explored.

## ACKNOWLEDGEMENTS

The research is supported by the Knowledge Innovation Program of the Chinese Academy of Sciences (kzcx2-yw-127) and National Natural Science Foundation of China (Grant 40672171). The authors wish to thank Xiaoming Zhou and Xinhe Jiang for their assistance with the field work.

## REFERENCES

- [1] SONG, Y., FAN, Z., LEI, Z., Research on Water Resources and Ecology of Tarim River, China, Xinjiang People's Press, Urumqi, China (2000) 481.
- [2] BAILLIE, M.N., HOGAN, J.F., EKWURZEL, B., WAHI, A.K., EASTOE, C.J., Quantifying water sources to a semiarid riparian ecosystem, San Pedro River, Arizona, J. Geophys. Res. **112** (2007).

- [3] CHEN, Y.N., et al., Response of riparian vegetation to water-table changes in the lower reaches of Tarim River, Xinjiang Uygur, China, *Hydrogeol. J.* **16** (2008) 1371–1379.
- [4] ZHU, Z., CHEN, Z., WU, Z., Studies on Aeolian Landforms in the Taklimakan Desert, Science Press, Beijing (1981) 110.
- [5] JIAO, P., WANG, E., LIU, C., Characteristics and origin of tritium in the potassium-rich brine in Lop Nur, Xinjiang, *Nuclear Techniques* **27** 9 (2004) 710–715.
- [6] INTERNATIONAL ATOMIC ENERGY AGENCY, WORLD METEOROLOGICAL ORGANIZATION, Global Network of Isotopes in Precipitation, The GNIP Database (2006), <http://www.iaea.org/water>.
- [7] LI, W., HAO, A., ZHENG, Y., LIU, B., YU, D., Regional environmental isotopic features of groundwater and their hydrogeological explanation in the Tarim Basin, *Earth Science Frontiers* **13** 1 (2006) 191–198.
- [8] PANG, Z., HUANG, T., CHEN, Y., Diminished groundwater recharge and circulation relative to degrading riparian vegetation in the middle Tarim River, Xinjiang Uygur, Western China, *Hydrol. Process.* **24** (2010) 147–159.
- [9] HUANG, T., PANG, Z., Changes in groundwater induced by water diversion in the Lower Tarim River, Xinjiang Uygur, NW China: Evidence from environmental isotopes and water chemistry, *J. Hydrol.* **387** (2010) 188–201.

# ORIGIN AND EVOLUTION OF REACTIVE AND NOBLE GASES DISSOLVED IN MATRIX PORE WATER

F. EICHINGER<sup>a,b</sup>, H.N. WABER<sup>b</sup>, J.A.T. SMELLIE<sup>c</sup>

<sup>a</sup> Hydroisotop GmbH,  
Schweitenkirchen, Germany

<sup>b</sup> Rock-Water Interaction,  
Institute of Geological Sciences, University of Bern,  
Bern, Switzerland

<sup>c</sup> Conterra AB,  
Stockholm, Sweden

## Abstract

Reactive and noble gases dissolved in matrix pore water of low permeable crystalline bedrock were successfully extracted and characterized for the first time based on drillcore samples from the Olkiluoto investigation site (SW Finland). Interaction between matrix pore water and fracture groundwater occurs predominately by diffusion. Changes in the chemical and isotopic composition of gases dissolved in fracture groundwater are transmitted and preserved in the pore water. Absolute concentrations, their ratios and the stable carbon isotope signature of hydrocarbon gases dissolved in pore water give valuable indications about the evolution of these gases in the nearby flowing fracture groundwaters. Inert noble gases dissolved in matrix pore water and their isotopes combined with their in situ production and accumulation rates deliver information about the residence time of pore water.

## 1. INTRODUCTION

In crystalline bedrock systems, gases occur dissolved in fracture groundwater, matrix pore water and in fluid inclusions of rock forming minerals such as quartz and feldspars. Fracture groundwater and pore water, the latter being present in the inter- and intragranular connected pore space of the rock matrix, interact with each other predominately via diffusion. In contrast, mineral fluid inclusions represent isolated reservoirs without exchange for most gases under ambient conditions.

Reactive and noble gases dissolved in pore water and their isotope signatures carry valuable information about the evolution of a hydrogeological system. Information about origin and fluxes of dissolved gases is also important within the context of the safety assessment of a nuclear waste repository. For example,

owing to their ability to buffer surface derived dissolved oxygen, the occurrence of small amounts of hydrocarbons in fracture groundwater might be beneficial to safety assessment. In contrast, large amounts of hydrocarbons (mainly CH<sub>4</sub>) in fracture groundwaters combined with dissolved sulphate may affect safety assessment adversely. This is because of the possibility of bacterially mediated sulphate reduction with the resulting formation of HS<sup>-</sup> potentially increasing the corrosion of artificial (and natural) barriers and repository materials. The expected heat production within and around a repository will, in addition, lower the dissolved gas solubility in matrix pore water and fracture groundwater what might result in degassing and other undesired chemical and physical processes in and around a repository system.

Similarly as for chemically conservative solutes, matrix pore water in crystalline rocks is a reservoir for dissolved gases. Due to the large volume of pore water present in the rock matrix compared to the volume of fracture groundwater it might even constitute an important endmember in the overall groundwater evolution given that the exchange pore water–fracture groundwater appears to be dominated by diffusion [1]. This demands a detailed characterization of dissolved gases in matrix pore water and fracture groundwater. The chemical and isotopic characterization of inert (noble gases) and reactive (hydrocarbon) gases in matrix pore water provides information about gas origin, gas fluxes over large time periods as well as more recent chemical processes induced by the exchange between pore water and fracture groundwater. Under special circumstances and combined with the noble gas in situ production in the bedrock, some information can be obtained about the residence time of such gases in the pore water and thus the long term stability of the hydrogeologic system.

Dissolved hydrocarbon and noble gases were successfully quantified and isotopically characterized for the first time in pore water extracted from the low permeable crystalline rock matrix. The investigations were carried out on drillcore material collected from a subhorizontal drill hole (ONK–PH9) drilled in the ONKALO access tunnel at a depth of 306 m b.s. at the Olkiluoto site, Finland. The borehole was designed to penetrate across a water conducting, regional fracture zone (HZ20B) into undisturbed bedrock of low permeability.

## 2. METHODS

Core samples for pore water dissolved gas characterization were collected at different intervals of few decimetres to several metres from the highly transmissive hydraulic zone HZ20B, which extends from 22–42 m along the borehole (a.b.), into the undisturbed bedrock to 97 m a.b. Immediately after recovery from the drillhole, core samples of a length of 7 to 10 cm were placed in vacuum sealed stainless steel cylinders, which were multiply flushed with nitrogen for noble gas samples or helium for reactive gas samples to remove all air. Subsequently the cylinders were evacuated

for a few seconds down to a pressure of about 0.1 mbar. Gases dissolved in the pore water were then allowed to equilibrate between the pore water and the void volume in the cylinder over a time period of 250 days at room temperature. After equilibration, the concentrations of the reactive gases were analysed in a Shimadzu GC 17A gas chromatograph. Possible air contamination was monitored and corrected for by the oxygen concentration measured in the gas mixture. Back-calculation of measured concentrations to pore water concentrations was performed with the pressure data collected at various stages of the experiment and the water content of the rock sample placed into the stainless steel cylinder. This water content was determined gravimetrically by drying the rock sample at 105°C until constant weight conditions after termination of the out-gassing experiment. The water content of the samples varies between 0.24 wt.% and 1.34 wt.% with the corresponding masses of pore water in the rock samples being about 1–3 mL.

The carbon isotope composition of methane was determined by GC-IRMS using a Varian MAT-250 equipped with a direct dual inlet system. The results are reported relative to the V-PDB standard.

The same experimental procedure was applied for noble gases as for reactive gases. It should be noted that the chosen equilibration time allowed the attainment of steady state conditions in the out-gassing process with respect to the light noble gases, but not with respect to the heavy noble gases due to the rather large differences in diffusion coefficients. The concentrations of noble gas isotopes in the gas mixture were measured using a GV5400 He noble gas mass spectrometer at the University of Heidelberg. For the noble gas samples, the degree of air contamination of the extracted gas was monitored and corrected for by the measured neon isotope contents. The back-calculation to noble gas concentrations in pore water was performed in the same way as for the reactive gases. A detailed description and evaluation of the applied methods can be found in [2].

### 3. GAS COMPOSITION OF FRACTURE GROUNDWATER AT OLKILUOTO

In the Olkiluoto fracture groundwater, sampled from various drill holes, total dissolved gas concentrations increase with depth, with nitrogen and methane making up the major portions of the total gas contents. Across the entire Olkiluoto island, fracture groundwater displays a distinct stratification of redox conditions with depth. Nitrogen is most abundant in the upper 300 m b.s., whereas below 300 m methane becomes the dominant component [3]. In the first 280 m b.s. dissolved methane concentrations are rather irregularly distributed and vary between about 0.1 and 30 mL/L STP (Standard Temperature, 0°C and Pressure, 1 bar). In the depth interval corresponding to the pore water samples (280–320 m b.s.), concentrations of CH<sub>4</sub> in fracture groundwaters range from 0.1–0.8 mL/L STP [3]. Towards greater depth dissolved CH<sub>4</sub> displays a regular increase reaching maximum concentrations of about

900 mL/L STP at around 1000 m b.s. Concentrations of higher hydrocarbons (HC) also increase below 300 m and HC mass and stable isotope ratios indicate that thermal abiogenic HCs dominate in the deepest fracture groundwaters collected from 500–1000 m b.s. In contrast, in the shallower groundwaters with lower CH<sub>4</sub> concentrations down to about 300 m b.s., the fraction of bacterially formed HCs dominates [3].

Helium in fracture groundwater also increases with depth, but already below about 100 m b.s. and in a more regular way compared to CH<sub>4</sub> [3]. In the depth interval corresponding to the pore water samples (280–320 m b.s.) dissolved <sup>4</sup>He in groundwater ranges from 0.3–1.4 mL/L STP. Below 800 m b.s. rather constant <sup>4</sup>He concentrations of around 22 mL/L STP are measured in the fracture groundwaters across the site [3].

## 4. RESULTS

### 4.1. Hydrocarbon (HC) gases in pore water

Dissolved HCs were successfully extracted and analysed from samples from within the highly transmissive HZ20B zone, in the first 9 m (42–51 m a.b.) adjacent to it and again from about 25 m to 50 m (70–97 m a.b.) further into the undisturbed bedrock. Unfortunately, samples from 10–25 m distance from HZ20B had too low gas contents and/or too high air contamination. In all samples CH<sub>4</sub> is the main hydrocarbon species dissolved in pore water. Its concentration, however, changes as a function of distance to the HZ20B zone: In the samples located within the water-conducting zone and at its border, the pore waters have CH<sub>4</sub> concentrations of around 0.2 mL/L<sub>PW</sub> STP (Fig. 1). These concentrations are very similar to that of the flowing fracture groundwater (0.6 mL/L STP) at this depth. In the first 9 m away from this zone into the bedrock, CH<sub>4</sub> concentrations in the pore water increase to 15.1 mL/L<sub>PW</sub> STP (Fig. 1). In the undisturbed bedrock zone between 25 m to 50 m away from the HZ20B zone (70–97 m a.b.) CH<sub>4</sub> concentrations decrease again from 13.2 to 5.6 mL/L<sub>PW</sub> STP. Across the entire profile, concentrations of higher saturated HCs (C<sub>2</sub>–C<sub>4</sub>) show less variation, being between 0.01 and 0.21 mL/L<sub>PW</sub> STP for ethane, 0.003 and 0.16 mL/L<sub>PW</sub> STP for propane, <0.001 and 0.21 mL/L<sub>PW</sub> STP for i-butane and 0.001 and 0.47 mL/L<sub>PW</sub> STP for n-butane [2]. The dominance of CH<sub>4</sub> and the low variations in the higher HCs in the pore water gas results in a similar spatial distribution of the C<sub>1</sub>/(C<sub>2</sub>+C<sub>3</sub>) ratio as that of CH<sub>4</sub> (Fig. 1).

The δ<sup>13</sup>C values of CH<sub>4</sub> dissolved in pore water were analysed for some samples and vary between –54 and –25‰ V-PDB (Fig. 1). Although the spatial distribution suggests some regularity, more data would be needed for a detailed interpretation regarding the dynamic exchange between pore water and fracture groundwater. However, the data available allow some statements about possible differences in the

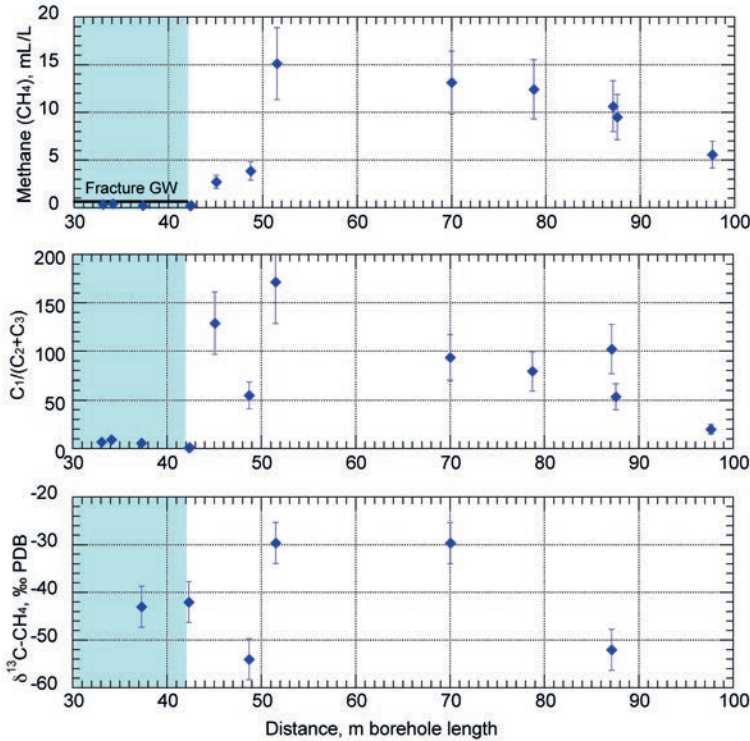


FIG. 1. Methane concentration (top), hydrocarbon mass ratios (centre) and  $\delta^{13}\text{C}$  values of methane (bottom) dissolved in pore water from core samples from the drill hole ONK-PH9 (306 m b.s.). The drill hole was drilled from the ONKALO access tunnel at Olkiluoto into the undisturbed bedrock across the high transmissive water conducting fracture zone HZ20B. The blue shaded area in the figure marks the end of this zone. The cumulated errors of pore water  $\text{CH}_4$  concentrations and  $\text{C}_1/\text{C}_2+\text{C}_3$  ratios are  $\pm 24\%$  and  $\pm 25\%$ , respectively. The analytical error of the  $\delta^{13}\text{C}$  ratios of  $\text{CH}_4$  dissolved in pore water is  $\pm 5\%$ .

origin of the hydrocarbons in the pore water. Except for two samples, the concentrations of higher hydrocarbons were too low to be analysed for their isotopic composition. The same accounts for the hydrogen isotope composition of methane.

The similarity of  $\text{CH}_4$  concentrations in groundwater sampled from the water-conducting HZ20B zone and pore water in rock samples from this zone suggests that fracture groundwater and pore water methane concentrations are at steady state within the HZ20B zone. Already at about 2 m distance and further into the rock matrix, however, a transient state between fracture groundwater and pore water is established with the  $\text{CH}_4$  concentrations in the pore water being higher by a factor of 10 or more. This transient state indicates that the circulation of present day low  $\text{CH}_4$  groundwater in the HZ20B zone has been too short to achieve equilibrium between the two

reservoirs and CH<sub>4</sub> is now transferred along a chemical gradient from the pore water into the fracture groundwater. In agreement with conservative chemical tracers [1, 2] and based on transport processes alone one could argue that the pore water HC concentrations in the sample located at greatest distance in the undisturbed rock matrix (i.e. at 50 m distance from HZB20 or 97 m a.b.) could represent some type of 'back-ground composition' that has not been influenced by recent fracture groundwaters.

#### 4.2. Origin of hydrocarbons (HC) in pore water

In natural hydrogeological systems different processes can lead to the generation of HCs. Different HC generating processes can be distinguished by the molecular ratio between methane (C<sub>1</sub>) and the sum of ethane (C<sub>2</sub>) and butane (C<sub>3</sub>) expressed as C<sub>1</sub>/(C<sub>2</sub>+C<sub>3</sub>), and the stable isotope signatures of carbon and hydrogen of the individual HC species [e.g. 4, 5]. Biogenic hydrocarbons have C<sub>1</sub>/(C<sub>2</sub>+C<sub>3</sub>) ratios of generally ≥1000 due to the limited formation of higher HCs in low temperature bacterial processes. In contrast, thermogenic hydrocarbons have molecular HC ratios of generally ≤10, depending on the precursor material. During the abiogenic hydrocarbon formation, higher hydrocarbons are produced by polymerization of methane [5]. The molecular ratio of such abiogenic HCs is considered to be in the same range as that of the thermogenic HCs. The δ<sup>13</sup>C signature of thermogenic CH<sub>4</sub> commonly varies between -25 and -50‰ PDB, depending on the maturity of decomposition of the original organic matter [4]. The δ<sup>13</sup>C values of CH<sub>4</sub> derived from methanogenesis tend to be depleted in <sup>13</sup>C, because bacteria prefer to metabolize lighter isotopes. The δ<sup>13</sup>C signature of bacterially produced CH<sub>4</sub> is typically lower than -50‰ PDB [4, 5]. In contrast, δ<sup>13</sup>C values of CH<sub>4</sub> from abiogenic sources are more enriched in <sup>13</sup>C compared to those of bacterially and thermogenically produced CH<sub>4</sub>, generally ranging between -25 and -30‰ PDB [4, 5].

The pore water samples collected from within and adjacent to the water-conducting HZ20B zone have a C<sub>1</sub>/(C<sub>2</sub>+C<sub>3</sub>) of around 1. Combined with the δ<sup>13</sup>C signature of dissolved CH<sub>4</sub> (-42‰ PDB), this suggests a thermogenic origin of CH<sub>4</sub> in these samples. Whereas CH<sub>4</sub> concentrations and isotope composition of these pore waters are well within the range of fracture groundwater at this depth, concentrations of higher HCs in the groundwater below the detection limit [3] prevent a further comparison. A similar unequivocal and complex situation is observed for the samples in the first 9 m away from the HZ20B. Here, pore water has greatly elevated C<sub>1</sub>/(C<sub>2</sub>+C<sub>3</sub>) of about 50–170 combined with increased CH<sub>4</sub> concentrations suggesting an increasing proportion of bacterially produced methane. However, this is only supported by the δ<sup>13</sup>C value of CH<sub>4</sub> in one sample (δ<sup>13</sup>C = -54‰ PDB), whereas the other sample has a signature more typical for thermogenic CH<sub>4</sub> (δ<sup>13</sup>C = -30‰ PDB). Based on the limited data set and considering the reactivity of hydrocarbons and the dynamics of the pore water – fracture groundwater system close to the water-conducting zone,

a more detailed interpretation regarding the origin of hydrocarbons in pore water close to the HZ20B fracture zone does not seem possible at this time.

A somewhat different case arises, however, for the hydrocarbons dissolved in pore water of samples collected at greater distance (>25 m) in the intact low permeable bedrock. In these samples, the CH<sub>4</sub> concentrations in pore water become similar and so do the C<sub>1</sub>/(C<sub>2</sub>+C<sub>3</sub>) values (Fig. 1). Furthermore, the two last samples, collected some 45 m and 55 m from the high transmissive zone show a surprisingly similar δ<sup>13</sup>C signature of CH<sub>4</sub> and C<sub>1</sub>/(C<sub>2</sub>+C<sub>3</sub>) ratio, respectively, as also observed in the fluids of fluid inclusions in quartz of the same rock. Such fluid inclusion fluids show δ<sup>13</sup>C values for CH<sub>4</sub> between -50 and -55‰ PDB and C<sub>1</sub>/(C<sub>2</sub>+C<sub>3</sub>) ratios between 7 and 25 and are interpreted to originate predominantly from thermogenic or abiogenic processes [6]. For the pore water this might indeed indicate that some 55 m away from the highly transmissive hydraulic zone HZ20B a similar HC signature is preserved, as it is present in the fluids entrapped in fluid inclusions. It should be noted that this similarity does not imply that the signatures in these two reservoirs have been established at the same time. However, it might indicate that the HCs in pore water in the rock matrix far away from active hydraulic zones and in mineral fluid inclusions have the same origin. In any case it appears that the HC signature observed in the pore water today is very old.

### 4.3. <sup>4</sup>He concentrations in pore water

Helium occurs in bedrock systems as radiogenic <sup>4</sup>He and nucleogenic <sup>3</sup>He with the latter having an about 10<sup>6</sup> lower abundance than <sup>4</sup>He. Radiogenic <sup>4</sup>He is produced by the natural decay of uranium and thorium residing in the minerals of the rock. Due to the strong activation energy during the production process most of the radiogenic <sup>4</sup>He is released to the surrounding interstitial pore water and from there to the groundwater and finally to the atmosphere [7]. In the low permeable rock matrix, interim storage of He isotopes may also occur in lattice imperfections of quartz and feldspar crystals allowing a determination of the pore water residence time under favourable conditions [8]. The chemical inert character of He and its continuous in situ production makes it a valuable tracer to investigate solute transport processes.

Along the profile in borehole ONK-PH9, <sup>4</sup>He concentrations in pore water vary between 0.4 and 5.7 mL/L<sub>pW</sub> STP (Fig. 2). These concentrations are well below the solubility of He of about 270 mL He/L at in situ conditions (ca. 10°C, 30 bar, IS 0.2M). Within the analytical uncertainty the <sup>4</sup>He concentrations of pore water from rock samples from within and adjacent to the water conducting HZ20B zone are equal to that measured for the groundwater (0.6 mL/L STP). In this highly fractured zone, diffusion dominated intact rock matrix domains are limited to the dm size. This means that a complete exchange between the two reservoirs and thus steady state conditions between pore water and fracture groundwater will be attained within a short time (years). The observed match between the <sup>4</sup>He concentrations in pore water and

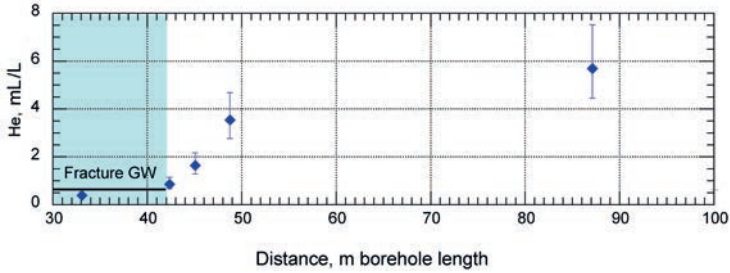


FIG. 2.  $^4\text{He}$  concentrations of pore water from core samples from the bedrock profile in the horizontal borehole ONK-PH9 (306 m b.s.) at Olkiluoto. The blue area marks the end of the highly transmissive fracture zone HZ20B. The cumulated errors are  $-22\%$  and  $+32\%$ .

groundwater is in agreement with such a steady state in the HZ20B zone. The match further supports the experimental and analytical procedures for the characterization of He in such small volumes of pore water (about 1–3 mL) in that the obtained results are hydrogeologically plausible even at the lowest concentrations observed for the pore water samples from this zone.

Away from the highly transmissive HZ20B zone into the intact bedrock,  $^4\text{He}$  concentrations in pore water increase from 0.9 to 3.6 mL/L<sub>pw</sub> STP in the first 7 m along the profile (Fig. 2). The highest  $^4\text{He}$  pore water concentration of 5.7 mL/L<sub>pw</sub> STP is recorded for the sample some 45 m from the HZ20B zone (87 m a.b., Fig. 2). Similarly to the HC gases above, the  $^4\text{He}$  concentration of this sample can be regarded as some type of ‘background’ concentration not influenced by recent groundwater. This is based on its location far inside the intact low permeable bedrock and results obtained from other chemically inert pore water tracers [1]. To produce the observed concentration by in situ production alone about  $10^6$  years would be required based on the U and Th contents of the rock.

The decrease of pore water  $^4\text{He}$  from more than an order of magnitude higher concentrations in great distance from the HZ20B zone to concentrations identical to those in the groundwater of this zone indicates that  $^4\text{He}$  is lost from the pore water system to the groundwater. In turn, the  $^4\text{He}$  concentrations approximately four times higher in the deep groundwaters below 500 m b.s. compared to the HZ20B fracture groundwater indicate a substantial He flux from great depth, which will also affect the  $^4\text{He}$  concentrations in pore water. The present data do not allow the quantification of the individual fluxes. However, they allow the discernment of the origins of He in the HZ20B groundwater as the adjacent pore water and a deep source at greater depth.

## 5. CONCLUSION

Reactive gases and noble gases dissolved in pore water from low permeable crystalline rocks were successfully extracted and quantified for the first time. The pore water in the low permeable rock matrix acts as a source of these compounds for the groundwater in the adjacent water-conducting zone as indicated by the spatial distribution of concentrations and isotope compositions of CH<sub>4</sub>, higher hydrocarbons and He. Hydrocarbons in the pore water appear to originate at least in part from the same abiogenic thermogenic source as HCs in mineral fluid inclusions, which have similar chemical and isotopic compositions. Helium in pore water originates from a deep seated source, in addition to the <sup>4</sup>He from the local rock produced in situ. Further data will be required to quantify the individual fluxes and time periods of pore water–fracture groundwater exchange.

## REFERENCES

- [1] EICHINGER, F., WABER, H.N., SMELLIE, J.A.T., Matrix pore water in low-permeable crystalline bedrock: An archive for the palaeohydrogeological evolution (this volume).
- [2] EICHINGER, F., HÄMMERLI, J., WABER, H.N., DIAMOND, L.W., SMELLIE, J.A.T., Chemistry and dissolved gases of matrix pore water and fluid inclusions in Olkiluoto bedrock from borehole ONK-PH9, Posiva Working Report 2011-63, Posiva Oy, Olkiluoto, Finland (2011).
- [3] PITKÄNEN, P., PARTAMIES, S., Origin and Implications of Dissolved Gases in Groundwater at Olkiluoto, Posiva report 2007–04, Posiva Oy, Olkiluoto, Finland (2007).
- [4] WHITICAR, M.J., Carbon and hydrogen isotope systematics of bacterial formation and oxidation of methane, *Chem. Geol.* **161** (1999) 291–314.
- [5] SHERWOOD LOLLAR, B., WESTGATE, T.D., WARD, J.A., SLATER, G.F., LACRAMPE-COULOUME, G., Abiogenic formation of alkanes in the Earth's crust as a minor source for global hydrocarbon reservoirs, *Nature* **416** (2002) 522–524.
- [6] EICHINGER, F., MEIER, D., HÄMMERLI, J., DIAMOND, L.W., Stable Isotope Signatures of Gases Liberated from Fluid Inclusions in Bedrock at Olkiluoto, Posiva Working Report 2010–88, Posiva Oy, Olkiluoto, Finland (2010)
- [7] BALLENTINE, C.J., BURNARD, P.G., Production, release and transport of noble gases in the continental crust, *Rev. Mineral. Geochem.* **47** (2002) 481–538.
- [8] TOLSTIKHIN, I., et al., Helium transfer from water into quartz crystals: A new approach for porewater dating. *Earth Planet. Sci. Lett.* **238** (2005) 31–41.



# MULTIPLE TRACER ( $^4\text{He}$ , $^{14}\text{C}$ , $^{39}\text{Ar}$ , $^3\text{H}/^3\text{He}$ , $^{85}\text{Kr}$ ) DEPTH PROFILE IN AN EXTENSIVELY EXPLOITED MULTILEVEL AQUIFER SYSTEM IN THE VENETIAN PLAIN, ITALY

A. MAYER<sup>a</sup>, R. PURTSCHERT<sup>b</sup>, J. SÜLTENFUSS<sup>c</sup>, C. CLAUDE<sup>a</sup>,  
Y. TRAVI<sup>d</sup>

<sup>a</sup> Centre Européen de Recherche et d'Enseignement  
des Géosciences de l'Environnement,  
Aix-en-Provence, France

<sup>b</sup> Climate and Environmental Physics,  
University of Bern,  
Switzerland

<sup>c</sup> Institute of Environmental Physics,  
University of Bremen,  
Germany

<sup>d</sup> UMR-EMMAH, Université d'Avignon et des Pays de Vaucluse,  
Avignon, France.

## Abstract

Individual dating tracers have their specific inherent properties, advantages and limitations. Apparent  $^4\text{He}$  accumulation ages are biased as a function of a prior unknown external helium influx;  $^{14}\text{C}$  ( $T_{1/2}$ : 5730 a) dating in groundwater requires suitable geochemical correction schemes and  $^{39}\text{Ar}$  ( $T_{1/2}$ : 269 a) may be affected by underground production. In a multiple tracer study in the Venetian Plain, Italy, using  $^4\text{He}$ ,  $^{14}\text{C}$ ,  $^{39}\text{Ar}$ ,  $^3\text{H}/^3\text{He}$  and  $^{85}\text{Kr}$  data, the groundwater residence times in a depth profile consisting of different separated aquifers between 50–350 m depth are estimated. Moreover, limitations and uncertainties of the applied tracer methods are identified, assessed and quantified.

## 1. INTRODUCTION

The Venetian Plain is the fore deep basin of the Southern Alps in NE Italy (Fig. 1). The upper part of this plain is made up by a coarse grain, undifferentiated alluvial fan, accumulated at the outlets of the alpine valleys. Due to the elevated permeability, the phreatic water table in this zone occurs at about 40–70 metres below

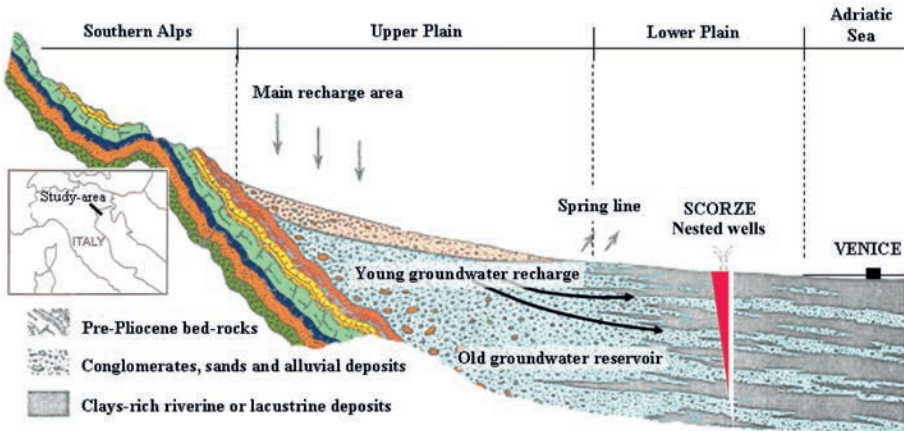


FIG 1. Location and simplified cross-section of the study area, in northeastern Italy.

surface. This part of the plain constitutes an important recharge area for the aquifers of the region. The lower plain is characterized by a multilayer aquifer system, with artesian aquifers separated by aquicludes. The contact with the basements Mesozoic and Tertiary rocks at the base of the sedimentary sequence deepens towards the southeast from 100 to several thousand metres below surface.

In this study we investigated the multilayer aquifer system near Scorzè, some 20 km northwest of Venice. This location was chosen because of the wealth of hydrogeological information available, including the access to various wells reaching the first ten artesian aquifers from the surface.

## 2. METHODS

At Scorzè, we sampled a vertical profile from nested wells at one location of groundwater from the first to the tenth aquifer, radiotracers and various chemical constituents. The investigated depths range from  $-40$  to  $-320$  m from surface. Two field campaigns were carried out in March 2008 and October 2010. Samples for the radio-noble gases  $^{85}\text{Kr}$  and  $^{39}\text{Ar}$ ,  $^{14}\text{C}$ , stable isotopes, majors (ICP–AES) and trace elements (ICP–MS)  $^3\text{H}$ ,  $^3\text{He}$  and  $^4\text{He}$  (gas mass spectrometry),  $^{34}\text{S}$ ,  $^{224}\text{Ra}$ ,  $^{223}\text{Ra}$ ,  $^{228}\text{Ra}$ ,  $^{226}\text{Ra}$ ,  $^{222}\text{Rn}$ , and  $^{36}\text{Cl}$  were taken. Here only the noble gas and radiocarbon data are discussed. For more details to the methods we refer to Ref. [1].

### 3. RESULTS

#### 3.1. General pattern of tracer concentrations with depth

In Fig. 2 we report the vertical profile for  $^3\text{H}$ ,  $^{85}\text{Kr}$ ,  $^{39}\text{Ar}$ ,  $^{14}\text{C}$  and  $^4\text{He}$ .  $^3\text{H}$  and  $^{85}\text{Kr}$  profile clearly shows the presence of groundwater recharged after the bomb pulses, at all levels beside 3, 7 and 10. These three aquifers are also characterized by lower  $^{14}\text{C}$  activities and higher  $^4\text{He}$  contents and thus definitely contain older groundwater.  $^{14}\text{C}$  data (corrected for the incorporation of dead carbon using various models) yield ages of about 13 kyr for the lowest aquifer.  $^{39}\text{Ar}$  data indicates, however, that this groundwater also contains a significant fraction of atmospheric  $^{39}\text{Ar}$  and even in the lowest aquifer its age cannot be older than about 1 kyr, assuming a simple decay from atmospheric  $^{39}\text{Ar}$ .

To solve this discrepancy, rather than using a dead carbon correction model based on chemistry and  $\delta^{13}\text{C}$ , we calculated the apparent rate of  $^{14}\text{C}$  decay due to matrix-exchange with dead carbon by combining  $^{39}\text{Ar}$  and stable  $^{13}\text{C}$  data as a proxy of the matrix-exchange (Fig. 3). In addition, we included diffusive exchange between the permeable aquifer layers and the quasi stagnant aquitards, [2, 3], a radiogenic production term of  $^{39}\text{Ar}$  in the calculation of  $^{39}\text{Ar}$  ages to take into account the presence of lithogenic  $^{39}\text{Ar}$  in groundwater. We also estimated the age effects of mixing and dispersion of groundwater in the aquifer under various dispersivity assumptions.

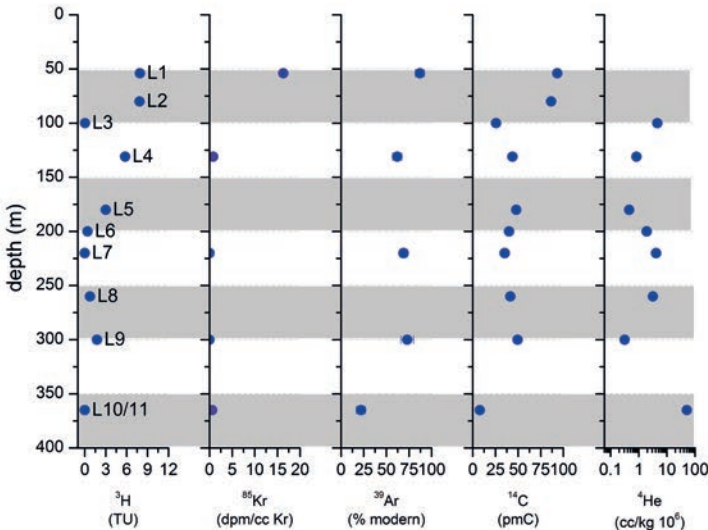


FIG. 2. Tracer concentrations as function of depth below surface. Labels indicate aquifer levels. Note the logarithmic scale for  $^4\text{He}$ .

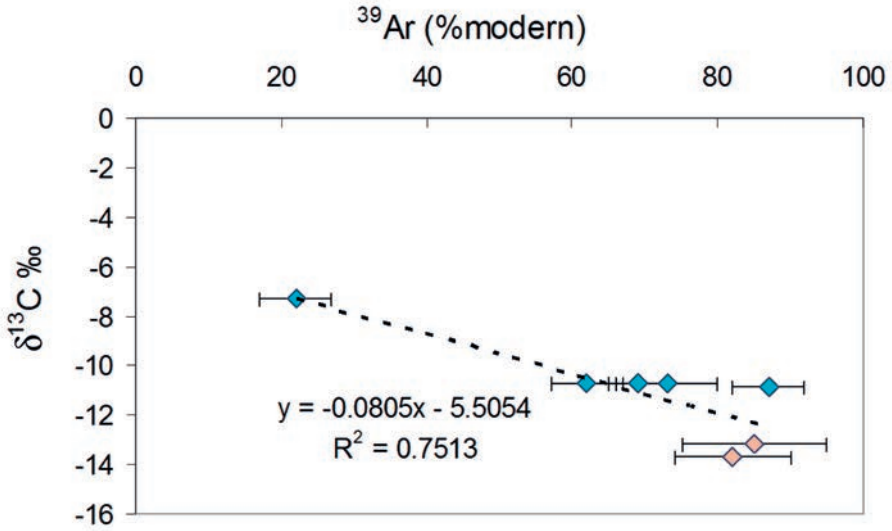


FIG. 3. Determination of the carbon exchange rate based on the  $^{39}\text{Ar}$ – $\delta^{13}\text{C}$  correlation (orange symbols: samples from the unconfined part).

### 3.2. Radiocarbon dating

We define a first order law relating the activity of  $^{14}\text{C}$  to the total decay due to radioactivity and mixing, both in the aquifer reservoir and with the aquifer matrix:

$$^{14}\text{C}(t) = ^{14}\text{C}_0 \exp(-\lambda_{\text{tot}}^{\text{C}} T_m)$$

$$\lambda_{\text{tot}}^{\text{C}} = \lambda_1^{\text{C}} + \lambda_2^{\text{C}} + \lambda_3^{\text{C}} + \lambda_4^{\text{C}}$$

where  $T_m$  is the mean residence time and  $^{14}\text{C}_0 = 50$  pMC is the initial  $^{14}\text{C}$  activity at the beginning of the flow path determined by the  $\delta^{13}\text{C}_0$  of the young waters [4] ( $\delta^{13}\text{C}_0 \sim -12\text{‰}$  (Fig. 3) and  $\delta^{13}\text{C}_{\text{soil}} = -24\text{‰}$ ).  $\lambda_1^{\text{C}}$  is the radioactive decay constant,  $\lambda_2^{\text{C}}$  is the chemical exchange rate along the flow path, estimated based on the base of the  $\delta^{13}\text{C}$ – $^{39}\text{Ar}$  relationship (Fig. 3). The data shows that an inverse correlation exists between  $^{39}\text{Ar}$  (radioactive) and  $\delta^{13}\text{C}$  (stable). Since  $\delta^{13}\text{C}$  changes in time only because of reaction with carbonates of the aquifer matrix (closed system assumption), the anti-correlation implies a matrix exchange rate for carbon  $\lambda_2^{\text{C}}$  of  $2.1 \times 10^{-4}$ /a.  $\lambda_3^{\text{C}}$  is the tracer exchange rate between the active aquifer levels and the adjacent stagnant zones, estimated on the base of (i) dimensions of a system of parallel aquifer and aquitards layers and (ii) diffusion coefficient from the literature [2].  $\lambda_4^{\text{C}}$  is

TABLE 1. FIRST ORDER DECAY CONSTANTS (AND CORRESPONDING HALF-LIVES) FOR  $^{39}\text{Ar}$  AND  $^{14}\text{C}$  CONSIDERING DIFFERENT PROCESSES (DECAY, DISPERSIVE MIXING, ISOTOPE EXCHANGE)

		Decay	Aquitar Exchange	Dispersion			Isotope Exchange	Total
				d=10 a	d=100 a	d=1000 a		
$^{39}\text{Ar}$	$\lambda_{39}(\text{a}^{-1})$	2.58E-3	1.90E-3	-1.65E-5	-1.48E-4	-7.94E-4	-	3.68E-3
	$T_{1/2}(\text{a})$	269	365	-42000	-4698	-873	-	188
$^{14}\text{C}$	$\lambda_{14}(\text{a}^{-1})$	1.21E-4	4.12E-4	-3.85E-8	-3.65E-7	-3.47E-6	2.09E-3	7.38E-4
	$T_{1/2}(\text{a})$	5730	1684	-18000000	-1900000	-200000	33.16	939
$^{39}\text{Ar}/^{14}\text{C}$	$\lambda_{39}/\lambda_{14}$	21.3						5.0

**Note:** If all processes are considered, the  $\lambda_{39}/\lambda_{14}$  decay constant ratio is reduced by a factor of ~4 (from 21.3 to 5).

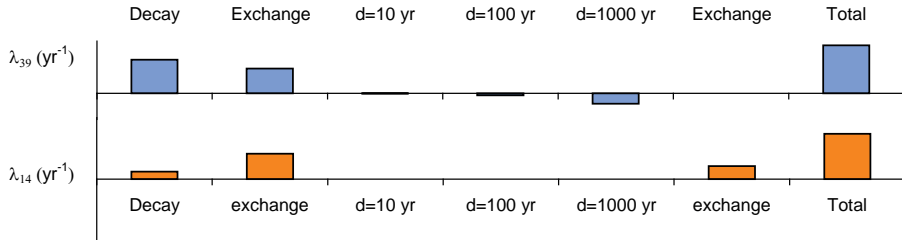


FIG. 4. First-order decay constants for  $^{39}\text{Ar}$  and  $^{14}\text{C}$ .

the apparent decay constant due to dispersive mixing. The resulting age distribution  $g$  can be expressed as:

$$g(t, T_m, d) = \frac{T_m}{\sqrt{\pi d t^3}} \exp\left(-\frac{(t - T_m)^2}{d t}\right)$$

and depends on the dispersion parameter  $d$  [a] (Table 1) and the mean residence time  $T_m$ . Mixing of water components with different ages leads to an apparent 'slower decay rate' as a function of half-life (concavity of decay curve) and extent of dispersive mixing ( $d$ ). On  $^{39}\text{Ar}$  relevant timescales this effect can be neglected for  $^{14}\text{C}$  but contributes to a further reduction of the discrepancy between  $^{14}\text{C}$  and  $^{39}\text{Ar}$  ages (Table 1).

### 3.3. $^{39}\text{Ar}$ dating

Similarly to  $^{14}\text{C}$  we define the decay law of  $^{39}\text{Ar}$  as:

$${}^{39}\text{Ar}(t) = ({}^{39}\text{Ar}_0 - P) \exp(-\lambda_{\text{tot}}^{\text{Ar}} T_m) + P$$

$$\lambda_{\text{tot}}^{\text{Ar}} = \lambda_1^{\text{Ar}} + \lambda_3^{\text{Ar}} + \lambda_4^{\text{Ar}}$$

Decay constants are defined as for  ${}^{14}\text{C}$ , except the chemical term that has not to be considered for the noble gas  ${}^{39}\text{Ar}$ . Instead an underground production term  $P$  (secular subsurface equilibrium activity in % modern) is included to account for lithogenic  ${}^{39}\text{Ar}$ . The lowest measured value of 22% modern (L10/11) indicates an upper limit of this term.

### 3.4. ${}^4\text{He}$ dating

In contrast to single layer aquifers, this system appears to be favourable for  ${}^4\text{He}$  dating because the deepest layer acts as a shield against an eventually occurring external crustal flux from below. The in situ production can easily be calculated based on an estimated  $U$  and  $Th$  concentration and on the porosity. In situ production ages are an upper age limit ( ${}^4\text{He}$  (in situ) in Fig. 5) because the accumulation rate is likely higher based on experience in other cases [5]. Any tracer ages above this threshold age are therefore suspicious.

In the deepest layer a lower age limit ( ${}^4\text{He}$  (ext-flux) in Fig.4) can be estimated using the ‘whole crustal flux’ defined e.g. in Ref. [6].

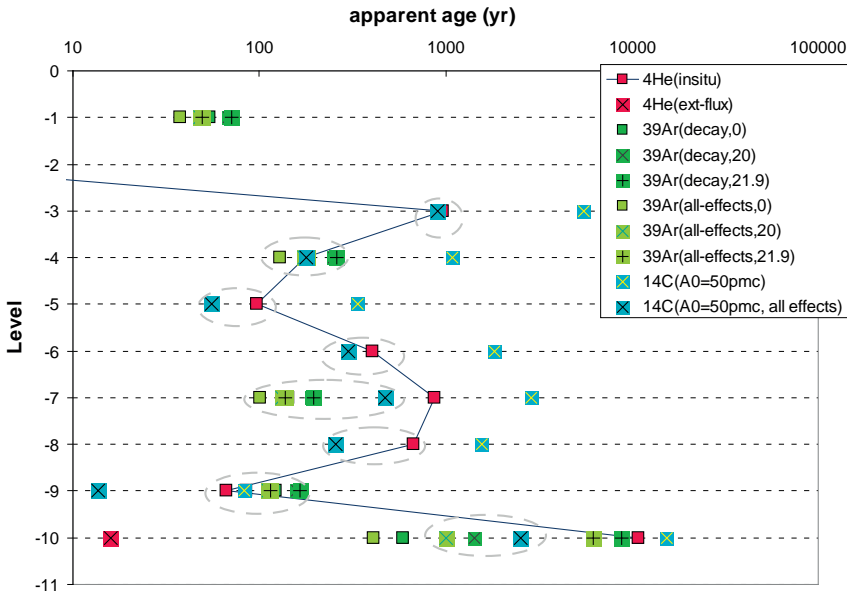


FIG. 5. Comparison of tracer ages at different depth levels (see Fig. 2).

#### 4. DISCUSSION

In Fig. 5 tracer ages are plotted as a function of depth below surface. The presence of young water components in the top levels and level 9 is demonstrated by  $^3\text{H}/^3\text{He}$  and  $^{85}\text{Kr}$  dating. For the old waters it is assumed (except for the deepest layer) that mixing of different water components is rather a continuous process than e.g. a two component mixture of a young and very old component. The  $^4\text{He}$  ages define an upper age limit as explained above.  $^{14}\text{C}$  ages ( $^{14}\text{C}_{\text{max}}$ ) calculated with an initial activity of 50 pMC (estimated from  $\delta^{13}\text{C}$ ) are generally too high in comparison to  $^4\text{He}$  and  $^{39}\text{Ar}$ . This discrepancy is significantly reduced if the above mentioned processes (Table 1) are included in the age calculation ( $^{14}\text{C}$  — all effects — in Fig.4).

For most levels, all tracers yielded comparable ages (dotted ellipses in Fig. 5). For the deepest layer,  $^{39}\text{Ar}$  ages approximate  $^{14}\text{C}$  and  $^4\text{He}$  ages only if the measured  $^{39}\text{Ar}$  of 22% modern is mostly attributed to underground production ( $^{39}\text{Ar}$  all effect, 21.9 in Fig. 4). However, this radiogenic contribution does not appear to affect  $^{39}\text{Ar}$  ages in the shallower levels. The age ranges found in all aquifers are also in qualitative agreement with hydraulic ages, calculated using Darcy's law, which tend, however, to be even lower by almost an order of magnitude. A possible reason for this discrepancy arises from the calculation of these hydraulic ages as groundwater transit times from the recharge area, without taking into account aging and admixture of waters originating from outside the 'confined flow tubes' depicted in Fig. 1.

#### 5. CONCLUSIONS

Diffusive exchange with aquitards, ongoing isotope exchange for carbon and dispersive mixing are all processes that have to be considered for  $^{14}\text{C}$  (and partly  $^{39}\text{Ar}$ ) dating. The most important effect seems to be isotope exchange (Table 1). Some discrepancies, however, remain (e.g. level 7). Considerable  $^{39}\text{Ar}$  underground production for the deep level cannot be excluded. This term can be constrained by means of multiple level measurements.  $^4\text{He}$ , in particular in multilayer systems, can provide very valuable age constrains. More work has to be carried out to achieve better understanding. This is another example of the strength and advantages of multitracer studies.

#### ACKNOWLEDGMENTS

The Water Authority of the Lagoon of Venice (Autorità d'Ambito Territoriale Ottimale della Laguna di Venezia) are warmly thanked for funding this work. Dr. T. Cambuzzi and E. Conchetto are thanked for fruitful discussion on the hydrology of the area. EMMAH Avignon is also acknowledged for cofunding this study.

## REFERENCES

- [1] SÜLTENFUß J., PURTSCHERT, R., FÜHRBÖTER, J.F., Age structure and recharge conditions of a coastal aquifer (northern Germany) investigated with  $^{39}\text{Ar}$ ,  $^{14}\text{C}$ ,  $^3\text{H}$ , He isotopes and Ne, *Hydrogeol. J.* **19** (2011) 221–236.
- [2] SANFORD, W., Correcting for diffusion in carbon-14 dating of ground water, *Groundwater* **35** (1997) 357–361.
- [3] SUDICKY, E.A., FRIND, E.O., Carbon-14 dating of groundwater in confined aquifers: Implication of aquitard diffusion, *Water Resour. Res.* **17** (1981)1060–1064.
- [4] INGERSON, E., PEARSON, F.J., JR., “Estimation of age and rate of motion of groundwater by the  $^{14}\text{C}$ -method”, *Recent Researches in the Fields of Hydrosphere, Atmosphere and Nuclear Geochemistry* (MIYAKE, Y., KOYAMA, T., Eds), Maruzen, Tokyo (1964) 263–283.
- [5] TORGERSEN, T., Continental degassing flux of  $^4\text{He}$  and its variability, *Geochem. Geophys. Geosyst.* **11** (2010) 15.
- [6] TORGERSEN, T., HABERMEHL, M.A., CLARKE, W.B., Crustal helium fluxes and heat flow in the Great Artesian Basin, Australia, *Chem. Geol.* **102** (1992) 139–152

# UNEXPECTED $\delta^{18}\text{O}$ AND $\delta^2\text{H}$ VARIABILITY OF GROUNDWATER IN THE EASTERN PARIS BASIN

L. GOURCY, E. PETELET-GIRAUD  
BRGM Service EAU,  
Orléans, France

## Abstract

The Paris Basin covers about one-third of the total surface area of France. In 2009, two campaigns sampling 25 boreholes tapping Tertiary aquifers were carried out in the Basin. These aquifers are recharged at a similar altitude and the groundwater age is too young to have registered climate change. In the past, regional studies included the use of isotopes to understand groundwater origin and dynamics. Both  $\delta^{18}\text{O}$  and  $\delta^2\text{H}$  as well as ages (CFC/SF<sub>6</sub>) and chemical components were determined in all collected samples. A noticeable stable isotope ‘anomaly’ appears in the south-western part of the Basin, where the average  $\delta^{18}\text{O}$  and  $\delta^2\text{H}$  values are more depleted and do not fit the pattern given by the continental effect in this area. A regional particularity of the spatial distribution of such isotopes in precipitation may be possible, but should be confirmed by additional work.

## 1. INTRODUCTION

Recent work on improving our knowledge of the natural geochemical background of water bodies in France has highlighted the presence of high concentrations of the natural trace elements F and Se in the Paris Basin [1]. Aquifers showing the highest concentrations are in Tertiary formations. A study was carried out in the most affected area, the eastern part of the Paris Basin, in a vast rectangle of about 47 000 km<sup>2</sup> from Orléans to Reims. This research project, which was started in 2008 together with the Seine-Normandy Water Agency, aimed to determine the origin of these elements and particularly of Se that commonly reaches concentrations exceeding drinking water limits (10 µg/L). A large number of geochemical elements (major and trace elements, stable water isotopes and CFC and SF<sub>6</sub> as age dating tools) were analysed for the chemical and isotopic characterization of each aquifer. Stable water isotopes ( $\delta^2\text{H}$  and  $\delta^{18}\text{O}$ ) are interesting natural tracers as they can indicate surface water influence, interconnection between aquifers, seasonal effects and recharge processes. All geochemical tools were used to understand time and space variations in dissolved element concentrations, factors needed for sustainable groundwater management.

## 2. SAMPLING AND ANALYSES

Two sampling campaigns, in April 2009 during the high water stage, and in October 2009 during low water, covered 23 points in the Chalk and Tertiary aquifers of the Paris Basin (Fig. 1). The wells were sampled after pumping at least three purge volumes and stabilization of the chemical groundwater parameters, such as pH and conductivity. Samples for chemical cation analyses were kept in polyethylene bottles after acidification with nitric acid, and 50 ml of raw water in HDPE bottles was used for  $\delta^2\text{H}$  and  $\delta^{18}\text{O}$  determinations. Samples for CFC and  $\text{SF}_6$  age dating were collected in 500 mL glass bottles [2].

Concentrations were measured on water samples by inductively coupled plasma atomic emission spectrometry (ICP-AES) for  $\text{Ca}^{2+}$ ,  $\text{Na}^+$ ,  $\text{K}^+$ ,  $\text{Mg}^{2+}$  (uncertainty 5–10%) and by ion chromatography for  $\text{Cl}^-$ ,  $\text{NO}_3^-$ ,  $\text{SO}_4^{2-}$ ,  $\text{PO}_4^{3-}$  (uncertainty 5–10%). Anion analyses were done by ion chromatography and cation ones by ICP-AES. The accuracy of both techniques is around 5–10%, depending on the concentration. Alkalinity was determined by HCl titration and the Gran method.

Isotopic ratios of both O and H are given in per mil (‰) versus VSMOW (Vienna Standard Mean Ocean Water) reference material in the usual  $\delta$ -scale defined as:

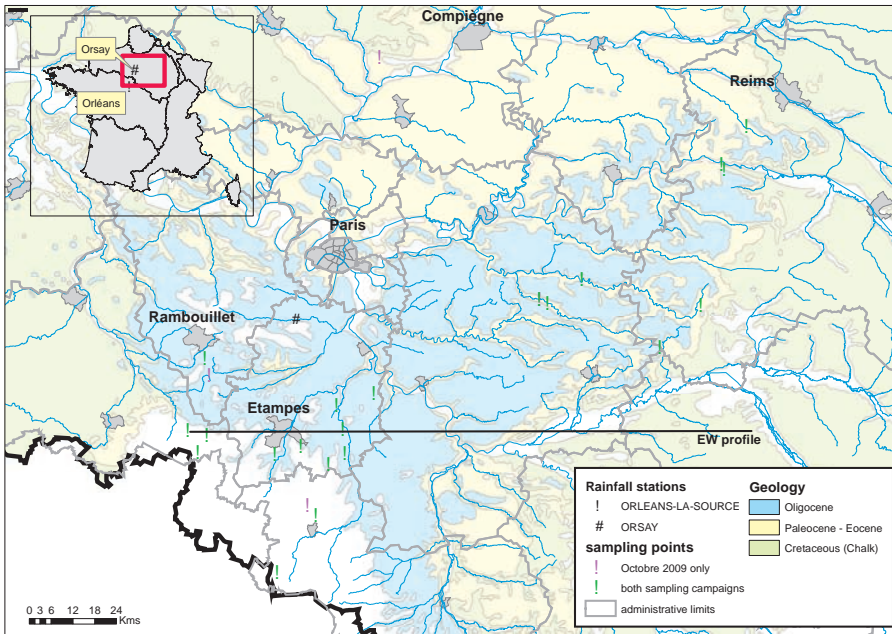


FIG.1. Location of sampling points and geological boundaries in the Paris Basin.

$$\delta_{\text{sample}} (\text{‰}) = \left\{ \left( \frac{R_{\text{sample}}}{R_{\text{standard}}} \right) - 1 \right\} \times 1000$$

where  $R$  is the  $^2\text{H}/^1\text{H}$  and  $^{18}\text{O}/^{16}\text{O}$  atomic ratios.

The O and H isotopic composition of water was measured using a Finnigan MAT-252 mass spectrometer with an uncertainty of  $\pm 0.1\text{‰}$  and  $\pm 0.8\text{‰}$  for  $\delta^{18}\text{O}$  and  $\delta^2\text{H}$ , respectively. All isotopic analyses were done by the BRGM Geochemistry Laboratory. For CFC and  $\text{SF}_6$ , to avoid any air contamination, each bottle was kept in a water filled metal box, and analyses were done by gas chromatography with an electron capture detector after pre-concentration using a purge-and-trap technique (Spurenstofflabor, Wachenheim, Germany). The detection limit was close to 10–4 pmol, allowing the measurement of CFC concentrations down to 0.01 pmol/L and of  $\text{SF}_6$  concentrations down to 0.1 fmol/L. The reproducibility was about  $\pm 5\%$  for water samples.

### 3. RESULTS AND DISCUSSIONS

#### 3.1. Hydrogeology of Paris Basin

Hundreds of aquifers exist in the Paris Basin, the major ones being in Jurassic (limestone), Cretaceous (Chalk and Green Sand), Tertiary (Brie and Beauce sandstones) and Quaternary (small alluvial aquifers) sedimentary formations. Tertiary aquifers are the most intensively exploited as well as being the most sensitive to groundwater contamination. The Paris Basin being a syncline, the extension and thickness of the sedimentary deposits are of variable size.

The oldest groundwater sampled in our case came from the Cretaceous Chalk aquifer, whose extension is very large, including the south of England. On top of this aquifer, Ypresian (Eocene) clay, sand and lignite form impermeable or semi-permeable layers, in turn overlain by the great multilayer ‘Champigny’ aquifer. This is composed of various calcareous and sandy aquifer layers of irregular horizontal extension that are commonly unconnected. The most productive aquifers are the Beauvais and Auvers sands, the St Ouen limestone and the Champigny (*sensu stricto*) limestone. Within this multilayer aquifer, impermeable or semi-permeable layers are formed by gypsum and marl. In the southwestern part of the Basin, these impervious layers do not exist, nor do the Ypresian layers.

Oligocene aquifers are, from bottom to top, Brie limestone, Fontainebleau sand, Etampes limestone and Beauce limestone, all of which are intensively exploited.

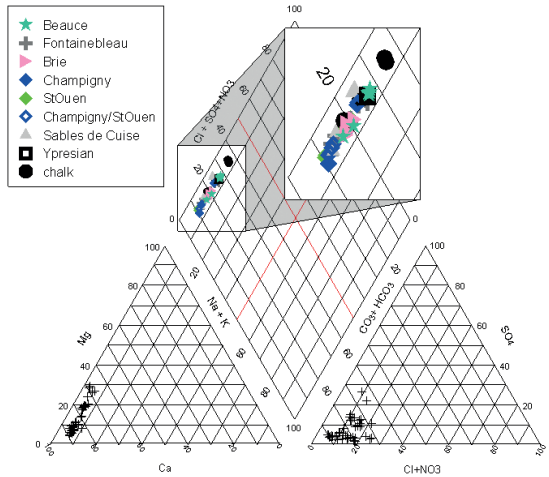


FIG. 2. Piper diagram for groundwater sampled in April and October 2009 in the Paris Basin.

### 3.2. Chemical groundwater characteristics

Each of the main aquifers was sampled for chemical and isotope analyses. Major chemical elements show a similarity for groundwaters of a quite different origin. The Ca-HCO<sub>3</sub> type dominates, as many of the sampled aquifers have a carbonate matrix. Groundwater from the Ypresian (Eocene) and Fontainebleau (Oligocene) aquifers, composed respectively of sandy clay and sand/sandstone, also has a Ca-HCO<sub>3</sub> chemical facies. In the Piper diagram of Fig. 2, only water from the Chalk aquifer appears slightly different, mainly due to higher sulphate concentrations.

Trace element concentrations (XY diagrams, principal component or discriminant function analyses) show no systematic association between elements, or between specific elements and aquifer lithology. It should be noted, however, that in view of the large size of the studied area only a few boreholes were sampled for each aquifer. Maps of the geochemical background anomalies in the Seine-Normandy basin [2] show Se and F anomalies in the Paris Basin, but do not specify in which aquifers.

Age dating using CFCs (CFC-11, CFC-12, CFC-113) and SF<sub>6</sub> tools shows that none of the Tertiary aquifers contain palaeowaters; apparent ages could not be defined for two wells in the Chalk aquifer due to contamination. For all other boreholes, the CFC ages are from 1955 (<8% of young water component) to 1986–1990. Groundwater has little or no present day recharge component, which partly explains the very low monthly variability of chemical element concentrations or isotope values.

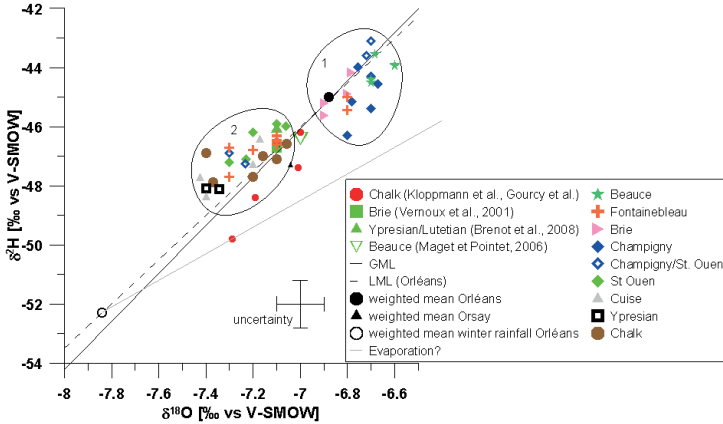


FIG. 3.  $\delta^2\text{H}$  vs.  $\delta^{18}\text{O}$  for groundwater collected in April and October 2009, rainfall data for the Orléans and Orsay stations, and some values from the literature (see text).

### 3.3. Stable Isotope data

Values of  $\delta^2\text{H}$  and  $\delta^{18}\text{O}$  were determined for all samples:  $\delta^2\text{H}$  values range from  $-43.1\text{‰}$  to  $-48.4\text{‰}$  and  $\delta^{18}\text{O}$  values range from  $-6.6\text{‰}$  to  $-7.4\text{‰}$ . Rainfall data were collected in Orléans [3] and Paris-Orsay (F. Barbecot, pers. comm.), i.e. in the south and centre west of the studied area. The weighted means for both stations are shown in Figure 3, as are the Global Meteoric and the Local Meteoric lines for Orléans ( $\delta^2\text{H} = 7.42 \times \delta^{18}\text{O} + 5.55$ ). The average weighted mean values at Orsay for the period 2003–2009 were  $-7.04\text{‰}$  for  $\delta^{18}\text{O}$  and  $-47.3\text{‰}$  for  $\delta^2\text{H}$ . For the period 1996–2009 in Orléans, the average weighted mean values are quite different at  $-6.88\text{‰}$  for  $\delta^{18}\text{O}$  and  $-44.8\text{‰}$  for  $\delta^2\text{H}$ . On a  $\delta^{18}\text{O}$  distribution map [4], the studied area falls in an area between  $-6.8$  and  $-7.5\text{‰}$   $\delta^{18}\text{O}$ . As the main aquifer recharge in the Paris Basin occurs in winter, the weighted mean of rainfall isotopes for the months November to April ( $-7.84\text{‰}$  for  $\delta^{18}\text{O}$  and  $-52.1\text{‰}$  for  $\delta^2\text{H}$ ) can be considered as representative of the input signal.

Very few literature data exist on the stable isotope composition of groundwater in the Tertiary aquifers of the Paris Basin. The values plotted in Fig. 3 are for Beauce [5] and Brie [6] limestones and for Ypresian/Lutetian sandy clay in the eastern Paris Basin [7]. In addition, some values from the Chalk aquifer [8, 9] are available (Fig. 3). Chalk aquifer water and some groundwater from the present study fall below the Local and Global Meteoric lines. Vachier [10] highlighted a similar pattern for Chalk groundwater near Reims (northern part of the study area) and suggested that some water may have evaporated while percolating through the unsaturated zone, before joining the aquifer. With these data we can draw an evaporation line from the weighted mean of winter precipitation (November to April) and intercepting the more

## GOURCY and PETELET-GIRAUD

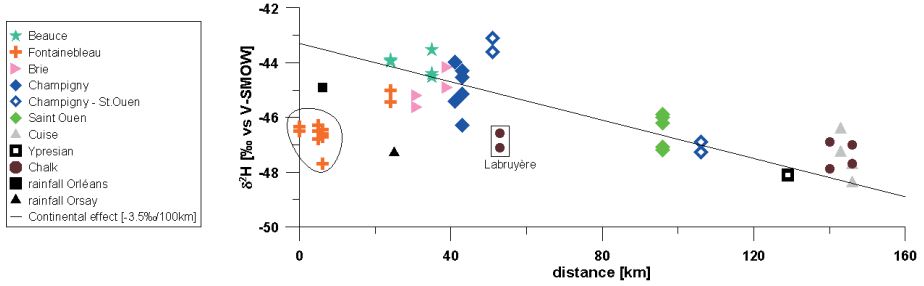


FIG. 4.  $\delta^2\text{H}$  of groundwater collected in April and October 2009 plotted vs. distance on an E–W profile.

$\delta^2\text{H}$  depleted groundwater. This evaporation line has a slope of 4.5 while the slope of the evaporation lines measured in previous work in the Paris Basin [9] is 4.3.

The sampled groundwater is divided into two groups. Most of the groundwater in the first group, including the weighted mean value of Orléans precipitation, falls between the ‘evaporation line’ and the Local Meteoric Line (LML). It is considered that most groundwater recharge occurs during winter, though this is not confirmed by the isotope composition of precipitation as demonstrated already by Ref. [11]. The weighted average of winter precipitation (65% of total precipitation) is isotopically more depleted than the average Tertiary aquifer water.

Groundwater from the second group is isotopically depleted and water from some boreholes has a higher d-excess and falls above the LML.

As expected when considering the CFC age, the sampled boreholes contained a variable part of young water. The isotope composition is far from that of the paleowaters in the Chalk aquifer:  $-7.9\text{‰}$  for  $\delta^{18}\text{O}$  and  $-50\text{‰}$  for  $\delta^2\text{H}$  [12]. The  $\delta^{18}\text{O}$  and  $\delta^2\text{H}$  range for groundwater is much narrower than the one for rainfall in Orléans ( $\delta^{18}\text{O}$  of  $-1.9\text{‰}$  to  $-9\text{‰}$  and  $\delta^2\text{H}$  of  $-11.9\text{‰}$  to  $-85.6\text{‰}$ ), indicating groundwater mixing over several hydrologic cycles. We can thus consider that the isotope variability is not due to any ‘paleo temperature’ effect.

Looking at the spatial distribution of stable isotope values (Fig. 4), a continental effect can be seen. An east–west profile can be drawn with plotted projections of all the sampled boreholes on a single line (see Fig. 1) with km 0 considered as the first sampling point. The east–west stable isotope depletion of groundwater from all aquifers except Fontainebleau sand can be estimated at  $-0.46\text{‰}/100\text{ km}$  for  $\delta^{18}\text{O}$  and  $-3.5\text{‰}/100\text{ km}$  for  $\delta^2\text{H}$ . This result is comparable to that obtained for the Chalk aquifers of the Paris Basin [8] and to the results obtained by [13] for winter precipitation in Europe ( $-3.3\text{‰}/100\text{ km}$  for  $\delta^2\text{H}$ ). In the figure, the superposed points are for April and October data. The ‘Labruyère’ point is located in the extreme north of the studied area.

Water from the Fontainebleau Sand aquifer in the western part of the studied area (km ‘0’) has a stable isotope composition that falls outside the overall pattern of

a decrease in heavy isotope content with inland distance. The weighted average value of rainfall at Orléans, located less than 80 km from the area bounded by five sampling points, is also isotopically enriched. Another borehole exploiting water from the Fontainebleau Sands aquifer, but located farther east, shows  $\delta^2\text{H}$  and  $\delta^{18}\text{O}$  values similar to the ones of other aquifers of the same sector and to Orléans precipitation. Weighted mean values of  $\delta^{18}\text{O}$  and  $\delta^2\text{H}$  at Orsay, located 45 km northeast from the anomalous points, are again more negative. The significant difference in  $\delta^2\text{H}$  and  $\delta^{18}\text{O}$  weighted mean values at Orsay and Orléans is probably due to local meteorological phenomena.

#### 4. CONCLUSIONS

Major dissolved elements do not allow chemical discrimination of the different Tertiary aquifers (and Chalk) of the Paris Basin. Even trace elements cannot be used, as no direct correlation exists between dissolved element concentrations in water and the exploited aquifer. This difficulty in chemically characterizing each aquifer may also be due to difficulties in determining the origin of water pumped from the sampled boreholes. To solve this uncertainty, stable isotope information was collected.

The isotopic composition of groundwater from Tertiary aquifers in the Paris Basin reflects the continental effect of precipitation and the stable isotope composition of the various Tertiary aquifers is similar. Therefore, this tool cannot be used for distinguishing the origin of Eocene and Oligocene groundwater.

An anomaly in the overall isotope pattern was highlighted for the groundwater of the Fontainebleau Sands aquifer in the southern part of the Beauce plain. This anomaly cannot be related to any rainfall amount or altitude effect. More detailed work is thus necessary in order to evaluate if a temperature anomaly or air mass dominating trajectories can influence the isotope composition of precipitation in the southeastern part of the Paris Basin. More regional groundwater data and precipitation monitoring stations are needed for a better understanding of the spatial distribution of  $\delta^{18}\text{O}$  and  $\delta^2\text{H}$  in this area.

#### REFERENCES

- [1] BRENOT, A., et al., Identification des zones à risque de fond géochimique élevé en éléments traces dans les cours d'eau et les eaux souterraines — Vol. 3: Bassin Seine-Normandie, Report BRGM/RP-55346-FR (2007).
- [2] INTERNATIONAL ATOMIC ENERGY AGENCY, Use of Chlorofluorocarbons in Hydrology: A Guidebook, IAEA, Vienna (2006).
- [3] INTERNATIONAL ATOMIC ENERGY AGENCY/WORLD METEOROLOGICAL ORGANIZATION, The Global Network of Isotopes in Precipitation, The GNIP Database (2006), <http://www.iaea.org/water>.

- [4] MILLOT, R., PETELET-GIRAUD, E., GUERROT, C., NÉGREL, P., Multi-isotopic composition ( $\delta^7\text{Li}$ - $\delta^{11}\text{B}$ - $\delta\text{D}$ - $\delta^{18}\text{O}$ ) of rainwaters in France: Origin and spatio-temporal characterization, *Appl. Geochem.* **25** (2010) 1510–1524.
- [5] MAGET, P., POINTET, T., “Beauce”, Aquifères et eaux souterraines en France, Vol. 1 (ROUX, J.-C., Ed), BRGM, Orléans, France (2006) 191–199.
- [6] VERNOUX, J.F., SANJUAN, B., BRACH, M., Analyse chimique de la nappe du Calcaire de Brie — Chailly-en-Bière (Seine-et-Marne), Report BRGM/RP-51263-FR (2001).
- [7] BRENOT, A., BARAN, N., PETELET-GIRAUD, E., NÉGREL, P., Interaction between different water bodies in a small catchment in the Paris basin (Brévilles, France): Tracing of multiple Sr sources through Sr isotopes coupled with Mg/Sr and Ca/Sr ratios, *Appl. Geochem.* **23** (2008) 58–75.
- [8] KLOPPMANN, W., DEVER, L., EDMUNDS, W.M., Residence time of Chalk groundwaters in the Paris Basin and the North German Basin: a geochemical approach, *Appl. Geochem.* **13** (1998) 593–606.
- [9] GOURCY, L., et al., Impact sur la qualité de la ressource en eau souterraine du surstockage dans la plaine alluviale de la Bassée, BRGM/RP-56695-FR (2008).
- [10] VACHIER, P., DEVER, L., FONTES, J.-C., “Mouvements de l’eau dans la zone non saturée et alimentation de la nappe de la craie de Champagne, (France): Approches isotopique et chimique”, *Isotope Techniques in Water Resources Development (Proc. Symp. Vienna, 1987), Proceedings Series, IAEA, Vienna (1987) 367–379*
- [11] GRABCZAC, J., et al., Estimation of the tritium input function with the aid of stable isotopes, *Catena* **11** (1984) 105–114.
- [12] SMITH, D.B., et al., The age of groundwater in the Chalk of the London Basin, *Water Resour. Res.* **12** (1976) 392–404.
- [13] ROZANSKI, K., SONNTAG, C., MUNNICH, K.O., Factors controlling stable isotope composition of European precipitation, *Tellus* **34** (1982) 142–150.

# USE OF ISOTOPIC TECHNIQUES FOR THE ASSESSMENT OF HYDROLOGICAL INTERACTIONS BETWEEN GROUND AND SURFACE WATERS — RIO MAN, CIÉNAGA COLOMBIA

P. PALACIO, C. DAPEÑA, T. BETANCUR

Universidad de Antioquia,  
Medellín, Colombia

## Abstract

The Man River basin is located in the lower foothills of the western and central ranges of the tropical Andes, Colombia. In this area hydrological studies and hydrochemical analyses were carried out and isotopic techniques applied to describe and understand the interactions between ground and surface waters. To expand this model and to include elements other than local hydrodynamics, relationships between regional precipitation, recharge, regional flow paths and hydraulic gradients controlling water flows from big rivers to groundwater are currently being explored. Accordingly, an isotope local meteoric water line was derived and it was discovered that the relationship between ground and surface waters is similar in wet and dry seasons. Precipitation constitutes the main recharge source, base flow is important in supporting flow in rivers, streams and wetlands, and evaporation causes effects over water systems in dry periods. A tendency towards increasing air temperatures has been detected in the Man River; this change may cause negative impacts over the hydrological system, affecting evapotranspiration–recharge processes.

## 1. INTRODUCTION

This paper integrates the first results obtained as part of the study Conceptual Hydrological Model for the Middle and Lower parts of the Man River basin using Hydrological, Hydrochemical and Isotopic Techniques with the results of the project Hydrochemical and Isotopic Techniques for the Assessment of Hydrological Processes in the Wetlands of Bajo Cauca Antioquia carried out by the University of Antioquia in the framework of a cooperative project with the International Atomic Energy Agency (IAEA). A hydrological model simulating the interaction between surface and groundwater in the lower reaches of the Man River basin was obtained through the use of hydrological techniques. This model was refined, adjusted and validated using isotope techniques mainly based on the analysis of spatial and temporal variance of stable isotopes measured in rainwater, surface water bodies such as streams and wetlands, and in an unconfined aquifer.

## 2. STUDY AREA

The Bajo Cauca Antioquia area, located in the foothills of the central and western ranges of the Andes in Colombia, is a flat region crossed by mountains, home to a complex hydrological system formed by the rivers Cauca, Nechí and Man, by two aquifers and by more than 350 wetlands (Fig. 1). The Man River originates within the jurisdiction of the Municipality of Taraza at 1050 m a.s.l. The basin covers an area of 688 km<sup>2</sup> and is located between the coordinates 75°12'36.0" and 75°33'50.4" W, 7°57'36 and 7°31'8.0'4 N. The relief in the lower part is characterized by a flat topography of low inclination and extensive valleys. In the middle part, the slopes are low to moderate, the valleys are of little depth and the hills are predominantly low. The region is distinguished by its warm and humid climate, with temperatures ranging from 25 to 30° C. The rainfall pattern is unimodal, with a dry period between December and March and a wet period between April and November. The average annual rainfall is 2800 mm, which peaks in October to reach 469 mm/month. The geology of the area is composed mainly of clastic sedimentary rocks of continental origin and of Tertiary age, represented by the Cerrito Formation, Sincelejo Group and the more recent alluvial deposits of the Quaternary period. These units have important attributes, constituting an important aquifer which has defined the region in the form of three hydrogeologic units; U<sub>123</sub>, an unconfined aquifer formed by alluvial deposits from the River Man and the slightly consolidated saprolite of the upper member of the Cerrito Formation; U<sub>4</sub>, a confining unit that underlies unit U<sub>123</sub> and is constituted by Tertiary sediments of the Middle Member of the Cerrito Formation,

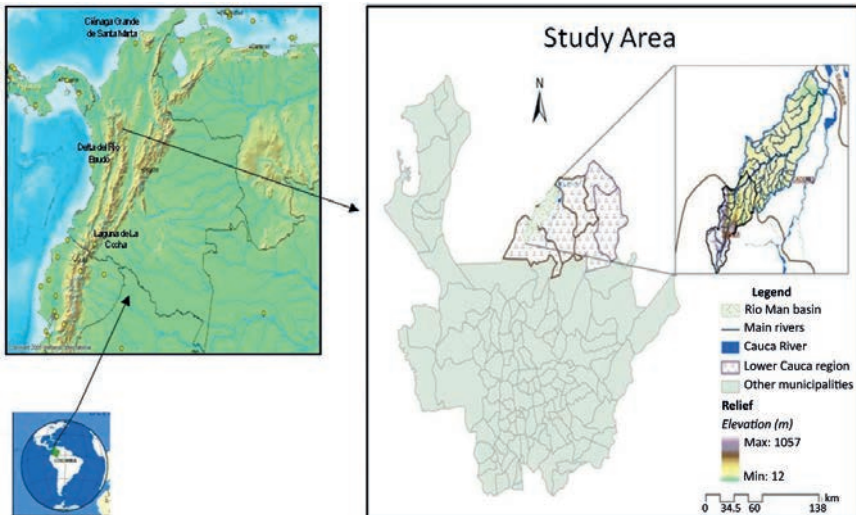


FIG. 1. Location of the study area.

and U<sub>5</sub>, which corresponds to a lower member of the Cerrito Formation and behaves regionally as a confined aquifer.

### 3. METHODOLOGY

Some years ago, Falkenmark and Chapman [1] stated “The conceptual framework common to every hydrologic analysis, regardless of its scale, is the systemic division of hydrological processes to a number of stores interconnected by water flow.” In this sense, a conceptual hydrological model could be defined as a pictorial representation of a water flow system that includes maps, block diagrams and cross sections which highlight the characteristics of its elements and describe the nature and magnitude of the processes that link its components. This model integrates information about the characteristics of surface, atmospheric and underground systems. Ref. [2], referring to the certainty of conceptual models, uses the term ‘surprise’, and relates it to the situation in which the collection of new information invalidates the original conceptual model. The surprise may arise as a result of revision of the scientific theory or as a result of new information obtained on a particular site. Uncertainty is rooted in the foundation of our knowledge and is a function of our limited ability to understand the natural world. Almost by definition, error cannot be quantified in a conceptual model. Ref. [3] argues that within the field of hydrogeology, one idea that can be generalized to every hydrological system is that: “it is even possible to have different conceptual models for the same system.” A conceptual hydrological model is built on information obtained from the interpretation of data from observation of reality (Fig. 2). Proof of its validity is achieved through the implementation of specific research techniques which include hydrochemistry and isotope hydrology [4]. Achieving the goal of having a set and validated conceptual model requires continuous monitoring of the natural and induced processes taking place in the system under study.

For this case study in the Man River Basin, the hydrologic data includes a series of daily hydroclimatic registries that spans more than 20 years, taken by the Institute of Meteorology and Environmental Studies of Colombia (IDEAM). Since 2007, the University of Antioquia, in the framework of an agreement with the IAEA, has been operating a monitoring network of groundwater level with monthly water level readings with accuracy to the centimetre. Within the same system there is also a monitoring network of hydrochemical and isotopic variables, for which water samples are collected during the two hydrological scenarios (rainy and dry) that occur annually in the basin within a normal cycle. The network consists of a station for precipitation, a weather station, 41 piezometric stations and 27 stations for sampling surface water. Hydrogeochemical variables analysed include major and minor ions and isotopic parameters correspond to <sup>18</sup>O and <sup>2</sup>H. Sampling was conducted following the protocols defined by certified laboratories and the IAEA. Chemical analyses were

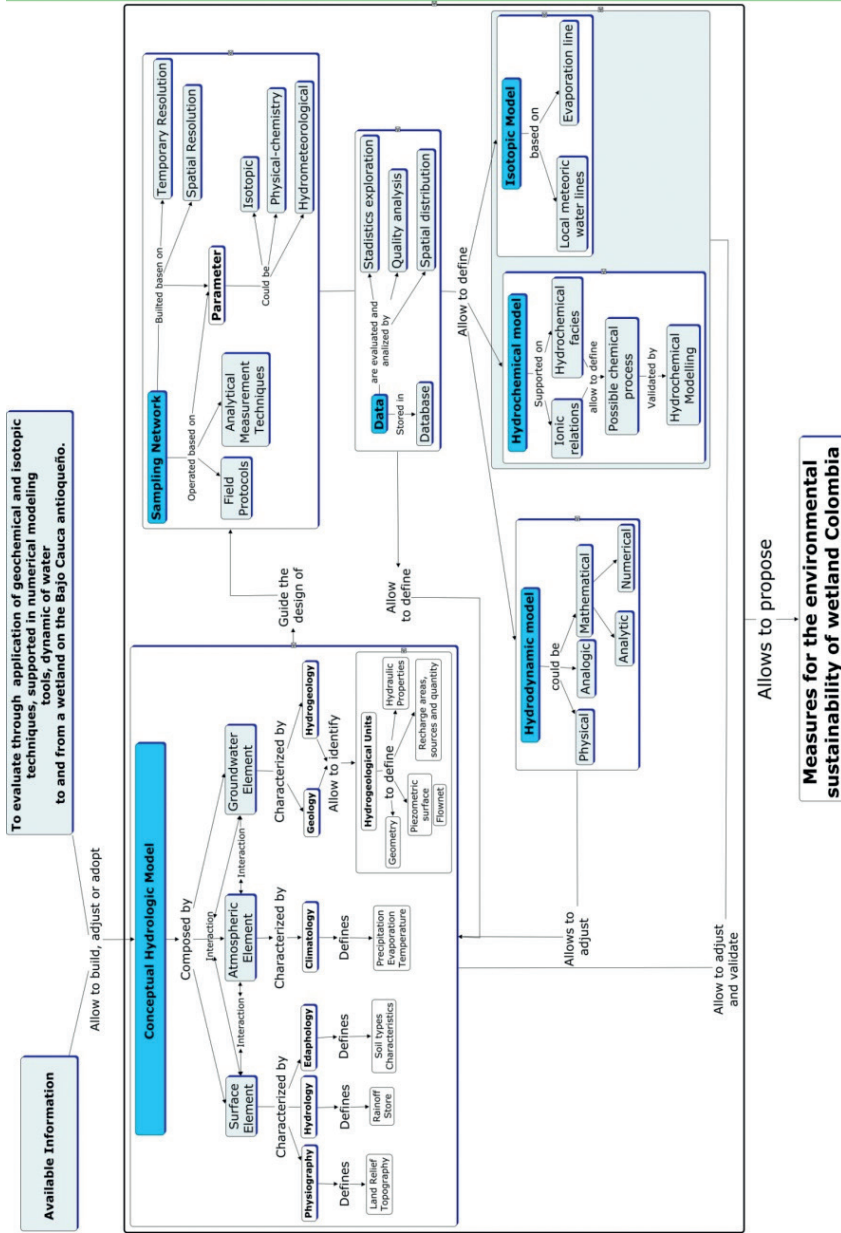


FIG. 2. Methodological framework.

performed in the Environmental Quality Laboratory CORANTIOQUIA using chromatography and atomic absorption. Isotopic analyses were made in the Geo laboratory in El Salvador using mass spectrometry and in the National University of Mar del Plata in Argentina using a spectrometry laser.

### 3.1. Hydrological interaction between surface water and groundwater in the man river basin

*Hydrological model.* Processing the hydroclimatological data of IDEAM and the piezometric levels obtained during three years of monthly monitoring, and, considering the hydrogeological model proposed by Ref. [4], a conceptual hydrological model for the lower middle of the Man River basin (Fig. 3) was developed. This map shows the principal surficial environments (Man River, Quebradona stream and the wetland Ciénaga Colombia) and underground environment (the piezometric surface of the unconfined aquifer); the directions of

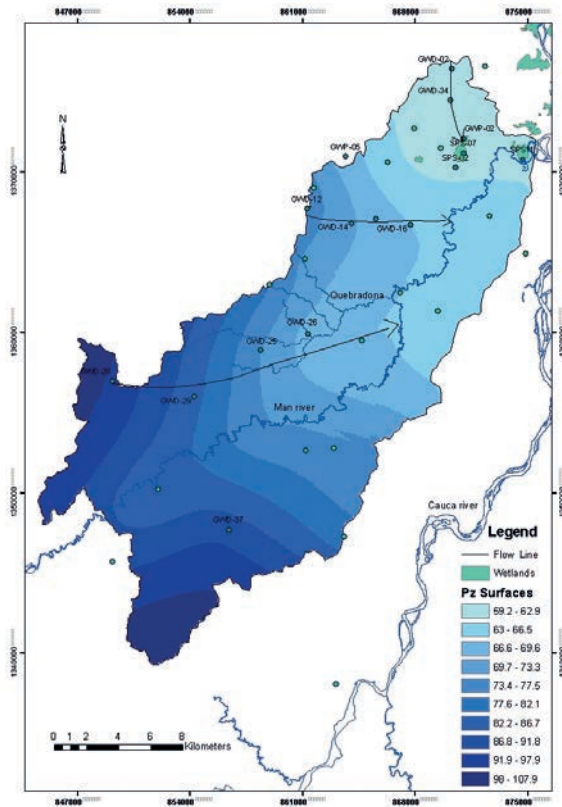


FIG. 3. Model of surface-groundwater interaction.

flow show the interaction that occurs between the surface and the underground. The unconfined aquifer contributes through the baseflow to the surface flow in the upper and lower sections of the Man River, in the Quebradona stream and towards the Ciénaga Colombia wetland; in the middle, the Man River acts as an influent stream on its left bank, giving water to the aquifer.

The magnitude of the processes of flow in the Man River basin was quantified by processes of mass balance applied over an observation period of 3 years (2007 to 2010). According to the results of this multi-year study, average monthly total run-off for the basin is 20.5 m<sup>3</sup>/s; the total recharge is in the order of 1300 mm/a, with base flow contributions taking place more than seven months a year that that would account for 40 to 60% of the estimated total recharge.

*Hydrochemistry.* We analysed a total of 131 samples (4 rain, 83 ground and 44 surface water samples) that met the condition of having an ion balance error of less than 10% (Table 1). Piper diagrams (Fig. 4) show a set of water types for groundwater that vary from calcium/magnesium bicarbonate, sodium bicarbonate to mixed, while surface water is mainly composed of calcium bicarbonate type. Rainwater was shown to be calcium bicarbonate type.

Following the routes marked by the directions of water flow defined in the hydrological model, the chemical evolution of water chemistry is expected to be confirmed (Table 2). A flow line drawn from north to south using the points GWD-02→GWD-34→GWP-02 shows a normal evolution consistent with the

TABLE 1. SYNTHESIS OF HYDROGEOCHEMICAL RESULTS (mg/L)

		Ca	Na	Mg	K	Cl	HCO <sub>3</sub>	SO <sub>4</sub>	NO <sub>3</sub>	pH	Cond. (µS/cm)
Ground- water	Min.	0.3	1.2	0.3	0.1	0.7	2.6	1.5	3.3	4.9	14.0
	Max.	98.5	301.0	54.4	5.7	278.0	974.0	27.8	198.8	8.5	1425.0
	Range	98.3	299.8	54.1	5.6	277.3	971.4	26.3	195.5	3.6	1411.0
	Average	20.4	32.3	9.6	1.8	22.6	145.9	2.1	13.2	6.5	258.8
	Std. Dev.	19.8	58.2	11.8	1.2	46.8	183.4	3.1	25.1	0.7	317.6
	Count	83.0	83.0	83.0	83.0	83.0	83.0	83.0	66.0	73.0	73.0
Surface water	Min.	1.6	1.9	1.5	0.5	0.8	0.0	1.5	0.0	5.7	2.6
	Max.	17.7	9.6	11.4	4.0	5.9	77.3	95.2	10.5	7.8	141.9
	Range	16.1	7.7	9.9	3.5	5.1	77.3	93.7	10.5	2.1	139.3
	Average	5.9	4.1	3.5	1.8	1.7	38.4	4.2	3.7	6.9	62.6
	Std. Dev.	3.3	1.7	1.8	0.7	1.2	15.7	14.1	1.8	0.5	31.1
	Count	44.0	44.0	44.0	44.0	44.0	44.0	44.0	38.0	40.0	39.0

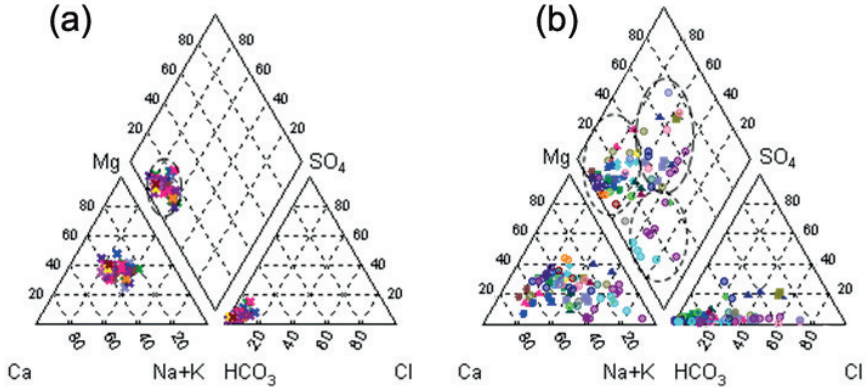


FIG. 4. Piper diagrams for surface (a) and groundwaters (b).

series of Chevotareb; water changes from calcium bicarbonate to sodium bicarbonate; the magnesium present in GWD-34 and GWP-02GWD could be due to the dissolution of dolomite present in the cement of the Cerrito Formation; the emergence of chloride in GWP-02 may be due to processes of evaporation. Other directions of flow along paths GWD-12→GWD-14→GWD-15→GWD-16 and GWD-28→GWD-29→GWD-25→GWD-26 suggest that processes of mixing occur between groundwater and a possible associated recharge source or with contributions from surface runoff. The sodium types at the beginning of line 2 near a recharge area can be explained by pollution associated with the domestic use of sodium hypochlorite, combined with processes of evaporation during recharge. There is exchange of cations between Na and Ca and dissolution of dolomite which results in the appearance of Mg. The presence of NO<sub>3</sub> may be due to the land use in the area, which is primarily cattle raising.

#### 4. ISOTOPE HYDROLOGY.

For stable isotopes of water, surveys conducted between 2007 and 2010 produced 32 rain water samples, 71 for surface water and 124 for groundwater; a summary of the analyses is presented in Table 3.

From rainwater data from station SPR-07 (Hacienda La Candelaria, University of Antioquia), we obtained the local meteoric water line, which basically coincides with the global meteoric line. The weighted value of the precipitation corresponds to  $-8\text{‰}$  for  $\delta^{18}\text{O}$  y  $-57\text{‰}$  for  $\delta^2\text{H}$ .

By considering the values obtained for samples of surface water during dry periods, particularly those taken in the Ciénaga Colombia wetland, it was possible

TABLE 2. MAIN TRENDS OF HYDROCHEMICAL EVOLUTION

Line	Code	Name	Depth	Type
L1	GWD-02	Costa Rica	5	Ca-HCO <sub>3</sub>
	GWD-34	La Siberia	10	Ca-Mg-HCO <sub>3</sub>
	GWP-02	Pz. Norte Ciénaga	6	Na-Mg-Ca-HCO <sub>3</sub> -Cl
L2	GWD-12	Mirador Las Brisas	5	Na-Mg-HCO <sub>3</sub> -Cl-NO <sub>3</sub>
	GWD-14	Charrascal	10	Ca-Na-HCO <sub>3</sub>
	GWD-15	Jesusalén	5	Na-Ca-HCO <sub>3</sub> -Cl
	GWD-16	El Topacio	10	Ca-Mg-Na-HCO <sub>3</sub> -Cl
L3	GWD-28	El Cortijo	12	Ca-Na-HCO <sub>3</sub>
	GWD-29	El Orgullo	5	Ca-Mg-Na-HCO <sub>3</sub>
	GWD-25	El Paraíso	5	Na-Mg-Ca-NO <sub>3</sub> -Cl
	GWD-26	La Bonita	5	Na-Mg-HCO <sub>3</sub>

to obtain an evaporation line for this water system. Understanding the relationship between the values obtained for water samples in the atmosphere, on the surface and underground, allows a better understanding of the interactions established in the form of flows in the hydrological model (Fig. 5). In general, the isotopic composition of groundwater is homogeneous and is found in the range  $-7.9$  to  $-5.1\%$  for  $\delta^{18}\text{O}$  and  $-55.5$  to  $-39.4\%$  for  $\delta^2\text{H}$ , with some samples being more enriched in some places and at some times, a situation that would correspond to processes of evaporation before recharging (GWD-31 in March 2010 and GWD-37 in samples from April 2008 and March 2010) or to sources of recharge other than local rainfall (Hotel Buenos Aires).

Making an evaluation of the isotopic ratios from year to year (Fig. 6), we can see that in samples collected in 2007, the isotopic content of groundwater is more enriched than that of the surface water, the latter being characterized by an isotopic signature very similar to the weighted value of the rain. The isotopic values of most groundwater catchments sampled during this period are below the evaporation line, which could mean that the water underwent processes of evaporation before reaching the aquifer system, a plausible situation considering that that year was unusually dry. For 2008 and 2009, surface water and groundwater had very similar isotopic signatures recorded at various points, showing the relationship between the two (SPR11 for 2008 and GWP-02, GWP-05 and SPS-02, GWD-16 and SPS-07 in 2009 are notoriously impoverished). In 2010, variability in the isotopic composition of groundwater was minimal and very similar to that of rain and surface water; this year was one of the wettest periods in the hydrology of the region.

TABLE 3. SYNTHESIS OF ISOTOPIIC INFORMATION

	<sup>2</sup> H (‰)	<sup>18</sup> O (‰)	<sup>2</sup> H 2007	<sup>18</sup> O 2007	<sup>2</sup> H 2008	<sup>18</sup> O 2008	<sup>2</sup> H 2009	<sup>18</sup> O 2009	<sup>2</sup> H 2010	<sup>18</sup> O 2010
Min.	-73.49	-10.59	-70.2	-9.6	-54.7	-7.7	-73.5	-10.6	-57.6	-8.6
Max.	-30.17	0.70	-41.4	-5.6	-30.2	0.6	-39.8	0.7	-33.4	-5.0
Range	43.32	11.29	28.8	4.0	24.6	8.3	33.7	11.3	24.2	3.6
Average	-47.44	-6.78	-48.9	-7.0	-47.8	-6.5	-47.1	-6.8	-46.6	-6.8
Std. Dev.	5.43	1.22	5.9	0.8	4.8	1.7	5.4	1.3	5.6	0.8
Count	124.00	124.00	23.0	23.0	23.0	23.0	49.0	49.0	29.0	29.0
Min.	-66.61	-9.50	-61.4	-8.9	-66.6	-9.5	-63.6	-9.5	-46.8	-6.9
Max.	17.29	4.17	17.3	4.2	-25.2	-4.0	-35.5	-5.1	3.8	0.9
Range	83.90	13.67	78.7	13.0	41.4	5.4	-46.5	-6.8	50.6	7.8
Average	-43.33	-6.00	-43.1	-5.5	-48.1	-6.6	28.1	4.4	-24.6	-3.4
Std. Dev.	17.22	2.82	23.5	4.1	10.3	1.4	7.7	1.1	20.2	3.0
Count	71.00	71.00	22.0	22.0	15.0	15.0	26.0	26.0	8.0	8.0
Min.	-89.0	-12.3	—	—	—	—	—	—	—	—
Max.	7.8	-0.1	—	—	—	—	—	—	—	—
Range	96.8	12.2	—	—	—	—	—	—	—	—
Average	-42.6	-6.5	—	—	—	—	—	—	—	—
Std. Dev.	27.0	3.4	—	—	—	—	—	—	—	—
Count	33.0	33.0	—	—	—	—	—	—	—	—

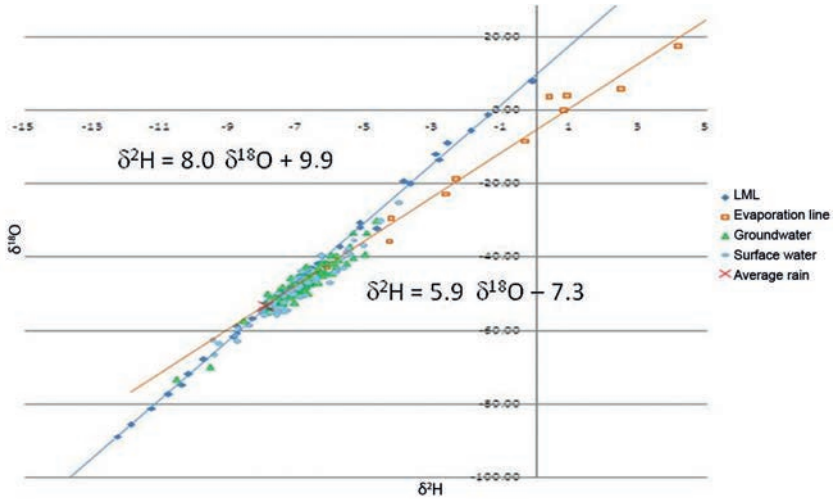


FIG. 5. Isotopic composition of rain, surface and ground water.

## 5. CONCLUSIONS

The isotopic analyses provided a better understanding of the interactions between the surface and ground water. The isotopic values of most groundwater catchments sampled during this period are below the evaporation line, which could mean that the water underwent processes of evaporation before reaching the aquifer system. The isotopic data reflects the groundwater role in the hydrological cycle in the zone of study during the sampling period.

## ACKNOWLEDGEMENTS

Our thanks to the IAEA, the University of Antioquia — GIGA group, the National University of the Mar del Plata, Daniel Martinez and the Community of Bajo Cauca.

## REFERENCES

- [1] FALKENMARK, M., CHAPMAN, T., Hidrología comparada, Comité Nacional Español para el Programa Hidrológico Internacional, Ministerio de Obras Publicas, Transporte medio Ambiente España, UNESCO, Spain (1993) 490.
- [2] BREDEHOEFT, J., The conceptualization model problem — surprise, Hydrogeol. J. **13** (2005) 37–46

- [3] CARRERA, J., ALCOLEA, A., MEDINA, A., HIDALGO, J., SLOOTEN, L., Inverse problem in hydrogeology, *Hydrogeol. J.* **13** (2005) 206–222.
- [4] BETANCUR, T., An approach to the knowledge of a tropical water-bearing system, Case study: Bajo Cauca antioqueño, University of Antioquia (2008).
- [5] SARAVANA KUMAR, S., et al., Recent studies on surface water–groundwater relationships at hydro-projects in India using environmental isotopes, *Hydrol. Proc.* **22** 23 (2008) 4543–4553.
- [6] VITALE, M.V., et al., Surface water–groundwater interaction and chemistry in a mineral-armored hydrothermal outflow channel, Yellowstone National Park, USA, *Hydrogeol. J.* **16** (2008) 1381–1393.



# **APPLICATION OF ENVIRONMENTAL ISOTOPES IN HYDROLOGICAL STUDIES ALONG THE RIVER NILE VALLEY, EGYPT**

A.A. NADA

Site and Environmental Dept. NCNSRC,

Atomic Energy Authority,

Cairo, Egypt

## **Abstract**

This paper reviews some of the contributions of isotope techniques to better understanding hydrological problems in Egypt and the Nile basin. The stable isotope composition of precipitation shows considerable variations both in time and space since it is controlled by climatic factors. Surface waters became enriched in deuterium and oxygen-18 relative to their initial isotopic composition as losses by evaporation occur. The GNIP sampling stations at Entebbe and Addis Ababa, which are located at the source of the Nile River, present relatively depleted isotopic contents. Assuming that the central Africa runoff (White Nile downstream from Sudan) represents 30% of the natural discharge of Egypt, and the remaining 70% is derived from Ethiopia (Blue Nile), we obtain a composite depleted stable isotope composition of the river Nile reaching upper Egypt under natural conditions (before the construction of the Aswan High Dam). Stable isotopes were used to estimate the evaporation rate from Lake Nasser, based on the isotopic content of the lake water. The lake can be divided into two sectors: the first sector, with remarkable vertical gradient in O-18 and deuterium, and a second sector, characterized by a lower vertical isotopic gradient. In order to detect this effect, surface Nile water samples have been collected at Cairo after a heavy storm event covering all Egypt at the beginning of November 1994, characterized by very negative deuterium and oxygen-18 contents. The isotopic content of Nile water samples fluctuated and slightly changed with time. The variation of the bomb tritium response of the Nile has been reconstructed using a model based on the contents in the catchment areas of the Nile. Pre-bomb tritium content in the Nile was about 5 TU, reaching a maximum level during the early sixties of about 500 TU. At present the tritium level content of the Nile is about 6 TU.

## **1. INTRODUCTION**

Within the framework of projects supported by the IAEA, environmental isotope studies have been carried out on surface and groundwater systems along the course of the River Nile in Egypt. The mixing between Nile water, virtually the only source of groundwater recharge, and adjacent groundwater has been studied in different areas

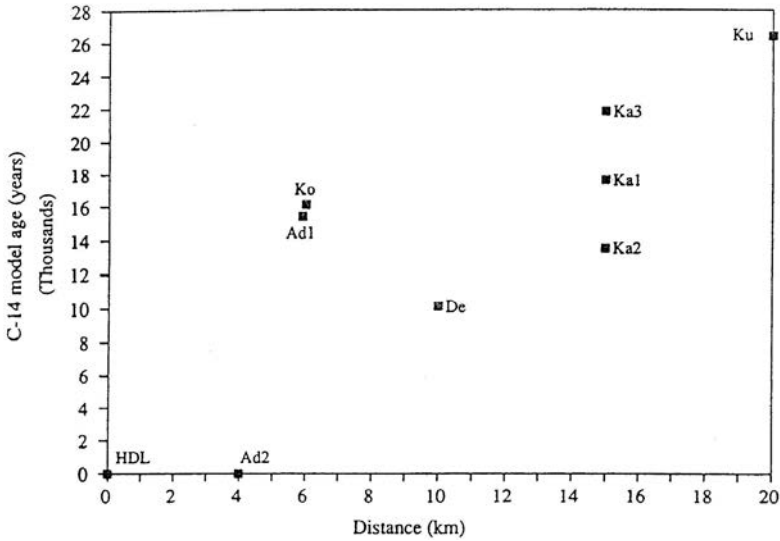


FIG. 1. C-14 model age of groundwater vs. distance from Nile River.

along the course of the Nile in Egypt. These areas include the High Dam Lake (HDL) Nasser, El Minia and Tahta Upper Egypt and Nile Delta area.

As far as is known about the isotopic composition of palaeowaters, previous investigations [1, 2] have shown that palaeowaters in Egypt commonly present stable isotope contents of about  $-10\text{‰}$  for  $\delta^{18}\text{O}$  and  $-75\text{‰}$  for  $\delta^2\text{H}$ . Since this groundwater was replenished during pluvial periods thousands of years ago, it is free of tritium and has a C-14 content of less than 25 pMC. These findings are in accordance with results obtained in the present study (Fig. 1). The Nile water generally consists of surface runoff and groundwater discharge from the Nile valley. In the past decades, this system has been subjected to several hydrological and environmental changes.

## 2. TEMPORAL VARIATION OF THE TRITIUM CONTENT OF THE RIVER NILE

The variation of the bomb tritium response of the Nile has been reconstructed [3] by using the model which is based on tritium data for precipitation in the catchment areas of the Nile in Uganda (Entebbe station) and of the Blue Nile (Addis Ababa station) taken from the IAEA GNIP database. Assuming that the main Nile receives 2/3 of its water from Ethiopian rains and 1/3 from Ugandan rains, the tritium model of Nile precipitation was run with inputs in the ratio of 2:1 respectively.

The results show that the pre-bomb tritium level of the Nile was approximately 5 TU. The maximum value during the early sixties, caused by bomb tritium, was about 500 TU. At present, the tritium content of the Nile is still higher than the tritium content of the rainfall in the region which reflects the presence of water fallen as rain in the period when the tritium content was higher than that of today.

### 3. TEMPORAL VARIATION OF THE STABLE ISOTOPE CONTENTS OF THE NILE BEFORE CONSTRUCTION OF THE HIGH DAM

Several of the IAEA sampling stations provide valuable information about the isotopic composition of rain within the Nile Basin. The first IAEA station is the Blue Nile in Addis Ababa, Ethiopia. According to IAEA precipitation station record the isotopic composition ranges from  $-8.4$  to  $+5.7\text{‰}$  for  $\delta^2\text{H}$  and from  $-2.7$  to  $-0.7\text{‰}$  for  $\delta^{18}\text{O}$ . A second IAEA precipitation station is the White Nile in central Africa at Entebbe, Uganda. The isotopic content ranges from  $-33$  to  $+4\text{‰}$  for  $\delta^2\text{H}$  and from  $-5.7$  to  $-1.1\text{‰}$  in  $\delta^{18}\text{O}$ . Assuming the central Africa runoff contribution to the White Nile downstream represents 30% of natural discharge to Egypt and 70% is derived from Ethiopian Highlands runoff (Blue Nile), we obtain a composite stable isotope composition of  $\delta^2\text{H} = -1\text{‰}$  and  $\delta^{18}\text{O} = -1.8\text{‰}$  as order of magnitude estimated after convolution in Sudan.

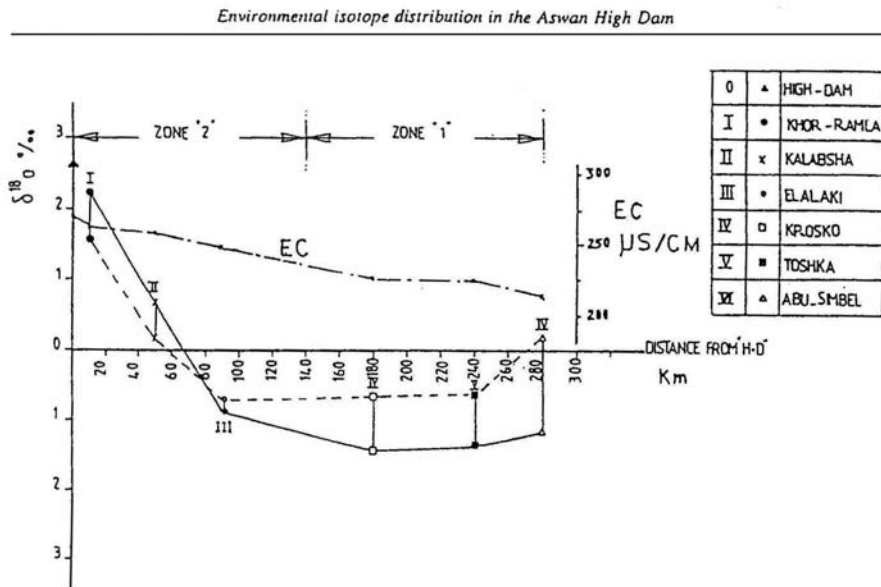


FIG. 2. Oxygen-18 content and electric conductivity (EC) of HDL water.

Due to evaporation,  $\delta^{18}\text{O}$  and  $\delta^2\text{H}$  are enriched up to  $-1.1\text{‰}$  for and  $+1\text{‰}$  respectively at the beginning of Aswan High Dam Lake, 300 km from Aswan Dam, and at the zero point of Aswan Dam these values reach values up to  $+2.4\text{‰}$  and  $+22\text{‰}$  respectively in December 1988 [4]. In fact, the river discharge is completely controlled by the High Dam reservoir. The increase of the isotopic content between Aswan and Cairo is given by a gradient of about  $+0.1\text{‰}/100\text{ km}$  for  $\delta^{18}\text{O}$  and  $+1\text{‰}/100\text{ km}$  for  $\delta^2\text{H}$ .

#### 4. ISOTOPE DISTRIBUTION IN THE ASWAN HIGH DAM LAKE (EGYPT)

Oxygen-18 and deuterium contents were used to estimate the evaporation rate from the Aswan High Dam Lake and to investigate the interrelation between the lake and the adjacent groundwater. According to changes in the isotopic contents, the lake can be divided into two sections. The first section, extending between Abu Simbel, El-Alaki and Krosko shows a vertical gradient of oxygen-18 and deuterium. The second section, in the northern section of the lake, extends up to the High Dam, and is characterized by a lower vertical isotopic gradient. In this sector, higher values of oxygen-18 and deuterium at the top and lower isotopic values at the bottom are found as shown in Fig. 2. To estimate the degree of evaporation from the lake using environmental isotopes, the natural conditions were simulated by putting an evaporation pan on a concrete installation. The evaporation pan was always surrounded by lake water from the bottom and also from the sides. The evaporation losses were estimated to be 19% using isotope techniques, in fairly good agreement with the values estimated at the High Dam hydrometeorological station in Aswan, ranging from 17.9 to 21.4%.

The isotopic contents of groundwater samples in the area indicate that recent recharge to nearby aquifers is limited to wells near to the lake and up to a maximum distance of about 10 km. Beyond this distance, palaeowater is observed, with highly depleted deuterium and oxygen-18 contents, which was also confirmed by C-14 dating of groundwater in this area, with ages of up to 26 000 years.

#### 5. ENVIRONMENTAL ISOTOPE CONTENTS OF GROUNDWATER IN UPPER EGYPT

Chemical and isotopic investigations indicate that the recharge source for the groundwater in the Tahta district, adjacent to the Nile, is mainly from the Nile water seeping from irrigation channels. The groundwater is of sodium bicarbonate type, with  $\delta^{18}\text{O}$  and  $\delta^2\text{H}$  values similar to those of the Nile water. The groundwater in the far west of the Nile bank is palaeowater, with a chemical composition of sodium sulphate and sodium chloride type [5].

Based on isotope data, groundwater in Minia Governorate can be classified into four groups [6]. The first group is characterized by a tritium content lower than 3.9 TU,  $\delta^{18}\text{O}$  between  $-1.3\text{‰}$  and  $0.9\text{‰}$ , and  $\delta^2\text{H}$  between  $-3.7\text{‰}$  and  $+13.6\text{‰}$ . The second group was distinguished by tritium contents ranging from 15.3 TU and 64 TU,  $\delta^{18}\text{O}$  between  $+2.3\text{‰}$  and  $+3.8\text{‰}$ , and  $\delta^2\text{H}$  between  $+20\text{‰}$  and  $+30\text{‰}$ . This second group corresponds to recently recharged waters, after the construction of the Aswan High Dam, affected by evaporation through Lake Nasser. The third group is characterized by depleted isotope values, having  $\delta^{18}\text{O}$  between  $-6.6\text{‰}$  and  $-8.4\text{‰}$ , and  $\delta^2\text{H}$  from  $-54\text{‰}$  to  $-64\text{‰}$ , which corresponds to palaeowater. The fourth group is represented by a mixture of waters of the previous three groups, principally the first two groups.

## 6. ENVIRONMENTAL ISOTOPE CONTENTS IN NILE WATER (CAIRO)

The isotope contents of surface water change with time and environmental effects. In order to determine the importance of these effects, surface Nile water samples have been collected at El-Gamma Bridge through the period from 08/11/1994 to 06/07/1996, just after the heavy storm that covered Egypt at the beginning of November 1994. The isotopic content of the heavy rainstorm was  $-44\text{‰}$  for  $\delta^2\text{H}$  and  $-6.5\text{‰}$  for  $\delta^{18}\text{O}$  at Cairo site. The isotopic content of that event may have different values in the south of Egypt where there is the main source of discharge to the Nile system. The fluctuations of isotopic content of Nile water samples are shown in Fig. 3 [7]. It is clear that isotopic contents change according to time, discharge and

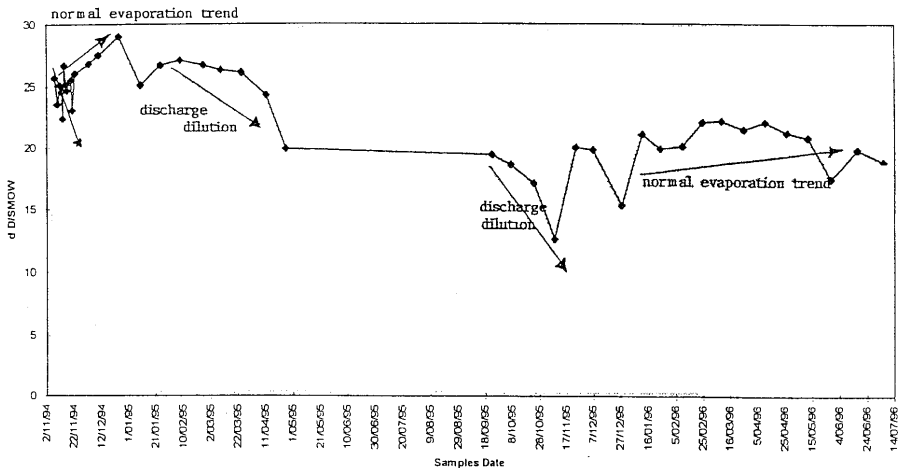


FIG. 3. Temporal variation of  $\delta^2\text{H}$  in the River Nile Water at El-Gamma Bridge, Giza, from 1994 to 1996.

the evaporation rate. The relation between  $\delta^{18}\text{O}$  and  $\delta^2\text{H}$  contents is represented by the equation:  $\delta^2\text{H} = 9.79 \delta^{18}\text{O} - 4.15$ .

7. ASSESSMENT OF GROUNDWATER RESOURCES IN NILE DELTA DESERT INTERFACE

The hydrogeological, hydrogeochemical and environmental isotopes studies of the Pleistocene and the Pliocene aquifers in Wadi El-Natron and Sadat City area were used to define the buffer characteristics of aquifers and delineate the groundwater flow patterns and the mixing of water of different origins.

The computer code MULTIS was used for the interpretation of environmental isotope data. The code estimates the mean residence time and mixing ratios between groundwater of the deeper aquifer and the Nile water. The mean residence times of the waters from the Pleistocene and the Pliocene aquifers range from 22 to 31.5 a respectively, reflecting the recent recharge to these aquifers, as shown in Fig. 4. The contribution of the deep palaeowaters (most probably from the Nubian Sandstone aquifer) to the Pleistocene aquifer amounts to 31.8%, while the contribution of the Nile water amounts to 68.2% in the Pliocene aquifer, the contribution of the paleowater is 38.6%, while the remaining 61.4% is from the Nile water. Um-Risha Lake receives 81.1% of its water from direct precipitation and the remaining 18.9% as seepage from the Pliocene aquifer.

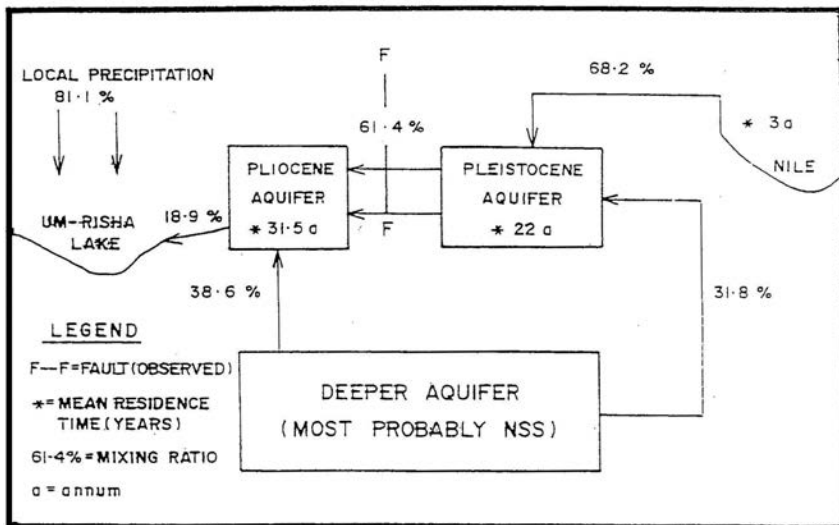


FIG. 4. Main characteristics of groundwater resources in the Nile Delta Desert Interface.

## 8. CONCLUSIONS

This paper presents examples of the use of isotope techniques to characterize aquifers and surface water bodies in Egypt and the Nile basin. Stable isotopes in precipitation over the Nile basin show large variability allowing the tracing of river waters contributing to the Nile river, as well as the estimation of evaporation losses from the Aswan High Dam. Carbon-14 and tritium have provided important insights into the groundwater dynamics of both shallow and deep aquifers

## REFERENCES

- [1] NADA, A.A., Evaluation of environmental isotopic and salinar composition of groundwater in oases of the Western Desert, Egypt, *Isotopes Environ. Health Studies* **31** (1995) 117–124.
- [2] THORWEIHE, U., SCHNEIDER, M., SONNTAG, C., New aspects of hydrology in southern Egypt, *Berliner Geowiss. Abh.* **A 50** (1984) 209–216.
- [3] RAGAA, E.S.A., Study of Environmental Isotopes and Trace Elements Abundance in Egyptian Waters, PhD Thesis, Faculty of Science, Cairo University (1980).
- [4] ALY, A.I.M., et al., Study of environmental isotope distribution in the Aswan High Dam Lake (Egypt) for estimation of evaporation of lake water and its recharge to adjacent groundwater, *Environ. Geochem. Health* **15** 1 (1993) 37–49.
- [5] AWAD, M.A., NADA, A.A. HAMZA, M.S., FROEHLICH, K., Chemical and isotopic investigation of groundwater in Tahta region, Sohag, Egypt, *Environ. Geochem. Health* **17** 3 (1995) 147–153.
- [6] EL-BAKRI, A., TANTAWI, M., BLAVOUX, B., DRAY, M., Water recharge sources identified by isotopes in Minia Governorate, Egypt, *Egypt J. Geol.* **37** 1 (1993) 91–109.
- [7] RAMADAN, E.E., Isotope and Chemical Composition of Surface and Groundwater in Northern Nile Valley Soils, M.Sc. Thesis, Cairo University (1998).



# ISOTOPE INVESTIGATIONS AT AN ALPINE KARST AQUIFER BY MEANS OF ON-SITE MEASUREMENTS WITH HIGH TIME RESOLUTION AND NEAR REAL-TIME DATA AVAILABILITY

A. LEIS<sup>a</sup>, R. SCHMITT<sup>b</sup>, A. VAN PELT<sup>c</sup>, M. PLIESCHNEGGER<sup>a</sup>,  
T. HARUM<sup>a</sup>, W. ZEROBIN<sup>d</sup>, H. STADLER<sup>a</sup>

<sup>a</sup> Joanneum Research,  
Institute for Water, Energy and Resources,  
Graz, Austria

<sup>b</sup> Meteorologie consult GmbH,  
Koenigstein, Germany

<sup>c</sup> Picarro Inc.,  
Sunnyvale,  
California, USA

<sup>d</sup> Vienna Waterworks,  
Vienna, Austria

## Abstract

For a lot of hydrological isotope investigations it would be helpful to conduct on-site measurements with a very high time resolution. Recent developments of a highly sensitive gas analyser on the basis of so called 'Cavity Ring Down Spectroscopy' (CRDS) has lead to a new class of on-site capable measuring devices, the wavelength scanned (WS)-CRDS. In the framework of a new project it succeeded for the first time in measuring the stable environmental isotopes of the water on-site and on-line at one of the most important karst springs in Austria. It was necessary, to adapt the WS-CRDS system for on-site application. Particularly the sampling device had to be adopted to get samples from the flow of the spring to the WS-CRDS system in real time. The system was installed at the spring during snowmelt with measuring intervals of fewer than 10 minutes. This measuring device was combined with a near real time data transmission system, based on LEO satellites. This allowed a dissemination of the data via the internet and, for registered users, also a download possibility of the data.

## 1. INTRODUCTION

The studied alpine karst system is located in the so called Northern Calcareous Alps in Austria reaching altitudes up to approx. 2300 m.a.s.l. The spring is situated in the Salza-valley at an altitude of approximately 650 m.a.s.l. (Fig. 1). The investigated karst spring is a typical limestone spring type according to Ref. [1], with well developed karst conduits [2]. The mean discharge is 5240 L/s (year 1995–2009), showing high variations with a  $Q_{max}/Q_{min}$  discharge ratio of 40. The mean water residence was estimated at between 0.8 to 1.5 years, using an exponential model. According to this, the discharge response after precipitation is very quick (some hours). The estimated alpine catchment covers an area of about 70 km<sup>2</sup>, with a mean altitude of 1780 m.a.s.l. [3]. Vegetation comprises summer pastures, natural calcareous alpine swards with open krummholz and forests [4].

## 2. METHODS

### 2.1. Measuring device

The isotopic composition of the water samples were measured by using Cavity Ring Down Spectroscopy [5] with a WS-CRDS (Wavelength Scanned Cavity

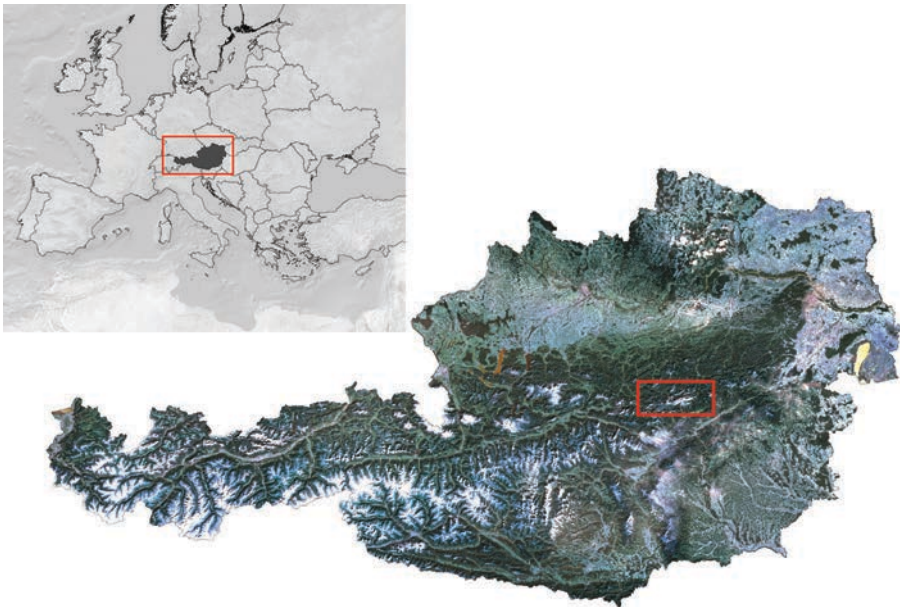


FIG. 1. Location of the investigation area.

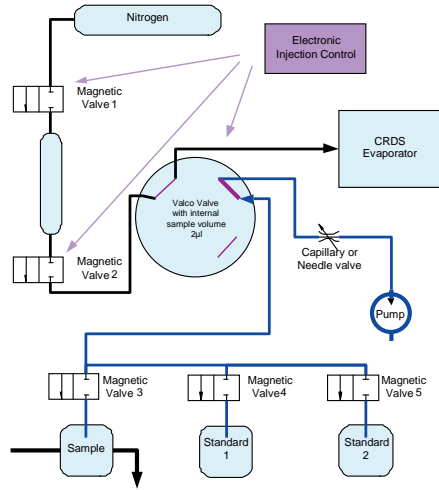
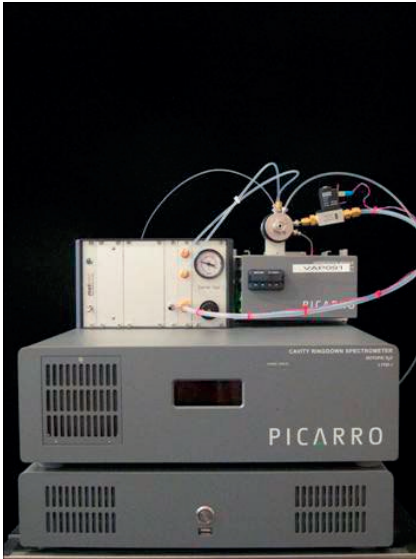


FIG. 2. Picarro System with online water injection module.

Ring-Down Spectroscopy) instrument (Picarro, Inc.). In order to adapt the System for on-site isotope measurements at the spring the laser spectrometer was coupled to an automatic injection module (Meteorologie consult GmbH) for continuous measurements of liquid samples based on a VALCO valve (Fig. 2).

The device replaces the auto-sampler and allows quasi-continuous injections of a 2  $\mu\text{L}$  water sample into the Picarro L1102 iso-water analyser via the Picarro vaporizer module. The water sample is sucked through the internal sample volume by a small pump (KNF, Neuberger). The sample volume is injected into the vaporizer of the system by a defined volume of dry nitrogen gas at 2–4 bars. The VALCO valve is also switched by the pressure actuator by nitrogen. The procedure of sampling and the injection into the vaporizer is controlled by the exchange of trigger signals between the Picarro analyser and the injection module. A USB data logger is used to actuate the valves and to communicate with the coordinator program of the analyser. The control software of the injection module is implemented on the PC of the analyser. The cycle time of the sample and the analysis is approximately 9.5 minutes, as defined by the analytical procedure of the L1102-I analyser. An unlimited number of samples can be injected into the analyser. The sample frequency and timing is controlled by a special version of the coordinator program of the analyser.

## 2.2. The LEO satellite system

Wireless data transmission is used for online transmission of the data measured at stations in the network [6] in order to avoid the costly needs for cable laying and

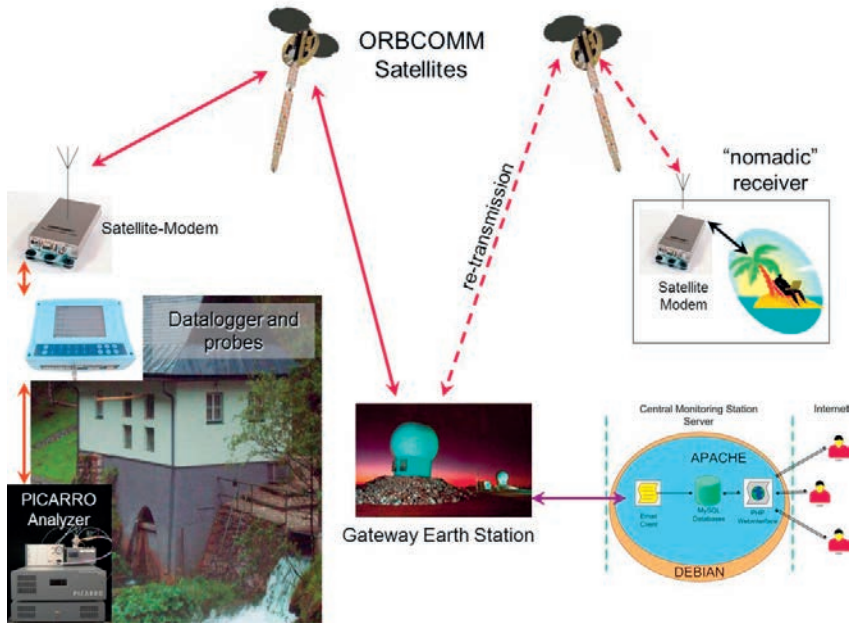


FIG. 3. Schematic of data streams via LEO Satellite system.

installation of power supplies. Due to recurrent coverage problems with land based systems (GSM/GPRS (General Packet Radio Service)/UMTS (Universal Mobile Telecommunications Service), as well as those arising from very restricted elevation angles in mountainous regions for GEO satellites (Geostationary Earth Orbit), for our applications LEO satellites (Low Earth Orbit) have proven preferable. Based on extensive technical and cost comparisons and the validation of measurements, e.g. Refs [7] and [8], the ORBCOMM LEO satellite system [9] was chosen for standard implementation with minor data transfer rates. ORBCOMM is a ‘Little LEO’ system, with 30 servicing satellites in six orbit planes of 800 km altitude. It provides bi-directional ‘short message’ data transfer at 2.4/4.8 kbps, with data blocks of preferably less than 100 Bytes. ORBCOMM operates at frequencies of about 140 MHz, providing large satellite footprints, and requires only low cost/low power equipment, allowing the use of simple whip antennas as well as small solar-panels for power supply. Transmitting in the VHF band means that the system can also work in forests.

The core and backbone of the application (Fig. 3) is a bi-directional, near real time data link via LEO satellites. This facilitates the monitoring of in situ measurements for all hydrological purposes, especially the quality monitoring of drinking water supplies and similar applications.

For this investigation, the connection possibilities of the system were expanded. The reason was that the Picarro System is a Windows based system, providing data

via file structures. So an interface between the data logger used, with different hydrological probes, and the new system was developed, to enable a near real time data transmission also in this case.

### 2.3. Central Monitoring Station (CMS) and web interface

The Central Monitoring Station (CMS) provides an online internet portal for access to the environmental data. It is built around a server running the operating system Debian, a very stable open source software, providing perfect interaction and performance with the server. Among others, the server comprises a RAID system (redundant array of independent disks) for fault tolerant operation. A dedicated email client and a ftp client were developed to decode and extract the compressed measurement data sets and to store them in the integrated MySQL database. The clients are fully automated and dynamically coded, so no user defaults are needed for these stand alone programs. They provide flexible and simple configuration e.g., of individual number of stations, types and coding of input data sets. Additionally, incorrect mails (syntax check) are detected automatically and stored in a specific database table. In

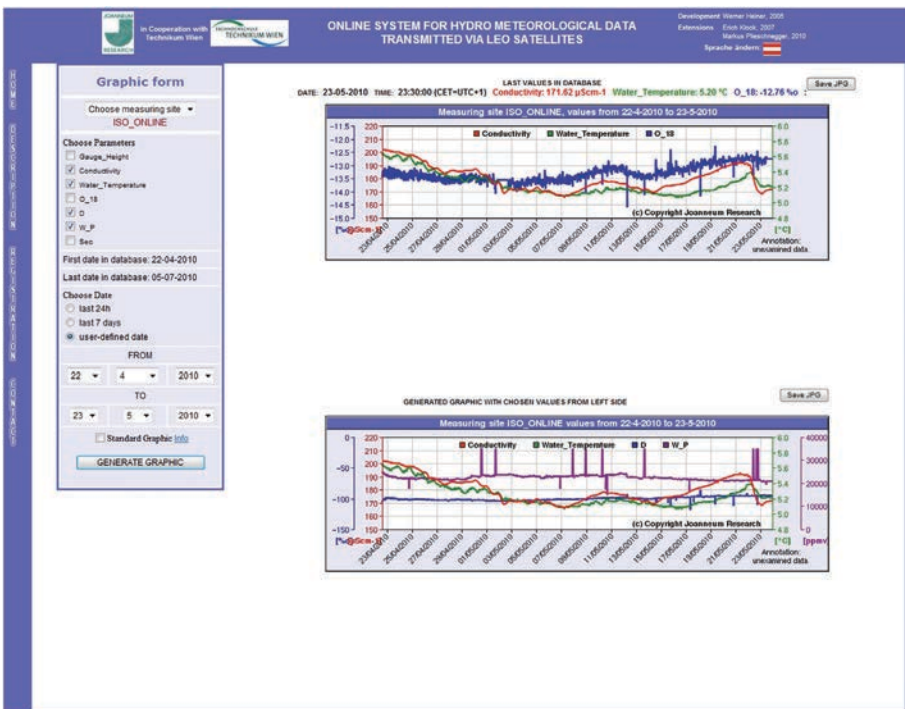


FIG. 4. The dynamically generated website for online data during event monitoring of stable isotopes.

this case, it can also automatically send an information mail to the user regarding this error. To provide on-line communication with access to the stored measurement data through the internet, an Apache-Webserver was implemented. The Internet portal concept comprises a dynamically generated website which allows 'real time' display of these data as graphics or tables. The dynamically generated online website is shown in Fig. 4.

The widely common freeware PHP was used for programming these interactions between internet users and the CMS. Furthermore, PHP can also interpret other interface languages, e.g. XML or JavaScript, using standardized modules, which makes the chosen implementation very flexible for on-line environmental communication. Additionally to the online graphical representation, all co-workers and public access users are also able to download these graphics or charts on their local machine, once they are registered. Using password protection, several access levels to the data and visualization are feasible for different user groups, e.g., general public access to environmental information vs. individual access for specific in depth data for research project co-workers. In combination with the encryption of the data transfer, the system is also prepared for sensitive non-public data. As there is the possibility of cross-linking the measuring sites, the system can also be used for precipitation triggered automated event sampling [10].

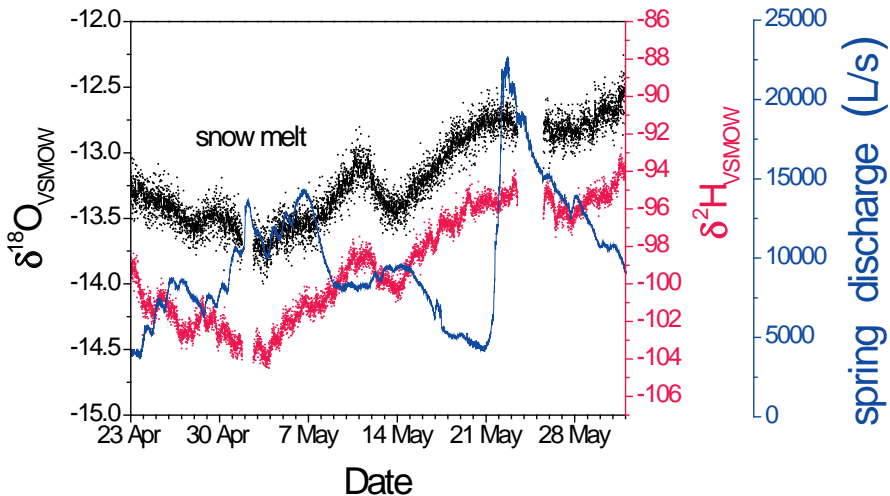


FIG. 5. Time series of isotopic composition and spring discharge during snowmelt at a karst spring.

### 3. RESULTS

#### 3.1. Time series

In Fig. 5 the course of deuterium, oxygen-18 and discharge is shown. The increase of discharge during the first days of May was caused by snowmelt, the rapid increase of discharge after May 21 was caused by a rain event, which brought approximately 100 mm precipitation during one day.

The different behaviour of the isotopes is clearly shown. The influence of the winter precipitation during snowmelt is obvious. The very damped reaction of  $^2\text{H}$  and  $^{18}\text{O}$  cannot be interpreted, due to missing analyses of the event causing precipitation.

### 4. DISCUSSION

As shown, it is possible to use the described system on-site, to enable near real time data availability with high time resolution. The measuring increment of the Picarro system was approximately 9.5 minutes. Data transmission was realized every 15 or 30 minutes. One motivation was to synchronize Picarro data with hydrological data available from other measuring systems. The first results were very promising and open up a new outlook for gathering important information about water resources and the possibilities of protection.

Further developments should improve the control mode of the Valco. It is planned to use an electric device. The on-site measuring of at least two standards has to be implemented. During our investigations reference samples were taken manually with different time increments.

### ACKNOWLEDGEMENTS

The work was carried out in close cooperation with the Vienna Waterworks (Dr. Wolfgang Zerobin) and supported by the area management of the Vienna Waterworks in Wildalpen (Ing. Christoph Rigler). Our thanks go also to Mr. Hermann Kain for the excellent technical assistance. The project was financially supported by the Austrian Federal Ministry for Transport, Innovation and Technology.

## REFERENCES

- [1] D'AMORE, F., SCANDIFFIO, G., PANICHI, C., Some observations on the chemical classification of ground water, *Geothermics* **12** (1983) 141–148.
- [2] STADLER, H., STROBL, E., Karstwasserdynamik und Karstwasserschutz Zeller Staritzen, Joanneum Research, Graz (1997), unpublished report (in German).
- [3] STADLER, H., STROBL, E., Karstwasserdynamik und Karstwasserschutz Hochschwab, Joanneum Research, Graz (2000), unpublished report (in German).
- [4] DIRNBÖCK, T., DULLINGER, S., GOTTFRIED, M., GRABHERR, G., Die Vegetation des Hochschwab — Alpine und Subalpine Stufe, *Mitt Naturwissen Verein Stmk.* **129** (1999) 111–251 (in German).
- [5] BERDEN, G., PEETERS, R., MEIJER, G., Cavity ring-down spectroscopy: Experimental schemes and applications (Review), *Int. Rev. Phys. Chem.* **19** 4 (2000) 565–607.
- [6] HEINER, W., Online-system for hydro-meteorological data transmission via LEO-satellites, Diploma Thesis, University of Applied Sciences Technikum-Wien, Vienna, (2005) (in German).
- [7] STADLER, H., SKRITEK, P., “Remote water quality monitoring ‘on-line’ using LEO Satellites”, *Proc. Int. Conf. on Automation in Water Quality Monitoring, Vienna* (2003) 155–162.
- [8] SKRITEK, P., PFLIEGL, R., “Near online vessel tracking on European waterways combining GPS and LEO-satellite transmission”, *Proc. ENC-GNSS2002 Conf., Amsterdam* (2002) CD-ROM.
- [9] ORBCOMM, Global M2M: Connecting the world’s assets, <http://www.orbcomm.com> (last visited 2011/01/20).
- [10] STADLER, H., et al., Microbiological monitoring and automated event sampling at karst springs using LEO-satellites, *Water Sci. Technol.* **58** 4 (2008) 899–909.

# RECHARGE RATES TO DEEP AQUIFER LAYERS ESTIMATED WITH $^{39}\text{Ar}$ , $^{85}\text{Kr}$ AND $^{14}\text{C}$ DATA: A CASE STUDY IN ODENSE (DENMARK)

R. PURTSCHERT

Climate and Environmental Physics,  
University of Bern, Switzerland

T.K. BJERRE, J. LINDERBERG

Odense Water,  
Odense, Denmark

K. HINSBY

Geological Survey of Denmark and Greenland (GEUS),  
Copenhagen, Denmark

## Abstract

The increasing pressure on groundwater resources due to overexploitation, contamination and also due to the effects of climate change leads to an increasing need and interest to investigate the recharge and flow dynamics of pre-modern groundwater (>50 a old). Knowledge about turnover times and groundwater age is crucial e.g. in vulnerability assessment studies as shallow and young groundwater is more susceptible to environmental changes than deeper and generally older groundwater. The presence and age of young water can be determined by a series of transient tracers (e.g.  $^3\text{H}/^3\text{He}$ , CFC's,  $\text{SF}_6$ , etc). However, with the need to exploit deeper unpolluted resources a tracer on timescales of hundreds of years is required.  $^{39}\text{Ar}$  ( $T_{1/2}$ : 269 a),  $^{85}\text{Kr}$  ( $T_{1/2}$ : 10.8 a) and  $^{14}\text{C}$  ( $T_{1/2}$ : 5730 a) results from 35 wells around the city of Odense (Denmark) are presented. The determined age spectra range from a few years to several hundreds of years. Based on the space–depth distribution of age gradients, renewal/recharge rates to the deep aquifer layers have been estimated. The comparison of  $^{39}\text{Ar}$  and  $^{14}\text{C}$  activities reveals a remarkably good correlation but with a distinct difference in age scale suggesting mixing due to broad age distributions and activity shifts due to rock–water interaction.

## 1. STUDY SITE

The investigated aquifer system is located in the central part the island of Funen, in the vicinity of the City of Odense (Fig. 1). The aquifer system has been used for water supply purposes for more than 100 years. Owing to increasing water quality problems in production wells in recent years, much attention has been given to the distribution of residence time in the aquifer system (e.g. Ref. [1]).

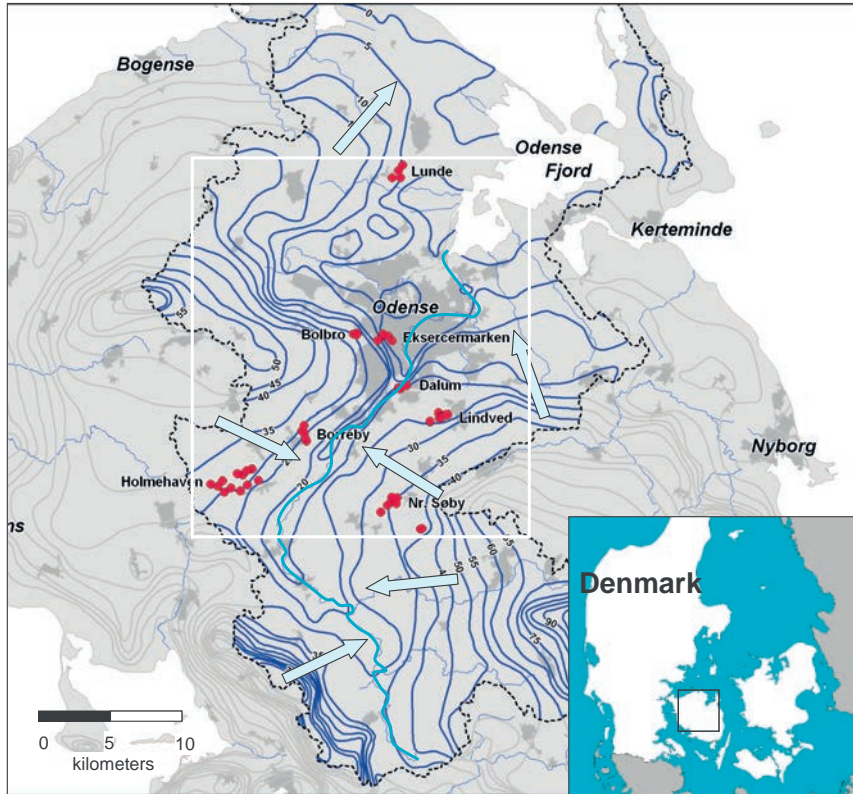


FIG. 1. Location of study area and sampled well fields (red dots). Main direction of groundwater flow (arrows) is towards the Odense river and the Odense Fjord. In blue, lines of constant groundwater head.

The main aquifers are found in semi-confined units of glacio-fluvial sand and gravel deposits at varying depths overlain by glacial till [2]. Tertiary marls and clay forms the lower boundary of the Quaternary aquifer system. The aquifer system is drained by Odense stream flowing in a northeasterly direction towards the sea. In most of the catchment area the sand/gravel units seem to be separated by glacial till of varying sand content. The extensive well log archive of lithological information shows that the geology of the quaternary deposits is rather complex and heterogeneous with interconnected hydrostratigraphic units with a typical thickness of 10–15 metres [2]. The catchment is characterized by an undulating surface cut by numerous tributaries and a relatively large topographical variation ranging from 2–120 metres within a radius of 10 km. Most of the area is artificially drained due to agricultural interests and the generally wet climate. Based on climatic records from 1991 to 2000, the yearly precipitation ranges from 580 to 1030 mm/a and the yearly potential evapotranspiration from 480 to 570 mm/a. Mean annual net precipitation is 390 mm and most of it (>90%) occurs in the cold season (Oct–Mar).

## 2. METHODS

During two field campaigns in 2008 and 2009, 35 wells from different well fields around the city of Odense were sampled for radio noble gases  $^{85}\text{Kr}$  and  $^{39}\text{Ar}$ ,  $^{14}\text{C}$ , stable isotopes and main chemical constituents.  $^{39}\text{Ar}$  is produced by the interaction of cosmic rays with nuclides of potassium and argon in the atmosphere. The resulting atmospheric equilibrium activity expressed as % modern in relation to recent air (100% modern) is unaffected by anthropogenic sources and constant at  $1.67 \times 10^{-2}$  Bq/m<sup>3</sup> of air [3], corresponding to an atmospheric  $^{39}\text{Ar}/\text{Ar}$  ratio of  $\sim 10^{-15}$ . With a half-life of 269 years,  $^{39}\text{Ar}$  fills the precision dating gap between the young residence time indicators (e.g.  $^3\text{H}$ - $^3\text{He}$ ,  $^{85}\text{Kr}$ ) and the radiocarbon method.

A possible complication is  $^{39}\text{Ar}$  produced in the subsurface due to neutron activation of potassium ( $^{39}\text{K}(\text{n,p})^{39}\text{Ar}$ ). If not considered in the age calculation this would lead to an underestimation of the calculated groundwater residence time.

$^{85}\text{Kr}$  is produced as a fission product of uranium and plutonium decay. Over the last 50 years the increasing release of  $^{85}\text{Kr}$  from nuclear fuel reprocessing plants (e.g. Sellafield, La Hague) has completely overwhelmed the natural activity of about  $10^{-7}$  Bq/cm<sup>3</sup><sub>STP</sub> Kr [4]. The current specific activity in the atmosphere is about 1.4 Bq/cm<sup>3</sup><sub>STP</sub> Kr or 80 dpm/cc Kr (decays per minute and cm<sup>3</sup><sub>STP</sub> krypton gas). The activities of the argon and krypton gas separated from groundwater is measured in high pressure proportional counters in an ultralow background environment [5] after gas purification by gas chromatographic methods [6].

Because of the low isotopic abundances of  $^{85}\text{Kr}$  and  $^{39}\text{Ar}$ , a relatively large amount of water (400 and >1500 litres for  $^{85}\text{Kr}$  and  $^{39}\text{Ar}$ , respectively) has to be degassed in the field to obtain a sufficient number of  $^{85}\text{Kr}$  and  $^{39}\text{Ar}$  atoms. The minimum detection level (MDL) for  $^{39}\text{Ar}$  is 3–10% modern for water volumes of 4–1.5 tons of air-saturated water respectively. The MDL of  $^{85}\text{Kr}$  including sampling and gas processing artefacts is  $\sim 1$  dpm/cc Kr.  $^{14}\text{C}$  samples were obtained by direct precipitation of TDIC dissolved in several tens of litres of water. For  $^{14}\text{C}$  analysis the precipitated  $\text{BaCO}_3$  was converted to  $\text{CO}_2$  by acidification and  $\text{CH}_4$  was synthesised for low level gas counting [7]. The achieved MDL is 0.5 pMC. Separate samples (1 L) were collected for  $^{13}\text{C}$  analysis by mass spectrometry.

## 3. RESULTS

### 3.1 $^{85}\text{Kr}$ and $^{39}\text{Ar}$ activities

The spatial and depth dependent distribution and activity ranges of  $^{39}\text{Ar}$  are shown in Fig. 2. Generally  $^{39}\text{Ar}$  activities decrease with depth with lowest values of  $\sim 40\%$  modern in 80 metres below surface. This corresponds to an uncorrected tracer age of up to 360 years. The mean activity depth gradient corresponds to a vertical

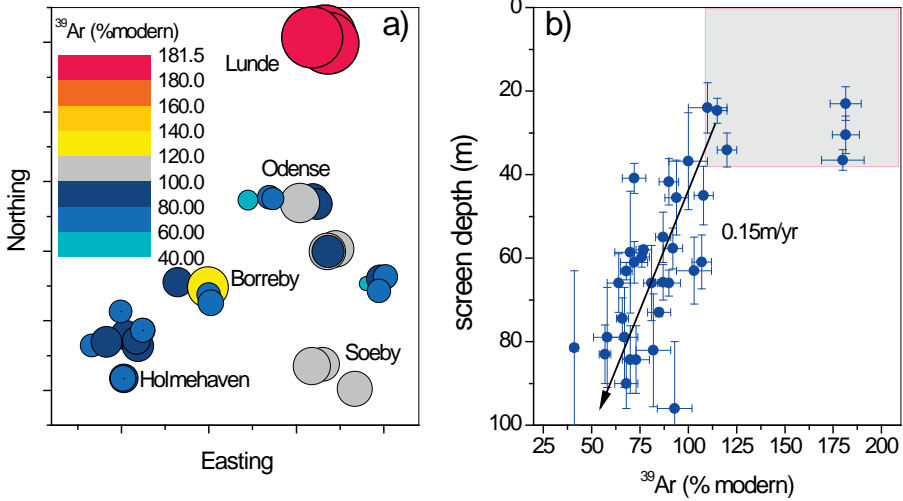


FIG. 2. (a) Spatial (compare with Fig. 2) and (b) depth related distribution of  $^{39}\text{Ar}$  activities. Three shallow samples from the Lunde well field and to a minor extent a sample in the Borreby well field show over-modern  $^{39}\text{Ar}$  values (activity and depth range indicated in grey in Fig. 2b). The arrow: average vertical flow velocity deduced from  $^{39}\text{Ar}$  age gradient.

seepage velocity of 0.15 m/a (arrow in Fig. 2). The  $^{85}\text{Kr}$  activities of all sampled wells (Fig. 3) are significantly depleted compared to the actual atmospheric level, indicating a minimal age of >20 years (Fig. 4c) or/and the admixture of old  $^{85}\text{Kr}$  free water components. In the upper part of the aquifer (<50 depth)  $^{85}\text{Kr}$  values range between the MDL and 14 dpm/cc Kr. Below 50 metres the water is mostly  $^{85}\text{Kr}$  free in accordance with depleted  $^{39}\text{Ar}$  values. There are, however, some exceptions, with  $^{85}\text{Kr}$  free waters in shallow depths and  $^{85}\text{Kr}$  active samples in the deeper part indicating mixing of water components of different ages.

Over modern  $^{39}\text{Ar}$  concentrations that are mainly observed in shallow depths and in the most northern well field near Lunde (Figs 1 and 2) where all three samples show values of ~180% modern are intriguing.

### 3.2. Radiocarbon dating

Seven selected wells were also sampled and analysed for  $^{14}\text{C}$  and  $\delta^{13}\text{C}$  concentrations.  $^{14}\text{C}$  activities range between 55 pMC and 39 pMC with a corresponding increase in  $\delta^{13}\text{C}$  from -14‰ to -11‰. Thus, the  $^{14}\text{C}$  variation is at least partly caused by dissolution of  $^{14}\text{C}$  dead carbonate originating from the aquifer rocks [8]. Bomb derived  $^{14}\text{C}$  [9] can be excluded based on  $^{85}\text{Kr}$  concentrations at or below the MDL.

## 4. DISCUSSION

The presence of over modern  $^{39}\text{Ar}$  activities in the northern part of the study area raises the question of how far the other samples are also affected by underground production. Final conclusions can only be drawn by means of detailed geophysical borehole logging and the analyses of the elemental composition of the different lithological units. The large range of  $^{39}\text{Ar}$  activities (40–180% modern) demonstrates that the strength of underground production varies spatially or with depth and is most pronounced in the Lunde area.

The quasi-linear correlation between  $^{14}\text{C}$  and  $^{39}\text{Ar}$  activities (Fig. 3) provides evidence that (i) aging causes a significant contribution to the concentration variation for both tracers and as a consequence (ii) that underground production of  $^{39}\text{Ar}$  is likely to be of minor importance in the southern part of the investigated area (it is unlikely that the subsurface neutron flux is linked with the carbon geochemistry). The lowest observed  $^{39}\text{Ar}$  values of ~40% modern defines an upper estimate of the subsurface equilibrium concentration, at least at that location.

After correcting for the carbon dilution effect [8] using the  $\delta^{13}\text{C}$  values and the simple mixing model of Ref. [11],  $^{14}\text{C}$  derived groundwater ages are nonetheless significantly older than the corresponding  $^{39}\text{Ar}$  piston flow ages (Fig. 3), a fact that has also been observed elsewhere [12, 13]. Three processes are believed to contribute to this discrepancy in our case: (i) diffusive exchange between the permeable sand zones with the less permeable silt layers or the underlying aquitards [10, 14], which have been observed to affect  $^{14}\text{C}$  dating results in other Danish aquifer systems

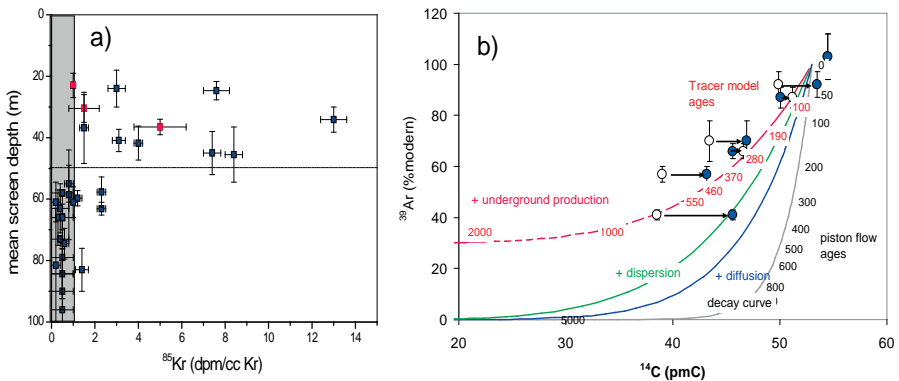


FIG. 3. (a)  $^{85}\text{Kr}$  activities as function of screen depth. The red samples correspond to the 'Lunde' samples with significant underground production. The grey shaded activity range corresponds to the methodological detection limit. (b) Measured  $^{39}\text{Ar}$  and  $^{14}\text{C}$  data (open symbols) for isotope dilution corrected values (solid symbols) and theoretical model curves cumulatively considering radioactive decay (grey line), diffusive exchange with stagnant zones using realistic parameters [2, 10] (blue line), dispersive mixing according DM2 in Fig. 4 (green line) and a secular underground  $^{39}\text{Ar}$  production equilibrium of 30% modern (red line).

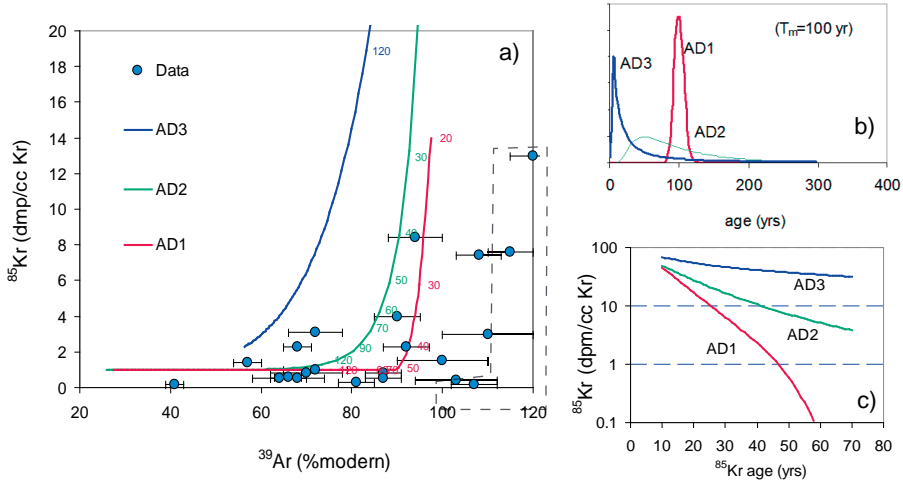


FIG. 4. Comparison of  $^{39}\text{Ar}$  and  $^{85}\text{Kr}$  activities for different strengths of dispersive mixing (or age distributions AD). The red curves (AD 1) represent low dispersion ('quasi-piston flow'), the green curve AD2 moderate dispersion and the blue curve very pronounced dispersion (AD3 'quasi-exponential model'). Labels in (a) indicate mean residence times. Samples within the dotted line (Fig. 4a) are suspicious for  $^{39}\text{Ar}$  underground production. (b) Examples of age distributions with mean residence time  $T_m=100$  years. (c)  $^{85}\text{Kr}$  values as a function of model age.

[17]. Mainly because of the shorter half-life of  $^{39}\text{Ar}$ , the resultant retardation for  $^{14}\text{C}$  is larger than for  $^{39}\text{Ar}$  causing a 'faster aging' of  $^{14}\text{C}$  compared to  $^{39}\text{Ar}$ . (ii) Mixing of different water components resulting in a broad age distribution. In particular in heterogeneous systems such as this one flow lines from different recharge areas (infiltration is spatially distributed) are mixed together when the water is extracted from extended screen intervals. As a first order approximation this effect can be parameterized by a dispersion model [15, 16] by means of a generalized dispersion parameter (Fig. 3b). If the age distribution AD2 is assumed, the disagreement between  $^{39}\text{Ar}$  and  $^{14}\text{C}$  ages is further reduced. (iii) Remaining deviations may be locally caused by underground production of  $^{39}\text{Ar}$  as indicated in Fig. 3b. The combined effects (i–iii: red line in Fig. 3) allows the consistent interpretation of the  $^{39}\text{Ar}$  and  $^{14}\text{C}$  data in terms of mean residence time (red labels in the figure) ranging up to 600 years.

Dispersive mixing and the resultant wide distribution of ages is also in accordance with the observed correlation of  $^{85}\text{Kr}$  and  $^{39}\text{Ar}$  activities (Fig. 4a). Whereas a piston flow scenario (AD1) contradicts with the presence of  $^{85}\text{Kr}$  in  $^{39}\text{Ar}$  depleted samples, AD2 is in agreement with most of the data pairs. For some samples the extreme mixing case AD3 has to be assumed.

## 5. CONCLUSIONS

Dating results of 35  $^{39}\text{Ar}$  and  $^{85}\text{Kr}$  and 7  $^{14}\text{C}$  samples from the quaternary sands aquifer in Odense have been presented. Activities of all tracers decrease with depth. The conclusive interpretation of tracer concentrations in terms of age or residence time requires the consideration of secondary effects, most importantly the dispersive mixing of different water components. Doing so results in mean residence times in the deepest wells of ~600 years in the frame of a model that assumes dispersion, diffusive exchange with stagnant zones and 30% modern underground production of  $^{39}\text{Ar}$ . Uncorrected  $^{39}\text{Ar}$  ages ranging up to 369 years define a lower age limit. The vertical seepage velocity ranges between 150 mm/a (with uncorrected  $^{39}\text{Ar}$  ages) and ~75 mm/a if the combined and corrected  $^{14}\text{C}$ - $^{39}\text{Ar}$  ages from Fig. 3b are used. With a mean aquifer porosity of 30% this corresponds to a spatially and temporally averaged recharge rate to the deep aquifer layers of ~50–25 mm/a. Because many wells were brought into operation in the recent past the system has not yet established a dynamic equilibrium and will likely evolve with time.

$^{39}\text{Ar}$  dating in the northern well field Lunde is impeded due to very high  $^{39}\text{Ar}$  production. The reason for this ‘hot spot’ is yet unknown and will be investigated further in the near future. The Lunde wells are supplied by water from a distinct recharge area (Fig. 1), are relatively shallow compared to most of the other wells and are nevertheless very low in  $^{85}\text{Kr}$  (red symbols Fig. 3). One hypothesis explaining this enhanced  $^{39}\text{Ar}$  values may be cosmic ray induced  $^{39}\text{Ar}$  production in this zone, which is shallow and decoupled from direct recharge.

## ACKNOWLEDGMENTS

This project was made possible thanks to the financial support of Odense Water. We wish also to thank Erik Borregaard Larsen and Jan Jæger for their professional joint effort and help throughout all sampling campaigns.

## REFERENCES

- [1] CORCHO ALVARADO, J.A., et al.,  $^{36}\text{Cl}$  in modern groundwater dated by a multi-tracer approach ( $^3\text{H}/^3\text{He}$ ,  $\text{SF}_6$ , CFC-12 and  $^{85}\text{Kr}$ ): A case study in quaternary sand aquifers in the Odense Pilot River Basin, Denmark, *Appl. Geochem.* **20** (2005) 599–609.
- [2] TROLDBORG, L., The influence of conceptual geological models on the simulation of flow and transport in Quaternary aquifer systems, PhD Thesis, Environment & Resources Techni- cal University of Denmark, Copenhagen (2004) 120 pp.
- [3] LOOSLI, H.H., A dating method with  $^{39}\text{Ar}$ , *Earth Planet. Sci. Lett.* **63** (1983) 51–62.

- [4] LEHMANN, B., LOOSLI, H.H., “Use of noble gas radioisotopes for environmental research”, Resonance Ionization Spectroscopy 1984 (Proc. Int. Symp. Knoxville, Tennessee, 1984) (HURST, G.S., PAYNE, M.G., Eds), Conference Series 71, The Institute of Physics, Bristol (1984).
- [5] LOOSLI, H.H., PURTSCHERT, R., “Rare Gases”, Isotopes in the Water Cycle: Past, Present and Future of a Developing Science (AGGARWAL, P.K., GAT, J.R., FROELICH, K., Eds), Springer, Dordrecht, The Netherlands (2005) 91–96.
- [6] CORCHO ALVARADO, J.A., et al., Constraining the age distribution of highly mixed ground- water using  $^{39}\text{Ar}$ : A multiple environmental tracer ( $^3\text{H}/^4\text{He}$ ,  $^{85}\text{Kr}$ ,  $^{39}\text{Ar}$  and  $^{14}\text{C}$ ) study in the semiconfined Fontainebleau Sands Aquifer (France), *Water Resour. Res.* **43** (2007).
- [7] OESCHGER, H., et al., “Recent progress in low level counting and other isotope detection methods”, Radiocarbon Dating: Proceedings of the Ninth International Conference, Los Angeles and La Jolla, 1976 (BERGER, R., SUESS, H.E., Eds), University of California Press, Los Angeles (1979).
- [8] FONTES, J.-C., “Chemical and isotopic constraints on  $^{14}\text{C}$  dating of groundwater”, Radiocarbon after Four Decades: An Interdisciplinary Perspective (TAYLOR, R.E., LONG, A., KRA, R.S., Eds), Springer, New York (1992) 242–261.
- [9] KALIN, R.M., “Radiocarbon dating of groundwater systems”, Environmental Tracers in Subsurface Hydrology (COOK, P., HERCZEG, A., Eds), Kluwer Academic, Boston (2000) 111–144.
- [10] SANFORD, W., Correcting for diffusion in carbon-14 dating of groundwater, *Ground Water* **35** (1997) 357–361.
- [11] INGERSON, E., PEARSON, F.J., Jr., “Estimation of age and rate of motion of groundwater by the  $^{14}\text{C}$ -method”, Recent Researches in the Fields of Hydrosphere, Atmosphere and Nuclear Geochemistry (MIYAKE, Y., KOYAMA, T., Eds), Maruzen, Tokyo (1964) 263–283.
- [12] LOOSLI, H.H., OESCHGER, H., Use of  $^{39}\text{Ar}$  and  $^{14}\text{C}$  for groundwater dating, *Radiocarbon* **22** (1980) 863–870.
- [13] ALTHAUS, R., ET AL., “Cross-border groundwater management: The contribution of deep groundwater to quaternary basins deduced from isotope data”, Advances in Isotope Hydrology and its Role in Sustainable Water Resource Management (IHS 2007) (Proc. Symp. Vienna, 2007), Vol. 2, Proceedings Series, IAEA, Vienna (2007) 111–120.
- [14] SUDICKY, E. A., FRIND, E.O., Carbon 14 dating of groundwater in confined aquifers: Implications of aquitard diffusion, *Water Resour. Res.* **17** (1981) 1060–1064.
- [15] ZUBER, A., MALOSZEWSKI, P., “Lumped parameter models”, Environmental Isotopes in the Hydrological Cycle: Principles and Applications, Vol. 6, IAEA/UNESCO, Vienna (2001) 497–515.
- [16] MALOSZEWSKI, P., ZUBER, A., “Lumped parameter models for the interpretation of environmental tracer data”, Manual on Mathematical Models in Isotope Hydrology, IAEA-TECDOC-910, IAEA, Vienna (1996) 9–58.
- [17] HINSBY, K., et al., “Use of isotopes ( $^3\text{H}$ ,  $^{14}\text{C}$ ,  $^{13}\text{C}$ ,  $^{18}\text{O}$ ) and CFCs for the analyses of groundwater flow and transport dynamics: Selected case and modelling studies from sand aquifers and a deep clay aquitard in Denmark”, Use of Isotopes for Analyses of Flow and Transport Dynamics in Groundwater Systems, IAEA, Vienna (2002) CD-ROM.

# USING ISOTOPE METHODS TO ASSESS GROUNDWATER RECHARGE IN SOME HYDRAULIC CATCHMENTS IN A SEMIARID REGION IN CENTRAL TUNISIA

K. ZOUARI, R. TRABELSI, A. KACEM

Laboratory of Radio-Analysis and Environment, ENIS,  
Sfax, Tunisia

## Abstract

Water resource issues constitute a major concern in arid and semiarid areas in Tunisia. To meet rising demand for different human activities considerable importance is being given to improving the natural groundwater recharge by the installation of hydraulic catchments. In central Tunisia, numerous retention sites and dams have been built since 1990, for example, the el Ogla dam in the Nadhour-Saouaf basin. In order to determine the implication of these hill reservoirs on the hydrodynamic functioning and water quality of the aquifer system, hydrochemical (major elements) and isotopic methods have been employed. The interpretation of these results showed that the shallow aquifer is recharged mainly by surface water and water dam infiltration from the el Ogla and Sahel catchments. A tentative isotopic mass balance based on stable isotope contents leads to the quantification of the artificial recharge rate, which ranges between 42% and 86% of precipitation in the humid period.

## 1. INTRODUCTION

The countries of the south of the Mediterranean Sea with semiarid climate are characterized by prolonged periods of dryness alternating with exceptional rainy episodes.

The temporal and spatial irregularity of precipitations in Tunisia and their potential variations in the future could have major hydrological impacts. Thus, in the centre of Tunisia, where precipitations are rare and intense, occurring mainly in autumn and spring [1], surface flows are very important. Since the natural recharge of the aquifer is discontinuous, an efficient management of the water resources in this region is required.

During 1990–2000, a strategy of mobilization and storage of surface water was planned in Tunisia in order to meet the water deficit during dry years and to satisfy water demand for different human activities. Accordingly a multitude of hydraulic catchments have been built in the centre of Tunisia [2], such as the el Ogla dam in the Nadhour-Saouaf basin.

In order to determine the implication of these hill reservoirs on the hydrodynamic functioning and the water quality of the aquifer system, hydrochemical (major elements) and isotopic methods have been employed.

2. STUDY AREA

The syncline of Nadhour-Saouaf is located at the centre of Tunisia between the latitudes 36° 04 and 36°15 N and longitudes 10° 00 and 10° 15 E. It represents a vast plain bordered by the reliefs of Ez zibidine and Toujjine, Fkirine, Bou slam, Krimir, Dghafra, Kef Naama, Klass, Mdeker and Garci (Figs 1–3). It is drained by a very dense hydrographic network consisting of wadis that originate on the slopes of the mountainous reliefs. The most significant wadis are el Ogla, the Sahel, Kseub and Zarzour (Fig. 1).

The study area is characterized by a semiarid climate with high spatial and temporal variation in rainfall. The average of precipitations is 350 mm/a in the plain of Nadhour and it increases with altitude to reach 450 mm/a in Saouaf located upstream of the basin. The annual average temperature varies between 18 and 20°C, the average moisture of the air varies between 60 and 70% and the potential evapotranspiration varies between 1400 and 1500 mm/a [3].

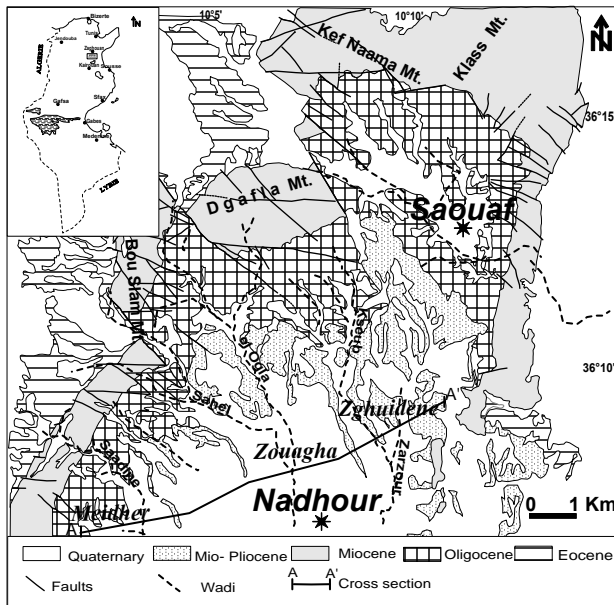


FIG. 1. Geological and location map of the study area.

### 3. GEOLOGY AND HYDROGEOLOGY

The Nadhour-Saouaf syncline recorded a delta-fluvial sedimentation organized as a set of sedimentary systems shaped by hydrodynamic regimes of waves, tides and rivers during the Oligocene [4]. However, in the late Miocene, major folds have resulted in a stop in the brackish-lagoonal sedimentation at the heart of the syncline. Thus, continental sediments of the Mio-Plio-Quaternary unconformably overlie the earlier deposits [5]. This basin is affected by faults of NW–SE direction [6].

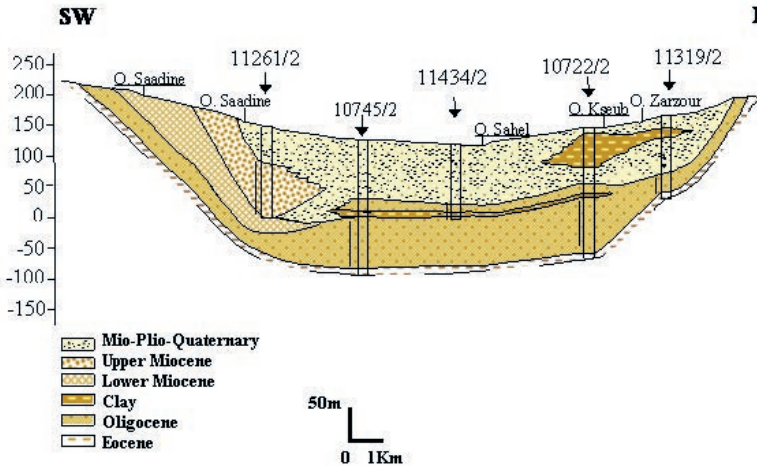


FIG. 2. Schematic cross section (AA') through the basin of Nadhour-Saouaf.

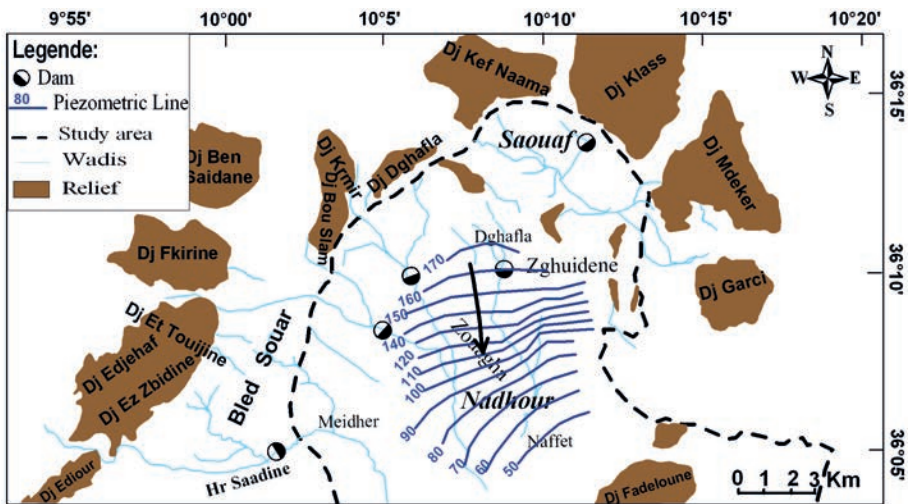


FIG. 3. Potentiometric map of the shallow aquifer of the Nadhour-Saouaf basin (January 2004).

The filling of the Nadhour-Saouaf basin by permeable deposits, with semi permeable caused by the wadis following the Oligocene one, explains the presence of several aquifer levels which constitute a lenticular system (Fig. 2). This study will focus on the shallow aquifer of this system.

The shallow aquifer is logged in the Mio-Plio-quadernary clayey sand deposits and gravel alternations, sands and clay. However, in the extreme north of the study basin, in the area of Saouaf, this aquifer is absent. The piezometric level of the shallow aquifer measured in January 2004 varies from 170 m to 50 m (Fig. 3).

#### 4. SAMPLING AND ANALYTICAL METHODS:

The location of collected water samples is presented in Fig. 4. Chemical analysis of major elements was carried out on five water samples from surface water and 10 samples from shallow wells (sampling in June 2004). These analyses were established by ionic chromatography in liquid phase at the Laboratory of Radio-analysis and Environment (LRAE) of the National School of Engineers of Sfax (Tunisia).

Stable isotopes ( $^{18}\text{O}/^2\text{H}$ ) were measured in a humid (December 2004) and a dry period (June 2004). These analyses were made by mass spectrometry and the results are expressed in ‰ compared to the international standard V-SMOW. Analytical uncertainties are of  $\pm 0.2\text{‰}$  for oxygen-18 and  $\pm 2\text{‰}$  for deuterium. The Carbon-14 activities measured on 9 samples by liquid scintillation on the  $\text{CO}_2$  obtained by the acid attack of  $\text{BaCO}_3$ , were analysed at the LRAE.

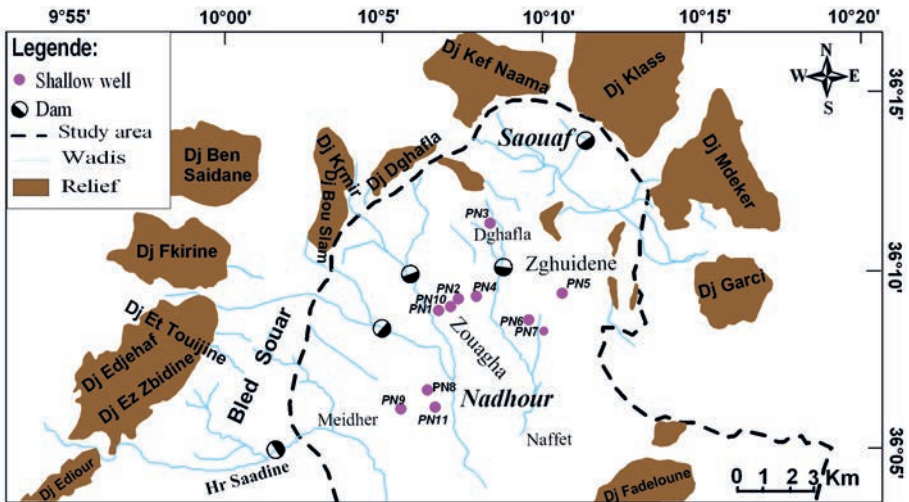


FIG. 4. Location of sampling points in Nadhour-Saouaf Basin.

## 5. RESULTS AND DISCUSSION

### 5.1. Hydrochemistry data

Chemical analyses of groundwater samples show that the total mineralization of the shallow aquifer varies between 700 mg/L and 3700 mg/L.

Downstream of El Oglâ dam groundwater salinity exceeds 2000 mg/L. This could be explained by an infiltration of relatively saline water (2490 mg/L) from the el Oglâ dam towards the shallow aquifer of Nadhour. The infiltration of this water could modify the chemical quality of groundwater such as in the case of the el Gouazine catchment located in central Tunisia, in the northwest of Kairouan [2].

The highest value of mineralization is measured in the region of Dghafâ. This high salinity of about 3700 mg/L is related to a variation in the lithological formation of the shallow aquifer. Although the depth of this well does not exceed 50 m, it collects a deep aquifer level assigned to the marine Miocene. The chemical water type of the shallow aquifer (Fig. 5) is  $\text{SO}_4\text{-Ca-Na}$ , which could be affected by the el Oglâ Dam characterized by the  $\text{SO}_4$  water type.

### 5.2. Isotopic study

The local meteoric line was calculated using precipitations higher than 5mm in the El Oglâ basin [7] by imposing a theoretical slope of 8 reflecting the thermodynamic equilibrium during condensation [8]. The equation of this local meteoric line is  $\delta^2\text{H} = 8 \delta^{18}\text{O} + 10.75$ .

According to the correlation diagram  $\delta^{18}\text{O}/\delta^2\text{H}$  (Fig. 6), the shallow groundwater and surface water of Nadhour are plotted under the local Meteoric water line. This suggests that these water samples are largely derived from evaporated rainwater and runoff. The isotopic composition of water dams presents a wide range of variation. The  $^{18}\text{O}$  and deuterium contents of the water collected in December 2004 vary between  $-1.01$  to  $-3.85\%$  in oxygen-18, and between  $-28$  and  $-9.9\%$  in deuterium. Moreover, the shallow aquifer groundwater presents an intermediate composition between that of the mean rainfall and dam water. In fact, they are aligned along a mixture line of equation  $\delta^2\text{H} = 5.39 \delta^{18}\text{O} - 5.09$  ( $n = 11$ ,  $r^2 = 0.98$ ).

In order to quantify the contribution of Dam water to the recharge of the shallow aquifer, the binary mixing equation was used:

$$\delta^{18}\text{O}_s = \delta^{18}\text{O}_B T_B + \delta^{18}\text{O}_P T_P$$

where  $\delta^{18}\text{O}_s$ ,  $\delta^{18}\text{O}_B$  and  $\delta^{18}\text{O}_P$  are the respective isotopic composition of shallow groundwater, of dam water and of rain water.  $T_B$  and  $T_P$  represent respectively the contribution of dam water and rainwater to the recharge of the shallow aquifer with  $T_B + T_P = 1$ .

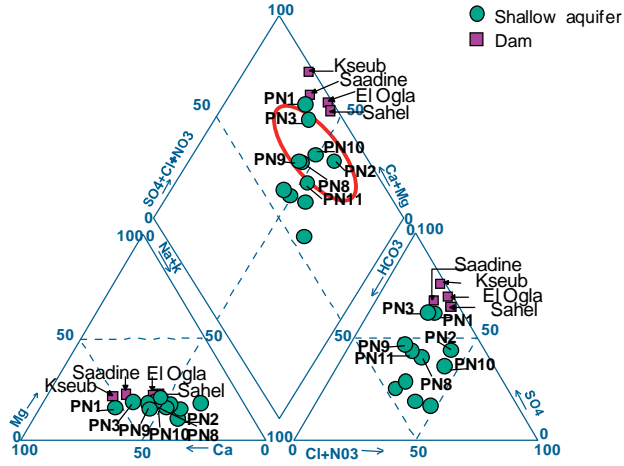


FIG. 5. Piper diagram of groundwater and surface water in the Nadhour-Saouaf basin.

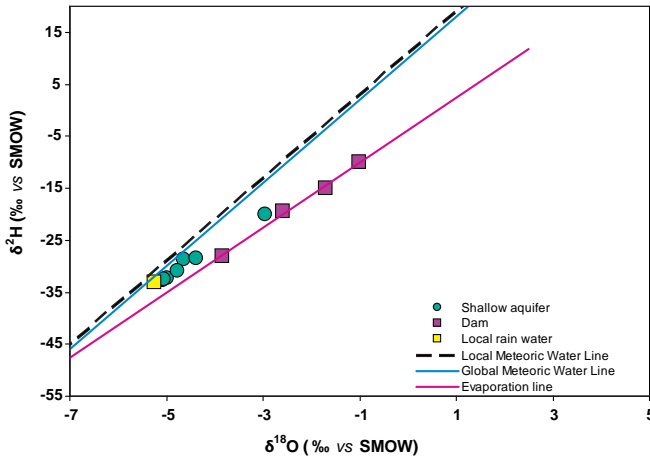


FIG. 6.  $\delta^{18}O/\delta^2H$  diagram of groundwater and surface water in Nadhour-Saouaf basin.

The assessment of this equation shows that the contribution of these dam waters to the recharge of the shallow aquifer is variable in time and space. It indicates that during the dry period (June 2004), dams do not contribute to the groundwater recharge, except for the well PN1, which shows a relatively small contribution (31%) of the El Ogla dam. However, during the wet season (December 2004), the contribution of these dams is significant. The participation of El Ogla dam in the recharge of the shallow aquifer reaches 86% (PN1). Furthermore, the contribution of the Sahel

dam is of less importance where it varies between 42 and 62%. However, the contribution rate of el Kseub dam does not exceed 7%.

The contribution of dam water to the recharge of the shallow aquifer becomes increasingly smaller while moving away from these catchments towards the downstream of the basin.

The carbon-14 activity measured in the water of the groundwater varies between 40 and 100 pMC. These relatively high activities of carbon-14 prove a recent contribution by infiltration of surface waters from el Ogla and Sahel to the recharge of the shallow aquifer.

## 6. CONCLUSION

The use of the hydrogeochemical tools allowed us to understand the overall functioning of the aquifer system of Nadhour-Saouaf and to characterize the relation between surface water and groundwater.

The chemical analyses show that the shallow groundwater is of the type  $\text{SO}_4\text{-Ca-Na}$ . The inversion of salinity gradient in this aquifer compared to the flow direction is explained by the infiltration of salt water from the El Ogla dam.

The stable isotope contents ( $^{18}\text{O}/^{16}\text{O}$ ) confirm the recharge of the shallow aquifer from El Ogla and the Sahel dam water. Their contribution to the recharge varies between 42 and 86% in the wet period. Moreover, the high carbon-14 activity downstream of the el Ogla dam confirms the hypothesis of the inversion of the salinity gradient as the result of a contamination by evaporated salt water of hydraulic catchments in the north of the basin.

## ACKNOWLEDGEMENTS

This study was carried out within the framework of the technical cooperation IAEA project TUN/8/019.

## REFERENCES

- [1] SLIMANI, M., CUDENNEC, C., FEKI, H., Structure du gradient pluviométrique de la transition Méditerranée-Sahara en Tunisie: déterminants géographiques et saisonnalité, *Hydrological Sciences Journal* **52** 6 (2007) 1088–1102.
- [2] MONTOROI, J.-P., GRÜNBERGER, O., NASRI, S., Groundwater geochemistry of a small reservoir catchment in Central Tunisia, *Appl. Geochem.* **17** (2002) 1047–1060.
- [3] HENIA, L., Climat et bilan de l'eau en Tunisie: Essai de régionalisation climatique par les bilans hydriques, Doctorat d'Etat, Université de Tunis, Tunisia (1993).

- [4] TURKI, M., SAADI, M., ZAGBIB- TURKI, D., RAMI, A., Notice explicative de la carte géologique de la Tunisie à 1/50.000: Jebibina et Ain Jelloula, Feuilles N° 48 et 55, Office National des Mines, Direction du service Géologique (2002) 34–37.
- [5] MENCIK, E., STRANIK, Z., SALAJ, J., Notice explicative de la carte géologique de la Tunisie à 1/50.000: Dj Fkirine, Feuille N° 42, Direction des Mines et de la géologie. Sous- Direction de la Géologie (1978) 47–48
- [6] HAMZA, M., Géologie du bassin sédimentaire de Sisseb El Alem, Direction Générale des Ressources en Eau, Tunis, Tunisie, Ministère de l’Agriculture, Tunisia (1992).
- [7] GAY, D., Fonctionnement et bilan de retenues artificielles en Tunisie: Approche hydrochimique et isotopique, Doctoral Thesis, University of Paris XI, Orsay (2004) 156.
- [8] CRAIG, H., Isotopic variations in meteoric waters, *Science* **133** (1961) 1702–1703.

# ISOTOPIC COMPOSITION AND AGE OF SURFACE WATER AS INDICATORS OF GROUNDWATER SUSTAINABILITY IN A SEMIARID AREA: CASE OF THE SOUSS BASIN (MOROCCO)

L. BOUCHAOU<sup>a</sup>, T. TAGMA<sup>a</sup>, W. NATHANIEL<sup>b</sup>, J.L. MICHELOT<sup>c</sup>,  
S. BOUTALEB<sup>a</sup>, Y. HSISSOU<sup>a</sup>, M. MASSAULT<sup>c</sup>, A. VENGOSH<sup>b</sup>,  
M. ELFASKAOU<sup>d</sup>

<sup>a</sup> LAGAGE Laboratory, Ibn Zohr University,  
Agadir, Morocco

<sup>b</sup> Duke University, USA

<sup>c</sup> UMR 'IDES', CNRS - Université Paris-Sud,  
Orsay, France

<sup>d</sup> Hydraulic Agency of Souss-Massa-Draa basins,  
Agadir, Morocco

## Abstract

This study aims to determine the surface water and groundwater interconnection in the Souss catchment of western Morocco by applying multiple isotopic tracers such as  $\delta^{18}\text{O}$ ,  $\delta^2\text{H}$ ,  $^3\text{H}$ , Ra,  $^{14}\text{C}$ ,  $^{87}\text{Sr}/^{86}\text{Sr}$  and CFCs. Stable water isotope data indicate that the High Atlas Mountains, with their high rainfall and low  $\delta^{18}\text{O}$  and  $\delta^2\text{H}$  values, constitute the major source of recharge to the Souss-Massa aquifer. Carbon-14 activities (34–94 pMC) and  $^3\text{H}$  indicate a long residence time of groundwater in some areas. The high  $^{14}\text{C}$  activities measured in the Ifni spring located at 2158 m a.s.l. and the Tiar spring at 711 m a.s.l. indicate a modern contribution, which is consistent with recharge from the High Atlas tributaries. In the upstream mountainous section, the mass balance mixing model suggest that groundwater contribution to stream flow is about 72% during the wet season and 36% during the dry season. In the downstream plain, 80% of surface flow infiltrates to the aquifer.  $^{226}\text{Ra}$  and  $^{87}\text{Sr}/^{86}\text{Sr}$  variations were indistinguishable for surface waters and groundwater.

## 1. INTRODUCTION

The Souss basin is located in western Morocco, between the High Atlas Mountains in the north and the Anti-Atlas Mountains in the south (Fig. 1). The climate is semiarid to arid and the rainy season extends from November to March and

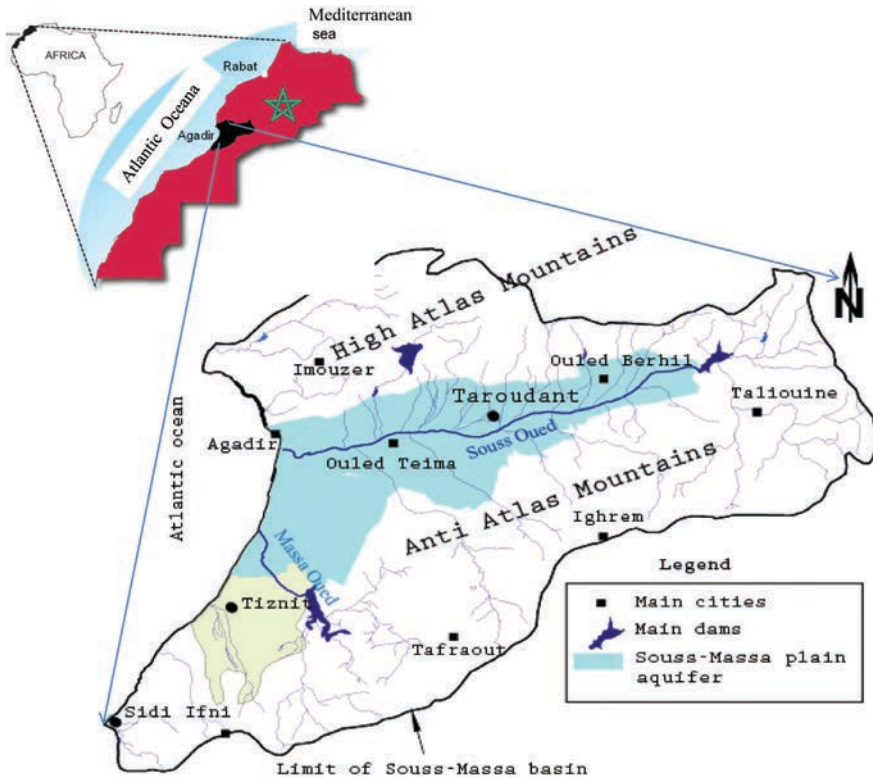


FIG. 1. Situation and geographical context of the Souss catchment.

the dry season from April to October. The rainfall and the average runoff vary in time and space, ranging from 200 mm/a in the plains (mean altitude: 460 m a.s.l.) to 600 mm/a in the mountains (altitude >700 m a.s.l.). The main Oued (wadi) in this basin is the Souss Oued, which has an intermittent flow regime, due to the length of the dry season (typically 6 to 8 months) every year. It receives many important tributaries, in particular from the High and Anti Atlas Mountains. The flow coming from a high altitude (rain and snowmelt) infiltrates in the piedmont area and in the beds of rivers, which is composed of high permeable conglomerate sediments. The plain hosts a large number of wells (more than 20 000) with depths varying from a few metres to nearly 300 m. Most of these wells, which penetrate a multilayered unconfined aquifer, are drilled into Plio-Quaternary sands and gravels and pump groundwater mostly for irrigation (94%). The exploitation rates, which are required to meet the increasing demands of the current agricultural practices, exceed the natural replenishment of these basins and have resulted in depletion of the groundwater resources and degradation of their quality.

In order to improve the management of water resources, several studies [1–3] were carried out in order to provide a better understanding of the hydrological system of the aquifer and to evaluate the relationship between surface runoff (rivers and dams) and groundwater. This paper reports a geochemical and isotopic investigation in the Souss catchment that utilizes tracers such as  $\delta^{18}\text{O}$ ,  $\delta^2\text{H}$ ,  $^3\text{H}$ , Ra,  $^{14}\text{C}$  and  $^{87}\text{Sr}/^{86}\text{Sr}$ . This study is focused mainly on the Souss River catchment in the southern margin of the High Atlas Mountains.

## 2. METHODS

Water samples were collected during several campaigns from surface water bodies (dams and rivers), wells, boreholes and springs in various parts of the basin, and were analysed for their chemical and isotopic compositions. Chemical and isotopic analyses were carried out in several laboratories including the Applied Geology and Geo-Environment Laboratory of the University of Agadir (Morocco), the IDES Laboratory of Paris-Sud University, Orsay, Paris (France), the IAEA laboratory in Vienna, Duke University (USA) and CNESTEN, Rabat (Morocco).

## 3. RESULTS AND DISCUSSION

The overall results are considered in relation to the flow direction along the river. The flow direction is from east to west towards the Atlantic Ocean.

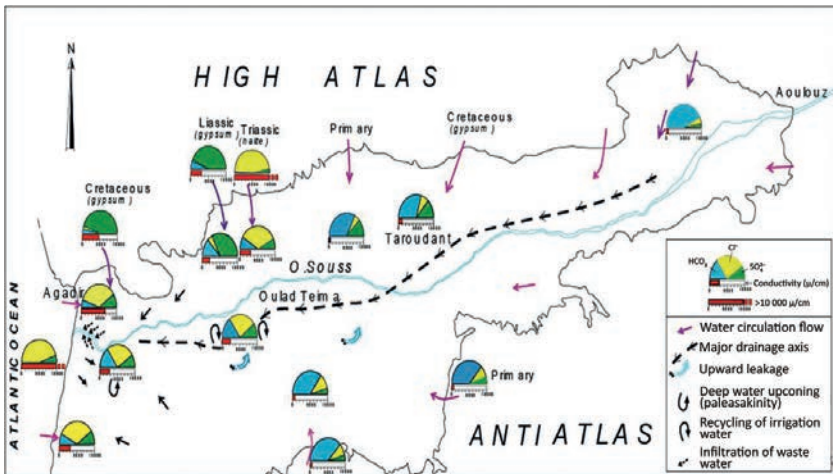


FIG. 2. Spatial distribution of water types in the Souss aquifer [4].

### 3.1. Chemical water types

A general evolution of major ion concentrations and overall salinity displays an increase in mineralization from the upstream to downstream sections.

This data indicates that:

- The mineralization of groundwater increases through interaction with limestone formations in the basin, which is a major process that affects the overall water chemistry in the upstream part of the basin.
- An influence of salt dissolution and sea water intrusion is observed in the downstream section of the aquifer. This observation is in concordance with the water types and geological formations of the Atlas Mountains, indicating that the water recharge is originating from the Atlas Mountains in the north.
- The presence of high nitrate concentration reflects the extensive impact of agriculture and recharge from irrigation return flows along the valley, thus inferring recycling of the water through pumping and irrigation, which is another component of the hydrological balance.

### 3.2. Isotopic characterization and origin of water

The  $\delta^2\text{H}$  ( $-56.8$  to  $-8.4\text{‰}$ ) and  $\delta^{18}\text{O}$  ( $-8$  to  $-0.5\text{‰}$ ) values vary along the global Meteoric Water Line (Fig. 3), which is consistent with the composition of local precipitation. This spatial variability may be caused by evaporation, altitude and seasonal effects of the recharge waters that recharge to the groundwater. The results show large and significant variations of  $\delta^2\text{H}$  and  $\delta^{18}\text{O}$  values during the period of investigation.

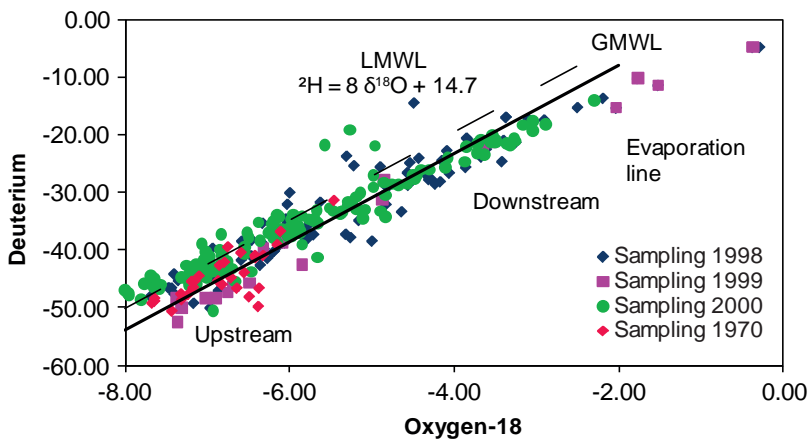


FIG. 3. Variation of stable isotopes (in ‰) from upstream to downstream along the Souss River compared to LMWL and GMWL [5].

In Fig. 3, most water samples plot close to the Global Meteoric Water Line (GMWL) and the Local Meteoric water line (LMWL). The more negative values are found in the upstream part (high altitude) while the most positive values are found in the downstream part. Hydrogen and oxygen isotope signatures reveal a significant infiltration of surface water before evaporation, indicating recharge through fractures in Atlas Mountain crystalline and limestone rocks and infiltration of surface water along rivers and/or in the alluvial cones at the margin of the Atlas basins. Stable isotopes indicate that the High Atlas Mountains, with their high rainfall and low  $\delta^{18}\text{O}$  and  $\delta^2\text{H}$  values ( $-6$  to  $-8\text{‰}$  and  $-36$  to  $-50\text{‰}$ ), constitute the major source of recharge to the Souss Basin while the contribution of precipitation in the plain itself, with its higher  $\delta^{18}\text{O}$  and  $\delta^2\text{H}$  values, is negligible.

According to the previous studies [1, 2], the  $^3\text{H}$  and  $^{14}\text{C}$  data suggest that the mean residence time (MRT) of water in the Souss aquifer ranges from the present to several thousands of years; hence old water is mined, particularly in the deep section of the aquifer towards the downstream. In the upstream part, carbon-14 activities (34–94 pMC) indicate a variable residence time. The  $^{14}\text{C}$  activities of 94 pMC measured upstream show a modern contribution, which also indicates the recharge effect from High Atlas tributaries.

Since tritium activities in present day precipitation in the region are not known, we used the surface water tritium signature as a representative of the modern meteoric signal, in the range of 5 to 10 TU [6]. As the water recharges vertically within the

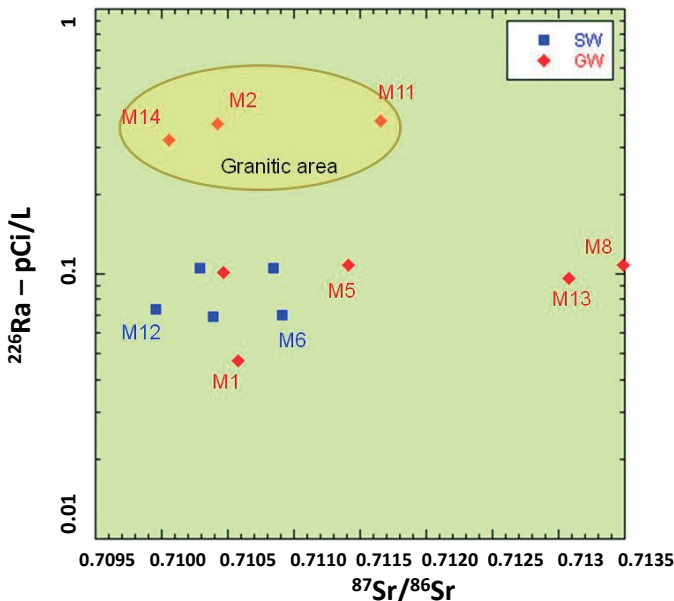


FIG. 4. Relationship between  $^{226}\text{Ra}$  and  $^{87}\text{Sr}/^{86}\text{Sr}$  in the upstream part of the Souss basin.

basin and laterally from the recharge zone adjacent to the aquifer basins, the tritium activities are expected to decrease with time. In contrast to the surface water, most of the groundwater samples have very low tritium, which indicates that both the vertical and lateral recharge process are longer than about 30 years, particularly in the shallow aquifer of the Souss plain. The lack of high tritium activities in groundwater suggests that the 1960s tritium peak [7, 8] has already diminished in that groundwater system. Alternatively, if all groundwater samples were very young (of the last decade), one would expect to have tritium levels similar to those measured in the surface waters. The values of CFCs measured in the two sites of the catchment indicate water recharge post 1945. The apparent residence time clearly indicates a mixing of old and recent contributions to stream flow, which confirms the results of stable and age dating isotopes.

In Fig. 4, data of  $^{226}\text{Ra}$  and  $^{87}\text{Sr}/^{86}\text{Sr}$  values are presented. These relationships show similar values in surface waters and groundwater. This similarity could be explained by hydraulic connection of stream flow and groundwater. Elevated Ra activities are associated with radiogenic values of  $^{87}\text{Sr}/^{86}\text{Sr}$  in granitic areas. This association indicates the sensitivity of these tracers for elucidating the nature of the aquifer rocks in which groundwater is in chemical equilibrium.

#### 4. CONCLUSION

This study presents the results of several isotopic and age dating isotopic tools in an attempt to reveal the origin of recharge water and the residence time of surface and groundwater resources in the semiarid area of the Souss Basin in western Morocco. The data indicate that the High Atlas Mountains constitute the main recharge area of the Souss catchment. Tritium and  $^{14}\text{C}$  data revealed modern and old groundwater in the contribution to baseflow. The presence of CFCs indicates a post-1945s recharge component. The apparent MRT clearly indicates a mixing of old and recent contributions to stream flow.

$^{226}\text{Ra}$  and  $^{87}\text{Sr}/^{86}\text{Sr}$  show indistinguishable values between surface water and groundwaters and are sensitive to the type of the aquifer lithology. Mass balance mixing model results suggest a significant contribution of groundwater to the stream flow. All the indicators suggest that the water resources in the studied area are very vulnerable to contamination processes.

The results of this study (recharge areas, residence time estimation), should be used not only to conceptualize, but should also be applied to calibrate groundwater flow models carried out by the Hydraulic department in Morocco. These factors should be taken into consideration in future water management plans.

## ACKNOWLEDGMENTS

This work is supported by CRP n 12893, NATO project (ESP.Md.SFP 983134) between Duke University (USA) and Ibn Zohr University (Morocco) and CNRS-CNRST cooperative project between LAGAGE laboratory (Agadir, Morocco) and IDES laboratory (Orsay, Paris, France).

## REFERENCES

- [1] BOUCHAOU, L., et al., Application of multiple isotopic and geochemical tracers for investigation of recharge, salinization, and residence time of water in the Souss-Massa aquifer, southwest of Morocco, *J. Hydrol.* **352** (2008) 267–287.
- [2] BOUCHAOU, L., et al., “Isotopic study of the relationship between surface water and groundwater under a semi-arid climate: Case of Souss-Massa basin (South-Western Morocco)” *Groundwater and climate in Africa* (TAYLOR, R., TINDIGMWA, C., OUOR, M., SHAMSUDDUHA, M., Eds), IAHS Red Book series **334** (2009) 76–81.
- [3] DINDANE, K., et al., Hydrochemical and isotopic characteristics of groundwater in the Souss Upstream Basin, southwestern Morocco, *J. African Earth Sci.* **36** (2003). 315–327.
- [4] HSISSOU, Y., et al., Use of chemical tracing to study acquisition modalities of the mineralization and behaviour of unconfined groundwaters under a semi-arid climate: The case of The Souss plain (Morocco), *Env. Geol.* **42** (2002) 672–680.
- [5] ROZANSKI, K., et al., “Isotopic patterns in modern global precipitation”, *Climate Change in Continental Isotopic Records* (SWART, P.K., et al., Eds), *Geophysical Monograph Series Vol. 78*, AGU, Washington, D.C.(1993) 1–36.
- [6] INTERNATIONAL ATOMIC ENERGY AGENCY, WORLD METEOROLOGICAL ORGANIZATION, *Global Network of Isotopes in Precipitation, The GNIP Database* (2004) <http://www.iaea.org/water>.
- [7] MICHEL, R.L., “Tritium in the hydrologic cycle”, *Isotopes in the Water Cycle: Past, Present and Future of a Developing Science* (AGGARWAL, P.K., GAT, J.R., FROEHLICH, K., Eds), Springer, Dordrecht, The Netherlands (2005) 53–66.
- [8] PLUMMER, L.N., “Dating of young groundwater”, *Isotopes in the Water Cycle. Past, Present and Future of a Developing Science* (AGGARWAL, P.K., GAT, J.R., FROEHLICH, K., Eds), Springer, Dordrecht, The Netherlands (2005) 193–218.



# ISOTOPES TRACING THE WATER CYCLE IN THE PAMPEANO AQUIFER AT THE SOUTHEAST OF BUENOS AIRES PROVINCE, ARGENTINA

D.E. MARTÍNEZ<sup>a,b</sup>, O.M. QUIROZ LONDOÑO<sup>a,b</sup>, E. BOCANEGRA<sup>a</sup>,  
H.E. MASSONE<sup>a</sup>, C. DAPEÑA<sup>b</sup>

<sup>a</sup> Instituto de Geología de Costas y del Cuaternario,  
U.N. de Mar del Plata, Argentina

<sup>b</sup> Consejo Nacional de Investigaciones Científicas y Técnicas, CONICET,  
Buenos Aires, Argentina

## Abstract

A sedimentary sequence of loess-like Quaternary deposits, with a thickness ranging from a few metres to about 100 m, covers about 1 500 000 km<sup>2</sup> in the Argentine Pampas. These deposits, named the Pampeano Sediments, constitute the main groundwater resource for the sustainability of agricultural production in Argentina. An isotope hydrology survey was carried out on a catchment area of about 10 000 km<sup>2</sup> covered by these sediments in order to improve the understanding of the hydrological cycle. Since 2005, stable isotopes (<sup>2</sup>H, <sup>18</sup>O) have been determined in: (a) rainwater collected at three points in the basin; (b) stream water continuously sampled weekly at three points in the main river; and (c) groundwater samples. Furthermore, <sup>3</sup>H concentration was determined in nearly 50 samples. Results show a seasonal effect in precipitation and the weighted average values as characteristic recharge water. A numerical flow model using the code MODFLOW was developed simultaneously and the isotopic results used to validate it. Groundwater is homogenous in its isotope composition indicating a dispersive flow model. Dominance of baseflow in the streamflow composition is another conclusion of the study.

## 1. INTRODUCTION

Pampa is the geographical denomination for a large plain in Argentina (Fig. 1) occupying about 1 500 000 km<sup>2</sup>. This large region was covered during the Pleistocene by loess deposits and loess-like silt and silt-sandy sediments transported by winds, mostly of SW-NE direction. The sequence of loessic sediments receives the generic denomination of Pampean Sediments [1]. A very important characteristic of these deposits is that they constitute aquifer systems which support about the 70% of the national GDP.

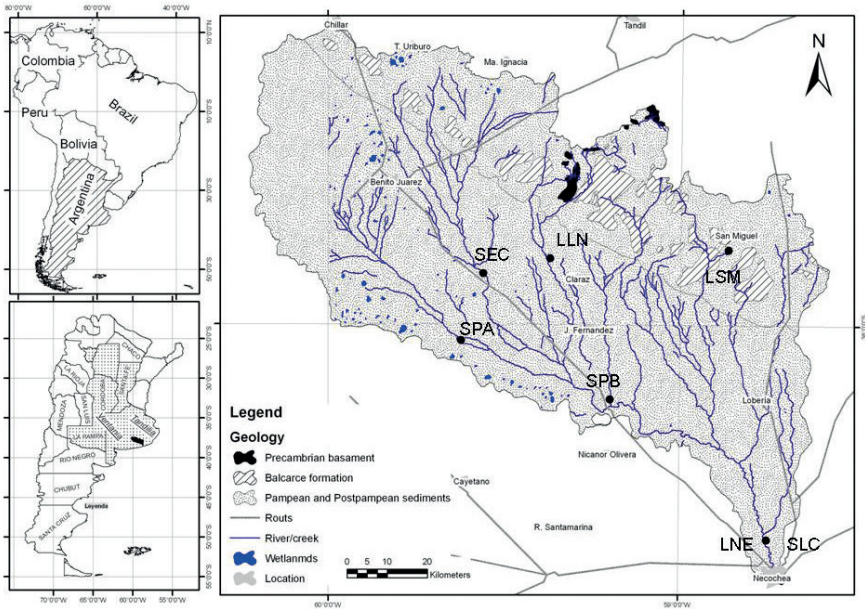


FIG. 1. Location of the Quequén Grande River catchment in the Buenos Aires province.

The Pampeano Sediments have sometimes been characterized as aquitards or poor-yield aquifers [2] because of the grain size distribution of the sediments. However, in practical terms, these sediments form widely distributed phreatic aquifers, sometimes with a thickness above 100 m, giving transmissivity values of up to 1400 m<sup>2</sup>/d [3]. Several groundwater flow models covering different areas of the Pampeano Aquifer System have been developed [3]. Additionally, solute transport models have been developed considering chemical element distribution in several sectors of the aquifer system [5].

In this contribution the results of a large isotope monitoring project, carried out as a part of an IAEA CRP, are coupled with a numeric flow model in order to improve the understanding of the aquifer systems and the consolidation of conceptual models. The study area is the catchment of the Quequén Grande River (QGR), located at the southeast of Buenos Aires province (Fig. 1) and occupying an area of 10 000 km<sup>2</sup>.

This catchment is a sedimentary basin located between the outcrop of two Paleozoic systems called Tandilia and Ventania (Fig. 1). The basin is filled with Pampeano Sediments, reaching a maximum thickness of 296 m near the coastal line. This large volume of sedimentary deposits form a shallow unconfined aquifer that is closely linked to surface waters [6].

## 2. METHODOLOGY

In order to characterize the isotopic composition of the different components of the local water cycle in the catchment, a sampling network was designed and developed, including three monthly composite rain water sampling points (LNE, LSM and LLN), five weekly stream water sampling points (SLC, STA, SPB, SPA and SEC) and a variable number of groundwater sampling points with a seasonal frequency (Fig. 1). The water isotope monitoring programme started in January 2005, resulting in about five years of continuous sampling, which constitutes an extraordinary record for a Latin American catchment. Isotope measurements were carried out at the Instituto Nacional de Geocronología y Geología Isotópica (INGEIS), in Buenos Aires. Stable isotopes  $^2\text{H}$  and  $^{18}\text{O}$  were analysed with a mass spectrometer Finnigan MAT Delta S. The results are expressed as isotopic deviations vs. Vienna Standard Mean Ocean Water (V-SMOW). Since 2007, stable isotope analyses are carried out by laser spectrometry using a Los Gatos Research LT-100 analyser at the Laboratory of the Hydrogeology Group of the National University of Mar del Plata.

On the other hand, a mathematical flow model was developed by using MODFLOW code [9]. The base map was imported from a (dxf) file containing the catchment contour and the stream network. A  $100 \times 100$  regular grid was discretized. The aquifer was modelled as one layer and the top and the bottom of the aquifer were obtained from surface maps. The model was calibrated using 60 observation wells. Hydraulic conductivity was distributed in 7 zones corresponding to geomorphologic zones, with values ranging from 1 to 30 m/d. A constant level condition of 0 m was stated at the coastal line. No flow boundaries were set on the east and west water divides. The streams' conductance was obtained from the equation:

$$C = LWK/M$$

where  $L$  is the cell length (1500 m assigned),  
 $W$  is the width of the river, variable from few metres to 100 m at the outlet into the ocean,  
 $K$  is the hydraulic conductivity of the river bed =  $2 \times 10^{-3}$  m/d,  
 $M$  is the thickness of the river bed = 0.1 m.

## 3. RESULTS

### 3.1. Stable isotope characterization

Rainwater isotopic composition was monitored through monthly composite precipitation samples. A previous isotope characterization of precipitation was carried out in the area [7] showing some differences in the weighted mean isotope

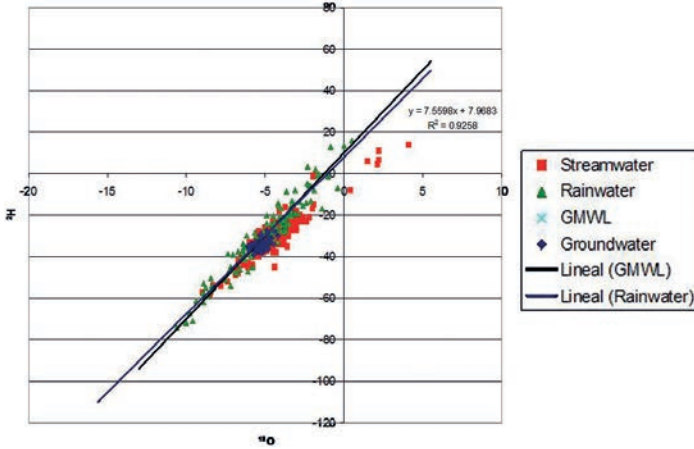


FIG. 2.  $\delta^2H$  vs.  $\delta^{18}O$  diagram including the GMWL.

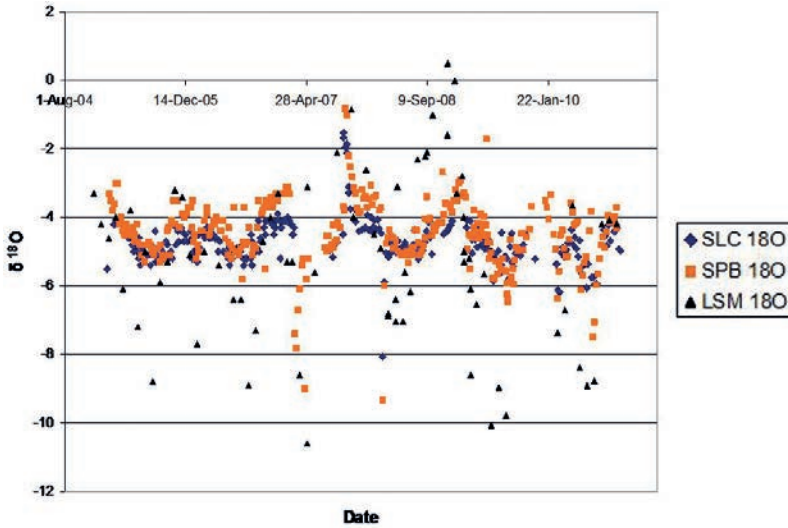


FIG. 3.  $\delta^{18}O$  records in river water at SLC and SPB and in rain at LSM.

content between the coastal (LNE) and the inland stations (LSM, LLO). The Local Meteoric Water Line corresponds approximately to the GMWL (Fig. 2) with an equation  $\delta^2H = 7.56 \delta^{18}O + 7.97$ . The average values for precipitation are  $\delta^2H = -29.8\text{‰}$  and  $\delta^{18}O = -4.99\text{‰}$ . Analysing the behaviour of the isotope composition of precipitation, a seasonal effect can be observed, which it is also strongly affected by an amount effect (Fig. 3). The more depleted isotope values correspond to heavy rain events.

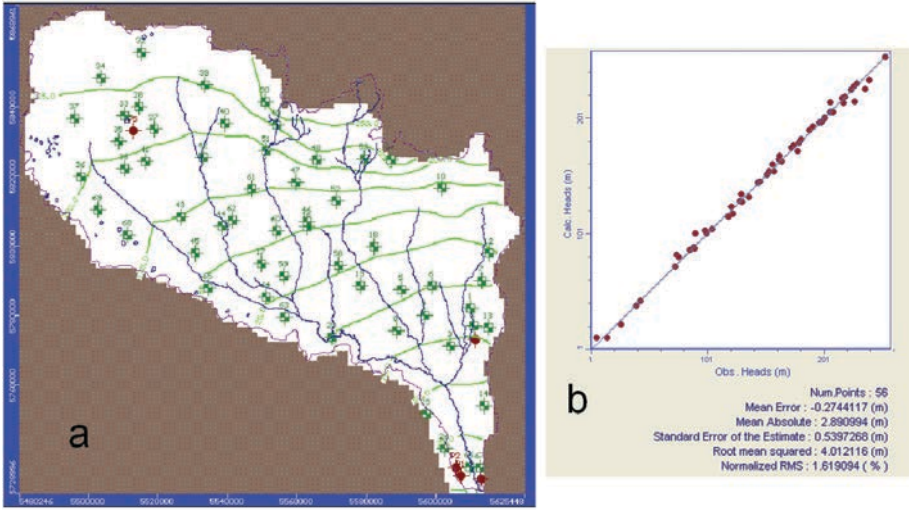


FIG. 4. (a). Modelled potentiometric map; (b). Calculated vs. observed groundwater levels.

Groundwater composition is very homogeneous, with all samples showing a narrow range of  $\delta^2\text{H}$  and  $\delta^{18}\text{O}$  values (Fig. 2). Average values are  $\delta^2\text{H} = -34.1\text{‰}$  and  $\delta^{18}\text{O} = -5.31\text{‰}$ .

Stream water isotope composition is more variable than groundwater, but not as much as rain water, indicating the participation of both components, direct runoff and baseflow, in its composition. A sinusoidal signal can be observed in river water composition, also indicating baseflow dominance in its composition and the seasonality effect in the fast flow component (Fig. 3).

### 3.2. Modflow modelling

The groundwater potentiometric map obtained from modelled values (Fig. 4a) fits adequately the measured piezometric records. The fit between observed water table levels and the level calculated by the model gives a mean error of  $-0.27$  m and a maximum absolute mean error of  $2.89$  m (Fig. 4b).

The budget calculation indicates that the discharge corresponding to the total net recharge to the aquifer is distributed in the following way:  $6.3\%$  discharges directly into the ocean,  $3.6\%$  is extracted by exploitation wells, and the remaining  $90.1\%$  discharges to the streams as baseflow. Mass balance indicates a groundwater contribution to the QGR of  $771\,000\text{ m}^3/\text{d}$ , which represents a discharge of  $14.4\text{ m}^3/\text{s}$ . Considering an average total discharge of  $17\text{ m}^3/\text{s}$ , the groundwater contribution calculated by modelling is a  $84\%$  of total streamflow.

#### 4. DISCUSSION AND CONCLUSIONS

Previous studies of the QGR catchment based on hydrograph separation demonstrated that more than 80 percent of total streamflow is baseflow [6]. The five years of weekly isotope data of the QGR water at two sites showed a sinusoidal behaviour, oscillating  $\pm 2\%$  in  $\delta^{18}\text{O}$  around the mean annual isotope content of local groundwater. This behaviour demonstrates the dominance of groundwater contribution on the streamflow isotope composition as well as the contribution of direct runoff to the isotope content of surface waters.

A significant coincidence exists between the calculated percentage of baseflow in streamflow from hydrograph separation and those calculated by using the flow model MODFLOW. Stable isotope composition also indicates the dominance of groundwater discharge on streamflow composition.

Focusing mainly on the Pampeano aquifer, the fact that the isotopic composition of groundwater is similar to the average long term isotope composition of precipitation indicates that recharge derives exclusively from precipitation in a well mixed behavior [10]. MODFLOW results indicate that discharge is mainly produced through the stream network. Stable isotopes indicate, as confirmed by MODFLOW and B flow results, that about 80% of baseflow in streamflow derives from groundwater. However, the proportion discharging to the rivers, directly to the sea or extracted through boreholes cannot be established with only isotope data.

The complementary use of the stable isotope monitoring programme and flow modelling of the Pampeano aquifer in the QGR catchment shows that this is a shallow aquifer which is recharged directly from local precipitation and discharges mainly to the surface waters. Groundwater discharge supports streamflow, baseflow being around 80% of the total river discharge.

#### ACKNOWLEDGEMENTS

This study was carried out as a part of the CRP supported by the IAEA. The National Agency of Scientific Promotion (ANPCyT) and the National Council of Scientific and Technological Research (CONICET) of Argentina supported the research through the projects PICT07-00390 and PIP5668 respectively. The local catchment management committee cooperated with sampling.

## REFERENCES

- [1] TERUGGI, M., The nature and origin of Argentine loess, *Journal of Sedimentary Petrology* **27** 3 (1957) 322–332.
- [2] SALA, J.M., “Recursos hídricos (Especial mención de las aguas subterráneas)”, *Relatorio Geología de la Provincia de Buenos Aires: VI Congreso Geológico Argentino*, Buenos Aires (1975) 169–193.
- [3] BOCANEGRA, E., et al., “Aplicación de cálculos de mezcla para evaluar el origen del agua en infraestructuras subterráneas en Mar del Plata, Argentina (Mixing indexes applied to assess water sources in flooding urban underground structures in Mar del Plata, Argentina)”, *Aportes de la hidrogeología al conocimiento de los recursos hídricos (MARIÑO, E.E., SCHULZ, C.J., Eds)*, Vol. 2., Asociación Civil GA-IAH, Buenos Aires (2009) 691–700.
- [4] VARNI, M., USUNOFF, E., Simulation of regional-scale groundwater flow in the Azul River basin, Buenos Aires Province, Argentina, *Hydrogeol. J.* **7** 2 (1999) 180–187.
- [5] MARTINEZ, D.E., MASCIOLI, S., BOCANEGRA, E.M., Determination of Zn partition coefficient and simulation of reactive transport from landfills in Mar del Plata, Argentina, *Environmental Geology* **51** (2006) 463–469.
- [6] MARTÍNEZ, D.E., et al., “Environmental isotopes in the water cycle in the catchment of the Quequen Grande River, Argentina”, *Advances in Isotope Hydrology and its Role in Sustainable Water Resources Management (IHS 2007) (Proc. Symp. Vienna, 2007)*, Vol. 1, Proceedings Series, IAEA, Vienna, Austria, (2007) 381–388.
- [7] QUIROZ LONDOÑO, O.M., MARTÍNEZ, D.E., DAPEÑA, C., MASSONE, H., Hydrogeochemistry and isotope analyses used to determine groundwater recharge and flow in low gradient catchments of the province of Buenos Aires, Argentina, *Hydrogeol. J.* **16** 6 (2008) 1113–1127.
- [8] SEILER, K-P., LINDNER, W., Near-surface and deep groundwaters, *J. Hydrol.* **165** (1995) 33–44.
- [9] GUIGER, N., FRANZ, T., *Visual MODFLOW: The integrated Modeling Environment for MODFLOW and MODPATH, Versión 2.00 — User’s Manual* (1996) 161.
- [10] GAT, J.R., TZUR, Y., “Modification of the isotopic composition of rainwater by processes which occur before groundwater recharge”, *Isotopes in Hydrology (Proc. Symp. Vienna, 1966)*, IAEA, Vienna (1967) 49–60.



# ISOTOPIC AND HYDROGEOCHEMICAL TECHNIQUES FOR THE SUSTAINABLE MANAGEMENT OF WATER RESOURCES IN AN ARID WATERSHED OF NORTHERN CHILE

R. OYARZÚN<sup>a,b</sup>, J.F. MUÑOZ<sup>c</sup>, E. AGUIRRE<sup>d</sup>, J. OYARZÚN<sup>a</sup>, C. ORTIZ<sup>c</sup>, S. MARÍN<sup>d</sup>, H. MATURANA<sup>a</sup>, N. KRETSCHMER<sup>b</sup>, E. JOFRÉ<sup>a</sup>.

<sup>a</sup> Departamento Ingeniería de Minas,  
Universidad de La Serena, Chile

<sup>b</sup> Centro de Estudios Avanzados en Zonas Áridas,  
La Serena, Chile

<sup>c</sup> Departamento de Ingeniería Hidráulica y Ambiental,  
Pontificia Universidad Católica, Chile

<sup>d</sup> Comisión Chilena de Energía Nuclear,  
Chile.

## Abstract

Water is the main limiting factor for the development of Northern Chile. South of 26°S, major conflicts are related to the allocation of water and the interaction between surface and shallow groundwater, when used by farmers. The conflict is aggravated due to little knowledge about these interactions. Isotope techniques can add valuable information for the assessment of water interactions and the definition of suitable integrated watershed management strategies. This is pursued in the Limarí basin within the ongoing CHI/8/029 project, mainly funded by the IAEA.

## 1. INTRODUCTION

Arid and semiarid zones cover approximately 40% of the earth's surface. Water is a limited resource in these areas, which are generally submitted to increasing demand due to factors such as population growth and water requirements from economic activities such as agriculture and mining. This increased demand may be aggravated by water shortage trends due to climate change. Within this situation, a proper understanding of surface water-groundwater (SW-GW) connectivity is a key issue in modern integrated water resources management, which is especially important in arid zones.

Agriculture is the largest water demanding activity (consumptive use) in Chile, with approximately 75% of the total water use. Chile is well known for having liberal water regulation. Once obtained, the ownership of a water right can be treated and managed separately to the land property initially assigned. Also, the Chilean legal body distinguishes surface from ground waters, and therefore, the rights associated with each of them. Recently, an amendment introduced to the Water Act in 2005 includes the mandatory justification for new requested water rights, the taxing of non-used water resources, and the faculty of the DGA (Chilean Water Authority) to restrict groundwater allocations and intervene during drought periods, as well as the promotion for the establishment of groundwater user organizations. At the same time, although still lacking a constitutional framework, several efforts of integrated watershed management have recently started. These refer to the CONAMA's National Watershed Strategy and the DGA's Regional Water Round Tables. Within this legal frame, the issue of SW-GW relations has attained special relevance.

In semiarid north central Chile (18°30'–32°15' S latitude), the Coquimbo Region is by far the one with the most important agricultural activity, with approximately 75 700 ha of irrigated crops, representing 77% of the irrigated agriculture in this part of the country. Within the Coquimbo Region, the Limarí basin (30°20'/31°15' S; 70°30'/71°49' W) includes over 50% of the irrigated agricultural surface of the Region. This is due to the existence of the largest irrigation oriented hydraulic infrastructure of Chile, the Paloma System, a set of three water reservoirs, La Paloma (750 Mm<sup>3</sup>), Recoleta (100 Mm<sup>3</sup>) and Cogotí (150 Mm<sup>3</sup>), and the existence of a dense irrigation channel network. These factors have determined a sustained increase in irrigated area through the years. This, and the change of crop type as well as the introduction of new crops, have further modified seasonal water consumption patterns and added additional stress on the limited water resources. This situation, after a request made by some of the Limarí basin water user organizations, motivated the official declaration by the DGA of Limarí as an 'overallocated' catchment. Thus, the Resolution DGA N° 72 of January 19, 2005, determined the fully allocated status of the Grande river, the Limarí river and their tributaries. After this, no new permanent consumptive surface water right can be granted in the basin. Thus, groundwater resources have become potentially susceptible to increased demand and use. This translates into a very complex situation when groundwater is extracted from shallow wells in the alluvial plane near the streams. Indeed, there have been already disputes between water users due to SW–GW interaction issues that have reached civil suit status. Moreover, as recognized in a recent DGA technical report [1], in general, in the Limarí basin, there is very limited information on the degree of interaction between rivers and aquifers.

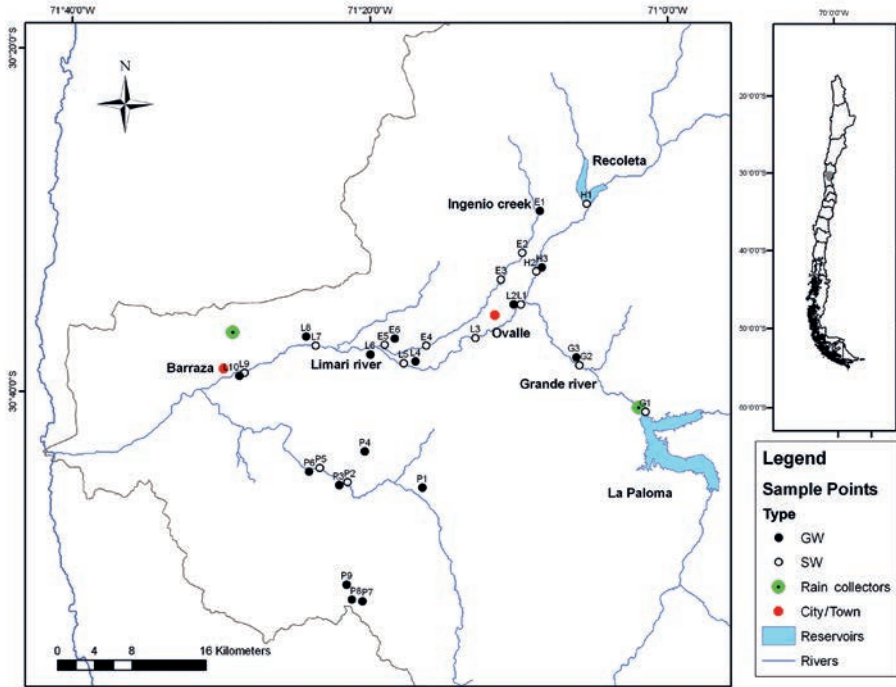


FIG. 1. Location of the study area.

## 2. STUDY AREA

As explained, the area of interest of this study corresponds to the Limarí river basin, downstream of the La Paloma and Recoleta reservoirs, in the Coquimbo Region, North Central Chile (Fig. 1).

## 3. METHODS

The approach includes the field assessment of SW–GW interactions based on water chemical data, water stable isotopes ( $^{18}\text{O}$ ,  $^2\text{H}$ ) and the radioactive isotope  $^{222}\text{Rn}$  content in water from samples taken in selected sites of the study area.

### 3.1. Data gathering and field study preparation

First, the available information of the study site has been complemented, especially in terms of existing wells in the area and their lithological characteristics. Also,

rural water committees were contacted and visited, in order to get authorization for groundwater sampling (see below).

### 3.2. Field study

Two sampling campaigns have been conducted, in autumn (April) and spring–summer (December) 2010. However, this contribution only considers results from the first campaign, as those of the second are not yet available, and excludes results for  $^{222}\text{Rn}$ , which were only obtained in the second campaign. Samples have been taken for both surface water and groundwater components in several locations of the study area. Following Ref. [2], groundwater sampling site selection criteria were: (a) operational groundwater well or observation well; (b) shallow well (less than 60 m maximum depth); (c) known production zone (screen interval); (d) short screen interval; (e) within 400 m of a stream; (f) preferably in close proximity to surface water sample locations (i.e. lake, reservoir, stream); (g) in topographic locations that enable groundwater interaction with stream; (h) accessible by road. For this, and based on previous experience and studies carried out in the neighbouring Elqui basin (e.g. Ref. [3]), rural drinking water wells (Agua Potable Rural) represent suitable locations for groundwater sampling and will be considered for this work. Surface sample site selection was: (a) preferably close to surface water gauging stations; (b) on higher order streams, above and below key stream junctions on the main stream or major tributaries; (c) within the range of influence of groundwater sampling site; (d) accessible by road. Samples will be taken in three rounds, in April, August and December, in order to include seasonal effects due to climate events and variable agricultural water demanding conditions.

#### 3.2.1. Groundwater sampling method

Prior to sampling, wells were purged of a volume of water equivalent to three times the volume of the well casing and/or until field parameters stabilize. Water samples for major and trace elements were obtained directly from the pump outlet and collected in 1 L plastic, double capped, rinsed bottles. At each sampling point two samples were obtained, one for cations and trace elements in pre-treated bottles (with 2% v/v  $\text{HNO}_3$ ) and another for anions (without acid). Samples for water stable isotopes were collected directly from the pump outlet and sealed in pre-rinsed Nalgene type 125 mL plastic bottles [2]. Samples for  $^{222}\text{Rn}$  (carried out during the second campaign only) were also collected directly from the well in glass bottles following the recommendations given in the  $^{222}\text{Rn}$  analyser equipment (i.e. RAD  $\text{H}_2\text{O}$ ) user manual. Samples were kept refrigerated during and after field work. Also, parameters such as temperature, pH, electrical conductivity, and dissolved oxygen, were determined in the field using a portable multi-parameter probe.

### 3.2.2. *Surface water sampling procedure*

Surface water samples were taken directly from rivers and creeks, as well as from water reservoirs (Recoleta and La Paloma dams). Field data determination and sampling protocols (i.e. types of bottles, sample amount) were the same as those mentioned for groundwater. In addition, rainfall water samples were taken monthly (maximum of four samples per year from May to August) during 2009 and 2010 at three collector stations placed at different heights in the basin, following the recommendations of the International Atomic Energy Agency. Precipitation samples were analysed for isotopes ( $^2\text{H}$ ,  $^{18}\text{O}$ ).

### 3.3. **Laboratory analysis**

Chemical (Ca, Na, K, Mg,  $\text{HCO}_3$ ,  $\text{CO}_3$ , Cl,  $\text{SO}_4$ ,  $\text{NO}_3$ ,  $\text{PO}_4$ , Al, As, Cd, B, Cu, Fe, Mn, Zn, F) and isotopic ( $^{18}\text{O}$ ,  $^2\text{H}$ ) analyses were carried out at the Chilean Nuclear Energy Commission (CCHEN) at Santiago. Radon determinations were carried out at the Environmental Laboratory, Mines Engineering Department, University of La Serena, using a RAD  $\text{H}_2\text{O}$  equipment.

### 3.4. **Data analysis**

#### 3.4.1. *Data screening*

Chemical and stable isotope data have been preliminarily evaluated using central tendency (mean, median and mode) and dispersion (standard deviation, skewness) statistics. Accuracy of laboratory analyses was checked by ionic balance [4].

#### 3.4.2. *Statistical and graphical analysis*

To determine the relation between water samples, and therefore SW–GW connectivity, multivariate analysis, in particular hierarchical cluster analysis (HCA; Ward's linkage method, Euclidean distance for similarity measurements) and principal component analysis (PCA; Varimax rotation, Kaiser criterion) will be carried out for each data set, i.e. each sampling round [3, 5, 6], using Minitab V.14. The relationship between sample clusters and geographic location throughout the watershed will be tested for spatial coherence. Hydrochemical facies and chemical differences between groups will be further analysed through graphical techniques such as Piper (ternary) and Stiff diagrams, using the code Aquachem.

3.4.3. Radioactive isotope data

Radioactive isotope information is used as a complementary tool to evaluate SW–GW connectivity and its nature. Indeed, based on <sup>222</sup>Rn profiles, i.e. presence/absence of spikes in stream water samples along the river, groundwater contribution to surface water (i.e. gaining reach) will be detected. Instead, for stream reaches where no spikes are found, this will be interpreted as zones of potential river water infiltration into nearby alluvial aquifers zones (i.e. losing stream), following Ref. [7].

4. PRELIMINARY RESULTS AND DISCUSSION.

4.1. Major ion chemistry

The results of chemical analyses of groundwater and surface water samples are represented in a Piper diagram (Fig. 2).

It is observed that, in general, surface waters and groundwaters do not exhibit major differences in their composition, and they correspond to Ca–Mg and Cl–SO<sub>4</sub>

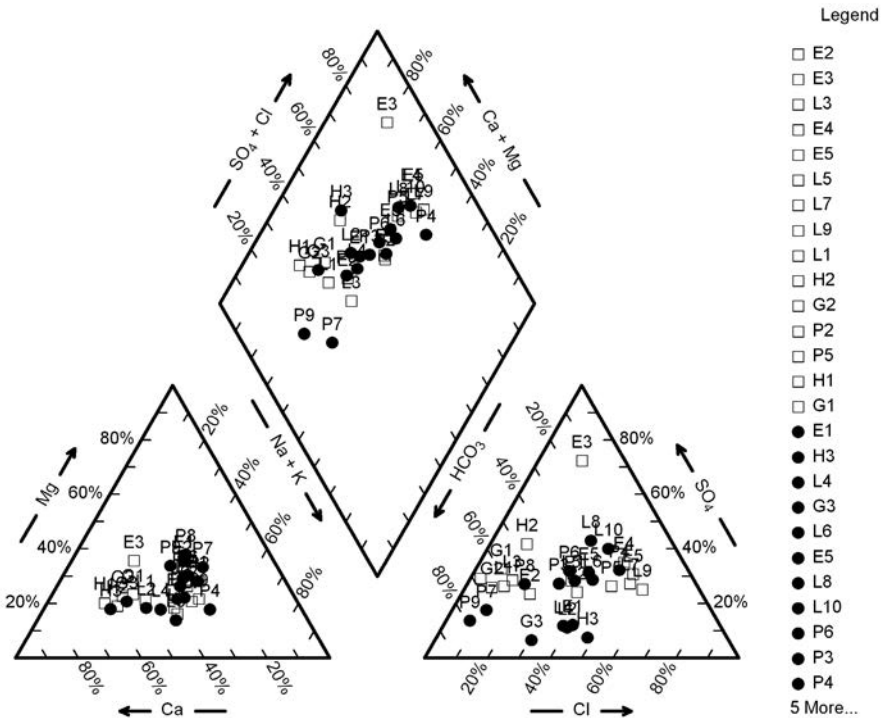


FIG. 2. Piper diagram for water samples in the Limari basin.

facies. The exception to this are the groundwater samples taken in the Punitaqui area (e.g. P7, P9) where the ion carbonate dominates, and the surface water sample taken in the El Ingenio creek, with sulphate content due to the existing mining activity in the area. However, it must be recalled that these results correspond only to the autumn sampling campaign, and the information from the second campaign (Spring–Summer) will allow a better understanding of the composition of surface waters and groundwater.

#### 4.2. Stable isotope composition

Fig. 3 shows the  $\delta^2\text{H}$  and  $\delta^{18}\text{O}$  composition of groundwater and river water. It also displays both the global and the local meteoric water lines (solid and dashed lines respectively). For the sake of clarity, the groundwater samples of the Punitaqui area (GWP) have been plotted separately from the other groundwater samples, as well as those of the water reservoirs, La Paloma and Recoleta (WR).

It can be seen that the samples from Punitaqui fall in the meteoric line. All the other samples display below the local meteoric line, which is a consequence of the strong effect of the water reservoirs on the isotopic fingerprint of both surface waters and groundwaters in the study area.

Three main clusters can be identified; the one with the more depleted values corresponds to the Hurtado river area. At the other extreme, the one with the more enriched isotope values corresponds to the area of Camarico (P1 to P6), which is irrigated by the La Paloma reservoir. Finally, the central cluster group samples of surface water and groundwater downstream of La Paloma, in the Limarí river, which do not exhibit great variation between them. This is verified when  $\delta^{18}\text{O}$  and Cl are considered simultaneously, as shown in Fig. 4.

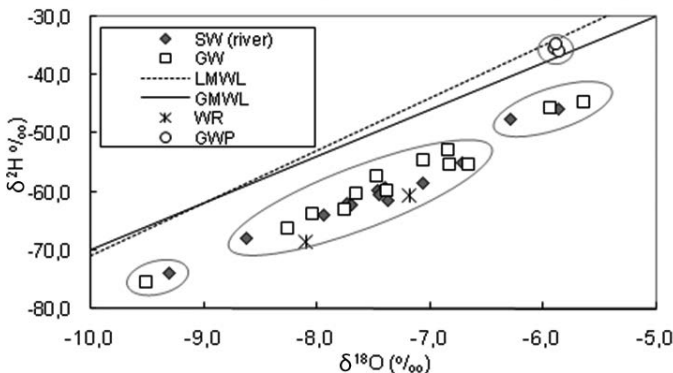


FIG. 3. Isotope relationship in surface and ground waters.

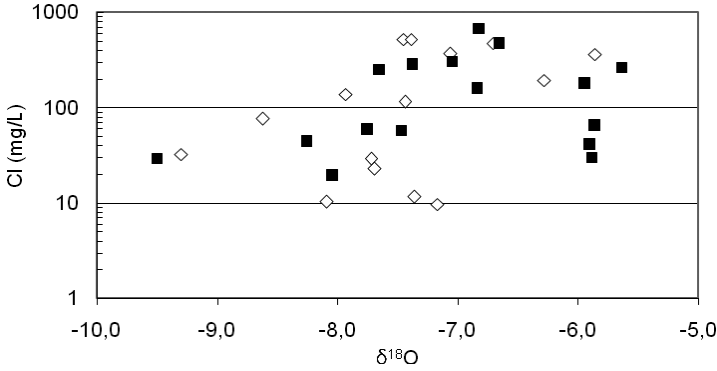


FIG. 4.  $\delta^{18}\text{O}$  vs. Cl in surface waters and groundwater samples.

### 4.3. Radon

Surface waters and groundwaters exhibited very different  $^{222}\text{Rn}$  values. While the average for the former was  $1407 \text{ Bq/m}^3$ , the figure for the latter reached  $16\,842 \text{ Bq/m}^3$ . The following graph correspond to a longitudinal transect through the Limarí river. Interestingly, there is a clear spike near L5, which could correspond to groundwater contribution to stream flow [7].

## 5. CONCLUSIONS

While only preliminary results are available, the combined use of water chemistry data, stable and radioactive isotopes has allowed the identification of distinctive zones in the studied area, especially in terms of groundwater–surface water connectivity. The interpretation will be sounder when data from both sampling campaigns have been analysed.

## ACKNOWLEDGMENTS

This work has been partially funded by the IAEA through the TC project CHI/8/029 and by the Dirección de Investigación of the Universidad de La Serena through grant DIULS CD093401.

## REFERENCES

- [1] DGA, Evaluación de los recursos hídricos subterráneos en la cuenca del río Limarí, Informe Técnico N° 268, Dirección General de Aguas (2008) 40 pp.
- [2] GREEN, G., STEWART, S., Interactions between Groundwater and Surface Water Systems in the Eastern Mount Lofty Ranges, DWLBC Report 2008/27, Department of Water, Land and Biodiversity Conservation, Adelaide, Australia (2008) 101 pp.
- [3] CARVAJAL ASTUDILLO, M.J., Caracterización química e isotópica del sistema hidrológico de la cuenca del Elqui, Graduation Project, University of La Serena (2009).
- [4] STELLATO, L., et al., Some limitations in using  $^{222}\text{Rn}$  to assess river-groundwater interactions: The case of Castel di Sangro alluvial plain (central Italy), *Hydrogeol. J.* **16** (2008) 701–712.
- [5] THYNE, G., GÜLER, C., POETER, E., Sequential analysis of hydrochemical data for watershed characterization, *Ground Water* **42** (2004) 711–723.
- [6] DEMIREL, Z., GÜLER, C., Hydrogeochemical evolution of groundwater in a Mediterranean coastal aquifer, Mersin-Erdemli basin (Turkey), *Environ. Geol.* **49** (2006) 477–487.
- [7] BASKARAN, S., RANSLEY, T., BRODIE, R.S., BAKER, P., Investigating groundwater-river interactions using environmental tracers, *Aust. J. Earth Sci.* **56** 1 (2008) 13–19.



# CONTRIBUTION OF ISOTOPIC TOOLS TO THE NUMERICAL SIMULATION OF THE MAR DEL PLATA COASTAL AQUIFER, ARGENTINA

E. BOCANEGRA<sup>a</sup>, M. POOL<sup>b</sup>, J. CARRERA<sup>b</sup>, D.E. MARTÍNEZ<sup>a</sup>

<sup>a</sup> Instituto de Geología de Costas y del Cuaternario  
UNMDP, Argentina.

<sup>b</sup> Instituto de Diagnóstico Ambiental y Estudios del Agua,  
CSIC, Spain.

## Abstract.

Over-exploitation in the coastal aquifer in Mar del Plata, Argentina, led to a seawater intrusion process affecting groundwater by salinization. The aim of this paper is to show the contribution of isotopic techniques to generate the numerical flow and transport model of the Mar del Plata aquifer. On the basis of the hydrogeological conceptual model, a numerical model was constructed. It consists of a multilayer aquifer in the urban area with 2 layers separated by an aquitard and a monolayer aquifer in the rest of the basin. The isotopic difference recorded in groundwaters allow the identification of the origin of the recharge and the confirmation of the presence of the hydrogeological environments incorporated in the numerical model. Flow simulation reflects the evolution of piezometric heads. Chloride transport simulation represents the salinization process due to seawater intrusion and the subsequent backward movement of the interface due to the abandonment of salinized wells. The results of numerical simulation confirm the conceptual model and reproduce the impact of the adopted management strategies.

## 1. INTRODUCTION

Mar del Plata, located in the northeastern coast of Argentina (Fig. 1), is the main tourist resort of the country, with a stable population of 700 000 inhabitants and a seasonal population of over 1 million. Water for urban, agricultural and industrial uses is supplied exclusively by groundwater resources. The city registered a massive migration process during the second part of the past century, at a rate of 100 000 new inhabitants per decade. This urban growth process led to an increase in population density, industrial activities (building, gastronomy, textiles and fishing) and tourism in the urban area. The intensive exploitation in order to satisfy the fresh water needs of the city eventually caused an important piezometric level drawdown, a consequent seawater intrusion in the urban area and a high number of salinized wells. The maximum extension of the salinized area was reached at the end of the 1960s, and then

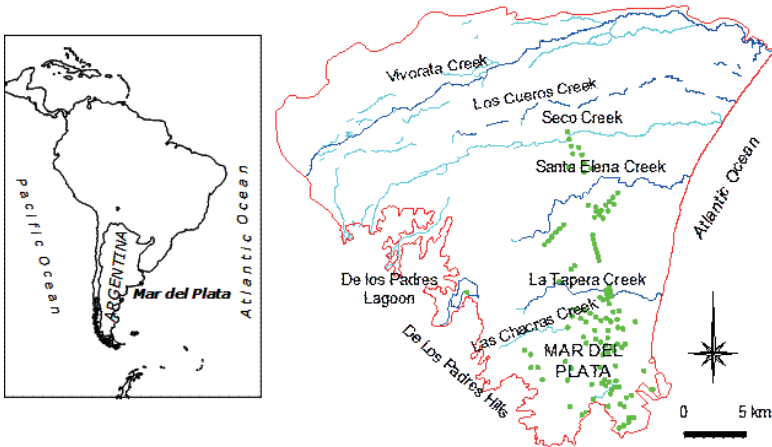


FIG. 1. Location map (green dots represent isotopic sampling).

a new exploitation zone was implemented to the north of the city. Since 1990, a battery of wells, located to the southwest of the basin coincident with the irrigated area, supplies water for consumption in the city. Recovery of phreatic heads due to the abandoned wells, a high increase of rainfall and leakage of running water and sewage owing to their obsolescence result in a water level rise leading to subsurface structure flooding and damage of reinforced concrete structures.

The geology consists of a quartzitic Palaeozoic bedrock overlain by a sedimentary cover of Upper Tertiary and Quaternary deposits [1]. Miocene clayey sandy sediments are found at 100 m depth, covered by Quaternary loess like sediments that, from a hydrogeological viewpoint, are the most important reservoir. Lithologic profiles allow the characterization of some hydrogeological environments in the basin. The urban zone presents a large number of discontinuous aquifer levels separated by aquitards, close to the beds of the creeks and to the hills, sediments are sandy or silt sandy, and the interfluvies, with a sequence of clayey silt sediments, show an aquitard behaviour. Transmissivity obtained from pumping tests is of about 600–800 m<sup>2</sup>/day in the urban area and between 1000 to 1400 m<sup>2</sup>/day in the rural area, the storage coefficient is 0.001, and porosity is approximately 0.15 [2]. The average rainfall in the period 1930–2009 was 910 mm/a in this city. Natural discharge is towards the sea. Artificial discharge due to pumping has historically led to a significant aquifer head decline.

The aim of this paper, as part of the IAEA ARCAL Project, Application of Isotopic Tools for Integrated Management of Coastal Aquifers (ARCAL XCII), RLA/8/041, is to show the contribution of isotopic techniques to generate the numerical flow and transport model of the Mar del Plata coastal aquifer.

## 2. METHODOLOGY

The formulation of the conceptual model was made after the collection, ordering, analysis and assessment of hydrogeological data, the spatial and temporal piezometric and hydrochemical evolution and the extractions for urban consumption and irrigation between 1913 and 2009. Available data include records of 451 wells or piezometers, 5486 piezometric levels, 122 transmissivity values, 3190 annual rainfall data and 7293 hydrochemical data.

The hydrochemical database allows the characterization of the state of groundwater and the processes that indicate the displacement of the freshwater–salt water front. In 2009, a groundwater sampling of 120 supply wells was performed in order to determine their stable isotopic composition.

Numerical simulation was carried out with the Visual TRANSIN code [3], which allows the user to solve and estimate the parameters of groundwater flow and solute transport equations. The solution of differential equations was achieved following the finite elements method.

## 3. ISOTOPIC TOOLS APPLIED TO THE CHARACTERIZATION OF THE RECHARGE PROCESS

An integrated analysis of the different hydrogeological environments and soil uses in relation to the distribution of  $\delta^{18}\text{O}$  and  $\text{Cl}^-$  allowed the identification of several recharge processes [4].

In the hilly area, toward the western zone of the basin, the main activity is an intensive fruti-horticultural farming with application of supplementary irrigation. In this area, values of  $\text{NO}_3$  between 10 and 45 mg/L were found, which indicates a process of anthropogenic affectation of the local water resources. The very low Cl contents in groundwater indicate a direct recharge of rain water in the higher elevation zone of the basin.

In the plain area, where the economic activity is basically dryland farming and cattle raising, values up to 25 mg/L  $\text{NO}_3$  indicate either absence or incipient contamination. Chloride concentration is also low (50 to 70 mg/L). The  $\delta^{18}\text{O}$  shows a differential behaviour; the palaeobeds of Seco Creek and Santa Elena Creek show depleted values, which imply rapid infiltration, whereas in the interfluves the values are enriched. Recharge in this area would then be affected by (a) the enriched water by evaporation during infiltration in a very flat relief that minimizes surface runoff and favours soil waterlogging, and (b) the water enriched by evaporation in Laguna de los Padres, which infiltrates in the aquifer's eastern edge. Close to La Tapera Creek, the isotopic enrichment could be related to a slow infiltration due to the presence of very fine sediments; this was later confirmed by the numerical model, which calibrated low transmissivity in this area.

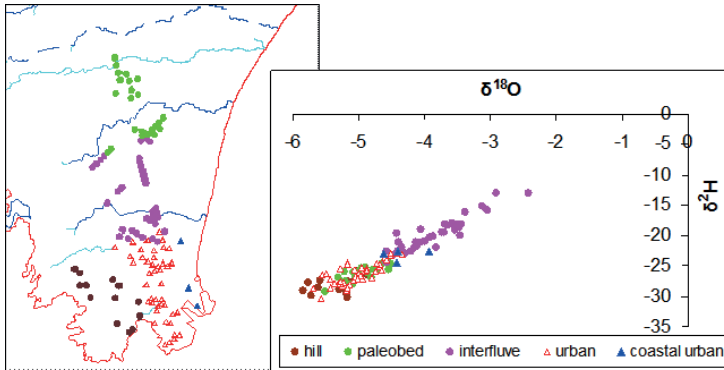


FIG. 2. Isotopic areal distribution and  $\delta^2H$  vs.  $\delta^{18}O$  diagram highlighting the hydrogeological environments and land uses.

The  $NO_3$  contents above 45 mg/L, beyond the norm for drinking water consumption, are located in the urban zone. Thus, they can be associated to the leakage of septic tanks and sewers and to the solute transport through regional flow. The concentration of  $Cl^-$  (70–200 mg/L) would confirm this hypothesis. Isotopic distribution shows values in a range from very low to low, which suggests the presence of direct rainwater recharge and losses of sanitary systems.

The  $\delta^{18}O$  values that are isotopically most enriched in the urban sector correspond to wells with a high content of  $Cl^-$  (up to 3500 mg/L), which shows interaction with seawater.

The areal distribution of wells with the common characteristics mentioned above is presented in Fig. 2. The isotopic difference recorded in the recharge terms allows the confirmation of the presence of the hydrogeological environments defined through lithological profiles.

#### 4. NUMERICAL MODEL

Taking into account the definition of hydrogeological environments, in the urban area the model is 2.5-D and comprises 3 layers, a 20 m width shallow aquifer and a 40 m deep aquifer separated by a 20 m aquitard, while in the rest of the basin the model is 2-D and simulates the phreatic, monolayer, 80 m width aquifer (Fig. 3). The aquitard is represented by 1-D elements that allow only vertical flow, is bidimensional. In the urban area, a portion of the deep aquifer submerged has been taken into consideration in order to evaluate interaction with seawater. The network of finite elements includes 17 363 elements and 7814 nodes.

In the monolayer aquifer, 3 zones of transmissivities were distinguished, corresponding to the hilly area, palaeobeds and interfluvies; in the multilayer

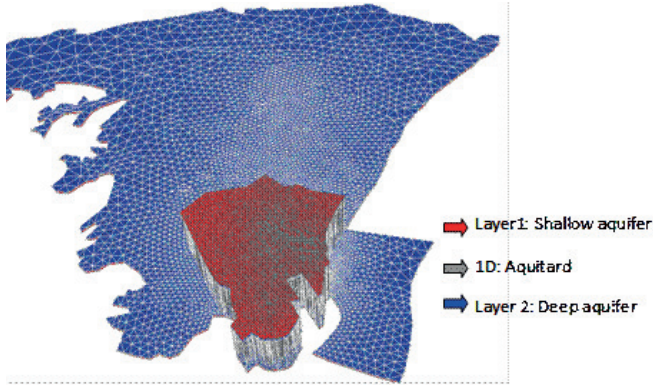


FIG. 3. Geometry and network of finite elements of the Mar el Plata aquifer model.

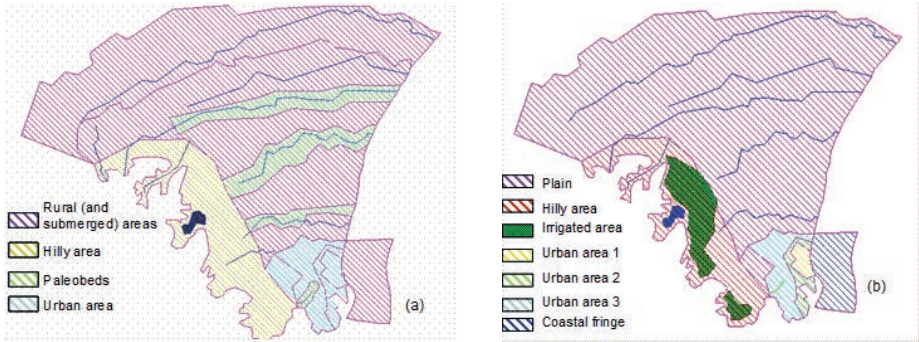


FIG. 4. (a) Areal distribution of transmissivities, (b) areal distribution of recharge.

TABLE 1. AUTOMATIC CALIBRATION OF TRANSMISSIVITIES

Hydrogeological environments	Estimated transmissivity (m <sup>2</sup> /d)	Previous estimate (m <sup>2</sup> /d)
Interfluves	780	730
Palaeobed in Seco Creek	950	1000
Palaeobed in Santa Elena Creek	820	1000
Palaeobed in La Tapera Creek	450	850
Palaeobed in Las Chacras Creek	700	850
Hilly area	1100	1000
Shallow aquifer in urban area	430	340
Deep aquifer in urban area	450	500

aquifer, different transmissivities were assigned to the surface layer and the deep layer (Fig. 4a). The recharge was represented by 6 zones: the plain area, which comprises interfluvial and palaeobeds, the hilly area, the irrigated zone, and 3 urban zones that contemplate the recharge related to the urban growth, taking into account especially the losses of the drinking water and sanitary systems and the infiltration by rain water runoff (Fig. 4b). A full description of the model can be found in Ref. [4].

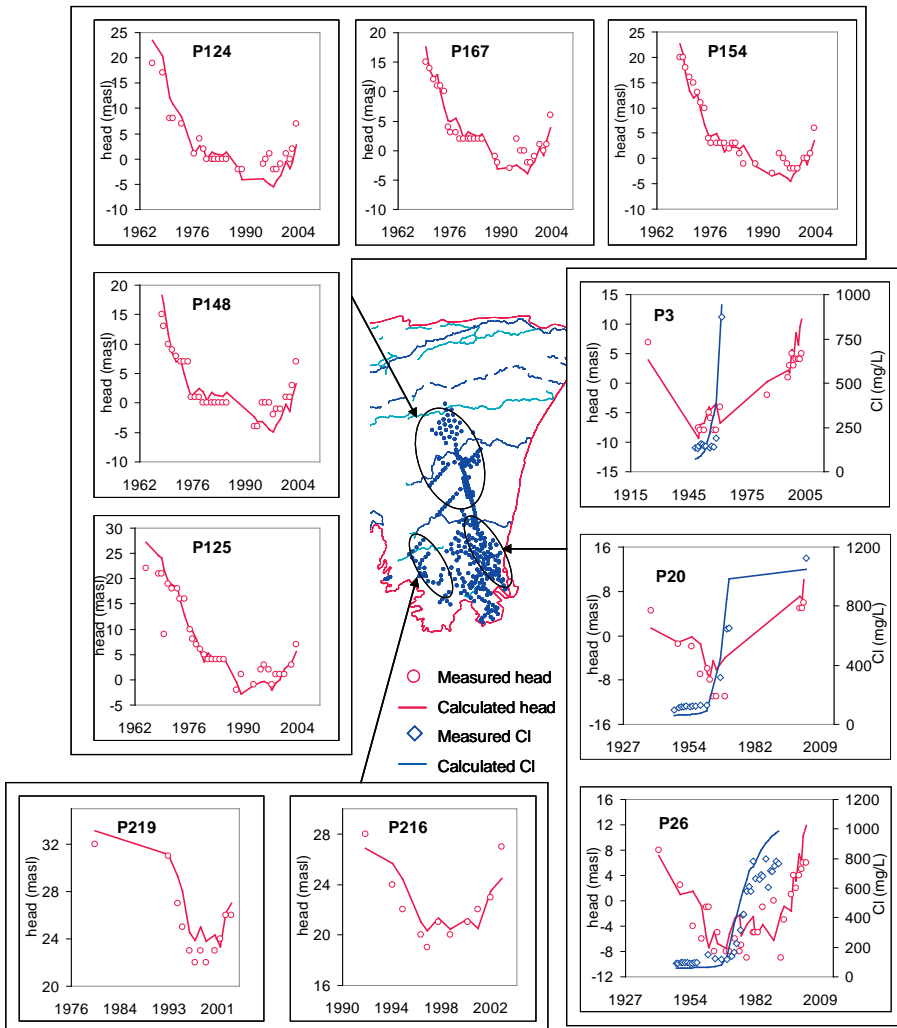


FIG. 5. Results of flow and seawater intrusion process simulation.

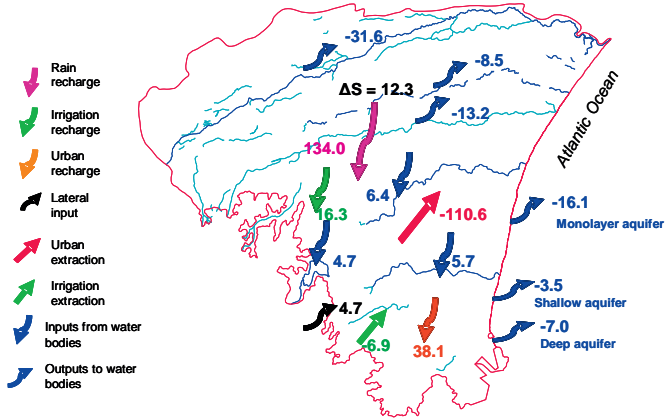


FIG. 6. Average water balance ( $\text{Mm}^3/\text{a}$ ), estimated for the period 1996–2005.

## 5. RESULTS

The calibration process consists in estimating the parameters of the model, so that the answer in terms of levels and concentrations fits the values measured and the values of the estimated parameters are coherent with the conceptual model. The results of the automatic calibration of transmissivities are shown in Table 1. Some similarities can be noticed with the previous estimate, which was made taking into account the pumping tests data.

Fig. 5 shows some results of flow simulation through hydrograms in different sectors of the basin and the simulation of the seawater intrusion process through the evolution of  $\text{Cl}^-$  in the urban area. A noticeable fitness can be observed between the simulated and the measured values.

The global mass balance for the period 1996–2005 (Fig. 6) indicates an input of  $134 \text{ Mm}^3/\text{a}$  rainwater recharge,  $38 \text{ Mm}^3/\text{a}$  recharge of urban origin,  $16.3 \text{ Mm}^3/\text{a}$  recharge in irrigated zones and a lateral input of some  $4.7 \text{ Mm}^3/\text{a}$ . The most significant output is the extraction for urban consumption of some  $110 \text{ Mm}^3/\text{a}$ , the extractions for irrigation of  $6.9 \text{ Mm}^3/\text{a}$ , the output through the creeks of  $41.2 \text{ Mm}^3/\text{a}$  and from the coastal areas of  $26.6 \text{ Mm}^3/\text{a}$ . The lagoon discharges  $4.7 \text{ Mm}^3/\text{a}$  into the aquifer. An increase of  $12.3 \text{ Mm}^3/\text{a}$  in storage takes place.

## 6. CONCLUSIONS

The integrated analysis of the different hydrogeological environments and soil uses in relation to the distribution of  $\delta^{18}\text{O}$  and  $\text{Cl}^-$  allowed the identification of different processes of recharge, such as rapid infiltration in aquifer sediments, slow infiltration of evaporated water in plain zones with an aquitard behaviour, recharge in the

urban zone influenced by the loss of sanitary systems or septic tanks, and the process of seawater intrusion.

The 2.5-D numerical model has been constructed in the urban area with two aquifer layers separated by an aquitard and the 2-D model in the rest of the basin. Calibration of the flow and chloride transport model in transient regime was performed by inverse simulation. Good fits have been obtained between the calculated and measured piezometric levels and the calculated and measured concentrations of Cl<sup>-</sup>. Results of numerical simulation allowing the confirmation of the conceptual model and the reproduction of the management strategies

The survey of the isotopic difference recorded in groundwaters constitutes a new contribution to the tools for aquifer management.

## REFERENCES

- [1] TERUGGI, M.E., KILMURRAY, J., "Tandilia", Geología de la Provincia de Buenos Aires, VI Cong. Geol. Arg., Relatorio, Buenos Aires (1975) 55–77.
- [2] BOCANEGRA, E.M., Modelo conceptual y simulación numérica del acuífero de Mar del Plata, Tesis de Maestría, Universidad Nacional de Rosario, Inédita (2008) 90 pp.
- [3] MEDINA, A., CARRERA, J., TRANSIN I.V., Fortran code for solving the coupled flow and transport inverse problem: User's guide, E.T.S.I. Caminos, Canales y Pueros, Barcelona (2005) 248.
- [4] BOCANEGRA, E.M., Desarrollo de herramientas hidrogeoquímicas y numéricas aplicadas a la evaluación de la explotación del acuífero de Mar del Plata, Tesis Doctoral, Universidad Nacional de Rosario (2011) 146 pp.

# HYDROCHEMICAL AND ISOTOPIC INVESTIGATION OF GROUNDWATER IN THE HAMMAMET-NABEUL AQUIFER SYSTEM, NORTH-EASTERN TUNISIA

A. BEN MOUSSA, K. ZOUARI

Laboratory of Radio-Analysis and Environment, ENIS,  
Sfax, Tunisia

T. KURTTAS

Isotope Hydrology Section  
International Atomic Energy Agency  
Vienna, Austria

## Abstract

The combination of major element geochemistry, stable ( $\delta^{18}\text{O}$ ,  $\delta^2\text{H}$ ) and radioactive ( $^3\text{H}$ ,  $^{14}\text{C}$ ) isotopes has provided a comprehensive understanding of the natural and anthropogenic processes that control groundwater mineralization as well as the sources of different groundwater bodies within the Hammamet-Nabeul unconfined aquifer (Cap Bon peninsula, northeastern Tunisia). The geochemical examination shows the dominance of Na-Cl and Ca-SO<sub>4</sub> water types resulting from the dissolution of halite and gypsum, the dedolomitization and the cation exchange process. Additionally, the return flow process in relation with the long term flood irrigation practice contributes to the mineralization by producing high amounts of nitrate. The stable isotope signatures reveal the existence of two groundwater groups. The non-evaporated groundwaters with relatively depleted contents, reflecting recharge at higher altitudes; and evaporated groundwaters with enriched contents highlighting the influence of return flow of irrigation waters. Tritium contents in these two groups provide evidence of the presence of pre-1950 and post-1960 recharge periods. Carbon-14 activities in shallow wells, in spite of their contamination by organic  $^{14}\text{C}$ , confirm the recent origin of the groundwaters in the study area.

## 1. INTRODUCTION

Throughout history, groundwater resources have played a fundamental role in meeting the challenge of growing water scarcity and facilitating economic development in northeastern Tunisia. During the last two decades in the Hammamet-Nabeul basin groundwater has been the only dependable source for agriculture production, which accounts for approximately 80% of all water supplies. Likewise, agricultural production that is based essentially on intense irrigation and application of fertilizer to improve the soils has permanently increased the risk of water scarcity and groundwater salinization [1]. On the other hand, tourism constitutes the second most

important economic activity in the region, with a total accommodation capacity of nearly 30 per cent of the national capacity. During the seasonal peak in tourism, the population of the county is estimated to be three times the year round population. Associated with this high rate of population growth is an increased demand for water resources with an average consumption of about 800 L per day [4]. Thus, there are crucial conflicting interests between tourism and agriculture as both sectors have most of their water needs during the summer months. The unconfined aquifer studied is of major economic importance and needs to be carefully assessed and managed. The general aim of the present hydrochemical and isotopic investigations is to provide relevant information concerning the main processes that control the groundwater composition as well as the sources of different groundwater bodies, which is often essential for best management and preservation of groundwater resources.

## 2. STUDY AREA

The Hammamet-Nabeul basin, which belongs to the Cap Bon peninsula in northeastern Tunisia, occupies an area extent of approximately 450 km<sup>2</sup> (Fig. 1). The climate of the study area is classified as Mediterranean, semiarid; with mild, wet winters and warm, dry summers. It is characterized by mean annual values of precipitation, temperature and potential evapotranspiration of about 450 mm, 20°C

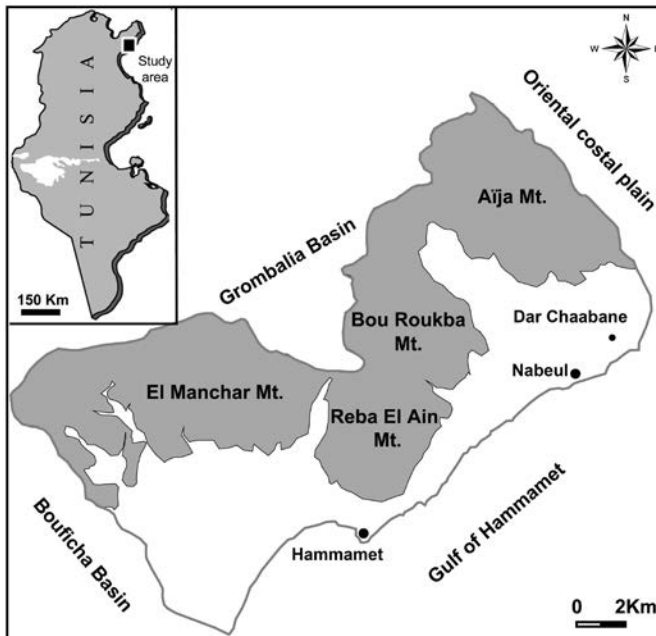


FIG. 1. Location of the Hammamet–Nabeul basin and units identified within.

and 1350 mm, respectively. The drainage network is relatively dense; it is constituted of several ephemeral Wadis, which collect and transport surface runoff from the surrounding highlands toward the Gulf of Hammamet discharge area.

### 3. GEOLOGY AND HYDROGEOLOGY

Geologically, the sedimentary outcrops in the Hammamet-Nabeul basin range from the Early Eocene to the Quaternary. In the depth, the Eocene series are constituted by thick Ypresian limestone units overlaid by the Lutetian–Priabonian marl. On the Eocene units lie the Oligocene, of coarse to medium-grained sandstone. This latter is covered by the Burdigalian clayey sand and sandstone deposit, which is overlain by the Langhian limestone and gypseous marl, fine to medium grained sand and the clay and marly clay series. On these deposits, there are the Tortonian sandy units, which are overlain by the sandy sandstone of the Oued el Bir Messinian Formation. The Plio-Quaternary deposits, which overlay the Miocene series, are represented by the Lower Tabianian clay of Potters, the Upper Tabianian sands of Nabeul, the Lower Plaisancian clay of Sidi Barka, the Upper Plaisancian sandstones of Hammamet and the Quaternary sands of the Rejich Formation [2].

Hydrogeologically, the Hammamet-Nabeul unconfined aquifer is hosted in the Plio-Quaternary detrital deposits, which vary from 20 to 300 m in thickness (Fig. 2). It consists mainly of varying proportions of sands, sandstones, clay, evaporates with dominant pedogenic calcite nodules. This unconfined aquifer represents

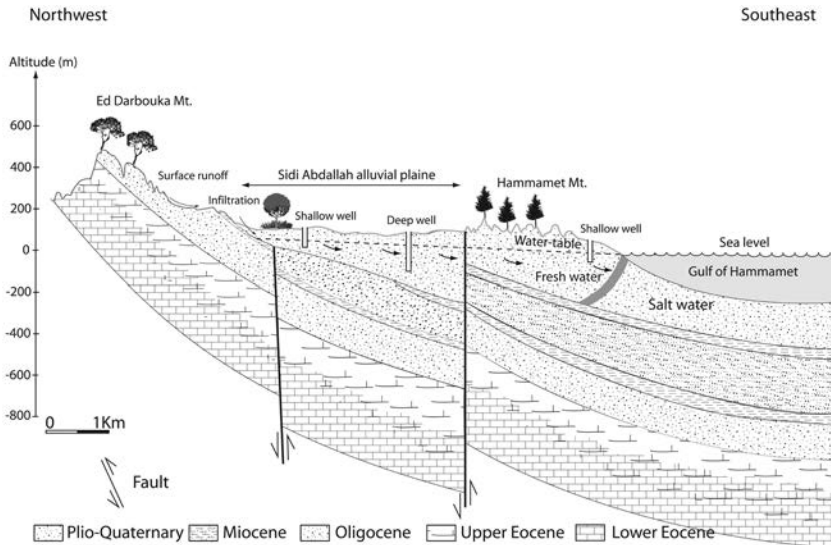


FIG. 2. Hydrogeological cross section in the Hammamet-Nabeul unconfined aquifer.

the largest groundwater storage in Tunisia, probably due to its high hydraulic conductivity. It is tapped by a high number of private and state owned wells located in the costal and central part of the basin. The bedrock of the Hammamet unconfined aquifer is constituted by the Miocene clayey deposits that separate this groundwater reservoir from the underlying confined aquifer of the Oligocene. The piezometric map of the shallow water table shows that groundwaters converge northwest–southeast from the northeastern high lands toward the Gulf of Hammamet, which constitutes the natural discharge area. This highlights the recharge of the unconfined aquifer in the foot of the mountains, limiting the basin in its northern part.

## 4. RESULTS AND DISCUSSION

### 4.1. Hydrochemical investigation

The  $p\text{CO}_2$  values, the physical parameters, total dissolved solids (TDS) and major ions of the groundwater samples are given in Table 1. The  $\log(p\text{CO}_2)$  values vary from  $-4.3$  and  $-1.9$  with an average of  $-2.5$ . The highest  $p\text{CO}_2$  levels are found in wells located downstream, suggesting an increasing saturation along the flow path. The lowest values are registered in the recharge area. Consequently, lower  $p\text{CO}_2$  levels are found in fresh groundwater upstream from the basin close to the recharge zones and around the Wadi courses. The groundwater samples with higher  $p\text{CO}_2$  levels have relatively longer residence times, which provides insight into the more extensive water–rock interaction and the microbial mediated reactions that produce  $\text{CO}_2$ . The  $T^\circ\text{C}$  values range from  $14.6$  to  $22.5^\circ\text{C}$ . The pH values vary from  $7.3$  to  $9.1$ . The EC and the TDS values vary across a wide range from  $0.73$  to  $10.12$  mS/cm and from  $0.43$  to  $7.32$  g/L respectively. The TDS values increase in the direction of groundwater flow. The highest values are measured upstream of the basin, indicating both the lack of rainwater infiltration and the relatively longer residence time that favours the dissolution of minerals.

#### 4.1.1. Natural mineralization process

The relationships between major ions indicate which chemical parameters are involved in mineralization processes. Dissolution of halite is confirmed by the well-defined relationship between Na and Cl ions. The spatial distribution of these two major ions shows the same evolution and the parabolic proportional evolution of the negative saturation indexes when correlated to the sum of ions (Na+Cl) deriving from the eventual dissolution of NaCl (Fig. 3).

Likewise, the dissolution of gypsum and/or anhydrite is highlighted through the 1:1 ratio of most samples in the plot of Ca versus  $\text{SO}_4$  and the proportional, parabolic, tendency observed in the correlation of the negative saturation indexes, with

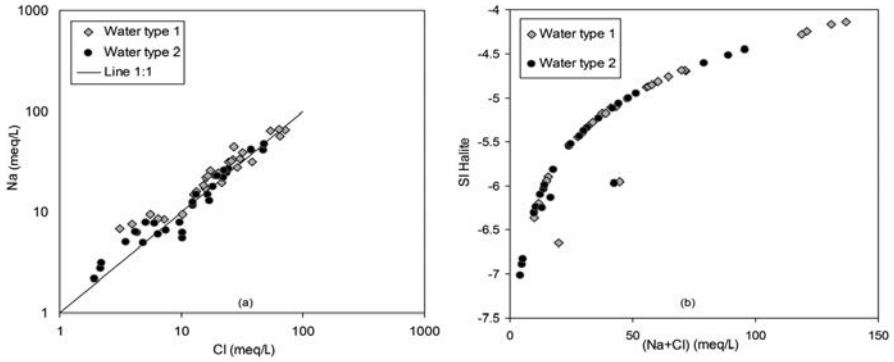


FIG. 3. Plots of Na versus Cl (a) and (Na+Cl) versus SI of halite (b).

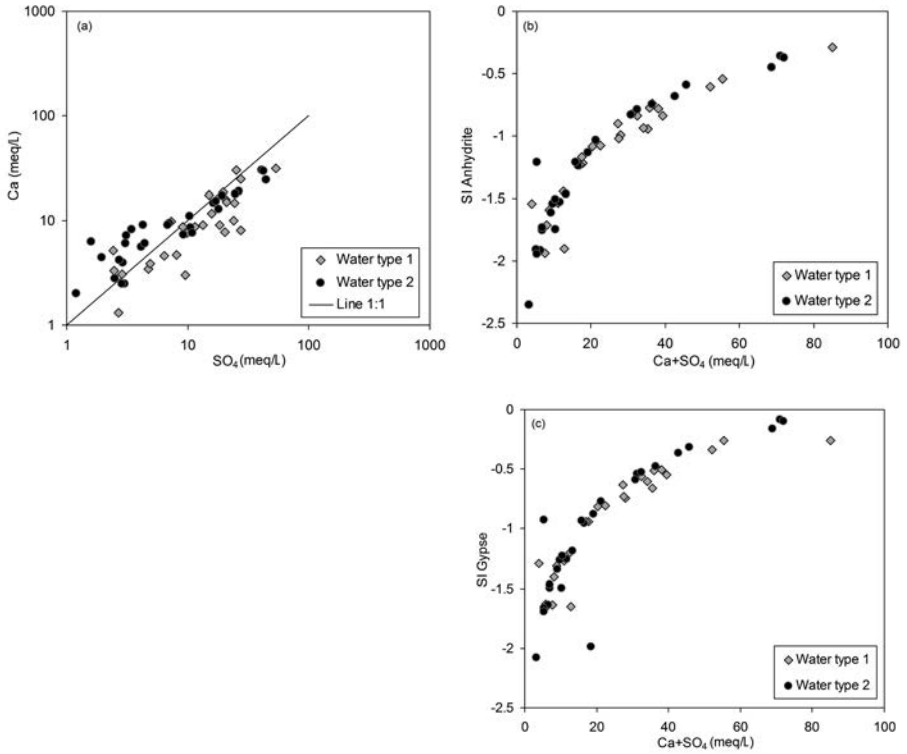


FIG. 4. Plots of Ca versus SO<sub>4</sub> (a); (Ca<sup>2+</sup> + SO<sub>4</sub><sup>2-</sup>) versus SI of anhydrite (b) and (Ca<sup>2+</sup> + SO<sub>4</sub><sup>2-</sup>) versus SI of gypsum (c).

TABLE 1. IN SITU MEASUREMENTS, GEOCHEMICAL AND ISOTOPIC DATA OF HAMMAMET-NABEUL SHALLOW GROUNDWATER

Well No.	T (°C)	pH	EC (µS/cm)	TDS (mg/L)	Na	Mg	Ca	Cl (meq/L)	NO <sub>3</sub>	SO <sub>4</sub>	HCO <sub>3</sub>	<sup>18</sup> O (%o vs. SMOW)	<sup>2</sup> H	<sup>14</sup> C (cm)	<sup>3</sup> H (UT)
1	20.2	7.7	2570	1940	11.7	4.5	8.2	12.5	3.0	3.4	4.0	-5.0	-27.7	84.6	2.5
2	19.8	7.6	1827	1370	5.0	5.0	5.6	4.9	2.0	4.2	4.6	-4.8	-27.9	96.2	1.7
3	20.1	7.6	1795	1350	6.0	3.2	6.1	6.5	1.1	3.1	4.2	-4.9	-29.5	83	1.5
4	18.5	7.8	8190	6660	41.3	26.7	24.3	47.6	0.5	44.6	10.2	-5.1	-30.6	-	-
5	19.2	7.3	2780	2160	12.5	7.6	9.5	12.4	2.1	7.1	6.2	-4.5	-26.7	124.8	3.5
6	20.7	8.12	3040	2520	15.1	6.8	11.0	16.5	3.3	10.4	3.0	-4.8	-27.5	-	-
7	19.8	7.32	3620	2480	13.1	8.3	9.0	17.1	5.6	4.3	4.4	-4.7	-27.5	-	-
8	18.8	8.03	3800	2840	18.0	10.9	14.9	18.2	2.2	16.4	4.6	-5.2	-27.7	-	-
9	19.4	7.9	2220	1760	8.0	4.7	9.0	9.7	1.3	6.8	3.0	-4.8	-24.6	-	-
10	21.2	7.7	3810	2680	15.0	9.0	8.6	13.3	3.1	10.5	6.4	-4.8	-24.6	-	-
11	20	7.8	1800	1210	7.7	4.0	6.0	6.0	0.2	4.4	7.0	-	-	-	2.9
12	19.6	7.9	1339	1020	6.6	3.6	4.5	7.5	0.1	2.0	4.0	-	-	89	0
13	19.7	7.8	5130	3820	24.4	12.2	19.0	23.7	0.9	26.7	5.3	-	-	-	-
14	16.2	8	4830	3790	22.9	16.9	17.9	19.1	2.7	24.8	6.8	-	-	-	-
15	20	9.16	733	430	2.2	2.1	2.0	1.9	0.0	1.2	3.2	-2.3	-8.1	-	-
16	20	7.4	4860	3580	27.1	12.3	17.3	24.5	4.3	19.2	7.8	-4.4	-26.25	-	-
17	20.8	7.8	4410	3150	22.1	10.5	15.3	22.1	2.9	17.3	5.0	-4.4	-23.2	-	-
18	19.4	7.6	6970	5240	41.5	19.4	30.3	37.6	6.9	40.8	5.0	-	-	-	-

19	19.7	7.5	7930	6720	47.5	22.6	29.4	48.2	2.9	42.6	6.2	-4.1	-23.1	-
20	21.3	7.9	1336	970	6.3	2.5	4.0	4.3	1.3	2.9	3.4	-	-	-
21	20.6	7.7	886	660	2.8	2.5	4.2	2.2	0.1	2.7	4.3	-5.05	-28.61	-
22	22.5	7.8	1069	700	3.2	2.7	2.8	2.2	0.0	2.5	4.7	-5.2	-28.93	-
23	22.6	7.2	4730	3170	25.8	11.3	13.0	22.5	0.5	17.9	5.0	-5.32	-32.33	-
24	21.6	7.7	1261	780	7.9	3.1	2.5	5.1	0.0	3.0	5.4	-5.25	-30.28	-
25	19	7.5	4380	2800	6.4	2.9	2.5	4.2	0.0	2.9	4.8	-5.21	-28.33	-
26	24.7	7.7	1534	880	22.8	9.0	7.7	19.8	0.0	10.9	6.6	-	-	-
27	22.4	7.5	2190	1430	5.5	6.0	6.3	10.3	0.3	1.6	5.4	-	-	-
28	22	7.5	1548	1090	6.3	4.6	7.2	10.3	0.0	3.1	4.0	-	-	-
29	23.2	7	1424	1090	5.0	4.4	7.4	3.5	0.0	9.2	1.0	-5.31	-32.16	-
30	19	7.7	5770	4040	44.4	10.2	8.1	27.1	0.0	27.3	6.6	-4.7	-23.5	117.6
31	22.5	7.5	4950	3660	33.4	8.0	7.7	26.8	3.1	20.3	4.6	-4.2	-24.0	-
32	19.8	8	1606	1190	8.5	3.2	3.3	7.2	1.5	2.5	3.9	-	-	111.7
33	17.4	8.01	1928	1360	8.6	4.1	3.4	6.4	0.2	4.7	5.2	-	-	115.4
34	19.7	7.8	1337	980	6.8	2.6	3.9	3.1	0.6	4.9	5.4	-4.6	-24.6	-
35	18.9	8	1463	970	7.7	3.3	3.1	4.0	1.3	2.9	5.0	-4.9	-30.8	73
36	21.1	7.4	3210	1790	17.4	6.8	4.7	15.7	1.1	6.4	5.4	-	-	-
37	19	7.5	9640	6520	56.1	12.5	30.0	64.8	5.3	25.4	4.7	-3.6	-25.2	-
38	19.8	8.24	6000	4810	39.4	15.4	18.6	31.9	2.2	19.5	15.8	-	-	-
39	20.5	7.6	3920	2570	25.8	10.8	9.0	17.4	4.5	13.4	6.0	-4.8	-26.3	-
40	19.8	7.6	10120	6700	65.6	17.8	24.6	71.5	0.5	27.6	8.4	-	-	-

respect to the referred minerals, versus  $(Ca+SO_4)$  resulting from the eventual dissolution (Fig. 4).

Cation exchange processes are highlighted, firstly through the relative excess of sodium that is compensated by the relative deficiency of calcium, and secondly by the two indices of base exchange (IBE), namely the Chloro-alkaline indices (CAI 1 and CAI 2) [5].

When there is an exchange between  $Na^+$  or  $K^+$  with  $Ca^{2+}$  or  $Mg^{2+}$  in the groundwater, both the above mentioned indices will be positive and if there is a reverse cation exchange prevalent then both these indices will be negative. Fig. 4 shows that these indices are all positive in the study area, suggesting that the cation exchange process became dominant in the study area and seems to occur along the groundwater flow path.

4.1.2. Anthropogenic process

The nitrate concentrations in the Hammamet–Nabeul groundwaters fluctuate between 8 and 425 mg/L, with an average value of 141 mg/L. The great majority of groundwater samples have very high nitrate concentrations, which exceed

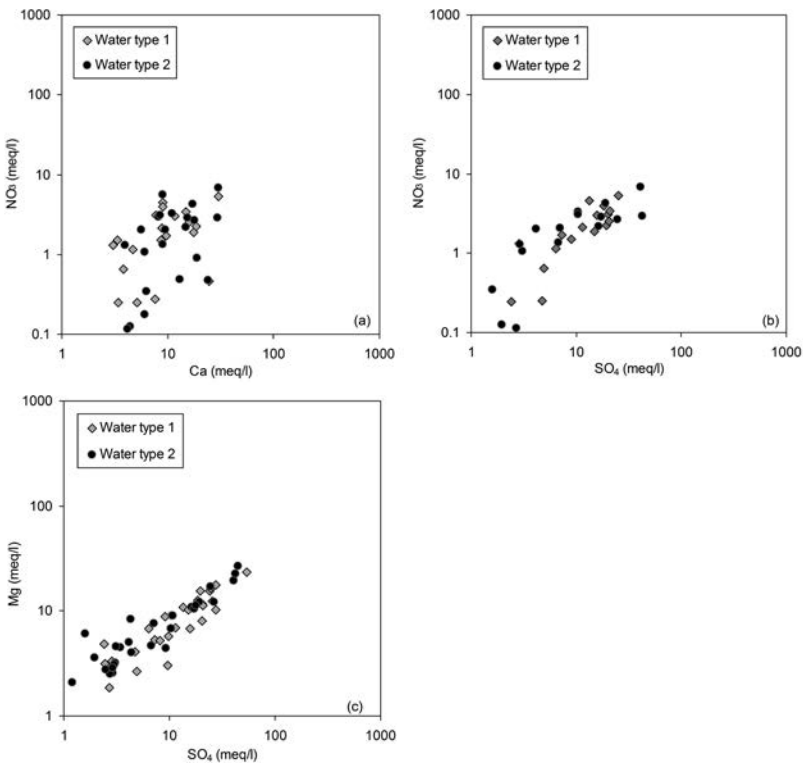


FIG. 5. Plots of Ca versus  $NO_3$  (a),  $SO_4$  versus  $NO_3$  (b) and Mg versus  $SO_4$  (c).

the maximum allowable concentration for human consumption (50 mg/L). These high concentrations of nitrate appear to be related to agricultural activities and may reflect intensive irrigation practices. In the agricultural areas, young, labile organic matter (OM), commercial complex nitrogen fertilizers, ammonium nitrate and other liquid fertilizers are used on a large scale. The fertilizers are applied essentially during the autumn and spring seasons. Furthermore, most of the agriculture areas are flood irrigated by inadequately managed irrigated systems. Hence, management practices of irrigated land, including nitrogen fertilizer application with the addition of labile OM to irrigated soil, contribute significantly to the degradation of groundwater quality. Subsequently, the long term groundwater abstraction for irrigation needs, combined with return flow, induces a recycling process that gradually increases the groundwater salinity and nitrate concentration that behave conservatively under aerobic conditions [6]. The evolution of  $\text{NO}_3^-$ , Ca, Mg and  $\text{SO}_4^{2-}$  ions is established in order to accurately assess the effect of the over-fertilization practices on groundwater quality. The  $\text{NO}_3^-$  and Ca ions show comparable evolution, suggesting that, for the agricultural samples, the  $\text{NO}_3^-$  and Ca ions derive from the same source, probably related to the large application of  $\text{Ca}(\text{NO}_3)_2$ -fertilizers [3] (Fig. 5). Likewise, the plot of Mg versus  $\text{SO}_4^{2-}$  ions exhibits a linear relationship, which may indicate a common origin, probably related to the overuse of fertilizers containing  $\text{MgSO}_4$  (Fig. 5). Moreover, the samples collected from agricultural areas display a strong relationship between nitrate and  $\text{SO}_4^{2-}$ , which might be due to the use of fertilizers containing N and S in the form of  $(\text{NH}_4)_2\text{SO}_4$  [5] (Fig. 5). Therefore, there is an urgent and crucial need for the assessment of fertilizer utilization, aquifer pollution vulnerability and subsurface contaminant load.

## 4.2. Isotopic investigation

### 4.2.1. Stable isotopes

The  $\delta^{18}\text{O}$  and  $\delta^2\text{H}$  contents of the groundwater studied range from  $-5.66$  to  $-2.27\text{‰}$  and from  $-30.7$  to  $-8.1\text{‰}$ , respectively. In the standard diagram of  $\delta^{18}\text{O}$  versus  $\delta^2\text{H}$  (Fig. 6), all groundwater samples are found globally on and below the RMWL, suggesting that they are derived from Mediterranean origin rainfall. However, when examined in detail, these groundwater samples can be divided into two groups. The first group, which includes 14 samples (about 40%), has relatively wide ranges of  $\delta^{18}\text{O}$  and  $\delta^2\text{H}$  values, varying from  $-5.22$  to  $-4.6\text{‰}$  and from  $-28.95$  to  $-23.5\text{‰}$ , respectively. These values define a regression line:  $\delta^2\text{H} = 7.83 \delta^{18}\text{O} + 12.25$  ( $R^2 = 0.86$ ). The slope of 7.83 is very similar to that of the RMWL, suggesting that this group of groundwater samples originates from direct condensation of atmospheric moisture [7]. Similarly, the intercept of 12.25, which is very comparable to the d-excess of the RMWL, suggests a modern origin of these groundwaters. On the other hand, the isotopic values of group 1 water samples are slightly depleted compared with

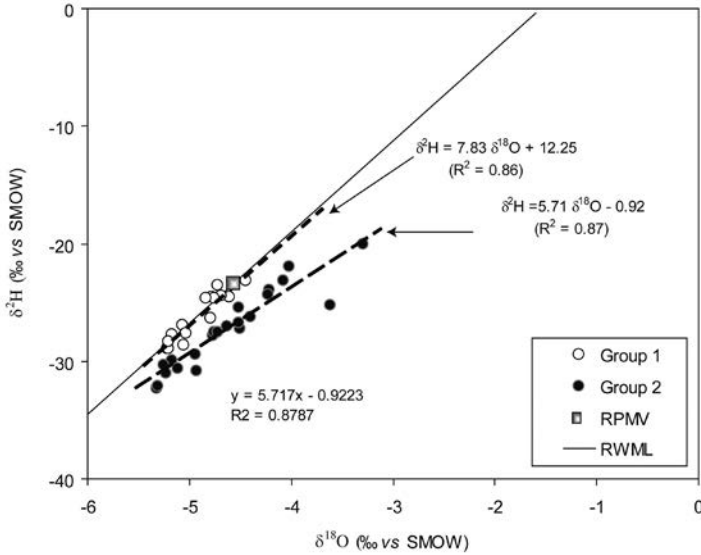


FIG. 6.  $\delta^{18}O/\delta^2H$  diagram.

those of the RPMV by up to 0.63‰ for  $\delta^{18}O$  and 5.65‰ for  $\delta^2H$ , suggesting that the Hammamet–Nabeul unconfined aquifer has been recharged at altitudes higher than the elevation of the GNIP station ( $E_{GNIP} = 10$  m a.s.l.). Considering the  $\delta^{18}O$  altitudinal gradient ( $G$ ) of 0.3‰/100 m, which is used in Ref. [7], the unconfined aquifer recharge altitude ( $RA$ ) can be estimated, using the equation:  $RA = E_{GNIP} + 100 \times (\delta^{18}O_{RPMV} - \delta^{18}O_{Groundwater} / G)$ , to be values (between 0 and 220 m a.s.l.) that coincide with the elevation of the aquifer outcrops in study area. The second groundwater group comprises 22 samples that are found below the RMWL with a regression line of  $\delta^2H = 5.7\delta^{18}O - 0.92$  ( $R^2 = 0.87$ ). The low values of the slope and the intercept of this regression line suggest the evaporation of group 2 groundwater samples. This evaporation is likely related to the return flow process in the zones where flood irrigation is applied on a large scale. In these zones, the long term practice of flood irrigation causes infiltration of water that largely fractionates on the ground surface and in the irrigation channels due to the long exposure to the atmosphere.

#### 4.2.2. Tritium and radio-carbon isotopes

Considering the data of the tritium contents in precipitation collected in the Tunisian GNIP stations (Tunis–Carthage, no 6071500 and Sfax city, no 7622500), the  $^3H$  contents in groundwater from the study area, which vary from 0 to 6.1 TU, suggest two recharge periods. Waters with  $^3H$  contents below 2 TU are likely to represent pre-nuclear recharge, i.e. recharge prior to thermonuclear testing in the 1950s and 1960s. However, waters with  $^3H$  contents between 2 and 6 TU

originate either from post-nuclear recharge, which infiltrated just before nuclear weapon tests, or from recharge occurring during the last two decades. On the other hand, the majority of groundwater samples show carbon-14 activities greater than 70 pMC; and about 45% of these samples have activities greater than 100 pMC. These relatively high activities support the existence of an important fraction of organic  $^{14}\text{C}$ , likely to be related to the infiltration of return flow waters, which highly affects the initial  $^{14}\text{C}$  contents. Nevertheless, they indicate the recent origin of the shallow groundwaters in the study area.

## 5. CONCLUSION

Major ion geochemistry and isotopic signatures of groundwaters from the Hammamet-Nabeul unconfined aquifer were used in conjunction with hydrogeological data to (1) provide a better understanding of the aquifers hydrodynamic functioning; (2) identify the natural and anthropogenic processes that control mineralization; (3) determine the origin of different water bodies and their sources of recharge. It has been demonstrated that groundwaters are mainly influenced by water–rock interaction processes i.e. dissolution of evaporates and cation exchange as well as by the dedolomitization process. Anthropogenic process in relation to the return flow of irrigation water also plays a significant role in groundwater salinization. The isotopic signatures enable the identification of two groups of groundwater samples. The first group corresponds to non-evaporated groundwater, which is characterized by depleted  $\delta^{18}\text{O}$  and  $\delta^2\text{H}$  contents highlighting the importance of modern recharge at higher altitudes. The second group corresponds to the evaporated groundwater that exhibits enriched stable isotope contents, reflecting the significance of infiltration of return flow irrigation waters. The second group is distinguished by relatively depleted contents of stable isotopes reflecting a palaeoclimatic origin. Tritium data show that recent groundwater originates from a mixture of contemporaneous and post-nuclear recharge. Carbon-14 activities in shallow wells, in spite of their contamination by organic  $^{14}\text{C}$ , confirm the recent origin of groundwater in the study area.

## ACKNOWLEDGEMENTS

The authors acknowledge the International Atomic Energy Agency (IAEA) for the financial support provided to the Technical Cooperation project (TUN 8/019) within this study was carried out.

## REFERENCES

- [1] BEN MOUSSA, A., et al., Hydrochemical and isotope evidence of groundwater salinization processes on the coastal plain of Hammamet–Nabeul, north-eastern Tunisia, *Phys. Chem. Earth* **36** 5–6 (2011) 167–178.
- [2] BEN SALEM, H., Évolution de la péninsule du cap Bon (Tunisie orientale) au cours du Néogène, *Notes Service Géologique, Tunisie* **61** (1995) 73–84.
- [3] BÖHLKE, J.K., SMITH, R.L., HANNON, J.E., Isotopic analysis of N and O in nitrite and nitrate by sequential selective bacterial reduction to N<sub>2</sub>O. *Anal. Chem.* **79** 384 (2007) 5888–5895.
- [4] CHAIBI, M.T., CHENINI, F., EPP, C., TONDI, G., *Renewable Energies (Italie), Une approche intégrée pour la gestion durable des ressources en eau dans le bassin méditerranéen, Colloque développement durable, Leçons et perspectives, Ouagadougou, Burkina Faso, 1–4 Juin 2004* (2006) 139–146.
- [5] GI-TAK, C, et al., Hydrogeochemistry of alluvial groundwaters in an agricultural area: An implication for groundwater contamination susceptibility, *Chemosphere* **55** (2004) 369–378.
- [6] STIGTER, T.Y., CARVALHO DILL, A.M.M., RIBEIRO, L., REIS, E., Impact of the shift from groundwater to surface water irrigation on aquifer dynamics and hydrochemistry in a semiarid region in the south of Portugal, *Agricultural Water Management* **85** (2006) 121–132.
- [7] BLAVOUX, B., Étude du cycle de l'eau au moyen de l'oxygène 18 et du deutérium, PhD Thesis, Université Paris-6 (1978) 316 pp.

# HYDROGEOCHEMICAL AND ISOTOPIC STUDIES OF GROUNDWATER IN THE CENTRAL REGION OF GHANA

S.Y. GANYAGLO<sup>a, b, 1</sup>, S. OSAE<sup>a, b</sup>, J.R. FIANKO<sup>a, b</sup>, A. GIBRILLA<sup>a</sup>,  
E. BAM<sup>a</sup>

<sup>a</sup> National Nuclear Research Institute,  
Ghana Atomic Energy Commission,  
Legon-Accra, Ghana

<sup>b</sup> School of Nuclear and Allied Sciences,  
University of Ghana, Legon-Accra

## Abstract

The hydrogeochemical and isotopic evolution of groundwater in the Central Region of Ghana has been studied in order to examine how hydrogeochemical processes control the overall groundwater chemistry in the study area. Two major hydrochemical facies have been identified as the Na-Cl and NaHCO<sub>3</sub> water types. The Na/Cl molar ratio indicates that silicate weathering is one of the major hydrogeochemical processes controlling groundwater water chemistry in the area. This is further confirmed by a plot of TDS against the Na/(Na+Ca) ratio. The Br/Cl ratio ranges from 0.00148 to 0.7087, suggesting minimal seawater intrusion in the area. Stable isotope values of the groundwater samples (<sup>18</sup>O and <sup>2</sup>H) are found around the global meteoric water line (GMWL), suggesting a direct infiltration of rainwater into the groundwater system. Elevated Cl<sup>-</sup> concentrations of the groundwater is probably due to sea spray and marine aerosols deposited on the top soil, though further studies are needed to determine the cause.

## 1. INTRODUCTION

Groundwater development in the Central Region of Ghana has been hindered by undesirable water quality in the majority of the boreholes. Elevated electrical conductivities (EC) in excess of 5000  $\mu$ S/cm have been reported in the area [1]. A significant number of boreholes have been abandoned because of high electrical conductivities. Since the study area is close to the coast, various hypotheses have been made to explain the high electrical conductivities in groundwater. The proposed explanations include seawater intrusion to groundwater, chloride and sodium ions

---

<sup>1</sup> Corresponding author: sganyaglo@yahoo.co.uk

from aerosols and the washing of salts accumulated in soils [2]. However, the exact source of the high electrical conductivity has not yet been determined.

Various geochemical models have been utilized to determine the sources of high electrical conductivities. Notably amongst them are Br/Cl, Na/Cl and Ca/Mg. Na, Cl and Br are found to be valuable for assessing the sources of high electrical conductivity in groundwater [3, 4]. In this research, major ions in groundwater and stable isotopes ( $^{18}\text{O}$  and  $^2\text{H}$ ) were used to examine the hydrogeochemical processes controlling the overall chemistry of groundwater in the area. This study aimed at assisting in developing effective management strategies to protect aquifers from contamination and over exploitation in the study area.

## 2. STUDY AREA

The study area is located between latitudes  $5^{\circ}10'$  and  $5^{\circ}30' \text{N}$  and longitudes  $0^{\circ}30'$  and  $1^{\circ}0' \text{W}$  (Fig 1). The area is underlain by gently rolling terrain and mostly drained by ephemeral rivers [1]. The major rivers draining the area are the Ochi-Narkwa and Ayensu rivers. The climate is of a tropical type and characterized by two rainy seasons with mean annual rainfall reaching about 1200 mm [1].

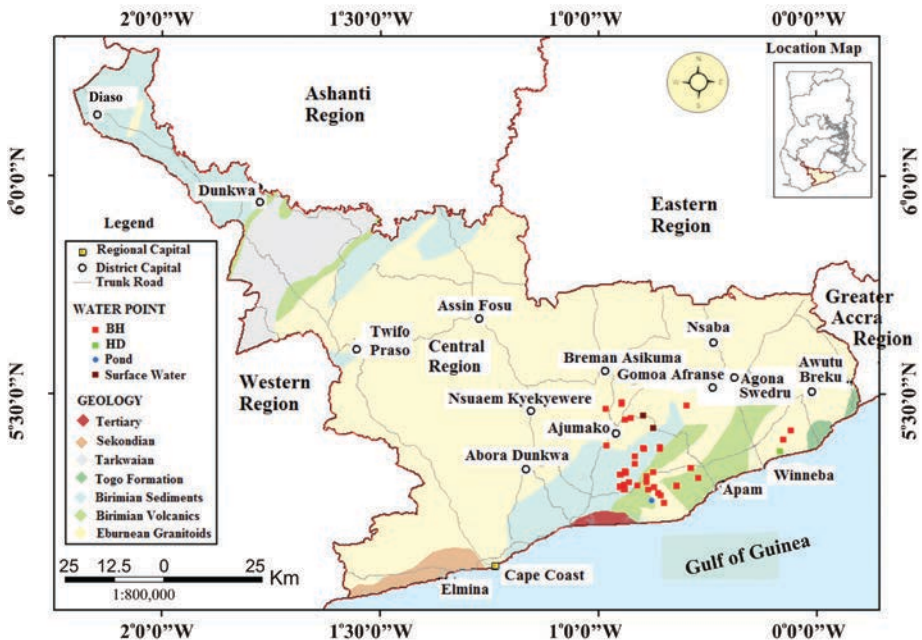


FIG. 1. Geological map of the study area showing sampling points.

The area is underlain by the Early Proterozoic Birimian rocks and associated Eburnean granitoids [5]. The Birimian is divided into two, a lower series termed the sedimentary basin and an upper series termed the volcanic belt. The sedimentary basin is comprised of phyllites, schists, tuffs and greywackes. The volcanic belt is comprised of basic and intermediate lavas and pyroclastic rocks, phyllites and greywackes [6]. The geological map of the study area is shown in (Fig 1). The Eburnean granitoids are found in both the sedimentary basin and the volcanic belt. Major rock types include quartz diorites, tonalities, trondhjemites, granodiorites, adamellites and granites.

### 3. MATERIALS AND METHODS

Water samples were collected at 39 sites across the study area, including 36 boreholes, 2 samples from the River Ochi-Narkwa and 1 sample from a pond, in December 2009. Water temperature, pH, electrical conductivity (EC), total dissolved solids (TDS) and oxidation reduction potential (Eh) were measured in-situ using a Hach Sension 2 portable pH/SE meter and a Sension 5 conductivity meter. Alkalinity was determined in the field by titrating with 1.6  $\text{NH}_2\text{SO}_4$  to pH 4.5 using a HACH Digital multi-sampler, Model AL-DT. The samples for the analysis of major ions were filtered into acid washed polyethylene bottles, using 0.45  $\mu\text{m}$  filters and placed in an ice chest with ice cubes in the field and in the refrigerator in the laboratory until analysis. The samples for cation analysis were acidified using 1%  $\text{HNO}_3$ , while those for anion analysis were not acidified. Calcium ( $\text{Ca}^{2+}$ ) and Magnesium ( $\text{Mg}^{2+}$ ) were determined using an Atomic Absorption Spectrophotometer (AAS). Sodium ( $\text{Na}^+$ ) and potassium ( $\text{K}^+$ ) were determined using the flame photometer. The anions chloride ( $\text{Cl}^-$ ), sulphate ( $\text{SO}_4^{2-}$ ), nitrate ( $\text{NO}_3^-$ ) and bromide ( $\text{Br}^-$ ) were measured with a Dionex 90 ion chromatograph. The ionic balance is estimated at  $\pm 10\%$ .

The stable isotopes oxygen-18 ( $^{18}\text{O}$ ) and deuterium ( $^2\text{H}$ ) of groundwater samples were determined using a Liquid Water Isotope Analyser at the Department of Chemistry of the National Nuclear Research Institute in Ghana's Atomic Energy Commission (GAEC). The results for both isotopes were expressed in ‰ deviation from the VSMOW standard. The reproducibility is better than 0.1‰ for  $\delta^{18}\text{O}$  and about 1‰ for  $^2\text{H}$ .

### 4. RESULTS AND DISCUSSION

#### 4.1. Hydrogeochemical Characteristics

A statistical summary of the analytical results of the groundwater samples from the Central Region of Ghana is given in Table 1. About 56% of the water samples

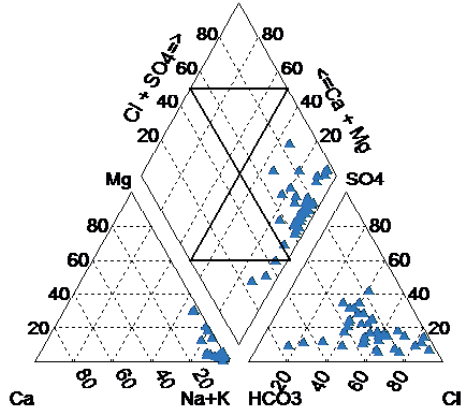


FIG. 2. Piper trilinear diagram showing the various hydrochemical facies in the Central Region groundwaters.

TABLE 1. STATISTICAL SUMMARY OF HYDROCHEMICAL PARAMETERS IN THE CENTRAL REGION GROUNDWATERS

Parameters	Units	Min.	Max.	Median	Mean
Temperature	°C	22.2	27.5	25.0	24.13
pH	pH units	5.47	7.76	6.49	6.50
EC	µS/cm	134.3	22210	1151	1783.01
TDS	mg/L	59.2	13910	724.4	1092.45
Eh	mV	-44	95	35	33.31
HCO <sub>3</sub> <sup>-</sup>	mg/L	36.60	602.60	182.00	233.26
Cl <sup>-</sup>	mg/L	22.50	1747.30	274.95	357.50
SO <sub>4</sub> <sup>2-</sup>	mg/L	18.10	407.19	108.33	121.69
Na <sup>+</sup>	mg/L	60.00	1055.75	300.00	328.19
K <sup>+</sup>	mg/L	15.00	92.50	26.00	31.60
Ca <sup>2+</sup>	mg/L	0.33	45.04	7.22	10.29
Mg <sup>2+</sup>	mg/L	0.68	71.63	6.24	10.66
NO <sub>3</sub> <sup>-</sup>	mg/L	< detection limit			
Br <sup>-</sup>	mg/L	1.2	219.30	25.53	41.77

have elevated concentrations of C<sup>-</sup> (>250 mg/L). SO<sub>4</sub><sup>2-</sup> concentration ranges between 18.00 mg/L and 407.19 mg/L. Most of the water samples have SO<sub>4</sub><sup>2-</sup> concentrations below 400 mg/L. Concentrations of NO<sub>3</sub><sup>-</sup> are below the detection limit. Br<sup>-</sup> ranges from 1.2 mg/L to 219 mg/L.

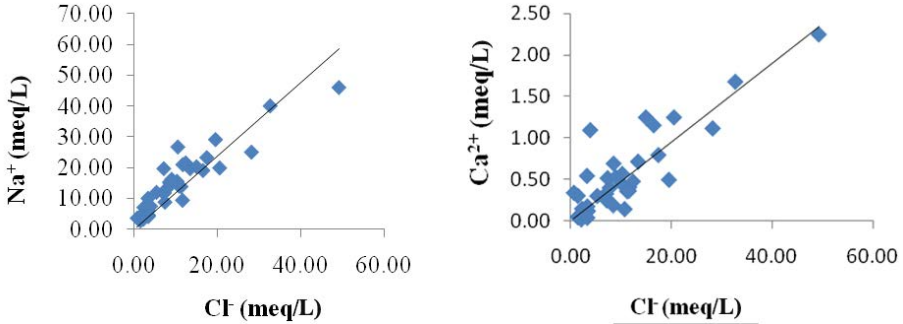


Fig. 3. Relationship between ions and  $\text{Cl}^-$  contents in the Central Region groundwaters.

Concentrations of major cations, such as  $\text{Na}^+$ ,  $\text{K}^+$ ,  $\text{Ca}^{2+}$  and  $\text{Mg}^{2+}$ , showed significant variations in the study area. The dominant cation in the area is  $\text{Na}^+$ , followed by  $\text{K}^+$ ,  $\text{Ca}^{2+}$  and  $\text{Mg}^{2+}$  whilst the dominant anion is  $\text{Cl}^-$  followed by  $\text{HCO}_3^-$  and then  $\text{SO}_4^{2-}$ . The main hydrochemical facies in the study area are  $\text{NaCl}$  and  $\text{NaHCO}_3$  water types (Fig. 2).

The relationships between the major ions of the groundwater samples were assessed to determine the sources of the ions accounting for the hydrochemical facies identified, as shown in Fig. 3. The Na and Ca ions were strongly related to  $\text{Cl}^-$  (correlation coefficient  $r^2 = 0.92, 0.87$ ), suggesting a common source of saline water (Fig. 4).  $\text{SO}_4^{2-}$  and  $\text{Cl}^-$  showed a moderate positive correlation  $r^2 = 0.67$ ).  $\text{HCO}_3^-$ ,  $\text{Mg}^{2+}$ ,  $\text{K}^+$  and  $\text{Br}^-$  showed a very weak correlation with  $\text{Cl}^-$  ( $r^2 = 0.03, 0.11$  and  $0.14$ ), suggesting that these ions may not be of a common source of saline water.

Reference [7] suggests that if the Na/Cl molar ratio is equal to 1, it can be considered that only the halite dissolution process is responsible for the supply of Na ions, but that if the molar ratio Na/Cl is more than 1, then silicate weathering is taking place. In the study area the Na/Cl molar ratio ranges from 0.80 to 5.54. This suggests that halite dissolution is not the sole hydrogeochemical process responsible for the supply of Na ions. In the study area, 59% of the samples have a Na/Cl molar ratio  $>1$  and 41% have a Na/Cl molar ratio close or equal to 1. Silicate weathering is therefore considered to be taking place in the area. This is further supported by a graph (Fig. 4) of TDS against  $\text{Na}/[\text{Na}+\text{Ca}]$ , according to Ref. [7]. This graph suggests that the Na and Ca ions are supplied by rock weathering processes. The major rock types in the area, as discussed in the section describing the study area, include mica-schist, granite, granodiorite and gneiss. Predominant minerals include plagioclase feldspars (albite and anorthite), micas and hornblende. Na rich plagioclase feldspar (albite) weathers to yield  $\text{Na}^+$  in groundwater, according to equation (1):



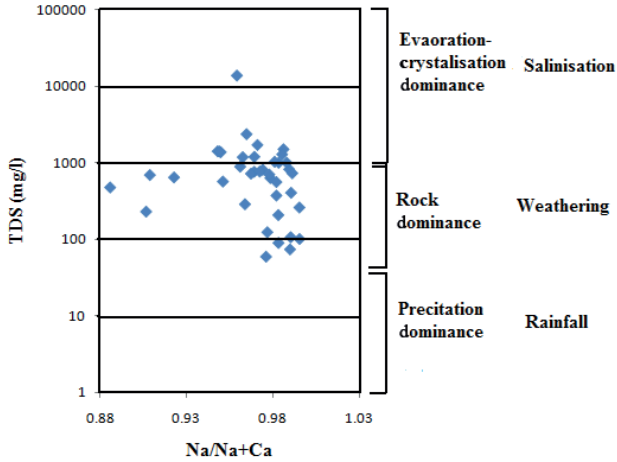


FIG. 4. Scatter plot between TDS and Na/(Na+Ca) showing rock dominant weathering and few of the samples plotting in the evaporation-crystallization dominance region.

Ca rich plagioclase feldspar will weather to yield  $\text{Ca}^{2+}$  in the groundwater water, according to equation (2):



The micas (muscovite and biotite) may weather to release  $\text{K}^+$  and  $\text{Mg}^{2+}$  in the groundwater.

The values of a few samples also are found in the evaporation-crystallization dominance region in Fig. 4. This suggests that evaporation may be also responsible for the salinization of groundwater in the study area.

The Br/Cl ratio has often been used as a reliable indicator of the origin of salinity due to its specific composition in various saline sources [8]. The Br/Cl ratio in seawater is  $0.0035 \pm 0.0002$  (weight ratio) and unpolluted maritime precipitation concentrations are close to this value [9]. The Br/Cl ratio of the groundwater samples ranges from 0.00148 to 0.7087. Only two of the 39 borehole samples collected at Gyangyanahadze and Ekumfi Owuyaw (CR 2 and CR 11) have a Br/Cl ratio below the seawater value, suggesting seawater intrusion. The rest of the samples are above the seawater value revealing minimal seawater intrusion in the area.

#### 4.2. Stable Isotopes

Stable isotopes ( $^{18}\text{O}$  and  $^2\text{H}$ ) of twenty-six groundwater samples and three surface water samples in the study area were evaluated. The  $^{18}\text{O}$  values of surface water vary from  $-2.37$  to  $-1.76\text{‰}$  V-SMOW. The  $^2\text{H}$  values of surface water vary from

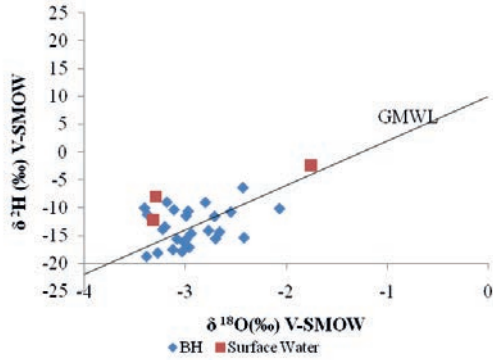


Fig. 5. Relationship between  $\delta^2\text{H}$  and  $\delta^{18}\text{O}$ .

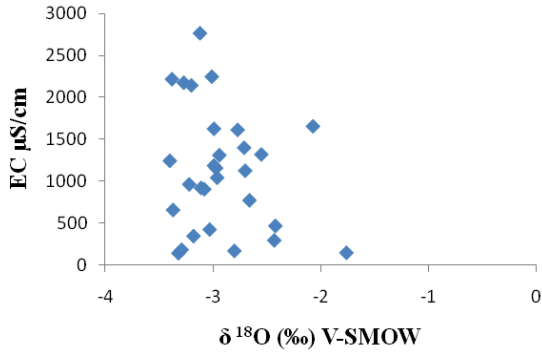


FIG. 6. Relationship between EC and  $\delta^{18}\text{O}$ ‰ V-SMOW.

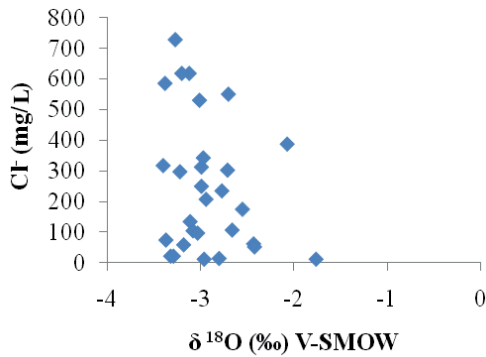


FIG. 7. Relationship between  $\text{Cl}^-$  and  $\delta^{18}\text{O}$ ‰ V-SMOW.

-12.21 to -2.37‰ V-SMOW. The  $^{18}\text{O}$  composition of groundwater ranges between -3.4 and -2.07‰ V-SMOW (mean: -2.94‰ V-SMOW). The  $^2\text{H}$  values of the groundwater vary from -18.68 to -6.33‰ with (mean: -13.36‰ V-SMOW). These values are comparable with those presented in Ref. [1] in the same terrain.

The relationships between  $\delta^2\text{H}$  and  $\delta^{18}\text{O}$  of both surface and groundwaters are presented in (Fig. 5). The surface and groundwater samples are found around the global meteoric water line (GMWL) after Ref. [10], suggesting that groundwater is recharged by direct infiltration of rain water. A few samples deviate slightly from the GMWL, indicating slight evaporation in the area. This confirms the observation made earlier in Fig. 4.

Fig. 6 shows the relationship between EC and  $\delta^{18}\text{O}$  values. The weak correlation between EC and  $\delta^{18}\text{O}$  suggests that evaporation may not be a possible cause of salinity in the area. Similarly, a weak correlation is observed for the relationship between  $\text{Cl}^-$  and  $\delta^{18}\text{O}$  (Fig. 7), indicating multiples sources of  $\text{Cl}^-$  in the area [9]. Enhanced  $\text{Cl}^-$  content of the groundwater may be due to the dissolution of salt from sea spray and marine aerosols deposited on the top soil, but further investigation on the high  $\text{Cl}^-$  concentrations is required.

## 5. CONCLUSION

The groundwater in the Central Region of Ghana is characterized by weakly acidic waters ( $5.34 \leq \text{pH} \leq 7.76$ ), high electrical conductivity (EC) along the coast and inland ( $134.3 \leq \text{EC} \leq 22\,210$ ) and total dissolved solids (TDS) within the range ( $59.2 \leq \text{TDS} \leq 13910$ ). Two major hydrochemical facies have been identified as Na-Cl and  $\text{NaHCO}_3$  water types. The Na/Cl molar ratio suggests that silicate weathering is one of the predominant hydrogeochemical processes controlling the chemical composition of groundwater in the area. The Br/Cl ratios of the majority of the groundwater samples revealed minimal seawater intrusion in the area.

The graph of stable water isotopes ( $^{18}\text{O}$  and  $^2\text{H}$ ) shows that the groundwater samples are found around the global meteoric water line, indicating that groundwaters in the study area are of meteoric origin with slight evaporation. The relationships of EC and  $\text{Cl}^-$  with  $\delta^{18}\text{O}$  suggest that evaporation is not a major cause of the salinity in the area. High  $\text{Cl}^-$  concentrations in groundwater might be due to the dissolution of salts from sea spray and marine aerosols deposited on the top soil, but further studies are needed to determine the cause.

## ACKNOWLEDGEMENT

The authors would like to thank the International Atomic Energy Agency (IAEA) for supporting the Technical Cooperation project GHA/8/009 by providing

equipments and technical expertise. We are also grateful to the National Nuclear Research Institute (NNRI) for logistical and financial support during the field programme. We appreciate the assistance by the staff of the chemistry department especially Nash Bentil, John Senu and Eunice Agyeman, for conducting laboratory analysis of the samples.

## REFERENCES

- [1] ARMAH, T.E.K., "Groundwater salinisation in parts of southern Ghana", Groundwater: Past Achievements and Future Challenges (SILOLO, O., et al., Eds), Balkema, Rotterdam, (2000).
- [2] UNITED NATIONS EDUCATIONAL, SCIENTIFIC AND CULTURAL ORGANIZATION., Groundwater in Hard Rocks: Project 8.6 of the International Hydrological Programme (LARSSON, I., Ed.), UNESCO, Paris (1984).
- [3] GROBE, M., et al., Saline groundwater in the Münsterland Cretaceous Basin, Germany: Clues to its origin and evolution, *Mar. Petrol. Geol.* **19** (2002) 307–322.
- [4] CARTWRIGHT, I., et al., Hydrogeochemical and isotopic constraints on the origins of dryland salinity, Murray Basin, Victoria, Australia, *Appl. Geochem.* **19** (2004) 1233–1254.
- [5] LEUBE, A., et al., The early Proterozoic Birimian Supergroup of Ghana and some aspects of its associated gold mineralization, *Precambrian Research* **46** (1990) 139–165.
- [6] KESSE, G.O., *The Mineral and Rock Resources of Ghana*, Balkema, Rotterdam (1985).
- [7] SINGH, C.K., et al., Integrating multivariate statistical analysis with GIS for geochemical assessment of groundwater quality in Shiwaliks of Punjab, India, *Environ. Earth. Sci.* **62** (2011) 1387–1405.
- [8] DE MONTETY, V., et al., Origin of groundwater salinity and hydrogeochemical processes in a confined coastal aquifer: Case of the Rhône delta (Southern France), *Appl. Geochem.* **23** (2008) 2337–2349.
- [9] HELSTRUP, T., *Environmental Isotopic and Hydrochemical Characteristics of Groundwater from the Cretaceous-Eocene Limestone Aquifer in the Keta Basin of Togo*, PhD Thesis, Geological Institute, University of Copenhagen (2006).
- [10] CRAIG, H., Isotopic variations in meteoric waters, *Science* **133** 3465 (1961) 1702–1703.



# URANIUM ISOTOPES AS A TRACER OF GROUNDWATER EVOLUTION IN THE COMPLEXE TERMINAL AQUIFER OF SOUTHERN TUNISIA

F. HADJ AMMAR<sup>a,b</sup>, P. DESCHAMPS<sup>b</sup>, N. CHKIR<sup>a</sup>, B. HAMELIN<sup>b</sup>,  
K. ZOUARI<sup>a</sup>

<sup>a</sup> Laboratory of Radio-Analysis and Environment,  
National School of Engineering of Sfax, Sfax, Tunisia

<sup>b</sup> Centre Européen de Recherche et d'Enseignement  
de Géosciences de l'Environnement,  
Aix en Provence, France

## Abstract

The Complexe Terminal (CT) aquifer system is the main water supply for remote areas of southern Tunisia. Its exploitation has resulted in significant draw-down of the water table. The CT aquifer is a multilayered aquifer lodged in Miocene sand deposits, Senonian limestones and Turonian carbonates. Little is known about the relationships and exchanges between the different layers. Here, uranium isotopic measurements carried out in groundwater samples from the CT aquifer are presented in order to constrain models for mixing of water masses, water-rock interaction and groundwater flow. Analyses were performed using a VG54 (TIMS) at the CEREGE. Results indicate a range in  $^{238}\text{U}$  concentration and  $^{234}\text{U}/^{238}\text{U}$  activity ratios of 1.5 to 8 ppb and 1.1 to 3.2 respectively. Together with major and trace analyses, uranium isotopic compositions provide important insights into the factors controlling the chemical evolution of groundwater and shows very distinct patterns between carbonate and sandstone layers.

## 1. INTRODUCTION

The mechanisms of entry of naturally occurring radioelements in the uranium and thorium decay series vary between the different parents and daughters or decay products. The decay of these radioelements ultimately leads to the formation of multiple radiogenic daughter products, including different isotopes of uranium ( $^{238}\text{U}$ ,  $^{234}\text{U}$ ), thorium ( $^{230}\text{Th}$ ,  $^{228}\text{Th}$ ), radium ( $^{228}\text{Ra}$ ,  $^{226}\text{Ra}$ ,  $^{224}\text{Ra}$ ), and radon ( $^{222}\text{Rn}$ ,  $^{220}\text{Rn}$ ) [1].

Uranium, which is the radioelement of interest in this study, is exceptionally complex in terms of hydrochemistry. The concentration and mobility of radioelements in groundwater are ultimately a function of a number of chemical and physical factors. Its solubility is affected by factors including Eh, pH and the presence of particular chemical compounds.

Uranium exists in U(IV) or U(VI) oxidation states in groundwater depending on the environmental conditions. The U(VI) state is highly soluble, unlike U(IV) which is sparingly soluble. In general, U is soluble in oxidizing natural waters, occurring as the uranyl cation, and tends to form stable carbonate complexes [2, 4].

The formation of carbonate complexes can change the stability field of U(VI). These U(VI) complexes may exist in alkaline conditions and high carbonate concentrations even in reducing conditions. As demonstrated also in Ref. [5], U behaves conservatively in oxygenated groundwaters such as those found in the southern Great Basin in North America [6]. In reducing waters, U is insoluble and exists as U(IV) [2, 3, 7].

Radioactive disequilibria among the uranium isotopes ( $^{234}\text{U}$ – $^{238}\text{U}$ ) is related to the different mobility of these two nuclides during water–rock interactions, which is seen as a consequence of  $\alpha$ -recoil; such processes enhance  $^{234}\text{U}$  mobility, inducing an enrichment of this isotope in surface water and geochemical sorting or differentiation processes [8].

The distribution and the patterns of environmental disequilibrium of naturally occurring uranium isotopes ( $^{234}\text{U}$  and  $^{238}\text{U}$ ) in waters suggest that variations in isotopes activity ratios and concentrations can be used to describe aquifer processes, to classify aquifers or to evaluate the mixing proportions of waters from different sources. Uranium is unique in its potential as a useful tracer in hydrologic investigations [9].

The objective of this study was to determine activity concentrations of uranium as a natural radioactive element in groundwater samples from the Complexe Terminal aquifer in southern Tunisia, by adopting advanced instrumental techniques as well as to identify parameters controlling the origin of the  $^{234}\text{U}$ – $^{238}\text{U}$  fractionation in groundwaters. From the observed uranium isotope disequilibria, we determined water–rock interactions, including precipitation and dissolution processes, and their influence on radionuclide transport and transit time of groundwater in the aquifer.

## 2. STUDY AREA

The investigated area is located in southern Tunisia (Fig. 1). This zone is characterized by an arid/semiarid climate and limited water resources. Meteorological records indicate irregular rainfall of 100 to 200 mm, high average annual evapotranspiration and that water deficit is particularly significant. The annual evaporation is even greater than 2500 mm and the mean annual temperature is of the order of 21°C. Therefore, fossil water constitutes the main part of the groundwater resources in the study area. It represents 58% of the total of deep aquifers in Tunisia. In these arid and semiarid regions, population is dispersed and groundwater has emerged as a vital source of water. Water needs are extensive and agriculture is the most important activity (oasis).

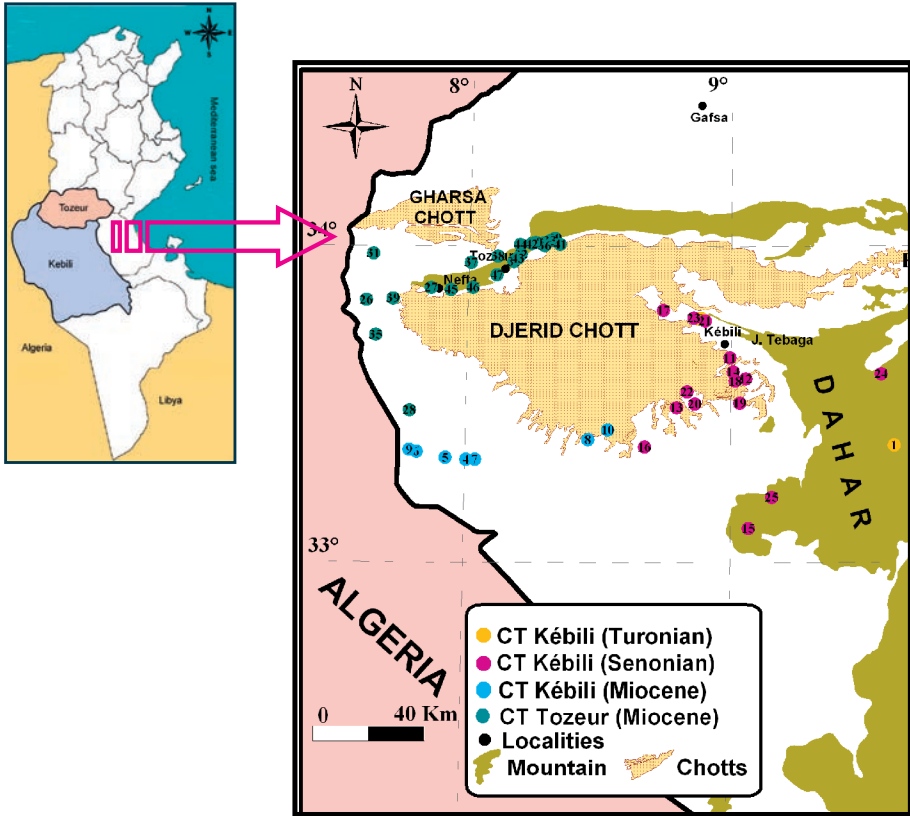


FIG. 1. Map of the studied area.

### 3. GEOLOGY AND HYDROGEOLOGY

The regional geology has been discussed by several authors [10–12]. The oldest geological formations are sandstone of the Continental Intercalaire, while the youngest are the detrital deposits of the Plio-Quaternary. The most common outcrops from the Middle and Upper Cretaceous are the Cenomanian and the Turonian formations, covered by the Senonian [10–12]. Upper Cretaceous sedimentary sequences extend over the Saharan platform and outcrop on surrounding uplands due to the presence of several N–S and W–E faults [13–15]. They are composed of alternations of thick shallow and deep marine clays, shales and carbonate deposits.

The CT aquifer is constituted of three stratigraphic units: the Miocene detrital aquifer, the Senonian limestone aquifer and the Turonian Carbonate/Dolomite aquifer.

In the Kébili region, hosting formations are mainly Cretaceous limestones (Senonian and Turonian). The Senonian aquifereous level is exploited in rural areas to supply domestic water and to meet agricultural needs [16]. Transmissivities of

the Senonian aquifer range between  $50 \times 10^{-3}$  and  $150 \times 10^{-3}$  m<sup>2</sup>/s [17]. The Turonian is relatively more homogeneous than the Senonian and is represented by limestone and dolomite/limestone. It is fractured and karstic with a mean thickness of about 50 m (rarely exceeding 100 m). Although, its thickness is limited, the Turonian aquifer is characterized by high transmissivity, generally around  $300 \times 10^{-3}$  m<sup>2</sup>/s. Turonian formations lodge an aquifer which quickly becomes confined under the Senonian and which is directly in contact with Plio-Quaternary at the bounds of the basin. This aquiferous level, exploited since the 80's by deep boreholes, constitutes the principal water bearing formation in the Kebili region.

In the Djérid region (Redjim Maâtoug and Tozeur areas), sandy Miocene formations make up the aquifer. Transmissivities of the Miocene aquifer range between  $10^{-3}$  and 100 m<sup>2</sup>/s. The aquifer is confined in its major part. It becomes unconfined only in the east of the Dahar regions and near the Tozeur uplift where the Pontian sands outcrop.

Over the last two decades, increasing water demand for agriculture, industry and domestic uses has led to the overexploitation of groundwater resources. Currently, the rate of water extraction far exceeds the rate of water recharge, resulting in the gradual depletion of the CT aquifer. Drilling exploiting the CT aquifer has been continuing in southern Tunisia since 1950, which resulted in an increase in pumped discharge from around 3000 L/s in 1974 to more than 14000 L/s in 2005. Artesian discharge disappeared due to the intensive exploitation of this aquifer. Only some wells situated in the low zones are still artesian. Indeed, since 2000 all springs have dried up and all water needs are exclusively met from the deep aquifers.

#### 4. SAMPLING AND ANALYTICAL METHODS

A sampling campaign of 47 wells was carried out during March 2009. Samples were collected at different depths. Polyethylene sample bottles were washed successively with diluted nitric acid and were triple rinsed with sample groundwater prior to filling. All the samples were filtered with a 0.45 µm cartridge filter and were preserved with nitric acid (HNO<sub>3</sub>) to prevent precipitation.

The uranium isotopic compositions were determined at the CEREGE using chemical separation and VG54 (TIMS) procedures. Enriched spikes of <sup>233</sup>U, <sup>236</sup>U (<sup>233</sup>U/<sup>236</sup>U) and <sup>229</sup>Th (<sup>230</sup>Th/<sup>229</sup>Th) were added to 200 mL of water samples. Uranium was pre-concentrated from filtered water samples by co-precipitation with Fe-hydroxide at pH 8 using ammoniac solution. The precipitate was recuperated by centrifugation and then dissolved in 4 M HNO<sub>3</sub>.

This solution was passed through an ion exchange using UTEVA [Uranium and Tetravalent Actinide] resin which is able to separate and concentrate uranium and tetravalent actinides from aqueous solutions. After being washed with Milli-Q

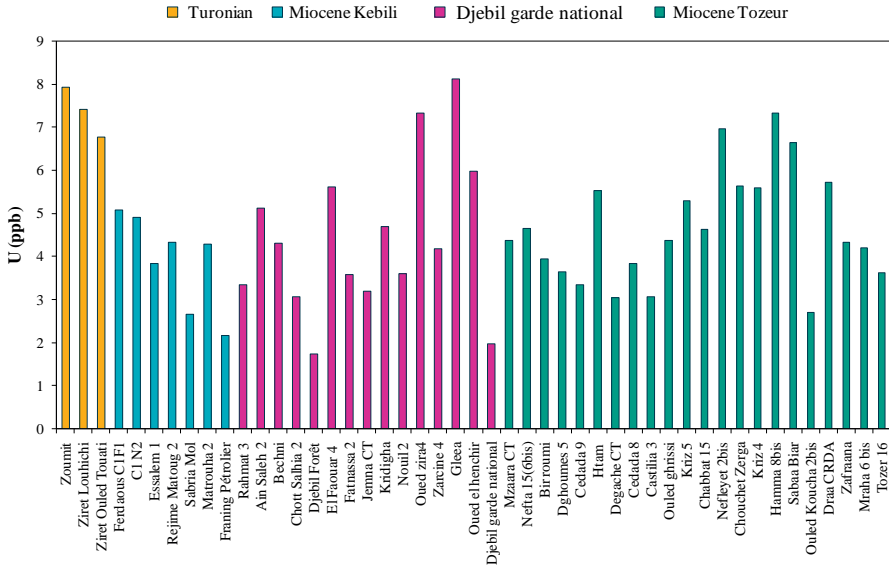


FIG. 2. U contents of all analysed water samples.

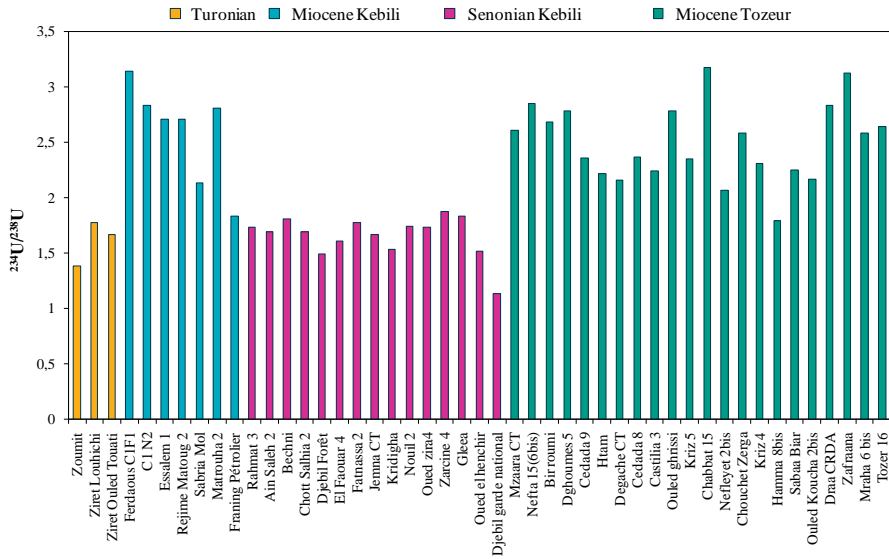


FIG. 3.  $^{234}\text{U}/^{238}\text{U}$  activity ratios of all analysed water samples.

water, uranium is directly eluted. The resulting solution was evaporated in order to be loaded on rhenium filament.

Major element analyses were carried out in the Laboratory of Radio-Analysis and Environment of the National School of Engineering of Sfax with liquid ion chromatography (HPLC) on a Waters chromatograph equipped with columns IC-PakTM CM/D for cations, using EDTA and nitric acid as eluents and on a Metrohm chromatograph equipped with columns CI SUPER-SEP for anions using phthalic acid and acetonitrilic as eluents. The overall detection limit for ions was 0.04 mg/L.

## 5. RESULTS

Groundwater sampled from the Complexe Terminal aquifer has a U content ranging from 1.5 to 8 ppb. The Carbonate (Senonian) and sandy (Miocene) aquifers both cover this entire range of variation (Fig. 2). The three samples collected from the Turonian levels have uranium contents in the upper range (6.7 to 7.93 ppb). The variability in U content in water samples is, therefore, in agreement with the lithological variability of the studied area. The large variation in U concentration also suggests varying degrees of water–rock interactions.

The lowest values of  $^{238}\text{U}$  (1.75 ppb and 1.98 ppb) have been obtained in water from Djebil Forêt and Djebil Garde National wells that are located near the recharge area of the aquifer.

All the groundwater samples have  $^{234}\text{U}/^{238}\text{U}$  activity ratios greater than 1, varying between 1.14 and 3.14 (Fig. 3). Such results indicate that  $^{234}\text{U}$  nuclides are leached preferentially to  $^{238}\text{U}$  from the mineral structures. This is usually attributed to recoil displacement of the daughter product  $^{234}\text{Th}$ , resulting from alpha decay in the radioactive series, which in consequence causes lattice destruction and bond breakage [18]. Moreover, oxidation of  $^{234}\text{U}$  from U (IV) to U (VI) may also occur during the process and the form  $^{234}\text{U}$  (VI) is then preferentially leached to the water [19].

The results illustrated in Fig. 3 also show that the Miocene sands bear higher and more variable  $^{234}\text{U}/^{238}\text{U}$  activity ratios (from 1.8 to 3.2) than the Senonian and Turonian carbonates (from 1 to 1.8).

The results from this study may provide important insights into the factors controlling uranium concentrations in CT groundwater in southern Tunisia.

U contents are broadly correlated with  $\Sigma$  cations (Fig. 4). The heterogeneity of the concentrations of most chemical elements confirms that the groundwaters' mineralization is the combined result of water–rock interaction and probable mixing relationships between the different aquifer horizons.

Uranium concentration has often been reported to be associated with carbonate concentrations in surface and underground water, as uranium has a higher solubility due to complexation with carbonates [20]. In this case, the concentration of  $\text{HCO}_3^-$ ,

which could be controlled by the dissolution or precipitation of calcite, is not correlated with the U content.

In contrast, as shown in Fig. 5, it seems that sulphate and uranium concentrations are correlated with each other in the CT groundwater. Sulphate also commonly forms soluble complexes with uranium and thereby increases its solubility [21]. So, the concentration of uranium in these groundwaters is probably influenced by the dissolution of evaporitic salts. Indeed, gypsum is present in the Cretaceous–Tertiary strata which are thought to overlie the Jurassic strata in the major part of the basin.

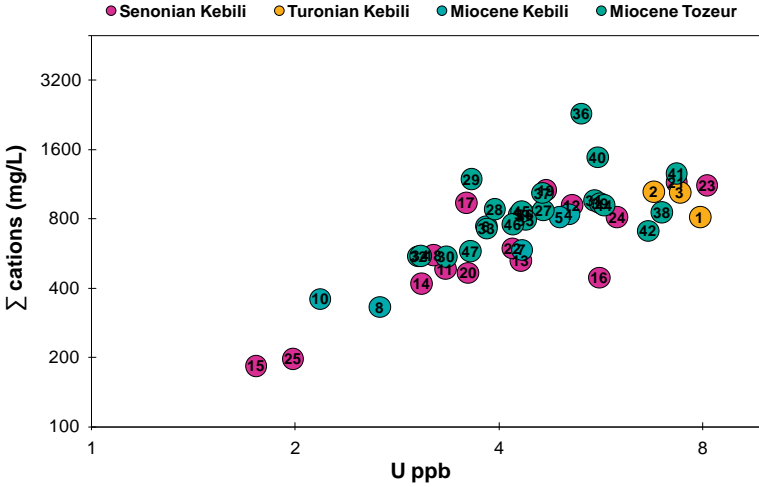


FIG. 4. Relation between  $\Sigma cations$  and U content.

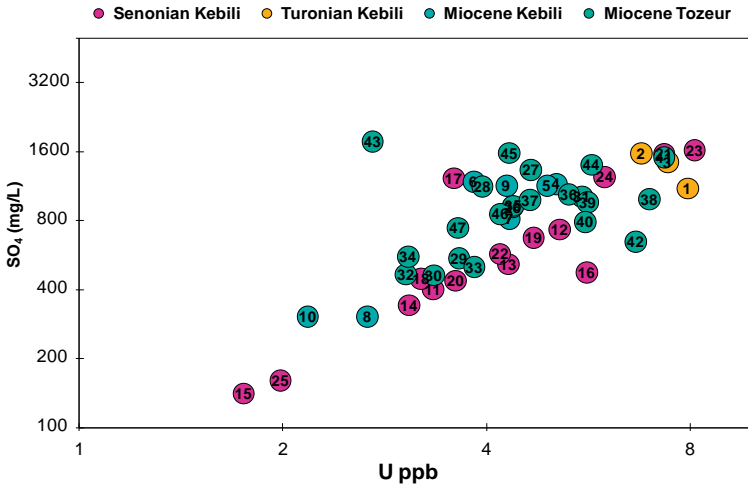


FIG. 5. Relation between  $SO_4$  concentration and U content.

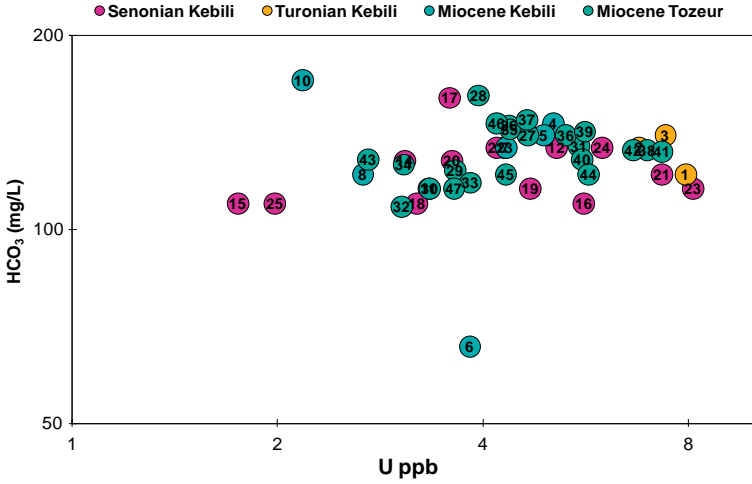


FIG. 6. Relation between  $HCO_3^-$  concentration and U content.

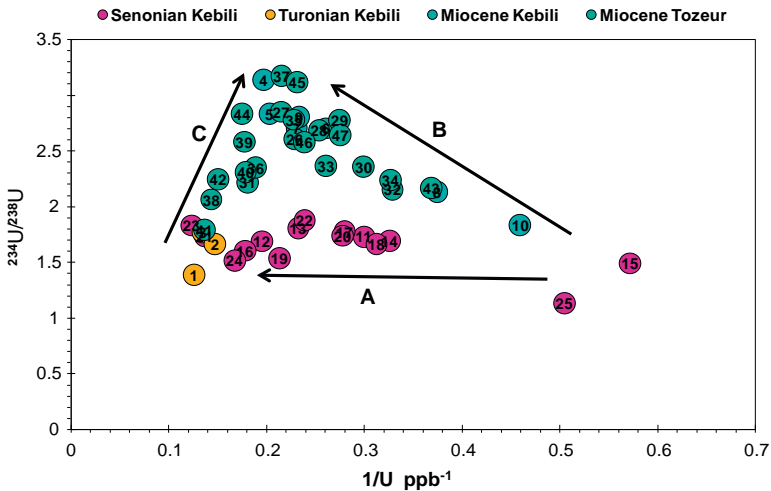


FIG. 7.  $^{234}U/^{238}U$  AR versus reciprocal U content.

$^{234}U/^{238}U$  activity ratios are represented in Fig. 7 as a function of a reciprocal function of concentrations of uranium, in order to define the mixing relationships between the different groundwater types [22]. Relationships between three different endmembers can be highlighted in the Complexe Terminal aquifer.

The samples from the carbonate formations of Senonian and Turonian aquifer lie along the lowest side of the three endmember triangle, with nearly constant  $^{234}U/^{238}U$  AR around 1.5. The samples closest to the recharge have the lowest uranium concentration along this trend (sample #15 and 25), while the highest is found in

the Turonian aquifer. This trend ('A' in Fig. 7) is thus compatible with a progressive leaching of uranium from the parent limestone, along the flow path of groundwater.

A third endmember with high  $^{234}\text{U}/^{238}\text{U}$  ( $>3$ ) and relatively high U content is represented by the sandy Miocene samples in Kebili (#4) and Tozeur (#35, #45). All other samples from the sandy miocene aquifer are then randomly scattered between those three endmembers, corresponding to mixtures in various proportions between different water bodies, along trend 'B' and 'C'.

Alternatively, trend 'B' may also be compatible with a possible hypothesis of a preferential dissolution of  $^{234}\text{U}$  from the matrix rock [23].

## 6. CONCLUSION

The CT represents a prime example of an overexploited aquifer since it is damaged by enhanced pumping for water supply. Isotopic measurements of U ( $^{238}\text{U}$  and  $^{234}\text{U}$ ) and major element content in groundwaters are used to provide reliable information about the processes that control the chemical evolution of groundwater and to identify parameters controlling the origin of the  $^{234}\text{U}$ - $^{238}\text{U}$  fractionation. Our results show that groundwater geochemistry is ultimately a result of lithologic variations associated with water-rock interaction and dissolution of limestone, dolomite, carbonate and gypsum found among the aquifer formations. Our results help us to elucidate the mixing relationships between the different aquifer horizons.

## ACKNOWLEDGEMENTS

We are grateful to both technical staffs of the Centre Européen de Recherche et d'Enseignement des Géosciences de l'Environnement and the Laboratory of Radio-Analysis and Environment of Sfax, who provided help with sample analysis.

## REFERENCES

- [1] COPENHAVER, S.A., KRISHNASWAMI, S., TUREKIAN, K.K., EPLER, N., COCHRAN, J.K., Retardation of  $^{238}\text{U}$  and  $^{232}\text{Th}$  decay chain radionuclides in Long Island and Connecticut aquifers, *Geochim. Cosmochim. Acta* **57** 3 (1993) 597–603.
- [2] LANGMUIR, D., Uranium solution-mineral equilibria at low temperatures with applications to sedimentary ore deposits, *Geochim. Cosmochim. Acta* **42** (1978) 547–569.
- [3] KLINKHAMMER, G.P., PALMER, M.R., Uranium in the oceans: Where it goes and why, *Geochim. Cosmochim. Acta* **55** (1991) 1799–1806.
- [4] READ, D., et al., The migration of uranium into peat-rich soils at Broubster, Caithness, Scotland, U.K., *J. Contam. Hydrol.* **13** 1–4 (1993) 291–308.

- [5] OSMOND, J.K., COWART, J.B., "Ground water", Uranium-series Disequilibrium: Applications to Environmental Problems (IVANOVICH, M., HARMON, R.S., Eds), Clarendon Press, Oxford (1982) 202–245.
- [6] WINOGRAD, I.J., ROBERTSON, F.N., Deep oxygenated ground water: Anomaly or common occurrence?, *Science* **216** (1982) 1227–1230.
- [7] DREVER, J.I., *The Geochemistry of Natural Waters*, Prentice Hall, Englewood Cliffs, New Jersey (1988).
- [8] IVANOVICH, M., HARMON, R.S., (Eds), *Uranium-Series Disequilibrium: Application to Earth, Marine and Environmental Sciences*, Clarendon Press, Oxford (1992).
- [9] OSMOND, J.K., RYDELL, H.S., KAUFMAN, M.I., Uranium disequilibrium in groundwater: An isotope dilution approach in hydrologic investigations, *Science* **162** 3857 (1968) 997–999.
- [10] CASTANY G., L'accident Sud-Tunisien, son âge et ses relations avec l'accident Sud-Atlasique d'Algérie, C.R. Séances Acad. Sc. Paris, V. 238 (1954) 916–918.
- [11] BUSSON, G., *Le Mésozoïque saharien*, 2 vols, Centre National de la Recherche Scientifique, Paris (1970).
- [12] BOUAZIZ, S., Etude de la tectonique cassante dans la plateforme et l'Atlas Sahariens (Tunisie Meridionale): Evolution des paleochamps de contraintes et implications géodynamiques, Thèse de Doctorat, Fac. Sc. De Tunis (1995) 301p.
- [13] BUROLLET, P.F., Contribution à l'étude stratigraphique de la Tunisie central, *Ann. Min. et Géol.* **18** (1956).
- [14] BUSSON, G., *Le Mésozoïque saharien. 1ère partie: L'Extrême Sud-tunisien*. Edit., Paris, «Centre Rech. Zones Arides», *Géol.*, 8 (1967) 194 pp.
- [15] BOUAZIZ, S., MELLO, J., Etude géologique de la région de Tataouine, internal report, Office National des Mines, Tunis (1987) 139 pp.
- [16] OSS, *Système Aquifère du Sahara Septentrional: Hydrogéologie*, Volume 2, OSS, Tunisia (2003).
- [17] MAMOU, A., Caractéristiques, évaluation et gestion des ressources en eau du Sud Tunisien, PhD Thesis, University of Paris South, Paris (1990).
- [18] OSMOND, J.K., COWART, J.B., IVANOVITCH, M., Uranium isotopic disequilibrium in ground water as an indicator of anomalies, *Int. J. Appl. Radiat. Isot.* **34** (1983) 283–308.
- [19] SUKSI, J., Natural Uranium as a Tracer in Radionuclide Geosphere Transport Studies, Academic Dissertation, University of Helsinki (2001).
- [20] OURAL, C.R., UPCHURCH, S.B., BROOKER, H.R., Radon progeny as sources of gross  $\alpha$  radioactivity anomalies in ground water, *Health Phys.* **55** (1988) 889–894.
- [21] BANKS, D., RØYSET, O., STRAND, T., SKARPHAGEN, H., Radioelement (U, Th, Rn) concentrations in Norwegian bedrock groundwaters, *Environ. Geol.* **25** (1995) 165–180.
- [22] OSMOND, J.K., COWART, J.B., The theory and uses of natural uranium isotopic variations in hydrogeology, *Atomic Energy Rev.* **144** (1976) 621–679
- [23] ANDREWS, J.N., et al.,  $^{234}\text{U}/^{238}\text{U}$  activity ratios of dissolved uranium groundwaters from a Jurassic limestone aquifer in England, *Earth Planet. Sci. Lett.* **57** (1982) 139–151.

# INSIGHT INTO GROUNDWATER FLOW WITHIN A CRYSTALLINE AQUIFER

*Case study of the Ursuya Mount, Northern Basque Country  
(France)*

J. JAUNAT <sup>a</sup>, F. HUNEAU <sup>a</sup>, A. DUPUY <sup>a</sup>, H. CELLE-JEANTON <sup>b</sup>,  
M. FRANCESCHI <sup>a</sup>, P. LE COUSTUMER <sup>a</sup>

<sup>a</sup> Université de Bordeaux, Institut EGID,  
EA Géoresources & Environnement,  
Pessac, France

<sup>b</sup> Université de Clermont-Ferrand, LMV UMR 6524,  
Clermont-Ferrand, France

## **Abstract**

Stable isotopes of the water molecule and tritium in conjunction with geochemistry have been used to understand the groundwater flow pattern and origin within the gneissic aquifer of the Ursuya Mount. This aquifer constitutes one of the main water supplies of the Northern Basque Country and improved knowledge about the water recharge, origin, quality and residence time is of strategic importance for a sustainable development of the resource. 16 springs, 4 boreholes and total rainfall have been sampled monthly since summer 2009. Preliminary results indicate complex and contrasted groundwater flows within the aquifer. Shallow groundwater restricted to the upper weathered horizons is characterized by a strong influence of anthropogenic inputs. At depth, groundwater mainly circulates along the major structural discontinuities of the gneiss in semi-confined conditions. These levels, providing the most promising resource for the water supply, show increased water mineralization caused by a longer residence time of groundwater and hence indicate a slower dynamic of the system.

## 1. INTRODUCTION.

The gneissic aquifer of the Ursuya Mount is one of the main water supplies of the Northern Basque Country. This geographical zone is subject to strong water needs constantly on the increase. A study has been conducted since 2009 on this aquifer in order to improve the knowledge of its potential and its hydrodynamic properties. The development of a general method relevant to all types of bedrock aquifers within the region will result from this work.

The fundamental characteristic of fractured rock aquifers is spatial variability in hydraulic conductivity and hence groundwater flow rate. Because of this

heterogeneity, a number of methods that are traditionally used for characterizing porous media aquifer systems are of limited relevance in fractured rock aquifers [1–3]. In this context, geochemical and isotopic tools are useful complements for understanding the functioning of this fractured aquifer and for hard rock aquifers in general.

## 2. FRAMEWORK AND OBJECTIVES

The Ursuya Mount is situated between the towns of Hasparren and Macaye and about 30 km from the city of Bayonne. Its area is about 45 km<sup>2</sup>. Because of the special situation of this mountain beside the Pyrenees, the crystalline formations (Precambrian gneiss) are affected by a strong regional metamorphism. Two separate units were identified by Ref. [4] (top of Fig. 1): paragneiss with biotites at the bottom and basic gneiss at the top.

The study area is often covered by a more or less important layer of weathered material (frequently more than 10 m; bottom of Fig. 1). Many authors agree with the capacitive function of those materials (e.g. Refs [5, 7]). The underlying fractured bedrock essentially has a transmission function.

At least two hydrological cycles are required to get the necessary data to meet the following objectives of: (a) clarifying the aquifer potential of the site both quantitatively and qualitatively; (b) determining geographic and seasonal variations; (c) understanding the origin and the flow pattern of the groundwater; (d) evaluating the groundwater residence times and the areas of preferential recharge. Various methods are used in this study. Here, we present only some geochemical and isotopic data. Thus, structural or hydrodynamic approaches will not be discussed here.

## 3. MATERIAL AND METHODOLOGY

Since summer 2009, water from 15 springs has been collected monthly (Fig. 1). Rainwater has also been collected. Four samplers are distributed across the catchment. One sequential precipitation collector (Eigenbrodt) is deployed at about 600 m altitude. It allows the sampling of rainwater for two days, avoiding evaporation after collection (Has; Fig. 1). 3 additional collectors allow the sampling of the total monthly precipitations (Zub, Cambo and Mend; Fig. 1). Electrical conductivity, temperature, pH and alkalinity are measured in the field at all sampling points. Major ion analyses (Cl<sup>-</sup>, NO<sub>3</sub><sup>-</sup>, SO<sub>4</sub><sup>2-</sup>, Ca<sup>2+</sup>, Mg<sup>2+</sup>, K<sup>+</sup> and Na<sup>+</sup>) are performed for all samples by ion chromatography in liquid phase in the laboratory of the EGID Institute at the University of Bordeaux. Analyses of the stable isotopes of groundwater and rainwater (<sup>18</sup>O and <sup>2</sup>H) are performed using a liquid-water stable isotope analyser (DLT-100 Los Gatos Research) respecting the analytical scheme

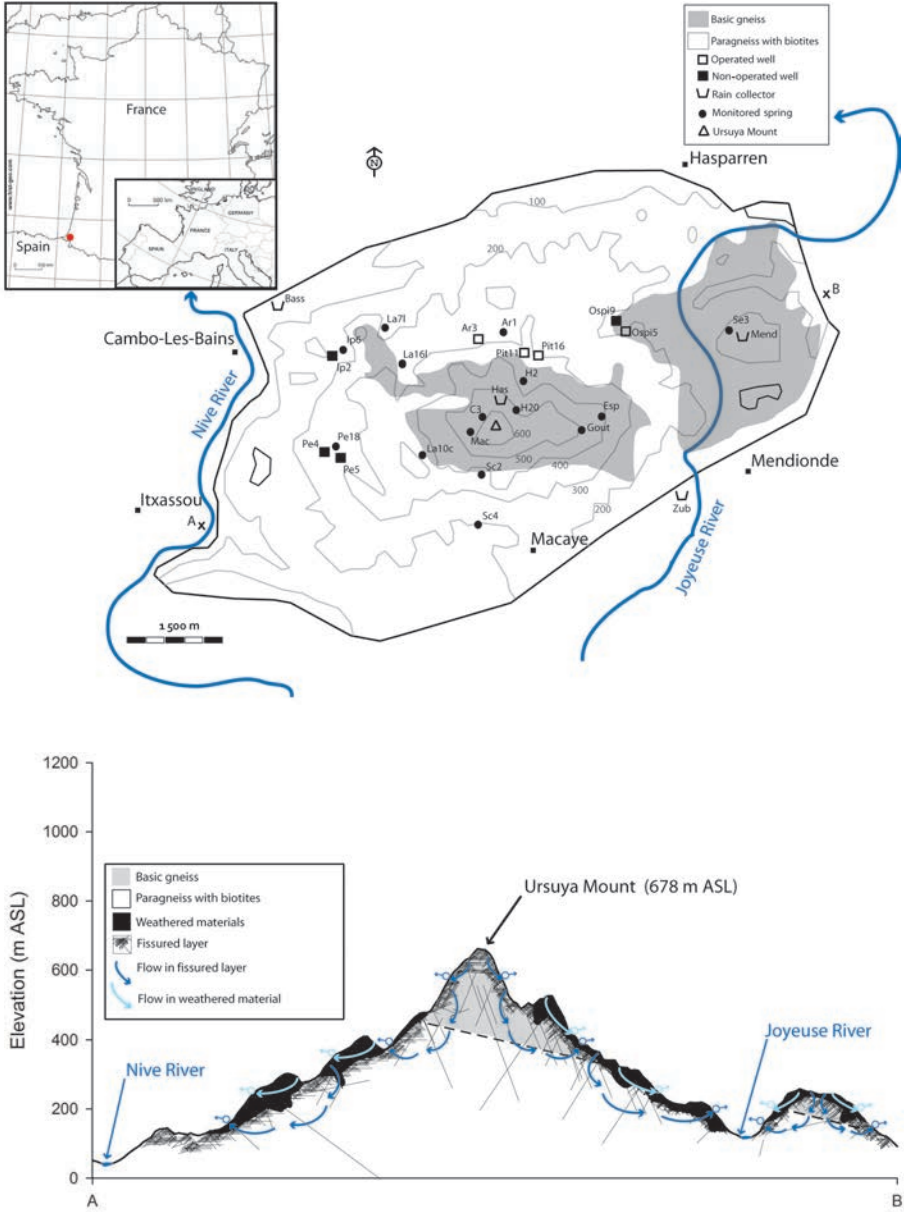


FIG. 1. Top: topography and geology of the site and location of the sampling points. Bottom: conceptual diagram of the Ursuya aquifer; see location of the cross section on the top figure; adapted from Refs [5] and [6].

recommended by the IAEA [8, 9]. The water of the 15 springs and 3 operated wells (Fig. 1) were also analysed for  $^3\text{H}$  content in September 2010. The analyses were conducted at the Hydrogeology Department of the University of Avignon by liquid scintillation counting.

#### 4. RESULTS AND DISCUSSION

##### 4.1. Geochemical data

Groundwater of the Ursuya Mount presents significant geochemical variations. Fig. 2 shows the Stiff Diagrams of the 15 monitored springs. These diagrams were drawn up using the average concentrations from measurements carried out since 2009 at each sampling point. Very low concentrations are observed (0.8 meq/L or less). This reflects the low mineralization of the groundwater in this aquifer. Indeed, the measured electrical conductivities range from 31.7  $\mu\text{S}/\text{cm}$  (SE3 on 2010/07/10) to 198.3  $\mu\text{S}/\text{cm}$  (SC4 on 2011/05/10) with an average value of 82.5  $\mu\text{S}/\text{cm}$ . The results indicate 4 different water types: Ca-Na (C3, H20, LA16l and SE3);  $\text{HCO}_3$ -Ca-Mg

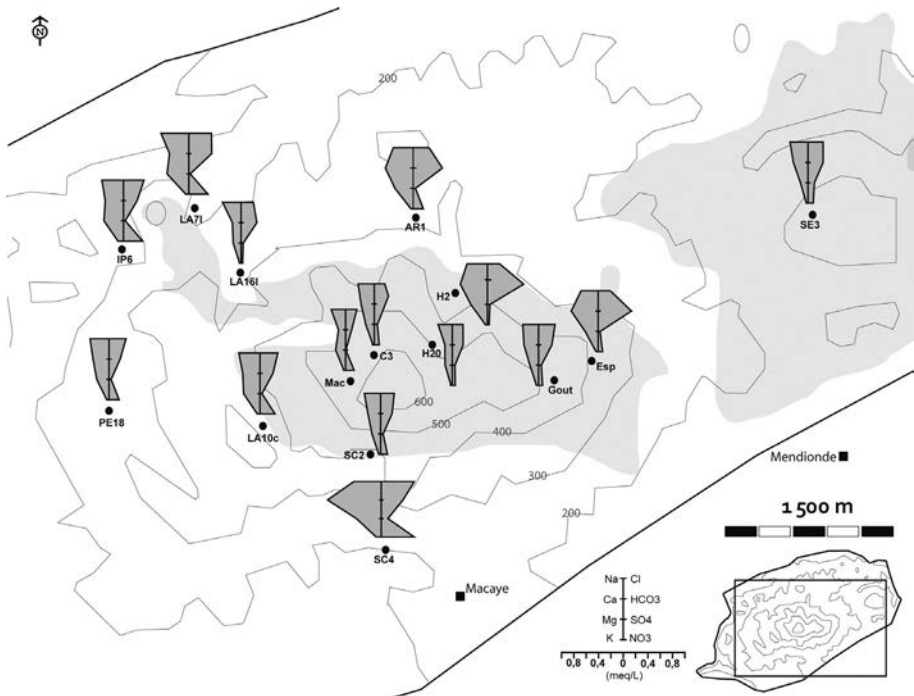


FIG. 2. Geographical distribution of the groundwater types (Stiff Diagrams) of the monitored springs.

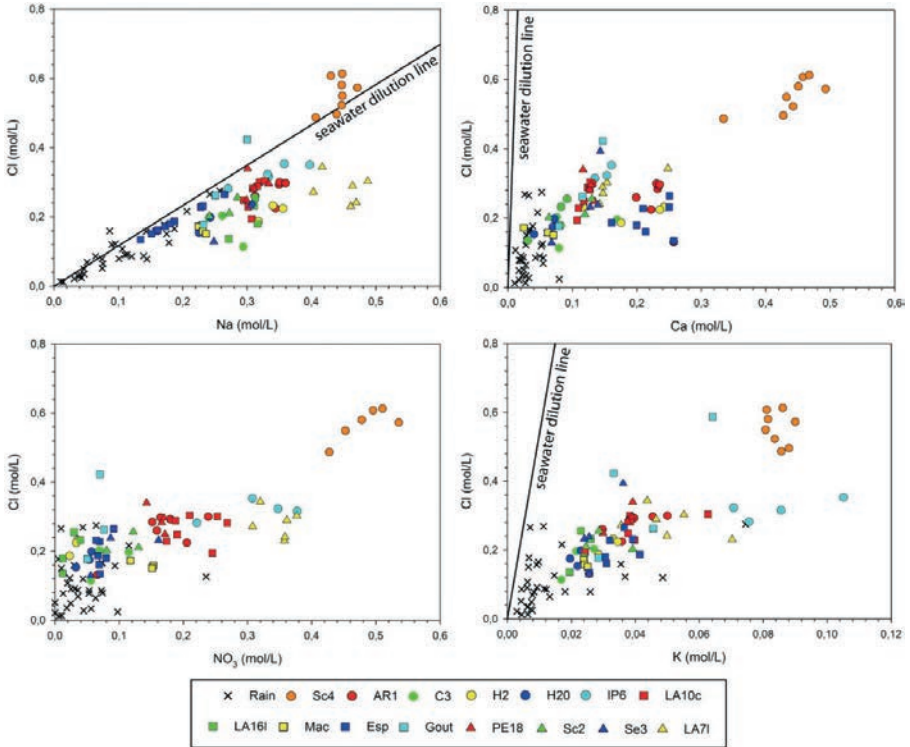


FIG. 3. Plot of chloride vs. major ion (Na, Ca,  $\text{NO}_3$ , K,  $\text{SO}_4$ ) content from the monitored springs and from the rainwater sampled at the Hasp station. The seawater dilution line is also displayed.

(AR1, Esp and H2); Cl-Na (IP6, LA7I, LA10c and Mac); Cl-Ca-Mg (Gout, Pe18 and SC2). SC4 stands out with a Cl-Ca water-type.

When comparing the concentrations with a conservative tracer of marine origin such as chloride the influence of the Atlantic Ocean is very marked. Fig. 3 shows Cl vs. Na, Ca,  $\text{NO}_3$  and K diagrams.

The Cl vs. Na diagram underlines the purely oceanic origin of the air masses at the origin of the precipitation. Indeed, rainwater data are plotted along the seawater dilution line. The rainwater is slightly enriched in Ca. Ca originates mainly from terrestrial sources (dissolution of regional limestone or alluvial carbonated sediments or Saharan dusts) [10]. Ca concentrations could also be associated with anthropogenic origin (traffic, cement factories) [11]. The Cl vs. K and Cl vs.  $\text{NO}_3$  charts show the anthropogenic influence on the composition of the rainwater with enrichment in K and  $\text{NO}_3$  compared to the seawater dilution line. K has its main origin in anthropogenic aerosols (wood fires) and the  $\text{NO}_3$  concentrations are explained by significant agricultural activity in the study area and its surroundings (meadows).

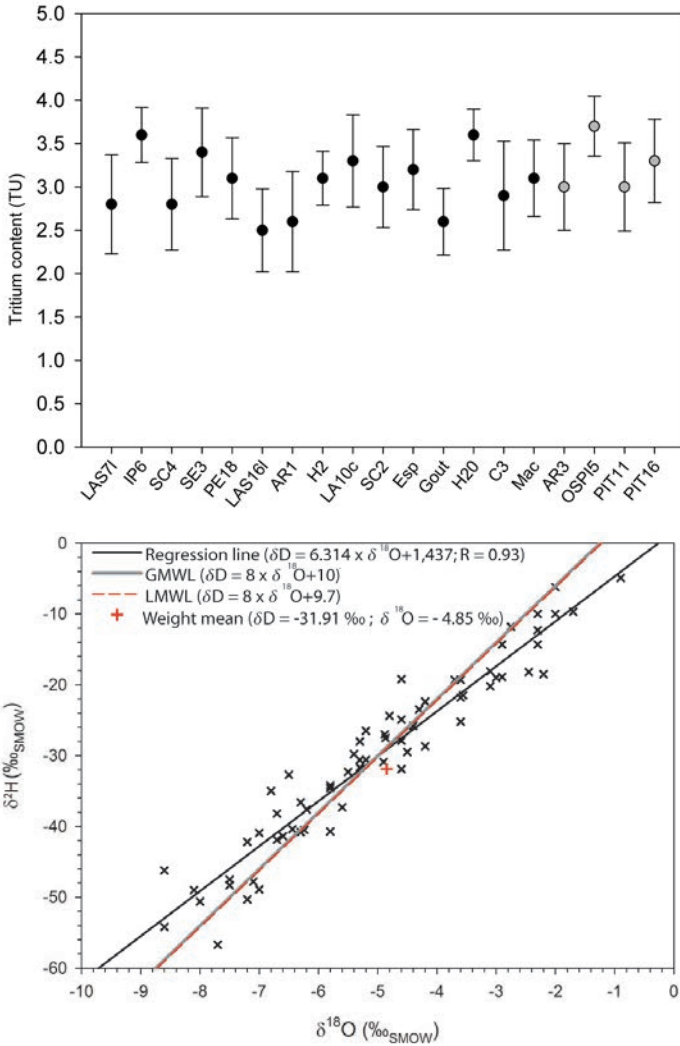


FIG. 4. Top: Tritium content from the monitored springs and the operated wells; Bottom:  $\delta^{18}\text{O}$  vs.  $\delta^2\text{H}$  in rainwater (monthly samples from the Dax station, France;  $43^{\circ}40'48''/ -1^{\circ}3'36''/ 9\text{ m A.S.L.}$ ) from 1999/01 to 2004/12 (GNIP Data). The local meteoric water line (LMWL) and the global meteoric water line (GMWL) are also drawn [12].

For all groundwater samples (except for SC4), in addition to anthropogenic sources, the enrichment in Na, Ca and K below the seawater dilution line and the rain-water could be partly related to silicate weathering processes [12].

The SC4 waters have very different characteristics (Figs 2 and 3). They are more enriched in Na, Ca,  $\text{NO}_3$  and K than the other sampled waters. Based on data from Ref. [6], we can assume that SC4 waters are circulating through weathered

porous horizons. All the other monitored groundwaters are more probably circulating through fissured levels (Fig. 1 bottom). The high concentrations observed in SC4 waters, particularly in  $\text{NO}_3$ , can be attributed to the reduced protection of the catchment from anthropogenic contributions. High concentrations in Ca may also indicate strong water–rock interactions with carbonate minerals of this weathered layer.

#### 4.2. Isotope hydrology

Tritium concentrations in groundwater may be used as indicators of groundwater age by comparison with historical records of elevated tritium levels in precipitation, which resulted from atmospheric thermonuclear testing in the early 1950s to late 1970s. All the samples measured contain a tritium concentration of 2 TU or greater with an average value of 3.08 TU, indicating that the water was recently recharged (Fig. 4 top).

The average tritium content of the Dax rainfalls measured between 1997 and 1998 is of 3.14 TU (7 samples), which is close to the value observed in our groundwater samples. Likewise, the stable isotopes of the water molecule from Ursuya groundwater will certainly be in the tendency of the long term chronicle of the Dax rainfalls (sampled from 1997; Fig. 4 bottom). This station is located about 50 km north of the study area and is under clear Atlantic influences. Linear regression calculated with the 68 samples of the Dax station (GNIP Data) gives the line equation:  $\delta^2\text{H} = 6.31 \times \delta^{18}\text{O} + 1.44$  ( $r^2 = 0.93$ ; Fig. 4 right).

Isotopes tend to show that the residence time of Ursuya Mount groundwaters are very limited and do not confirm ages of more than fifty years old. The recharge, which is clearly of local and recent origin, must now be compared with the geochemical indicators to evaluate the dynamic of the silicate weathering processes to explain the different water types encountered.

### 5. CONCLUSIONS AND PROSPECTS

The first results on the Ursuya Mount show significant geographic variability in the composition of groundwater and demonstrate the influence of the Atlantic on rainwater as on groundwater. Anthropogenic inputs also seem to have a strong impact on the chemical concentrations. Geochemical tools confirm the information provided in 2010 by well logs and pumping tests carried out in the 4 non-operated boreholes (top of Fig. 1). Indeed, these measurements showed the existence of two levels with different hydrodynamic characteristics. A level near the surface, in close relation with the atmosphere, reacting quickly to rainfall inputs and an underlying level slightly confined.

Analyses of stable isotopes in rainwater and in groundwater are expected to confirm these conclusions and to provide additional information on the preferential

recharge areas and on the flow pattern. Finally, the residence time of groundwater will be determined at low resolution level by additional measurements of CFC and SF<sub>6</sub> concentrations.

### ACKNOWLEDGEMENTS

This work is financially supported by the European Union via the FEDER programme, the Agence de l'Eau Adour-Garonne and the Conseil Général des Pyrénées Atlantiques.

### REFERENCES

- [1] COOK, P.G., A Guide to Regional Groundwater Flow in Fractured Rock Aquifers, CSIRO, Adelaide (2003).
- [2] BERKOWITZ, B., Characterizing flow and transport in fractured geological media: A review, *Adv. Water Resour.* **25** (2002) 861–884.
- [3] PRAAMSMA, T., NOVAKOWSKI, K., KYSER, K., HALL, K., Using stable isotopes and hydraulic head data to investigate groundwater recharge and discharge in a fractured rock aquifer, *J. Hydrol.* **366** (2009) 35–45.
- [4] BUREAU DE RECHERCHES GÉOLOGIQUES ET MINIÈRES, Carte géologique d'Iholdy au 1/50 000, n° 1027, BRGM, Pessac, France (1974).
- [5] WYNS, R., ET AL., Application of proton magnetic resonance soundings to groundwater reserve mapping in weathered basement rocks (Brittany, France), *Bull. Soc. Géol. France* **175** 1 (2004) 21–3.
- [6] CHÉRY, L., Qualité naturelle des eaux souterraines: Méthode de caractérisation des états de référence des aquifères français, BRGM, Orléans (2006) 238 pp.
- [7] COURTOIS, N., et al., Large-scale mapping of hard-rock aquifer properties applied to Burkina Faso, *Ground Water* **48** (2010) 269–283.
- [8] PENNA, P., et al., On the reproducibility and repeatability of laser absorption spectroscopy measurements for  $\delta^2\text{H}$  and  $\delta^{18}\text{O}$  isotopic analysis, *Hydrol. Earth Syst. Sci.* **14** (2010) 1551–1566.
- [9] INTERNATIONAL ATOMIC ENERGY AGENCY, Laser Spectroscopic Analysis of Liquid Water Samples for Stable Hydrogen and Oxygen Isotopes, Training Course Series 35, IAEA, Vienna (2009).
- [10] CELLE-JEANTON, H., TRAVI, Y., LOÏYE-PILOT, M.-D., HUNEAU, F., BERTRAND, G., Rainwater chemistry at a Mediterranean inland station (Avignon, France): Local contribution versus long-range supply, *Atmos. Res.* **91** (2009) 118–126.
- [11] SANUSI, A., WORTHAM, H., MILLET, M., MIRABEL, P., Chemical composition of rainwater in Eastern France, *Atmos. Environ.* **30** 1 (1996) 59–71.
- [12] PETELET-GIRAUD, E., CASANOVA, J., CHÉRY, L., NÉGREL, P., BUSHAERT, S., Attempt of isotopic characterisation ( $\delta^{18}\text{O}$  and  $\delta^2\text{H}$ ) of present

rainwater signature using lakes and reservoirs: application to south-western France,  
*La Houille Blanche* **2** (2005) 57–62.



# **HYDROGEOCHEMICAL AND ISOTOPIC CHARACTERIZATION OF THE HYDROGEOLOGICAL MODEL OF THE PARRITA AQUIFER, CENTRAL PACIFIC OF COSTA RICA**

R. MATAMOROS-ARGUEDAS

Servicio Nacional de Aguas Subterráneas, Riego y Avenamiento (SENARA),  
San José, Costa Rica

## **Abstract**

A combined study of hydrology, hydrochemistry and environmental isotopes has been carried out by SENARA in the Parrita River basin, Costa Rica's Pacific coast, with the assistance of the IAEA's Technical Cooperation Project RLA/8/041. This region presents a high water demand due to agricultural activities and tourism. Deuterium and oxygen-18, in conjunction with the major ions, were used to assess the overall hydrological functioning of the basin, including the relationships between different water bodies. Preliminary results indicate that groundwater is recent, the transit time of water in the aquifer is very fast and that there is a strong hydraulic connection between surface waters and the aquifer. This information has been incorporated into the first version of the vulnerability map of the Parrita aquifer, which is being used as a land management tool by local authorities.

## **1. INTRODUCTION**

The Parrita aquifer is located at the lower reaches of the Parrita River basin, which flows into the Central Pacific region of Costa Rica. The study area covers about 236 km<sup>2</sup>. The Parrita aquifer area corresponds to one of the coastal regions with higher population growth and economic development in Costa Rica. The economy has traditionally focused on agriculture, but today's development is targeting trade and tourism.

The water demand in the area has increased in recent years due to growing needs for public water supply, trade, irrigation, industry and tourism. This increase could lead to problems when trying to improve quality of life. For this reason, organizations such as the Servicio Nacional de Aguas Subterráneas, Riego y Avenamiento (SENARA), the Instituto Costarricense de Acueductos y Alcantarillados (A y A) and the Escuela Centroamericana de Geología (ECG) at the University of Costa Rica (UCR) have made strategic alliances in order to generate information about the hydrogeology and hydrochemistry of the zone of Parrita. It is expected that these

## MATAMOROS-ARGUEDAS

studies will serve as practical tools for planning and decision making according to the properties and hydrogeological characteristics of the aquifer.

In the framework of the regional Technical Cooperation Project RLA/8/041, the International Atomic Energy Agency (IAEA), SENARA and the UCR carried out a combined study of hydrochemistry (major ions) and isotope hydrology (deuterium and oxygen-18), complementary to other tools used such as geology and hydrogeology, in order to improve the first hydrogeological model of the Parrita River basin.

### 2. HYDROGEOLOGICAL CONCEPTUAL MODEL

The Central Pacific area of Costa Rica is protected to the north by high mountain ranges that prevent the incursion of trade winds and cause a drying effect. The local rainfall (station La Ligia) ranges from 2070 mm/a, the driest year in the last ten years is 2070.5 mm and 3260.8 mm for the northern part (station Playón). Potential evapotranspiration, calculated by the Blaney and Criddle equation [1], is about 1820 mm/a.

The regional geological setting is controlled by the chronostratigraphic analysis of the Parrita sedimentary basin. The basement of the basin includes ocean floor igneous rocks associated with pillow lavas from the Cretaceous period, formally associated to the Nicoya Complex [2, 3], while the overlying sedimentary

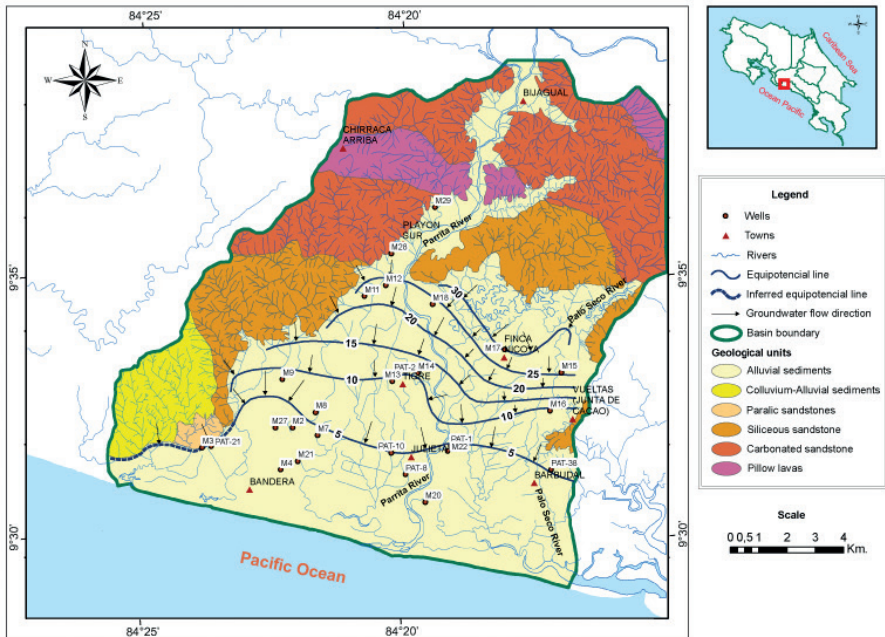


FIG. 1. Hydrogeological map of the Parrita aquifer.

rocks are deposited in a platform environment, and, parallel to the coast, the Punta Judas, Chires and Río Negro formations crop out. These formations are composed of finegrained sandstones and carbonate rocks of Oligocene to Quaternary age [4]. Overlying sedimentary rocks are colluvium-alluvial and alluvial deposits of recent Quaternary age, the latter corresponding to the main aquifer (Fig. 1).

The aquifer extends over an area of 133.5 km<sup>2</sup>, corresponding to granular sediments, comprising silt, clay, sand and gravel, with the presence of lateral variations in grain size. The thickness ranges from 5 to 25 m. Groundwater levels are shallow, with static levels between 0 and 35 m a.s.l. The direction of groundwater flow is predominantly towards the south (Fig. 1). The average hydraulic gradient is 0.0019 and hydraulic conductivity is between 32 and 41 m/day. The roof of the aquifer is covered to the south by a layer of fine sediments (mostly silt and clay in some sectors), with a thickness ranging from 2 to 21 m. This layer of fine sediments may lead to the development of confined or semiconfined hydraulic conditions, or simply cover the aquifer without creating confinement. Other areas of the aquifer are covered by layers of variable grain size, ranging from fine sediments to gravel. In these areas, the aquifer is unconfined.

In order to elaborate a map of intrinsic vulnerability to pollution for the aquifer, the GOD method [5] was used. Four vulnerability categories were obtained: Low, medium, high and extreme (Fig. 2).

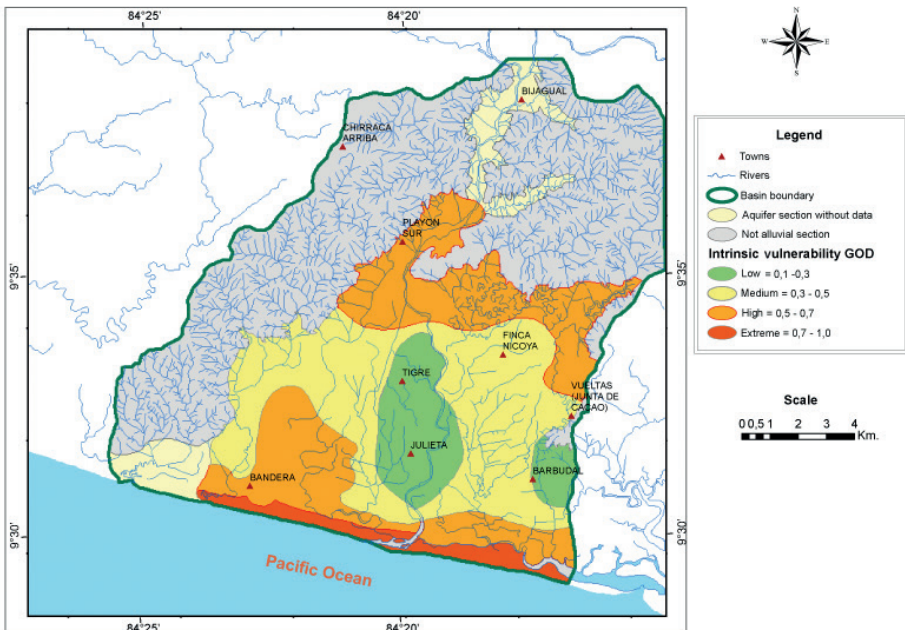


FIG. 2. Intrinsic vulnerability to pollution map for the Parrita aquifer.

**MATAMOROS-ARGUEDAS**

**TABLE 1. GENERAL INFORMATION ABOUT THE SAMPLING POINTS IN THE PARRITA AQUIFER**

Hydrochemical zone	Sampling station code	Geographic Coordinates		Altitude (m)	Type of sampling	Filters location / Dug well depth (m)
		West Longitude	North Latitude			
1	P06	9.577412	-84.338206	30.98	Dug well	9
1	P07	9.549335	-84.327763	16.01	Drilled well	
1	P10	9.601699	-84.308199	16	Drilled well	
1	P11	9.325517	-84.508155	8.09	Drilled well	
1	P12	9.524627	-84.318217	19.64	Drilled well	
1	R02	9.520696	-84.324206	23	River	
1	R03	9.60204	-84.308273	59	River	
2	P14	9.602307	-84.322279	38	Drilled well	
2	R04	9.60204	-84.321914	40	River	
3	P08	9.549896	-84.549896	30	Drilled well	
3	R01	9.535464	-84.279092	20	River	
4	P01	9.53174	-84.368194	16	Drilled well	
4	P02	9.51845	-84.371937	20	Drilled well	
4	P03	9.529681	-84.360145	17.67	Drilled well	6.00
4	P04	9.536794	-84.360707	14	Drilled well	
4	P05	9.547463	-84.371563	13.7	Drilled well	
5	P09	9.557009	-84.299873	20.64	Drilled well	
	E01	9.511973	-84.402008	4	Lagoon	
	L01	9.600198	-84.343381	320	Rain	

Source: Data collected by SENARA

Potential groundwater recharge calculated for the bottom of the basin into the aquifer is 6.29 m<sup>3</sup>/a [6] and the potential recharge volume is 4230 L/s. Most of the recharge occurs laterally into the aquifer, from the sedimentary formations and the Nicoya Complex (pillow lavas), but an important quantity of this recharge occurs directly through the alluvial sediments to reach the aquifer.

### 3. HYDROGEOCHEMICAL AND ISOTOPIC MODEL

For the analysis of aquifer hydrochemistry, four sampling campaigns, including groundwater (wells), surface water (rivers) and precipitation, were conducted. One campaign was conducted during the dry season (December to April) and the other three during the rainy season (May to November). The four sampling campaigns were conducted by staff of the Centro de Investigación en Contaminación Ambiental (CICA) at UCR. Analyses included the determination of major and minor ions, physical properties such as electrical conductivity, temperature, acidity and hardness. For the analysis of the origin and chemical characterization of water, a Piper diagram was used [7]. The information about each sampling station is presented in Table 2. According to the Piper graphic (Fig. 3), both groundwater and surface waters are of the bicarbonate-calcium type, suggesting a recent origin and a direct relation between groundwater and surface water. Fig. 4 shows the relation Mg vs. Ca/Mg, also showing the existence of nine samples with Mg contents, for sampling sites P11, P14, R02 and R03.

Isotopic analyses were carried out at the Mass Spectrometry Laboratory of the National Autonomous University of Mexico (UNAM), to determine the isotope contents deuterium ( $\delta^2\text{H}$ ) and oxygen-18 ( $\delta^{18}\text{O}$ ) for a total of 55 samples.

Fig. 5 presents the relationships between  $\delta^{18}\text{O}$  and  $\delta^2\text{H}$  for the Parrita River basin, considering the different sample types. The mangrove samples are out of

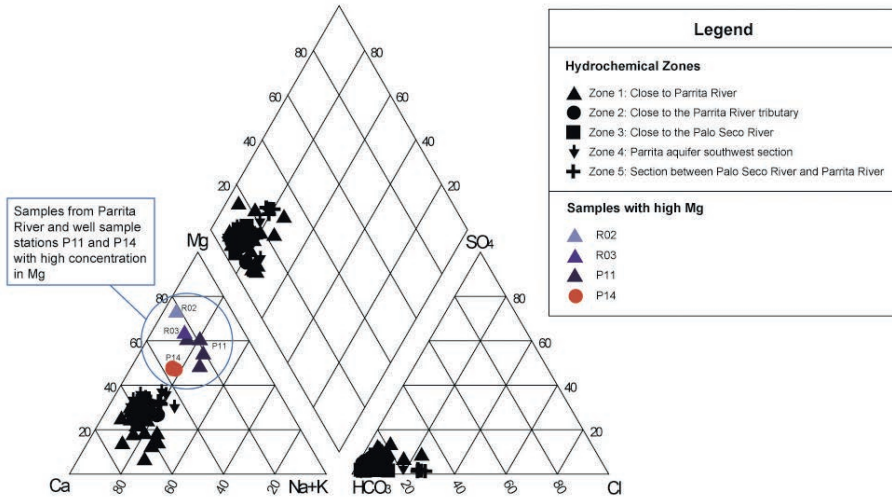


FIG. 3. Piper diagram.

# MATAMOROS-ARGUEDAS

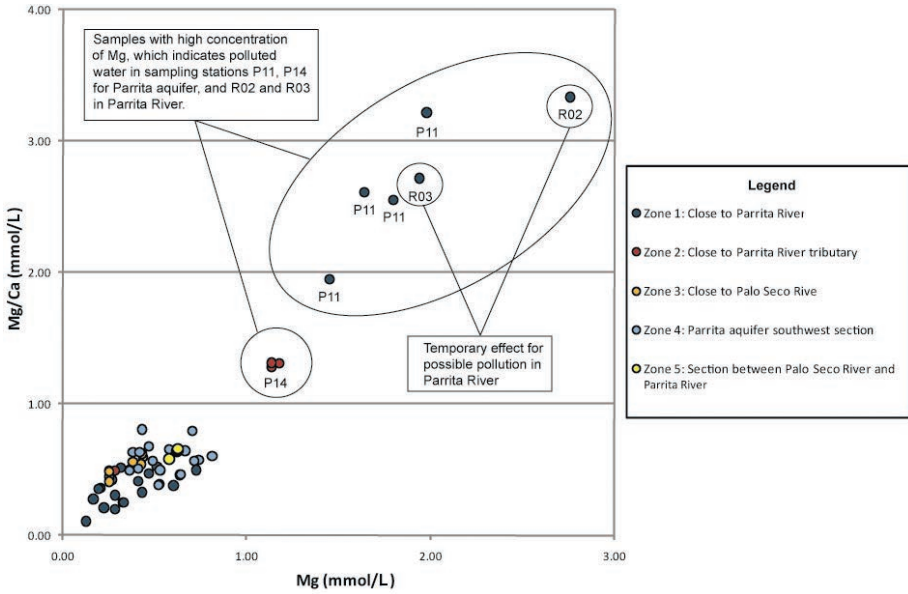


FIG. 4. Relation Mg vs. Mg/Ca.

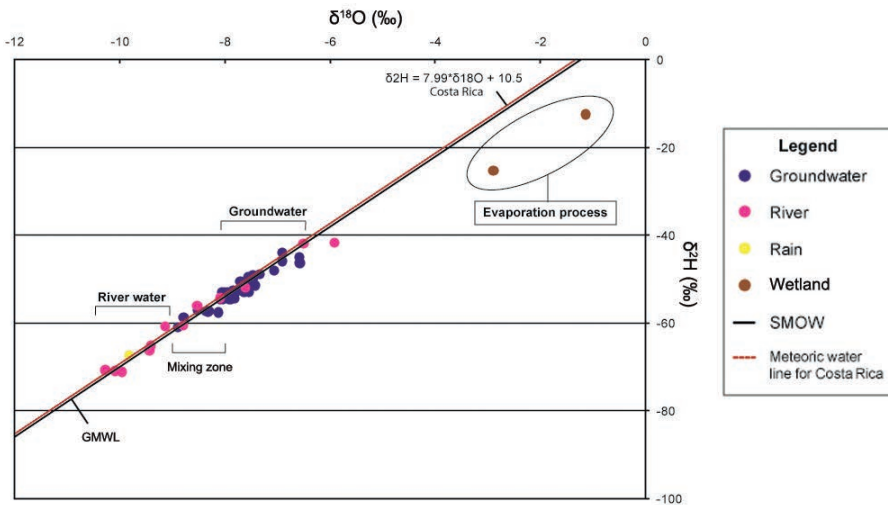


FIG. 5. Relationship  $\delta^{18}O$  vs.  $\delta^2H$  for different water types.

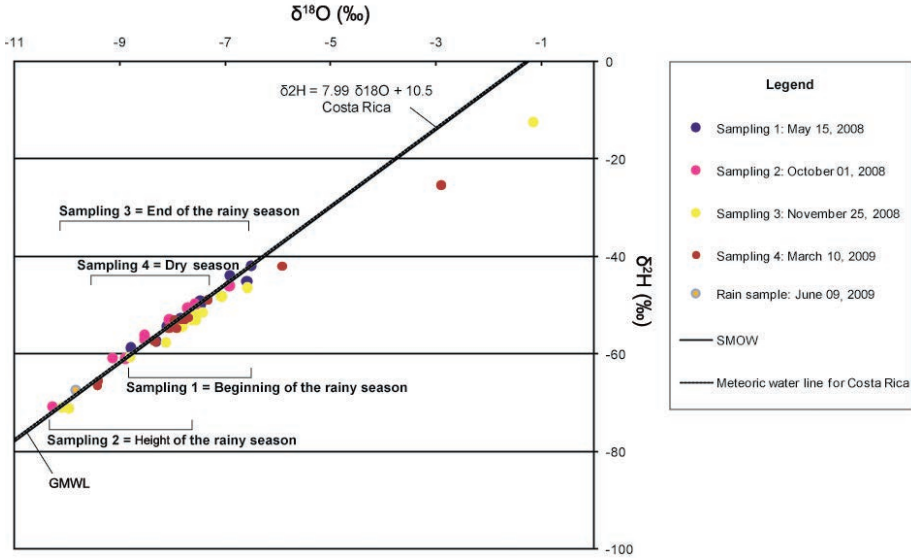


FIG. 6. Relationship  $\delta^{18}\text{O}$  vs.  $\delta^2\text{H}$  for different sampling campaigns.

the GMWL, due to the importance of the evaporation process. Groundwater samples are more enriched than surface water; however, there is a mixing process between these types of samples, which is shown in the centre of the sample group and reaffirms the existence of hydraulic connection between the surface waters and groundwater.

Fig. 6 shows the relationship between  $\delta^{18}\text{O}$  and  $\delta^2\text{H}$  considering all samples grouped by the sampling campaign. According to this graphic, there is not an apparent isotopic evolution for the isotopic contents over time. However, progressive isotopic depletion during the rainy season is seen for sampling campaigns 1 and 2.

In order to assess the existence of spatial variations in the isotopic contents, the aquifer area was divided into five zones, considering the drainage pattern and the chemical and isotopic characterization (Fig. 7). Table 2 indicates the sampling sites for groundwater and surface waters.

The groundwater and surface water samples were grouped by each hydrochemical zone and were plotted into a  $\delta^{18}\text{O}$  and  $\delta^2\text{H}$  graphic (Fig. 8). Zones 4 and 5 present similar isotopic behaviour, taking into account the expected difference between groundwater and surface waters.

Groundwater in zones 1 and 3 presents a strong influence by Parrita and Palo Seco rivers. Fig. 8 shows common features for zones 1, 3, 4 and 5, which evidence the relationship between groundwater and surface waters, which indicates high vulnerability to groundwater pollution.

MATAMOROS-ARGUEDAS

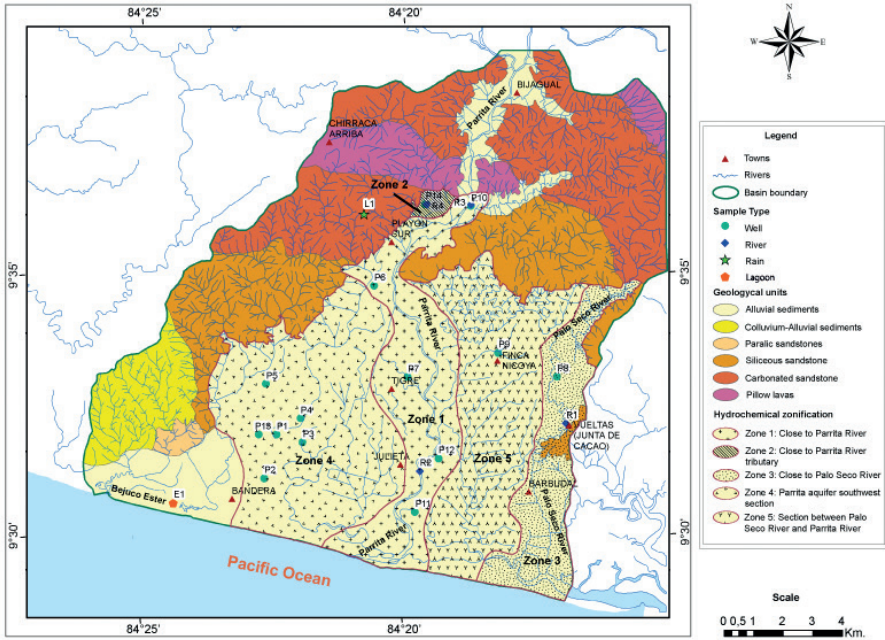


FIG. 7. Hydrochemical zones identified in the study area.

TABLE 2. HYDROCHEMICAL ZONES IN THE PARRITA AQUIFER

Hydrochemical zone	Zone name	Sampling sites
1	Close to Parrita River	P01, P10, P11, P12, R02, R03
2	Close to Parrita River tributary	P14, R04
3	Close to Palo Seco River	P08, R01
4	Parrita aquifer southwest section	P01, P02, P03, P04, P05
5	Section between Palo Seco River and Parrita River	P09

Groundwater in zone 2 shows a different isotopic pattern, with isotopically enriched values than in the other zones, possibly due to higher precipitation conditions at the northern part of the aquifer, or due to the high aquifer recharge conditions that exist for this zone.

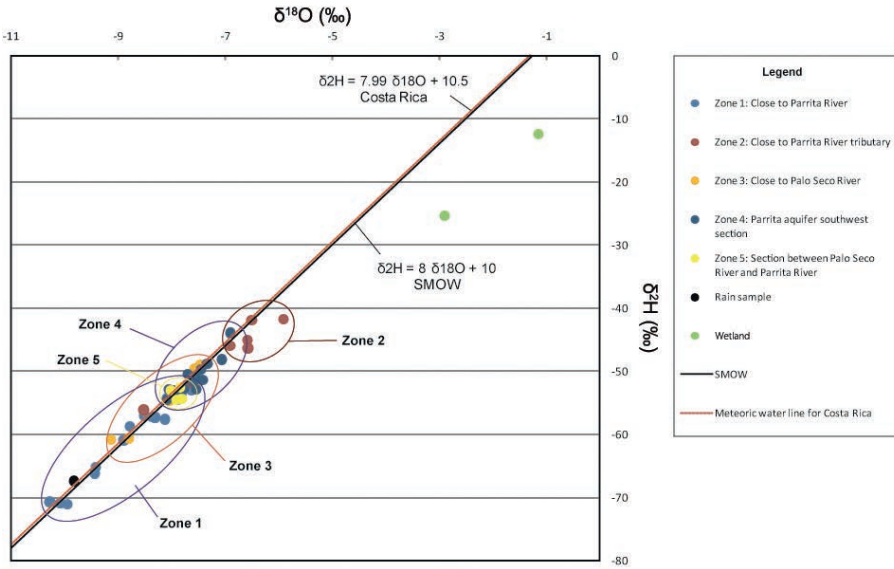


FIG. 8.  $\delta^{18}O$  versus  $\delta^2H$  relationship based on the identified hydrochemical zones.

#### 4. CONCLUSIONS

The groundwater system in the Parrita River basin evidences rapid infiltration conditions and therefore the presence of recent groundwaters due to fast transit time of water in the aquifer. There is a strong hydraulic connection between groundwater and surface water. Due to the high permeability of the aquifer and the shallow water level, the aquifer presents a high vulnerability to pollution, which can occur either from the surface by direct infiltration and through the surface water courses to the aquifer.

Thus, it is necessary not only to use the vulnerability to pollution as a territorial planning tool to protect the aquifer, but also for the establishment of policies for the management and protection of surface water courses.

#### REFERENCES

- [1] CUSTODIO, E., LLAMAS, M.R., Hidrología Subterránea, Omega, Barcelona, Spain (2001).
- [2] BAUMGARTNER, P.O., “El complejo ofiolítico de Nicoya (Costa Rica): Modelos estructurales analizados en función de las edades de los Radiolarios (Calloviense a Santoniense)”, Manual de Geología de Costa Rica (SPRECHMANN, P., Ed.), Editorial Universidad de Costa Rica, San José (1984) 115–123.
- [3] HAUFF, F., HOERNLE, K., VAN DEN BOGAARD, P., ALVARADO, G.E., GARBE-SCHÖNBERG, D., Age and geochemistry of basaltic complexes in western

## MATAMOROS-ARGUEDAS

- Costa Rica: Contributions to the geotectonic evolution of Central America, *Geochem. Geophys. Geosyst.* **1** 5 (2000).
- [4] GUARÍA CÁRDENES, S., Sedimentología de los ambientes costeros y continentales actuales y sus implicaciones geológico-ambientales en la región de Parrita, Pacifico Central de Costa Rica, University of Costa Rica, San José (2002).
- [5] FOSTER, S., “Fundamental concepts in aquifer vulnerability, pollution risk and protection strategy”, *Vulnerability of Soil and Groundwater to Pollutants* (VAN DUIJVENBOODEN, W., VAN WAEGENINGH, H.G., Eds), Proceedings and Information No. 38, TNO Committee on Hydrogeological Research, The Hague (1987) 69–86.
- [6] SCHOSINSKY, G., LOSILLA, M., Modelo analítico para determinar la infiltración con base en la lluvia mensual, *Revista Geológica de América Central* **23** (2000) 43–55.
- [7] FREEZE, R.A., CHERRY, J.A., *Groundwater*, Prentice Hall, New York (1979).

# DETERMINING MRT OF GROUNDWATER BY MODELLING THE DISTRIBUTION OF ENVIRONMENTAL (HYDROGEN AND OXYGEN) ISOTOPES

E. ANOVSKA-JOVCHEVA<sup>a</sup>, Z. JOVCHEV<sup>b</sup>, T. ANOVSKI<sup>a</sup>, V. POPOV<sup>c</sup>

<sup>a</sup> Faculty of Technology and Metallurgy,  
University of Sts Cyril & Methodius,  
Skopje, The FYR of Macedonia

<sup>b</sup> Faculty of Electrical Engineering and Information Technology,  
University of Sts Cyril & Methodius,  
Skopje, The FYR of Macedonia

<sup>c</sup> Wessex Institute of Technology,  
Southampton, UK

## Abstract

The distribution of environmental isotopes ( $^3\text{H}$ ,  $\delta^2\text{H}$  and  $\delta^{18}\text{O}$ ) into the local hydrological cycle within the Ohrid–Prespa Lake hydro system, has been investigated. By using an appropriate model, relevant hydrogeological and hydrometeorological data and a computer code which implements an adequate recursive equation, the mean residence time (MRT) of groundwater infiltrating from Lake Prespa towards the Galichica Mountain and recharging the series of springs along the southeastern coastline of Lake Ohrid (recognized by UNESCO as a World Heritage site) has been determined. A value of approximately 6 a has been obtained.

## 1. INTRODUCTION

In the southeastern part of the Former Yugoslav Republic of Macedonia there are three lakes shown in Fig. 1: Lake Ohrid, shared with Albania, and the Great and Small Prespa Lakes, shared with Albania and Greece. The Galichica and Dry mountains separate the lakes. According to an existing hypothesis by Cvijic [1], water from Lake Prespa, which is shared by the three neighbouring countries, is drained through the Galichica and Dry Mountains into Lake Ohrid. This drainage is shown schematically in Fig. 2. Field research conducted first by Anovski and collaborators [2] and later by other scientists [3–4], confirmed this hypothesis.



FIG. 1. Investigated area of interest.

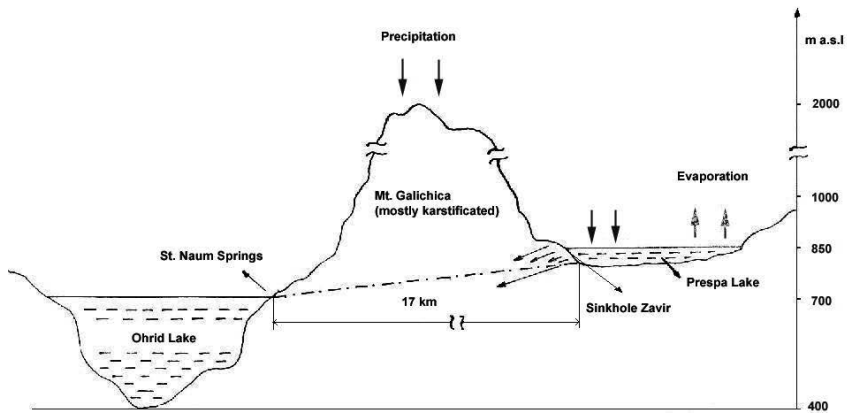


FIG. 2. Schematic diagram of the cross-section of the profile: Sinkhole Zavir-St Naum Spring.

The lakes Great Prespa (253.6 km<sup>2</sup>) and Small Prespa (47.4 km<sup>2</sup>) are at a reference altitude of 847.68 and 850 m a.s.l., respectively and are linked by a small channel with a sluice that separates the two lakes. In the past, periodical oscillations of the lake's level were in the range of one to three metres, depending on the amount of rain in the season. Since the mid-1980s, a steady decrease of the water level has been recorded that endangers the ecological balance of the lake and the watershed area resulting in serious consequences for the fishing and tourist industry in the transborder Prespa region.

The importance of Lake Prespa as an area of high ecological significance has been widely recognized by the national Governments of the three countries sharing

the lake (several national projects have been financially supported) and by international organizations and bodies (IAEA, NATO SPS, UNESCO and others) not only because of its natural beauty, but also because of its high biodiversity, including populations of rare water birds, such as, for example, the Dalmatian pelican, categorized as an internationally vulnerable species, as well as for its cultural values, including Byzantine monuments.

The willingness of the three governments to co-operate in order to promote the protection of the entire Prespa area was established on the 2nd February 2000, when the Prime Ministers of Albania, Greece and the FYRO Macedonia issued a trilateral declaration recognising the international importance of the Prespa Lakes as well as the need for cooperation in order to promote conservation of its natural and cultural values.

That is why the fulfilment of various projects' objectives (definition of the quality and quantity of the lake water, lake water balance, hydrological relationship between the three Lakes and others), made a significant contribution to the protection of the Ohrid-Prespa hydrosystem and reinforced the peace and stability in the region.

## 2. METHODOLOGY

Though in the recent years a joint research programme between the three border countries has been conducted, the cause for this water level drop was not known, mainly because the data collected has not been processed in a systematic way and advanced computer simulation tools have not been used in previous studies.

The novel aspects of the last project, NATO SPS Project No 981116 [5], relate to the way of dealing with water resources in karstic regions under the influence of changing weather patterns. A full evaluation of the data available in the previous years combined with the data collected over the project's duration was used to estimate the implications for a complex system such as the Prespa Lake where parameters such as sinkholes, precipitation and evaporation, water inflow through rivers and streams and water used in agriculture have been taken into account. The research advanced the scientific basis in this area, which will find its application in the future in related research worldwide.

The modelling part of the study aimed to determine the hydrological relationship between the Prespa and Ohrid lakes as well as to estimate the MRT of the infiltrated Prespa Lake waters through the Galichica Mountain by using environmental isotopes ( $^3\text{H}$ ,  $\delta^2\text{H}$  and  $\delta^{18}\text{O}$ ).

## 2.1. Distribution of environmental isotopes

### 2.1.1. Determination of $\delta^2H$ and $\delta^{18}O$ in water samples

After the physicochemical pretreatment, using standard procedures for the determination of  $\delta^{18}O$ , water samples were subject to exchange with  $CO_2$  gas. For the determination of  $\delta^2H$ , the reduction technique with Zn shots was used. Mass spectrometric measurements were carried out using a VG Micromass 602C mass spectrometer.

### 2.1.2. Determination of $^3H$ concentration in water samples

Considering the relatively low concentrations of tritium in environmental water samples (precipitation, ground and surface waters), water samples were enriched by an electrolytic process and then measured on a beta liquid scintillation counter (Packard Instrument, M 3320).

## 2.2. Determination of the MRT by a mixing model

Taking into consideration the local geological conditions, relevant hydrometeorological and isotope data and by using an appropriate two component mixing model, shown in Fig. 3, supported by a computer program which implements an adequate recursive equation, the MRT of the infiltrated Prespa Lake waters through Galichica Mountain, which recharge the St. Naum and other springs located on the southeastern coastline of the Ohrid Lake has been determined.

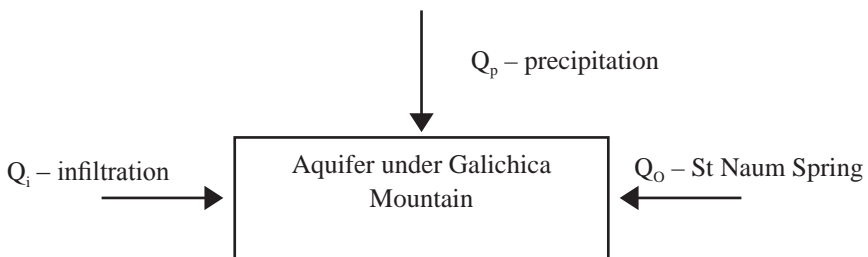


FIG. 3. One cell model including mixing of two components (precipitation and infiltration of Prespa Lake waters).

### 3. RESULTS AND DISCUSSION

#### 3.1. Stable isotope distribution

##### 3.1.1. Distribution of $\delta^2H$ values

On the basis of the isotope results obtained so far, the investigated waters within the local hydrological cycle can be divided into three groups:

- Galichica Spring at 1200 m a.s.l. as an average for the precipitation over Galichica Mt. with an average altitude of 1600 m a.s.l., depleted in heavier stable isotope, showing  $\delta^2H$  values ranging from  $-88$  to  $-64\%$  vs. VSMOW, fitting the LMWL (Local Meteoric Water line), according to the following equation,  $\delta^2H = 8 \delta^{18}O + 14$ ;
- Lake Prespa waters showing enriched values, ranging from  $-32$  to  $-20\%$  vs. VSMOW;
- St. Naum Spring water with  $\delta^2H$  values ranging from  $-56$  to  $-40\%$  vs. VSMOW, as intermediate between the values of precipitation and those of lake water (see Fig. 4).

##### 3.1.1. Distribution of $\delta^{18}O$ values

Similar distribution for the heavier stable isotope of oxygen ( $\delta^{18}O$ ) is observed:

- Precipitation, showing  $\delta^{18}O$  values ranging from  $-11.4$  to  $-9.8\%$  vs. VSMOW;
- Prespa lake waters showing enriched values ranging from  $-2.6$  to  $-1.4\%$  vs. VSMOW;
- St. Naum Spring water showing  $\delta^{18}O$  values ranging from  $-7.0$  to  $-6.6\%$  vs. VSMOW, as intermediate values between those of precipitation and those of Prespa lake water.

According to these results, it can be concluded that water in St. Naum and other surrounding springs is a mixture of these two components, with the following ratios:

- In the St. Naum Spring, 40% of the spring waters derive from the Prespa Lake and 60% from precipitation;
- For the Tushemiste Spring, the respective values of 55 and 45% were estimated.

By analysing the water balance in the hydrological system it was determined that  $8.7 \text{ m}^3/\text{s}$  into the St. Naum, Tushemiste and other springs on the south-eastern coast of the Ohrid Lake are result of infiltration of water from the Prespa Lake.

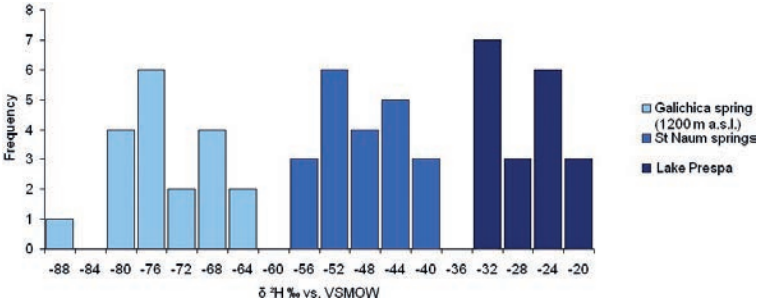


FIG. 4. Frequency distribution of δ²H value in observed water samples.

### 3.2. Modelling of the distribution of tritium contents

Taking into account the measured discharges and precipitations and discharges of St. Naum and other springs of interest, enrichment of Tritium content due to evaporation within Lake Prespa [5], as well as the above defined isotope ratios, it can be concluded that 19.6 m³/s of water is infiltrated through the Galichica Mountain into Lake Ohrid.

Apart from the above mentioned model and available hydro-meteorological and stable isotope data, a computer code was developed in order to simulate the tritium concentrations in the water from the St. Naum Spring, shown in Fig. 5, by solving the following recursive equation of Ref. [6]

$$S_n = (S_{n-1} + BRF \times CBRF - BOF \times CBOF) \alpha \tag{1}$$

where:

$S_n$  is the simulated tritium concentration in the St. Naum Spring waters, for the current year of observation, (TU);

$S_{n-1}$  is the calculated tritium concentration in the St. Naum Spring waters, for the previous year of observation, (TU);

$BRF$  is the boundary recharge fraction (precipitation and groundwater);

$CBRF$  is the concentration of the boundary recharge fraction. This value is derived from the measured or estimated tritium in precipitation over the FYR of Macedonia for the corresponding year of observation. When groundwater is considered, this value is multiplied by the enrichment factor due to evaporation within the Lake Prespa;

$BRF \times CBRF$  is the product of the boundary input mass within the cell;

$BOF$  is the boundary outlet fraction (precipitation and groundwater), equal to  $BRF_{\text{precipitation}} + BRF_{\text{groundwater}}$ ;

$CBOF$  is the concentration boundary outlet fraction for the first year (TU);

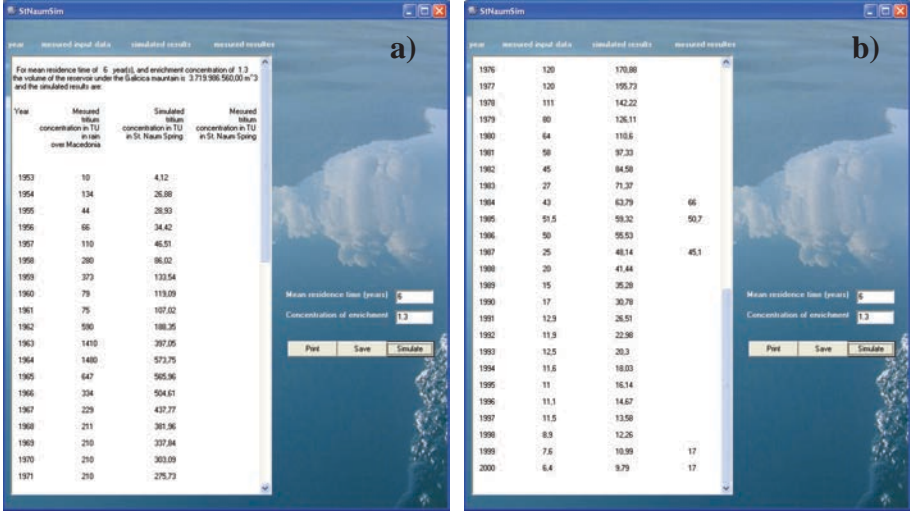


FIG. 5. C Computer program; (a) top half, (b) bottom half.

$BOF \times CBOF$  is the product that gives the boundary outlet mass leaving the cell;  
 $\alpha$  is the radioactive decay constant, which for one year is equal to 0.945.

After comparing the results for the different MRT and concentration of enrichment, it has been confirmed that by taking into account 6 a for MRT and 1.3 for the enrichment factor due to the evaporation within Lake Prespa, the measured and the simulated results differ with acceptable minor deviations.

The determined MRT of the groundwater with the value of 6 a has also been confirmed by recently performed tracer experiments by injection of artificial tracer in the Zaveri sinkhole in 2001 and its appearance in Tushemishte Spring, approximately 6 years later, i.e. in 2007 [5]. The volume of the reservoir under the Galichica Mountain that recharges the St. Naum Spring has been determined and a value of  $3.7 \times 10^9 \text{ m}^3$  has been obtained.

#### 4. CONCLUSIONS

On the basis of the performed study of the Prespa/Ohrid Hydro system, the following conclusions could be drawn:

- The distribution of environmental isotopes within the hydrological cycle was used as an effective hydrological tool, especially in the region where isotope fractionations can occur, i.e. involving surface water accumulations;

- Although the tritium content in precipitation is approaching the natural level, 4–6 TU, it still can be used as an efficient tool in hydrological investigations and particularly for the observed hydrosystems where historical tritium data are available;
- For the water reaching the underground reservoir and supplying the St. Naum and other springs located at the southeastern coast of Lake Ohrid, a value of  $MRT = 6$  a has been calculated and confirmed by artificial tracer experiments recently performed;
- Taking into account the value of the MRT, 6 years, and other relevant hydrological parameters and isotope data (spring discharge, participation of Lake Prespa water into the water of the observed springs), a value of approximately  $3.7 \times 10^9 \text{ m}^3$  has been estimated for the volume of the groundwater reservoir (under the Galichica Mountain).

### ACKNOWLEDGEMENT

This work is supported by the NATO Science for Peace and Security programme (Project No. Sfp 981116); IAEA REG Project RER 8/008 and UNESCO (Project No. 37542103 MCD).

### REFERENCES

- [1] CVIJIC, J., Fundamentals of Geography and Geology of Macedonia and Old Serbia, Special Edition VIII+680, Serbian Academy of Sciences, Belgrade (1906) (in Serbian).
- [2] ANOVSKI, T., et al., A study of the origin of water in the St. Naum's Springs, Lake Ohrid, FIZIKA: A Journal of Experimental and Theoretical Physics **12** (1980) 76–86.
- [3] EFTIMIR, ZOTO, J., "Isotope study of the connection of Ohrid and Prespa lakes", Proc. Intern. Symp. Towards Intergrated Conservation and Sustainable Development of Transboundary Macro and Micro Prespa Lakes, PPNEA, Korça, Albania (1997) 32–37.
- [4] LEONTIADIS, I.L., STAMOS, A., Isotope hydrology Study of the Region upstream of Aliakmona, 5th Panhellenic Symposium on Hydrogeology, Limasol, Cyprus (1999).
- [5] NORTH ATLANTIC TREATY ORGANIZATION, Sustainable Management of the International Waters — Prespa Lake, Final Report (SPS No. 981116), NATO (2010).
- [6] BARANYI, S., "The use of tritium measurement in the investigation of Lake Balaton", Proc. Intl Symp. on the Hydrology of Lakes, Helsinki, IAHS Publ. No. 109 (1973).

# UNDERSTANDING THE HYDROGEOLOGY OF RAYA VALLEY BASIN, NORTHERN ETHIOPIA USING STABLE ISOTOPES OF WATER

M. GEBRE EGZIABHER, T. AYENEW, S. KEBEDE

Department of Earth and Planetary Sciences,  
Addis Ababa University,  
Addis Ababa, Ethiopia

## Abstract

The Raya valley is located in the northern part of Ethiopia. The study area is connected to the Ethiopian rift system and bounded by the Ethiopian plateau to the west and Cherecher Mountain to the east. The study area is characterized by its semiarid climate. In order to investigate isotopic characteristics of different water bodies and groundwater recharge, water samples were collected in the summer rainy season and analysed for stable isotopes of oxygen and hydrogen by a laser based liquid water isotope analyser. Most of the groundwater samples are plotted just below the LMWL, which indicates that the origin is meteoric water and affected by secondary evaporation. There are highly depleted water samples in the eastern side of the study area, which could be attributed to the existence of palaeowater. Groundwater is mainly recharged by rain water and intermittent rivers. Open water bodies (the lake Ashenge and Gerjale swamp area) show enrichment due to high rate of evaporation. Isotopically the flood water in the highland area is depleted as a result of high rate of rainfall, high humidity and low rate of evaporation.

## 1. INTRODUCTION

During the last four decades the use of isotopes, either naturally occurring (environmental isotopes) or artificial isotopes (injected) have shown their value in studies related to water development and management [1]. The isotopes:  $^2\text{H}$ ,  $^3\text{H}$  and  $^{18}\text{O}$  are the components of water molecules,  $\text{H}_2\text{O}$ , which can offer a broad range of possibilities for studying processes within the water cycles [2].  $^{13}\text{C}$  and  $^{14}\text{C}$  are stable and radioactive isotopes of carbon, which provide information on water travel time, the interaction of water in soil and subsurface water.

The Raya valley catchment is an intermountain area, which is located in the northern part of Ethiopia. It is bounded in the west by the northwestern Ethiopian Plateau and in the east by the Afar Rift (Fig. 1). The geomorphology of the study area is dominated by the western mountains and central graben having small isolated hills. The study area is highly affected by tectonic activity. In the western highland

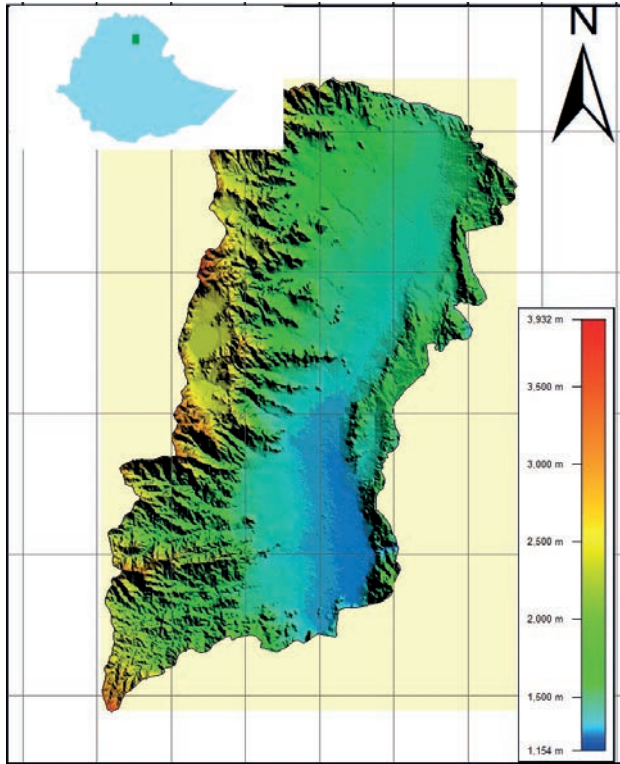


FIG. 1. Location map of the Raya valley basin.

the elevation varies from 1800 to 3800 m.a.s.l, while on the low lying graben or lowland it ranges from 1400 to 1800 m.a.s.l.

The classification of the climate regime used in this study is based on the information of UNESCO [3]. Using the ratio of annual precipitation to annual evapotranspiration the climate regime can be classified in several groups. Therefore, the western highland is classified as humid and the central graben is semiarid.

Surface water features in the study area are Ashenge Lake, Gerjale swampy area, Korem flood plain and several intermittent rivers. Most of the streams emerge from the western highland and then automatically disappear when they reach the basin fill graben due to the fact that the slope drops instantly from highland to the graben and also because the porosity of the sediments in the graben is higher than the highland.

The basin fill lowland graben is eco-environmentally fragile and scarce in surface water resources. However, the groundwater is the perennial source of water supply for domestic and other uses. Recent studies [4–8] have confirmed that the basin fill graben is a promising area for groundwater development. As a result, recent activities are being implemented to use groundwater as a principal source for agro-economical

development for the country. Such extensive projects could result in groundwater mining. Therefore, isotope hydrology can give a better understanding of the groundwater.

In arid–semiarid regions, it is vital to know the rate of groundwater recharge and discharge to insure the sustainable management of the resource. In this case study, an attempt is made to trace stable isotope signals from rain water and groundwater, to know where recent recharge has taken place. Also special emphasis is given to Lake Ashenge, the Gerjale swamp and the Korem flood plain.

## 2. STUDY AREA

The Raya valley basin is located in between UTM 539690–599690 east and UTM 1338650–1428650 north. It extends 80 km in a N–S direction and 29–38 km in an E–W direction, covering a total area of 2741 km<sup>2</sup>. The elevation of Raya valley decreases from 3800 m.a.s.l. in the highland to 1600 m.a.s.l. in the low lying graben and it rises to small extent towards Chercher Mountain in the eastern side of the graben (Fig. 1).

The annual precipitation and annual potential evapotranspiration (PET) for the highland are estimated to be 921 mm/a and 1260 mm/a, respectively. For the graben the annual precipitation and annual PET is 717 mm/a and 1625 mm/a, respectively. The climate is semiarid for the lowland and humid for the highland with a high rate of rainfall.

There are eleven major intermittent rivers in the study area [7], which contribute to groundwater recharge from the runoff by infiltration. These rivers generate floods from the mountainous volcanic rock of the western plateau and, when they reaches the low lying alluvial graben, the runoff is easily infiltrated to the porous part of the valley. Therefore, the intermittent river floods are the principal source of groundwater recharge.

The western highlands are mainly composed of Tertiary volcanic rocks. These rocks are highly disturbed by tectonic movement. The valley is composed of loosely compacted sedimentary basin fill deposits, which have the capability of holding and transmitting groundwater.

The loosely compacted sedimentary basin fill deposit has a high potential for agricultural development but the main problem is the scarcity of surface water and recurrent draught. Agriculture in this area is based on rain fed irrigation using the flood flowing from the western side of the mountain chains [4–6].

## 3. METHOD

Rainfall samples, lake samples, well samples, hand dug well samples, flood water samples and swamp water samples were collected during 25

August–5 September 2010 and several isotopic data are adopted from a previous study [8].

Samples were taken in 1000 mL IAEA sample bottles with screw cap and sealed tightly to prevent evaporation. Temperature, pH, static water level, dissolved oxygen and electric conductivity were measured in the field for all samples except for the precipitation sample.

All the samples were analysed by Liquid Water Isotope Analyser for oxygen-18 and deuterium in the isotope hydrology laboratory of Addis Ababa University and identical sample were sent to LHA (Laboratory of Hydrogeology in University of Avignon, France) to cross check. In the previous study [8], the samples were analysed in the Isotope Hydrology Laboratory, Vienna, Austria.

## 4. RESULT AND DISCUSSION

### 4.1. $\delta^2\text{H}$ , $\delta^{18}\text{O}$ composition of Ethiopian precipitation

The isotopic compositions ( $\delta^2\text{H}$  and  $\delta^{18}\text{O}$ ) of Ethiopian rainfall have been monitored in monthly composite samples by the International Atomic Energy Agency (IAEA) within the framework of the GNIP (Global Network of Isotopes in Precipitation) programme since 1965 [9], which makes Ethiopia the longest record holder of data on rainfall in Africa. From this record, a local meteoric water line (LMWL) was established to understand the isotopic composition of water body in the study area.

In the  $\delta^2\text{H}$ - $\delta^{18}\text{O}$  plot, the precipitation samples are aligned along the LMWL and the best fit equation is given as  $^2\text{H} = 7.14 \text{ }^{18}\text{O} + 11.96$  with a regression coefficient i.e.  $R^2 = 0.9141$  (Fig. 2). The remarkable feature of the  $\delta^2\text{H}$  and  $\delta^{18}\text{O}$  composition of Ethiopian meteoric water is its enrichment despite the high altitude of the country [10]. The isotopic composition of Ethiopian rainfall is the most enriched compared to other East Africa regions, which is a known phenomenon [11]. The enrichment is attributed to the contribution of already enriched moisture from the transpired moisture of the vegetated Congo basin. However, a satisfactory explanation for the enrichment of the rainfall is yet to be found [10].

### 4.2. Isotopic composition of water bodies

The isotopic compositions of the water sample that have been collected from the Raya valley basin including Lake Ashenge, springs from the western highland, bore-hole and hand dug well samples, swamp water, flood water and rainfall water were analysed and showed distinct differences. The isotopic composition of the water varies from isotopically depleted groundwater and flood water lying in the Korem highlands to highly enriched lake water in the northwestern part of the study area (Fig. 2).

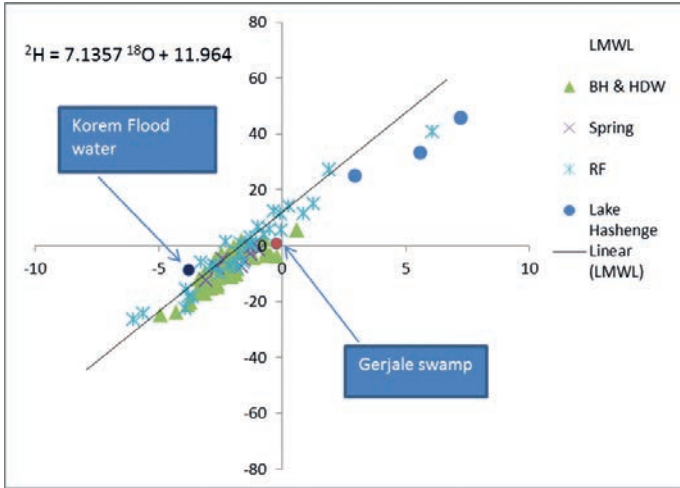


FIG. 2.  $\delta^2\text{H}$  vs.  $\delta^{18}\text{O}$  plot of all the water samples collected from the study area.

### 4.3. Hydrogen and oxygen isotope composition in precipitation

There are several effects that influence the distribution of stable isotopes in rainfall. These effects include altitude, temperature and amount. The isotopic composition of precipitation is in the range of  $-6.03$  to  $1.92\text{‰}$  for  $\delta^{18}\text{O}$  and  $-26.4$  to  $27.2\text{‰}$  for  $\delta^2\text{H}$ . The average values of  $\delta^2\text{H}$  and  $\delta^{18}\text{O}$  in precipitation are  $-2.18\text{‰}$  and  $-1.78\text{‰}$  respectively. The deuterium values are linearly and positively correlated with the  $\delta^{18}\text{O}$  values.

The study area is a semiarid region and is characterized by intense evaporation, therefore secondary evaporation during rainfall is expected. When rain falls through a dry air column, evaporation takes place [12]. Evaporation during rainfall would shift the water away from the Global Meteoric Water Line (GMWL) [12, 13]. The slope of the LMWL is smaller than the slope of the GMWL, which indicates secondary evaporation during rainfall.

### 4.4. Hydrogen and oxygen isotope composition in groundwater

Considering all the groundwater data, the distribution of the  $\delta^{18}\text{O}$  ranges from  $-4.93$  to  $0.6\text{‰}$  and the  $\delta^2\text{H}$  ranges from  $-24.6$  to  $5.6\text{‰}$ . The mean values of  $\delta^2\text{H}$  and  $\delta^{18}\text{O}$  are  $-7.9\text{‰}$  and  $-2.22\text{‰}$  respectively. The  $\delta^2\text{H}$  is linearly and positively correlated to the  $\delta^{18}\text{O}$ . All the groundwater samples are plotted (Fig. 2) around the LMWL, which implies that the groundwater is of meteoric origin.

In the study area, the  $\delta^2\text{H}$ – $\delta^{18}\text{O}$  compositions of groundwater plot below but almost parallel to the LMWL. This deviation can be used to understand the recharge

mechanism. Evaporation prior to the recharge mechanism is an important process. Therefore, two assumptions can be made: either the aquifer gets its water from already enriched evaporated streams and/or the evaporated soil moisture mixes with the subsequent rain, which infiltrates the soil and displaces the residual soil water downwards to become groundwater.

#### 4.5. Hydrogen and oxygen isotope composition in open water body

The average stable isotopic values for the lake Ashenge sample were found to be +4.27‰ for  $\delta^{18}\text{O}$  and +29.23‰ for  $\delta^2\text{H}$ . Lake water samples plotted below the LMWL, which shows that there has been fractionation by evaporation. Therefore, the lake undergoes a high level of enrichment by evaporation.

The Gerjale swamp area is located near the small town of Gerjale, where the water lies within a low lying semiarid area characterized by low annual precipitation and high PET. The water body gives  $\delta^2\text{H}$  and  $\delta^{18}\text{O}$  values of -0.24‰ and +0.89‰ respectively. The data plotted just below the LMWL which suggests that the swamp area is under a high rate of evaporation resulting in highly saline water.

In the highland Korem town, there was flood water lying on the plain in the mountainous area. The  $\delta^2\text{H}$  and  $\delta^{18}\text{O}$  values are -3.79 and -8.69‰ and plotted above the LMWL, depleted isotopically. A possible reason for this phenomenon could be low evaporation due to high humidity. The western highland is characterized by high rainfall and relatively low PET.

## 5. CONCLUSION

Stable isotope data have been used to trace the interaction of meteoric water and groundwater. Most of the groundwater samples plot just below the LMWL, which indicates that the origin is meteoric water and affected by secondary evaporation. There are highly depleted water samples in the eastern side of the study area, which could be attributed to the existence of palaeowater. Groundwater is mainly recharged by rain water and intermittent rivers. Open water bodies (the lake Ashenge and Gerjale swamp area) show enrichment due to high rate of evaporation. Isotopically the flood water in the highland area is depleted as a result of high rate of rainfall, high humidity and low rate of evaporation.

## ACKNOWLEDGMENTS

We acknowledge the financial support provided by International Water Management Institute and AAU, Department of Earth Sciences for logistic supply

during the field work. We would like to express our deepest gratitude to Sileshi Mamo and Tilahun Azage for their priceless help during the study.

## REFERENCES

- [1] UNITED NATIONS EDUCATIONAL, SCIENTIFIC AND CULTURAL ORGANIZATION, INTERNATIONAL ATOMIC ENERGY AGENCY, Environmental Isotopes in the Hydrological Cycle: Principles and Applications, UNESCO, Paris (2000), <http://www.iaea.org/water>.
- [2] GONI, I.B., Tracing stable isotope values from meteoric water to groundwater in the southwestern part of the Chad basin, *Hydrogeol. J.* **14** (2006) 742–752.
- [3] UNITED NATIONS EDUCATIONAL, SCIENTIFIC AND CULTURAL ORGANIZATION, Map of the World Distribution of Arid Regions, UNESCO, Paris (1979).
- [4] RELIEF SOCIETY OF TIGRAY (REST), Raya valley development study project — Phase I: Reconnaissance Phase Report, Vol I, REST, Ethiopia (1996).
- [5] HAGOS, M.A., Groundwater Flow Modelling assisted by GIS and RS Techniques (Raya Valley-Ethiopia), M.Sc. Thesis, International Institute for Geo-information Science and earth Observation, Enschede, The Netherlands (2010).
- [6] NEDAW, D., Aquifer Characterization and Hydrochemical Investigation in Raya Valley, PhD Thesis, University of Natural and Applied Life Sciences (“BOKU”), Vienna (2003).
- [7] WATER WORKS DESIGN AND SUPERVISION ENTERPRISE, Raya pressurized irrigation project feasibility study on water resource and hydrology, unpublished report (2008).
- [8] MAMO, S., Hydrogeology, Hydrogeochemistry and Isotope Hydrology of Raya and Kobo Valleys, Adjacent Plateau, Escarpment and Part of Afar Rift, Ethiopia: Hydrogeological Mapping, Recharge Evaluation and Water Quality Assessment, Geological Survey of Ethiopia, Addis Ababa (2007).
- [9] AYALEW BELAY, E., Growing Lake with Growing Problems: Integrated Hydrogeological Investigation on Lake Beseka, Ethiopia. Ph.D thesis University of Bonn, Germany (2009).
- [10] KEBEDE, S., et al., Groundwater origin and flow along selected transects in Ethiopian rift volcanic aquifers, *Hydrogeol. J.* **16** (2008) 55–73.
- [11] ROZANSKI, K., et al., “Isotope patterns of precipitation in the East African region”, *The Limnology, Climatology and Paleoclimatology of the East African Lakes* (JOHNSON, T.C., ODADA, E.O., Eds), Gordon and Breach, Toronto (1996) 79–93.
- [12] YIN, L., et al., Isotopes ( $\delta D$  and  $\delta^{18}O$ ) in precipitation, groundwater and surface water in the Ordos Plateau, China; Implications with respect to groundwater recharge and circulation, *Hydrogeol. J.* **19** (2011) 429–443.
- [13] FRIEDMAN, I., et al., Water-vapor exchange between a water droplet and its environment, *J. Geophys. Res.* **67** (1962) 2761–2766.



# **GROUNDWATER AGES AND HYDROCHEMICAL EVOLUTION ALONG A FLOW-PATH IN THE NORTHEASTERN SECTOR OF THE GUARANI AQUIFER SYSTEM (GAS) DERIVED FROM STRUCTURAL GEOLOGY, ISOTOPES AND HYDROCHEMICAL DATA**

D. GASTMANS<sup>a</sup>, H.K. CHANG<sup>a</sup>, P.K. AGGARWAL<sup>b</sup>, N. STURCHIO<sup>c</sup>,  
L. ARAGUÁS ARAGUÁS<sup>b</sup>

<sup>a</sup> LEBAC, UNESP Rio Claro  
Rio Claro (SP), Brazil

<sup>b</sup> Isotope Hydrology Section, IAEA  
Vienna, Austria

<sup>c</sup> Department of Earth and Environmental Sciences,  
University of Illinois at Chicago,  
Chicago, IL, USA

## **Abstract**

A 400 km transect in the Northeastern part of the Guarani Aquifer System (GAS) was selected to evaluate the geochemical evolution, groundwater ages and assess past recharge conditions. The analysis is based on the revision of the geological settings and the results of water chemistry, stable isotopes (<sup>2</sup>H, <sup>18</sup>O and <sup>13</sup>C) and carbon-14 determined in selected groundwater samples. GAS groundwater evolves from Ca-Mg-HCO<sub>3</sub> type near the recharge areas to Na-HCO<sub>3</sub> type and then to Na-HCO<sub>3</sub>/Na-Cl-SO<sub>4</sub> waters, indicating the relevance of the dissolution and exchange processes with the aquifer matrix. More negative water stable isotope contents (up to 3‰ in O-18, compared to present day recharge) are found in large portions of the study area, indicating distinct climatic recharge conditions in the past. Carbon-14 contents range from 80 pMC in the outcrop area to values below the detection limit at relatively short distances from the recharge zones, suggesting the existence of very old groundwaters in the central portion of the aquifer. Dating using the long lived isotope Kr-81, He-4 accumulation rates and hydrodynamic modelling is being conducted.

1. INTRODUCCION

The sustainable exploitation of very old groundwaters in large regional aquifers, which present residence times over 40 000 years, represents a challenge for responsible agencies of groundwater resource management. An integrated research approach is required to understand water recharge rates, flow paths, interactions between groundwater and the geological framework and residence time distributions in these complex hydrogeological systems. The use of multiple stable and radioactive isotope tracers combined with chemical data can certainly help in this endeavour.

The Guarani Aquifer System (GAS) is one of the most important groundwater reservoirs in South America, and it represents a typical example of a transboundary aquifer, shared by Argentina, Brazil, Paraguay and Uruguay. The GAS represents an important source of potable water for more than 90 million people that live in the area. It extends for about 1 100 000 km<sup>2</sup> in the territory of Argentina (228 255.26 km<sup>2</sup>), Brazil (735 917.75 km<sup>2</sup>), Paraguay (87 535.63 km<sup>2</sup>) and Uruguay (36 170.51 km<sup>2</sup>).

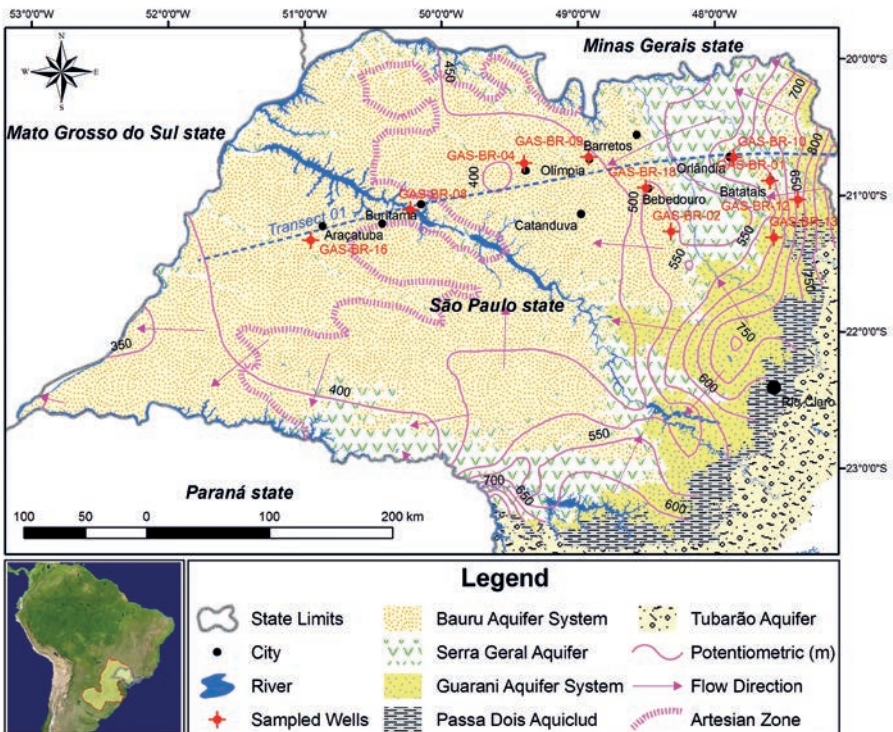


FIG. 1. Map showing GAS potentiometric surface, main flow directions, outcrops of aquifers in study area and the location of sampled wells.

On this continental scale, aquifer groundwaters aged over 30 000 years were recognized in the confined portion of the aquifer during isotopic studies carried out by several authors [1–4]. These age values are related to the C-14 dating limit, giving rise to age uncertainties for the older GAS groundwater. Estimations using U-isotopes were carried out in Ref. [5], which estimated groundwater residence times in the order of 640 ka, in dependence of the approach used to calculate this ages, very close to ages estimated using hydrodynamic data from the aquifer.

The groundwater age uncertainties in the deeper portions of the GAS are difficult to validate considering the accepted conceptual flow model defined for the Guarani Aquifer Project [4]. A research project was proposed to the IAEA to be carried out by UNESP — Campus de Rio Claro, the IAEA and the University of Illinois at Chicago, with the aim of evaluating the ages of very old groundwater in the GAS. This paper presents the preliminary results of the study, focusing on aspects related to the geochemical evolution and the assessment of past recharge conditions, using water chemistry, stable isotopes ( $^2\text{H}$ ,  $^{18}\text{O}$  and  $^{13}\text{C}$ ) and carbon-14 along a 400 km transect in the northeastern portion of the GAS (Fig. 1).

## 2. METHODS

Two groundwater sampling campaigns were conducted in April and October 2010 where samples were collected from selected wells along the transect shown in Fig. 1. The electrical conductivity, pH and temperature of each water sample were measured in the field. Samples were filtered (0.45  $\mu\text{m}$ ) and aliquots were acidified using nitric acid to pH <2, for cation analysis, while other aliquots were refrigerated (approximately 4°C) for anion analysis. The cation and anion concentrations in groundwater samples were determined at the Hydrogeology and Hydrogeochemistry Laboratory of the Applied Geology Department (UNESP-Campus Rio Claro). Sodium, potassium and anions were analysed using ion chromatography, and silicon, magnesium and calcium were determined by ICP-AES. Samples for  $\delta^2\text{H}$  and  $\delta^{18}\text{O}$  were collected in polyethylene bottles, and for  $\delta^{13}\text{C}$  and  $^{14}\text{C}$  in amber glasses bottles directly from the wells. Stable isotopes ratios in water ( $\delta^2\text{H}$  and  $\delta^{18}\text{O}$ ) and  $\delta^{13}\text{C}$  in total dissolved inorganic carbon (TDIC) were analysed at the Isotope Hydrology Laboratory at the IAEA using routine mass spectrometry measurements. C-14 determination in TDIC was made using standard AMS methods. Results are presented in Table 1.

## 3. RESULTS AND DISCUSSION

The hydrochemical evolution of groundwater in the part of the Guarani aquifer is similar to what has been previously reported [2, 4], starting from Ca-Mg- $\text{HCO}_3$  in

TABLE 1. ISOTOPIC AND HYDROCHEMICAL RESULTS (in mg/L)

Site	GAS- BR-01	GAS- BR-02	GAS- BR-04	GAS- BR-08	GAS- BR-09	GAS- BR-10	GAS- BR-12	GAS- BR-13	GAS- BR-16	GAS- BR-18
	Batatais	Jaboticabal	S.J.Rio Preto	Buritama	Olimpia	Orlândia	Altinópolis	Serra Azul	Valparaíso	Bebedouro
pH	6.25	6.90	9.59	9.49	9.39	6.62	6.21	5.85	9.37	9.60
EC ( $\mu\text{S}/\text{cm}$ )	64.80	189.00	354.00	498.00	434.00	145.6	40.2	31.5	719.00	307.00
Temp. ( $^{\circ}\text{C}$ )	29.7	32.4	44.4	43.8	50.2	nm	nm	nm	nm	43.7
Mg	1.29	2.91	0.36	0.04	0.03	1.90	1.12	0.81	<0.025	<0.025
Ca	4.22	23.70	2.05	0.96	1.30	17.40	2.28	1.96	0.77	1.07
Na	2.56	8.63	74.10	101.00	89.30	3.30	1.45	1.17	153.00	63.10
K	6.44	2.11	0.42	0.48	0.30	3.70	1.76	1.52	0.79	0.30
$\text{HCO}_3$	38.00	119.00	120.00	158.00	120.00	81.00	13.30	14.60	204.00	93.80
$\text{CO}_3$	<2.00	<2.00	35.80	9.61	34.50	<2.00	<2.00	<2.00	43.50	34.80
$\text{NO}_3$	0.14	0.06	6.76	30.40	18.20	0.05	2.31	0.47	44.50	2.59
Cl	0.10	0.10	0.10	0.10	0.10	<0.10	5.80	2.91	<0.10	0.46
$\text{SO}_4$	<0.15	0.93	4.17	33.20	16.70	0.13	<0.15	<0.15	40.50	4.31
F	0.04	0.08	0.42	0.63	0.32	0.08	0.03	0.02	1.77	0.14
$\text{SiO}_2$	11.30	6.67	14.80	12.10	15.00	7.26	6.80	8.43	12.40	14.80
$\delta^{18}\text{O}$ (‰)	-6.75	-9.71	-8.56	-8.50	-8.76	-8.40	-6.59	nm	-6.91	-8.39
$\delta^2\text{H}$ (‰)	-45.82	-68.30	-58.23	-57.85	-60.15	-58.44	-49	nm	-47.6	-56.8
$\delta^{13}\text{C}$ (‰)	-17.51	-9.00	-9.64	-8.61	-7.75	-12.02	-13.2	nm	-6.6	-11.2
C-14 (pMC)	68.99	1.11	3.43	1.02	0.84	15.84	98.8	nm	1.8	3.2

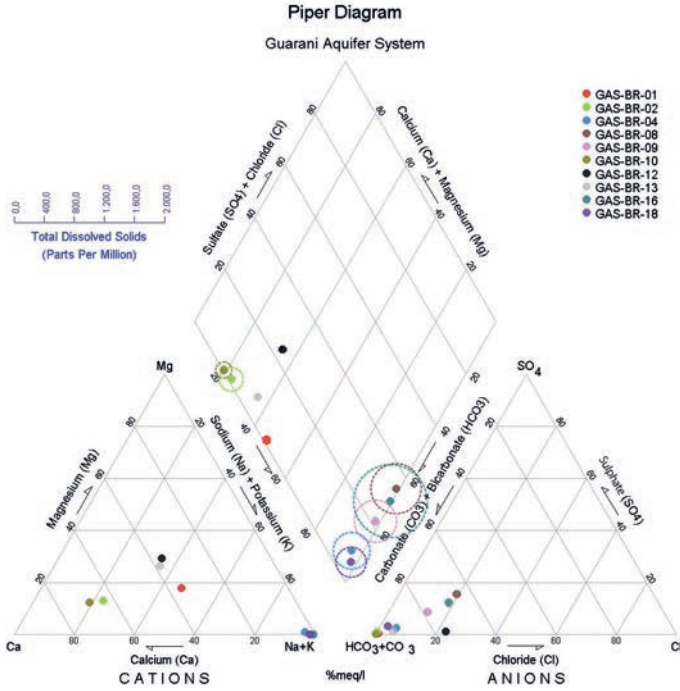


FIG. 2. Piper diagram for SAG groundwaters.

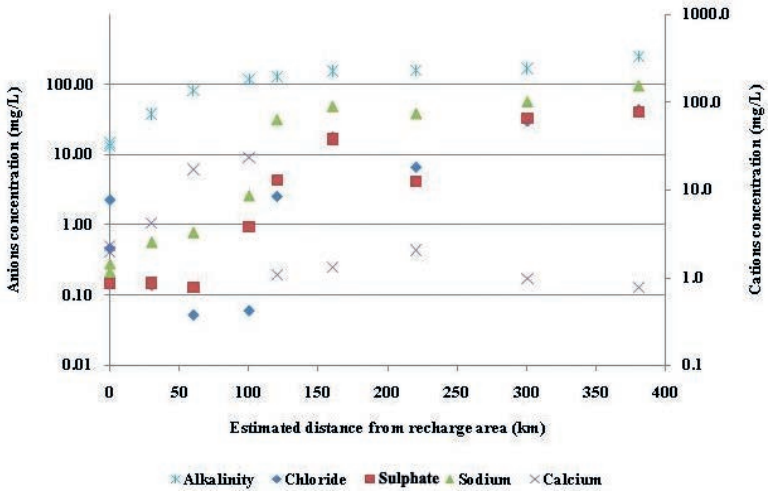


FIG. 3. Evolution of the concentration of major cations and anions along the transect.

the recharge zones located in the outcrop areas of the sandstone layers (Altinópolis; GAS-BR-12, Serra Azul; GAS-BR-13, Batatais; GAS-BR-01; Jaboticabal; GAS-BR-02, Orlândia; GAS-BR-10). These waters evolve to Na-HCO<sub>3</sub> type (São José do Rio Preto; GAS-BR-04, Olímpia; GAS-BR-09 and Bebedouro; GAS-BR-18) and then to Na-HCO<sub>3</sub>/Na-Cl-SO<sub>4</sub> waters (Buritama; GAS-BR-08 and Valparaíso; GAS-BR-16) in the deeper, more confined parts of the aquifer (Fig. 2).

Along the transect an increase in alkalinity, chloride, sulphate and sodium concentrations is observed, while calcium concentrations decrease along the transect. This decrease can be explained by ion exchange as proposed by several authors [6–8], leading to the evolution from Ca-HCO<sub>3</sub> to Na-HCO<sub>3</sub> groundwaters (Fig. 3).

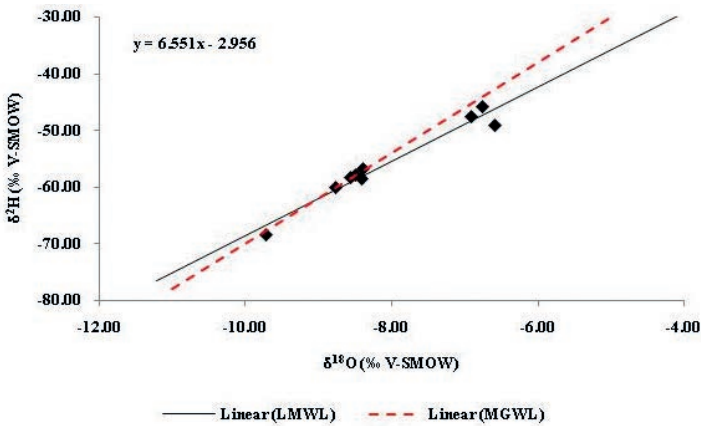


FIG. 4.  $\delta^{18}O$  vs.  $\delta^2H$  relationship for groundwater samples collected along the transect.

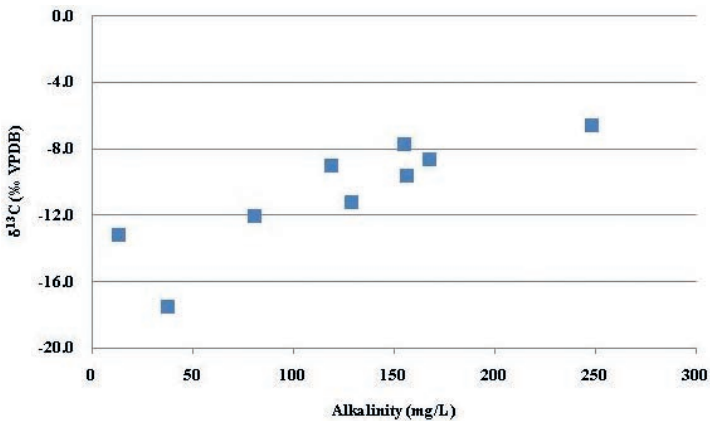


FIG. 5. Variation of  $\delta^{13}C$  contents vs. alkalinity.

The  $\delta^{18}\text{O}$  values vary from  $-6.75\text{‰}$  to  $-9.71\text{‰}$  vs. V-SMOW and those of  $\delta^2\text{H}$  vary from  $-45.8\text{‰}$  to  $-68.3\text{‰}$  vs. V-SMOW. The  $\delta^{18}\text{O}$  vs.  $\delta^2\text{H}$  relationship and the Global Meteoric Water Line (GMWL) is presented in Fig. 4. This diagram shows that most groundwater samples collected in the recharge area or near the outcrop areas (GAS-BR-01, GAS-BR-12 and GAS-BR-13) show an isotopic signature similar to average present day rainwater, (about  $-6\text{‰}$ ). A marked isotopic shift (up to  $-3\text{‰}$   $\delta^{18}\text{O}$ ) is observed in the first sections of the confined part of the aquifer. Further down-dip along the transect,  $\delta^{18}\text{O}$  values remain around  $-8\text{‰}$ .

The marked  $\delta^{18}\text{O}$  variability of groundwaters sampled in a short distance, from the recharge area to the confined part of the GAS, suggests changing climatic conditions during recharge of these waters, as suggested by other authors in the northwestern part of the GAS [2, 9]. However this point needs to be evaluated after obtaining noble gas concentrations in groundwater, which may indicate palaeotemperature values during groundwater recharge.

Along the transect  $\delta^{13}\text{C}$  values in GAS groundwater vary from  $-17.5\text{‰}$  to  $-6.6\text{‰}$  vs. VPDB, with a trend to more positive values along the transect. The progressive enrichment in  $\delta^{13}\text{C}$  ratios in the TDIC is proportionally related to the gradual increase in alkalinity along the flow path, and could be related to the dissolution and exchange with the carbonate cement in the GAS sandstones in the centre of the Paraná Basin [8–10] (Fig. 5).

C-14 activities of 80 pMC are found in present day recharge areas. Along the transect the C-14 activities decrease abruptly, reaching about 1 pMC in wells placed over 50 km from the recharge area (Fig. 6).

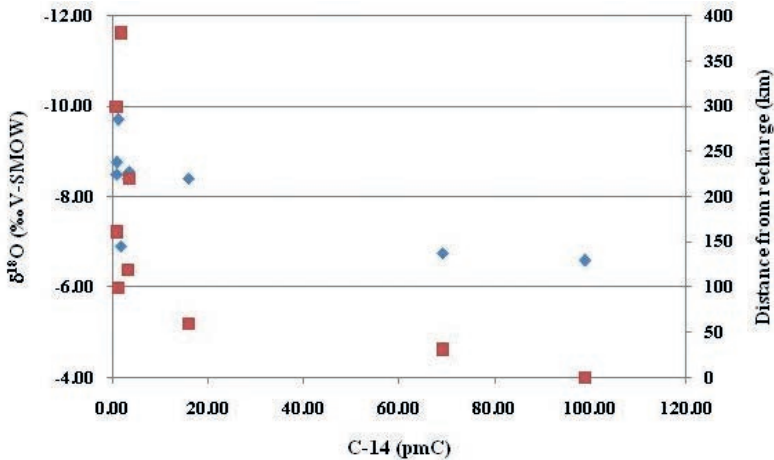


FIG. 6. Variation of C-14 activities related to the distance from the recharge (red squares) areas and  $\delta^{18}\text{O}$  (blue diamonds).

#### 4. CONCLUSION

Preliminary results of the research project show that groundwaters evolve from Ca-Mg-HCO<sub>3</sub> waters in recharge areas to Na-HCO<sub>3</sub> and then to Na-Cl-SO<sub>4</sub> waters in the confined zone of the aquifer. The main geochemical processes responsible for this evolution are mineral dissolution and ion exchange.

In the outcrop area, groundwaters present a stable isotopic content comparable to present day rains. More depleted water isotopic contents (up to -3‰ in δ<sup>18</sup>O) are found westward, probably indicating distinct climatic conditions during recharge in the past. These isotopically depleted groundwaters present C-14 activities very close to the detection limit, which suggests the existence of very old groundwater in the central portion of the aquifer, where hydraulic gradients are much smaller than those near the recharge areas.

These features have important implications for the exploitation of groundwater in the confined zone of the GAS, because very low recharge rates could be expected and the replenishment rate of the reservoir is different than that of extraction. It is important to understand the distribution of residence time of groundwater, in order to construct and validate numerical hydrodynamic models that can be used for developing and improving groundwater management strategies, which will ensure the optimal use of these resources. To obtain this information about the ages of very old groundwater in the GAS, in the next step of the project is focusing on the determination of groundwater ages, using long lived isotopic tracer measurements such as <sup>81</sup>Kr, <sup>36</sup>Cl and/or <sup>4</sup>He and also improve the knowledge about the past recharge temperature conditions using noble gas determinations.

#### ACKNOWLEDGEMENTS

The authors would like to thank the staff of the water supply companies which authorized our access to the wells sampled during this project.

#### REFERENCES

- [1] GALLO, G., SINELLI, O., Estudo Hidroquímico e Isotópico das Águas Subterrâneas na Região de Ribeirão Preto, *Revista Brasileira de Geociências* **10** (1980) 130–139.
- [2] DA SILVA, R.B.G., Estudo Hidroquímico e Isotópico das Águas Subterrâneas do Aquífero Botucatu no Estado de São Paulo, PhD Thesis, Universidade de São Paulo, Brazil (1983) 133 pp.
- [3] KIMMELMANN, A.A.S., REBOUÇAS, A.C., SANTIAGO, M.M.F., DA SILVA, R.B.G., “Isotopic study of Botucatu aquifer system in the Brazilian portion of the Parana Basin”, *Isotope Hydrology Investigations in Latin America*, IAEA-TECDOC-502, IAEA, Vienna (1989) 51–71.

- [4] ORGANIZATION OF AMERICAN STATES, Aquífero Guarani: Programa Estratégico de Ação, OAS, Washington D.C. (2009).
- [5] BONOTTO, D.M., Hydro(radio)chemical relationships in the giant Guarani Aquifer, Brazil, *J. Hydrol.* **323** (2006) 353–386.
- [6] SRACEK, O., HIRATA, R., Geochemical and stable isotopic evolution of the Guarani Aquifer System in the state of São Paulo, Brazil, *Hydrogeol. J.* **10** (2002) 643–655.
- [7] MENG, S.X., MAYNARD, J.B., Use of statistical analysis to formulate conceptual models of geochemical behavior: Water chemical data from the Botucatu Aquifer in São Paulo State, Brazil, *J. Hydrol.* **250** (2001) 78–97.
- [8] GASTMANS, D., CHANG, H.K., HUTCHEON, I., Groundwater geochemical evolution in the northern portion of the Guarani Aquifer System (Brazil) and its relationship to diagenetic features, *Appl. Geochem.* **25** 1 (2010) 16–33.
- [9] GASTMANS, D., CHANG, H.K., HUTCHEON, I., Stable isotopes ( $^2\text{H}$ ,  $^{18}\text{O}$  and  $^{13}\text{C}$ ) in groundwaters from the northwestern portion of the Guarani Aquifer System (Brazil), *Hydrogeol. J.* **18** (2010) 1497–1513.
- [10] FRANÇA, A.B., ARAÚJO, L.M., MAYNARD, J.B., POTTER, P.E., Secondary porosity formed by deep meteoric leaching: Botucatu eolianite, southern South America, *AAPG Bulletin* 87 7 (2003) 1073–1082.



# ROLE OF ISOTOPES IN THE DEVELOPMENT OF A GENERAL HYDROGEOLOGICAL CONCEPTUAL MODEL OF THE GUARANI AQUIFER SYSTEM (GAS)

H.K. CHANG<sup>a</sup>, R. ARAVENA<sup>b</sup>, D. GASTMANS<sup>a</sup>, R. HIRATA<sup>c</sup>,  
M. MANZANO<sup>d</sup>, L. VIVES<sup>e</sup>, L. RODRIGUES<sup>f</sup>, P.K. AGGARWAL<sup>g</sup>,  
L. ARAGUÁS ARAGUÁS<sup>g</sup>

<sup>a</sup> LEBAC, UNESP Rio Claro  
Bela Vista, Rio Claro (SP), Brazil

<sup>b</sup> Department of Earth and Environmental Sciences,  
University of Waterloo,  
Waterloo, Ontario, Canada

<sup>c</sup> IG-USP São Paulo,  
Cidade Universitária, São Paulo (SP)

<sup>d</sup> Escuela Universitaria de Ingeniería Civil,  
Universidad Politécnica de Cartagena,  
Cartagena, Spain

<sup>e</sup> Instituto de Hidrología de Llanuras, IHLLA,  
Azul, Argentina

<sup>f</sup> Facultad de Ingeniería y Ciencias Hídricas,  
Universidad Nacional del Litoral,  
Santa Fé, Argentina

<sup>g</sup> Isotope Hydrology Section, IAEA,  
Vienna, Austria

## Abstract

The Guarani Aquifer System (GAS) is one of the most important groundwater reservoirs in South America, and it represents a typical example of a large transboundary aquifer, shared by Argentina, Brazil, Paraguay and Uruguay. Groundwater flow shows a regional trend from north to south, controlled by the topography and regional hydraulic gradients. Recharge occurs in outcrop areas, mainly in the northern and eastern borders of the GAS. Discharge zones were identified in the southern and western borders. Four main hydrodynamic domains are recognized, related to the major tectonic structures of the Paraná Basin. The spatial distribution and

the large range of stable isotope contents of groundwater in the confined part of the GAS indicate that recharge has occurred under different climatic conditions. Carbon-14 contents above the detection limit are only found along a narrow band parallel to the outcrop areas, indicating the existence of very old groundwaters in the central portion of the aquifer.

## 1. INTRODUCTION

The use of environmental isotopes in hydrogeological investigations, complementing geochemical and hydrodynamic information, is now routine, and could be

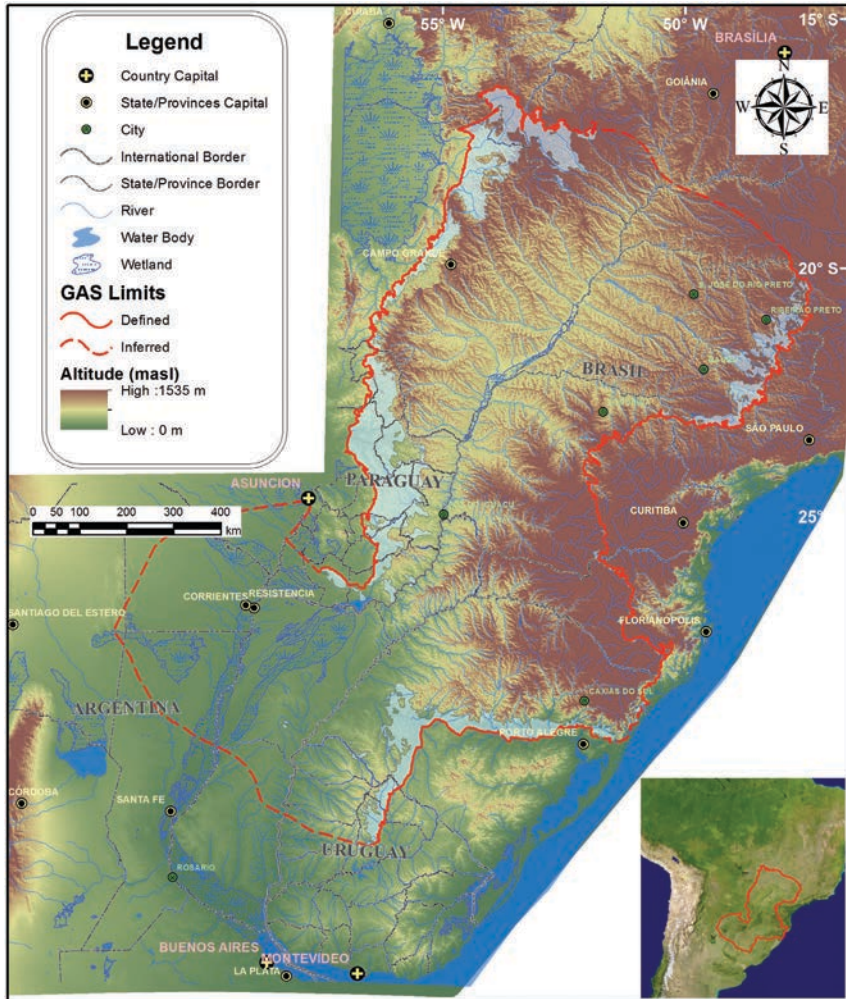


FIG. 1. Location of the Guarani Aquifer System in South America and its hydrological boundaries.

helpful to understand patterns of groundwater flow and to validate hydrogeological continental scale aquifers such as the Guarani Aquifer System (GAS), one of the most important groundwater reservoirs in South America, representing a typical example of a large transboundary aquifer, shared by four countries: Argentina, Brazil, Paraguay and Uruguay. The GAS constitutes an important source of potable water for more than 90 million people that live above it. It extends for about 1 100 000 km<sup>2</sup> in the territory of: Argentina (228 255.26 km<sup>2</sup>), Brazil (735 917.75 km<sup>2</sup>), Paraguay (87 535.63 km<sup>2</sup>) and Uruguay (36 170.51 km<sup>2</sup>) (Fig. 1).

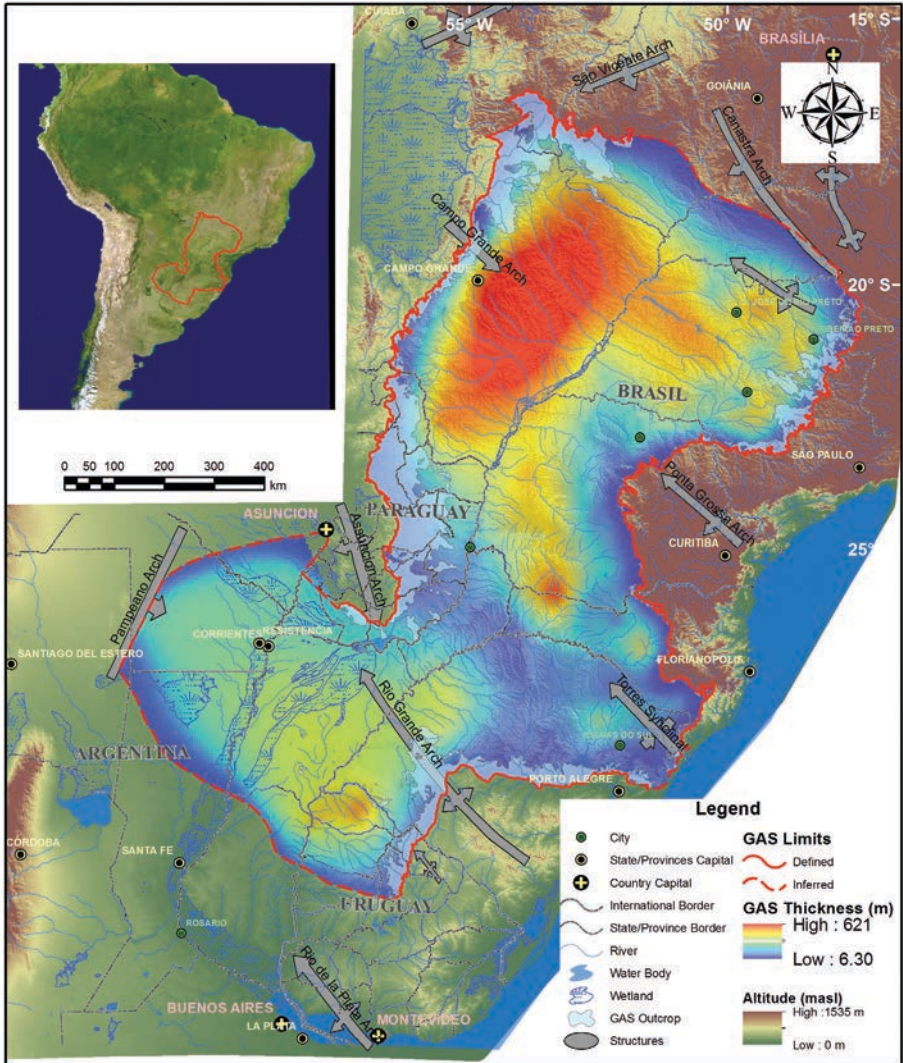


FIG. 2. Thickness of the Guarani Aquifer System and main geological structures in the Parana and Chacoparanaense Basins.

Due to its importance for the region, a Global Environmental Facility (GEF) funded project ‘Environmental Protection and Sustainable Integrated Management of the Guarani Aquifer’ was carried out to produce a comprehensive hydrogeological study of the GAS. This project has been funded by the GEF, the World Bank and the Organization of American States (OAS). Since the early phases of the project, the IAEA was involved in the implementation of the project by providing technical assistance on the use of isotope and hydrochemical tools in characterizing the main hydrogeological features of this continental scale aquifer.

The main purpose of this article is to present the conceptual hydrogeological model for the GAS developed during the project and the role of isotope tools in the delineation of major sectors within the aquifer, the characterization of recharge areas and mechanisms of the shallow and deep parts of the GAS and the definition of groundwater dynamics.

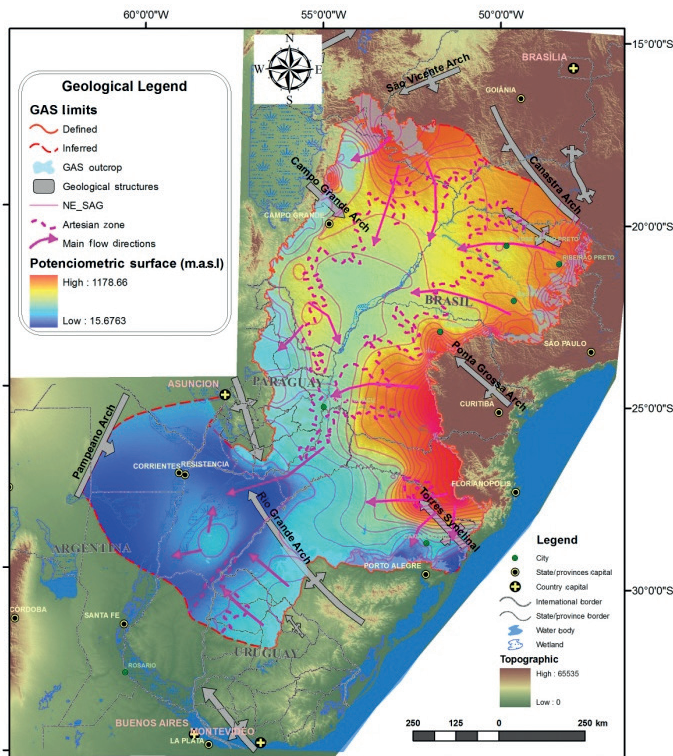


FIG. 3. Potentiometric map of the Guarani Aquifer System.

## 2. GEOLOGICAL SETTING

The GAS is formed by a package of Mesozoic sedimentary continental clastic rocks that occur in the Chacoparanaense and Parana Sedimentary Basins. The base is bounded by a Permo-Eotriassic regional unconformity and the top by lava flows of the Serra Geral Formation. It includes the Misiones (Argentina and Paraguay), Tacuarembó (Uruguay), Santa Maria, Caturrita, Guará and Botucatu (Brazil — south portion of Paraná Basin) and Pirambóia and Botucatu (Brazil — north portion of the Parana Basin) formations [1].

The aquifer crops out along its western and eastern boundaries, but most of the GAS is confined by basaltic layers of Cretaceous age (in some places covered by more than 1500 m). The aquifer units show important differences in thickness (from less than 50 to more than 600 m, with a mean thickness of 250 m). Spatial distribution of the units constituting the GAS and its limits are controlled by several faults and tectonic structures, however, important structures within the Paraná Basin are supposed to control groundwater flow, such as the Ponta Grossa Arch, the Rio Grande and Asunción Arches and the Torres Syncline (Fig. 2).

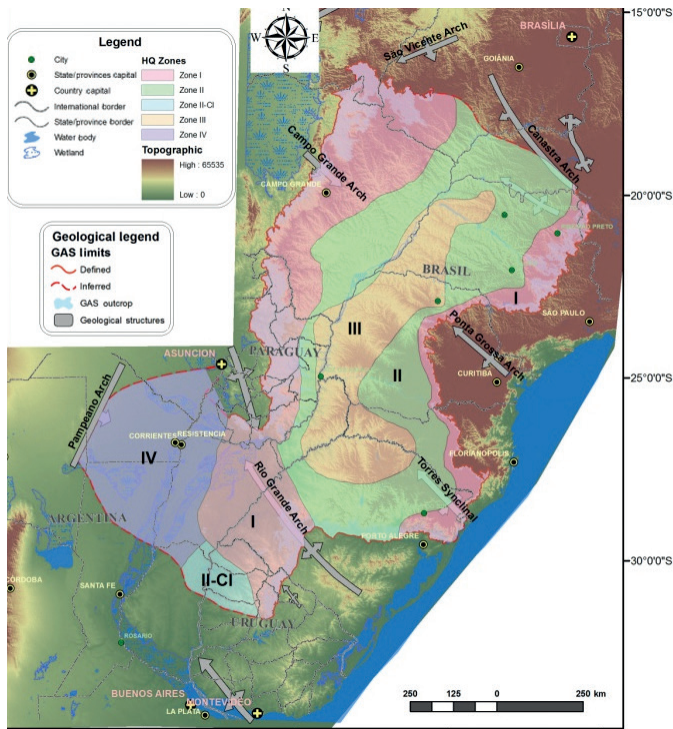


FIG. 4. Main hydrochemical facies identified in GAS groundwater.

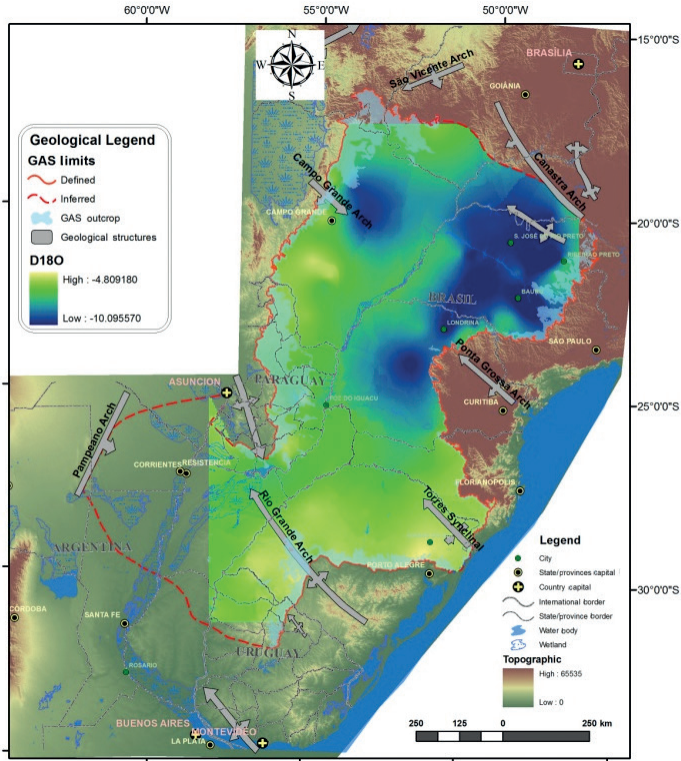


FIG. 5.  $\delta^{18}\text{O}$  distribution map of the Guarani Aquifer System.

### 3. HYDROGEOLOGICAL SETTING

The topography and the geological structure suggest the presence of recharge areas in most of the outcrop areas. The potentiometric map delineates, among various flow lines, a main flow path from the north and NW to the south, following the axis defined by the Paraná River (Fig. 3). Some of the outcrop areas function as recharge areas of local shallow groundwater flows and, at the same time, discharge areas of the deep confined aquifer, especially in the western and southern borders of the GAS. Due to the important amount of precipitation over the aquifer (1000–2000 mm/a) there is active groundwater circulation in the outcrop areas and in the shallow part of the aquifer. These local flows generally discharge to local rivers crossing the outcrop of the GAS

Important hydrodynamic features are observed along the Paraná river, in the northern part of the GAS, and along the Uruguay river, close to the national border between Argentina and Uruguay; these two important zones are located in zones where the aquifer is artesian.

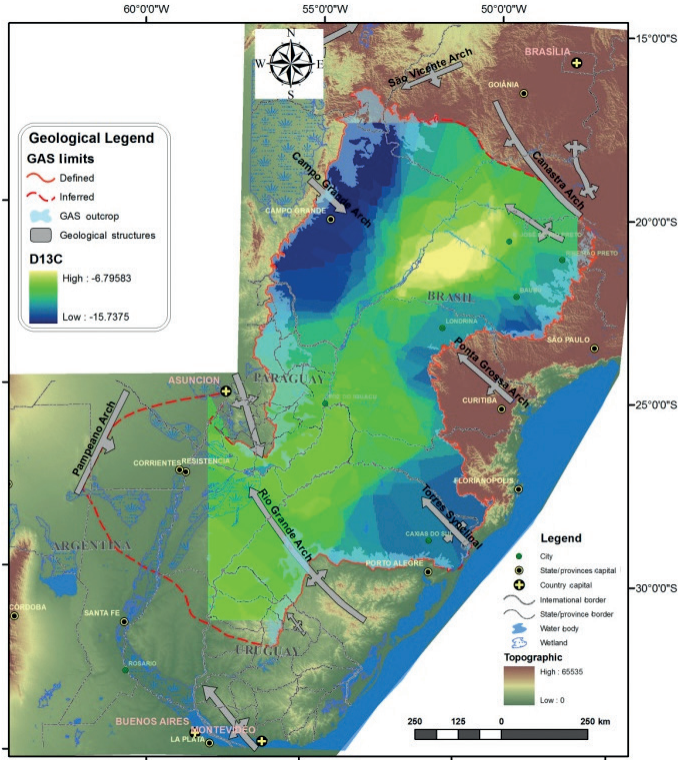


FIG. 6.  $\delta^{13}\text{C}$  distribution map of the Guarani Aquifer System.

The GAS presents relatively high hydraulic conductivity (in the order of 1–5 m/d) but the low hydraulic gradients found in the deeper parts of the aquifer (0.2 m/km) lead to very low groundwater velocities of the deep system. Higher hydraulic gradients (3–5 m/km) are only found in the boundaries of the GAS.

#### 4. HYDROCHEMISTRY OF THE GUARANI AQUIFER SYSTEM

The groundwater quality of the GAS is generally very good, with very low mineralization levels in most areas. In general, four main hydrochemical facies are recognized along the GAS, related to the geochemical evolution from recharging waters in the outcrop areas towards the deep central parts of the aquifer. Zone I is characterized by Ca-Mg-HCO<sub>3</sub> waters, Zone II by Na-Ca-HCO<sub>3</sub> waters and Zone II-Cl by an increase in chloride content, Zone III by Na-SO<sub>4</sub>-Cl waters and finally Zone IV by high salt content. The distribution of these hydrochemical facies are shown in Fig. 4.

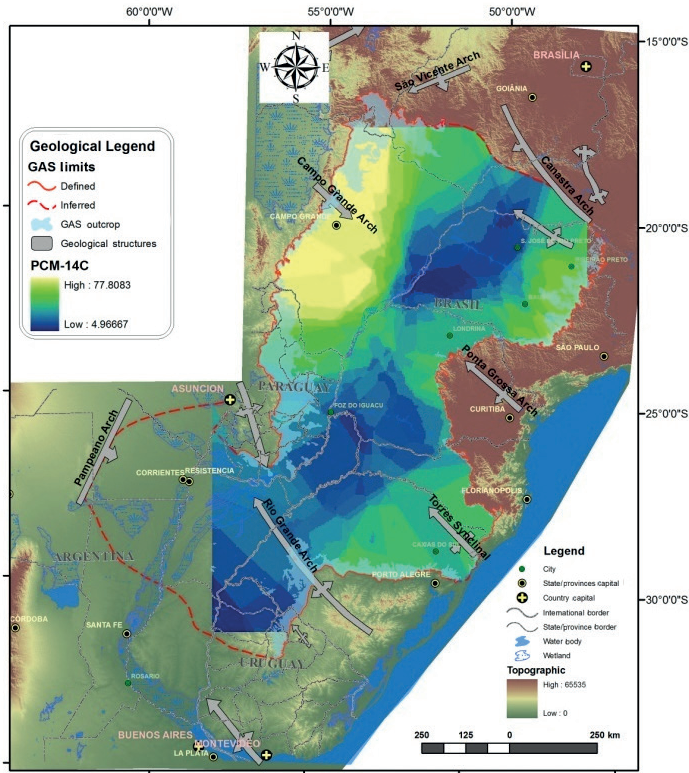


FIG. 7. Distribution of  $^{14}C$  map of the Guarani Aquifer System.

Generally the evolution observed along the flow lines is due to the dissolution of carbonates and to ion exchange processes, as presented by several authors [2, 3]. In most cases, the increase in salinity and other trace elements has been related to contributions from saline waters and aquitards found at greater depth. Temperature and pH values also increase from approximately 20°C and 6.8 units in the recharge areas, to 50°C and 9.5 units in the deepest boreholes drilled in the centre of the Paraná basin. In the southern part of the aquifer increasing levels of chloride and sulphate are found locally, changing the hydrochemical facies of the deepest water samples towards the sodium chloride type.

## 5. ISOTOPES IN THE GUARANI AQUIFER SYSTEM

The spatial distribution of the  $\delta^{18}O$  and  $\delta^2H$  contents of GAS groundwater showed marked contrasts between different sectors of the GAS, delineating zones of the GAS with particular origin and dynamics. In most of the recharge areas, the stable

isotope contents of precipitation matched the stable isotope values found in present day precipitation and tritium values in the range of 0 to 3 TU, similar to present day contents. However, several zones in the confined part of the aquifer, such as the GAS in the Sao Paulo State, are characterized by the presence of more negative isotope contents than present day precipitation (up to 3‰ in  $\delta^{18}\text{O}$ ). These unusual isotope values are not found in the Southern part of the aquifer and are still a topic of debate in terms of palaeoclimatic significance as proposed by several authors [4, 5] (Fig. 5).

In general, a progressive trend towards more positive  $\delta^{13}\text{C}$  values is also found along the main flow paths. This geochemical trend confirms the importance of carbonate dissolution and exchange in the hydrochemical evolution of groundwaters, as indicated above. Analysis of the spatial distribution of carbon isotopes helped to confirm previous ideas about the existence of local recharge in the outcrop areas and discharge flows as well as discharge of regional flows.

Carbon isotopes in the DIC have also been measured in a systematic way along several flow lines. The available isotope results confirm the presence of recently recharged waters in the outcrop areas. A rapid decline of  $^{14}\text{C}$  activities is observed along the mentioned flow paths towards the confined part of the aquifer. Most deep boreholes in the central part of the aquifer present  $^{14}\text{C}$  activities below the detection limit, in agreement with hydrodynamic ages derived from numerical models of flow in the GAS. Some  $^{14}\text{C}$  activities found in the deep confined part of the GAS, in the range 0–10 pMC, are supposed to be the result of mixing of deep groundwater with shallow groundwater present in the post-GAS sediments. Based on hydrodynamic considerations and the result of the radiocarbon analyses, it is assumed that most groundwaters in the deep confined part of the aquifer present groundwater residence times well above the range of the radiocarbon dating method.

## 6. CONCLUSIONS

The combined use of piezometric, hydrochemical and isotope data allowed the delineation of the boundary conditions for the GAS, identifying areas of recharge, discharge and no-flow. For example, present day recharge was confirmed in outcrop areas. However, isotope data and numerical modelling indicated that active groundwater recharge to the deep confined system is very limited, probably in the order of 1% of annual precipitation, over the recharge area (10–15 mm/y). On the other hand, the discharge mechanisms have not been fully studied, due to the difficulties in measuring small groundwater discharges in areas with a large runoff. Besides the discharge along the outcrop area in the border zones of the aquifer, other options have been suggested but not yet proved. In areas characterized by the presence of dikes (Ponta Grossa Arch), a number of springs discharging into major rivers have chemical compositions similar to the GAS waters. Additionally, groundwater discharge through extensive wetland located in Argentina has been suggested but never studied.

In a recent field trip to the area salt rich water has been collected, which support this discharge hypothesis.

The revised conceptual model of the GAS has important implications for the exploitation of groundwater in the GAS sectors identified by hydrochemical and isotope data. Groundwater extracted from the unconfined part of the aquifer is fully renewable due to the potential for enhanced recharge under intensive pumping. Consideration of the water balance indicates potential recharge in the order of 300–500 mm/a. However these areas are vulnerable to pollution and other impacts of human activity. Groundwater extracted in the confined portion is economically feasible to certain depths (about 400 m), and therefore, a substantial part of the water resources from deep horizons are not available for extraction. Exploitation of the deep confined groundwater is controlled by the storage coefficient of the GAS. These groundwaters usually present higher mineralization and are well protected against pollution, although they demand a planned extraction.

## REFERENCES

- [1] SINELLI, O., et al., Texto Explicativo – Mapa Hidrogeológico do Sistema Aquífero Guarani, Escala 1:3.000, Rio Claro, Consórcio Guarani (2008) 57.
- [2] SRACEK, O., HIRATA, R., Geochemical and stable isotopic evolution of the Guarani Aquifer System in the state of São Paulo, Brazil, *Hydrogeol. J.* **10** (2002) 643–655.
- [3] BONOTTO, D.M., Hydro(radio)chemical relationships in the giant Guarani Aquifer, Brazil, *J. Hydrol.* **323** (2005) 353–386
- [4] GALLO, G., SINELLI, O., Estudo Hidroquímico e Isotópico das Águas Subterrâneas na Região de Ribeirão Preto, *Revista Brasileira de Geociências* **10** (1980) 130–139.
- [5] DA SILVA, R.B.G., Estudo Hidroquímico e Isotópico das Águas Subterrâneas do Aquífero Botucatu no Estado de São Paulo, PhD Thesis, Universidade de São Paulo, Brazil (1983) 133 pp

# APPLICATION OF ISOTOPIC TOOLS FOR THE INTEGRATED MANAGEMENT OF THE SANTA ELENA COASTAL AQUIFER, ECUADOR

P. CARRIÓN<sup>1</sup>, S. JIMÉNEZ, P. ROMERO

Centro de Investigaciones y Proyectos Aplicados a las Ciencias de la Tierra,  
Escuela Superior Politécnica del Litoral,  
Guayaquil, Ecuador

## Abstract

In 2007, two technical cooperation projects, RLA/8/041 'Application of Isotopic Tools for Integrated Management of Coastal Aquifers, Ecuador' and ECU/8/026 'Characterization of Coastal Aquifers of the Santa Elena Peninsula' were launched to better assess groundwater resources and possible marine intrusion in the Santa Elena coastal area. Groundwater constitutes the main source of drinking water in the area, complemented by surface water resources derived from the Santa Elena reservoir. The Escuela Superior Politécnica del Litoral (ESPOL), through the Centro de Investigación y Proyectos Aplicados a las Ciencias de la Tierra (CIPAT), implemented these projects in collaboration with other local institutes. Strategic planning is designed to promote the sustainable use of groundwater, based on a solid characterization of groundwater bodies using hydrogeological, hydrochemical and isotopic techniques. ESPOL currently works in the isotopic characterization of the main water types and their interactions in the Santa Elena aquifer.

## 1. INTRODUCTION

The field of groundwater hydrology is a recent topic of study in Ecuador. It has been greatly promoted in recent years through the technical cooperation programme of the IAEA. The development of this field has involved working with local communities to set up strategies and plans to increase the knowledge and interest in the monitoring, evaluation and conservation of the water resources. Creating a water culture is a process that needs time and a number of factors to mature.

The study area of these two projects is located in the Santa Elena province (PSE in Spanish), a coastal region of Ecuador. This area is part of a dry to arid climatic belt. The annual mean temperature ranges from 17°C to 35°C. The variable rainfall rates determine that evaporation exceeds annual precipitation, with values of real

---

<sup>1</sup> Present address: Facultad de Ingeniería en Ciencias de la Tierra, Km 30.5 Vía perimetral, Campus Gustavo Galindo, Guayaquil, Ecuador

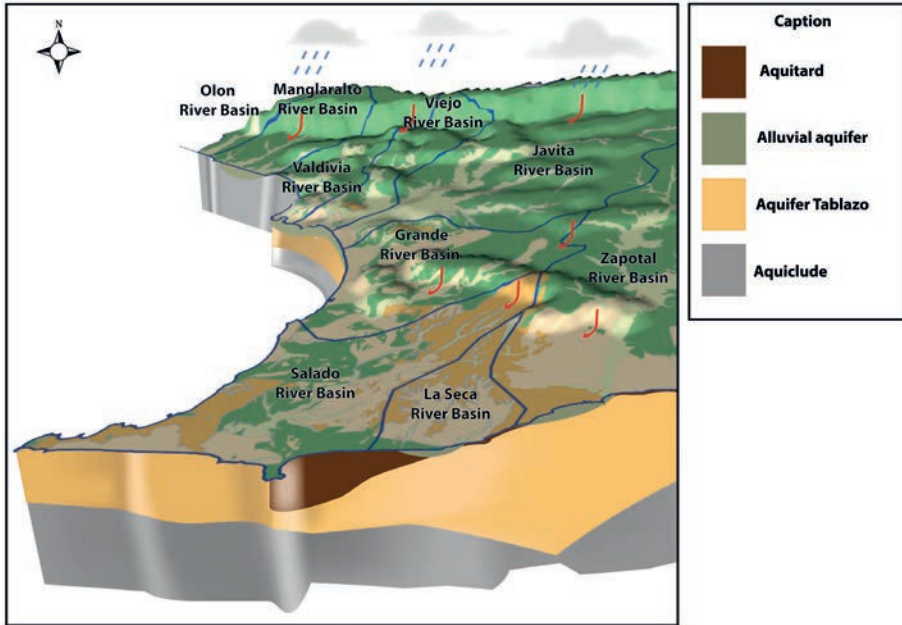


FIG. 1. Conceptual hydrogeological model of study area.

evaporation exceeding 1100 mm/a, and precipitation values in some sectors below 450 mm/a. However, local rainfall is the only source of water recharge to the aquifers in the area.

The study area extends over 3762 km<sup>2</sup>, in which there are about 240 000 inhabitants, with approximately 100 000 inhabitants in rural areas. It consists of nine river basins. This area has been divided into two sectors: northern and southern, based on the diverse climatic and hydrogeological characteristics.

In the northern sector, most of aquifers correspond to unconfined aquifers which are located in floodplains of rivers. They are mainly composed of gravels, silts and sands. On the other hand, in the southern sector, there are important deeper aquifers that are being used for water supply which are mainly located in the Tablazo Fm., which consist of calcareous sandstones and conglomerates.

The conceptual hydrogeological model of the area considers the alluvial aquifers (gravel and sands) in the basins located in the northern sector: Olón, Manglaralto and Valdivia. The aquifers in the southern sector are linked to the Tablazo Formation and are formed by unconsolidated sands, sandstones and calcareous conglomerates: Salado, La Seca and Zapotal in the communities Sayá, Atahualpa, Prosperidad, Santa Elena, Río Verde, Pechiche, El Real and Manantial de Chanduy.

## 2. METHODOLOGICAL APPROACH

In the present study, interdisciplinary studies involving hydrogeology, geology, geophysics, hydrochemistry and isotope techniques ( $^{18}\text{O}$ ,  $^2\text{H}$  and  $^3\text{H}$ ) were used. Within the monitoring programme established at the beginning of the project, a total of 200 wells have been sampled during three sampling campaigns. However, after a check-up of the ionic balance of the hydrochemical analysis, a number of results were discarded due to errors above 10%.

In the hydrochemical study of groundwater in the PSE, we have considered the chemical analysis of major ions:  $\text{Na}^+$ ,  $\text{Mg}^{2+}$ ,  $\text{Ca}^{2+}$ ,  $\text{K}^+$ ,  $\text{CO}_3^{2-}$ ,  $\text{NO}_3^-$ ,  $\text{SO}_4^{2-}$  and  $\text{Cl}^-$ . The results are shown in Piper and Stiff diagrams, distinguishing samples from the northern and southern sectors. This graphic representation has been made on the geological map presented in Fig. 2.

Parallel to physical and chemical sampling, samples were collected for isotopic analysis of deuterium and oxygen-18. In two campaigns, a total of 116 samples were collected, which were analysed in Mexico and Chile. A smaller set of samples for tritium analysis were collected. Table 1 summarizes the general hydrological data, physical and chemical parameters and the results of the isotopic analyses.

## 3. RESULTS

### 3.1. Hydrochemistry

Based on the Piper diagram shown in Fig. 1, the following water types can be defined:

- Most of the samples collected belong to the  $\text{Ca}^{2+}/\text{Na}^+-\text{HCO}_3^-$  type, which have not been influenced by sea water. In this group groundwater from areas far from the coastal sites are found, as well as rain and river runoff.
- A second group is formed by samples showing the  $\text{Na}^+-\text{Cl}^-$  type with  $\text{Cl}^- > \text{SO}_4^{2-} > \text{HCO}_3^-$ : These samples show important marine influence.
- The third type is formed by those samples of the  $\text{Na}^+-\text{Cl}^-$  type, but with  $\text{Cl}^- > \text{HCO}_3^- > \text{SO}_4^{2-}$ , with possible thermal influence.

The waters of the  $\text{Ca}^{2+}/\text{Na}^+-\text{HCO}_3^-$  type correspond to samples collected in the northern part of the PSE, while the  $\text{Na}^+-\text{Cl}^-$  type waters correspond to those sampled in the southern sector.

As indicated above, the northern and southern areas show significant differences in the chemical composition of groundwater. Groundwater in the northern sector shows greater similarity to the water chemistry of precipitation and surface waters, characterized by low mineralization and chemical composition of the  $\text{Ca}^{2+}/\text{Na}^+-\text{HCO}_3^-$  type (except the sample Palmar1, which is water evaporated and

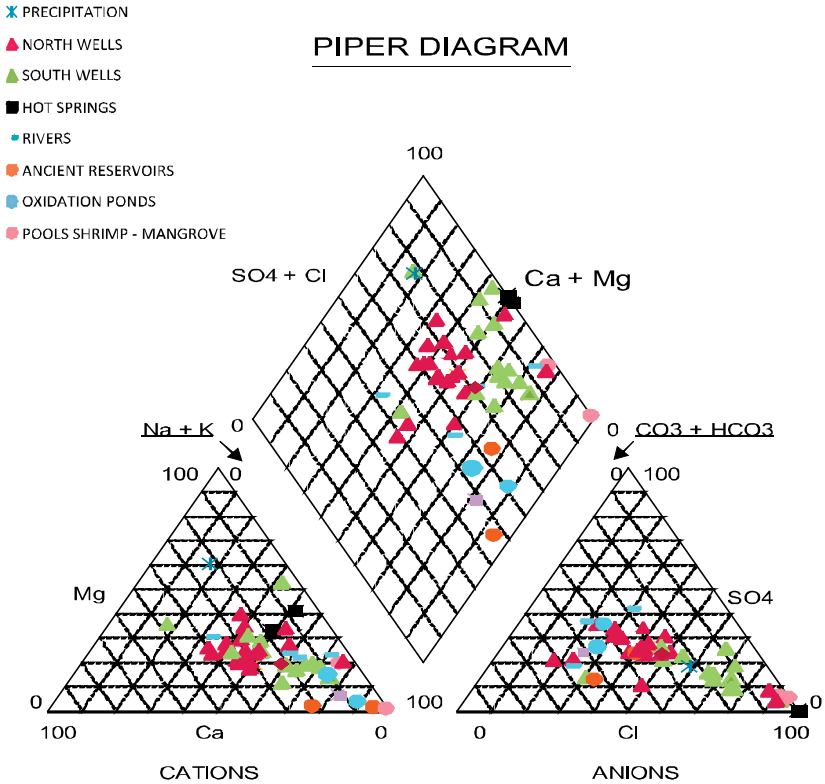


FIG. 2. Piper diagrams of water samples collected in PSE.

is very close to the coastline), although there are some wells in the coastline that have been influenced by seawater intrusion, as in sectors of Manglaralto and Olón.

In the southern sector, most of the samples show a predominantly  $\text{Na}^+ - \text{Cl}^-$  composition, with variations in  $\text{Ca}^{2+}$ ,  $\text{Mg}^{2+}$ ,  $\text{SO}_4^{2-}$  and  $\text{HCO}_3^-$ , which have been classified into two types:  $\text{Na}^+ - \text{Cl}^-$ , with  $\text{Cl}^- > \text{SO}_4^{2-} > \text{HCO}_3^-$ , with marine influence and  $\text{Na}^+ - \text{Cl}^-$ , with  $\text{Cl}^- > \text{HCO}_3^- > \text{SO}_4^{2-}$ , with thermal influence, finding a smaller set of samples with similar composition to recharge water (Prosperidad and Atahualpa), which demonstrate the infiltration of water from rivers. It should be noted that the well QT2 in the Tablazo Formation shows a high level of salinity because the area is characterized by saline environments.

### 3.2. Isotope hydrology

Using the results of the analysis of  $^{18}\text{O}$  and  $^2\text{H}$  isotopes, two water bodies with different isotopic signatures have been identified. In the northern sector, isotopically

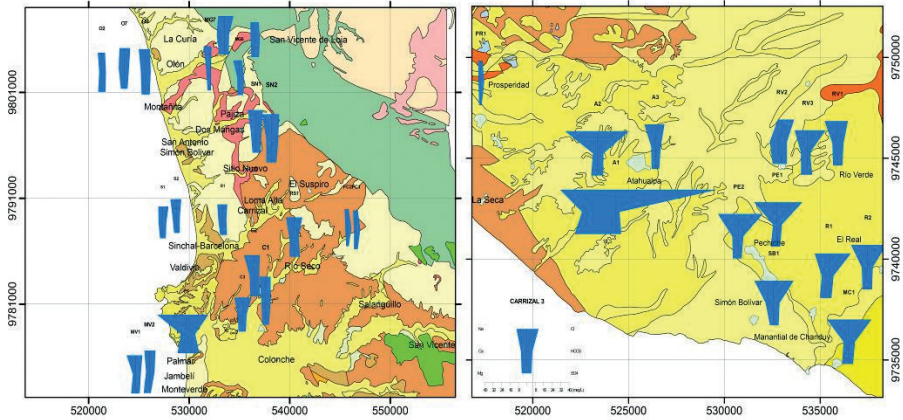


FIG. 3. Stiff Diagrams for groundwater samples in the northern (left) and southern (right) sectors of PSE.

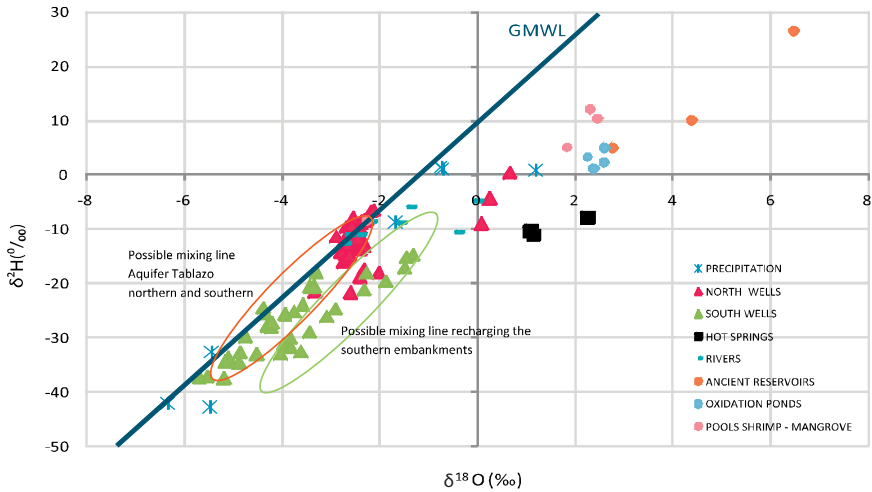


FIG. 4. Isotopic composition of surface and groundwaters in PSE.

more enriched groundwaters were mapped, while more depleted isotopic values were found in the southern sector. Probably the two aquifers are related to present day precipitation, but results of Carbon-14 analyses are not yet available.

The difference found between the two sectors may be due to the fact that in the southern sector recharge is limited to the wettest months, leading to more negative isotopic values of the infiltrating waters, while recharge in the northern sector occurs in most months of the year, resulting in the contribution of more enriched

TABLE 1. SUMMARY RESULTS. HYDROCHEMISTRY AND ISOTOPE CONTENTS

Zone	Aquifer Name	Status.	n (chem-stb-T)	Ca <sup>2+</sup>	Mg <sup>2+</sup>	K <sup>+</sup>	Na <sup>+</sup>	Cl <sup>-</sup>	HCO <sub>3</sub> <sup>-</sup>	NO <sub>3</sub> <sup>-</sup>	SO <sub>4</sub> <sup>2-</sup>	EC	pH	Temp	δ <sup>18</sup> O (‰)	δ <sup>2</sup> H (‰)	Tritium (TU)
North	Alluvial	X	38-41-02	90	37	7	169	183	328	0.3	206	1345	7.5	26.1	-2.54	-11.9	1.0
		s	38-41-03	48	22	2	107	145	76	0.4	115	729	0.4	1.2	0.22	3.0	-
South	Alluvial	X	NA	138	293	34	1730	3128	477	0.2	510	9869	8.0	26.0	-1.18	-12.8	-
		s	NA	90	349	37	2611	4639	318	0.4	572	12595	0.5	0.8	1.45	8.4	-
	X	30-23-03	147	83	11	477	853	312	34.0	302	3595	7.5	27.2	-4.03	-26.8	0.3	
	s	30-23-03	135	76	7	306	795	66	176.4	166	2733	0.4	1.4	1.05	6.2	0.3	
	Tablazo (thermal spring)	X	06-04-01	1481	529	12	2587	8124	24	0.7	5	18404	8.1	31.9	1.41	-10.1	0.0
		s	06-04-01	732	460	9	303	571	7	1.0	4	8025	0.3	1.3	0.57	1.4	-

X = mean; s = standard deviation; n = number of analyses for major ions – stable isotopes – Tritium; ion concentrations in mg/L; electrical conductivity in μS/cm. stable isotopes (deuterium and oxygen-18) in ‰ vs. VSMOW; tritium in Tritium Units; temperature in °C.

values of precipitation to recharge. Fig. 4 shows isotopic signature of the two sectors, as well as the open water cisterns, which are obviously evaporated and heavily enriched in stable isotopes.

Among the evaporated groundwaters, several wells representing small alluvial aquifers in the south are found in Fig. 4. These isotopic numbers may indicate that water cisterns contribute to the recharge of these shallow aquifers.

Thermal waters appear to show isotopic signatures similar to those of the most enriched samples (+1 to +2‰ in  $\delta^{18}\text{O}$ ), although lower deuterium values, indicating a different origin of the deep fluids flowing in the thermal springs.

### 3.3. Tritium

Tritium contents in groundwaters are higher in the northern sector, with a mean value of about 1.0 TU, similar to the estimated present day value in precipitation (1.5 TU based on the nearby stations in Ecuador and Peru). A number of samples in the southern sector show tritium levels below the detection limit, with a mean value of about 0.2 TU. The lower values in the southern sector are consistent with reduced recharge rates and longer residence time of groundwater in the aquifers in the southern sector. Carbon-14 will be measured in those groundwater samples showing lack of tritium.

## 4. CONCLUSIONS

Isotope tracers were used to characterize shallow and deep aquifers in the Santa Elena peninsula, Ecuador. Stable isotope and tritium data showed significant differences in the hydrological regime of the basins and aquifers located in the northern and southern parts of the study area. More favourable conditions for groundwater recharge and sustainable use of underground water resources are found in the northern part of the Santa Elena peninsula.

## REFERENCES

- [1] INTERNATIONAL ATOMIC ENERGY AGENCY, Estudios de Hidrología Isotópica en América Latina 2006, IAEA-TECDOC-1611, IAEA, Vienna (2009).
- [2] TORO, L., Mission Report: Preliminary Hydrogeological Assessment of the Peninsula of Santa Elena, Ecuador, Guayaquil (2007) 1–51
- [3] ARAGUÁS ARAGUÁS, L.J., QUEJIDO, A.J., Identification of the mechanisms and origin of groundwater salinity in coastal aquifers using isotope techniques, *Vértices Magazine (CIEMAT)* (2007) 28–32
- [4] VENGOSH, A., GIESKES J., MAHN, C., New evidence for the origin of hypersaline pore fluids in the Mediterranean basin, *Chem. Geol.* **163** (2000) 287–298.

- [5] YINGKAI XIAO, DEZHONG YIN, WEIGOU LIU, QINGZHONG WANG, HAIZHENG WEI, Boron isotope method for study of seawater intrusion, Science in China Series E: Technological Sciences **44** supplement (2001) 62–71.
- [6] CUSTODIO, E., HERRERA, C., Utilización de la relación Cl/Br como trazador hidrogeoquímico en hidrología subterránea, Bol. Geol. Min. (Madrid) **111** 4 (2000) 49–67.

# THE USE OF MULTIPLE ENVIRONMENTAL TRACERS IN AGE INTERPRETATION OF THE MOUNT AMBA AQUIFER, KINSHASA, DEMOCRATIC REPUBLIC OF CONGO

L.J. NDEMBO

Commissariat Général à l'Energie Atomique,  
Centre Régional d'Etudes Nucléaires de Kinshasa,  
Kinshasa, Democratic Republic of the Congo

N. PLUMMER

U.S. Geological Survey,  
Reston, VA, USA

Y. RAVI

EMMAH, University of Avignon,  
Avignon, France

T. VITVAR

Isotope Hydrology Section, IAEA,  
Vienna, Austria

## Abstract

The apparent tracer ages and mean residence time of recently recharged groundwater from the Mount Amba aquifer (Kinshasa, DR Congo) were evaluated using measurements of radiocarbon ( $^{14}\text{C}$ ), tritium ( $^3\text{H}$ ), sulphur hexafluoride ( $\text{SF}_6$ ), chlorofluorocarbons (CFCs: CFC-11, CFC-12, CFC-113), using tracer input functions suitable for the Southern Hemisphere. The apparent tracer age (assuming unmixed groundwater samples) is discussed and compared with different mixing models in age interpretation. Using a binary mixing model, a wide range of mixtures with young fraction ages of 0–30 years was found. Exponential mixing models indicated mean residence times from 12–42 years. In age interpretation, radiocarbon was used as a stable isotope tracer on the anthropogenic timescale (past 50 years) in this carbonate free aquifer.

## 1. INTRODUCTION

The multi-tracer approach seems to be the most powerful approach for groundwater dating [1–4], providing unique insights for dating groundwater in particular hydrogeological contexts, such as the Mount Amba aquifer. This aquifer is formed by

carbonate free, high permeability detritic materials and it is located in a wet area in the province of Kinshasa, Democratic Republic of Congo.

Fast circulation of groundwater implying a very short residence time of water is the main hydrodynamic feature of the aquifer. Thus, this study compares the relevance of the various methods used for dating groundwater using environmental tritium, carbon-14 (used as a stable isotope, due to the groundwater circulation of this aquifer [5]), chlorofluorocarbons (CFCs) [6, 3] and sulphur hexafluoride (SF6).

These dating methods are compared and discussed within this particularly favourable framework to evaluate the average apparent age of water. The study evaluates the proportion of the younger and older groundwater components in the mixtures of water according with the recharge periods and their respective ages and rates of recharge.

## 2. THE STUDY AREA

The study area extends over 9 965 km<sup>2</sup> and is located near the city of Kinshasa. The area represents only about 0.42% of the surface area of the Democratic Republic of the Congo and it extends around latitude: 3.9 to 5.1° S and longitude: 15.2 to 16.6° E. This zone is occupied, with approximately 7 000 000 inhabitants with a density of 700 inhabitants/km<sup>2</sup> in 20% of the area (outside of plateau des Bateke; see Fig. 1).

In the study area three physiographic zones have been identified:

- Plateau of Bateke, with an elevation ranging from 600 to 700 m and located in the east of the city of Kinshasa (covering about 80% of the study area);
- Plains area, in the north, with an elevation from 300 to 350 m, along the Congo river;
- Hills area, in the south and the west part of the region, with an elevation from 350 to 600 m.

Major rivers in the area are: (i) Bombo–Lumene, (ii) Lufimi (plateau of Bateke), (iii) Ndjili (and its tributary Lukaya) and (iv) Nsele, crossing through the hills and the plains of the study area. Rivers flow generally from south to north and all are tributaries of the Congo River.

From the geological point of view, the study area is characterized by the presence of two main geological units: (a) Quaternary sands (with different grain sizes or colours, sometimes with clay, gravel or silt lenses, especially in the Pool Malebo and the wetlands), (b) overlying sandstone material with different geological ages (Cretaceous sandstone, polymorphic sandstone and Palaeozoic feldspathic sandstone (Inkisi sandstones), constituting the basement of the aquifer. Few localized clayey

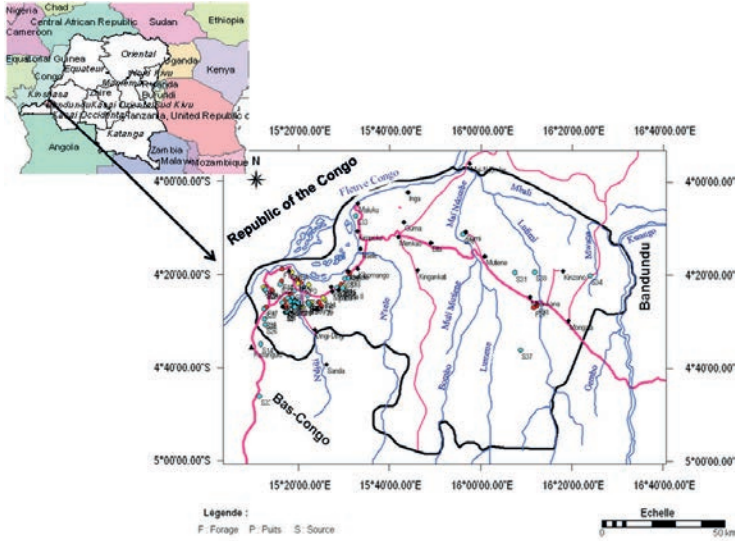


FIG. 1. Location of the study area and sampling points for the study.

interlayers above the soft sandstone in the west and within the Quaternary sands were identified in the south of the hill zone.

The main aquifer is constituted by the Quaternary sands and the soft sandstone overlying bedrock in the study area. It mainly consists of coarse grain sands with higher permeability, especially in the hill zone in the western part of the region. The aquifer is phreatic or semiconfined due to its lateral variability. Its thickness can reach 175 m in the plain and hill zones of Kinshasa, 225 m in the West and more than 250 m in the plateau of Bateke.

### 3. METHODOLOGY

Groundwater ages or apparent ages are modelled on the basis of simplifying assumptions applied to the process of transport which affects the tracer along its transit along the flow paths in the aquifer. The simplest approach to simulate transport processes relevant to groundwater dating is the piston flow model, which supposes that the concentration of the tracer is not modified by the processes related to transport (such as mixing or dispersion) starting from the recharge zone to the measurement point. However, groundwater age as determined with the piston model is often too simplistic, because the dispersion and the mixture process do occur during groundwater transit in the aquifer. Additionally younger water frequently lies at the top of the aquifer while older groundwater dominates at greater depths. If the well is rather deep, groundwater can be mixed from several aquifer levels during pumping. This

mixture of water types leads to the mixing of ages, which can complicate the modelling of apparent age. However, the simplest case is a binary mixture with old water (characterized by the lack of CFCs) and recent water. Groundwater dating becomes more complex when more than two water types are mixed, because the majority of the models estimating apparent age of groundwater are based on binary mixtures. In the case of exponential models, apparent age of water varies with the depth.

## 4. RESULTS AND DISCUSSION

### 4.1. Input functions: tritium, chlorofluorocarbon, SF<sub>6</sub> and radiocarbon in precipitation

The input function for tritium in precipitation was reconstructed with data from the World Meteorological Organization/International Atomic Energy Agency (WMO/IAEA) GNIP based on the approach proposed by Doney et al. [8] and with available tritium in precipitation measurements from the WMO/IAEA GNIP and the ZAI/8/013 Project [5].

In constructing the Southern Hemisphere atmospheric input functions for CFCs (CFC-11, CFC-12 and CFC-113), pre-1976 values were based on emissions and production records. Post-1976 Southern Hemisphere atmospheric mixing ratios were based on ALE/GAGE/AGAGE and data from Cape Grimm, Tasmania in ppt on the SIO-2005 scale [9].

Air curves for SF<sub>6</sub> in the northern and southern hemispheres were compiled by Busenberg [9] based on published data primarily from NOAA sources. The Southern Hemisphere curve was adjusted for latitudinal effects to approximate that of the Congo and is slightly higher than marine air from Cape Grimm, Tasmania and other data from the South Pole.

The radiocarbon atmospheric input function for CO<sub>2</sub> was based on measurements from Wellington, New Zealand [10]. A fitting procedure was used to estimate values of δ<sup>14</sup>C post 1994 in the Southern Hemisphere.

### 4.2. Interpretation of the apparent age of water and the fractions of binary mixture

Fig. 2 and Fig. 3 show examples of the dating methodology used. Fig. 2 compares ppt values of CFC-113 to CFC-12. The heavy dashed line corresponds to the atmospheric input of CFC-113 relative to CFC-12 and dates are labelled at the plus signs. The light dashed line corresponds to dilution of modern (2008) water with old, CFC blank water. In Fig. 3, tracer plots utilizing δ<sup>14</sup>CO<sub>2</sub> in relation to CFCs

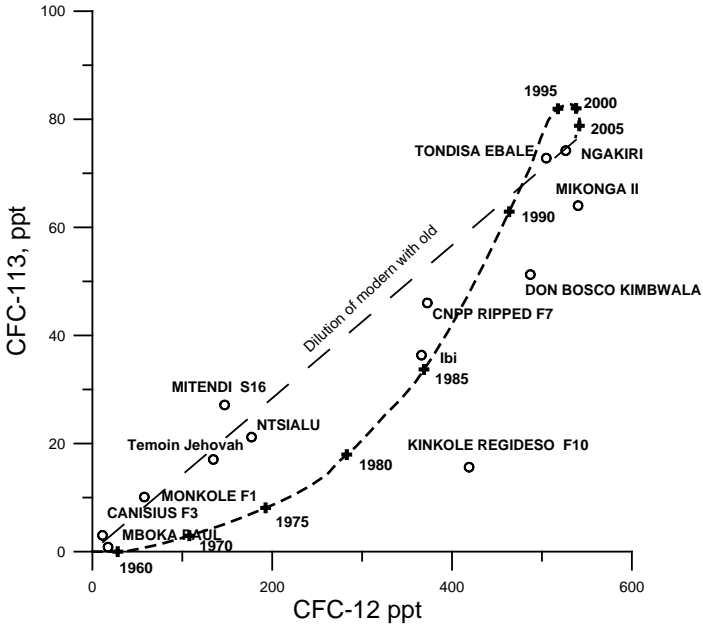


FIG. 2. Comparison of CFC-113 concentration (in ppt) relative to CFC-12.

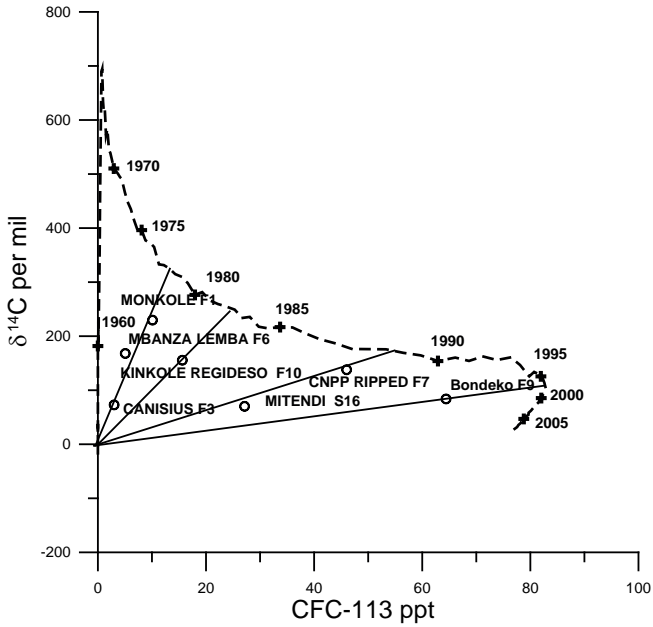


FIG. 3.  $\delta^{14}\text{CO}_2$  in the Southern Hemisphere in relation to CFC-113 concentration (in ppt). Hypothetical mixing lines are shown (solid lines).

TABLE 1. SUMMARY OF AGE INTERPRETATIONS

Sample code	date	CFC-11 apparent date	CFC-12 apparent date	CFC-113 apparent date	SF <sub>6</sub> apparent date	<sup>14</sup> C apparent date 1	<sup>14</sup> C apparent date 2	CFC- 113/ CFC12 date 1
OLE F1	24-Apr-08	1969	1965.5	1976.5	1979	1962	1983	np
CANISIUS F3	24-Apr-08	1964.5	1954	1970	1972.5	1958	2001.5	np
MBANZA LEMBA F6	30-Apr-08	np	np	1972.5	1976.5	1960	1989	1964
CNPP RIPPED F7	24-Apr-08	1985.5	1985	1987.5	1991.5	1959.5	1994	1989
DON BOSCO	25-Apr-08	1984	1991.5	1988	1999	nd	nd	1987
BONDEKO F9	30-Apr-08	np	np	1990	2004	1958.5	2000	1973
KINKOLE REGI F10	27-Apr-08	1977	1987.5	1979	1999.5	1959.5	1990	1974
CMSCJ	23-Apr-08	np	np	1987.5	1995	nd	nd	1968
TONDISA EBALE	23-Apr-08	1989	1993	1992	1992	nd	nd	1991
MIKONGA II	27-Apr-08	np	2001.5	1990	1998	nd	nd	1988
TEMOIN JEHOVAH	30-Apr-08	np	1972	1979.5	2000.25	nd	nd	1989
MBOKA PAUL	23-Apr-08	1959.5	1956.5	1965.5	1980	nd	nd	1977
MITENDI S16	23-Apr-08	1972	1972.5	1983	1983.25	1958	2002	np
MISSION	25-Apr-08	np	np	1979.5	nd	nd	nd	np
NTSIALU	23-Apr-08	1972.5	1974	1981	1991.75	nd	nd	1988
IBI	23-Apr-08	1976	1985	1985.5	1994	nd	nd	1986
NGAKIRI	27-Apr-08	1988	1996.5	1992	2008	nd	nd	1991

**Note:** % young CFC-113/SF<sub>6</sub> 1 not possible.

Green — Best estimate of groundwater recharge year and percentage of water of that age. In some cases a range of ages are possible, depending on the choice of tracers.

Yellow — Terrigenous SF<sub>6</sub>, cannot be dated using SF<sub>6</sub>.

nd— not determined.

np — not possible.

CFC-113/ CFC12 date 2	% young CFC- 113/ CFC12 date 1	% young CFC- 113/ CFC12 date 2	CFC- 113/SF <sub>6</sub> date 1	CFC- 113/SF <sub>6</sub> date 2	% young CFC-113/ SF <sub>6</sub> 2	<sup>14</sup> C/ CFC- 113 date	% young <sup>14</sup> C/113	<sup>14</sup> C/SF <sub>6</sub> date	% young <sup>14</sup> C/SF <sub>6</sub>
np	np	np	1971	2002	12.5	1978.5	73.0	1980.5	81.6
np	np	np	1968	>2008	4.0	1978.0	22.4	1982.5	29.2
np	np	np	1968	>2008	6.7	1976.5	46.0	1980.5	59.7
np	86.0	np	1972.5	1999.5	55.9	1989.0	81.5	1967.0	22.4
np	125.0	np	1968.5	2008	66.8				
np	np	np	1968.5	2008	83.9	1997.0	76.6	2001.5	113.7
np	np	np	1963.5	>2008	terrigenic	1982.5	62.4	1996.0	132.3
np	np	np	1970	2004	59.7				
2007	106.0	93.6	1987	1994	90.2				
np	127.6	np	1971	2002.5	79.6				
np	30.2	np	1963.5	>2008	terrigenic				
np	8.0	np	1962	>2008	1.1				
np	np	np	1978	1995.5	33.0	1990.0	45.6	1992.0	45.0
np	np	np							
np	42.2	np	1966	>2008	terrigenic				
np	94.4	np	1968.5	2007.5	47.2				
>2008	112.3	np	1968	>2008	97.6				

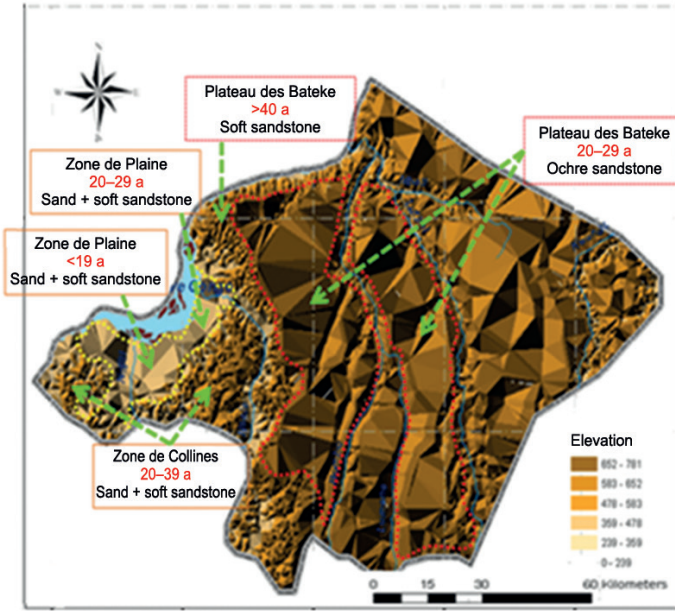


FIG. 4. Spatial distribution of apparent groundwater ages in Kinshasa.

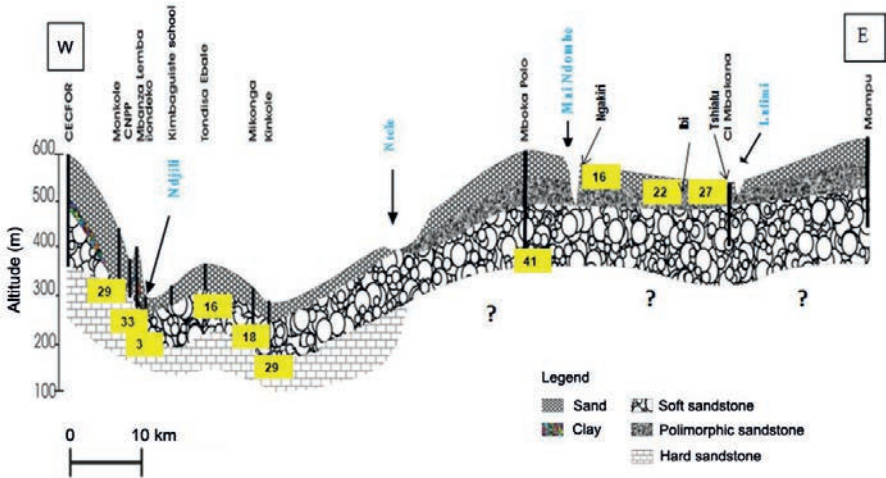


FIG. 5. Spatial distribution of groundwater ages as a function of geological facies in the study area.

to refine estimates of mixing and young fraction age, particularly for the samples with low fractions of young water.

Values expressing percentage of young water >100% are considered to be near 100%, within analytical uncertainties. Only one valid tracer measurement was obtained from the Mission sample, CFC-113. The apparent date of 1979.5 assumes an unmixed sample. Assuming mixing, the Mission sample contains less than 100% of water younger than 1979.5.

Table 1 summarizes currently available information on age estimation for the 17 samples collected in the Mount Amba aquifer. Only two age interpretation models were considered: the apparent tracer age of an unmixed sample, as if the sample were piston flow, and the binary dilution of a young fraction. In the latter case, the age of the young water fraction was based on the ratio of two atmospheric tracers and the percentage of the young fraction was computed choosing one of the two tracers used to calculate the ratio. In the binary dilution model, it is assumed that the old fraction is tracer free.

The comparison of each tracer to the evolution of a second tracer in the study zone shows that certain samples are not mixed: Mboka Paul (pre-1960); Ibi (1986) and CNPP (approximately recharged in 1987) and two other sites contain very recent water (Ngakiri and Tondisa Ebale). Other sites contain water which approaches the dilution line between modern water and old water (Mitendi, Ntsialu, Témoin of Jéhovah, Monkole and Canisius). Three sites which are likely to be dated with CFC-12 contain a light excess of it (Mikonga II, Don Bosco and Kinkole); the CFC-113 suggests for these sites the apparent dates of recharge 1991, 1988 and 1980 respectively, as long as they are not diluted by mixing with other waters. Apparent groundwater age varies from 3 to 41 a. Spatial variability of apparent age in the study area is shown in Figs 4 and 5.

In addition, it appears on the basis of analysis of this study,  $\delta^{14}\text{C}$  seems to give more relevant information than  $\text{SF}_6$  or CFC-113. Indeed, the nuclear pulse (after 1960s) still remains intact with a timescale of the Mount Amba aquifer (small decay for  $\delta^{14}\text{C}$ ) and the atmospheric concentration of  $\text{SF}_6$  is still increasing, while the CFC-113 contents appear less degraded than the other CFCs. This tracer constitutes a good tool for the development of the multi-tracer method with these three elements. It should be noted that the graph  $\delta^{14}\text{C}$  vs. CFC-113 has a broader scale in the lower part of the curve of the model piston, which allows an easy estimate of the ages and the mixtures.

## 5. CONCLUSION

In the Mount Amba aquifer, groundwater apparent age varies from 3 to 41 a and is directly correlated with the depth of boreholes, the static level position of the water table and the thickness of the aquifer. The oldest groundwater is found in the areas where soft sandstones crop out. Groundwater residence time varies between 20 and

39 a on the Hill zone of Kinshasa. On the Kinshasa plain, the residence time is generally lower than 19 a, except for the Kinkole area, located to the east of Kinshasa, which collects water from fractured sandstones. The residence time in this sector lies between 20 and 29 years. Groundwater age under the plateau of Bateke is higher than 40 years.

Groundwater renewal rate is a function of the transit time of infiltrating waters through the unsaturated zone and of the volume of the recharge. It varies from 30 to 100% in the Mount Amba aquifer, with an average rate of 64%. However, the plateau of Bateke shows a very low renewal rate (1% to 8%).

## REFERENCES

- [1] SZABO, Z., et al., Age dating of shallow groundwater with chlorofluorocarbons, tritium/helium-3, and flow path analysis, Southern New Jersey coastal plain, *Water Resour. Res.* **32** 4 (1996) 1023–1038.
- [2] PLUMMER, L.N., et al., Groundwater residence times in Shenandoah National Park, Blue Ridge Mountains, Virginia, USA: A multi-tracer approach. *Chem. Geol.* **179** (2001) 93–111.
- [3] PLUMMER, L.N., BÖHKLE, J.K., BUSENBERG, E., “Approaches for groundwater dating”, Residence Times and Nitrate Transport in Ground Water Discharging to Streams in the Chesapeake Bay Watershed (LINDSEY, B.D., et al.), *Water-Resources Investigations Report 03-4035*, U.S. Geological Survey, New Cumberland, Pennsylvania (2003) 12–24.
- [4] DUNKLE, S.A., et al., Chlorofluorocarbons (CCl<sub>3</sub>F and CCl<sub>2</sub>F<sub>2</sub>) as dating tools and hydrologic tracers in shallow groundwater of the Delmarva Peninsula, Atlantic Coastal Plain, United States, *Water Resour. Res.* **29** 12 (1993) 3837–3860.
- [5] NDEMBO LONGO, J., Apport des outils hydrogéochimiques et isotopiques à la gestion de l’aquifère du Mont Amba, Doctoral Thesis, Université d’Avignon, France (2009) 204 pp.
- [6] PLUMMER, L.N., BUSENBERG, E., “Chlorofluorocarbons”, *Environmental tracers in subsurface hydrology* (COOK, P.G., HERCZEG, A., Eds), Kluwer, Dordrecht, The Netherlands (2000) 441–478.
- [7] BUSENBERG, E., PLUMMER, L.N., Dating young groundwater with sulphur hexafluoride: Natural and anthropogenic sources of sulphur hexafluoride, *Water Resour. Res.* **36** 10 (2000) 3011–3030.
- [8] DONEY, S.C., GLOVER, D.M., JENKINS, W.J., A model function of the global bomb tritium distribution in precipitation, 1960–1986, *J. Geophys. Res.: Oceans* **97** C4 (1992) 5481–5492.
- [9] INTERNATIONAL ATOMIC ENERGY AGENCY, *Use of Chlorofluorocarbons in Hydrology: A Guidebook*, IAEA, Vienna (2006).
- [10] MANNING, M., MELHUIISH, W.H., “Atmospheric  $\delta^{14}\text{C}$  record for Wellington”, *Trends: A compilation of data on Global Changes*, The Carbon Dioxide Information Analysis Center, Oak Ridge National Laboratory, Oak Ridge, TN (1990).

# QUANTIFICATION OF SUBMARINE GROUNDWATER DISCHARGE IN SOUTHEASTERN BRAZIL USING NATURAL AND CONSERVATIVE TRACERS

T.A. SOUZA<sup>a</sup>, J.M. GODOY<sup>a,b</sup>, M.L.D.P. GODOY<sup>b</sup>, I. MOREIRA<sup>a</sup>,  
Z.L. CARVALHO<sup>b</sup>

<sup>a</sup> Departamento de Química,  
Pontifícia Universidade Católica, PUC–Rio,  
Rio de Janeiro, RJ, Brazil

<sup>b</sup> Instituto de Radioproteção e Dosimetria, IRD,  
Comissão Nacional de Energia Nuclear,  
Rio de Janeiro, RJ, Brazil

## Abstract

Growing evidence suggests that submarine groundwater discharge (SGD) is an important source of materials for the coastal ocean, including nutrients, particularly when originating from contaminated continental aquifers. The objective of this work is to consolidate the application of naturally occurring radium isotopes ( $^{223}\text{Ra}$ ,  $^{224}\text{Ra}$ ,  $^{226}\text{Ra}$  and  $^{228}\text{Ra}$ ) and other tracers (such as salinity,  $^{222}\text{Rn}$ ,  $^{18}\text{O}$ ,  $^2\text{H}$ , Ba, Si, U and nutrients) in the study of water mixing in coastal regions, including the SGD (Submarine Groundwater Discharge). About 120 seawater and groundwater samples were collected between the months of March and September 2009 in Arraial do Cabo, southeastern Brazil. Seawater samples (100–200 L) were obtained along offshore transects, as were groundwater samples (20 L) and both were filtered through columns packed with manganese-coated acrylic fibre.  $^{223}\text{Ra}$  and  $^{224}\text{Ra}$  activities were measured using a delayed coincidence counter system.  $^{226}\text{Ra}$  and  $^{228}\text{Ra}$  activities were determined by the technique of total alpha and beta counting.

## 1. INTRODUCTION

During the last few years, several studies assessing the significance of submarine groundwater discharge (SGD) in different environments have been conducted [1–4]. In such intertidal areas, tidal and wave oscillations can cause submarine groundwater discharge (SGD) by (a) producing pressure and height gradients between the land and seawater levels and (b) forcing seawater to flow through coastal permeable sediments [5].

SGD is particularly important to the coastal zone because a variety of chemical constituents (nutrients, metals, etc.) tend to be enriched in groundwater relative to

seawater [1, 4, 6–8]. These substances can be natural or anthropogenic (sewage, mining waste, etc.) and are eventually carried by the groundwater to surface waters [9].

The SGD fluxes usually present high spatial and temporal variability, a characteristic which has historically hindered their assessment [10]. The development of indirect techniques that allow an integrated measurement of this process in the water column has been very helpful. Among these methodologies, radium isotopes have been proven to be very useful to estimate submarine groundwater discharge fluxes [8, 11–13].

The method is based on the four naturally occurring radium isotopes ( $^{223}\text{Ra}$ ,  $^{224}\text{Ra}$ ,  $^{226}\text{Ra}$  and  $^{228}\text{Ra}$ ), the so called ‘radium quartet’ [4], which are enriched in SGD and behave conservatively once introduced to coastal regions. These isotopes belong to three different decay series ( $^{235}\text{U}$ ,  $^{232}\text{Th}$  and  $^{238}\text{U}$ ) and their range of half-lives ( $^{226}\text{Ra}$ : 1600 a;  $^{228}\text{Ra}$ : 5.75 a;  $^{223}\text{Ra}$ : 11.4 d and  $^{224}\text{Ra}$ : 3.66 d) allows the examination of processes that occur during mixing and transport.

## 2. STUDY LOCATION AND FIELD SAMPLING

### 2.1. Arraial do Cabo, southeastern Brazil

The city of Arraial do Cabo, located around 150 km distant of the city of Rio de Janeiro, has the form of a small peninsula and is surrounded by 30 kilometres of beaches.

In Arraial do Cabo, the northeast winds predominate all year [14]. These winds cause resurgence, a very important phenomenon that occurs in the region during the spring and summer. When blowing parallel to the coast, the northeast winds cause the warm water of the stream of Brazil to move away from the coast, allowing the upwelling of the cold and deeper waters of the South Atlantic (CWSA — Central Water of the South Atlantic, at 18°C). The deeper water is enriched with inorganic compounds that had not suffered photosynthesis owing to the absence of light in this layer. When arriving at the sea surface, these nutrients lead to an abundance of fish and in proportion to that they promote the development of the planktonic communities [15].

The upwelling of the cold waters is associated with other secondary factors such as the presence of the Serra do Mar close to the coast line, being the main factor controlling the climate of the region of Cabo Frio, differentiating it from the remaining portion of the southeastern Brazilian coast [16, 17].

Different from the predominantly humid tropical climate on the southeastern coast [17], the climate of Arraial do Cabo is considered hot semiarid by the Köppen classification, with five months of drought [18]. The annual precipitation increases by 823 mm in the region of Cabo Frio to a maximum of 3035 mm in the northwest portion of the Serra do Mar [16]. The majority of the climatic elements (temperature relative

humidity, evaporation and precipitation) of the region of Arraial do Cabo presents uniformity throughout the year and only the element insolation is more changeable.

The average temperature oscillates around 5°C between the summer (25.0°C to 25.3°C) and the winter (21.4°C to 21.5°C), with seasonal regularity in the temperature and is the lowest in the state due to the constant winds [19]. The relative humidity of the air is about 80% during the year. The distribution of the rains is irregular, but they normally occur in the spring and the summer [14].

## 2.2. Sampling Campaigns

In this work, 118 seawater and groundwater samples were collected during six sampling campaigns between the months of March and September 2009 in the region of Arraial do Cabo. At a sampling depth of one metre, high volume (100–200 L) seawater samples were obtained along offshore transects and groundwater samples (20 L) were also collected in kiosks located in the shoreline and stored in plastic tanks.

The water was pumped at flow rates of <1.0 L/min through two sequential columns, one containing pure acrylic fibre and the other containing MnO<sub>2</sub> coated acrylic fibre, to remove particulate and to quantitatively adsorb Ra [20]. Samples for nutrient analyses were collected in polyethylene amber bottles of 500 mL and congealed. Sub-samples for barium, silicon, uranium and salinity were collected in Falcon tubes of 50 mL and kept cooled at 4°C until the analyses. Salinity was



FIG. 1. Geographic map showing the sampling points in the Arraial do Cabo region.

measured in the field using portable meters allowing temperature compensation and calibration with appropriate standards.

### 3. METHODOLOGY

#### 3.1. Radium isotopes

Each Mn fibre sample containing radium was partially dried (~50% water) and connected to a RaDeCC system (Scientific Instruments). Helium was circulated through the manganese fibre to remove  $^{219}\text{Rn}$  and  $^{220}\text{Rn}$  generated by the decay of  $^{223}\text{Ra}$  and  $^{224}\text{Ra}$ . Both isotopes passed through a scintillation cell, where the alpha particles emitted from the Rn and from its daughter products were detected by a photomultiplier tube (PMT) coupled to the cell. The pulses generated in the PMT were then directed to a delayed coincidence system proposed by Ref. [21] and adapted for the measurements of radium by Ref. [22].

The delayed coincidence counting system (RaDeCC) uses the difference between the decay constants of isotopes of short half-life Po, daughter of  $^{219}\text{Rn}$  and  $^{220}\text{Rn}$ , for the identification of deriving particles alpha of the decay of  $^{219}\text{Rn}$  and  $^{220}\text{Rn}$  and thus determines the activities of the restrained  $^{223}\text{Ra}$  and  $^{224}\text{Ra}$  in the manganese fibre.

The samples were measured shortly after sampling, for a second time about of two weeks afterwards and a third time one month later. The first measurement was used to calculate the  $^{224}\text{Ra}$  concentration, the second measurement to calculate the  $^{223}\text{Ra}$  concentration and the last measurement to calculate  $^{228}\text{Th}$ . The activity of  $^{228}\text{Th}$  is needed for the necessary corrections of the results regarding supported  $^{224}\text{Ra}$ .

After these determinations, the manganese fibres were leached with concentrated HCl and hydroxylamine hydrochloride, so that the long half-life radium isotopes could be quantitatively removed. Radium was co-precipitated with  $\text{BaSO}_4$  and the alpha count of  $^{226}\text{Ra}$  was measured using a spectrometer of total alpha and beta counting (Berthold, model LB 770). After approximately 21 days of precipitation, necessary so that the balance of Ra-Rn was reached, as well as for  $^{224}\text{Ra}$  and  $^{223}\text{Ra}$  to decay, as described by Ref. [23],  $^{228}\text{Ra}$  was determined by beta counting of the same precipitate, covering the system with a filter paper of equal diameter, to blind the detector to alpha particles from  $^{226}\text{Ra}$  and to count the beta particles of the isotope of interest.

#### 3.2. Silicon, barium, uranium, salinity and nutrients

The silicon and barium concentrations in the seawater and groundwater samples were determined by Inductively Coupled Plasma-Optical Emission Spectroscopy

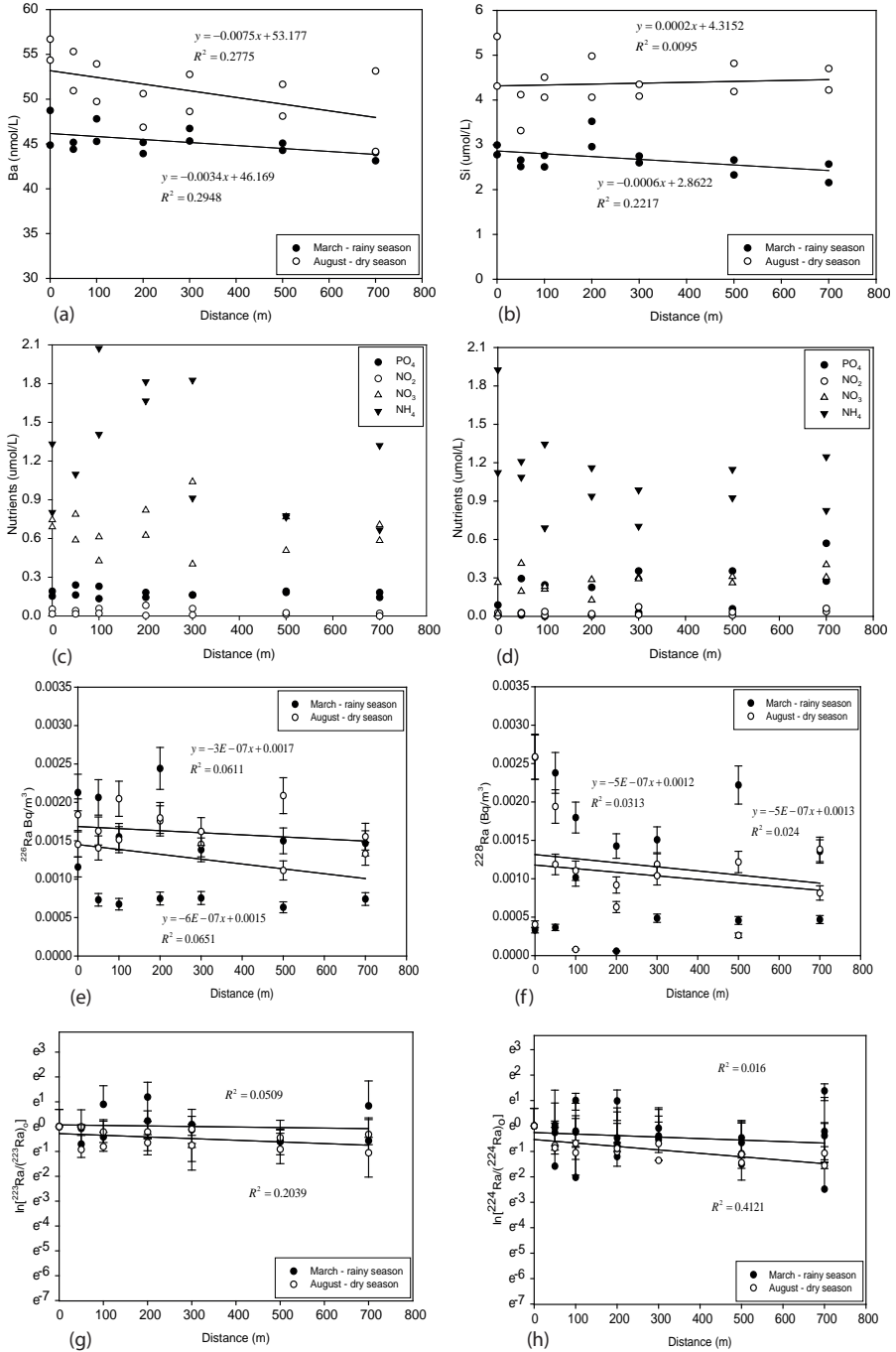


FIG. 2. Tracer (Ba, Si, nutrients, <sup>223</sup>Ra, <sup>224</sup>Ra, <sup>226</sup>Ra, <sup>228</sup>Ra and U) concentration distributions in dry and rainy seasons against distance offshore in the Arraial do Cabo region.

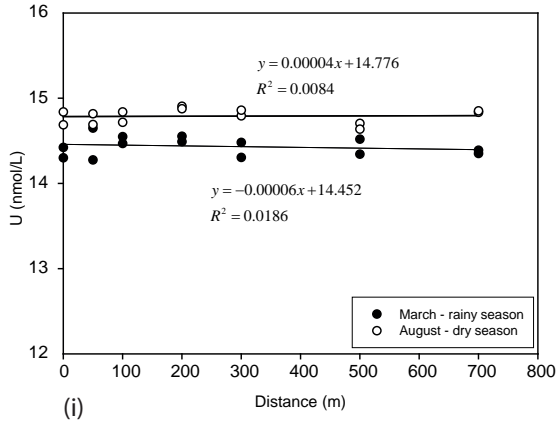


FIG. 2. (cont.) Tracers (Ba, Si, nutrients,  $^{223}\text{Ra}$ ,  $^{224}\text{Ra}$ ,  $^{226}\text{Ra}$ ,  $^{228}\text{Ra}$  and U) concentrations distributions in dry and rainy seasons against the distance offshore in the Arraial do Cabo region.

(ICP-OES Perkin Elmer, model: Optima 4300 DV) using direct analysis without dilution and scandium as an internal standard.

The uranium concentrations in the seawater and groundwater samples were determined by inductively coupled plasma mass spectrometry (ICP-MS Varian, model: 820 MS) after dilution 1:100 and applying Tl as an internal standard.

The salinity of the samples was measured using a pH/conductivity pocket meter (WTH, model: pH/Cond 340i) calibrated with a solution of KCl (35 g/kg). All salinity measurements were performed at 25 °C.

The congealed samples kept were used for the determination of the nutrient concentrations (phosphate, nitrate, nitrite and ammonium), according to the methodology described in Ref. [24].

#### 4. RESULTS AND DISCUSSION

Among the samples collected in six sampling campaigns between March and September 2009, consisting of two transects each, results obtained during the months of March and August were selected, since these months were the most representative of the rainy and dry seasons respectively. Concentration distributions of Ba, Si, nutrients,  $^{223}\text{Ra}$ ,  $^{224}\text{Ra}$ ,  $^{226}\text{Ra}$ ,  $^{228}\text{Ra}$  and U in relation to the distance offshore at the Arraial do Cabo area are presented in Fig. 2.

Graphs (2a) and (2b) present the barium and silicon concentrations as a function of the distance offshore. The results of analysis of these tracers indicate an inverse correlation. The barium concentrations become closer the greater the distance offshore and for the silicon, the observed behaviour indicates that the trend of the

results becomes more distinct for each season. In graphs (2c) and (2d) the results obtained from the analysis of nutrients (phosphate, nitrate, nitrite and ammonia) are presented separately in order to better observe changes in concentrations in relation to distance in both seasons. It was observed that the  $^{226}\text{Ra}$  and  $^{228}\text{Ra}$  activities presented in graphs (2e) and (2f) did not vary significantly with distance offshore, resulting in extremely low correlation coefficients.

## 5. CONCLUSIONS

According to the results, it was possible to verify that the long life radium isotopes activities did not vary between the different seasons considered. Verifying the data obtained from the half-life radium isotopes activities ( $^{223}\text{Ra}$  and  $^{224}\text{Ra}$ ) in relation to the distance offshore, according showed in graphs (2g) and (2h), it was possible to observe that the correlation coefficients were low. There was no significant variation between the results of the dry and rainy seasons. In graph (2i) it could be observed that for the seasons investigated, uranium concentrations showed no significant variations with distance offshore.

## ACKNOWLEDGEMENTS

The authors thank IEAPM (Instituto de Estudos do Mar Almirante Paulo Moreira) for support during the field work and nutrient analysis, the IRD/CNEN for the logistical support needed for the accomplishment of the analysis, Maurício Dupim and André Vechi (Departamento de Química, PUC-Rio) for the silicon and barium determinations by ICP-OES. This project was also partially supported by the CNPq, through the INCT 'Transferência de matéria continente-oceano'.

## REFERENCES

- [1] CHARETTE, M.A., et al., Utility of radium isotopes for evaluation the input and transport of groundwater-derived nitrogen to a Cape Cod estuary, *Limnol. Oceanogr.* **46** 2 (2001) 465–470.
- [2] HWANG, D.-W., et al., Estimating submarine inputs of groundwater and nutrients to a coastal bay using radium isotopes, *Marine Chemistry* **96** (2005) 61–71.
- [3] MOORE, W.S., Sources and fluxes of submarine groundwater discharge delineated by radium isotopes, *Biogeochemistry* **66** (2003) 75–93.
- [4] RAMA, MOORE, W.S., Using the radium quartet for evaluating groundwater input and water exchange in salt marshes, *Geochim. Cosmochim. Acta* **60** 23 (1996) 4645–4652.

- [5] CHARETTE, M.A., et al., “Uranium- and thorium-series nuclides as tracers of sub- marine groundwater discharge”, U–Th Series Nuclides in Aquatic Systems (KRISHNASWAMI, S., COCHRAN, J.K., Eds), Elsevier, Oxford (2008) 155–192.
- [6] KREST, J.M., et al.,  $^{226}\text{Ra}$  and  $^{228}\text{Ra}$  in the mixing zones of Mississippi and Atchafalaya Rivers: Indicators of groundwater input, *Marine Chemistry* **64** (1999) 129–152.
- [7] KREST, J.M., et al., Marsh nutrient export supplied by groundwater discharge: Evidence from radium measurements, *Global Biogeochem. Cycles* **14** 1 (2000) 167–176.
- [8] MOORE, W.S., Large groundwater inputs to coastal waters revealed by  $^{226}\text{Ra}$  enrichments, *Nature* **380** (1996) 612–614.
- [9] BURNETT, W.C., et al., Groundwater and pore water inputs to the coastal zone, *Biogeochemistry* **66** (2003) 3–33.
- [10] BURNETT, W.C., et al., Measurement and significance of the direct discharge of groundwater into the coastal zone, *J. Sea Res.* **46** (2001) 109–116.
- [11] BECK, A.J., et al., Importance of geochemical transformations in determining submarine groundwater discharge-derived trace metal and nutrient fluxes, *Appl. Geochem.* **22** (2007) 477–490.
- [12] BURNETT, W.C., et al., Radon and radium isotopes as tracers of submarine groundwater discharge — Results from the Ubatuba, Brazil SGD assessment intercomparison, *Est. Coast. Shelf Sci.* **76** (2008) 501–511.
- [13] SWARZENSKI, P.W., et al., Ra and Rn isotopes as natural tracers of submarine groundwater discharge in Tampa Bay, Florida, *Marine Chemistry* **104** (2007) 69–84.
- [14] BARBIÉRE, E.B., Ritmo climático e extração do sal em Cabo Frio, *Rev. Bras. Geografia* **37** 4 (1975) 23–109.
- [15] DA SILVA, G.L., et al., “Estudo preliminar da climatologia da ressurgência na região de Arraial do Cabo, RJ”, XIV Congresso Brasileiro de Meteorologia, Florianópolis (2006).
- [16] BARBIERI, E., COELHO-NETO, R.C., “Spatial and temporal variation of rainfall of the east Fluminense coast and Atlantic Serra do Mar, State of Rio de Janeiro, Brazil”, *Environmental Geochemistry of Coastal Lagoon Systems of Rio de Janeiro, Brazil* (KNOPPERS, B.A., et al., Eds), UFF, Niterói (1999) 47–56.
- [17] TURCQ, B., et al., “Origin and evolution of the quaternary coastal plain between Guaratiba and Cabo Frio, State of Rio de Janeiro, Brazil”, *Environmental Geochemistry of Coastal Lagoon Systems of Rio de Janeiro, Brazil* (KNOPPERS, B.A., et al., Eds), UFF, Niterói (1999) 25–46.
- [18] DUARTE, A.C., Condições morfoclimáticas e vegetação do ambiente estépico da região de Cabo Frio, RJ, Brasil: Avaliação atual para uma perspectiva de preservação, Masters Dissertation, Universidade Federal Fluminense, Niterói, Rio de Janeiro (1998).
- [19] SECRETARIA DE PLANEJAMENTO E URBANISMO, Prefeitura Municipal de Armação dos Búzios, Plano diretor de desenvolvimento sustentável, Armação dos Búzios, RJ, Perfil do Município, Armação dos Búzios, Secretaria de Planejamento e Urbanismo (2003).

- [20] MOORE, W.S., Sampling  $^{228}\text{Ra}$  in the deep ocean, *Deep-Sea Research* **23** (1976) 647–651.
- [21] GIFFIN, C., et al., Delayed coincidence counter for the assay of actinon and thoron, *J. Geophys. Res.* **68** 6 (1963) 1749–1757.
- [22] MOORE, W.S., ARNOLD, R., Measurement of  $^{223}\text{Ra}$  and  $^{224}\text{Ra}$  in coastal waters using a delayed coincidence counter, *J. Geophys. Res.* **101** C1 (1996) 1321–1329.
- [23] GODOY, J.M., et al., Development of a sequential method for the determination of  $^{238}\text{U}$ ,  $^{234}\text{U}$ ,  $^{232}\text{Th}$ ,  $^{230}\text{Th}$ ,  $^{228}\text{Th}$ ,  $^{228}\text{Ra}$ ,  $^{226}\text{Ra}$ , and  $^{210}\text{Pb}$  in environmental samples, *J. Radioanal. Nucl. Chem.* **182** 1 (1994) 165–169.
- [24] STRICKLAND, J.D.H., PARSONS, T.R., *A Practical Handbook of Seawater Analysis* (Bulletin 167), Fisheries Research Board of Canada, Ottawa (1972).



# GEOSTATISTICAL ANALYSIS OF SPATIAL ISOTOPE ( $\delta^{18}\text{O}$ , $\delta^2\text{H}$ AND $^3\text{H}$ ) VARIABILITY OF GROUNDWATER ACROSS MOROCCO

H. MARAH <sup>a</sup>, N. ZINE <sup>b</sup>, M. QURTOBI <sup>a</sup>, B. OUDA <sup>a</sup>, F. TAOUS <sup>a</sup>, F. RAIBI <sup>a</sup>

<sup>a</sup> Water and Climate Unit,  
National Centre for Nuclear Energy,  
Sciences and Technology – CNESTEN,  
Rabat, Morocco

<sup>b</sup> Secretariat of State for Water and Environment  
at the Ministry of Energy, Mines,  
Water and the Environment,  
Rabat, Morocco

## Abstract

Environmental isotopes are increasingly being used for a variety of applications in the fields of the Earth's water cycle and climate change. This paper reports the first national level survey of  $\delta^{18}\text{O}$ ,  $\delta^2\text{H}$ ,  $^3\text{H}$  and  $^{14}\text{C}$  in groundwater across Morocco, including the analysis of the spatial distribution of stable ( $\delta^{18}\text{O}$  and  $\delta^2\text{H}$ ) and radioactive (tritium and carbon-14) isotopes used to assess eleven groundwater basins distributed across Morocco. The interpolations were carried out using ESRI ArcGIS 9.2 with spatial analyst extension. The methods used are ordinary kriging inverse distance weighting (IDW). The maps showing the spatial variability of tritium and radiocarbon in the basins are used to visualize the presence of modern and old groundwater, while the stable isotope maps show that the age of groundwater, the type (shallow or deep groundwater), the distance of the basin from the sea (Atlantic and Mediterranean) and the altitude are the main factors influencing the isotopic composition of groundwater. Those thematic maps will provide a valuable contribution for sustainable groundwater management of resources for drinking water supplies, agriculture and industry, which is a prime concern in countries dominated by arid and semiarid climates such as Morocco.

## 1. INTRODUCTION

Morocco is primarily characterized by semiarid to arid climate conditions, excluding a humid zone in the north. This difficult situation requires the application of new technologies to supplement conventional hydrological methods in order to improve water resources assessment and management in Morocco. Of these technologies, we used hydrochemistry and environmental isotopes as natural tracers of

water and its dissolved components. In this work we report the first national-level survey of  $\delta^{18}\text{O}$ ,  $\delta^2\text{H}$  and  $^3\text{H}$  in groundwater across Morocco [1]. The major objectives are of this study are:

- Compilation of existing hydrogeochemical data across Morocco into a national isotope database;
- Provision of short syntheses describing key findings and conclusions of previous groundwater studies in a number of certain aquifer units in Morocco, based on isotope results;
- Development of isotope maps using geostatistical methods and GIS tools to visualize the spatial variability of groundwater isotopes across Morocco;
- Contribution of a valuable resource for national and international scientific and practical applications involving the water cycle, climatology and ecology.

## 2. METHODS

### 2.1. Sampling network

Over 1200 water samples were collected from surface water, groundwater, springs and precipitation from 11 basins and 8 meteorological stations distributed across Morocco and analysed for their chemical and isotopic contents. Temperature, pH, conductivity and total alkalinity were measured in the field. Chemical analyses of major elements and isotope analyses for  $^3\text{H}$ ,  $\delta^{18}\text{O}$  and  $\delta^2\text{H}$  were measured at the Water and Climate Unit, CNESTEN. Fig. 1 shows the location of water points sampled for isotope analysis. Precipitation samples for isotope analyses have been systematically collected in 8 meteorological stations as part of studies conducted. Fig. 2 shows the geographical distribution of isotope rainfall stations.

### 2.2. Analytical methods

- The  $\delta^{18}\text{O}$  and  $\delta^2\text{H}$  values are reported in per mille units (‰) relative to VSMOW. Samples were analysed using a double inlet mass spectrometer. Precision at the CNESTEN laboratory is better than  $\pm 0.1\text{‰}$  and  $\pm 1.5\text{‰}$  for  $\delta^{18}\text{O}$  and  $\delta^2\text{H}$ , respectively.
- Tritium concentration is expressed in tritium units (TU). Tritium content is measured by counting its radioactive decay, using liquid scintillation spectrometers and electrolytic enrichment. The analytical uncertainty in the CNESTEN laboratory is  $\pm 0.3$  TU for tritium levels lower than 5 TU.

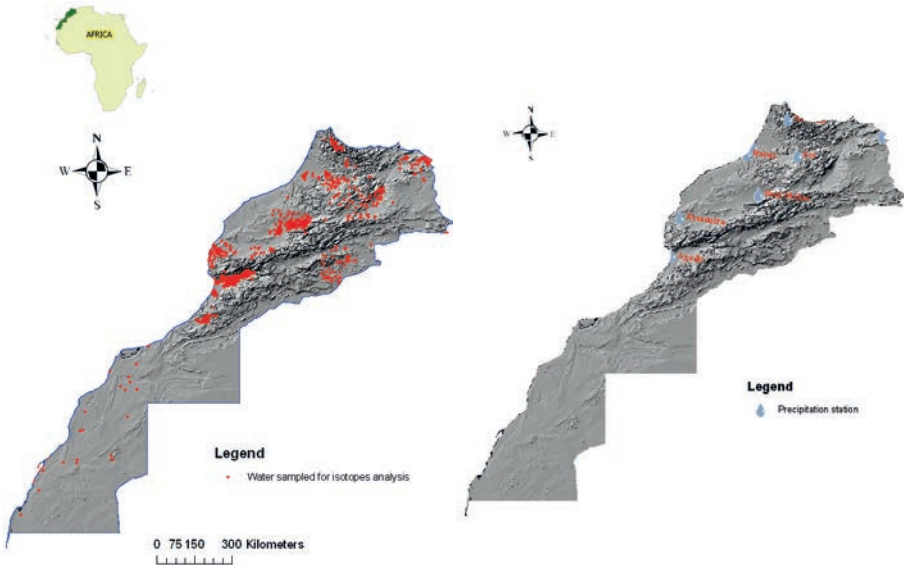


FIG. 1. Location of sampling sites for isotope analysis.

FIG. 2. Geographical distribution of isotope rainfall stations.

### 3. RESULTS

#### 3.1. Geostatistical analysis of spatial isotope ( $\delta^{18}\text{O}$ , $\delta^2\text{H}$ ) variability

The scatter plot in Fig. 3a shows the  $\delta^2\text{H}$  vs.  $\delta^{18}\text{O}$  relationship for different water types (springs, borehole and dug wells). The Global Meteoric Water line  $\delta^2\text{H} = 8 \delta^{18}\text{O} + 10$  and a characterization of the average global precipitation has also been included [2]. Figs 3b and 3c present frequency distribution diagrams for the individual isotope ratios and the mean values for each isotope ratio for the entire data set. The range of stable isotope ratios of these samples spans from  $-0.37$  to  $-10.21\text{‰}$  for  $\delta^{18}\text{O}$  and  $-4.75$  to  $-71.60\text{‰}$  for  $\delta^2\text{H}$ . Average values for the samples are  $-41.30\text{‰}$  for  $\delta^2\text{H}$  and  $-6.54\text{‰}$  for  $\delta^{18}\text{O}$ . The groundwater data clusters near the Global Meteoric Water Line characterizing average global precipitation, but most samples are above this line owing to two main sources of atmospheric moisture (Atlantic and Mediterranean). Deuterium excess ( $\delta = \delta^2\text{H} - 8\delta^{18}\text{O}$ ) values for the sample set range from  $0.1$  to  $31.9\text{‰}$ , with an average value of  $11.27\text{‰}$ .

Figs 4–7 show the spatial variability of  $\delta^{18}\text{O}$  and  $\delta^2\text{H}$  across Morocco, respectively. Figs 8a and 8b show the spatial variability of  $\delta^{18}\text{O}$  in precipitation across Morocco as well as the Local Meteoric Water line. The interpolation in Fig. 8a was conducted using ESRI ArcGIS 9.2 with the spatial analyst extension. An ordinary

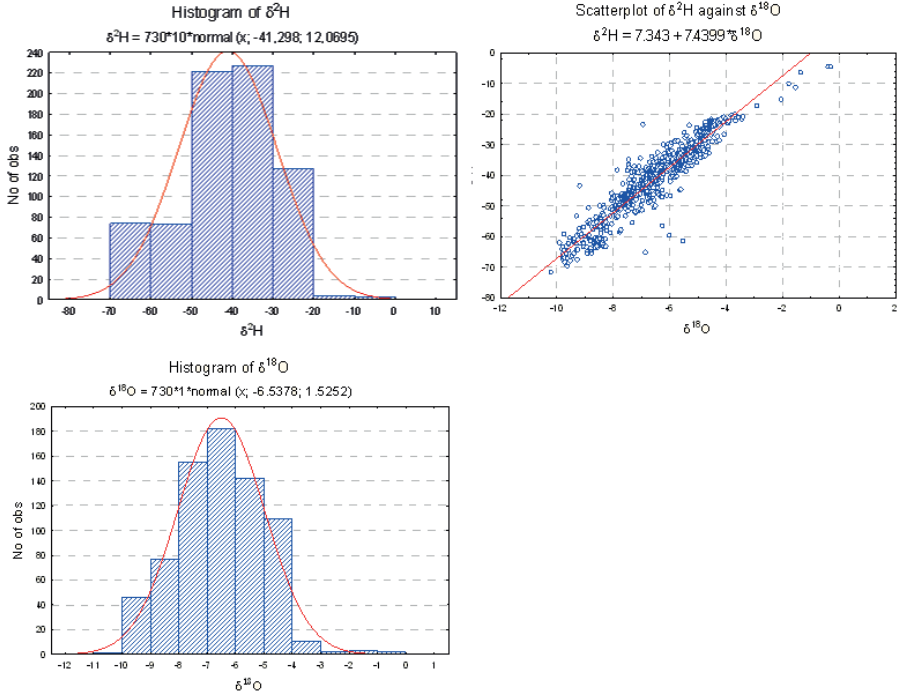


FIG. 3. Deuterium versus oxygen-18 for all samples analysed across Morocco.

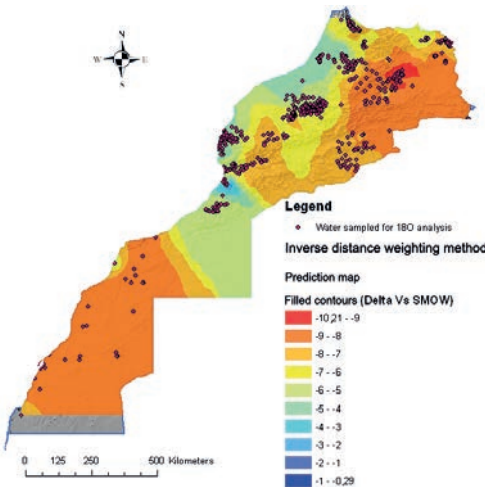


FIG. 4. Spatial variability of  $\delta^{18}\text{O}$  in groundwater across Morocco.

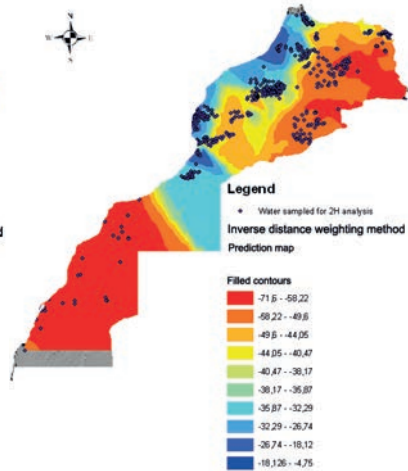


FIG. 5. Spatial variability of  $\delta^2\text{H}$  in groundwater across Morocco.

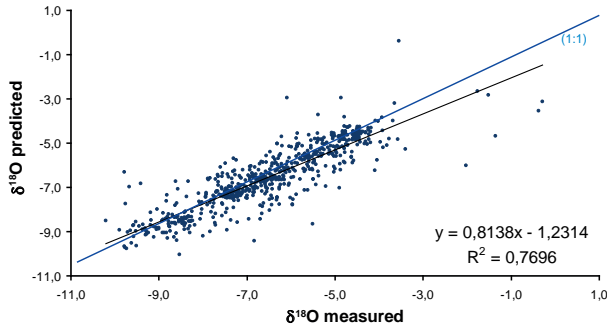


FIG. 6. Interpolation error for  $\delta^{18}\text{O}$  map.

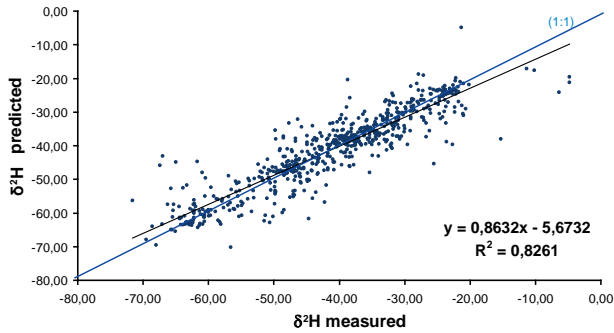


FIG. 7. Interpolation error for  $\delta^2\text{H}$  map of Morocco.

inverse distance weighting (IDW) was employed [3]. IDW interpolation explicitly implements the assumption that the elements that are close to each other are likely to be more similar than those that are farther apart. To predict a value for any unmeasured location, IDW will use the measured values surrounding the prediction location [4]. Those measured values closest to the prediction location will have more influence on the predicted value than those located farther away.

There appears to be a trend of lighter isotope values from west to east (Figs 4 and 5) due to the continental and altitude isotope effect, but in the south and east most groundwaters show a  $\delta^{18}\text{O}$  content of about  $-8$  to  $-10\%$ , suggesting a palaeoclimatic effect.

Figs 6 and 7 show the uncertainty of the predicted maps of Fig. 4 and 5. The blue regression function should fall close to the 1:1 line. This tendency can be found for  $\delta^2\text{H}$  and  $\delta^{18}\text{O}$  values of water samples. Visual inspection suggests that the deviation from the 1:1 relation between measured and modelled values is similar for both elements ( $R^2=0.77$  for  $\delta^{18}\text{O}$  and  $R^2=0.83$  for  $\delta^2\text{H}$ ).

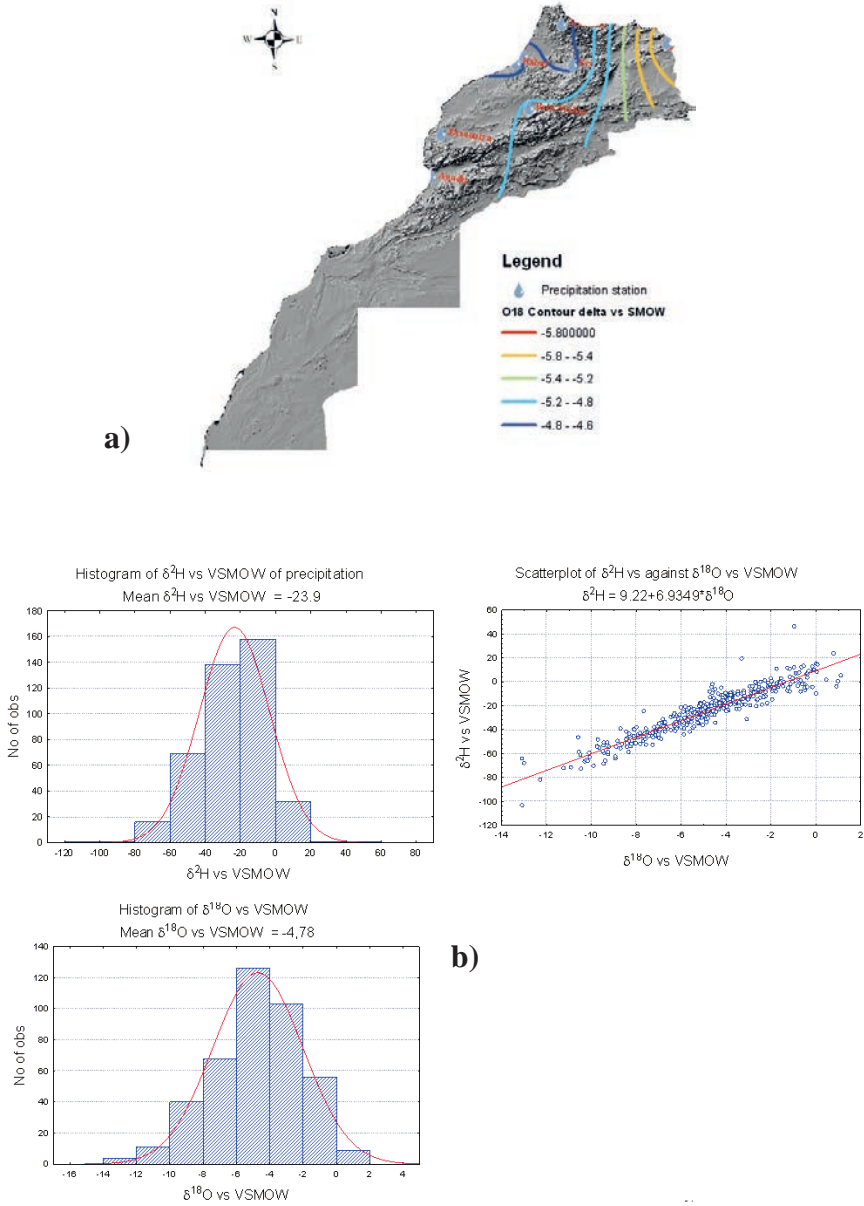


FIG. 8. (a) Spatial variability of  $\delta^{18}\text{O}$  in precipitation across the north of Morocco; (b) Deuterium versus oxygen-18 in precipitation (LMWL).

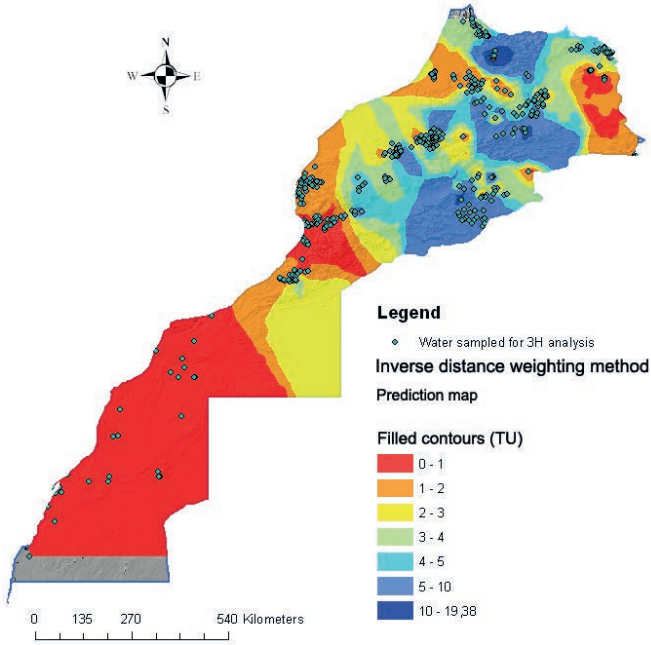


FIG. 9. Spatial variability of  $^3\text{H}$  in groundwaters across Morocco based on studies conducted in recent years.

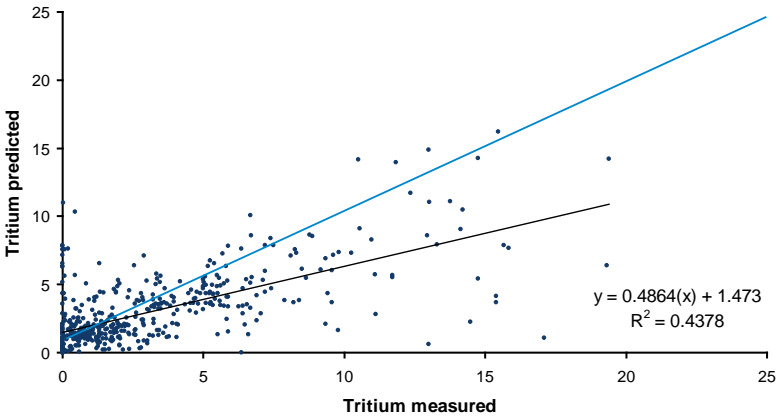


FIG. 10. Interpolation error for  $^3\text{H}$  map.

### 3.2. Geostatistical analysis of spatial isotope ( $^3\text{H}$ ) variability

Fig. 9 shows the spatial variability of tritium in groundwater across Morocco. Interpolation was conducted using ESRI ArcGIS 9.2 with the spatial analyst extension and ordinary IDW was also employed. The lowest tritium contents are found throughout the south of Morocco, indicating that old groundwater dominates in the area. The highest  $^3\text{H}$  values occur throughout the north, north east and northwest of Morocco, indicating modern recharge and the mixing of recent and old waters. The interpolation error graph (Fig. 10) shows the measured vs. the predicted values, in which can be seen a tendency for tritium values to be higher than predicted values. Visual inspection suggests that additional isotope data is required for mapping.

## 4. CONCLUSIONS

Ordinary kriging and inverse distance weighting methods have been use to map the isotope variability of groundwater across Morocco. The elaborated map using tritium and carbon-14 data in different hydrological settings provided excellent results to visualise areas of present day recharge and location of palaeowaters. The stable data of springs was used to visualise areas under the influence of different air masses contributing to the recharge of groundwater.

## REFERENCES

- [1] INTERNATIONAL ATOMIC ENERGY AGENCY, Atlas of Isotope Hydrology: Morocco, IAEA, Vienna (2010).
- [2] UNITED NATIONS EDUCATIONAL, SCIENTIFIC AND CULTURAL ORGANIZATION, INTERNATIONAL ATOMIC ENERGY AGENCY, Environmental Isotopes in the Hydrological Cycle: Principles and Applications, UNESCO, Paris (2000).
- [3] WEBSTER, R., OLIVER, M.A., Geostatistics for Environmental Scientists, 2nd edn, John Wiley & Sons, Chichester, UK (2007).
- [4] MARAHA, H., et al., "Improving understanding of hydrogeology in Morocco's Tadla Basin", Water and Environmental News **27** (2010) 9–11.

# USING ISOTOPE TECHNIQUES $^{34}\text{S}/^{32}\text{S}$ ( $\delta^{34}\text{S}$ ) TO DETERMINE THE ORIGIN OF DISSOLVED SULPHATE IN THUAN MY MINERAL WATER

VO THI TUONG HANH

Isotope Hydrology Laboratory,  
Institute for Nuclear Science and Technology,  
Hanoi, Vietnam

## Abstract

The application of the sulphur isotope ( $\delta^{34}\text{S}$ ) values of dissolved sulphate in groundwater provided the information necessary to evaluate the source of sulphate in the Thuan My mineral water. The  $\delta^{34}\text{S}$  of dissolved sulphate in water samples of the 33 wells (the depth from 30 m to 80 m), the river Da in the study area, the Hoa Binh Lake (upstream of the Da river), the Red River (downstream of the Da River) and the precipitation collected during both rainy and dry seasons in the Thuan My, Ha Noi and Lang Son was analysed. The concentrations of dissolved sulphate ( $\text{SO}_4^{2-}$ ) in these wells range from 674 to 2197 mg/L and the  $\delta^{34}\text{S}$  values in the wells are in a narrow range from +15.7 to +17.7‰. These values along with the chemical composition of water in this area allows one to explain the source of  $\text{SO}_4^{2-}$  in water from these wells as the dissolution of gypsum mineral ( $\text{CaSO}_4 \cdot 2\text{H}_2\text{O}$ ).

## 1. INTRODUCTION

The origin and the fate of sulphate in groundwater have concerned hydrogeologists for many decades. With increasing industrialization throughout this century, the differentiation between natural and manufactured sulphate became important. A particular challenge is the evaluation of potential and existing additions of the latter to groundwater and drinking water supplies. A research program on the effects of atmospheric sulphate deposition on terrestrial and aquatic ecosystems was initiated. For the delineation of various sources of groundwater sulphate, the application of stable isotope techniques has proven the most useful.

In the north of Vietnam, there are many mineral waters, some of them are mineral waters with high sulphate concentration and temperature and some of them are mineral waters with high sulphide concentration and temperature. Many mineral waters are on the market with brand names such as Vinh Hao, My Lam, Vital, etc. But the origin of sulphate in these waters is not well explained by the classical techniques. In order to explain the origin of sulphate in Thuan My mineral water, hydrochemical and sulphur isotope studies have been carried out in the area.

Most of the mineral waters in the North of Vietnam come from discontinuity planes and mineral water is contained in the deep layers and upwells along the fault as mineral waters.

The discontinuity presents in the Thuan My area with a length of 750 m and a width of 20 m. A mineral water as a hot spring is created from this discontinuity in a mushroom shape. The chemical composition of this mineral water at a high temperature is Ca-SO<sub>4</sub> while other fresh water around the Thuan My area is HCO<sub>3</sub>-Na-K-Ca at normal temperature.

The isotope composition of sulphate dissolved in water has many applications in the study of the chemistry and evolution of hydrologic systems and groundwater pollutions. Some of the most important applications include (1) determining the source of dissolved sulphur species, including natural sources such as gypsum or pyrite in rocks and anthropogenic sources such as fertilizer and acid rain, (2) understanding chemical reaction occurring in groundwater systems, such as the oxidation of sulphide or the microbial reduction of sulphate.

Sulphur has four stable isotopes: <sup>32</sup>S, <sup>33</sup>S, <sup>34</sup>S and <sup>36</sup>S with approximate abundances of 95.02%, 0.75%, 4.21% and 0.02% respectively. The ratio of <sup>34</sup>S to <sup>32</sup>S is most commonly measured. Stable isotopic ratios of unknowns are reported in parts per thousand (per mille, also ‰) relative to a standard, according to the following equation:

$$\delta = \frac{R_s - R_{Std}}{R_{Std}} 1000 (\text{‰})$$

where  $R_s$  is <sup>34</sup>S/<sup>32</sup>S of unknown samples and  $R_{Std}$  is <sup>34</sup>S/<sup>32</sup>S of standard.

## 2. STUDY AREA

A hot mineral water spring is located in Thuan My village, Ba Vi, 70 km north-west of Hanoi capital. The study area extends over 1.5 km<sup>2</sup> in area and lies between the dyke and the Da river. Hoa Binh Dam Lake is upstream of the Da river and the Red river is downstream. Land use is dominated by non-irrigated crops, such as corn and sweet potato. The hot mineral water spring was discovered 10 years ago by UNESCO with the dissolved SO<sub>4</sub><sup>2-</sup> concentration in water of the wells (deeper than 30 m) from 674 to 2197 mg/L and the temperature of water in these wells is also high at up to 45 °C. The villagers in this area have been using this mineral water with its high concentration of dissolved SO<sub>4</sub><sup>2-</sup> and high temperature as a spa as well as for physical therapy. There are currently more than 40 families who have exploited this water for spa purposes.

### 3. FIELD METHODS

Groundwater samples of Thuan My mineral water (deeper than 30m) were collected during two seasons in 2009 — dry, in March, and rainy, in September — from small family wells by small pumps. All wells were drilled for physical therapy. The deepest well (Trung Toan) is 80 m deep and has the highest temperature of 43°C, while the shallowest well is 38 m deep with a temperature of 36°C. The temperature of surface water is around 26–27°C. Temperature, pH, Eh, EC and total dissolved solids (TDS) were constantly monitored during pumping and a sample was collected after the reading stabilized. Alkalinity was measured immediately after sampling by titration with 0.1 N HCl to an end point between pH 4.5 and 5.1, depending on the amount of alkalinity present. The samples for major ion analysis were filtered through a 0.45 µm membrane, while the samples for cation analysis were acidified with ultra-pure HNO<sub>3</sub> and returned to the laboratory. Samples for laboratory chemical and isotopic analyses were stored in high density polyethylene bottles. All the samples were tested for the presence of sulphide (H<sub>2</sub>S, HS<sup>-</sup> and S<sup>2-</sup>) using a Hach field kit. In addition, samples from the Da River in the study area, the Hoa Binh Dam Lake, the Red River and precipitation were also collected during both the rainy and dry seasons in the Thuan My, Hanoi and Lang Son regions.

### 4. LABORATORY METHOD

The anions SO<sub>4</sub><sup>2-</sup>, NO<sub>3</sub><sup>-</sup>, Cl<sup>-</sup>, F<sup>-</sup>, PO<sub>4</sub><sup>3-</sup>, NO<sub>2</sub><sup>-</sup> and the cations Na<sup>+</sup>, K<sup>+</sup>, Mg<sup>2+</sup>, Ca<sup>2+</sup> and NH<sub>4</sub><sup>+</sup> were determined by DIONEX 600 ion chromatography. Bicarbonate concentrations were calculated as alkalinity titration values. The sulphate δ<sup>34</sup>S was determined on BaSO<sub>4</sub> at the Isotope Hydrology Laboratory, Institute for Nuclear Science and Technology, Hanoi, using a MicroMass Spectrometer (IsoPrime, GV Instruments, UK) equipped with an Eurovector elemental analyser (EuroEA 3000, Italy). Data processing was performed using the Masslynx Program supplied by GV Instruments Com., UK. BaSO<sub>4</sub> was precipitated with BaCl<sub>2</sub> and collected on a 0.45 µm filter. The pH was lowered to approximately 3 to 4 to prevent precipitation of BaCO<sub>3</sub>. BaSO<sub>4</sub> samples were weighed into 3–5 mm tin capsules and introduced into a Euro-Vector elemental analyser, reacted for SO<sub>2</sub> in an oxidation/reduction column, heated to 1050 °C in high purity oxygen (99.999%), transported by high purity helium (99.999%) through a pre-packed 0.8 m PTFE GC column and heated to 90 °C to produce SO<sub>2</sub>. The SO<sub>2</sub> from the sample was transported by helium (100 mL/min) into an IsoPrime continuous flow isotope ratio mass spectrometer. Isotope ratios are reported as δ-values relative to the standard meteoritic Canyon Diablo Troilite (CDT). The international standards used in this study were NBS-127, IAEA-SO-5 and IAEA-SO-6 with δ<sup>34</sup>S(‰) = +20.3, +0.5 and -34.1, respectively. The precision (1σ) for δ<sup>34</sup>S is better than 0.2‰.

A reliable sulphur isotope analysis depends first of all on collecting a sufficiently large, unfractionated, uncontaminated sample in the field. The methods for collecting samples depend upon the dissolved sulphate in the samples. For samples with sufficiently high sulphate concentration (equal to or greater than 20mg/L  $\text{SO}_4^{2-}$ ), dissolved sulphate is typically collected by direct precipitation as  $\text{BaSO}_4$ . Five litre water is collected in bottles and brought to the laboratory for  $\text{BaSO}_4$  precipitation. Anion exchange resin is used to collect sufficient dissolved sulphate from 5 litres (less than 20 mg/L  $\text{SO}_4^{2-}$ ). The samples were collected and preserved at the field site by the addition of 1 mL of  $\text{Zn}(\text{CH}_3\text{COO})_2$  saturated solution for precipitation of all  $\text{H}_2\text{S}$  (if present) in the samples and then the samples were brought to the laboratory for chemical processing. On the return to the laboratory, the water samples were heated

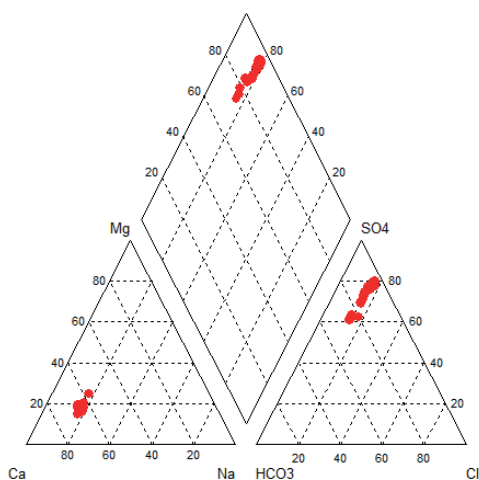


FIG. 1. Piper diagram of groundwater samples collected from Thuan My mineral water.

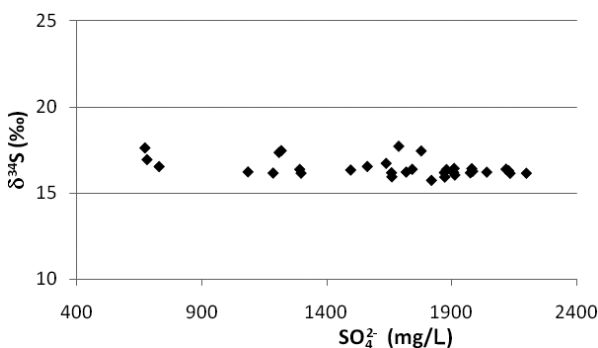


FIG. 2.  $\delta^{34}\text{S}$  in sulphate vs. concentration of  $\text{SO}_4^{2-}$  collected from Thuan My mineral water.

to boiling point to ensure the removal of  $\text{CO}_2$  and thus minimize co-precipitation of  $\text{BaCO}_3$ . Sulphate was precipitated as  $\text{BaSO}_4$  by the addition of 50 mL of 10%  $\text{BaCl}_2$  solution and the precipitate was washed with warm, deionised, distilled water and dried overnight in an oven at  $90^\circ\text{C}$ . The dried  $\text{BaSO}_4$  was then scraped and used for determining the  $\delta^{34}\text{S}$  [1].

## 5. RESULTS

The water characteristics of the samples collected from the 33 wells in rainy and dry seasons as explored in a Piper diagram (Fig. 1) are the same for all samples,  $\text{Ca-SO}_4$ . Total dissolved solids (TDS) values calculated from chemical analysis of these samples range from 2500–3900 mg/L and pH values range from 6.4 to 7.4. The sulphate concentration in 15 samples collected in the dry season and 18 samples in the rainy season ranges from 674 to 2197 mg/L. The sulphate concentration and temperature in these wells are slightly higher than shallower wells. The  $\delta^{34}\text{S}$  values in these wells fall in a narrow range from +15.7 to +17.7‰, with an average of  $+16.2 \pm 0.5\%$  (Fig. 2). The  $\delta^{34}\text{S}$  values in Ha Noi, Lang Son and Thuan My precipitation, the Da and Red rivers and the Hoa Binh Dam Lake range from 1.1 to 8.8‰. Sulphide was not detected in any of the samples.

## 6. DISCUSSION

The  $\delta^{34}\text{S}$  values of the wells are found in a narrow range from +15.7 to +17.7‰ with an average value of  $+16.2 \pm 0.5\%$  ( $1\sigma$ ) and chemistry results indicate that the origin of sulphate in groundwater of this area comes from a single source.

Six potential sources of high sulphate concentration in the wells could be:

- (1) Recharge from precipitation or river close to the study area: The hypothesis of these potential sources is easily dismissed because their sulphate concentration is very low compared to that of the deep wells. The  $\delta^{34}\text{S}$  values of wells are around  $+16.2 \pm 0.5\%$  and that of precipitation and river samples around this area range from 1.1 to 8.8‰ [2, 3].
- (2) Anthropogenic, such as industrial and agricultural activities: The  $\delta^{34}\text{S}$  values of these sources are from +1 to +10‰, therefore industrial and agricultural activities are an unlikely potential source of sulphate [4, 5].
- (3) Seawater intrusion: Seawater incursion is relatively easy to detect because high sulphate waters would also be high in chloride; the corresponding chloride/sulphate ratios (in mg/L) being approximately 7.8. The chloride/sulphate ratios for these wells are much lower than that, ranging from 0.12 to 0.22 (Fig. 3), thus seawater intrusion can be ruled out as a source of sulphate [3, 5–9].

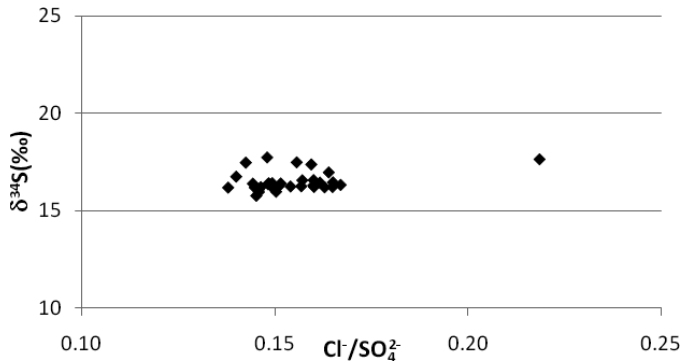


Fig. 3. The relationship between  $\text{Cl}^-/\text{SO}_4^{2-}$  ratio and  $\delta^{34}\text{S}$  in sulphate collected from Thuan My mineral water.

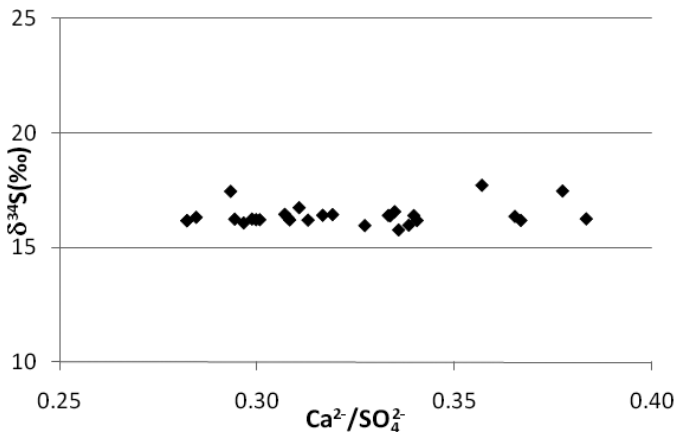


Fig. 4. The relationship between  $\text{Ca}^{2+}/\text{SO}_4^{2-}$  ratio and  $\delta^{34}\text{S}$  in sulphate collected from Thuan My mineral water.

- (4) Reduced inorganic sulphur in minerals such as pyrite and reduced inorganic sedimentary sulphur compounds by microbial activity: Microbial activity, in particular sulphate reduction has the potential to dramatically alter the isotopic composition of sulphate [3–9]. In the deep wells, the absence of sulphide rules out any significant microbial activity.
- (5) Magma volcano: Sulphur from volcanic emissions often has  $\delta^{34}\text{S}$  values close to +5‰ [3–7] so a magma volcano as the source of sulphate cannot be plausible.
- (6) Local dissolution of gypsum: The local dissolution of gypsum seems to be a good explanation of the high sulphate concentration in these wells because gypsum ( $\text{CaSO}_4 \cdot 2\text{H}_2\text{O}$ ) is a major source of sulphate and the  $\text{Ca}^{2+}/\text{SO}_4^{2-}$  ratio (in mg/L) in these wells is from 0.3 to 0.44 (Fig. 4) and the  $\delta^{34}\text{S}$  values of  $\text{SO}_4^{2-}$  are

very close to that of the gypsum. Thus a potential source of sulphate in these wells is the dissolution of gypsum [3–12].

## 7. CONCLUSION

Discontinuities in the area are very important for thermal springs there. These discontinuities are also associated with the formation of Thuan My sulphate mineral water, which has a ‘mushroom’ shape.

Hydrochemical analysis results suggest that the water type in the Thuan My area is Ca-SO<sub>4</sub>.

The chemical and  $\delta^{34}\text{S}$  isotope analyses assume that the origin of dissolved sulphate in the Thuan My mineral water is derived from a single source which is locally dissolved gypsum mineral.

## ACKNOWLEDGEMENTS

I would like to thank Prof. Dr. Dang Huu On for advice in designing the experiments. I am also thankful to Ms. Nguyen Thi Hong Thinh, Nguyen Thi Thai and Eng. Ha Lan Anh for analytical work. The study was supported by the Ministry of Science and Technology, code 06/08/NLNT.

## REFERENCES

- [1] CARMODY, R.W., PLUMMER L.N., BUSENBERG, E., COPLEN, T.B., Methods for Collection of Dissolved Sulphate and Sulfide and Analysis of their Sulfur Isotopic Composition, Open-File Report No. 97-234, U.S. Geological Survey, Virginia (1998).
- [2] HERUT, B., et al., Sources of sulfur in rainwater as indicated by isotopic  $\delta^{34}\text{S}$  data and chemical composition, Israel, Atmos. Environ. **29** (1995) 851–857.
- [3] MAYER, B., “Assessing sources and transformations of sulphate and nitrate in the hydrosphere using isotope techniques”, Isotopes in the Water Cycle (AGGARWAL, P.K., GAT, J.R., FROEHLICH, K.F.O., Eds), Springer, Dordrecht, The Netherlands (2005) 67–89.
- [4] ROBINSON, B.W., BOTTRELL, S.H., Discrimination of sulfur sources in pristine and polluted New Zealand river catchments using stable isotopes, Appl. Geochem. **12** (1997) 305–319.
- [5] INGRI, J., TORSSANDER, P.S., ANDERSSON, P., MÖRTH, C.-M., KUSAKABE, M., Hydrogeochemistry of sulfur isotopes in the Kalix River catchment, northern Sweden, Appl. Geochem. **12** (1997) 483–496.

- [6] KROUSE, H., “Sulphur and oxygen isotopes in sulphate”, *Environmental Tracers in Sub- surface Hydrology* (COOK, C.G., HERCZEG, A.L., Eds) Kluwer Academic, Boston, MA (2000) 195–231.
- [7] CLARK, I., FRITZ, P., *Environmental Isotopes in Hydrogeology*, Lewis, Boca Raton, FL (1997).
- [8] HUDAK, P.F., Sulphate and chloride concentrations in Texas aquifers, *Environ. Int.* **26** (2000) 55–61.
- [9] OTKAY, C., Usability and Origin of Geothermal Water Around Beypazarı Region Ankara, Turkey, *Proc. World Geothermal Congress 2010 Bali, Indonesia*, 25–29 April 2010.
- [10] PICHLER, T.,  $\delta^{34}\text{S}$  isotope values of dissolved sulfate ( $\text{SO}_4^{2-}$ ) as a tracer for battery acid ( $\text{H}_2\text{SO}_4$ ) contamination in groundwater, *Environ. Geol.* **47** (2005) 215–224.
- [11] TORFSTEIN, A., GAVRIELI, I., KATZ, A., KOLODNY, Y., STEIN, M., Gypsum as a monitor of the paleo-limnological–hydrological conditions in Lake Lisan and the Dead Sea, *Geochim. Cosmochim. Acta* **72** (2008) 2491–2509.
- [12] DE CARITAT, P., KROUSE, H.R., HUTCHEON, I., Sulphur isotope composition of stream water, moss and humus from eight arctic catchments in the Kola Peninsula Region (NW Russia, N Finland, NE Norway), *Water, Air, and Soil Pollution* **94** (1997) 191–208.

# **FEASIBILITY OF CHEMOMETRICS ASSISTED EXPLORATION AND MANAGEMENT OF GEOTHERMAL RESOURCES IN THE KENYA RIFT SYSTEM UTILIZING STABLE ISOTOPE AND RELATED MEASUREMENTS**

K.H. ANGEYO, P.O. OGWARI

Applied Nuclear and Radiation Physics Group,  
Department of Physics, University of Nairobi,  
Nairobi, Kenya.

## **Abstract**

The utility of isotopes is more effective if combined with chemical monitoring. Trace radiogenic and element characteristics of geothermal field matrices associated with the high background radiation areas (HBRA) of Kenya were studied and the combined potential of their profiles and multivariate relationships in surficial hydrothermal expressions system matrices of geothermally active HBRA were exploited for resource prospecting and environmental impact modelling. Some results are reported and it is shown how chemometrics and geostatistics assisted measurements could be combined with stable isotope studies. It is outlined how this work, part of the IAEA Project RAF/8/047 (“Introducing Isotope Hydrology for Exploration and Management of Geothermal Resources in the African Rift System”), will build on and enrich Kenya’s previous participation in IAEA supported projects on the sustainable development of groundwater resources which aimed to facilitate the integration of isotope techniques with non-nuclear techniques for water resource development.

## **1. INTRODUCTION**

Although isotope techniques are powerful tools for geothermal reservoir exploration and management, their utility in Kenya is limited [1, 2]. However, isotope techniques are more effective if integrated with regular chemical analytics [3]. We exploit the combined potential of trace radiogenic and element profiles of surficial hydrothermal expressions system matrices associated with high background radiation areas (HBRA) for geothermal resource prospecting and environmental impact modelling by use of chemometrics and geostatistics. Each geothermal system has a unique ‘marker’ signature and thus characterizing signatures can aid in prospecting the field based on the results of a few measurements [4]. Geothermal energy has the best prospects for development in Kenya [5]. Trace chemical characteristics have potential as intrinsic tracers for geochemical processes [6–9].

We present initial results for the Kerio geothermal field (mid Rift Valley, Kenya) which lies in a high background radiation area (HBRA) and thus is a ‘natural laboratory’ to not only study its trace element and radiogenic characteristics but also to explore their multivariate relationships [10, 11]. In certain places around the world local geology and geochemical processes have resulted in highly enhanced levels of radiation (HBRA) [12–15]. Besides Kerio, there are many other HBRA in Kenya such as Mrima Hill, Gwasi, Ruri, Homa Bay and Koru; in these areas we investigate the behaviour and possible fractionation and transportation of the radionuclides from ‘hot’ spots to the surroundings and determine transportation processes and spatial distribution and variability patterns [3]. In Kerio, there are several hot springs, at Kureswa, Soro and Arus [16]. Evidence of geothermal recharge has also been found in Lake Baringo, which neighbours Kerio [17].

## 2. MATERIALS AND METHODS

### 2.1. Sampling and Analysis

Standard sampling procedures were used. Rocks served as a control matrix in the evaluation of thermal fluid interaction with soil. Plants were used to evaluate the intake of the field’s toxic elements. Sample pellets were irradiated in a Cd-109 XRF system for 3000 seconds live time and analysed using the fundamental parameters method. The AXIL/QXAS software was used. Method validation was performed using IAEA Soil-7 certified reference standard. TXRF analysis was also used, based on a tube excited Mo target, operating at 40 KV and 20 mA.

### 2.2. Data Analysis and Interpretation

Although analytical spectrometry has high versatility, its practical utility to environmental analysis is limited by the complexity of data analysis and interpretation. We apply machine learning (especially multivariate chemometrics, including geostatistics) techniques to help reduce the complexity and increase the information gained. For instance, artificial neural networks are useful for nonlinear ordination and visualization of ecological data by Kohonen networks and ecological time-series modelling by recurrent networks [18]. In order to understand the geothermal prospect and to interpret the anisotropies we derived ‘knowledge’ of the spatial distribution of the geothermal signature, starting from a limited number of unevenly spaced samples via geostatistical analyses using ArcMap 9.3. The ‘marker’ geothermal signatures were trace elements in thermal water. The geostatistics methods [19, 20] that we used include description of single element frequency and spatial distribution, followed by investigation of multi-component associations and patterns, and finally, modelling

and interpretation. Semi-variograms of Rb, Sr and Cr and respective spatial dependence results were used to produce Kriging maps.

But we are not interested merely in maps that show the regional distribution for each variable separately, but to find combinations of the variables that reflect the underlying cause of the contribution. A more important challenge is to find the reasons for the regional distribution. We fulfil this objective by an initial investigation of the variables with multivariate chemometrics techniques. By means of chemometrics the dimension of data is reduced while keeping most of the information [21, 22]. This was realized via principal component analysis (PCA) and partial least squares (PLS). PCA is essentially a compression and display method which models an original multivariate data matrix using limited number of latent variables. The method eliminates redundant variables and deals with uncorrelated variables thus making data interpretation easier and enabling the visualization of the distribution of groupings based on underlying factors, which permits the evaluation of correlations between different elements and samples [23]. PLS, on the other hand, is a generalization of regression applicable to the analysis of (mostly noisy) or strongly correlated (collinear) data with numerous variables (property descriptors). The power of PLS lies in the fact that it decomposes a multivariate regression problem into a number of uncorrelated univariate regressions. A model is built which expresses the response variables  $Y$  (e.g. element concentration) as a function of the  $X$  variables (e.g. X ray spectral intensities).

### 3. RESULTS AND DISCUSSION

#### 3.1. Kerio Valley Geothermal Reservoir Diagnostics

Sixteen trace elements were measured in rock and soil; in water only 10 and in plants the number measured varied between 11–13. PLS results of water showed a strong positive correlation of temperature with Sr, K, Br, Rb, Ca and Cr (and negative for pH). The negative correlation found between U, Sr, Ni, Pb and most samples means that since U and Pb are radioactive elements, the reported Kerio Valley ‘HBRA’ cannot be due to radiogenic driven geothermal activity. Sr, K, Br are lithophile elements which concentrate in silicon phases: these elements were found to be the ‘marker’ trace element signatures of the Kerio Valley geothermal field. PLS results also indicated that the Kerio geothermal field is composed of acid sulphate aquifers.

In the PCA analysis, for instance, the sample KH11R (Fig. 1a) has higher Sr, U, Pb and Ni. KR10R has higher Ca, Cu and low K and thus originates from mafic magma (depleted of silica). K and Ca in rocks had a high influence on the PCA model. Excluding KH11R, KR10R and Fe, K, Ca, Ti (Fig. 1b) shows, as expected, a significant difference between SR12R (control sample) and the rest of the samples. KR9R, KR10R are basaltic in nature and are rich in Mn. The PLS plots in Fig. 2

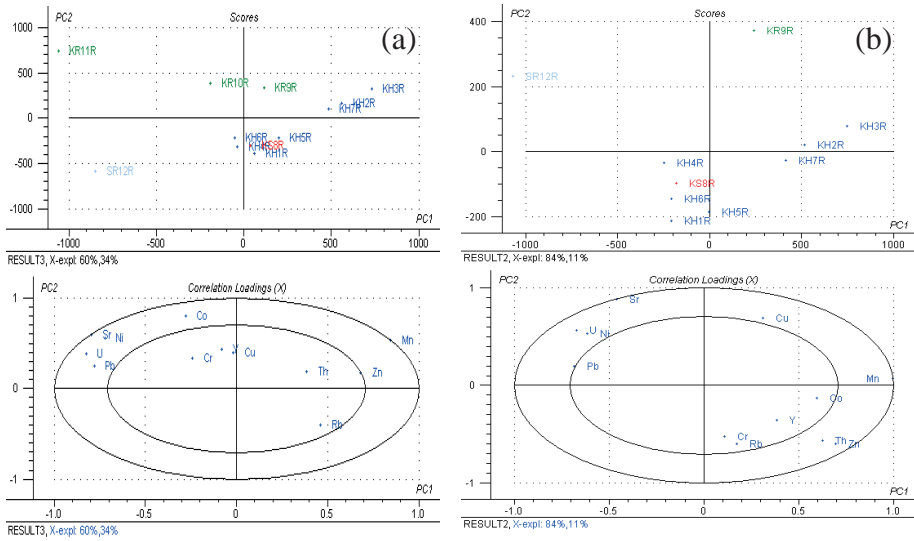


FIG. 1. PCA plots for trace element composition of all rock samples. The plots include scores and correlation loadings plots. (a) PCA plot including samples KR10R and KR11R; (b) PCA plot excluding samples KR10R and KR11R.

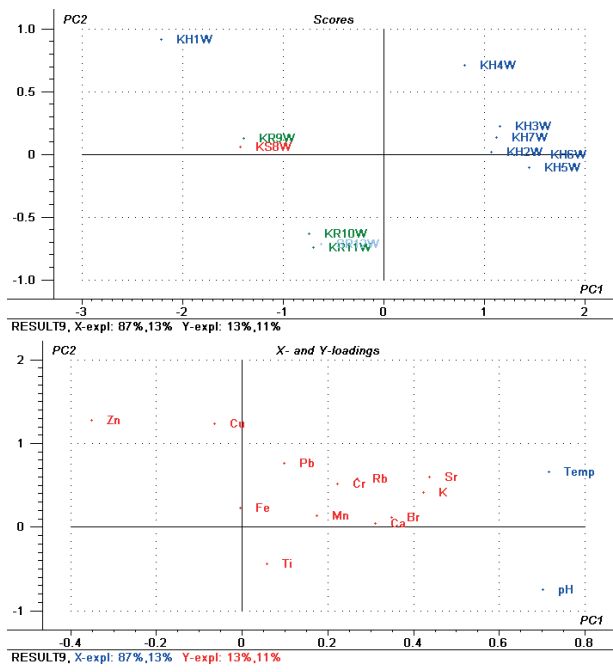


FIG. 2. PLS regression plots for trace element composition of water samples.

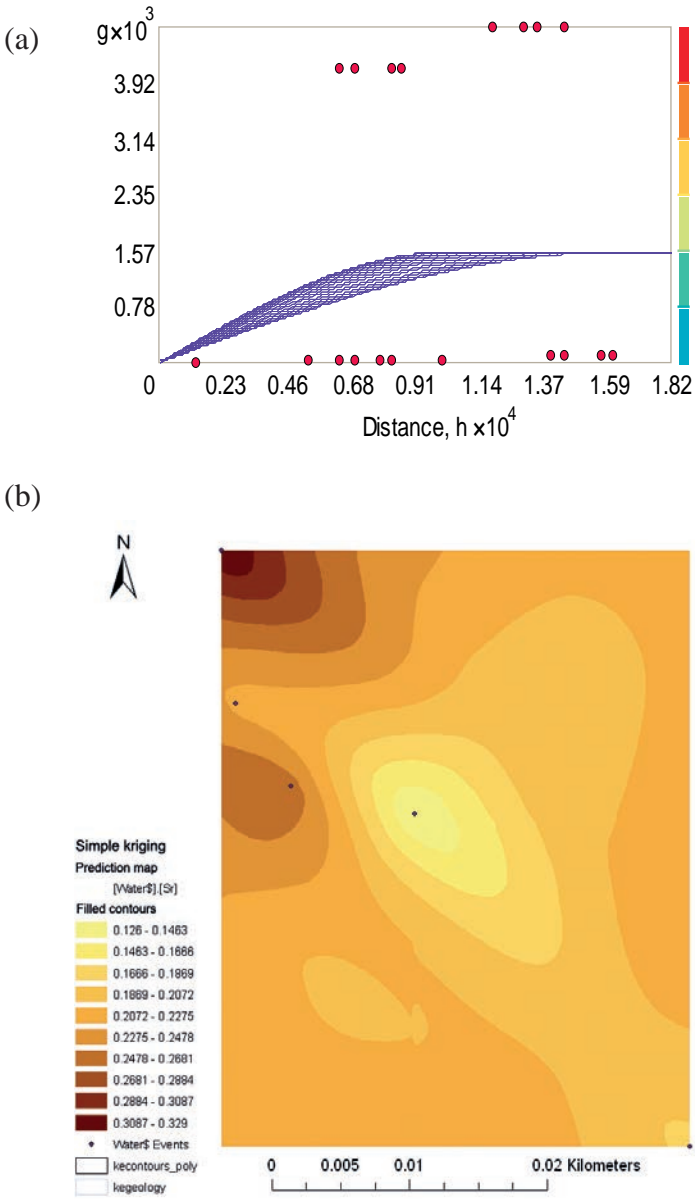


FIG. 3. (a) Rb experimental omnidirectional semi-variogram and fitting curves of spherical model and (b) Sr prediction map for thermal water dataset: the filled contour values are in ppm.

show scores of samples projection and correlation loading weights between the elements and physical properties of water.

Owing to the skewed sampling and the small area covered by geothermal springs, only Rb, Sr and Cr fit the geostatistical model (Fig. 3). The prediction is therefore based on linearly oriented sample points, which translates to a one dimensional projection instead of an area. This, however, indicates some existence of spatial correlation which diminishes with distance, with a high degree of spatial dependence, providing optimism in finding better models.

Taking this sampling as the first phase (for identification of the most significant matrices, their physical properties and 'marker' elements), meteoric water and respective emergence sediments were identified as the right matrices for geothermal prospect mapping. The hot spots should be springs which have minimal or no integration with run off or any other surface water, preferably with elevated temperature. From the elemental composition of the samples we can make a regression model for temperature and salinity/acidity and infer the expected region's thermal gradient.

This study therefore serves as a base for the design and systematic sampling approach for the sparse nature of the Kerio Valley geothermal field. Using PCA and PLS analysis of the data, springs of elevated thermal gradient have been identified as the sampling points. We recently joined the RAF/8/047 project (Introducing Isotope Hydrology for Exploration and Management of Geothermal Resources in the African Rift System) on which we intend to build to enrich Kenya's previous participation in IAEA supported projects on the sustainable development of groundwater resources. A profound knowledge of regional water recharge is a prerequisite for a sustainable usage of local groundwater reservoirs.

By determining how rapidly the water is moving and where in the system is being recharged, isotopes provide critical information to guide decisions. The stable isotope composition of equatorial high altitude precipitation and surface water bodies was studied on Mt. Kenya by Rietti-Shati et al. [2]. The study demonstrated the importance of characterizing local hydrological settings when interpreting lacustrine equatorial isotopic records of past climate and that for East Africa, the total range in oxygen and hydrogen isotopic composition of meteoric waters is smaller than in high latitudes. Stable oxygen and hydrogen isotopes are independent tracers that can be used to study the hydrological cycle, including groundwater pollution. Normally, ground, surface and rainwater are analysed for oxygen-18 and deuterium and various analytical and graphical techniques are then be used to analyse the data and to develop conceptual models to quantify flows between different regions within the site or surface water infiltration and migration into aquifers.

#### 4. CONCLUSION

We have derived knowledge of the spatial distribution of the geothermal signature, starting from a limited number of unevenly spaced samples via geostatistical analyses. The results show that the spatial distribution of the sampling points is insufficient to map the whole area of interest. This study therefore serves as a base for the design and systematic sampling approach for the sparse nature of the Kerio Valley geothermal signatures. Springs of elevated thermal gradient have been identified as the sampling points. The markers have shown a strong positive correlation with thermal gradient in water and the soil has provided the same correlation pattern as the water. Therefore in cases of dried springs, soil samples can provide a good model. Most of the rock samples were identified to originate from felsic magmas (i.e. have higher concentration of K with decreased Ca content). The thermal waters are most likely acid sulphate waters. They are probable vapour condensates which form steam heated waters.

#### REFERENCES

- [1] INTERNATIONAL ATOMIC ENERGY AGENCY, IAEA Regional Model Project RAF/8/029: Sustainable Development of Groundwater Resources in Southern and Eastern Africa, Internal Report, IAEA, Vienna (1995).
- [2] RIETTI-SHATI, M., YAM, R., KARLEN, W., SHEMESH, A., Stable isotope composition of tropical high-altitude fresh-waters on Mt. Kenya, Equatorial East Africa, *Chem. Geol.* **166** 3 (2000) 341–350.
- [3] ANGEYO, et al., “Status and Prospects in Research Infrastructure Development in Nuclear Analytical Spectrometry and Radiometric Instrumentation Methodologies for Environmental Radiation and Associated Radioactivity Measurements and Modelling Studies in Kenya”, Proc. IAEA Technical Meeting on Establishing a Network of Laboratories in the Field of Nuclear Instrumentation for Environmental Monitoring and Related Applications, 27–30 Sept. 2010, Krakow, Poland (2010), unpublished report.
- [4] OGWARI, P.O., Chemometrics-Assisted X-Ray Fluorescence and Geostatistical Analysis of Trace Element Characteristics of a High Background Radiation Area Geothermal Field, MSc Thesis, University of Nairobi (2010).
- [5] KENYA GOVERNMENT, Draft National Energy Policy (2004).
- [6] MATSUDA, S., KOIKE, K., Three-dimensional analysis of temperature distribution in a geothermal area using well-logging data set, *Geoinformatics* **15** 1 (2004) 15–24.
- [7] NICHOLSON, K., *Geothermal fluids: Chemistry and techniques*, Springer, Berlin (1993).
- [8] DUNBAR, N.W., HERVIG, R.L., Petrogenesis and volatile stratigraphy of the Bishop Tuff: evidence from melt inclusion analysis, *J. Geophys. Res.* **97** B11 (1992).
- [9] HIRST, B., et al., Oil and gas prospecting by ultra-sensitive optical gas detection with inverse gas dispersion modelling, *Geophys. Res. Lett.* **31** (2004) 112–115.

- [10] INTERNATIONAL ATOMIC ENERGY AGENCY, Occupational Radiation Protection: Protecting Workers against Exposure to Ionizing Radiation (Proc. Int. Conf. Geneva, 2002), Proceedings Series, IAEA, Vienna (2003).
- [11] NDERITU, S.K., “Natural gamma radiation levels, indoor and water  $^{222}\text{Rn}$  concentrations in SOI, Division of Kerio Valley, Kenya”, Proc. 3rd Intl Symp. Nuclear and Related Techniques, 22–26, October 2001, Havana, Cuba (2001).
- [12] MOHANTY, A.K., SENGUPTA, D., DAS, S.K., VIJAYAN, V., SAHA, S.K., Natural radioactivity in the newly discovered high background radiation area on the eastern coast of Orissa, India, *Radiation Measurements* **38** (2004) 153–165.
- [13] MALANCA, A., PESSINA, V., DALLARA, G., Assessment of the natural radioactivity in the Brazilian state of Rio Grande do Norte, *Health Phys.* **65** 3 (1993) 298–302.
- [14] RAMLI, A.T., HUSSEIN, A.W., WOOD, A.K., Environmental  $^{238}\text{U}$  and  $^{232}\text{Th}$  concentration measurements in an area of high level natural background radiation at Palong, Johor, Malaysia, *J. Environ. Radioact.* **80** (2005) 287–304.
- [15] TARITS, C., et al, Geochemical evidence of hydrothermal recharge in Lake Baringo, central Kenya Rift Valley, *Hydrol. Process.* **20** (2006) 2027–2055.
- [16] RECKNAGEL, F., Applications of machine learning to ecological modelling, *Ecological Modelling* **146** 1–3 (2001) 303–310.
- [17] DUTTER, R., “Robust statistical methods applied in the analysis of geochemical variables”, Contributions to Stochastics (SENDER, W., Ed.), Physica Verlag, Heidelberg (1987) 89–100.
- [18] MATSUDA, S., KOIKE, K., OHMI, M., Spatial estimation of geologic data using a neural network and detection of influence factors on their distribution, *J. Mining and Materials Processing* **119** 6/7 (2003) 359–369.
- [19] HOETING, J.A., DAVIS, R.A., MERTON, A.A., THOMPSON, S.E., Model selection for geostatistical data, *Ecol. Appl.* **16** (2006) 87–98.
- [20] VISWANATHAN, H.S., ROBINSON, B.A., GABLE, C.W., CAREY, J.W., A geostatistical modelling study of the effect of heterogeneity on radionuclide transport in the unsaturated zone, Yucca Mountain, *J. Contam. Hydrol.* **62–63** (2003) 319–336.
- [21] MEGLEN, R.R., Examining large databases: A chemometric approach using principal component, *J. Chemometrics* **5** (1991) 163–179.
- [22] MARK, H., WORKMAN, J., *Chemometrics in Spectroscopy*, Elsevier, Amsterdam (2007).
- [23] BRERETON, R.G., *Chemometrics: Data Analysis for the Laboratory and Chemical Plant*, Wiley, Bristol (2003).

# **DETECTION OF WATER LEAKS IN THE BENI-HAROUN DAM (ALGERIA)**

N. HOCINI, M. MAMI

Hydrology and Sedimentology Laboratory,  
Centre de Recherche Nucléaire d'Alger (CRNA),  
Algiers, Algeria

## **Abstract**

The main objective of this work was to identify the origin of water leakage in the Beni-Haroun dam by combining conventional, tracing and isotope techniques. The investigation was performed by a research team from the Algiers Nuclear Research Centre in collaboration with engineers from the National Agency for Dams. The chemical and isotopic results have shown no influence of dam water on the water sampled at the piezometers and drains that are present in the close neighbourhood of the dam. However, the water flowing at drain D15 has exhibited the closest quality to that of the reservoir. Dye tracing has shown a water circulation through complex pathways for the left bank.

## **1. INTRODUCTION**

This work was carried out within the framework of a Technical Cooperation project supported by the IAEA (ALG/5/021). This project aims to strengthen and develop scientific knowledge in African countries, mainly in the area of the detection of dam leakage and safety. The main objective of this work consisted in detecting water leakage combining classical and nuclear techniques (isotopic and radiotracer). Classical methods concerned the follow up of physico-chemical parameters (conductivity, temperature and chemical composition). Isotopic and radiotracer techniques concerned the isotopic composition (oxygen-18 and tritium) and labelling of the reservoir (fluorescent tracers), respectively [1–6].

## **2. DESCRIPTION OF THE STUDY AREA**

The Beni-Haroun Dam is located in the northeastern part of Algeria, at about 40 km north of the city of Constantine (Fig. 1). The Beni-Haroun Dam is a rectangular gravity concrete dam of initial capacity equal to 963 Mm<sup>3</sup>, the use of which is intended for both water allocation and irrigation of the neighbouring provinces including the main city of Constantine. The dam was first filled in August 2003 and the exploitation showed immediate leaks in the downstream part of the dam.

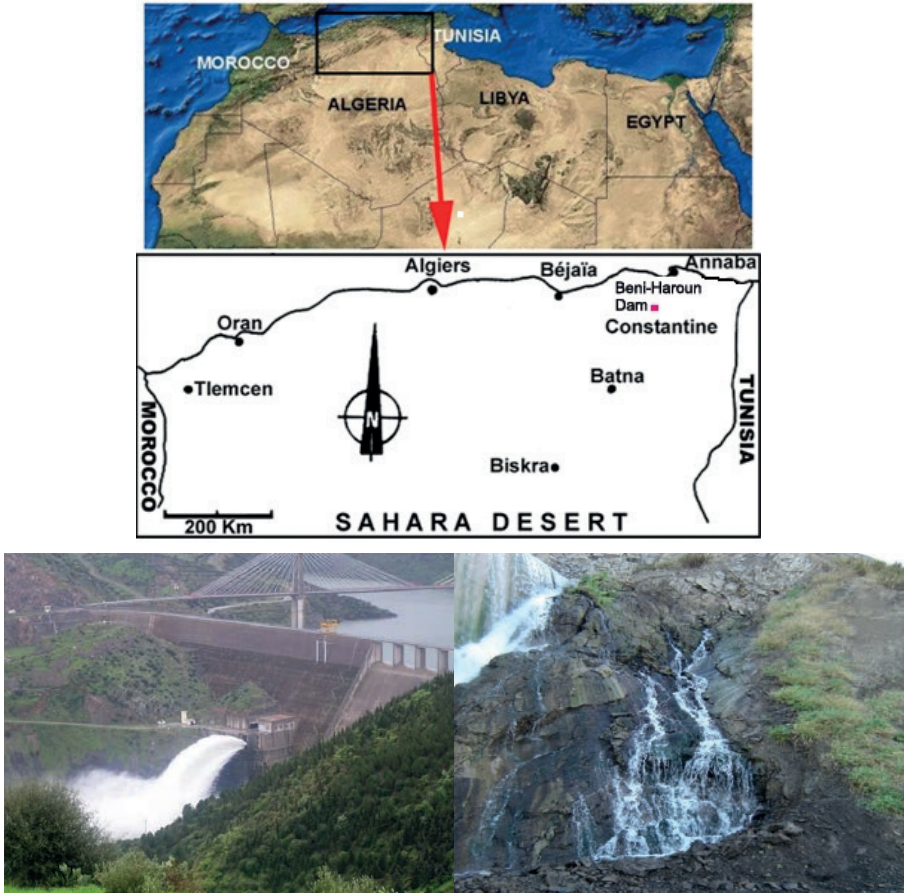


FIG. 1. Map showing location of dam site, and photographs of the same.

The installation of a cementation curtain does not seem to be fully successful and further investigations are required.

The 700 wide, 118 m high structure sits on an Eocene carbonate base that is NE–SW oriented and that plunges towards the upstream region. These highly fractured carbonate base formations are surrounded by black marly formations of Paleocene age in the downstream area and by marly formations of Eocene age in the upstream area. The left bank seems to be more fissured than the right one.

The carbonate base exhibits also rock fractures that are parallel to the axis of the dam structure rather than perpendicularly oriented. A previous study conducted in June 2002 and data from exploration boreholes have demonstrated the existence of a karstic zone with clayey fillings that extends over the whole bottom of the valley in the area comprised between both banks. Moreover, the presence of a spring tapping

a thermal aquifer has additionally complicated the question of the waterproofness of the dam site.

### 2.1. History of the leakage phenomenon

The first filling of the dam was completed in 5th August, 2003. The region experienced an exceptional and very brutal rainy event on the 25th of January 2003. Dam monitoring data has clearly shown the relationship between the rise of level in the lake and the increasing flowrate at the drains and sub-pressure readings. Also water levels at some piezometers have thus attained worrying limits. Low pressure springs have also appeared in the fissured carbonates on the left bank at the bottom of the structure between 116 m and 124 m. These were the consequence of the short floods at the beginning of December during which the level in the lake attained 145 m. The temperature that was recorded at the springs was 24°C whereas that in the lake was 14°C. The drains in the structure foundations were under pressure.

One year later and due to exceptional floods on 4th January 2004, the water level in the lake reached 162 m and the flowrate at the gates of the dam was 404 m<sup>3</sup>/s. Some other anomalies were also noticed:

- Relatively high flow through the concrete joints within the 100, 120, 134 and 140 galleries and deterioration of some joints in the foundation.
- Following the last floods on 30th and 31th December 2004, the level reached 165.23 m in the lake:
  - A spring appeared on the left bank close to the structure at 129 m, with an important flowrate and a temperature around 20°C;
  - The flow rate decreased to 100 L/s in the provisional derivation flowing injection and drainage works that were previously undertaken;
  - The pressure that was recorded at the drains of gallery 100 decreased compared with the values measured during the previous flood event;
  - An increase of the aquifer static water table as recorded in the downstream piezometers. One piezometer became artesian (PO.V-1).

## 3. EXPERIMENTAL WORK

An investigation at the dam was conducted by the CRNA in collaboration with ANBT at the Beni-Haroun Dam, during which the following activities were carried out.

The first field campaign, sampling for all water bodies within the immediate vicinity of the dam that were affected. Samples taken will be analysed for hydrochemistry, stable isotopes (oxygen-18 and deuterium) as well as tritium. In addition, conductivity and temperature profiles were recorded for accessible piezometers in both banks and measurements of conductivity and temperature were made at the drains

and for some points in the lake itself. Two samples were taken at the thermal spring at the Hammam (thermal baths) a couple of kilometres downstream of the dam site.

During the second field campaign, besides recording profiles in the same way as during the first field trip, tracer experiments using fluorescein on the width of limestone outcrop on the left bank of the dam were performed.

#### 4. RESULTS AND CONCLUSIONS

The achievements and the results gathered from the field campaigns allowed us to identify the problems affecting this dam through the overall observation of the features of the physical medium (geology) where it has been built.

Conductivity and temperature measured in the available piezometers is shown in Figs 2a and 2b. There is a definite zone of low temperatures and lower conductivity between piezometers P-RD4 and P-VII-2. This trend is confirmed by temperature

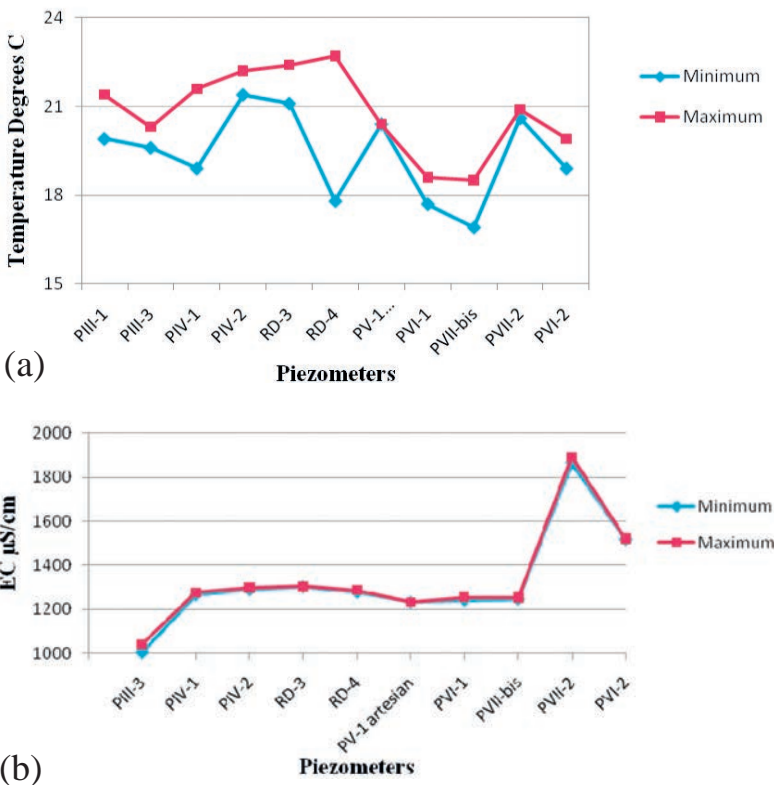


FIG. 2. (a) Maximum and minimum temperatures measured in the piezometers; (b) Maximum and minimum conductivities measured in the piezometers.

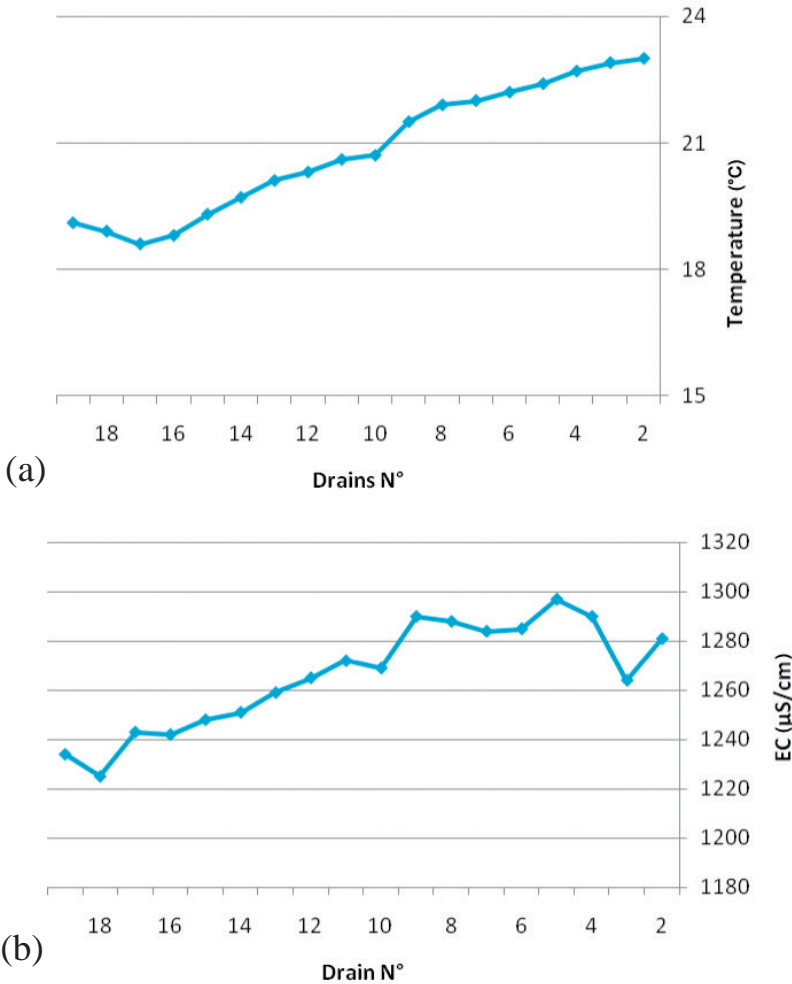


FIG. 5. (a) Temperatures measured along drains; (b) Conductivities measured along drains.

and conductivity in the drains shown in Figs 3a and 3b. Temperature is increasing from drain D17 to the right and towards the left. We know that temperatures increase towards the left bank. The main area of leakage is therefore in this zone.

With regard to the chemical composition, a Piper diagram (Fig. 4) showed that water sampled at the piezometers and drains that are present in the close proximity of the dam was not similar to the dam water but could be mixtures. However, the water flowing at the drain D15 has exhibited the closest quality to that of the dam. This was further confirmed by the isotopic results through oxygen-18 and tritium contents as summarized in Table 1.

TABLE 1. ISOTOPIC COMPOSITION OF SELECTED WATER SAMPLES

Sample	Tritium (TU)	$\delta^{18}\text{O}$ (‰)
Piezometer (PV.1)	8.9	-6.32
Drain D26	<LD	-5.91
Drain D15	<LD	-5.52
R1 left bank (re-emergence flow)	<LD	-5.60
Hammam (thermal spring)	0.3	-7.88
Reservoir	3.4	-4.72

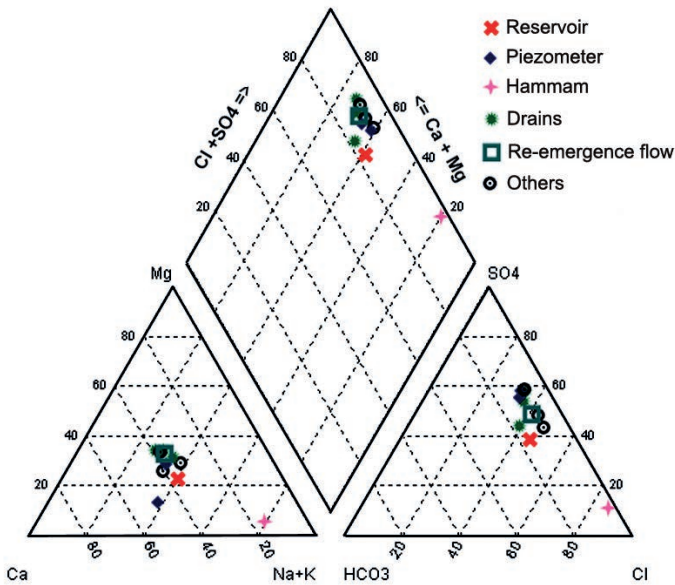


FIG. 6. Chemical classification of samples according to the Piper diagram.

The determination of potential zones of infiltration on the width of the limestone outcrop on the left bank of the dam was performed using a fluorescein tracer at a distance of 2 m from the shores of the reservoir. The tracer monitoring at the springs showed that fluorescein tracer was detected one week later at the left bank.

The investigation described in this paper leads us to the conclusion that the implementation of such a pilot study and its associated preliminary findings seems to be satisfactory. However, according to the complexity of the geological

site, more experiments need to be performed in order to better understand and assess the leakage phenomena.

### ACKNOWLEDGEMENTS

The above investigation was carried out within the framework of the IAEA-ALG/5/021 technical cooperation project. The authors are very grateful to the staff and colleagues of the 'Agence Nationale des Barrages et Transferts' for their fruitful co-operation and logistic assistance during field missions. All analyses were performed at the Hydrology and Sedimentology laboratory, Algiers Nuclear Research Centre, the contribution of whose staff is gratefully acknowledged.

### REFERENCES

- [1] PLATA BEDMAR, A., "Detection of leakage from reservoirs and lakes", Use of Artificial Tracers in Hydrology, IAEA-TECDOC-601, IAEA, Vienna (1991).
- [2] REMINI, B., HOCINI, N., MOULLA, A.S., "La problématique des fuites d'eau dans le barrage de Foug-el-Gherza (Biskra)", Premier Séminaire National sur le Développement des Zones Arides et Semi-arides, University of Djelfa, Algeria (1999).
- [3] REMINI, B., HOCINI, N., MOULLA, A.S., Water leaks in Foug-el-Gherza dam (Algeria), *EIN-International* **6** (2001) 55–59.
- [4] HOCINI, N., "Etude des fuites dans les barrages au moyen des techniques isotopiques", Premières Journées d'Etudes sur les Applications des Techniques Nucléaires en Ressources Hydriques et en Agriculture, COMENA/CDTN, Alger (1999).
- [5] MOULLA, A.S., "Détection du cheminement des fuites dans les barrages et autres réservoirs artificiels: Cas du barrage de Foug El-Gherza", Seminar on Nuclear Techniques et Applications in socio-economic fields: Water Resources, held on the fringe of the 13th AFRA Working Group Meeting of the African National Coordinators, Algiers (2002).
- [6] PLATA BEDMAR, A., ARAGUÁS ARAGUÁS, L., Detection and Prevention of Leaks from Dams, A.A. Balkema, The Netherlands (2002).



# **APPLICATION OF ISOTOPE AND DYE TRACING METHODS IN HYDROLOGY (CASE STUDY: HAVASSAN DAM CONSTRUCTION)**

Y. KHALAJ AMIRHOSSEINI

Water Research Institute,  
Tehran, Iran,  
Yousefkhajaj@yahoo.com

## **Abstract**

Iran, with its annual average precipitation rate of 260 mm, is considered among the arid and semiarid regions of the world. So, water scarcity as a primitive problem has hindered development in agricultural, economic, social and industrial fields. Constructing dams across the rivers is one of the most accepted methods to control and exploit surface waters. Reservoirs formed by constructing dams change fluvial morphology from a river course to a lake. This causes changes in groundwater flow behaviour at the dam site, i.e. a kind of conversion takes place from the role of the aquifers as a recharge source for the rivers before dam construction, into the role of the river-reservoir as the recharge source for the aquifer. As a result, water leakage might occur in the reservoir. Isotope and dye tracing methods could be used to investigate questions such as the present condition of the river, the process of surface water leakage into aquifers, the specification of water leakage locations, the relationships between different water resources, age, class, type, velocity and direction of groundwater flows, the status of permeability of formations of the reservoir, karst development, etc. The paper presents the study on application of environmental isotopes and dye tracers to investigate interaction between surface water and groundwater and possible threats of water leakage from the reservoir at the Havassan Dam site.

## **1. INTRODUCTION**

No attempts have been made yet in Iran to inject radioactive materials to investigate the artificial recharge of groundwater aquifers. However, several studies have been performed on the application of natural isotopes and dye tracing following recent development in dam construction activities and consequent problems such as water leakage from dam reservoirs. The present paper presents a case study in this field.



FIG. 1. Location of the study area. Based on UN map Iran, Map No. 3891 Rev. 1, January 2004.

## 2. STUDY AREA

The study area (590 km<sup>2</sup>) of the Havassan Dam construction site (Fig. 1) is located on the eastern part of the Iran–Iraq border between longitudes 45°40′–46°7′ N and latitudes 34°35′–34°55′ in Kermanshah Province, west of Iran. The dam is designed to be constructed on the River Havassan, which is formed where Ablima and Abzalan forks — originating from the east and northeastern heights — join. The annual average precipitation rate in the drainage area of the Havassan River is estimated at 663 mm, while the annual average temperature is recorded as 16.5°C. Baghva Mountain with 1217 m a.s.l. and Baghveisi with 450 m a.s.l. heights form the highest and lowest parts of the area, respectively.

### 3. PROBLEM ANALYSIS AND RESEARCH METHOD

Primitive observations confirm the probability of fractures and karst development in the area, which may cause water leakage from the reservoir. Isotope and dye tracing methods are used to investigate questions such as the origin of water resources and the relationships between these resources, the likely permeability of the dam site and the hydraulic relationship among calcareous aquifers in the area.

#### 3.1. Isotope tracing analysis

Stable isotopes ( $^2\text{H}$  and  $^{18}\text{O}$ ) and radioisotopes (tritium and  $^{14}\text{C}$ ) have been used in isotope studies of the dam construction site. These studies are performed to investigate the recharge mechanism and flow pattern in permeable formations and also to define the classes of waters. Two sets of samples were collected during the dry and wet seasons from 11 streams, rivers and boreholes in order to perform isotope and water chemistry analyses. The findings of isotope and chemical analyses of water resources in the area are summarized in Table 1.

In the  $\delta^2\text{H}$ - $\delta^{18}\text{O}$  diagram (Fig. 2), the river water samples are plotted below the Global Meteoric Water Line (GMWL) showing evaporation, while the samples of springs are plotted above the GMWL and are relatively depleted compared to the river waters but also depict an evaporation trend. The overall trend indicates that the groundwater contributes to the rivers in this area. High tritium values of springs indicate that the groundwater is very young and movement is quick.

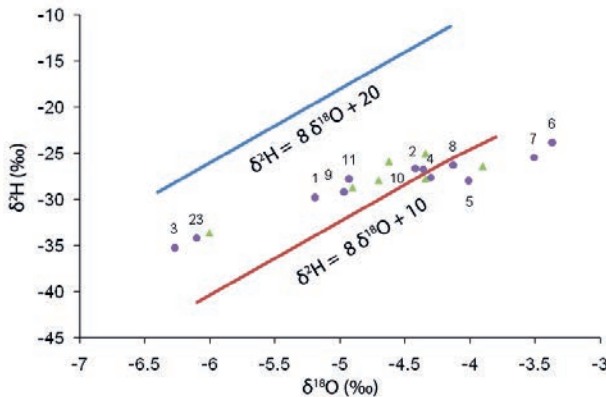


FIG. 2.  $\delta^2\text{H}$  vs.  $\delta^{18}\text{O}$  relationship of groundwaters in the study area.

TABLE 1. RESULTS OF ISOTOPE ANALYSES IN DYE TRACING STUDIES OF THE HAVASSAN DAM SITE

Sample code	Sampling point	May 1998			October 1998			
		Tritium (TU)	$\delta^{18}\text{O}$ (‰)	$\delta^2\text{H}$ (‰)	Tritium (TU)	$^{14}\text{C}$ (PMC)	$\delta^{18}\text{O}$ (‰)	$\delta^2\text{H}$ (‰)
1	Baghe Mansoor Spring	11.1±0.8	-4.90	-28.71	10.1±0.8	57±0.96	-5.19	-29.77
2	Hosseinabad Spring	12.8±0.9	-4.70	-27.92	10.3±0.8	61.59±0.94	-4.36	-26.75
10	Kuzerud Spring	12.0±0.9	-4.34	-27.75	9.8±0.9	-	-4.42	-26.62
11	Sarghale Spring	12.0±0.8	-4.62	-25.86	13.2±0.9	-	-4.93	-27.76
3	Dam axis Spring	12.3±0.9	-6	-33.66	2.6±0.8	-	-6.27	-35.23
6	Havassan River (inlet)	11.6±0.9	-3.90	-26.38	6.3±0.9	-	-3.37	-23.82
4	Havassan River (outlet)	9.7±0.9	-4.34	-25.0	11.8±1.5	-	-4.3	-27.65
8	Kani shirin River	-	-	-	5.7±1.4	81.26±1.6	-4.13	-26.27
7	Cahm saree River	-	-	-	10.4±1.5	-	-3.51	-25.47
5	Dar zangene River	-	-	-	10.6±1.5	-	-4.01	-27.95
9	Sifid savar Spring	-	-	-	9.9±1.5	-	-4.97	-29.19
23	HVG1 borehole	-	-	-	2.27±0.8	-	-6.1	-34.2

### 3.2. Dye tracing analysis

Nowadays, fluorescent materials are mostly used by hydrogeologists in ground-water tracing studies. Qualities such as their high sensitivity for detection (~0.01 ppb), high solubility and low side effects for the environment have made them the most common tracers.

Uranine, also known as sodium fluorescein (Merck, Germany), was selected as the most appropriate tracer for this study. The amount of tracer used is one of the main factors to be considered in order to perform a successful dye tracing process, so that it can be used to explore any relationship existing between the injection point and sampling points. The major effective factors in determining the amount of tracer

TABLE 2. SOME SPECIFICATIONS OF DYE SAMPLING POINTS OF HAVASSAN DAM SITE (INITIAL STAGE)

No.	Sampling point	Date of measurement	Temp. (°C)	Conductivity (µs/cm)	Salinity* (sal)	Water surface depth (m)	Water level in borehole (m)
1	HV <sub>3</sub> borehole	Oct.5, 1998	23.4	484	0.2	32.45	450.05
2	HV <sub>4</sub> borehole	Oct.4, 1998	24.8	392	0.1	–	444.5
3	HV <sub>6</sub> borehole	Oct.4, 1998	22.9	593	0.2	23.15	452.8
4	HV <sub>7</sub> borehole	Oct.5, 1998	23.3	415	0.1	17.9	470
5	HV <sub>8</sub> borehole	Oct.5, 1998	22.6	490	0.2	18.78	447.2
6	HV <sub>9</sub> borehole	Oct.4, 1998	24.5	330	0.1	35.30	448.5
7	HV <sub>13</sub> borehole	Oct.5, 1998	26.6	320	0.1	59.18	447.5
8	HV <sub>15</sub> borehole	Oct.5, 1998	26.5	770	0.3	7.0	441.6
9	HV <sub>16</sub> borehole	Oct.4, 1998	18	–	–	41.25	441.3
10	HV <sub>17</sub> borehole	Oct.4, 1998	25.2	329	0.1	41.1	444
11	Dam axis spring	Oct.2, 1998	19.6	409	0.1	–	–
12	Down-stream river	Oct.2, 1998	20.7	822	0.3	–	–
13	Kuzerud spring	Oct.3, 1998	23.6	277	0.2	–	–
14	Sarghale spring	Oct.3, 1998	23.3	362	0.1	–	–
15	HVG <sub>1</sub> borehole (injection point)	Oct.5, 1998	22.3	400	0.1	94.35	–

\* Salinity: is defined as the amount of salt in the water which is directly proportionate to conductivity.

are: the distance between the injection point and sampling points and the discharge rate of springs and rivers. In this case, 8 kg of tracer was used. Considering the initial field study, the hydraulic gradient and also the results of ditching activities, the HVG1 borehole on the right bank of the dam reservoir was selected as the injection point. On the other hand, in order to recognize general conditions and the background of water resources in the area, field measurements (temperature, conductivity, water level etc.) as well as the chemical analysis of water resources were performed prior to tracer injection (Table 2).

The injection process was performed by dissolving 8 kg of tracer in 200 L of water and 16 L of alcohol was also added to raise the dissolving speed. The activities were started on October 6, 1998, and the tracer was injected in the HVG1 borehole, which had a water table of approximately 95 m. In order to wash the internal wall of the borehole and also to make sure that all the tracer is transferred to the groundwater, the river water was pumped into the borehole for 24 hours. Also, in order to prevent unnatural pollution of the area and error occurrence, dishes and clothes used during injection activities were destroyed and the injection activities team left the area. The method of sampling from water resources in the area was adopted according to the type, distance and importance of the resources and location through both direct and indirect (by means of sampler) methods using activated carbon. Samples were taken from the streams behind the camp and dam axis, the river within the axis and downstream area, boreholes on the left bank of the river (HV3, HV4, HV6, HV8, HV11 and HV16) and boreholes on the right bank of the river (HV7, HV9, HV13, HV15 and HV17). The tracer monitoring activities continued up to December 17, 1998. Over 1770 samples were analysed. The tracer was found in HV7, HV8, HV9, HV13 and HV15 boreholes, in the stream in the dam axis and in the river within the downstream area. The tracer response curves vs. time are shown in Figs 3–8. Connections between the injection well and nearly all the sampling points within the right coast (in the dam axis), which are situated lower than the injection region,

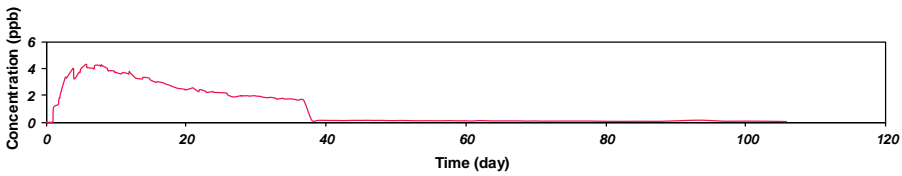


FIG. 3. Breakthrough curve in borehole HV8.

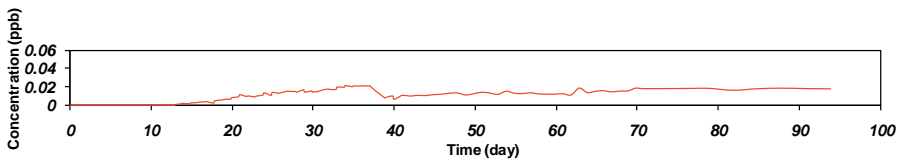


FIG. 4. Breakthrough curve in borehole HV9.

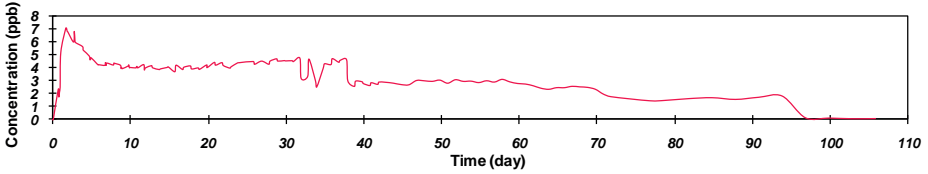


FIG. 5. Breakthrough curve in borehole HV13.

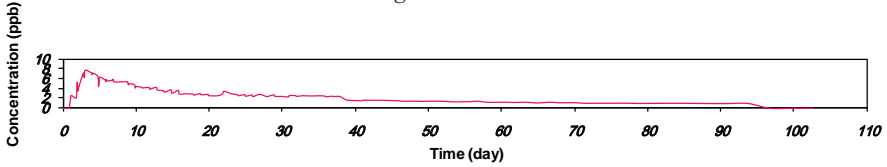


FIG. 6. Breakthrough curve in borehole HV15.

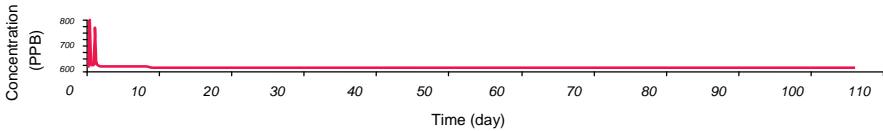


FIG. 7. Breakthrough curve in dam Axis.

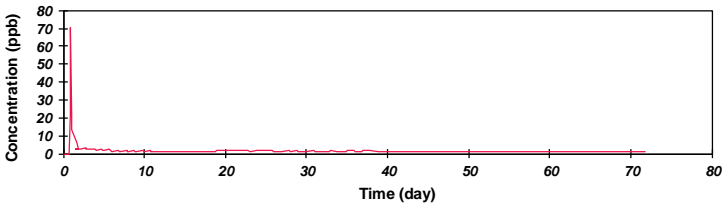


FIG. 8. Breakthrough curve in river Havassan.

indicate the existence of numerous fractures, pores and joints. This information reveals the active zone for water leakage from the dam reservoir to groundwater and flow patterns in this part. Different values of velocity (1–88.3 m/h) determined on the basis of the breakthrough time of the tracer to the sampling points indicate the existence of different notch and joint systems which, in turn, indicates karst development in the right bank.

#### 4. CONCLUSIONS AND RECOMMENDATIONS

The wide range of recorded values of groundwater velocity on the right coast represents the number of failures, notches, joints and likely karst development in this area. Therefore, the following should be taken into more careful consideration:

- Conducting geophysical studies in order to have a more accurate concept of the quality and the process of forming aquifers under the dam construction site.
- Paying more attention to the subsurface geology of water in the area and the petrological features of the area.
- Regular measurement of the water level of the boreholes, the discharge of streams and rivers as well as considering values obtained with respect to the rate of precipitation in order to determine the effect of precipitation on the water resources in the area.
- The information on the notches, joints and likely karst development which could lead to failures have to be considered in future planning.

### **REFERENCES**

- [1] WATER RESEARCH CENTER, Reports on tracing in experiments on dams sites in Iran, Internal report, Teheran (1990–1995).
- [2] WATER RESOURCE RESEARCH CENTER, Field Workshop on Tracing methods in Karst resources (1995).
- [3] MAHAB GHODS CONSULTING COMPANY, Design of dam reservoir, irrigation and drainage network for Havassan river – Geological Report (1996), unpublished report.
- [4] MEMARIAN, H., Geology and Geotechnics, Tehran University Press, Tehran (1995).
- [5] SEPASSI, M., Etude hydrogéologique et ressources en eau de la région de Saveh (Iran), PhD Thesis, Bordeaux University (1979).
- [6] SHARIATPANAHI, M., The principles of water quality and wastewater treatment, Tehran University Press, Teheran (2003), (in Farsi).

# ANALYTICAL METHODS AND INSTRUMENTATION



# NEW HYDROLOGICAL AGE-DATING TECHNIQUES USING COSMOGENIC RADIONUCLIDES BERYLLIUM-7 AND SODIUM-22

S. FREY, C. KÜLLS

Institute of Hydrology,  
Albert-Ludwigs-University of Freiburg,  
Germany

C. SCHLOSSER

Bundesamt für Strahlenschutz,  
Freiburg, Germany

## Abstract

Since atmospheric tritium levels have nearly reached the natural background, there is a need for further development of existing or additional methods for the age dating of young water. Non-gaseous age dating tracers are especially needed for hydrological applications in lakes, rivers and springs and for surface-groundwater interaction studies. Cosmogenically produced isotopes of sodium and beryllium ( $^{22}\text{Na}$ ,  $^7\text{Be}$ , half-lives of 2.602 years and 53.29 days respectively) have been investigated as potential environmental tracers for residence time analysis of surface water. A simple chemical separation scheme for both radionuclides was established and  $^7\text{Be}$  was detected in both surface and groundwater samples. The ions were extracted from 500 L water using an ion exchange resin. The water samples were dated to ages of about 165 and 323 days for riverine samples and 475 days for a groundwater sample. Measurement was performed using a lead covered HPGe detector. These ages match ages previously reported using stable isotopes and tritium.

## 1. INTRODUCTION

While tracers applied to estimate long residence times (hundreds to thousands of years) have been widely used — with their respective particular limitations — most of the tracers used to estimate short residence times (weeks to several years) have major limitations posing challenges related to their application [1]. Residence time analysis of recent groundwater is mainly based on or involves gases such as  $^{85}\text{Kr}$ , CFCs,  $\text{SF}_6$ , H/He, only providing reliable data if atmospheric contact or degassing can be prevented [2]. Since atmospheric tritium concentrations have almost dropped to their natural levels there is a need to further develop these methods or to develop new tracers applicable for short residence times (i.e. <10 a).  $^{22}\text{Na}$  and  $^7\text{Be}$

have adequate half-lives of 2.602 years and 53.29 days, respectively. Their potential application and specific limitations have been investigated in this study.

Because sodium is an alkaline metal, cation exchange processes are expected to at least partly affect transport in soil and bedrock. Bjerg & Christensen [3] were able to show in a tracer experiment that in a sandy aquifer after a distance of 35 m the mobile fraction still amounts to ~70% and to ~50% after 100 m, compared to injected chloride.  $^{22}\text{Na}$  was reportedly first detected in fresh water by Marquez et al. [4] in Rio de Janeiro. Arnold & Al-Salih [5] were the first detecting  $^7\text{Be}$  in rain water samples in Chicago and Lafayette. While Beryllium exhibits high sorption in the soil layer at  $\text{pH} > 6$  [6], no obvious limitations have been reported for  $^{22}\text{Na}$  [7]. Both  $^7\text{Be}$  and  $^{22}\text{Na}$  have rather short half-lives of 53.29 days and 2.602 years, respectively [8].  $^{22}\text{Na}$  and  $^7\text{Be}$  are produced simultaneously in the upper atmosphere by spallation reactions with argon ( $^{22}\text{Na}$ ) and nitrogen or oxygen ( $^7\text{Be}$ ) [9]. Production rates for  $^7\text{Be}$  vary from  $0.2 \text{ nuclei min}^{-1} \text{ m}^{-3}$  at sea level to  $80 \text{ nuclei min}^{-1} \text{ m}^{-3}$  at 30 km elevation. Moving at a constant altitude below 5 km, production rates vary only slightly from  $40^\circ$  to  $90^\circ$  on both hemispheres, whereas, at the respective altitude, production rates close to the equator are lower [10]. On an annual timescale both radionuclides have a maximum input in winter (December–February) and a minimum input in summer (June–August) [11].

This paper presents a modified method for the enrichment and chemical separation of sodium and beryllium with their respective stable and unstable isotopes presented in Ref. [12]. Using this method it was possible to detect both  $^{22}\text{Na}$  and  $^7\text{Be}$  in water samples.

## 2. SAMPLING SITES

All sampling sites are nested in the catchment of the river Dreisam, close to Freiburg, Germany (see Fig. 1). This mesoscale catchment ( $258 \text{ km}^2$ ) is located in the southern Black Forest in southwestern Germany. Elevations within the catchment range from 309 m to 1493 m a.s.l. Mean annual precipitation amounts to ~1500 mm/a generating an annual discharge of ~820 mm/a and a groundwater discharge of ~60 mm/a. Mean annual actual evapotranspiration is ~600 mm/a. The permeability of topsoils in this area is large enough ( $K_{\text{sat}} > 10^{-4} \text{ m/s}$ ) to prevent infiltration excess overland flow [13]. While the groundwater sampling site ‘Hungerbrunnen’ (334 m a.s.l.) and the river Dreisam gorge (316 m a.s.l.) are located in the shallow part of the catchment (‘Zartener Becken’), the river Brugga gorge (434 m a.s.l.) and the groundwater sampling site ‘Schauinsland’ (1284 m a.s.l.) are located in the steep headwater of the basin. Snow was collected in the direct vicinity of the Institute of Hydrology in Freiburg.

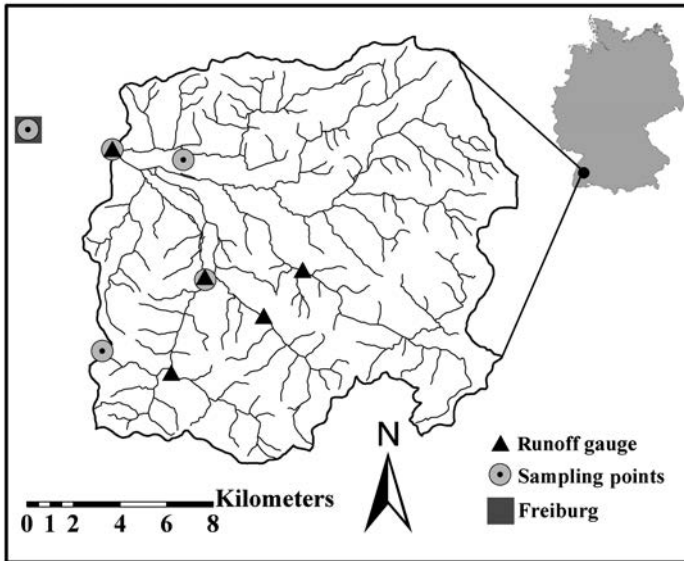


FIG. 1. Catchment of the river Dreisam and locations of the sampling sites.

### 3. SAMPLING AND MEASUREMENTS

In order to measure extremely low levels of short lived cosmogenically produced radionuclides in water, three barriers must be overcome: (1) The dissolved solids of a large water sample taken during a short time need to be extracted, (2) a rapid chemical separation of cosmogenically produced radionuclides from other elements that can disturb the detection and (3) a rapid measurement using a low background detector. Such analyses have been conducted as described below.

Large water samples of 500 litres per sample have been taken using a mixture of 1:1 anion and cation exchange resin (Amberlite® IR-120 /Amberlite® IRA-416). A 12 V non-adjustable pump, pumping 6 L/min was supplied via a 12 V DC battery. A Y pipe was installed as a bypass in order to reduce inlet flow to the resin column. The resin itself was packed in a glass column. Flow velocity through the resin was adjusted to 2 L/min using a valve to adjust bypass flow and checked via a flow meter located before the column. Before inflow to the pump, the water was filtered to prevent coarse material getting into the system and damaging it. A diagram of the sampling system is shown in Fig. 2.

In the field pH, electric conductivity and temperature of water were monitored before and after passing the exchange resin. Samples of both fresh and demineralised water have been taken to analyse principle components.

In the laboratory the resin was washed with two litres of 4M HCl and the eluate was evaporated to one litre. At this stage 30 gram were separated and the pH was adjusted to 7 using  $\text{NH}_4\text{OH}$  to determine principle components. The rest of

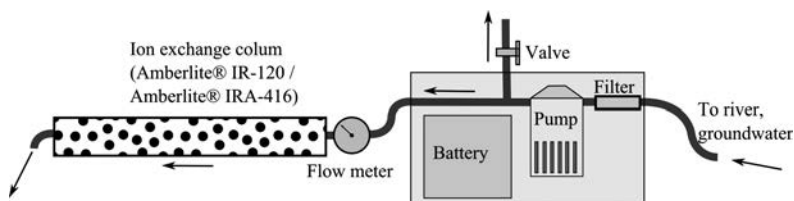


FIG. 2. Sampling system for collecting ions from large water samples.

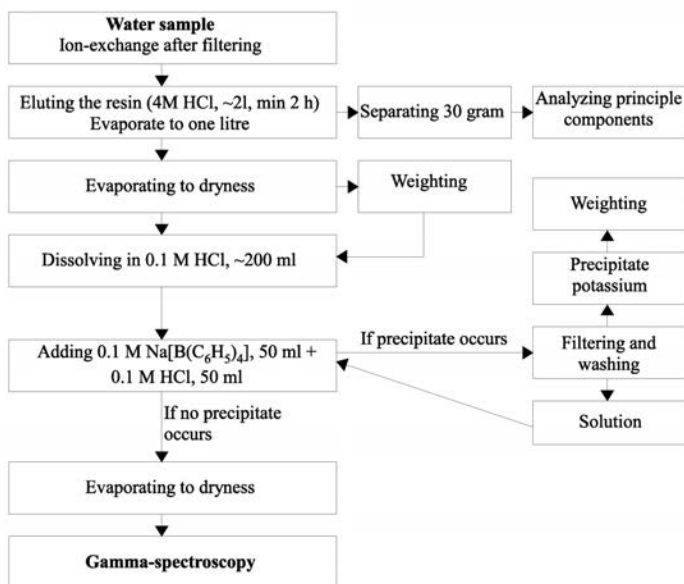


FIG. 3. Chemical separation scheme of potassium.

the solution was evaporated to dryness, weighed and dissolved in 0.1 M HCl. To precipitate potassium 0.1 M  $\text{Na}[\text{B}(\text{C}_6\text{H}_5)_4]$  (NaTPhB) and 0.1 M HCl (1:1) were added. The colourless precipitate (primarily KPhB, in addition PbTPhB, CsTPhB and  $\text{NH}_4\text{TPhB}$  [14]) was separated using a 45 nm pore size filter, evaporated to dryness and weighed. This procedure was repeated until no precipitate was observed. The solution was evaporated to dryness and analysed via gamma spectroscopy using a lead covered HPGe detector of a relative efficiency of 30%. Fig. 3 gives an overview of this chemical separation. In addition, pure NaTPhB was analysed to make sure no  $^{22}\text{Na}$  was added during the procedure.  $^{22}\text{Na}$  was detected by its 1275 keV peak,  $^7\text{Be}$  by its 477 keV peak.

#### 4. RESULTS AND DISCUSSION

Measured activities were used to estimate the age of sampled water. When one or both radionuclides could not be detected in a sample the detection limit represents the lower bound of the residence time. Age dating was done in two different ways: (1) input data was taken from snow measurements setting the age of snow to zero and (2) input data was taken from Ref. [15] for  $^7\text{Be}$  and from Ref. [11] for  $^{22}\text{Na}$ . In both cases Eq. 1 was used.

Free fluoride could be responsible for an increased mobility of beryllium ( $\text{BeF}_3$  and  $\text{BeF}_4^-$ ) observed as well as DOC [6]. In column experiments carried out by Hohwieler [13, 16] about 10% of mobile beryllium was found. This was attributed to sorption of beryllium to fine particulate matter or to complexation. Thermodynamic modelling indicates that in aqueous solutions containing dissolved fluoride, mobile beryllium-fluoride complexes develop with an activity ratio that corresponds to the observed mobile fraction. Therefore, age dating using  $^7\text{Be}$  was done under the assumption that 90% of the atmospheric input was held in the soil layer. However, this assumption should be validated by further experimental work and associated modelling in order to ascertain the geochemical process and narrow the activity ratio. In addition, the effective activity given by Eq. 2 of a sample was considered. The relative efficiency of the resin for sodium was calculated by comparing analyses of sodium before and after the water passed the resin. For beryllium, ten litres of melted snow were evaporated to dryness without passing the resin and analysed via gamma spectroscopy. The relative efficiencies for sodium and beryllium were found to be 70% and 50%, respectively. However, these values are still highly uncertain and need to be confined by spiking the input. The value for beryllium was estimated by only sample. For sodium, analyses of principle components of the eluate (see Fig. 3) were done by flame spectroscopy. Although the eluate was diluted by a factor of 100, the huge amount of chloride and ammonia disturbed the measurement.

$$N_{(t)} = N_{(0)} \times e^{-\lambda t} \quad \text{with} \quad \lambda = \ln(2)/T_{1/2} \quad (1)$$

$$N_{\text{eff}} = N_{(t)} \times (V \times E)^{-1} \quad (2)$$

$N_{(t)}$	is actual activity of a sample (mBq);
$N_{(0)}$	Activity of a sample at time 0 (mBq)
$N_{\text{eff}}$	Effective activity (mBq/L)
$\lambda$	Decay constant ( $\text{d}^{-1}$ )
$t$	Time (d)
$T_{1/2}$	Half-life (d)
$V$	Volume of water passing the resin (L)
$E$	Efficiency of the exchange resin (-)

TABLE 1. AGE DATING USING  $^7\text{Be}$  ACTIVITIES

Sample	Activity (mBq)	Activity (mBq/L)	Activity (eff) (mBq/L)	Age (d) related to		
				Literature	Literature (effective)	Obtained data
Brugga	830	1.66	3.32	360	308	323
Hungerbrunnen	110	0.22	0.44	512	460	475
Snow	61400	122.80	245.60	209	157	0
Dreisam	6820	13.64	27.28	201	149	165
Schauinsland	<62	<0.12	<0.25	>555	>503	>518

TABLE 2. AGE-DATING USING  $^{22}\text{Na}$  ACTIVITIES

Sample	Activity (mBq)	Activity (mBq/L)	Activity (eff) (mBq/L)	Age (d) related to		
				Literature	Literature (eff)	Obtained data
Brugga	<14.93	<0.03	<0.04	>3066	>2578	>340
Hungerbrunnen	<17.52	<0.04	<0.05	>2847	>2358	>121
Snow	19.14	0.04	0.06	2726	2237	0
Dreisam	<33.13	<0.07	<0.10	>1974	>1485	0
Schauinsland	<18.63	<0.04	<0.05	>2763	>2274	>37

Results of the gamma spectroscopy analyses and the respective age dating of samples are shown in Table 1 for  $^7\text{Be}$  and in Table 2 for  $^{22}\text{Na}$ . While  $^{22}\text{Na}$  could be detected in melted snow only,  $^7\text{Be}$  was found in all samples but Schauinsland.

According to Ref. [11] the deposition rates of  $^{22}\text{Na}$  vary between 0.1 and 0.3 mBq/L. Implicating the residence times derived from  $^7\text{Be}$  measurements and the resulting radioactive decay it should have been detectable. Possible reasons for not detecting that radionuclide are: (1) the efficiency of the exchange resin for sodium was lower than expected and (2) there may be sodium–sodium exchange processes between sodium stored in soil and bedrock and cosmogenically produced sodium increasing the residence time without influencing the mass balance of sodium, but changing the isotope signature.

For groundwater in the river Dreisam basin preliminary work using  $^{85}\text{Kr}$  and  $^{39}\text{Ar}/^{37}\text{Ar}$  showed a double maximum age distribution with one maximum at ~70 days and a second one at 3 to 4 years [17]. According to Uhlenbrook et al. [18] the age

of shallow groundwater was ~2–3 years whereas deep groundwater was found to be younger than 10 years old. Estimated groundwater ages using  $^7\text{Be}$  agree well with ages obtained using other independent methods.

## 5. CONCLUSIONS

Cosmogenically produced isotopes of sodium and beryllium ( $^{22}\text{Na}$ ,  $^7\text{Be}$ , half-lives of 2.602 years and 53.29 days, respectively) have been investigated as potential environmental tracers for residence time analysis of surface water. These two isotopes were detected in groundwater and river water samples using ion exchange resins in lead covered HPGe detectors. Water ages ranging from 165 to 475 days have been obtained for river and groundwater samples.

## ACKNOWLEDGEMENTS

Thanks to Barbara Herbstritt, Hermann Schür, Pablo Davila, Udo Gerstmann and Markus Weiler.

## REFERENCES

- [1] ROSE, S., Utilization of decadal tritium variation for assessing the residence time of base flow, *Ground Water* **45** (2007) 309–317.
- [2] SOLOMON, D.K., POREDA, R.J., SCHIFF, S.L., CHERRY, J.A., Tritium and helium-3 as groundwater age tracers in the Borden aquifer, *Water Resour. Res.* **28** (1992) 741–755.
- [3] BJERG, P.L., CHRISTENSEN, T.H., A field experiment on cation exchange-affected multicomponent solute transport in a sandy aquifer, *J. Contam. Hydrol.* **12** (1993) 269–290.
- [4] MARQUEZ, L., COSTA, N.L., ALMEIDA, I.G., The formation of  $^{22}\text{Na}$  from atmospheric argon by cosmic rays, *Il Nuovo Cimento* **6** (1957) 1292–1295.
- [5] ARNOLD, J.R., AL-SALIH, H.A., Beryllium-7 produced by cosmic rays, *Science* **121** (1955) 451–453.
- [6] SAKAGUCHI, A., et al., Cosmogenic radionuclide  $^{22}\text{Na}$  in the Lake Biwa system (Japan): Residence time, transport and application to the hydrology, *Earth Planet. Sci. Lett.* **231** (2005) 307–316.
- [7] SAKAGUCHI, A., et al., Cosmogenic radionuclide  $^{22}\text{Na}$  in the Lake Biwa system (Japan): Residence time, transport and application to the hydrology, *Earth Planet. Sci. Lett.* **231** (2005) 307–316.
- [8] KOMURA, K., et al., Measurements of short-lived cosmic-ray-produced radionuclides in rainwater, *J. Environ. Radioact.* **96** (2007) 103–109.

- [9] JASIULIONIS, R., WERSHOFEN, H., A study of the vertical diffusion of the cosmogenic radionuclides,  $^7\text{Be}$  and  $^{22}\text{Na}$  in the atmosphere, *J. Environ. Radioact.* **79** (2005) 157–169.
- [10] LAL, D., PETERS, B., “Cosmic ray produced radioactivity on the Earth”, *Handbuch der Physik* 46 (FLÜGGE, S., Ed.), Springer, Berlin, (1967) 551–612.
- [11] TOKUYAMA, H., IGARASHI, S., Seasonal variation in the environmental background level of cosmic-ray-produced  $^{22}\text{Na}$  at Fukui City, Japan, *J. Environ. Radioact.* **38** (1998) 147–161.
- [12] SAKAGUCHI, A., et al., Low-level measurement of the cosmogenic  $^{22}\text{Na}$  radionuclide in fresh water by ultra low-background gamma-ray spectrometry after simple radio-chemical separation, *J. Radioanal. Nucl. Chem.* **258** (2003) 101–105.
- [13] WISSMEIER, L., UHLENBROOK, S., Distributed, high-resolution modelling of  $^{18}\text{O}$  signals in a meso-scale catchment, *J. Hydrol.* **332** (2007) 497–510.
- [14] WITTIG, G., KEICHER, G., RÜCKERT, A., RAFF, P., Über Bor-alkalimetallorganische Komplexverbindungen, *Justus Liebigs Annalen der Chemie* **563** (1949) 110–126.
- [15] KNIES, D.L., et al.,  $^7\text{Be}$ ,  $^{10}\text{Be}$  and  $^{36}\text{Cl}$  in precipitation, *Nucl. Instrum. Methods Phys. Res.* **B 92** (1994) 340–344.
- [16] HOHWIELER, N., Beryllium-7 als neuer Tracer in der hydrologischen Prozessforschung — eine Machbarkeitsstudie, Masters Thesis. Institut für Hydrologie der Universität Freiburg (2005) 109 pp.
- [17] ADOLPH, G., Kombination von Isotopenmethoden und Grundwassermodellen in der Altlastenbearbeitung, *Freiburger Schriften zur Hydrologie* 28, Institut für Hydrologie der Universität Freiburg (2009) 206 pp.
- [18] UHLENBROOK, S., FREY, M., LEIBUNDGUT, C., MALOSZEWSKI, P., Hydrograph separations in a mesoscale mountainous basin at event and seasonal timescales, *Water Resour. Res.* **38** (2002) 1–14.

# ADVANCES IN RADIOCARBON MEASUREMENT OF WATER SAMPLES

R. JANOVICS<sup>a</sup>, M. MOLNÁR<sup>a</sup>, I. SVĚTLÍK<sup>b</sup>, I. MAJOR<sup>a</sup>, L. WACKER<sup>c</sup>

<sup>a</sup> Institute of Nuclear Research (ATOMKI),  
Hungarian Academy of Sciences,  
H-4001 Debrecen, Hungary

<sup>b</sup> Department of Radiation Dosimetry,  
Nuclear Physics Institute AS CR,  
Prague, Czech Republic

<sup>c</sup> Institute for Particle Physics,  
ETH Hönggerberg,  
Zürich, Switzerland

## Abstract

In this paper two very different and novel methods for the  $^{14}\text{C}$  measurement of water samples are presented. The first method uses direct absorption into a scintillation cocktail and a following liquid scintillation measurement. Typical sample size is 20–40 L and overall uncertainty is  $\pm 2\%$  for modern samples. It is a very cost effective and easy to use method based on a novel and simple static absorption process for the  $\text{CO}_2$  extracted from groundwater. The other very sensitive method is based on accelerator mass spectrometry (AMS) using a gas ion source. With a MICADAS type AMS system we demonstrated that you can routinely measure the  $^{14}\text{C}$  content of 1 mL of water sample with better than 1% precision (for a modern sample). This direct  $^{14}\text{C}$  AMS measurement of water takes less than 20 minutes including sample preparation.

## 1. INTRODUCTION

Sustainable groundwater management is one of the most important tasks for human civilization. Subsurface resources with very old and clean water can be affected by mixing with much younger and possibly polluted modern surface waters. Groundwater recharge usually originates from the surface [1]. If recharge is rapid, the contamination by younger water may lead to problems; however, if it is slow the water yielding capacity may rapidly decrease leading to the premature termination of the water resource. To trace these conditions an investigation of the  $^{14}\text{C}$  age of the water resources can be undertaken.  $^{14}\text{C}$  is generated from  $^{14}\text{N}$  by cosmic radiation in

the atmosphere with an approximately constant rate and decays with a half-life of 5730 years. The  $^{14}\text{C}$  isotope generated is dissolved by precipitation in the form of  $\text{CO}_2$  molecules and falls from the atmosphere. A part of the precipitation infiltrates the soil and reaches the groundwater within a certain time which depends on the porosity of the rocks [2]. Therefore, changes in the radiocarbon activity of the water resources over time give information on the connection of the water resources to the surface waters. Using radiocarbon activity data of the water resources it is easier to model the subsurface flow conditions of the water.

Radiocarbon emitted from nuclear facilities may reach the groundwater in the form of dissolved  $\text{CO}_2$ , therefore to explore the possible infiltrations the most effective way, besides tritium, is to measure the  $^{14}\text{C}$  activity of the groundwater in the groundwater monitoring wells settled in the vicinity of nuclear facilities. With the help of the radiocarbon activity data of the groundwater a contamination propagation model describing the flow conditions of the area can be established making the localisation of the source of the contamination much easier [3].

Radiocarbon activity in hydrological samples has been measured in the ATOMKI since the 1980's by gas proportional counter (GPC) [4]. The GPC method is one of the most accurate methods even today; however, a large amount of sample is needed and the sample preparation and the measurement require a lot of time. Besides, GPC is nowadays very rarely applied due to its difficulty and the troublesome manufacture of the device. If high precision measurement is to be taken by liquid scintillation counting, benzene should be prepared from the carbonaceous sample. Benzene production requires very sophisticated and time consuming sample preparation and also requires a large amount of samples [5]. The most high profile and expensive method to measure  $^{14}\text{C}$  is accelerator mass spectrometry (AMS) requiring significantly shorter measurement time compared to the decay counting methods. It requires a smaller amount of samples by orders of magnitude than the previous two methods; however, sample preparation is time consuming even for this method. As a first step, graphite should be generated from the  $\text{CO}_2$  liberated from the water sample. There are several graphite production methods (hydrogen or zinc reduction,  $\text{TiH}_4$  reduction in sealed tube etc.) [6], which are all relatively expensive and slow.

A cheaper and commonly available LSC method or a simpler AMS preparation method would be preferable, which would be faster and cheaper than the methods based on graphite production. We developed a combined approach to solve both problems. During the development of the methods intercomparisons were performed with the conventional GPC technique in both cases.

## 2. DIRECT ABSORPTION LSC COUNTING METHOD

A new chemical sample preparation method for liquid scintillation  $^{14}\text{C}$  measurements was implemented at the ATOMKI modifying previous routines [7, 8].

Several tests were executed with old borehole  $\text{CO}_2$  gas without significant content of  $^{14}\text{C}$  and were also performed on samples of known  $^{14}\text{C}$  activities between 29 and 7000 pMC, previously measured by GPC. The  $^{14}\text{C}$  activities of all prepared samples were measured by an ultra-low background LSC (TRI-CARB 3170 TR/SL, Perkin Elmer) including quenching parameter (tSIE).

We used pure  $\text{CO}_2$  gas for LSC measurements after the same purification procedure in the same chromatographic system as for radiocarbon dating in our GPC. The carbonate containing samples were treated with acid (85%  $\text{H}_3\text{PO}_4$ ). Then the  $\text{CO}_2$  gas obtained was purified in a chromatographic system [9]. After this the  $\text{CO}_2$  gas was frozen into a special plastic gas storage bag (Plastigas, Linde) equipped with a freezing finger for the quantitative gas input. We connected the gas storage bag to the vacuum line designed for  $\text{CO}_2$  absorption (Fig. 1).

The line consists of the following parts: the  $\text{CO}_2$  sample in a Plastigas (labelled 'PG' in Fig. 1) bag equipped with a freezing finger (FF) and a finely adjustable teflon valve (VG) for  $\text{CO}_2$  flow regulation. The bubbler (Hg) filled with Hg ensures the visibility of the gas flow rate and precludes the intrusion of absorbent vapour into the Plastigas. A 20 mL low-potassium glass vial with 11 mL of Carbosorb-E<sup>®</sup> absorbent (CS) is connected to the quick vial-connector (VF). The vial during the absorption is cooled about  $-10^\circ\text{C}$  degree using a cooling flask (CF). The initial pressure reduction is ensured by an evacuated puffer glass bulb (PB) with teflon valve (VB).

The valve of the Plastigas (VG) was slightly opened after the system was evacuated. Then the  $\text{CO}_2$  was continuously absorbed in the Carbosorb until it became saturated. The amount of  $\text{CO}_2$  absorbed in the Carbosorb was determined by direct weighing of the glass vial with the absorbent before and after the absorption. After

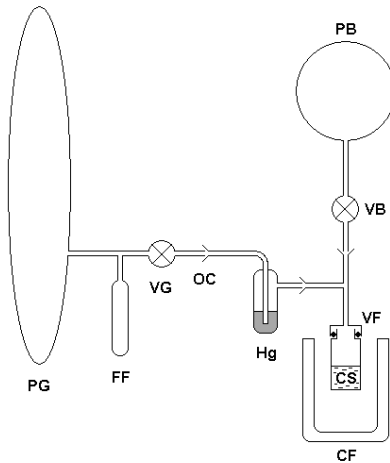


FIG. 1. Schematics of  $\text{CO}_2$  absorption line.

TABLE 1. LSC VS. GPC INTERCOMPARISON WITH SAMPLES OF DIFFERENT C-14 ACTIVITIES

Sample Nr.	$^{14}\text{C}$ activity (pMC), $\delta^{13}\text{C}$ uncorrected	
	GPC	LSC
1	6940 $\pm$ 23	6891 $\pm$ 61
		6996 $\pm$ 62
2	5147.7 $\pm$ 8.9	5140 $\pm$ 46
		5158 $\pm$ 46
3	759.2 $\pm$ 1.4	756.3 $\pm$ 7.8
4	581.3 $\pm$ 1.4	577.2 $\pm$ 6.3
5	219.5 $\pm$ 0.7	222.3 $\pm$ 3.2
		222.3 $\pm$ 3.1
6	113.8 $\pm$ 0.3	112.6 $\pm$ 2.2
		113.7 $\pm$ 2.2
7	112.7 $\pm$ 0.3	116.4 $\pm$ 2.2
8	28.6 $\pm$ 0.3	27.6 $\pm$ 1.5

the absorption 11 mL PermaFlour-E cocktail was added into each sample vial. Subsequently, the samples were counted by TriCarb 3170.

To test the sample preparation technique we performed absorption treatment on 8 samples (Table 1.). These samples were previously measured by the GPC technique.

The measured pMC values with LSC technique were very similar to the values of GPC method. To test the time stability of the mixtures we repeated the measurements of a higher activity sample after a long period of time (99 days). There was no significant ageing effect. We concluded that the measurements could be performed some time after the sample preparation. To estimate the uncertainty of the blank sample preparation we prepared six parallel blank (C-14 free) samples. The measured background count rates for the six blanks were very similar. The average count rate was  $1.869 \pm 0.020$  cpm. The preparation of blank samples shows a good reproducibility and no uncontrolled contamination was observed.

### 3. AMS TECHNIQUE

We investigated the applicability of a new method to prepare samples from dissolved inorganic carbonate (DIC) in ground-water for radiocarbon AMS analysis. This method does not require graphite generation and a small volume of water sample

is sufficient for the radiocarbon measurement. The procedure is very similar to pre-treatment of carbonate contained sample preparation for stable isotope measurement with the Gasbench technique. We applied a MICADAS type accelerator mass spectrometer (AMS) with gas ion source for C-14 analysis.

The radiocarbon preparation includes adding phosphoric acid to the water sample and then He purge gas is flowed through the sample vial to remove liberated  $\text{CO}_2$  from the vial headspace. The developed pre-treatment method does not require sample preparation under vacuum, which significantly reduces the complexity. Reaction time and conditions can be easily controlled, as the  $\text{CO}_2$  content of a water sample is extracted by acid addition in a He atmosphere using a simple septum sealed test tube. A double needle with flow controlled He carrier gas is used to remove  $\text{CO}_2$  from the test tube (Fig. 2). The  $\text{CO}_2$  extraction yield is less than 80% mainly because a large portion of the gas remains in solution in accordance with Henry's law.  $\text{CO}_2$  is then trapped on zeolite without using liquid  $\text{N}_2$  freezing.

The new method can be combined with an automated graphitization system such as AGE from ETHZ [10] in order to have a fully automated water preparation line for AMS graphite targets. In this case, about 5–12 mL of water is needed for an AMS sample.

The greatest advantage of the new groundwater pre-treatment method is the possibility to connect the extraction line directly to an AMS system using a gas ion source interface (Fig. 3). Preparation is vastly reduced compared to the other AMS methods and principally allows fully automated measurements of groundwater samples with an autosampler.

With our MICADAS AMS system we demonstrated that the  $^{14}\text{C}$  content in 1 mL of water could be routinely measured with more than 1% precision (for

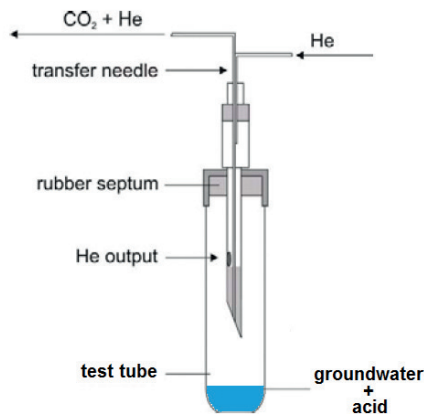


FIG. 2.  $\text{CO}_2$  transfer method using He carrier gas flushing through a double needle (Thermo, Gasbench) in a septum sealed test tube (Labco, UK).

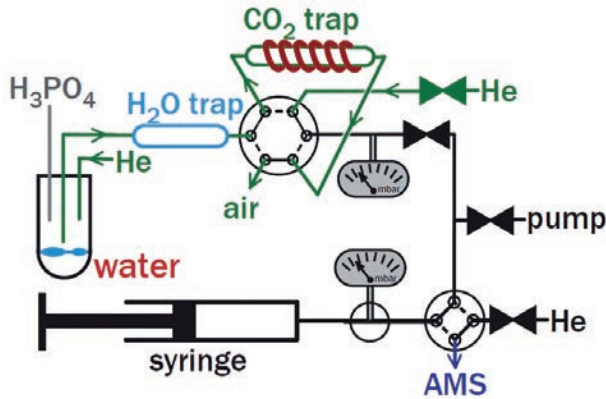


FIG. 3. Layout of the connection of groundwater preparation line to the existing ETHZ AMS gas ion source interface [11].

a modern sample). The AMS measurement of one water sample including sample preparation takes only about 20 minutes.

The method was tested on real groundwater samples and C-14 reference carbonate materials provided by the IAEA as well. We used IAEA carbonates as references because C-14 reference water samples do not exist and the new AMS method can be applied not only for dissolved inorganic carbon but also for solid carbonates in the same way. Because water sample transfer using a classical plastic medical syringe from the sample holder into the septa vial has the possibility to acquire atmospheric CO<sub>2</sub> contamination in the sample we tested the process blank level using high purity deionized (MilliQ®) water added to solid IAEA C1 carbonate to have a better estimation of the processed blank level. Groundwater samples (1 to 4), whose age ranges from very old to modern, were taken from real groundwater wells. The groundwater samples were measured by the conventional GPC method as a reference (see \* results in Table 2). The radiocarbon activity of the CO<sub>2</sub> gas was measured in 60 litre water samples in the case of the GPC method and in 1 mL water in the case of the AMS GI method. Table 2 shows the radiocarbon data of the samples measured by the two different methods.

The reproducibility of AMS GI measurement is excellent as shown by the 3 IAEA-C1, IAEA-C2 and 6 Groundwater-1 parallel measurements. The blank level is very low (< 1.0 pMC). The processed blank (C1 carbonate + MilliQ water) gave just a slightly higher level above the pure IAEA C-1 blank C-14 results (plus 0.1–0.6 pMC, depending on the carbon content of the sample) which could also result from the trace carbon in the MilliQ water used. The IAEA C-2 reference with a known C-14 level has shown an excellent match with the expected value. The presented inter-comparison between our conventional GPC and the new AMS GI methods was also satisfying. Only one sample (Groundwater-1) with the lowest C-14 level (~ 20 pMC) gave a slightly larger difference than the acceptable measurement error. It means that

TABLE 2. RADIOCARBON DATA OF GROUNDWATER TEST AND CARBONATE REFERENCE MATERIALS MEASURED BY AMS GAS ION SOURCE VS. REFERENCE VALUES (IAEA REFERENCE DATA OR WATER WITH KNOWN C-14 LEVEL AS MEASURED BY CONVENTIONAL GPC METHOD)

Sample type	Carbon ( $\mu\text{g}$ )	Measured by AMS GI (pMC)	Reference (GPC*) (pMC)
	55	$0.74 \pm 0.05$	
IAEA-C1 carbonate	52	$0.79 \pm 0.06$	blank
	39	$0.82 \pm 0.07$	
IAEA-C1 carbonate + 1mL deionised water	40	$1.37 \pm 0.11$	processed blank
	81	$0.89 \pm 0.05$	
IAEA-C2 carbonate	40	$41.16 \pm 0.49$	$41.14 \pm 0.03$
	20	$41.14 \pm 0.59$	
	40	$41.19 \pm 0.54$	
		$21.52 \pm 0.37$	
Groundwater-1	73	$21.21 \pm 0.39$	$18.70 \pm 0.13^*$
		$21.81 \pm 0.38$	
		$21.45 \pm 0.36$	
Groundwater-2	126	$21.19 \pm 0.37$	$30.00 \pm 0.10^*$
		$30.21 \pm 0.51$	
Groundwater-3	46	$66.00 \pm 1.20$	$67.00 \pm 0.15^*$
Groundwater-4	73	$91.92 \pm 0.89$	$90.50 \pm 0.30^*$

**Note:** All reported AMS GI results are background subtracted except IAEA-C1 results as they represent the background level.

it is very important to investigate the sample storage effect on AMS samples and other error sources affecting C-14 analyses of groundwater in more detail even for the conventional GPC method.

#### 4. CONCLUSION

A new LSC sample preparation method for liquid scintillation  $^{14}\text{C}$  measurements was implemented at the ATOMKI. The developed  $\text{CO}_2$  absorption method is fast, inexpensive and simple. The corresponding limit of  $^{14}\text{C}$  dating is 31 200 a. The combined uncertainty of the described determination is about 2% in the case of recent carbon.

A very sensitive and high throughput preparation technique for AMS measurement was also developed. The new AMS gas ion source water C-14 analyses require only 1 mL of water sample. The whole measurement takes only 20 min for each

sample. A MICADAS AMS system with online sample preparation line is able to measure  $^{14}\text{C}$  content from 1 mL water. The precision of measurement is more than 1% (for modern samples). The preparation is vastly reduced compared to the other AMS methods and principally allows fully automated measurements of groundwater samples with an auto-sampler.

The two new methods presented can be suitable for  $^{14}\text{C}$  measurements and the dating of hydrological and environmental samples as well. The new AMS facility at the ATOMKI (Debrecen, Hungary) using an EnvironMICADAS AMS system with gas ion source has a great potential for groundwater  $^{14}\text{C}$  analyses.

## REFERENCES

- [1] MITCHELL-BRUKER, S., HAITJEMA, H.M., Modelling steady state conjunctive ground- water and surface water flow with analytic elements, *Water Resour. Res.* **32** 9 (1996) 2725–2732.
- [2] ZHU, C., Estimate of recharge from radiocarbon dating of groundwater and numerical flow and transport modeling, *Water Resour. Res.* **36** 9 (2000) 2607–2620.
- [3] SVINGOR, Ě., MOLNÁR, M., PALCSU, L., Monitoring system with automatic sampling units in the surrounding Paks NPP, *Czechoslovak Journal of Physics* **56** (2006) D133–D139.
- [4] HERTELENDI, E., et al., A counter system for high-precision  $^{14}\text{C}$  dating, *Radiocarbon* **31** 3 (1989) 399–406.
- [5] BELLUOMINI, G., DELFINO, A., MANFRA, L., PETRONE, V., Benzene synthesis for radiocarbon dating and study of the catalyst used for acetylen trimerization, *Int. J. Appl. Radiat. Isot.* **29** 7 (1978) 453–459.
- [6] XIAOMEI, XU., et al., Modifying a sealed tube zinc reduction method for preparation of AMS graphite targets: Reducing background and attaining high precision, *Nucl. Instrum. Methods Phys. Res.* **B259** 1 (2007) 320–329.
- [7] WOO, H.J., et al., Optimization of liquid scintillation counting techniques for the determination of carbon-14 in environmental samples, *J. Radioanal. Nucl. Chem.* **239** 3 (1999) 649–655.
- [8] HORVATINČIĆ, N., BAREŠIĆ, J., BRONIĆ, I.K., OBELIĆ, B., Measurement of low  $^{14}\text{C}$  activities in a liquid scintillation counter in the Zagreb Radiocarbon Laboratory, *Radiocarbon* **46** 1 (2004) 105–116.
- [9] CSONGOR, Ě., SZABÓ, I., HERTELENDI, E., Preparation of counting gas of proportional counters for radiocarbon dating, *Radiochem. Radioanal. Lett.* **55** (1982) 303–310.
- [10] WACKER, L., NĚMEC, M., BOURQUIN, J., A revolutionary graphitization system: Fully automated, compact and simple, *Nucl. Instrum. Methods Phys. Res.* **B 268** (2010) 931–934.
- [11] RUFF, M., et al., A gas ion source for radiocarbon measurements at 200 kV, *Radiocarbon* **49** 2 (2007) 307–314.

# THREE NEW OFFSET $\delta^{11}\text{B}$ ISOTOPE REFERENCE MATERIALS FOR ENVIRONMENTAL BORON ISOTOPE STUDIES

M. ROSNER <sup>a,b</sup>, J. VOGL <sup>a</sup>

<sup>a</sup> BAM Federal Institute for Materials Research and Testing,  
Berlin, Germany

<sup>b</sup> IsoAnalysis UG,  
Berlin, Germany

## Abstract

The isotopic composition of boron is a well established tool in various areas of science and industry. Boron isotope compositions are typically reported as  $\delta^{11}\text{B}$  values which indicate the isotopic difference of a sample relative to the isotope reference material NIST SRM 951. A significant drawback of all of the available boron isotope reference materials is that none of them covers a natural boron isotope composition apart from NIST SRM 951. To fill this gap of required  $\delta^{11}\text{B}$  reference materials three new solution boric acid reference materials were produced, which cover 60‰ of the natural boron isotope variation (–20 to 40‰  $\delta^{11}\text{B}$ ) of about 100‰. The new reference materials are certified for their  $\delta^{11}\text{B}$  values and are commercially available through European Reference Materials® (<http://www.erm-crm.org>). The newly produced and certified boron isotope reference materials will allow straightforward method validation and quality control of boron isotope data.

## 1. INTRODUCTION

Boron isotope composition is a well established chemical quantity allowing important conclusions for scientific and industrial applications. Most of the currently available analytical procedures for the determination of boron isotope compositions, however, are complicated and suffer from difficulties related to the physical and chemical properties of boron (e.g. low mass, volatile boron species).

Despite the complicated analysis techniques, the interest in using boron isotope compositions in the earth and environmental sciences is steadily growing. The natural isotope variation of boron is large ( $\delta^{11}\text{B}$  –30 to +50‰) [1] and therefore enables studies on natural and anthropogenic issues through isotope fractionation or mixing processes. Depending on the pH-value the  $\text{B}(\text{OH})_3$  species and the  $\text{B}(\text{OH})_4^-$  species coexist in different proportions, whereby  $^{11}\text{B}$  prefers the triangular planar structure of  $\text{B}(\text{OH})_3$  and  $^{10}\text{B}$  prefers the tetrahedral structure of  $\text{B}(\text{OH})_4^-$ . The relationship between

pH-value, speciation and coordination of boron is being used to reconstruct palaeo-pH values of the ocean water by means of boron isotope data of marine carbonate phases. Apart from hydrologic studies boron isotopes have been successfully used for classical geo- and cosmo-chemical research [1]. Additionally boron isotopes have been used to study the origin of food products [2].

Because all mass spectrometric measurements are affected by mass discrimination or mass fractionation, the determined isotope ratios are biased relative to the true value. To obtain comparable isotope data, the measurements have to be carried out in a way that the results are traceable either to the International System of Units (SI) or to an internationally accepted standard. This means that the determination of isotope abundance ratios has to be corrected for mass discrimination or mass fractionation by applying an isotope reference material. The determination of relative differences or so called  $\delta$ -values can be related to  $\delta$ -reference materials [3].

Until 2001 only IRMM and NIST offer boron isotope reference materials in solid form either with natural isotopic composition (NIST SRM 951  $\delta^{11}\text{B} = 0\text{‰}$ , IRMM-011) or highly enriched in  $^{10}\text{B}$  (NIST SRM 952). Only IRMM offers two isotope reference materials in liquid form, one with natural boron isotopic composition (IRMM-611) and one enriched in  $^{10}\text{B}$  (IRMM-610), both certified for their elemental amount content.

To enable a more robust validation and quality control for boron isotope analyses of geochemical and environmental samples, this article describes the production and characterization of three  $\delta$ -reference materials (ERM-AE120, -AE121 and -AE122). The reference materials presented here are certified for their  $\delta^{11}\text{B}$  values and can be purchased from European Reference Materials ([www.erm-crm.org](http://www.erm-crm.org)).

## 2. PREPARATION AND CHARACTERIZATION OF THE ISOTOPE REFERENCE MATERIALS

The target values of ERM-AE120, -AE121 and -AE122 have been selected so that together with NIST SRM 951 most of the natural boron isotope variation is covered in equidistant intervals. The target  $\delta^{11}\text{B}$ -values have been selected as  $-20$ ,  $+20$  and  $+40\text{‰}$ . ERM-AE120 has been mixed from two boric acid solutions, one with natural like isotope composition and one enriched in  $^{10}\text{B}$ ; ERM-AE121 and -AE122, have been mixed from two boric acid solutions, one with natural-like isotope composition and one enriched in  $^{11}\text{B}$ . All mother solutions have been analysed for their boron mass fraction as well as their boron isotopic composition by TIMS using IDMS as a calibration technique

The isotopic compositions of all candidate reference materials have been calculated on basis of the gravimetric data as well as on the basis of the TIMS boron isotope measurement results obtained with the  $\text{Na}_2\text{BO}_2^+$  and  $\text{Cs}_2\text{BO}_2^-$ -graphite techniques. Instrumental mass fractionation during TIMS measurements was

TABLE 1. CERTIFIED  $\delta^{11}\text{B}$  VALUES OF ERM-AE120, -AE121 AND -AE122

ERM	B mass fraction (mg/kg)	$\delta^{11}\text{B}$ <sup>a</sup> (‰)
AE120	100.0 (2.0) <sup>a</sup>	-20.2 (6) <sup>b</sup>
AE121	100.0 (2.0) <sup>a</sup>	19.9 (6) <sup>b</sup>
AE122	100.0 (2.0) <sup>a</sup>	39.7 (6) <sup>b</sup>

**Note:** Expanded uncertainties ( $k = 2$ ) are given in brackets: a — informative quantity value; b — certified quantity value.

corrected with a correction factor obtained from concurrently measured IRMM-011 or NIST SRM 951.

ERM-AE120, -AE121 and -AE122 are certified for their respective  $\delta^{11}\text{B}$ -values (vs NIST SRM 951) only. These certified  $\delta^{11}\text{B}$ -values are the arithmetic mean of the gravimetric value, the  $\text{Na}_2\text{BO}_2$  TIMS value and the  $\text{Cs}_2\text{BO}_2$  TIMS value with their corresponding uncertainties (Table 1).

The boron mass fractions in all materials, as well as the boron isotopic composition of ERM-AE120, -AE121 and -AE122 are informative values only (Table 1). The relative expanded uncertainties of the boron mass fractions have been set to 2% based on the results of the stability study.

### 3. CONCLUSION

The  $\delta$ -reference materials ERM-AE120, -AE121 and -AE122 are primarily in-tended to be used for quality control and for validation of chemical and mass spectro-metric procedures for the determination of  $\delta^{11}\text{B}$  values. The three  $\delta$  reference materials are the first reference materials worldwide with natural  $\delta^{11}\text{B}$  values  $\neq 0$ ‰. The certified  $\delta^{11}\text{B}$  values are -20.2‰ for ERM-AE120, 19.9‰ for ERM-AE121 and 39.7‰ for ERM-AE122, each with an expanded uncertainty ( $k = 2$ ) of 0.6‰. The achieved expanded uncertainties of these materials enable reasonable quality control of analytical procedures for  $\delta^{11}\text{B}$  determinations in environmental and geochemical studies. Because they show  $\delta^{11}\text{B}$  values different from 0 and in parallel cover nearly all naturally occurring isotopic variation, these new  $\delta$ -reference materials are particularly useful as secondary reference materials. The equidistant  $\delta^{11}\text{B}$ -values of these materials (incl. NIST SRM 951 for  $\delta^{11}\text{B} = 0$ ) allow several additional features, such as localization of the blank  $\delta^{11}\text{B}$ -value or bracketing approaches.

REFERENCES

- [1] GREW, E.S., ANOVITZ, L.M. (Eds), Boron: Mineralogy, Petrology and Geochemistry, Rev. Mineral. Geochem. **33**, Mineralogical Society of America (1996).
- [2] ROSNER, M., PRITZKOW, W., VOGL, J., VOERKELIUS, S., Development and validation of a method to determine the boron isotopic composition of crop plants, Anal. Chem. **83** (2011) 2562–2568.
- [3] VOGL, J., PRITZKOW, W., Isotope dilution mass spectrometry — A primary method of measurement and its role for RM certification, MAPAN **25** (2010) 135–164.

# ISOBORDAT: AN ONLINE DATABASE ON BORON ISOTOPES

M. PENNISI<sup>a</sup>, A. ADORNI-BRACCESI<sup>a</sup>, D. ANDREANI<sup>a</sup>, L. GORI<sup>a</sup>,  
P.F. SCIUTO<sup>b</sup>, R. GONFIANTINI<sup>a</sup>

<sup>a</sup> Istituto di Geoscienze e Georisorse, CNR,  
Pisa, Italy

<sup>b</sup> Servizio Geologico, Sismico e dei Suoli,  
D.G. Ambiente e Difesa del Suolo e della Costa,  
Regione Emilia Romagna, Bologna, Italy

## Abstract

From 1986, boron isotope data in natural substances increased sharply in scientific publications. Analytical difficulties derived from complex geochemical matrices have been faced and interlaboratory calibrations reported in the boron literature. Boron isotopes are nowadays applied to investigate boron origin and migration in natural waters, sources of boron contamination, water–rock interactions and also contribute to water resource management. This is especially important in those areas where boron content exceeds the local regulations for drinking water supply and boron sources need to be identified. ISOBORDAT, an interactive database on boron isotope composition and content in natural waters is presented to the wider community of boron isotope users. The database's structure, scope and applications are reported, along with a discussion on  $\delta^{11}\text{B}$  values obtained in Italian waters. In the database boron data are structured in the following categories: rainwater, rivers, lakes, groundwater and potential contaminants. New categories (medium and high enthalpy fluids from volcanic and geothermal areas) are anticipated. ISOBORDAT aims to be as interactive as possible and will be developed taking into account information and suggestions received. The database is continually undergoing revision to keep pace with continuous data publication. Indications of data that are missing at present are greatly appreciated.

## 1. INTRODUCTION

Boron has two isotopes:  $^{10}\text{B}$  and  $^{11}\text{B}$ , with relative natural abundances of 20 and 80%, respectively. Boron occurs in nature almost exclusively as boric acid and derivatives and is mainly concentrated in the upper part of the earth's crust. Its high solubility in water and the steric configurations of boric acid and borate ions, coupled with the large relative mass difference between the two isotopes (10%)

and consequent wide isotopic fractionations, make this element a powerful tool to investigate fluid–rock interactions and transport processes in natural waters [1–4].

There are clear indications of significant contributions from human activities in the boron biogeochemical cycle. Anthropogenic boron contaminates the atmosphere through combustion of biomasses and coal and natural waters through releases from mining activities, industrial processing and animal wastes [5–8]. It has been estimated that anthropogenic boron has more than doubled the boron fluxes in the environment, as revealed particularly by boron transport in rivers.

Boron isotopes have contributed considerably to the understanding of the biogeochemical cycle of this element. The variations of the  $^{11}\text{B}/^{10}\text{B}$  ratio have a span of almost 100‰ – which is huge for an element not undergoing redox reactions in nature. The main process determining the isotopic fractionations takes place in two steps:

(i) Hydration of dissolved boric acid:



In the above pH dependent equilibrium, the borate anion  $\text{B(OH)}_4^-$  is depleted by about 30‰ in  $^{11}\text{B}$  with respect to  $\text{B(OH)}_3$  at room temperature;

(ii) Removal of  $\text{B(OH)}_4^-$  by adsorption on clay minerals in soils and aquifers. Adsorption of  $\text{B(OH)}_4^-$  is promoted by its tetrahedral configuration; trigonal  $\text{B(OH)}_3$  is not, or is much less, adsorbed. Adsorption of  $\text{B(OH)}_4^-$  implies a continuous shift to the right of equilibrium [1] with consequent large isotopic fractionations due to a Rayleigh-type mechanism.

The isotopic fractionations of boron and interactions with silicate matrices in water systems are currently investigated both in the laboratory and in different natural settings. The isotopic effects of boron adsorption by organic matter and oxides and hydroxides also represent a recent field of interest and a key point in understanding the behaviour of boron isotopes in weathering processes and related hydrological applications [9].

Over the past two decades the significant improvements achieved in the determination of the boron isotope ratio in geologic materials mainly concern thermal ionization spectrometry, inductively coupled plasma mass spectrometry (ICP-MS) and secondary ion mass spectrometry or ion microprobe. In particular, in environmental studies the advent of multiple collector ICP-MS offers new possibilities in the precision and range of materials that can be analysed, with more rapid analysis and smaller sample sizes. However, chemical procedures cannot be avoided and their efficiency is complicated when boron separation by organic matter is required.

The interest and application of boron isotopes in environmental studies has been rapidly growing, in parallel with technical procedure advances. Boron is used also in combination with other environmental isotopic fingerprints [5]. Surface waters and groundwater are major fields of application for boron isotopes, which help

in identifying natural and anthropogenic sources of dissolved boron, studying processes that remove it from its original reservoir and redistribute it in natural waters, and investigating interactions and ionexchange processes with rocks.

## 2. BORON ISOTOPE DATABASE: ISOBORDAT

On the basis of its twenty years' experience in boron isotope geochemistry [10–12], the Institute of Geochemistry and Georesources of Pisa has started to compile a database (<http://isobordat.igg.cnr.it/>) aiming to include all the isotopic data on boron in natural waters reported in the scientific literature. The database is here submitted for the first time to the wider community of boron isotope users. It includes currently values on about 400 'cold' natural waters, but its extension to medium and high enthalpy fluids from volcanic and geothermal areas is anticipated.

Compilation of a database is by nature a permanent 'work in progress', as data continue to be produced and others wait to be discovered in obscure publications addressed to a limited circle of readers. In order to have a database as complete as possible, the collaboration of the whole boron isotope community is necessary. We would appreciate, therefore, if our colleagues would supply us with any boron isotope data in their possession that are missing in the database, together with the basic information needed for its use in science and practical applications. The inclusion of unpublished data — all laboratories have set aside data which are, so to say, 'lost' to the scientific community because they most probably will never be published — is also envisaged: anyone wishing to use these unpublished data is required to quote the source.

We give below some basic information on the structure of the database.

The data are grouped in five categories, according to the sample nature: rainwaters, surface waters — rivers, surface water — lakes, groundwater, natural and anthropogenic contaminants. The last category has been added because boron isotopes are frequently used in water resources contamination studies.

For each sample, the data reported are:

- Sampling site: geographical location, main characteristics. E.g.: for groundwater: well, spring, shallow or deep (confined) aquifer.
- Sampling date.
- $\delta^{11}\text{B}$  ‰, expressed vs. the reference material NBS SRM–951. No measurement uncertainty is quoted, however, data of questionable quality will not be included in the database.
- Analytical technique. E.g.: PTIMS, NTIMS, etc.
- B concentration, expressed for waters in mg/L and for solid compounds in mg/kg.
- Bibliographic reference(s).

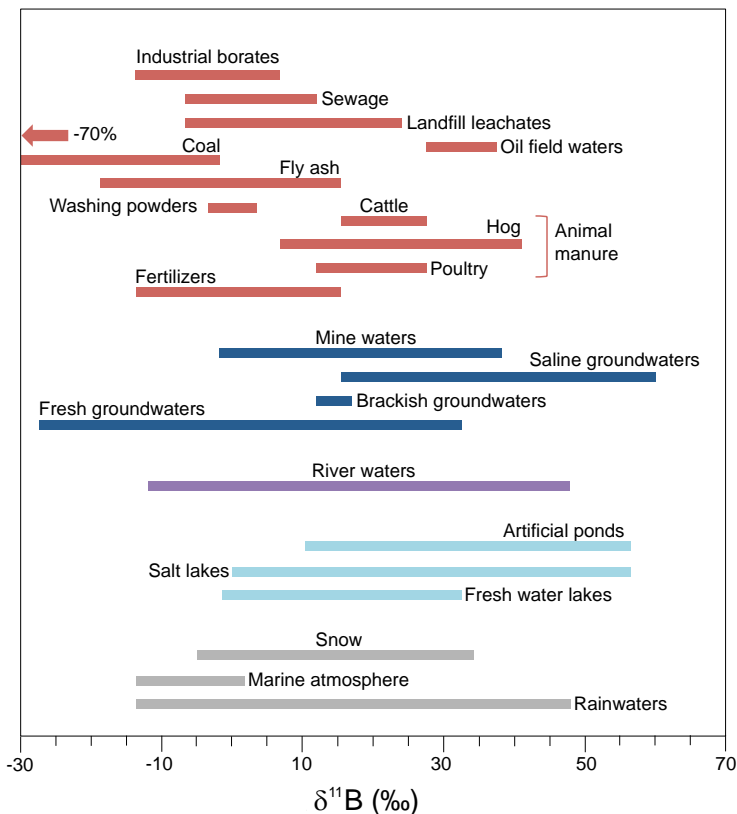


FIG. 1. Variability of  $\delta^{11}\text{B}$  (‰) in the different ISOBORDAT categories.

Isotopic data on potential boron contaminants of natural waters are gathered together in a section of the Isobordat database. These contaminants include: detergents, chemical fertilizers and manures, mining tailings and wastes of industrial processing of boron minerals. The isotopic composition of potential contaminants, which spans over a wide range, helps in identifying boron contamination sources and geochemical processes undergone in natural waters.

The ISOBORDAT web page has been created with the open CMS Joomla! 1.5 and Jx List Files v1.3 on a small xampp server (thanks to all open communities

Although  $\delta^{11}\text{B}$  values are all expressed vs. the same reference, comparison of data obtained in different laboratories and/or in different time periods may not be so straightforward. Experience has shown that interlaboratory calibration of boron isotope data is sometimes questionable, especially when different analytical techniques are involved [11–12]. The problem, however, cannot be tackled in this database.

Data on natural waters collected in ISOBORDAT show variations on  $^{11}\text{B}/^{10}\text{B}$  ratio of almost 60% in the categories Rainwaters, Rivers, Lakes, that reaches 90%

in the category Groundwater (Fig. 1). The observed span is huge for an element not undergoing redox reactions in nature. The variations on  $^{11}\text{B}/^{10}\text{B}$  ratio observed for the category Contaminants is also wide and spans about 25‰ for inorganic products and 110‰ for organic products.

### 3. ISOBORDAT: THE ITALIAN DATA

Statistical treatment of data is the most straightforward use of a database. We show below a simple statistical elaboration of more than hundred boron isotopic data on Italian groundwaters from disparate geological settings. All data have been obtained by positive thermal ionization mass spectrometry (PTIMS) in our institute

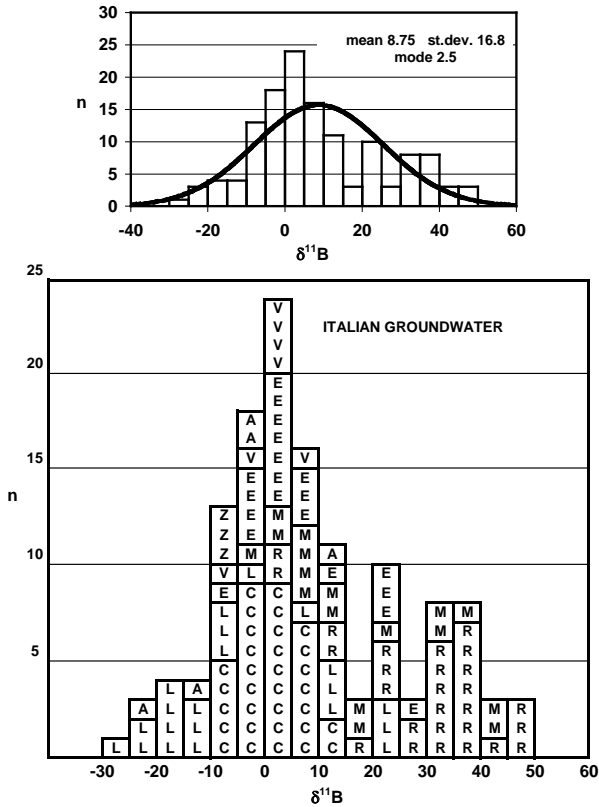


FIG. 2. Frequency distribution of  $\delta^{11}\text{B}$  values (‰) in Italian groundwaters. Letters indicate sampling areas: A – Arezzo (Tuscany), C – Val di Cornia (Tuscany), E – Etna (Sicily), L – Larderello-Val di Cecina (Tuscany), M – Modena (Emilia-Romagna), R – Ravenna (Emilia Romagna), V – Vesuvio (Campania), Z – Roma (Lazio). Data from A, M, V, Z are unpublished (P. Conti, G. Martinelli, R. Somma and D. Amicizia).

in the last two decades and are perfectly comparable [10–12]. Part of the data derive from on going investigations and are unpublished.

The  $\delta^{11}\text{B}$  values scan from  $-30\text{‰}$  to  $+50\text{‰}$ , i.e. over a  $80\text{‰}$  range and their frequency distribution is shown in the histogram of Fig. 2. The distribution is skewed towards the positive values and therefore the mean value is about  $7\text{‰}$  higher than the mode (upper part of Fig. 2). The asymmetric distribution is in part due to the number of samples analysed in different investigations. However, a close inspection of Fig. 2 reveals:

- (1) Most  $\delta^{11}\text{B}$  values span from  $-10\text{‰}$  to  $+25\text{‰}$ , which appears the most frequent range for groundwater boron. Data from all investigated areas are found within this range. The explanation of boron isotope variations within each studied area demands a closer examination of the specific geological and geochemical characteristics of aquifers, which is beyond the scope of this simple statistical treatment. The interested reader can find details in Refs [13–16]. In this range fall data from C (Cornia area, EU Boremed project), where the complex interaction of groundwater with geothermal fluids, seawater and sediments was recognized [15].
- (2)  $\delta^{11}\text{B}$  values more negative than  $-10\text{‰}$  have been found in groundwater exposed to boron contamination (investigations L and A). In particular, L values derive from shallow groundwater contaminated by industrial wastes from boron mineral processing in Larderello released in surface waters. Subsequently, after releases were stopped, boron was further depleted in  $^{11}\text{B}$  through progressive desorption of borate adsorbed on clay minerals of the aquifer [13].  $^{11}\text{B}$  is preferentially removed in desorption and thus the remaining adsorbed boron stock becomes enriched in  $^{10}\text{B}$ : this Rayleigh type mechanism is capable of producing very negative  $\delta^{11}\text{B}$  values.
- (3) The  $\delta^{11}\text{B}$  values more positive than  $+30\text{‰}$  mostly derive from shallow groundwater in coastal aquifers (investigation R). The R area is interested by diffuse salinization of soils and waters, carrying dissolved boron with a typical  $\delta^{11}\text{B}$  of  $+40\text{‰}$ . Thus, high  $\delta^{11}\text{B}$  values indicate the prevalent marine origin of dissolved boron [14]. Partial adsorption of borate ions  $\text{B}(\text{OH})_4^-$  results in an additional  $^{11}\text{B}$  enrichment of residual dissolved boron.

#### 4. CONCLUSION

We intend to compile a database including all — that is, as many as possible — data on the isotopic composition and concentration of boron dissolved in natural waters. In order to reach our objective, the cooperation of the whole boron isotope community is necessary. We believe that such a database will be of great help to boron isotope hydrologists and geochemists by speeding up the research of, and the comparison with, data already existing in the scientific literature.

## ACKNOWLEDGEMENTS

The authors are grateful to Elisa Sacchi for encouraging the ISOBORDAT startup.

## REFERENCES

- [1] PALMER, M.R., SWIHART, G.H., Boron isotope geochemistry: An overview, *Rev. Mineral. Geochem.* **33** (1996) 709–744.
- [2] FARBER, E., et al., The origin and mechanisms of salinization of the Lower Jordan river, *Geochim. Cosmochim. Acta* **68** (2004) 1989–2006.
- [3] VENGOSH, A., et al., A multi-isotope (B, SR, O, H, and C) and age dating ( $^3\text{H}$ – $^3\text{He}$  and  $^{14}\text{C}$ ) study of groundwater from Salinas Valley, California: Hydrochemistry, dynamics and contamination processes, *Water Resour. Res.* **38** (2002) 1–17.
- [4] LEMARCHAND, D., et al., Boron isotope systematics in large rivers: Implications for the marine boron budget and paleo-pH reconstruction over the Cenozoic, *Chem. Geol.* **190** (2002) 123–140.
- [5] WIDORY, D., et al. Nitrate in groundwater: An isotopic multi-tracer approach, *J. Contam. Hydrol.* **72** (2004) 165–188.
- [6] EINSENHUT, S., et al., Determination of boron isotopic variations in aquatic systems with negative thermal ionization mass spectrometry as a tracer for anthropogenic influences, *Fresenius J. Anal. Chem.* **354** (1996) 903–909.
- [7] BARTH, S., Application of boron isotopes for tracing sources of anthropogenic contamination in groundwater, *Water Res.* **32** (1998) 685–690.
- [8] LEENHOUTS, J.M., et al., Utilization of intrinsic boron isotopes as co-migrating tracers for identifying potential nitrate contamination sources, *Ground Water* **36** (1998) 240–250.
- [9] LEMARCHAND, E., et al., How surface complexes impact boron isotope fractionation: Evidence from Fe and Mn oxides sorption experiments, *Earth Planet. Sci. Lett.* **260** (2007) 277–296.
- [10] TONARINI, S., et al., Precise boron isotopic analysis of complex silicate (rock) samples using alkali carbonate fusion and ion-exchange separation, *Chem. Geol.* **142** (1997) 129–137.
- [11] TONARINI, S., et al., Intercomparison of boron isotope and concentration measurements — Part I: Selection, preparation and homogeneity tests of the intercomparison materials, *Geostandards Newsletter* **27** 1 (2003) 21–39.
- [12] GONFIANTINI, R., et al., Intercomparison of boron isotope and concentration measurements, Part II: Evaluation of results, *Geostandards Newsletter* **27** 1 (2003) 41–57.
- [13] PENNISI, M., et al., Boron, Sr, O, and H isotope geochemistry of groundwaters from Mt. Etna (Sicily) — Hydrologic implications, *Geochim. Cosmochim. Acta* **64** (2000) 961–974.

- [14] PENNISI, M., et al., The utilization of boron and strontium isotopes for the assessment of boron contamination of the Cecina River alluvial aquifer (central-western Tuscany, Italy), *Appl. Geochem.* **21** (2006) 643–655.
- [15] PENNISI, M., et al., Behaviour of boron and strontium isotopes in groundwater–aquifer interactions in the Cornia Plain (Tuscany, Italy), *Appl. Geochem.* **21** (2006) 1169–1183.
- [16] PETRINI, R., et al., “Application of O–H–B–Sr isotope systematics to the exploration of salinization and flushing in coastal aquifers: Preliminary data from the Pia-lassa Baiona ecosystem (Adriatic Sea)”, *Proc. Intl Congress on The Air, Water and Soil Quality, Imola 2009, Environmental Quality* **3** (2009) 37–42.

# **NORMALIZATION METHODS AND SELECTION STRATEGIES FOR REFERENCE MATERIALS IN STABLE ISOTOPE ANALYSES – REVIEW**

G. SKRZYPEK

West Australian Biogeochemistry Centre,  
John de Laeter Centre of Mass Spectrometry,  
School of Plant Biology, University of Western Australia,  
Crawley, Australia

R. SADLER

School of Agricultural and Resource Economics,  
University of Western Australia,  
Crawley, Australia

D. PAUL

Department of Civil Engineering (Geosciences),  
Indian Institute of Technology Kanpur,  
Kanpur, India

I. FÓRIZS

Institute for Geochemical Research,  
Hungarian Academy of Sciences,  
Budapest, Hungary

## **Abstract**

Stable isotope ratio mass spectrometers are highly precise, but not accurate instruments. Therefore, results have to be normalized to one of the isotope scales (e.g., VSMOW, VPDB) based on well calibrated reference materials. The selection of reference materials, numbers of replicates,  $\delta$ -values of these reference materials and normalization technique have been identified as crucial in determining the uncertainty associated with the final results. The most common normalization techniques and reference materials have been tested using both Monte Carlo simulations and laboratory experiments to investigate aspects of error propagation during the normalization of isotope data. The range of observed differences justifies the need to employ the same sets of standards worldwide for each element and each stable isotope analytical technique.

## 1. INTRODUCTION

The stable isotope scales have been primarily defined as SMOW [1] for hydrogen and oxygen, and PDB [2] for carbon and oxygen. These scales have been later revised and more precisely calibrated, when the exhausted original reference materials (e.g. PDB) were replaced by new primary reference materials (e.g. Refs [3–7]). For the new redefined scales it is recommended that  $\delta$ -values be measured and expressed relative to two international primary reference materials, e.g. NBS 19 and L-SVEC for  $\delta^{13}\text{C}$  (VPDB [8, 9]) and VSMOW–2 and SLAP for  $\delta^{18}\text{O}$  (VSMOW [10]). However, these primary reference materials cannot be always used for normalization of analysed samples owing to technical reasons [10, 11], and in keeping with the principle of identical treatment [12]. Therefore, several other secondary reference materials have been calibrated by the International Union of Pure and Applied Chemistry (IUPAC), the International Atomic Energy Agency (IAEA), the United States Geological Survey (USGS) and others (e.g. Refs [8–10]). These reference materials are now available from the IAEA and the National Institute of Standards and Technology (NIST) for all stable isotope laboratories.

A stable isotope analyst has to make a number of important decisions regarding how to best determine the ‘true’ stable isotope composition of analysed samples in reference to an international scale. It has to be decided which reference materials should be used, the number of reference materials and how many repetitions of each standard is most appropriate for a desired level of precision, and what normalization procedure should be selected. In this paper we summarize what is known about propagation of uncertainties associated with normalization procedures and propagation of uncertainties associated with reference materials used as anchors for the determination of ‘true’ values for  $\delta^{13}\text{C}$  and  $\delta^{18}\text{O}$ .

## 2. DISCUSSION

Several normalization methods transforming the ‘raw’ value obtained from mass spectrometers to one of the internationally recognized scales have been developed. However, as summarized by Paul et al. [13], different normalization transforms alone may lead to inconsistencies between laboratories. The most common normalization procedures are: single point anchoring (versus working gas and certified reference standard), modified single point normalization, linear shift between the measured and the true isotopic composition of two certified reference standards and two point and multi point linear normalization methods. The accuracy of these various normalization methods has been compared by using analytical laboratory data by Paul et al. [13], with the single point and normalization versus tank calibrations resulting in the largest normalization errors, which also exceed the analytical uncertainty recommended for  $\delta^{13}\text{C}$ . The normalization error depends greatly on

the relative differences between the stable isotope composition of the reference material and the sample. On the other hand, the normalization methods using two or more certified reference standards produces a smaller normalization error, if the reference materials are bracketing the whole range of isotopic composition of unknown samples. These conclusions are in agreement with the approach proposed by Coplen et al [8, 9] for the stable carbon isotope referencing. These studies strongly support the use of two point or multipoint normalisation methods based on regression line as producing the most reliable results [13].

However, even when a multipoint normalization method is used, the final normalization error still depends highly on the selection of reference materials, their  $\delta$ -values and the number of their replicates. Furthermore, the uncertainties associated with the calibration of each of the reference materials influences the overall normalization error. Skrzypek et al. [14] performed both Monte Carlo simulations and laboratory experiments to investigate aspects of error propagation during the normalization of stable carbon isotope data. The normalization error can be reduced by approximately 50% for  $\delta^{13}\text{C}$  (compared to the two point normalization) if either two standards are analysed four times each, or four standards two times each. It has been concluded that increasing both the number of different reference standards and the number of repetitions of each of these standards reduces the normalization error. For instance, for stable carbon isotope analyses using the EA technique, the optimal set of reference materials would be IAEA-CO-9, L SVEC, NBS 19 and IAEA-CO-1, with the next best option being L SVEC, NBS 22, USGS24 and NBS 19 [14]. Despite the availability of several other reference materials, these two sets should be used to best minimize the errors.

The level of reduction in errors is especially visible when the reference materials employed have relatively high uncertainty, due to the precision of the analytical technique (e.g. high temperature conversion) or its chemical composition (e.g.,  $\delta^{18}\text{O}$  yield as CO from nitrate materials) [10, 15]. Similarly, for stable carbon isotope composition, a much lower uncertainty in stable oxygen isotope analyses can be easily achieved through an optimal selection of reference materials. Skrzypek and Sadler [15] calculated that the best performing pairs, minimizing the errors for nitrates, are USGS35 and USGS34; for sulphates IAEA-SO-6 and IAEA-SO-5; and for organic materials IAEA-601 and IAEA-602. For both carbon and oxygen analyses, the observed errors were lowest when reference materials were located closest to the extremes of the considered range, and highest for reference materials covering only a narrow range of  $\delta$ -values. However, the difference is especially distinct for  $\delta^{18}\text{O}$  solid reference materials due to their higher uncertainties. A possible memory effect should also be taken into account during the selection of reference materials.

### 3. CONCLUSIONS

We argue that the optimal selection of reference materials and an increase in the numbers of their replicates will significantly improve the overall uncertainty in analysed samples. However, of greater importance is that the same set of standards should always be employed in stable isotope laboratories given the high degree of variability in normalization errors when the selection of reference materials is varied. A unified protocol for the normalization procedures, including a clearly defined optimal set of reference materials, would improve significantly the interlaboratory comparison of results by eliminating inconsistencies resulting from application of differing sets of reference materials by separate laboratories.

### ACKNOWLEDGEMENTS

G.S. was supported as the John de Laeter Research Fellow at the John de Laeter Centre of Mass Spectrometry, Western Australia.

### REFERENCES

- [1] CRAIG, H., Standard for reporting concentrations of deuterium and oxygen-18 in natural waters, *Science* **133** (1961) 1833–1834.
- [2] UREY, H.C., LOWENSTAM, H.A., EPSTEIN, S., MCKINNEY, C.R., Measurement of paleotemperatures and temperatures of the Upper Cretaceous of England, Denmark and the Southeastern United States, *Geological Society of America Bulletin* **62** (1951) 399–416.
- [3] COPLEN, T.B., Normalization of oxygen and hydrogen isotope data, *Chem. Geol.: Isotope Geoscience Section* **72** (1988) 293–297.
- [4] COPLEN, T.B., KENDALL, C., HOPPLE, J., Comparison of stable isotope reference samples, *Nature* **302** (1983) 236–238.
- [5] WERNER, R.A., BRAND, W.A., Referencing strategies and techniques in stable isotope ratio analysis, *Rapid Commun. Mass Spectrom.* **15** (2001) 501–519.
- [6] GONFIANTINI, R., Standards for stable isotope measurements in natural compounds, *Nature* **271** (1978) 534–536.
- [7] EPSTEIN, S., MAYEDA, T., Variation of O<sup>18</sup> content of waters from natural sources, *Geochim. Cosmochim. Acta* **4** (1953) 213–224.
- [8] COPLEN, T.B., et al., New guidelines for  $\delta^{13}\text{C}$  measurements, *Anal. Chem.* **78** (2006) 2439–2441.
- [9] COPLEN, T.B., et al., After two decades a second anchor for the VPDB  $\delta^{13}\text{C}$  scale, *Rapid Commun. Mass Spectrom.* **20** (2006) 3165–3166.
- [10] BRAND, W.A., et al., Comprehensive inter-laboratory calibration of reference materials for  $\delta^{18}\text{O}$  versus VSMOW using various on-line high-temperature conversion techniques, *Rapid Comm. Mass Spectrom.* **23** (2009) 999–1019.

- [11] HALAS, S., et al., Inter-laboratory calibration of new silver orthophosphate comparison materials for the stable oxygen isotope analysis of phosphates, *Rapid Commun. Mass Spectrom.* **25** (2011) 579–584.
- [12] BRENNAN, J.T., et al., High-precision continuous-flow isotope ratio mass spectrometry, *Mass Spectrom. Rev.* **16** (1997) 227–258.
- [13] PAUL, D., SKRZYPEK, G., FÓRIZS, I., Normalization of measured stable isotopic compositions to isotope reference scales — A review, *Rapid Comm. Mass Spectrom.* **21** (2007) 3006–3014.
- [14] SKRZYPEK, G., SADLER, R., PAUL, D., Error propagation in normalization of stable isotope data: A Monte Carlo analysis, *Rapid Comm. Mass Spectrom.* **24** (2010) 2697–2705.
- [15] SKRZYPEK, G., SADLER, R., A strategy for selection of reference materials in stable oxygen isotope analyses of solid materials, *Rapid Commun. Mass Spectrom.* **25** (2011) 1625–1630.



# IAEA REFERENCE MATERIALS FOR QUALITY ASSURANCE: A STUDY IN THE QUALITY CONTROL OF MARINE RADIOACTIVITY

PHAM MAI KHANH<sup>a</sup>, J. BARTOCCI<sup>a</sup>, E. CHAMIZO<sup>b</sup>, J. GASTAUD<sup>a</sup>,  
J.-M. GÓMEZ-GUZMÁN<sup>b</sup>, H. NIES<sup>a</sup>, E. VASILEVA<sup>a</sup>, M. BETTI<sup>a</sup>

<sup>a</sup> International Atomic Energy Agency,  
Environment Laboratory, Monaco

<sup>b</sup> Centro Nacional de Aceleradores,  
Seville, Spain

## Abstract

The IAEA's Marine Environment Laboratories has assisted laboratories in Analytical Quality Control Services (AQCS) for the analysis of radionuclides in the marine environment since the early seventies. The AQCS programme, now named Reference Products for Environment and Trade, is recognized as an essential component of quality assurance and control and for the development and validation of analytical methods, through its worldwide and regional interlaboratory comparisons and the provision of reference methods and Reference Materials/Certified Reference Materials (RMs/CRMs). A total of 49 interlaboratory exercises were organized and 42 RMs/CRMs were produced for marine radioactivity studies. Different techniques such as radiometric methods with X ray, gamma spectrometry, alpha spectrometry, beta counter, liquid scintillation counter as well as mass spectrometry (ICP-MS, AMS, TIMS...) are applied for the characterization during certification process. An overview of prepared Certified Reference Materials (CRMs) for radionuclides in marine matrices will be presented as well as lessons learned from interlaboratory comparisons (ICs) and Proficiency Tests (PTs). A characterization of a new CRM for radionuclides in IAEA-446, Baltic Sea seaweed (*Fucus vesiculosus*), as well as a specific case of using Accelerator Mass Spectrometry (AMS) technique to characterize I-129 in sea water (IAEA-418) and seaweed sample (IAEA-446), will be discussed. Available RMs/CRMs are listed and can be ordered and purchased through the IAEA website <http://nucleus.iaea.org/rpst/>.

## 1. INTRODUCTION

Reference materials (RM) represent samples of well established properties used for the assessment of analytical methods. With the aims of increasing the importance of the quality of data, of providing the required traceability to SI standard and of improving the accuracy and precision of Member State (MS) laboratories, the AQCS

programme, now named Reference Products for Environment and Trade, should also concentrate on the production of Certified Reference Material (CRM). The CRM should be available for different marine environmental matrices (sediment, water, biota...) [1–3]. Both RM and CRM have great impact on the development of methods of known accuracy. They represent an important benchmark in quality assurance (QA) and quality control (QC), helping identify weak methodologies, detecting training needs, upgrading the quality of laboratories' performance and assessing the validity of analytical methods. The reference methods or international standard methods can only be accepted on the basis of interlaboratory tests performed on selected CRM.

The IAEA Marine Environment Laboratory (MEL) has produced RM and CRM as the final products of their worldwide interlaboratory comparison exercises during the last 40 years. A total of 49 interlaboratory comparison exercises were organized and 42 reference materials and certified reference materials were produced for radionuclides in the marine environment. The production of CRM was performed according to ISO standards [3], using mostly the data contributed from these exercises and combined with high quality data supplied from further expert laboratories [4–9]. The required long term availability of CRM (over 10 years) necessitates their long term stability and the collection and preparation of large volume samples (over 100 kg, depending on the activity concentration of sample originating from different places).

We report here some results obtained from a characterization campaign of a new CRM for radionuclides in Baltic Sea seaweed (*Fucus vesiculosus*) (IAEA-446), as well as a specific case of using AMS technique to characterize I-129 in sea water (IAEA-418) and seaweed sample (IAEA-446). An overview of prepared RMs and CRMs for radionuclides in marine matrices will be presented as well as lessons learned from interlaboratory comparisons (ICs) and Proficiency Tests (PTs)

## 2. MATERIALS AND METHODS

### 2.1. Characterization of Baltic Sea seaweed (IAEA-446)

#### 2.1.1. Material description

The seaweed known as bladder wrack, with the Latin name '*Fucus vesiculosus*', was sampled 11–27 July 2006 from a coastline in the western part of the Baltic Sea (54°57' N, 11°59' E). The total mass of the wet sample was 718 kg. The seaweed was first dried in the open air and subsequently in heating cabinets at 85°C leaving a total dry weight of 105 kg. The sample was then ground into powder, passed through a 250 µm sieve, homogenized by mixing in a nitrogen atmosphere, bottled and sealed in polyethylene flasks (100 g units) and coded as IAEA-446. A total of 900 bottles was

produced. All these bottles, each containing 100 g of seaweed powder, were sterilised at 10 kGy ( $^{60}\text{Co}$ ) in an irradiation facility (Isotron, France). The moisture content of the sample was found to be not negligible (5.5%). This important moisture content of the samples should be checked prior to sample use by drying at  $60^\circ\text{C}$  in an oven until a constant weight is obtained. It is expected that moisture will be absorbed again after open exposure.

### 2.1.2. Homogeneity tests

The first homogeneity test, between bottles, has been done through gamma spectrometry and alpha spectrometry. The results of 16–20 aliquots for different weights of samples (10–60 g depending on the technique used for different radionuclides) showed a sufficient homogeneity for Cs-137, K-40, Pu-238,

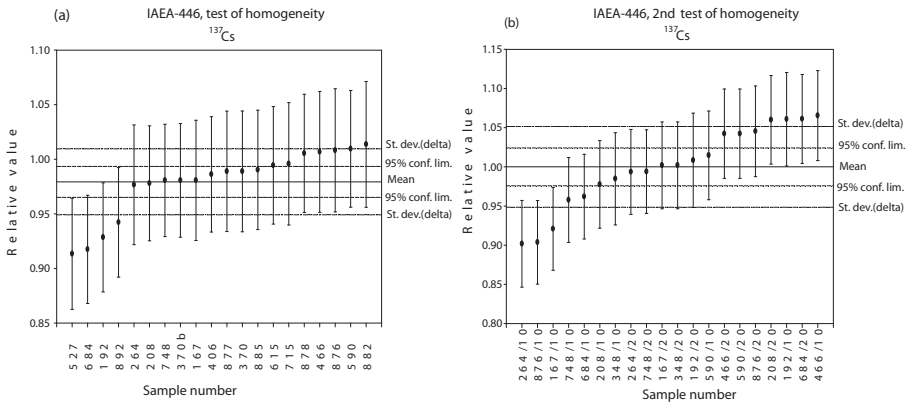


Fig. 1. Homogeneity test for Cs-137 in IAEA-446 (a) between bottles, (b) within bottle.

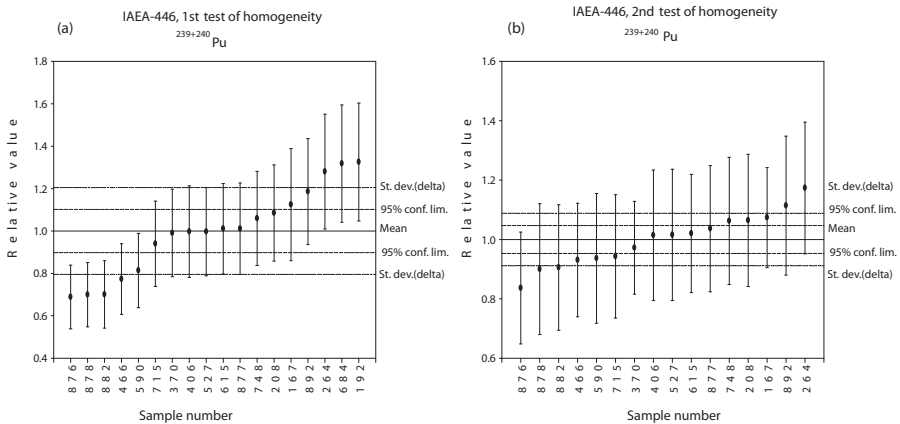


Fig. 2. Homogeneity test for Pu-239+240 in IAEA-446 (a) between bottles, (b) within bottle.

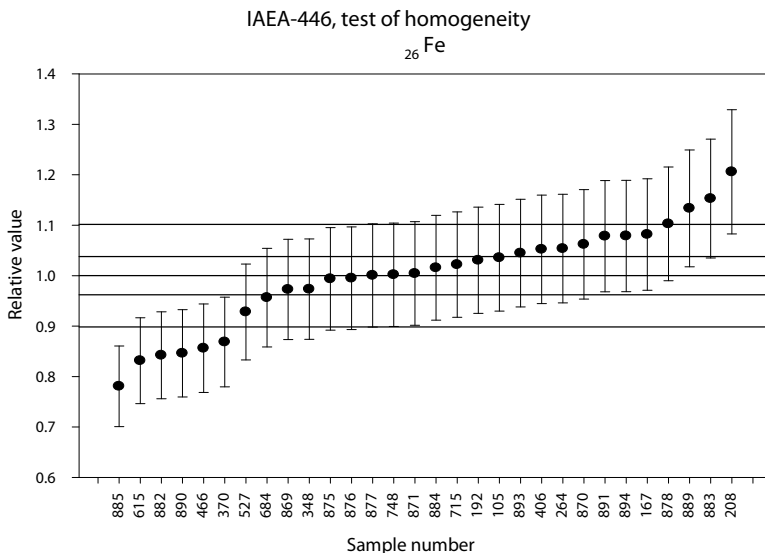


Fig. 3. Homogeneity test for stable isotope Fe in IAEA-446.

Pu-239+240, Th-228, Th-230, Th-232, Po-210 with the coefficient of variation below 15%–20%, depending on the activity range. The second test, within bottles, was done for a further 16–20 aliquots, through gamma spectrometry and through alpha spectrometry and ICP-MS for the determination of Cs-137, Pu-238, Pu-239+240 and U activities respectively. The ‘between samples’ variances showed no significant differences from the ‘within sample’ variances for the radionuclides tested. Results were identical within statistical uncertainties. Thus, the material can be considered sufficiently homogeneous for the radionuclides tested. Below are two examples of homogeneity test results for Cs-137 (determined by gamma spectrometry for 60 and 10 g of samples, Fig. 1a and Fig. 1b respectively) and Pu-239+240 (determined by alpha spectrometry with prior radiochemical separation for 50 g and 15g, Fig. 2a, Fig. 2b respectively).

An additional homogeneity test for major and trace elements (P, S, Cl, K, Ca, Fe, Ni, Cu, Zn, As, Br, Sr, I, Ba, Pb) for 4g of Fucus sample was done by XFR. The coefficient of variation was below 10% for XFR determined elements. Below is one example of the element iron as determined by XFR (Fig. 3).

## 2.2. Using AMS technique to characterization of reference material

AMS is a powerful mass spectrometry technique which is being recently used for the characterization of  $^{129}\text{I}$  and other isotopes in new RM candidate materials. This is the case for seawater sample (IAEA-418) from the Mediterranean Sea and

for the *Fucus* sample (IAEA-446) from the Baltic Sea. The details of a former case study can be found in a recent IAEA publication [10] and in a scientific paper [9]. Following the discussion during the International AMS Conference held in Vienna in 2000, the AMS scientific community strongly recommended the production of a low level  $^{129}\text{I}$  seawater RM, which could be used by AMS laboratories in their radiological assessment and oceanographic studies. Due to the behaviour of  $^{129}\text{I}$  in the marine environment (it is dissolved in seawater), and its long half-life ( $1.57 \times 10^7$  a), it is an ideal tracer for studying the mixing and transport of water masses in the world oceans. However, the detailed study of the latter case is ongoing and the results of Pu isotopes obtained from AMS (Seville, Spain) will be discussed later on when the feedback from the participants in the interlaboratory comparison of RM IAEA-446 are available.

### 3. AVAILABLE CRMs FOR RADIONUCLIDES IN MARINE SAMPLES AND LESSONS LEARNED FROM INTERLABORATORY COMPARISONS (IC) AND PROFICIENCY TESTS (PT)

The list of available CRMs, which has been recently released, with a large range of radionuclides for different matrices of marine samples, is summarized in Table 1. Available RMs/CRMs can be ordered and purchased through the IAEA website <http://nucleus.iaea.org/rpst/>.

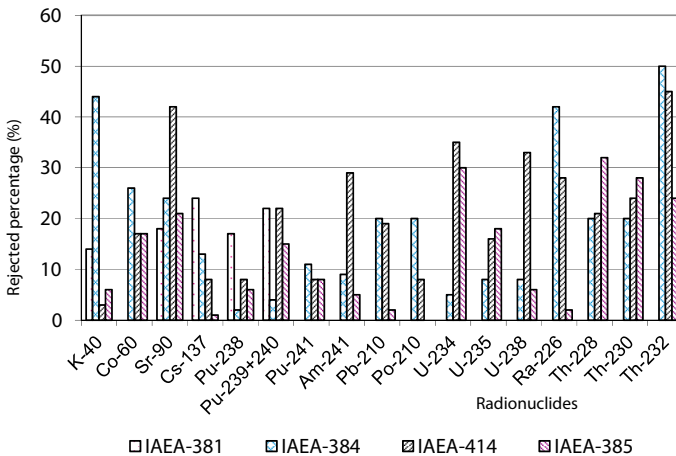


Fig. 4. Laboratory performance obtained from some most recent interlaboratory comparison exercises for radionuclides in different matrix of marine samples organized by IAEA-MEL.

TABLE 1. REFERENCE MATERIALS RECENTLY PRODUCED BY THE RADIOMETRICS LABORATORY OF IAEA-MEL FOR RADIONUCLIDES IN THE MARINE ENVIRONMENT

Code	Matrix, place of the origin	Radionuclide values	
		Reference	Information
IAEA-381	Seawater, the Irish Sea	$^{40}\text{K}$ , $^{90}\text{Sr}$ , $^{137}\text{Cs}$ , $^{237}\text{Np}$ , $^{238}\text{Pu}$ , $^{239}\text{Pu}$ , $^{240}\text{Pu}$ , $^{239,240}\text{Pu}$ , $^{241}\text{Am}$	$^3\text{H}$ , $^{235}\text{Sb}$ , $^{234}\text{U}$ , $^{235}\text{U}$ , $^{236}\text{U}$ , $^{238}\text{U}$ , $^{241}\text{Pu}$ , $^{244}\text{Cm}$
IAEA-384	Sediment, Fangataufa lagoon	$^{40}\text{K}$ , $^{60}\text{Co}$ , $^{155}\text{Eu}$ , $^{210}\text{Pb}$ , $^{210}\text{Po}$ , $^{230}\text{Th}$ , $^{234}\text{Th}$ , $^{234}\text{U}$ , $^{235}\text{U}$ , $^{238}\text{U}$ , $^{238}\text{Pu}$ , $^{239,240}\text{Pu}$ , $^{241}\text{Am}$	$^{90}\text{Sr}$ , $^{137}\text{Cs}$ , $^{214}\text{Bi}$ , $^{214}\text{Pb}$ , $^{226}\text{Ra}$ , $^{228}\text{Ac}$ , $^{232}\text{Th}$ , $^{237}\text{Np}$ , $^{239}\text{Pu}$ , $^{240}\text{Pu}$ , $^{241}\text{Pu}$
IAEA-414	Fish flesh, the Irish and North Seas	$^{40}\text{K}$ , $^{137}\text{Cs}$ , $^{226}\text{Ra}$ , $^{232}\text{Th}$ , $^{235}\text{U}$ , $^{238}\text{U}$ , $^{238}\text{Pu}$ , $^{239,240}\text{Pu}$ , $^{241}\text{Am}$	$^{90}\text{Sr}$ , $^{208}\text{Tl}$ , $^{210}\text{Po}$ , $^{210}\text{Pb}$ , $^{212}\text{Bi}$ , $^{212}\text{Pb}$ , $^{214}\text{Bi}$ , $^{214}\text{Pb}$ , $^{228}\text{Ac}$ , $^{228}\text{Ra}$ , $^{228}\text{Th}$ , $^{230}\text{Th}$ , $^{234}\text{Th}$ , $^{234}\text{U}$ , $^{239}\text{Pu}$ , $^{240}\text{Pu}$
IAEA-385	Sediment, Irish Sea	$^{40}\text{K}$ , $^{137}\text{Cs}$ , $^{226}\text{Ra}$ , $^{232}\text{Th}$ , $^{234}\text{U}$ , $^{238}\text{U}$ , $^{235}\text{U}$ , $^{238}\text{Pu}$ , $^{239+240}\text{Pu}$ , $^{241}\text{Am}$	$^{90}\text{Sr}$ , $^{208}\text{Tl}$ , $^{210}\text{Po}$ , $^{210}\text{Pb}$ , $^{212}\text{Bi}$ , $^{212}\text{Pb}$ , $^{214}\text{Bi}$ , $^{214}\text{Pb}$ , $^{228}\text{Ac}$ , $^{228}\text{Ra}$ , $^{228}\text{Th}$ , $^{230}\text{Th}$ , $^{234}\text{Th}$ , $^{234}\text{U}$ , $^{239}\text{Pu}$ , $^{240}\text{Pu}$
IAEA-437	Mussel, Mediterranean Sea	$^{40}\text{K}$ , $^{234}\text{U}$ , $^{238}\text{U}$ , $^{239+240}\text{Pu}$	$^{90}\text{Sr}$ , $^{208}\text{Tl}$ , $^{210}\text{Po}$ , $^{210}\text{Pb}$ , $^{212}\text{Bi}$ , $^{212}\text{Pb}$ , $^{214}\text{Bi}$ , $^{214}\text{Pb}$ , $^{228}\text{Ac}$ , $^{228}\text{Ra}$ , $^{228}\text{Th}$ , $^{230}\text{Th}$ , $^{232}\text{Th}$ , $^{234}\text{U}$ , $^{239}\text{Pu}$ , $^{240}\text{Pu}$
IAEA-418	Seawater, Mediterranean Sea	$^{129}\text{I}$	

Fig. 4 shows the performance of laboratories, or precisely the rejected percentage of results obtained from some interlaboratory comparison exercises for radionuclides organized by IAEA-MEL in the last 10 years in different matrices of marine samples. It can be seen that from different matrices (seawater, biota, sediment from different origins, see Table 1) and at different levels of activity in each sample, the laboratory performance can be different. It is difficult to go into details for each case due to the complexity of different techniques of measurement as well as the radiochemical separation procedure used. Each laboratory can address or check their

potential analytical problems through these interlaboratory comparison exercises and through the use of established reference materials.

#### 4. CONCLUSIONS

To ensure AQCS of marine radioactivity studies it is recommended to participate frequently in the ICs and PTs organised by the IAEA in order to (i) continue the improvement in performance through provision of feedback on the results, (ii) to be assisted further with reference methods and protocols to improve feedback from the IC and PT and to understand laboratories' analytical problems, and (iii) to be assisted with QA/QC programmes and manuals and to organise more QA/QC oriented training and missions if needed.

#### ACKNOWLEDGEMENTS

The International Atomic Energy Agency is grateful to the Government of the Principality of Monaco for the support provided to its Environment Laboratories.

#### REFERENCES

- [1] POVINEC, P.P., PHAM, M.K., IAEA reference materials for quality assurance of marine radioactivity measurements, *J. Radioanal. Nucl. Chem.* **248** 1 (2001) 211–216.
- [2] SANCHEZ-CABEZA, J.A., PHAM, M.K., POVINEC, P.P., IAEA programme on the quality of marine radioactivity data, *J. Environ. Radioact.* **99** (2008) 1680–1686.
- [3] INTERNATIONAL STANDARD ORGANIZATION, Guide 35: 2006 — Reference Materials — General and Statistical Principles, ISO, Geneva (2006).
- [4] POVINEC, P.P., et al., Certified reference material for radionuclides in seawater IAEA-381 (Irish Sea Water), *J. Radioanal. Nucl. Chem.* **251** 3 (2002) 369–374.
- [5] PHAM, M.K., et al., Certified reference material for radionuclides in fish flesh sample IAEA-414 (mixed fish from the Irish Sea and North Sea), *Appl. Radiat. Isot.* **64** (2006) 1253–1259.
- [6] POVINEC, P.P., et al., Reference material for radionuclides in sediment IAEA-384 (Fangataufa Lagoon sediment), *J. Radioanal. Nucl. Chem.* **273** 2 (2007) 383–393.
- [7] PHAM, M.K., et al., A new Certified Reference Material for Radionuclides in Irish Sea Sediment (IAEA-385), *Appl. Radiat. Isot.* **66** (2008) 1711–1717.
- [8] PHAM, M.K., et al., A new reference material for radionuclides in the mussel sample from the Mediterranean Sea (IAEA-437), *J. Radioanal. Nucl. Chem.* **283** (2010) 851–859.
- [9] PHAM, M.K., et al., Certified reference material IAEA-418:  $^{129}\text{I}$  in Mediterranean Sea water, *J. Radioanal. Nucl. Chem.* **286** (2010) 121–127.

- [10] INTERNATIONAL ATOMIC ENERGY AGENCY, Certified Reference Material IAEA-418: I-129 in Mediterranean Sea Water, Analytical Quality in Nuclear Applications Series 9, IAEA, Vienna (2009).

# OPTIMIZATION OF PLASTIC SCINTILLATOR THICKNESSES FOR ONLINE BETA DETECTION IN MIXED FIELDS

K. POURTANGESTANI, R. MACHRAFI  
University of Ontario Institute of Technology,  
Oshawa, Ontario, Canada

## Abstract

For efficient beta detection in a mixed beta-gamma field, Monte Carlo simulation models have been developed to optimize the thickness of a plastic scintillator used in whole body monitor. The simulation has been performed using MCNP/X code and different thicknesses of plastic scintillators ranging from 150 to 600  $\mu\text{m}$  have been used. The relationship between the thickness of the scintillator and the efficiency of the detector has been analysed. For 150  $\mu\text{m}$  thickness, an experimental investigation has been conducted with different beta sources at different positions on the scintillator and the counting efficiency of the unit has been measured. Evaluated data along with experimental ones have been discussed. A thickness of 300  $\mu\text{m}$  to 500  $\mu\text{m}$  has been found to be an optimum thickness for better beta detection efficiency in the presence of low energy gamma ray.

## 1. INTRODUCTION

This project is a cooperative effort between two organizations, the University of Ontario Institute of Technology and the CANBERRA Company. The working group deals with the optimization of plastic scintillators as a fundamental base of a whole body monitor to improve the efficiency of the detector to detect beta particles in mixed field of radiations.

The CANBERRA Company, as a large worldwide company manufacturing radiation instruments by using plastic scintillators of different kinds in a large proportion of its products, launched a further investigation to improve the performance and ISO standard functionality of its products. One of the CANBERRA products using plastic scintillators is the 'Argos' whole body monitor (5). The monitor uses several units composed of thin plastic scintillators. However, with the current configuration and layer thicknesses, the system has low detection efficiency for detecting beta radiation and consequently, a long counting time is required.

In this study, a thin plastic scintillator was characterized by simulating its response functions by means of detailed MCNPx<sup>1</sup> simulation and calculations as well

---

<sup>1</sup> MCNPx: Monte Carlo N Particle extended (simulation code).

as by calibration measurements for betas and photons at fixed energies. Tests were also conducted at the Canberra facility in order to compare the results with simulation of the response in a mixed radiation beta/gamma field. It is demonstrated that these detectors can be characterized sufficiently enough to serve their function as radiation monitors.

## 2. METHODOLOGY

The methodology consists of separate steps:

- Characterizing the existing unit by measuring its efficiency;
- Start modelling by MCNPx simulation (Monte Carlo N Particle) based on the data obtained from experiments with the existing unit;
- Further investigation by increasing the thickness of the scintillation layer and irradiate simulated model by different sources of beta.

## 3. EXPERIMENT WITH EXSITING UNIT

At the Canberra site, the existing unit, consisting of one plastic scintillator mounted on a simple plastic EJ-500, uses a clear and colourless epoxy cement with a refractive index at 1.57 for light collection in the whole body monitor. Thin plastic scintillators are the major sensors used in many detectors and monitors manufactured by CANBERRA. The recently designed detector under the name of Argos TPS monitor 5PB, uses a plastic scintillator of 150  $\mu\text{m}$  in thickness.

Measurements with the detector unit have been performed for different sources that create a mixed beta-gamma field. The main goal of this testing was to measure the efficiency of the detector with a 150  $\mu\text{m}$  thickness scintillation layer and later, to guide the MCNPx calculations for better optimization. Furthermore, testing was repeated by increasing the irradiation time and increasing the distance between the source and detector unit as well. The radiation sources such as  $^{14}\text{C}$ ,  $^{60}\text{Co}$ ,  $^{137}\text{Cs}$  and  $^{36}\text{Cl}$  have been chosen to match the ones encountered at work places where the monitors are deployed.

This experiment has been performed for only one thickness of 150  $\mu\text{m}$  for two rea-sons: the first one is to guide the further MCNPx simulation and the second one is because the unit is a functioning unit at the CANBERRA site. Finally we should mention that this test was performed in a low gamma radiation field, which considerably simplifies the experimental conditions.

## 4. SIMULATION

The existing unit at CANBERRA has a thickness of 150  $\mu\text{m}$ . The goal in this simulation is to determine the optimum thickness of the plastic scintillator to efficiently stop beta radiation and let gamma rays pass through. The Monte Carlo model was designed and employed to determine the transmission of beta particles and gamma rays through the scintillation material and to match the physical device as faithfully as possible. Prior to the development of the generic methodology shown in this research, it was appropriate to identify the types of models to achieve the highest rate of photons that reach the PMT when beta radiation interacts with the plastic scintillator.

### 4.1. Different models

At this stage, by using MCNPx code, we built a simple model of the existing detector unit which matches the exact dimension of the unit. The model consists of calculating the integrated average flux in the whole plastic box when the unit is irradiated with beta as well as with gamma and then comparing the number of photons for both cases. However, this model was very generic and doesn't help to optimize the position of the PMT (Photo Multiplier) in the plastic box. Therefore, a second model has been set up consisting of dividing the unit in 55 cells. Each cell has the same dimension as the entrance windows of the PMT. Furthermore, this model has been used not only for photon counting in different cells but also by calculating the deposited energy in each cell. The number of photons calculated in the entire plastic box (first model) or in a single cell (second model) didn't help to make a decision regarding the optimization of the thickness of the scintillation layer. Then the last model came out with the application of fundamental physics principle of energy deposition. Since the number of photons created in the plastic scintillator depends on

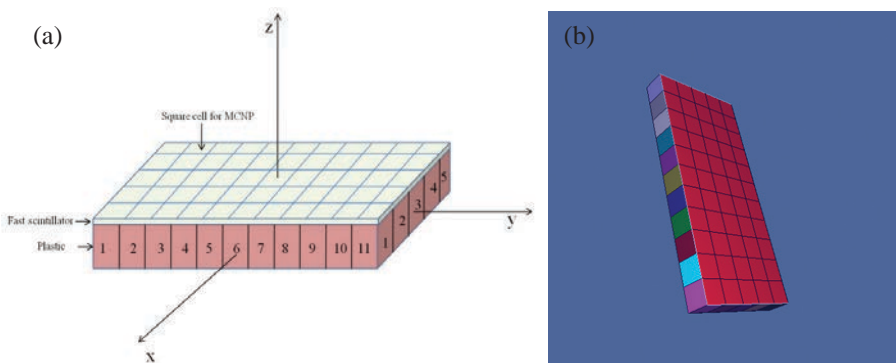


FIG. 1. a) 55 cells model to match the size of the PMT; b) Snap shot from MCNPx Visual Editor.

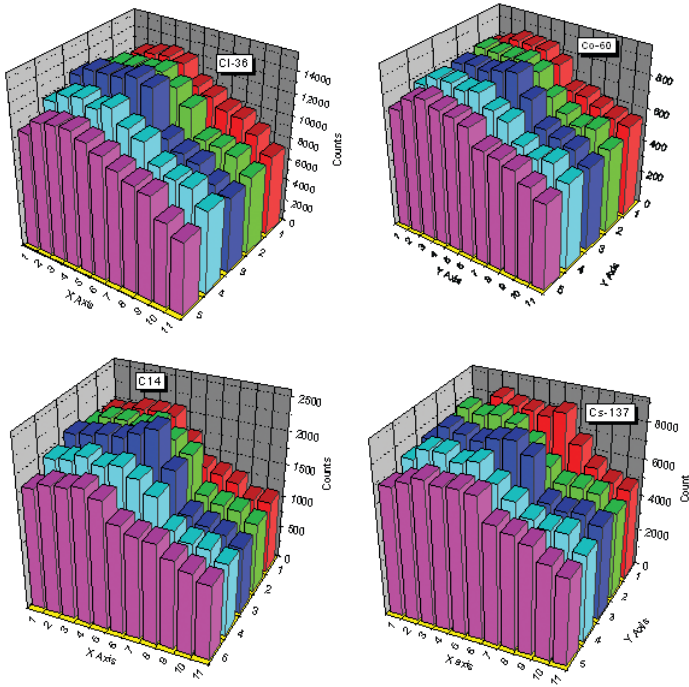


FIG. 2. Variation of the photon number as a function of the position on the x and y axis for different sources of beta particles located on the existing unit.

the deposited energy which itself depends on the incoming particles and the thickness of the scintillation layer, thus, the last model has been created based on calculating the deposited energy in the scintillation layer for different thickness for beta as well as for gamma with different energies. One of the eight tallies of MCNPx, namely the F8 tally that records the electron and photon energy deposition in each plastic cell was carried and code was ran in different modes: gamma source only, beta radiation only and mixed of beta and gamma.

## 5. RESULT, ANALYSIS AND DISCUSSION

### 5.1. Experimental data analysis and discussion

To analyse the performance of the detector, the experimental data measured with different beta sources placed on the top of the scintillation layer at different positions were converted into three dimensional graphs for each experiment. The variation of the photon number as a function of the position on the X and Y axis are

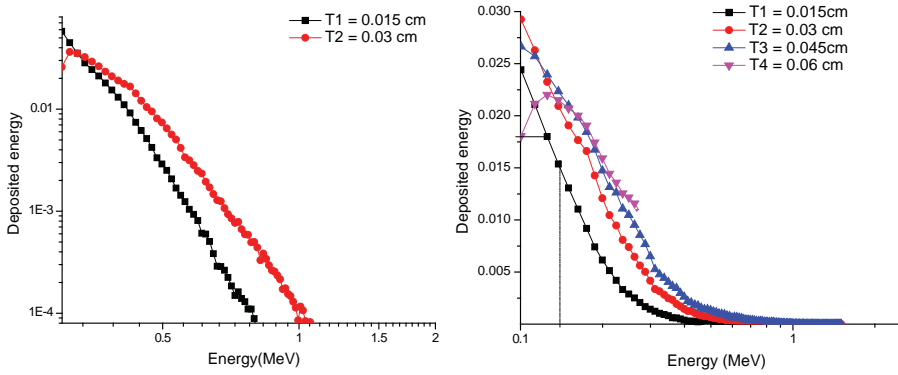


FIG. 3. Deposited energy for high beta energy: a) by doubling the thickness of the scintillation layer, b) by increasing thickness from 150  $\mu\text{m}$  to 600  $\mu\text{m}$ .

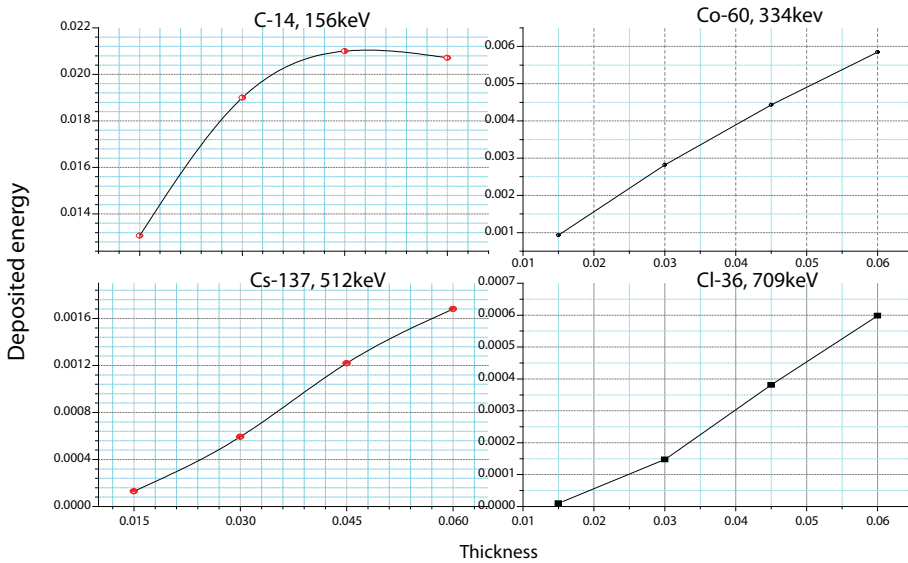


FIG. 4. Comparison for different beta energies with different thicknesses.

presented in the following figures. The further the source is from the entrance window (PMT position), the lower the number of counted photons is.

## 5.2. Simulated data analysis and discussion

### 5.2.1. Beta simulation

By increasing the thickness of scintillation layer, as energy increases, beta-particles deposit more energy in the scintillation layer. But for low beta particles, there is

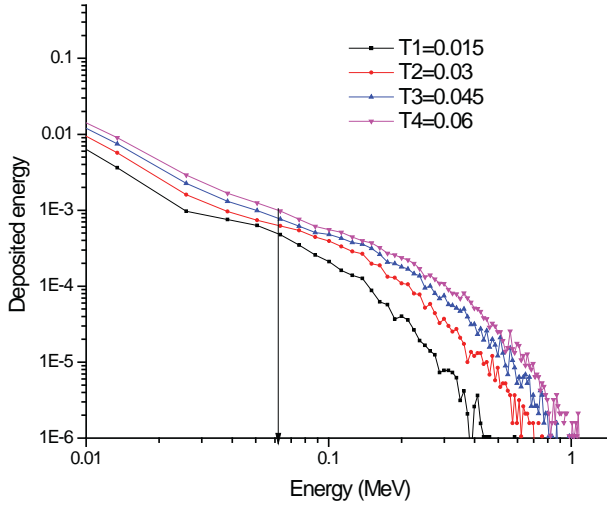


FIG. 5. Deposition energy in scintillation material as a function of gamma and the thickness of the scintillation layer.

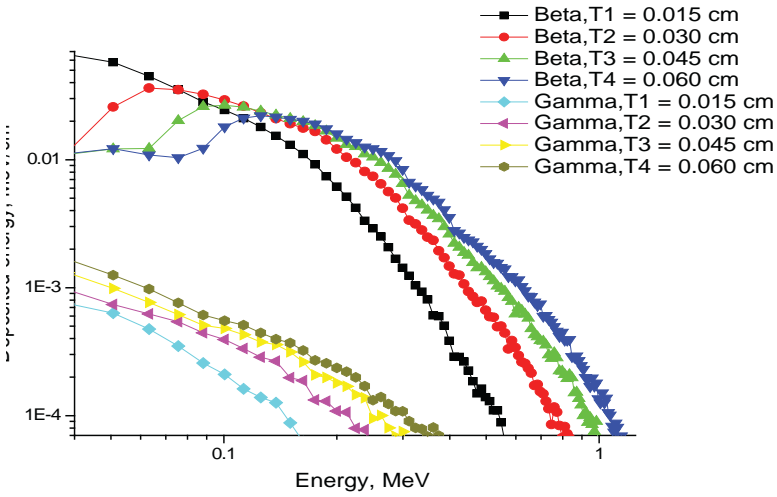


FIG. 6. Difference in deposition energy for beta particle and gamma ray by increasing thickness of scintillator layer.

TABLE 1. BETA AND GAMMA DEPOSITED ENERGY COMPARISON

Thickness cm	D <sub>1</sub> = deposition energy Am, 60keV	D <sub>2</sub> = deposition energy C14, 156 keV	D <sub>1</sub> /D <sub>2</sub>
0.03	$6.2215 \times 10^{-4}$	$190 \times 10^{-4}$	3.2%
0.045	$7.6659 \times 10^{-4}$	$210 \times 10^{-4}$	3.6%

no difference as shown in Fig. 3a by doubling the thickness and in Fig. 3b by increasing the thickness from 150  $\mu\text{m}$  to 600  $\mu\text{m}$ .

As can be seen from the figures above, we reached saturation in the energy deposition once we tripled the thickness. Therefore, there is no sense in increasing the thickness any further. At the same time these two thicknesses should be tested against lowest energy gamma. For this we propose to simulate 60 keV gamma energy.

### 5.2.2. Gamma simulation

The model was used when the unit was irradiated by gamma sources and as is shown in Fig. 5 with low gamma energy the amount of deposited energy is high, and all energy could be deposited by increasing the thickness.

### 5.2.3. Comparison between gamma and beta deposition energy

One can see that the energy deposition of beta particles is much higher than that one of the gamma quants, especially when the energy of gammas is above 200 keV.

The comparison between  $^{14}\text{C}$  (156 keV) beta and low energy gamma  $^{241}\text{Am}$  (62 keV) is shown in Table 1; the ratio of photons arising from gamma is only 3.6% of photons deriving from beta energy, after interaction with the 450  $\mu\text{m}$  thickness of the scintillation layer.

## 6. CONCLUSION

Monte Carlo simulation of radiation transport and light collection has been performed to optimize design parameters for a replacement detector module to increase the detector efficiency of beta-particles in plastic scintillators. MCNPx simulations have been used to evaluate the energies expected at various locations. A similar approach has been applied to a more complicated case of coincident events of maximizing the beta particle interaction with the scintillation layer and minimizing the gamma ray interaction and the relationship between the thickness of the detector and

the efficiency of the detector have been analysed. So far we can recommend the value between 0.03 cm and 0.045 cm as the best thickness of the scintillation layer for this detector. By increasing the thickness to 0.03 cm for gamma the deposited energy in the scintillation layer will be 3.2% and at 0.045 cm it will be 3.6%. As we see for the lowest gamma energy (Am-241, 56 keV) we found the best thickness for lowest adsorption to be the scintillation layer with the lowest deposit energy in this layer besides the fact of having enough thickness for beta particles to deposit most of their energies after interaction with the scintillation layer.

### ACKNOWLEDGEMENTS

K. Pourtangestani would like to thank her co-author Dr. Rachid Machrafi for his supervision, the CANBERRA Company which provided the opportunity to work on the whole body monitor and UOIT for support during this experiment.

### REFERENCES

- [1] LEO, W.R., *Techniques for Nuclear and Particle Physics Experiments*, 2nd rev. edn, Springer, Berlin (1994).
- [2] KNOLL, G.F., *Radiation Detection and Measurement*, John Wiley & Sons, Hoboken, NJ, 4th Ed. (2010) 860 pp.
- [3] VO, H.H., et al., Energy resolution of plastic scintillation detector for beta rays, *IEEE Transaction on Nuclear Science* **55** 6 (2008) 3717–3724.
- [4] LEROY, C., RANCOITA, P.-G., *Principles of Radiation Interaction in Matter and Detection*, World Scientific Publishing, Singapore (2004).
- [5] CANBERRA COMPANY, *Measurement Solution for Nuclear Safety and Security*, [www.canberra.com](http://www.canberra.com).
- [6] *Organic Scintillation Products*, Saint-GOBAIN. OH, [www.detectors.saint-gobain.com](http://www.detectors.saint-gobain.com); ELJEN TECHNOLOGY, Sweetwater, TX, [www.eljentechnology.com](http://www.eljentechnology.com).
- [7] STEPHENSON, R., *Introduction to Nuclear Engineering*, 2nd edn, McGraw-Hill, New York (1958) 491 pp.

# DETERMINATION OF Pu, Am AND Cm IN ENVIRONMENTAL SAMPLES

G. LUJANIENĖ

SRI Centre for Physical Sciences and Technology,  
Vilnius, Lithuania

## Abstract

The determination of actinides in the environmental samples at a lower detection limit is required for monitoring purposes and for environmental research. The method for Pu, Am and Cm measurements in soil and sediment samples provides high recoveries and good decontamination from interfering radionuclides. The main steps of the method involve digestion of the samples, separation of radionuclides from matrix using the TOPO/cyclohexane extraction and final purification using extraction Eichrom resins (TEVA, TRU). The accuracy and precision of Pu, Am and Cm analyses were tested using IAEA RM No 135, NIST SRM No 4350b, No 4357 and in intercomparison runs organized by the Risø National Laboratory, Denmark, and in the proficiency tests organized by National Physical Laboratory, UK. The method was applied for measurement of radionuclides in aerosol samples (ashes ~30 g), bottom sediments (50–80 g dr. wt) and soil (including Chernobyl soil) samples.

## 1. INTRODUCTION

The discovery of nuclear fission as well as the development of nuclear weapons and nuclear energy resulted in significant releases of radionuclides to the environment. Actinides were introduced into the environment due to the global fallout after nuclear tests, discharges from reprocessing and nuclear power plants as well as following accidents [1–2]. Nowadays, the development of reliable methods, capable of measuring actinide activity concentrations in environmental samples at a lower detection limit is required for monitoring purposes and for environmental research, e.g. application of actinides in tracer studies. Several overviews have been published recently on the analytical methods for environmental monitoring of actinides [3–5]. Published data indicate that separation yield decreases or varies across a wide range as the amount of samples taken for analysis increased. In addition, a lower chemical yield of americium separation was observed. As an exception the methods developed by Lee and Maxwell III, who extracted Pu and Am from large soil and sediment samples of 10–50 g and 100–200 g with a chemical yield about of 70–90% and 60–100%, respectively, should be mentioned [6–8]. Mineral acids are commonly used for sample digestion – most frequently leaching with 8 mol/L HNO<sub>3</sub> or mixtures of HNO<sub>3</sub>/HCl is performed [9]. Large soil and sediment samples require

a rather complex pre-treatment and macro-components separation prior to the final actinide cleaning. A large number of radio-analytical methods based on ion exchange, liquid-liquid extraction and precipitation techniques have been widely used for separation and pre-concentration of actinides. However, these traditional methods are time consuming and generate large amounts of acidic and organic waste. Recently, analytical methods based on extraction chromatography have become popular owing to the high selectivity of Eichrom resins which allow an efficient analytical procedure to be performed. In addition, they produce significantly less acidic waste and hazardous organic solvents than the most traditional procedures. Although there are a limited number of analytical procedures available, the replacement of traditional methods with new rapid extraction column methods can improve recoveries and the efficiency and accuracy of actinide determination [10]. However, there is still a lack of available methods based on extraction chromatography for the separation of actinides from large (up to 100 g) samples with typically low environmental concentrations. The purpose of this study was the development of a method which would make possible the handling of a variety of difficult sample matrices to reduce the time required for separation and the cost of actinide determination.

## 2. EXPERIMENTAL

All reagents used in the separation procedures were of analytical grade. The water used was obtained from a Milli-Q Synthesis A10 (Millipore) water purification system.  $^{242}\text{Pu}$  and  $^{243}\text{Am}$  were obtained from Isotrak, QSA Amersham International (AEA Technology UK), diluted to (1.06 Bq/ml and 1.11 Bq/ml) and employed as tracers in radiochemical procedures to enable yield corrections.

TEVA Resin (Aliquat<sup>TM</sup> 336), TRU-Resin (tri-*n*-butyl phosphate (TBP) and *N,N*-diisobutylcarbamoylmethylphosphine oxide (CMPO)), UTEVA Resin (diamylmethylphosphonate), available from Eichrom Europe, Paris, France) were employed for Pu and Am/Cm separation and cleaning. The tri-*n*-octylphosphine oxide (TOPO) was obtained from Fluka AG and was purified prior to extraction. The standard reference materials NIST No 4350b, No 4357, IAEA reference material IAEA-135, bottom sediments and soil and aerosol samples were used in this study. Environmental samples were dried, ground, homogenized and sieved. Then a suitable quantity of solids were weighed and ignited at 550 °C in an electric furnace overnight (~16 h). After the addition of  $^{242}\text{Pu}$  and  $^{243}\text{Am}$ , yield tracers and leaching with 8 mol/L  $\text{HNO}_3$  or aqua regia or reverse aqua regia the remaining solids were separated by centrifugation, solutions were diluted or evaporated and the sample redissolved. The final sample solution was made in 6 mol/L  $\text{HNO}_3$  – 0.15 mol/L  $\text{NaNO}_2$ . Pu(IV) was quantitatively extracted with 0.2 mol/L TOPO/cyclohexane ( $V_0/V = 1/20$ ,  $t = 15$  min, twice repeated). The extraction solutions were combined and washed twice with 3 mol/L HCl. Plutonium was reextracted by shaking the separated organic fraction

with 0.5 mol/L ascorbic acid/1 mol/L HCl ( $V_0/V = 1/1$ , twice repeated) for 15 min. The aqueous phase was twice washed with  $\text{CHCl}_3$  and transferred to the PTEF centrifuge bottles.  $\text{Nd}^{3+}$  ( $\text{Nd}(\text{NO}_3)_3$  solution, 15 mg/mL) and 40% HF was added to the aqueous phase, after vigorous stirring, the fine precipitate was separated by centrifugation at 6000 rpm for 5 min. The precipitate was washed with 1.5 mol/L HF and dissolved in the saturated  $\text{H}_3\text{BO}_3/\text{conc. HNO}_3$  solution. Then  $\text{NaNO}_2$  was added, the solution was left to stand for 15 min and  $\text{Nd}(\text{OH})_3$  was precipitated. After centrifugation for 5 min the precipitate was dissolved in  $\text{HNO}_3$ , a solution was made in 2 mol/L  $\text{HNO}_3 - 0.1$  mol/L  $\text{NaNO}_2$  and passed through the preconditioned TEVA resin column, followed by washing with 2 mol/L  $\text{HNO}_3$ . The Th was eluted with 9 mol/L HCl and 5 mol/L HCl. The Pu was eluted with 2 mol HCl - 0.1 mol/L  $\text{NH}_2\text{OH}\cdot\text{HCl}$ . The solution was evaporated, and the organic phase was destroyed with  $\text{HNO}_3/\text{H}_2\text{O}_2$ .

After Pu separation the pH of the aqueous solution was adjusted to 1.0–1.3 with  $\text{NH}_4\text{OH}$  and Am/Cm-fraction was extracted with 0.5 mol/L TOPO/cyclohexane ( $V_0/V = 1/10$ ,  $t = 15$  min, twice repeated). The extraction solutions were combined and washed twice with 0.1 mol/L  $\text{HNO}_3$ . The Am and Cm were back extracted with 2 mol/L  $\text{HNO}_3$ . ( $V_0/V = 2/1$ , twice repeated) for 15 min. The aqueous phase was twice washed with  $\text{CHCl}_3$  and evaporated. The residue was dissolved in 2 mol/L  $\text{HNO}_3$  and ascorbic acid was added to reduce Fe(III) to Fe(II). The solution was passed through the column, which was preconditioned with 2 mol/L TRU. The column was washed with 2 mol/L  $\text{HNO}_3$  and 9 mol/L HCl, and then Am and Cm were eluted with 4 mol/L HCl. The solution was evaporated, the residue was wet ashed with  $\text{HNO}_3/\text{H}_2\text{O}_2$ , sulphuric acid, and then a few drops of concentrated formic acid were added and evaporated to dryness. The residue was dissolved in 4 mol/L  $\text{NH}_4\text{SCN}/0.1$  mol/L  $\text{HCOOH}$  and passed through the preconditioned TEVA column. The column was washed with 4 mol/L  $\text{NH}_4\text{SCN}/0.1$  mol/L  $\text{HCOOH}$  then with 1.5 mol/L  $\text{NH}_4\text{SCN}/0.1$  mol/L  $\text{HCOOH}$  and the Am/Cm-fraction was eluted with 1 mol/L HCl. The solution was evaporated to dryness, fumed off with aqua regia and concentrated HCl.

Pu and Am/Cm fractions were electroplated after cleaning onto stainless steel discs and alpha spectrometry was performed in an alpha spectrometry system with passivated implanted planar silicon (PIPS) detectors, with an 450 mm<sup>2</sup> active area (AMETEK, Oak Ridge, Tenn, USA).

### 3. RESULTS AND DISCUSSION

A comparison of leaching methods indicated that for samples derived from global fallout the leaching ability of 8 mol/L  $\text{HNO}_3$  was similar to that of aqua regia and  $\text{HNO}_3/\text{HF}$  acids. However, the application of strong acids and HF for samples originating from the nuclear installation environment is reasonable although it is a more complicated procedure. Studies performed using the Chernobyl soil indicated that the amount of extracted Pu could vary by a factor of 10 in samples containing ‘hot’

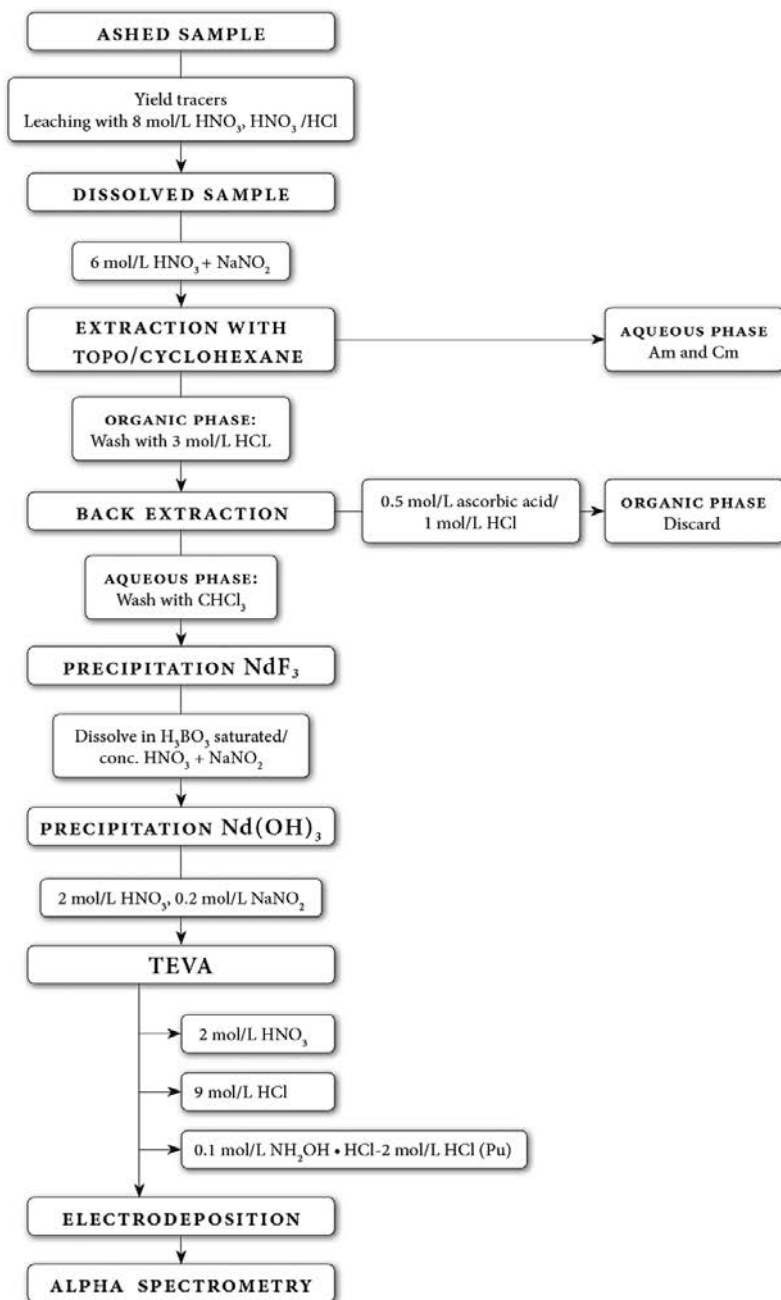


FIG. 3. Flow chart of the procedure for separation of Pu.

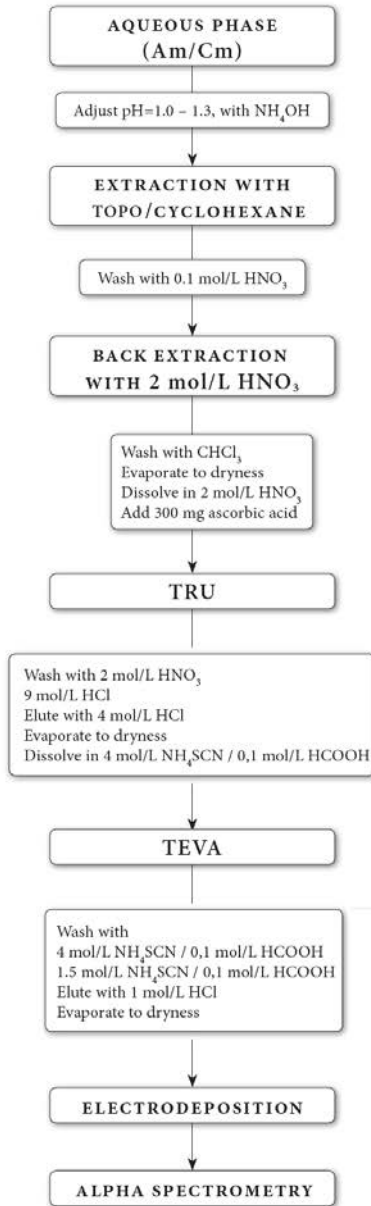


FIG. 4. Flow chart of the procedure for separation of Am/Cm.

particles depending on the leaching method. Figures 1 and 2 summarize the analytical procedure for environmental samples (e.g., bottom sediments up to 80 g) in a flow chart.

Plutonium was nearly quantitatively separated from the leaching solution using 0.2 mol/L TOPO/cyclohexane while most of the U and Th were extracted together [10]. The further Pu cleaning was performed using  $\text{NdF}_3$ ,  $\text{Nd}(\text{OH})_3$  precipitation followed by extraction chromatography using a TEVA column. U was separated during the  $\text{NdF}_3$  precipitation step. The recovery of  $^{242}\text{Pu}$  was close to 100%. The Th was removed from the column with 9 mol/L / 5mol/L HCl and then Pu(IV) was reduced to Pu(III) and eluted with 2 mol/L HCl – 0.1 mol/L  $\text{NH}_2\text{OH}\cdot\text{HCl}$ . The overall recovery of  $^{242}\text{Pu}$  tracer was found to be about 80% (75–95%) and an increase of the sample mass up to 100 g did not affect the recovery.

Am/Cm were extracted with 0.5 mol/L TOPO/cyclohexane and back extracted with 2 mol/L  $\text{HNO}_3$ . Then the Am/Cm fraction was cleaned from Pu, U, Th, Fe and rare earth impurities using a slightly modified method published by Pimpl et al [11]. The overall recovery of  $^{243}\text{Am}$  tracer was about 70% (73–89%), while the recovery decreased to 60% when 100 g samples were analysed. The decontamination factors (DF) were estimated as follows: for the Pu fraction  $\text{DF}_\text{U}=6\cdot 10^5$ ,  $\text{DF}_\text{Th}=5\cdot 10^4$ , For the Am/Cm fraction  $\text{DF}_\text{U}=2\cdot 10^6$ ,  $\text{DF}_\text{Th}=10^6$ .

The standard reference materials IAEA135, NIST SRM 4350b and 4357 were used to validate Pu and Am determination. The results of these measurements are shown in Table 1. The ratio of measured/reference values for  $^{239,240}\text{Pu}$  varied from 0.96 to 1.02 and for  $^{241}\text{Am}$  from 0.97 to 1.06. The measured values are in good agreement with recommended values and confidence tolerance limits. In addition, the accuracy and precision of Pu, Am and Cm analysis were tested in intercomparison

TABLE 1. Pu AND Am MEASUREMENTS IN THE STANDARD REFERENCE MATERIALS

Reference material (date)	$^{239,240}\text{Pu}$ , Bq/kg measured value	$^{239,240}\text{Pu}$ , Bq/kg reference value	$^{241}\text{Am}$ , Bq/kg measured value	$^{241}\text{Am}$ , Bq/kg reference value
NIST SRM 4350b (09/1981)	$0.506 \pm 0.026$ (0.500 – 0.512)	$0.508 \pm 0.030$	–	–
NIST SRM 4350b (09/1981)	$10.5 \pm 0.3$ 10.2 – 10.6	$10.4 \pm 0.2$ 9.3 – 13.2	$10.5 \pm 0.4^*$ (9.7 – 10.6)	$10^{**}$ (7 – 8)
IAEA 135 (01/01/1992)	$213 \pm 6$ (208 – 216)	$213 \pm 13$ (205 – 226)	$317 \pm 8^*$ (315 – 320)	$318 \pm 8$ (310 – 325)

\* uncertified value

\*\* corrected to the reference date

runs organized by the Risø National Laboratory, Denmark, for Pu and Am and in the proficiency test organized by the National Physical Laboratory, UK, for Pu, Am and Cm [12, 13].

The method was applied for measurements of radionuclides in aerosol samples (ashes ~30 g), bottom sediments (50–80 g dr. wt), soil (including Chernobyl soil) samples and low activity operational waste of various matrixes at Ignalina NPP, Lithuania. After determination of  $^{238}\text{Pu}$  and  $^{239,240}\text{Pu}$  by means of alpha spectrometry, plutonium isotopes were removed from the stainless steel disc using  $\text{HNO}_3$  and, following additional purification, the  $^{241}\text{Pu}$  and  $^{240}\text{Pu}/^{239}\text{Pu}$  ratio was measured using liquid scintillation and ICP-MS, respectively. The activity concentrations of  $^{239,240}\text{Pu}$  and  $^{241}\text{Am}$  determined in monthly aerosol samples ranged from 1 to 500 and from 0.3 to 500  $\text{nBq/m}^3$ , respectively [14]. The  $^{240}\text{Pu}/^{239}\text{Pu}$  ratio varied from 0.14 to 0.40 in aerosol samples collected in 1995–2005. The exponential decrease in the  $^{240}\text{Pu}/^{239}\text{Pu}$  ratio down to the global fallout value was found.

#### 4. CONCLUSIONS

The results obtained have shown that the analytical method is suitable for the determination of Pu, Am and Cm in environmental samples (bottom sediment, soil) and provides accurate data on their massic activities.

The method was applied for determination of actinides in bottom sediment, suspended matter, soil and aerosol samples. The method provides a low detection limit of about 0.005 Bq/kg and good chemical recoveries and excellent decontamination from interfering radionuclides.

#### REFERENCES

- [1] LIVINGSTON, H.D., POVINEC, P.P., A millennium perspective on the contribution of global fallout radionuclides to ocean science, *Health Phys.* **82** (2002) 656–668.
- [2] AARKROG, A., et al., Environmental radioactive contamination in Greenland: A 35 years retrospect, *Sci. Total Environ.* **245** (2000) 233–248.
- [3] VAJDA, N., KIM, C.K., Determination of Pu isotopes by alpha spectrometry: a review of analytical methodology, *J. Radioanal. Nucl. Chem.* **283** (2010) 203–233.
- [4] VAJDA, N., KIM, C.K., Determination of  $^{241}\text{Am}$  isotope: A review of analytical methodology, *J. Radioanal. Nucl. Chem.* **284** (2010) 341–366.
- [5] QIAO, X., et al., Determination of plutonium isotopes in waters and environmental solids: A review, *Anal. Chim. Acta* **652** (2009) 66–84.
- [6] LEE, S.H., et al., The development of sequential separation methods for the analysis of actinides in sediments and biological materials using anion-exchange resins and extraction chromatography, *J. Radioanal. Nucl. Chem.* **263** (2005) 419–425.

- [7] MAXWELL, S.L., Rapid method for determination of plutonium, americium and curium in large soil samples, *J. Radioanal. Nucl. Chem.* **275** (2008) 395–402.
- [8] LEE, S.H., et al., Analysis of plutonium isotopes in marine samples by radiometric, ICP-MS and AMS techniques, *J. Radioanal. Nucl. Chem.* **248** (2001) 757–764.
- [9] GOUTELARD, F., et al., Alpha-spectrometry measurement of Am and Cm at trace levels in environmental samples using extraction chromatography, *Journal of Alloys and Compounds* **271–273** (1998) 25–30.
- [10] PIMPL, M., SCHUETTELKOPF, H., “The measurement of Pu in Environmental samples and in gaseous and liquid effluents of nuclear installations”, Report SLU-REC-61 (Proc. Conf.), Swedish University of Agricultural Sciences, Uppsala (1986) 53–62.
- [11] PIMPL, M., HIGGY R.H., Improvement of Am and Cm determination in soil samples, *J. Radioanal. Nucl. Chem.* **248** (2001) 537–541.
- [12] NIELSEN, S.P., Intercomparison of Laboratory Analyses of Radionuclides in Environmental Samples, NKS-144, NKS, Roskilde (2006).
- [13] HARMS, A., GILLIGAN, C., Environmental Radioactivity Proficiency Test Exercise 2008, NPL Report IR 15, National Physical Laboratory, Teddington, England (2009).
- [14] LUJANIENĖ, G., et al., Artificial radionuclides in the atmosphere over Lithuania, *J. Environ. Radioact* **100** (2009) 108–119.

# ANALYSIS OF A SINGLE HOT PARTICLE BY A COMBINATION OF NON-DESTRUCTIVE ANALYTICAL METHODS

E. HRNECEK, L. ALDAVE DE LAS HERAS, M. BIELEWSKI, R. CARLOS  
EC JRC Institute for Transuranium Elements, Karlsruhe, Germany

M. BETTI  
IAEA Environment Laboratories, Monaco

## Abstract

Radioactive substances are often released to the environment in the form of particles. The determination of their chemical composition is a key factor in the overall understanding of their environmental behaviour. The aim of this investigation was to identify the source of one single radioactive particle collected from the Irish Sea and to understand its fate in the environment and in human body fluids. As the particle was supposed to be analysed for its dissolution behaviour in humans after ingestion, it was necessary to gain as much information as possible beforehand on the chemical and isotopic composition by means of non-destructive analysis such as SEM, SIMS,  $\mu$ -XRF and  $\mu$ -XANES. In this paper, an overview of the different non-destructive methods applied for the analysis of this particle and the results obtained is given. Additionally, the dissolution behaviour in human digestive solutions is discussed.

## 1. INTRODUCTION

Radionuclides released to the environment from anthropogenic activities can be in different physicochemical forms determining their mobility and possible biological uptake [1]. In many cases it has been shown that these releases are associated with radioactive particles whose morphology and chemical composition can influence the transport mechanisms of radionuclides in the environment as well as their bioavailability [2, 3].

In this work, one single radioactive particle collected from the Irish Sea has been investigated with a combination of non-destructive methods to determine its chemical speciation and isotopic composition before analyzing its dissolution behaviour in human digestive solutions. Results from measurements by SEM, SIMS,  $\mu$ -XRF and  $\mu$ -XANES are presented as examples for the information obtainable by these methods and details of the measurements and instrumentation used for analysis can be found in Ref. [4].

## 2. NON-DESTRUCTIVE ANALYSIS

Non-destructive analysis methods provide an opportunity to obtain information on sample composition without altering the sample, thus conserving it for further investigations. In these methods, either a signal emitted by the sample itself is observed, e.g.  $\gamma$  radiation emitted by radioactive elements, or the signal is produced by probing the sample with a beam of ions, or with radiation focused on the sample.

A scanning electron microscope (SEM) images the sample surface by scanning it with a high energy beam of electrons. These beam electrons interact with the atoms that make up the sample, producing signals which contain information about surface topography and composition. The signals produced by a SEM include secondary electrons, back scattered electrons (BSE), characteristic X rays and transmitted electrons. SEM can produce very high resolution images of a sample surface, revealing details of about 1 to 5 nm in size. Back scattered electrons (BSE) are beam electrons that are reflected from the sample by elastic scattering. These BSE are often used in analytical SEM together with the spectra obtained from the characteristic X rays of the sample elements hit by the high energy electron beam (energy dispersive X ray analysis, EDX). Because the intensity of the BSE signal is strongly related to the atomic number ( $Z$ ) of the specimen, BSE images can provide information about the distribution of different elements in the sample.

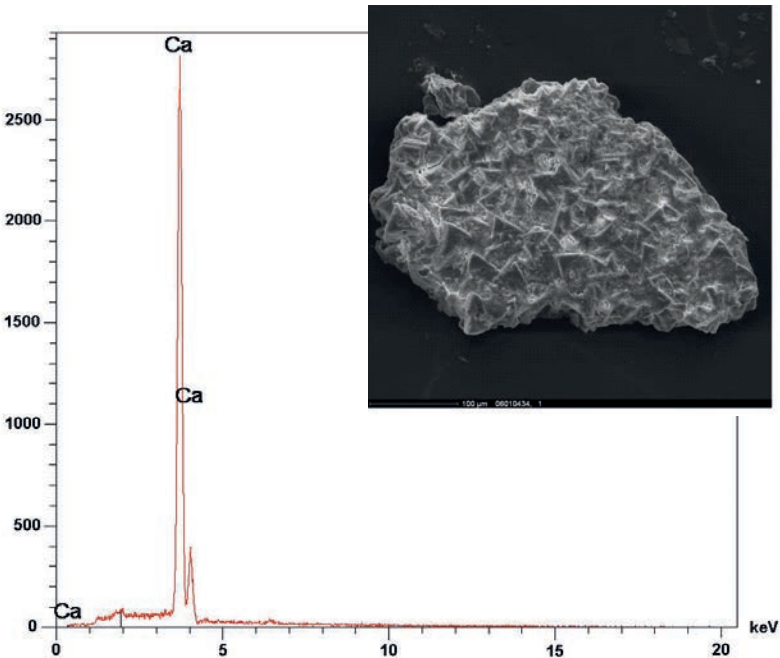


FIG. 1. SEM Picture showing an overview of a radioactive particle and an EDX spectrum.

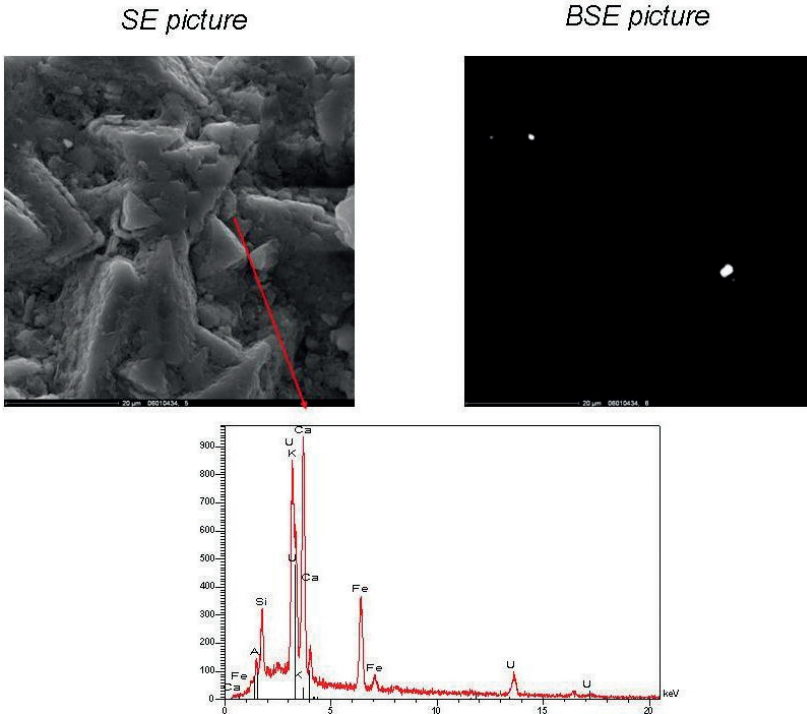


FIG. 2. SEM and back scattered electron (BSE) picture and EDX spectrum of an area of the particle.

Fig. 1 shows an image of the radioactive particle analysed by this technique. In this case, scanning electron microscopy with energy dispersive X ray analysis was used to determine the topology and the elemental composition of the particle. The diameter of the particle investigated corresponds to 400  $\mu\text{m}$  and the composition of the major part of the particle, mainly calcium, is a potential indication of calcite. Small grains of silicates are also present.

Zooming in on the sample, a secondary electron picture of an area of the same particle and its corresponding back scattered electron picture is shown in Fig. 2. Spots of high atomic number ( $Z$ ) elements become visible. The analysis of one of these spots by EDX reveals a high content of uranium. The study of this magnified area shows a uranium particle of about 1.5  $\mu\text{m}$  size sitting in the large calcite particle shown in Fig. 1.

Synchrotron radiation based X ray techniques are another advanced tool to look straight into a particle in a non-destructive manner. X ray fluorescence in confocal setup (confocal  $\mu\text{-XRF}$ ) can provide information on the presence and distribution of the elements. The usefulness of spectrometric, synchrotron radiation based techniques

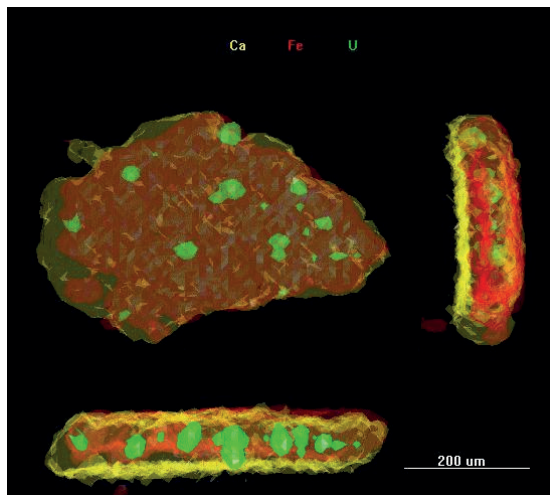


FIG. 3. Distribution of elements Ca, Fe and U in the particle reconstructed using XRF data.

for the characterization of radioactive particles by X ray microtomography [5, 6] or confocal  $\mu$ -XRF has been already reported [7, 5].

In our example, confocal  $\mu$ -XRF was used to determine the spatial distribution of elements in the particle. Three dimensional reconstructions of Ca, Cr, Mn, Fe, Ni, Cu, Zn, Sr, Ba, Pb and U distribution were performed. Fig. 3 shows the pattern of Ca, Fe and U in the particle. The most abundant element present was calcium, which is uniformly distributed and constitutes the matrix of the particle. The second most widespread element is iron. Its distribution is not homogeneous; it is principally placed on the surface of the grain. Uranium is present in the form of inclusions with sizes not exceeding 20  $\mu$ m.

From X ray absorption studies information on the oxidation state of selected elements can be obtained. If the setup is working in confocal geometry (confocal  $\mu$ -X ray Absorption Near Edge Spectroscopy,  $\mu$ -XANES) information on the oxidation state is collected only from specific areas of the sample. The knowledge of the oxidation state distribution can provide useful information on the release conditions [6] or the fate of particles in the environment. Results of these experiments are also of high importance for the radiological assessment of the contaminated areas from where the particles originate, as information on the oxidation state of a particle obtained by  $\mu$ -XANES can give information on its chemical stability against dissolution.

The oxidation state of uranium was determined at four locations in the hot particle by  $\mu$ -XANES. Two of the locations were in the inner part of the particle; the others were close to the surface. Higher oxidation states of uranium were found at

the surface (6.01 and 6.04) than in the inner part of the particle (5.40 and 5.63) indicating a better solubility at the surface of the particle.

Although not strictly a non-destructive method, secondary ion mass spectrometry (SIMS) is another valuable instrument to extract further information from a small sample. In this case, a primary beam of Cs<sup>+</sup> ions is used to atomize and ionize a small part of the sample surface. The sample ions are transmitted to a mass spectrometer, where the isotopic composition of the chemical elements from the sample can be determined. By knowing the isotopic composition of elements like uranium and plutonium, conclusions can be drawn on the irradiation history and thus the origin of the sample can be determined [8, 9]. For the investigated particle, the isotopic composition shows that the uranium is depleted in <sup>235</sup>U with a mass fraction of 0.312%. <sup>236</sup>U found with a mass fraction of 0.057% indicates that the depleted uranium contained in the particle originates from the reprocessing of uranium previously irradiated in a nuclear reactor.

Finally,  $\gamma$  radiation emitted by the radionuclides present in a sample can be analysed directly by Gamma spectrometry. This allows the quantification of the content of fission and activation products in the radioactive particle. For our particle, the analysis was performed with a Compton suppression gamma spectrometer specially designed for low level applications [10]. The gamma spectrum of the radioactive particle showed a large contribution of bremsstrahlung, indicating the presence of a strong beta emitter (e.g. <sup>90</sup>Sr). Except from a small contribution of <sup>137</sup>Cs, no other fission products could be detected.

In conclusion, the results show that the radioactive particle contains inclusions of depleted uranium previously irradiated in a nuclear reactor. The oxidation state of the uranium inclusions is higher at the surface of the particle. The uranium is embedded in a calcite matrix.

### 3. IN VITRO LEACHING IN SIMULATED HUMAN STOMACH AND INTESTINE SOLUTIONS

On the basis of the results obtained by non-destructive analysis, in vitro leaching of the radioactive particle was performed to simulate processes taking place in the human stomach and small intestine.

A micromanipulator was used to extract the particle from the surface of carbon tape used for the SIMS measurements. Then the leaching in the simulated stomach and intestine solutions was carried out. The system consisted of a 'stomach compartment' in which the particle is exposed to a synthetic gastric juice for a defined period, after which the contents of this compartment are transferred into a simulated 'small intestine compartment' in which they are allowed to react with small intestinal fluids for a further period. At the end of the procedure, an additional step in 1% HNO<sub>3</sub> was added in order to completely dissolve the particle. A flow chart of the leaching

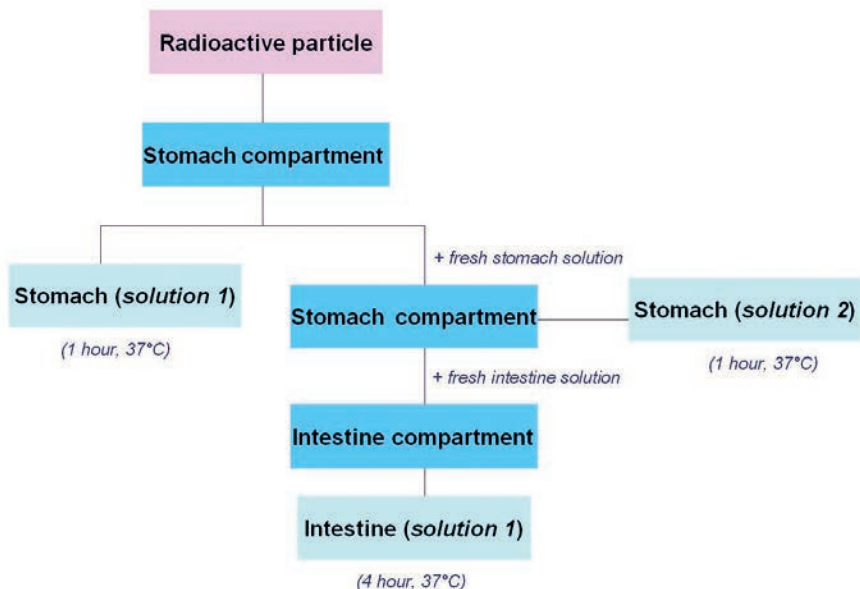


FIG. 4. Flow chart of the leaching procedure used in the simulated stomach and small intestine solutions.

procedure is given in Fig. 4 and details of the procedure can be found in Ref. [11]. In order to better simulate the kinetics of the digestion process, the leaching in the stomach compartment was repeated twice.

The leaching solutions were analysed by gamma spectrometry, liquid scintillation counting and inductively coupled plasma mass spectrometry for their content of  $^{90}\text{Sr}$ ,  $^{137}\text{Cs}$ ,  $^{234}\text{U}$ ,  $^{235}\text{U}$ ,  $^{236}\text{U}$ ,  $^{238}\text{U}$  and  $^{99}\text{Tc}$  radionuclides. The  $^{137}\text{Cs}$  concentrations were determined by  $\gamma$  spectrometry. The activity concentration of  $^{90}\text{Sr}$  was determined in the different leaching solutions using Sr specific extractive columns for radiochemical separation. Directly after column separation, the solutions containing  $^{90}\text{Sr}$  were measured by Liquid Scintillation Counting (LSC). Screening of  $^{99}\text{Tc}$  and determination of the uranium concentration and its isotopic composition in the different leachates were done by ICP-MS.

For the particle investigated, more than 99% of both  $^{137}\text{Cs}$  and  $^{90}\text{Sr}$  were found dissolved in the stomach compartment. The total  $^{90}\text{Sr}$  content of the particle was 24.4 kBq.  $^{99}\text{Tc}$  was not detected in any leaching solution samples by ICP-MS, with typical detection limits for  $^{99}\text{Tc}$  of 0.02 pg/g.

The total uranium content found in the particle was 43.6 ng. 76.3% was found in the leaching fractions corresponding to the stomach compartment. Another 2.8% was dissolved in the small intestine compartment. 20.9% of the uranium from the particle was not soluble under biological conditions and could be recovered in the final  $\text{HNO}_3$

step. The isotopic composition found in the uranium fractions was in agreement with that obtained by SIMS.

#### 4. SUMMARY

By choosing the right combination of tools, a great deal of information can be extracted even from a small sample. By using SEM and SIMS, information on elemental and isotopic composition can be obtained in a non-destructive way. Recent developments in synchrotron based techniques allow three dimensional mapping of element content at a micrometre scale and the extraction of information on oxidation states of elements in sub-regions of a small sample.

Leaching experiments provide valuable information on the behaviour of hot particles in biological fluids. For this purpose, mass spectrometric methods such as ICP-MS and radiometric methods like gamma spectrometry and LSC are the choice for determination of low concentrations of actinides and fission products.

### ACKNOWLEDGEMENTS

This investigation was financially supported by BNFL under Contract number 22318. The IAEA is grateful for the support provided to its Marine Environment Laboratories by the Government of the Principality of Monaco.

### REFERENCES

- [1] SALBU, B., et al., Characterisation of radioactive particles in the environment, *Analyst* **123** (1998) 843–850.
- [2] BETTI, M., et al., “Environmental radioactive particles: A new challenge for modern analytical instrumental techniques in support of radioecology”, *Analysis of Environmental Radionuclides* (POVINEC, P.P., Ed.), Elsevier, Amsterdam (2008) 355–370.
- [3] SALBU, B., Speciation of radionuclides — Analytical challenges within environmental impact and risk assessments, *J. Environ. Radioact.* **96** (2007) 47–53.
- [4] BIELEWSKI, M., et al., Nondestructive spectrometric study on a radioactive particle embedded in a marine sediment, *Microsc. Microanal.* **14** (2008) 321–327.
- [5] ERIKSSON, M., et al., Source term identification of environmental radioactive Pu/U particles by their characterization with non-destructive spectrochemical analytical techniques, *Spectrochim. Acta B* **60** (2005) 455–469.
- [6] SALBU, B., et al., High energy X-ray microscopy for characterization of fuel particles, *Nucl. Instrum. Meth. Phys. Res. A* **467** (2001) 1249–1252.
- [7] JERNSTRÖM, J., et al., Non-destructive characterization of low radioactive particles from Irish Sea sediment by micro X-ray synchrotron radiation techniques:

- Micro X-ray fluorescence ( $\mu$ -XRF) and micro X-ray absorption near edge structure ( $\mu$ -XANES) spectroscopy, *J. Anal. At. Spectrom.* **19** (2004) 1428–1433.
- [8] JERNSTRÖM, J., et al., Characterization and source term assessments of radioactive particles from Marshall Islands using non-destructive analytical techniques, *Spectrochim. Acta B* **61** (2006) 971–979.
- [9] RANEBO, Y., et al., The use of SIMS and SEM for the characterization of individual particles with a matrix originating from a nuclear weapon, *Microsc. Microanal.* **13** (2007) 179–190.
- [10] PEERANI, P., et al., Assessment of a Compton-event suppression  $\gamma$ -spectrometer for the detection of fission products at trace levels, *Nucl. Instrum. Meth. Phys. Res. A* **482** (2002) 42–50.
- [11] STEWART, A., COOK, G.T., MacKENZIE, A.B., Simulation of Human Stomach and Intestine Leaching of Dounreay Hot Particles, Scottish Environmental Protection Agency (2003), [http://www.sepa.org.uk/radioactive\\_substances/publications/dounreay\\_reports.aspx](http://www.sepa.org.uk/radioactive_substances/publications/dounreay_reports.aspx) (accessed Jan. 15, 2013).

# URANIUM SERIES RADIONUCLIDES IN THE WATER COLUMN OF THE NORTHEAST ATLANTIC OCEAN

F.P. CARVALHO

Nuclear and Technological Institute,  
Department of Radiological Protection and Nuclear Safety,  
Sacavém, Portugal

## Abstract

Naturally occurring radionuclides, namely  $^{238}\text{U}$ ,  $^{234}\text{U}$ ,  $^{230}\text{Th}$ ,  $^{226}\text{Ra}$ ,  $^{210}\text{Pb}$ ,  $^{210}\text{Po}$  and  $^{232}\text{Th}$ , were analysed in water samples from ocean vertical profiles in three major abyssal basins of the NE Atlantic (Porcupine, Iberia and Tejo Basins), from the surface to the deep sea water layer. Concentrations were determined in the dissolved and particulate phases. The profiles of uranium isotopes in the water column, mostly in dissolved phase, showed nearly homogenized concentrations with  $^{238}\text{U}$  averaging  $37 \pm 4$  mBq/L and  $^{234}\text{U}/^{238}\text{U}$  activity ratios averaging  $1.13 \pm 0.04$ , while  $^{226}\text{Ra}$  concentrations were 2–3 times higher in the bottom than at the ocean surface.  $^{230}\text{Th}$  activity concentrations were four orders of magnitude lower than  $^{234}\text{U}$ , confirming rapid Th scavenging from solution by the particulate matter.  $^{210}\text{Pb}$  and  $^{210}\text{Po}$  activity concentrations in the soluble phase were much lower than dissolved  $^{226}\text{Ra}$ . Modelling the distribution of these radionuclides in the water column leads to an average residence time of dissolved  $^{210}\text{Pb}$  and  $^{210}\text{Po}$  in the upper layer of 5 a and 1 a, respectively, and 0.6 a in the particulate phase for both radionuclides. In the deep water layer, soluble  $^{210}\text{Pb}$  and  $^{210}\text{Po}$  mean residence times were  $42 \pm 20$  a and 2 a, respectively. The calculated  $^{210}\text{Pb}$  deposition flux at the abyssal sea floor is comparable with the flux derived from the  $^{210}\text{Pb}$ -excess inventory measured in sediments, and about  $100 \text{ Bq}\cdot\text{m}^{-2}\cdot\text{a}^{-1}$ . The  $^{210}\text{Pb}$  atmospheric deposition flux at the ocean surface in this region was estimated at about  $74 \text{ Bq}\cdot\text{m}^{-2}\cdot\text{a}^{-1}$  and the  $^{210}\text{Pb}$  sink in the Northeast Atlantic is discussed.

## 1. INTRODUCTION

The naturally occurring radionuclides of the uranium and thorium series have been used as tools to investigate oceanographic processes including, for example, the mixing of water masses, oceanic circulation, particle flux, and sedimentation rates [1–8]. Thanks to sediment dating, geochronologies and time scales provided by the radionuclides and the radioactive decay mechanism, many natural processes could be investigated. The knowledge of radionuclide behaviour and their fate in the oceans is still in many cases a key piece in the understanding of complex natural processes, including atmosphere–ocean and sea water–sea floor exchanges as well as past climate changes [9–12].

In spite of great progress made in chemical oceanography and marine radioactivity research in the last decades, not all oceanic basins have been investigated as yet. This paper presents the distribution of the main uranium series radionuclides in the northeast Atlantic Ocean and the computed mean residence times for key radionuclides in the ocean layers of this region.

## 2. MATERIALS AND METHODS

Water samples were collected with 400 L stainless steel Gerard barrels (Hydrobios) with accurate readings of the water sampling depth measured with a pinger. Water samples were immediately filtered on board ship through large diameter (120 mm) membrane Millipore filters (0.45  $\mu\text{m}$ ) held in Teflon coated filter systems, and pressure application. Filtered waters were collected into polyethylene drums, acidified with  $\text{HNO}_3$  to  $\text{pH} < 2$ , and transported to the laboratory for analyses. Membrane filters were pre-washed with deionized water, dried, and pre-weighed in the laboratory. After seawater filtration on board, the filters with suspended particulate matter were folded and stored in sterile plastic bags until analysis.

For radionuclide analyses, internal tracers ( $^{232}\text{U}$ ,  $^{229}\text{Th}$ ,  $^{224}\text{Ra}$ ,  $^{209}\text{Po}$ , and 10 mg  $\text{Pb}^{2+}$ ) were added to measured volumes of filtered water samples of about 25 L for determination of the chemical yield. Radioelements were oxidized with potassium permanganate and, after prolonged homogenization with bubbling nitrogen gas, co-precipitated with  $\text{MnCl}_2$ . Precipitate was recovered and dissolved in order to separate the radioelements using ion exchange resins and column chromatography. The separate fractions with purified radioelements were transferred into plating solutions and electrodeposited onto stainless steel polished discs. Polonium was spontaneously plated onto silver discs, and lead precipitated as lead chromate, and the yield of recovery was determined by gravimetry. Lead-210 was determined through  $^{210}\text{Po}$ , after 6 months ingrowth and dissolution of the lead chromate precipitate to allow for  $^{210}\text{Po}$  plating onto a silver disc [13, 14]. Radionuclide measurements were made by alpha spectrometry using silicon surface barrier detectors (ORTEC EG&G).

The quality assurance of the results was ensured through periodic analysis of IAEA certified reference materials and participation in radioanalytical intercomparison exercises [15, 16].

## 3. RESULTS AND DISCUSSION

### 3.1. Surface open sea water: soluble and particulate radionuclides

To determine radionuclides in surface sea water and assess their partitioning between dissolved and particulate fractions, a large volume (400 L) of near surface

sea water (–5 m) was collected in the open sea, B area, off the continental shelf. The sea water sample, filtered on board, had a suspended load of 4.97 mg/L (dry wt), mostly of microscopic phytoplankton. Results indicated that uranium in the suspended particulate matter was 0.04% of the total uranium in sea water, and displayed a  $^{234}\text{U}/^{238}\text{U}$  activity ratio of  $0.83 \pm 0.10$ . Most of the uranium in seawater was, therefore, in the soluble phase and the U partitioning coefficient ( $K_d$ ) was computed as  $86 \pm 9$ .

In the same sea water sample,  $^{232}\text{Th}$  activity concentration was  $4.5 \pm 0.7$  mBq/L in solution and  $9.0 \pm 0.9$  Bq/kg in the suspended particulate matter, which corresponds to 91%  $^{232}\text{Th}$  in the particulate phase and to an in situ partitioning coefficient  $K_d = 2 \times 10^6$ . In the suspended particulate matter the ratio of specific activities  $^{232}\text{Th}/^{238}\text{U}$  was 2.8, signalling the terrigenous origin of  $^{232}\text{Th}$ . In suspended particulate matter the activity ratio  $^{230}\text{Th}/^{232}\text{Th} = 7.6 \pm 0.1$  was higher, for example, than in the Tagus River suspended particulate matter discharged into the sea, which indicated a  $^{230}\text{Th}$  enrichment in the particles with additional  $^{230}\text{Th}$  scavenging from sea water [17].

These two radioelements, uranium and thorium, represent amongst the natural radioactive decay series elements the two extremes of solubility and partitioning coefficients in sea water.

### 3.2. Oceanic vertical profiles

Sea water samples from vertical profiles of the NE Atlantic were analysed from three regions: A, the Tejo Abyssal Basin; B, the Iberian Abyssal Basin and C, the Porcupine Abyssal Basin (Fig. 1).

#### 3.2.1. Uranium

The average dissolved uranium concentrations were slightly lower in the Porcupine Basin compared with the other two basins closer to the continental margin. In each basin, the uranium concentrations in the water column were roughly similar at different depths, although not at a constant value from the surface to the bottom layer, which probably reflects the different origins of water masses (Table 1). Nevertheless, concentrations of  $^{238}\text{U}$  and total uranium in the water column varied slightly only with the water depth. The average of these determinations for  $^{238}\text{U}$  was  $37 \pm 4$  mBq/L ( $3.2 \pm 0.4$   $\mu\text{gU/L}$ ) and the average  $^{234}\text{U}/^{238}\text{U}$  activity ratio was  $1.13 \pm 0.04$ . This average uranium concentration and isotope activity ratio are similar to the average values  $3.3 \pm 0.02$  mBq/L and  $1.14 \pm 0.03$ , respectively, proposed for the world ocean [18, 19].

This distribution of uranium in the water column has two important implications. Firstly, a nearly constant vertical distribution implies that dissolved uranium is only slightly scavenged by settling particles and a vertical gradient of uranium

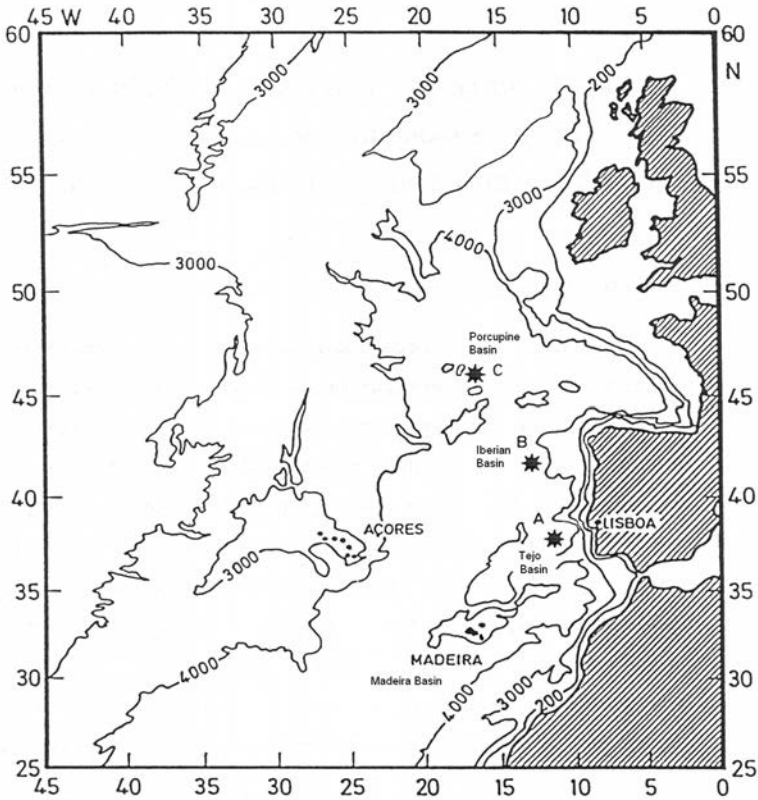


FIG. 1. The Northeast Atlantic Ocean and the sampling stations A, B, and C for radionuclide determinations. Bathymetry lines in metres.

concentration is not originated. Secondly, the uranium residence time in sea water must be very long, allowing for the homogenization of uranium (mostly from river discharges) to take place in ocean waters.

The uranium in river discharges was estimated at about  $2 \times 10^{10}$  g/y based on the average U concentration of  $0.3 \mu\text{g/L}$  in large rivers, and this global discharge corresponds to an average U discharge of  $5.8 \times 10^{-5} \text{ g}\cdot\text{m}^{-2}\cdot\text{a}^{-1}$  into the ocean [12]. Taking into account the uranium concentration in the air above the North Atlantic,  $4.1 \pm 1.2 \text{ pgU/m}^3$  ( $0.10 \pm 0.03 \text{ mBq/m}^3$ ), and using the mean deposition velocity of  $^{210}\text{Pb}$  in aerosol particles determined near the Atlantic coast at Lisbon, we can estimate the uranium deposition flux onto the ocean surface at  $1.3 \mu\text{g}\cdot\text{m}^{-2}\cdot\text{y}^{-1}$  ( $0.32 \text{ Bq}\cdot\text{m}^{-2}\cdot\text{a}^{-1}$ ) [20, 21]. This atmospheric flux is only about 2% of the uranium in the annual river discharges. The stability of uranium concentrations in sea water is well established and a global mean residence time of uranium in the ocean has been estimated at  $2 \times 10^5$  a [12]. Uranium removal from the upper layer of the ocean was

INVITED PAPER

TABLE 1. URANIUM CONCENTRATIONS IN THE NORTHEAST ATLANTIC OCEAN WATER COLUMN

Station	Sample depth (m)	<sup>238</sup> U (mBq/L)	<sup>234</sup> U (mBq/L)	μgU/L	<sup>234</sup> U/ <sup>238</sup> U
Zone A (St.E5)	0	38.2	43.8	3.3	1.14
Lat. 38° 40' N	10	38.0	43.3	3.3	1.14
Long. 10° 30' W	50	40.1	45.4	3.4	1.13
Bottom - 4500 m	150	38.1	44.2	3.3	1.16
	250	36.3	43.2	3.2	1.19
	500	37.7	43.8	3.3	1.16
	1000	41.2	46.8	3.5	1.14
	2000	38.4	40.8	3.2	1.06
	3000	39.4	46.0	3.4	1.16
	4000	39.8	45.0	3.4	1.13
Mean ± 1 SD		38.7±1.3	44.2±1.6	3.3±0.1	1.14±0.03
Zone B (St.S5)	0	40.2	44.0	3.4	1.09
Lat.40° 50' N	10	40.0	46.6	3.5	1.16
Long. 11° 55' W	250	38.2	43.8	3.3	1.15
Bottom -5100m	500	39.1	44.9	3.4	1.14
	2000	33.9	37.3	2.9	1.10
	3000	35.1	41.8	3.1	1.18
	4000	42.9	48.8	3.7	1.14
Mean ± 1 SD		38.5±2.9	43.9±3.4	3.3±0.2	1.14±0.03
Zone C (St. W2)	0	38	43	3.2	1.13
Lat. 46° 02' N	500	32	35	2.7	1.10
Long. 16° 39' W	1000	37	39	3.1	1.05
Bottom -4800m	2080	35	40	3.0	1.14
	3300	28	30	2.3	1.08
	3780	24	27	2.05	1.10
	4600	35	41	3.1	1.17
Mean ± 1 SD		32.7±4.7	36.4±5.6	2.8±0.4	1.11±0.04
Grand mean		37±4	42±5	3.2±0.4	1.13±0.04

**Note:** Relative uncertainties of activity concentrations were about 5% of the concentration value.

predicted as minor, and U measurements in the bio authigenic fraction collected in sediment traps indicated that the flux of uranium leaving the epipelagic zone is about 0.2 mBq·m<sup>-2</sup>·a<sup>-1</sup> (7.6 µg·m<sup>-2</sup>·a<sup>-1</sup>) and accounts for about 12% of the uranium annual discharge by rivers [19, 22]. This uranium in the oceanic particle flux has a biogenic origin, mostly redissolves during the particle fall in the water column, and it is not sufficient to generate a significant gradient in the vertical U distribution [22].

3.2.2. Thorium

It is well known that <sup>232</sup>Th (thorium series) in the ocean has a continental origin and it is delivered by river discharges, coastal erosion and wind transport. Th-234 and <sup>230</sup>Th isotopes are <sup>238</sup>U daughters (uranium series), and mainly originate in the radioactive decay of uranium dissolved in seawater. Most thorium produced in seawater is rapidly scavenged from the soluble phase and becomes associated with the particulate phase, as verified by the high Th partitioning coefficient determined above [23, 24].

In the water column at the Porcupine Abyssal area, <sup>230</sup>Th concentrations were always 1.2–3.6 times higher than <sup>232</sup>Th in the soluble phase (Table 2). In the same water samples, the average <sup>230</sup>Th/<sup>234</sup>U activity concentration ratio was (2.6 ± 1.5) × 10<sup>-4</sup>. Taking into account the high residence time of uranium in sea water, this ratio <sup>230</sup>Th/<sup>234</sup>U highlights the rapid scavenging of the daughter radionuclide <sup>230</sup>Th from the soluble phase in the water column. For an average depth of 4500 m in the NE Atlantic region and using the average <sup>230</sup>Th concentration 10 ± 6 mBq/L, the inventory of dissolved <sup>230</sup>Th in the water column is 45 ± 27 Bq/m<sup>2</sup>. The inventory of <sup>234</sup>U in the same water column, assuming an average concentration of 36 mBq/L, is 1.6 × 10<sup>5</sup> Bq/m<sup>2</sup>. From these inventories and using the mass balance equation for this parent-daughter pair of radionuclides

TABLE 2. CONCENTRATIONS OF THORIUM ISOTOPES IN FILTERED WATER (<0.45 µM) IN ZONE C (PORCUPINE BASIN) OF THE NORTHEAST ATLANTIC

Sample depth (m)	<sup>232</sup> Th		<sup>230</sup> Th	<sup>230</sup> Th/ <sup>232</sup> Th
	µBq/L ± 1 SD	pg/g	µBq/L ± 1 SD	
500	4.1 ± 1.0	1.0	15 ± 2	3.6
1000	5.1 ± 2.1	1.3	14 ± 2	2.7
2080	1.3 ± 0.1	0.3	1.7 ± 0.2	1.3
3300	9.6 ± 3.2	2.4	12 ± 3	1.2
3780	0.9 ± 1.2	0.2	3 ± 1	3.3
Mean ± 1 SD	4.2 ± 3.1	1.0 ± 0.8	9 ± 6	2.4 ± 1.0

$$\lambda_U N_U = \lambda_{Th} N_{Th} + \lambda_s N_{Th}$$

and converting into activity and resolving for  $\lambda_s$

$$\lambda_s = \lambda_{Th} [(A_U/A_{Th}) - 1]$$

where

- $A_U$  is the inventory of  $^{234}\text{U}$ ,
- $A_{Th}$  is the inventory of  $^{230}\text{Th}$  dissolved,
- $\lambda_{Th}$  is the radioactive decay constant of  $^{230}\text{Th}$ ,
- $\lambda_s$  is the scavenging rate of soluble  $^{230}\text{Th}$  by the particulate matter.

From  $\lambda_s$ , the mean residence time for  $^{230}\text{Th}$  in the soluble phase is computed at 32 a in the water column of this region of the Atlantic. This is comparable to a mean residence time of 20–35 a reported for the open Pacific Ocean [25]. In the open ocean, where  $^{232}\text{Th}$  supply is provided by atmospheric depositions, the  $^{234}\text{Th}$ ,  $^{230}\text{Th}$  and  $^{232}\text{Th}$  mean residence times in the exchangeable phase are likely to be identical. It may be noted that much shorter residence times for Th isotopes were reported in shallow waters containing higher suspended matter concentrations and with higher water mixing.

In the oceanic water column, dissolved  $^{238}\text{U}$  radioactive decay generates  $^{234}\text{Th}$  that is rapidly removed from the dissolved phase, as well as the  $^{230}\text{Th}$  atoms that may be formed by further decay [8, 23]. Therefore, in the seawater column very small amounts of  $^{226}\text{Ra}$  and  $^{210}\text{Pb}$  will indeed be generated from the dissolved uranium.

### 3.2.3 Radium

Radium ( $^{226}\text{Ra}$ ) concentrations were determined in the water column of the three NE Atlantic basins. Vertical profiles of  $^{226}\text{Ra}$  showed increasing concentrations from the ocean surface to the bottom. Comparing  $^{226}\text{Ra}$  concentrations with those of the radioactive parent  $^{230}\text{Th}$  it is clear that  $^{226}\text{Ra}$  does not originate from  $^{230}\text{Th}$  in situ decay. Vertical profiles of  $^{226}\text{Ra}$  with concentrations in deep layers 2–3 times higher than those at the surface have been previously reported in the literature and the increase of concentrations towards the bottom is ascribed to  $^{226}\text{Ra}$  dissolution from the sea floor sediments [26].

The  $^{226}\text{Ra}$  dissolved in ocean water is a source of  $^{210}\text{Pb}$  through  $^{222}\text{Rn}$  production and decay. Deviations from the  $^{226}\text{Ra}$ – $^{222}\text{Rn}$  radioactive equilibrium may occur near the ocean surface with some radon exhalation to the atmosphere and near the sea floor with radon exhalation from the bottom sediments into the sea water. Notwithstanding, the departure of  $^{222}\text{Rn}/^{226}\text{Ra}$  radioactive equilibrium seems to play a minor influence only on the  $^{210}\text{Pb}$  in-growth in the water column [12, 26].

### 3.2.4. $^{210}\text{Pb}$ and $^{210}\text{Po}$

The concentrations of  $^{226}\text{Ra}$ ,  $^{210}\text{Pb}$  and  $^{210}\text{Po}$  were also determined at different water depths in the three NE Atlantic basins. The common features of the vertical profiles of their concentrations are the following:

- Ra-226 activity concentrations increased from the ocean surface towards the bottom. This is a result of  $^{226}\text{Ra}$  dissolution from bottom sediments. The minimum values of  $^{226}\text{Ra}$  were always measured in the ocean surface layer, 0.9–1.2 mBq/L, while in ocean deep layers concentrations varied from 2.6 to 3.7 mBq/L, i.e. about 3 times higher than in surface sea water.
- Pb-210 concentrations in solution always displayed their maximal values in the surface layer, above 250 m depth, and decreased downwards to the ocean floor. The higher concentrations in the upper layer are from the atmospheric  $^{210}\text{Pb}$  depositions at the ocean surface.
- Dissolved Po-210 also displayed the higher concentrations in the ocean surface layer, with maximal values around 250–500 m depth, and decreasing downwards to the ocean floor.
- The activity concentration ratios  $^{210}\text{Pb}/^{226}\text{Ra}$  were always  $>1$  in the ocean surface layer and became  $<1$  in the deep ocean layers. The crossover, i.e.  $^{210}\text{Pb}/^{226}\text{Ra} = 1$ , occurred at around 300 m depth in regions A and C, and at around 1000 m depth in region B (Iberian Abyssal Basin).
- The  $^{210}\text{Pb}$  excess in the ocean surface layer from atmospheric depositions is scavenged and removed in such a way that the  $^{210}\text{Pb}$ - $^{210}\text{Po}$  radioactive equilibrium in that layer is never attained. Below the ocean surface layer the  $^{210}\text{Pb}/^{226}\text{Ra}$  ratio was always  $<1$ , and a removal mechanism of  $^{210}\text{Pb}$  and  $^{210}\text{Po}$  also prevented the formation of the  $^{226}\text{Ra}$ - $^{210}\text{Pb}$ - $^{210}\text{Po}$  radioactive equilibrium in the deep ocean layers. Similar profiles of vertical distribution of these radionuclides in the water column were reported for the subtropical and high latitudes of the North Atlantic, and for the Pacific Ocean [27, 30]. The sources of these radionuclides to the ocean water column and the mechanisms controlling their concentrations in, and removal from the water column have been reviewed by several authors [1, 6, 26].

### 3.3. $^{210}\text{Pb}$ and $^{210}\text{Po}$ mean residence times and fluxes

Radionuclide concentrations determined in the NE Atlantic water column were used to compute the mean residence time of these radionuclides, as well as their deposition rates at the sea floor. Computations were made using box models and the assumption of a dynamic equilibrium of radionuclide concentrations in the water column. The ocean was represented by three layers: the surface mixed layer (0–150 m depth), the intermediate layer (150–500 m depth), and the deep ocean layer (500 m to the sea floor, average depth 4500 m) [6, 28, 30]. The average concentrations for

$^{226}\text{Ra}$ ,  $^{210}\text{Pb}$  and  $^{210}\text{Po}$  in these layers were used to compute the radionuclide inventories in the water column ( $\text{Bq m}^{-2}$ ) for each layer (Table 3).

Figure 2 depicts the ocean layers, the radionuclide inventories, mean residence times and calculated radionuclide fluxes including atmospheric deposition rates at the ocean surface and deposition rates at the abyssal sea floor. The average  $^{210}\text{Pb}$  atmospheric flux needed to explain the  $^{210}\text{Pb}$  excess over  $^{226}\text{Ra}$  in the ocean surface layer is about  $74 \text{ Bq}\cdot\text{m}^{-2} \text{ a}^{-1}$ . This value of the atmospheric deposition flux may vary with seasons of the year and the  $^{210}\text{Pb}$  excess determined in the ocean surface layer is likely to vary also with the seasonal primary production in the ocean. For comparison, the average annual  $^{210}\text{Pb}$  deposition in the Lisbon area is  $56 \pm 12 \text{ Bq}\cdot\text{m}^{-2}\cdot\text{a}^{-1}$  (unpublished data). The average residence time of  $^{210}\text{Pb}$  in the soluble phase in the ocean surface layer is about 5 years and the  $^{210}\text{Po}$  residence time is about 1 a. The mean residence time of the particulate radionuclides in the ocean surface layer was computed at 0.6 a. The mean residence times of dissolved  $^{210}\text{Pb}$  and  $^{210}\text{Po}$  in the deep ocean layer were computed at  $42 \pm 20$  a, and 2 (1.6–2) a respectively. The removal of these radionuclides from the deep water column can be theoretically explained by the sedimentation of fine particles with a settling velocity of 900 m/a. These values

TABLE 3. RADIONUCLIDE STOCKS (A) IN THE NE ATLANTIC OCEAN ( $\text{Bq}/\text{m}^2$ )

Station	Boundaries of water layer (depth, m)	$A_{\text{Ra}}$	$A_{\text{Pb}}^d$	$A_{\text{Pb}}^p$	$A_{\text{Po}}^d$	$A_{\text{Po}}^p$
Surface mixed layer:						
Zone A	0–150	165	338	41	240	71
Zone B	0–150	180	287	11	–	–
Zone C	0–150	150	363	37.5	216	97
Intermediate layer:						
Zone A	150–500	466	511	70	546	175
Zone B	150–500	456	783	9	–	–
Zone C	150–500	423	626	82	635	150
Deep sea layer:						
Zone A	500–4500	9010	5200	900	4100	1700
Zone B	500–5000	10690	7155	120	–	–
Zone C	500–4725	9490	3125	621	2325	1298

**Note:** Subscripts Ra, Pb and Po refer to  $^{226}\text{Ra}$ ,  $^{210}\text{Pb}$  and  $^{210}\text{Po}$ , respectively; superscripts *d* means dissolved and *p* means particulate.



can be compared with published data for other regions of the Atlantic Ocean, which are not very different, and for the Mediterranean Sea [1, 28, 29, 31, 32]. Seasonality in the primary production and in the particle flux are expected to control residence times and fluxes of these radionuclides in the ocean [33, 34].

Based on the sea water radionuclide inventories and deficiencies the annual deposition fluxes of  $^{210}\text{Pb}$  and  $^{210}\text{Po}$  at the sea floor of the NE Atlantic were also computed (Fig. 2). These model computations assumed that all particulate  $^{210}\text{Pb}$  exported from the epipelagic zone and 50% of the exported particulate  $^{210}\text{Po}$  are transferred to the abyssal sea floor, and add to the  $^{210}\text{Pb}$  and  $^{210}\text{Po}$  produced from dissolved  $^{226}\text{Ra}$  in the intermediate and deep water layers. This provides an upper limit for the  $^{210}\text{Pb}$  flux and a likely estimate for  $^{210}\text{Po}$  based on its higher assimilation and higher retention in biota. However, this is probably still an overestimation of radionuclide transfer fluxes to the deep sea, and it is likely that some  $^{210}\text{Pb}$  and maybe even more  $^{210}\text{Po}$  is recycled in the epipelagic and mesopelagic zones where most of the oceanic biomass may be found. With those assumptions, the annual deposition fluxes at the abyssal floor would be  $125 \pm 38 \text{ Bq}\cdot\text{m}^{-2}\cdot\text{a}^{-1}$  for  $^{210}\text{Pb}$  (an upper limit) and about  $270 \text{ Bq}\cdot\text{m}^{-2}\cdot\text{a}^{-1}$  for  $^{210}\text{Po}$ . Assuming recycling of the downward particle flux with 50% retention of  $^{210}\text{Pb}$  in the epipelagic and mesopelagic zones, as applied to  $^{210}\text{Po}$ , the annual  $^{210}\text{Pb}$  deposition rate at the abyssal sea floor would be  $100 \text{ Bq}\cdot\text{m}^{-2}\cdot\text{a}^{-1}$ .

Sediment samples from the Iberian Abyssal Basin and from the Porcupine Basin were analysed for  $^{226}\text{Ra}$  and  $^{210}\text{Pb}$  excess in the sediment [35]. The inventory of  $^{210}\text{Pb}$  excess (there are no data for  $^{210}\text{Po}$ ) required average deposition fluxes of  $108 \pm 33$  ( $n=8$ ) and  $100 \pm 20$  ( $n=5$ )  $\text{Bq}\cdot\text{m}^{-2}\cdot\text{a}^{-1}$  in these basins, respectively. Therefore, there is a good agreement between the  $^{210}\text{Pb}$  deficiency in the deep sea water layer maintained by the sinking particulate matter, and the  $^{210}\text{Pb}$  excess found in the abyssal sea floor sediments.

#### 4. CONCLUSIONS

The average uranium concentration in the NE Atlantic water column is  $3.2 \pm 0.4 \mu\text{g/L}$ , with a  $^{234}\text{U}/^{238}\text{U}$  isotopic activity concentration ratio of  $1.13 \pm 0.04$ , similar to values proposed as the world ocean average [18–19]. Uranium concentrations were lower in the Porcupine Basin at greater distance from the continental margin than in the other regions investigated. Most of the uranium in open sea water is in the soluble phase, and only about 0.04% was associated to suspended particles ( $K_d=86 \pm 9$ ). The vertical profile of uranium concentrations in the water column showed minor variations with depth.

The  $^{232}\text{Th}$  present in the Atlantic water originates in the lithosphere and enters the ocean with atmospheric depositions. Thorium displays very low solubility and the  $^{232}\text{Th}$  measured in the ocean water was 91% in the particulate phase ( $K_d=2 \times 10^6$ ). The  $^{230}\text{Th}$  isotope is produced in the water column from dissolved  $^{234}\text{U}$  decay, but it

is rapidly scavenged by particles and the  $^{230}\text{Th}/^{234}\text{U}$  activity concentrations ratio in the soluble phase is maintained very low, at  $2.6 \times 10^{-4}$ .

Ra-226 in the oceanic water column is in excess relative to  $^{230}\text{Th}$  due to radium dissolution from bottom sediments. The vertical profile of  $^{226}\text{Ra}$  showed lower concentrations of about 1.2 mBq/L at the surface, and 2–3 times higher near the abyssal sea floor.

Pb-210 in seawater is partly due to in situ production from dissolved  $^{226}\text{Ra}$  decay, but very little  $^{210}\text{Pb}$  actually originates from uranium decay in sea water due to  $^{234+230}\text{Th}$  scavenging and removal from the water column. In the upper layer,  $^{210}\text{Pb}$  and  $^{210}\text{Po}$  concentrations are higher than those of  $^{226}\text{Ra}$  due to  $^{210}\text{Pb}$  and  $^{210}\text{Po}$  atmospheric depositions. In the deep ocean layers,  $^{210}\text{Pb}$  and  $^{210}\text{Po}$  concentrations are much lower than  $^{226}\text{Ra}$  and are maintained at a low level by particle scavenging.

Pb-210 and  $^{210}\text{Po}$  in the ocean surface layer are mainly from continental origin and enter the open ocean with atmospheric depositions. Their residence times in the soluble phase were 5 and 1 a respectively. Once associated to particles their residence time in the surface layer is lower, at about 0.6 years, being partly released again in the water column from decomposing biogenic debris. These debris seem to be largely recycled in the intermediate ocean layer, probably by the many midwater species that live in the mesopelagic region and form the sonic scattering layer. In the bathyal and abyssal depths, where suspended particles and biota are much less dense,  $^{210}\text{Pb}$  and  $^{210}\text{Po}$  mean residence times in the soluble phase from in situ  $^{226}\text{Ra}$  decay, and especially  $^{210}\text{Pb}$ , were likely to be much higher and actually computed at  $42 \pm 20$  a and 2 a, respectively.

The accumulation of  $^{210}\text{Pb}$  and  $^{210}\text{Po}$  in the abyssal sea floor generates an inventory much above the radionuclide inventory supported by autochthonous  $^{226}\text{Ra}$  decay, at least for  $^{210}\text{Pb}$ . The  $^{210}\text{Pb}$  excess in the top sediment layers is usually a good tracer for sediment accumulation in shallow waters, but in the deep sea it is not a suitable tracer for sedimentation rate studies. Nevertheless, the analyses of  $^{210}\text{Pb}$  in sediments of the NE Atlantic indicated an inventory of  $^{210}\text{Pb}$  excess that implies a deposition flux at around  $100 \text{ Bq}\cdot\text{m}^{-2}\cdot\text{a}^{-1}$  [35]. The  $^{210}\text{Pb}$  flux from the water column needed to maintain the inventory of  $^{210}\text{Pb}$  excess measured in the abyssal sediments was thus in good agreement with  $^{210}\text{Pb}$  model flux computations and with an upper limit of  $125 \pm 38 \text{ Bq}\cdot\text{m}^{-2}\cdot\text{a}^{-1}$ . This agreement indicates a vertical transport and on site deposition of  $^{210}\text{Pb}$  from the oceanic water column, without significant  $^{210}\text{Pb}$  export to, or import from other ocean basins.

## ACKNOWLEDGEMENTS

Thanks are due to Mr. J. M. Oliveira and Ms. G. Alberto for the sample collection and analyses, and to the crews of RV 'A. Carvalho' (Hydrographic Institute, Portugal) and RV 'W. Herwig' (Federal Institute of Fisheries Research, Institute

## INVITED PAPER

of Fishery Ecology, Hamburg, Germany) for collaboration with the sampling and work at sea.

## REFERENCES

- [1] BACON, M.P., BELASTOCK, R.A., TECOTZKY, M., TUREKIAN, K.K., SPENCER, D.W., Lead-210 and polonium-210 in ocean water profiles of the continental shelf and slope south of New England, *Cont. Shelf Res.* **8** (1988) 841–853.
- [2] THOMSON, J., COLLEY, S., ANDERSON, R., COOK, G.T., MACKENZIE, A.B.,  $^{210}\text{Pb}$  in the sediments and water column of the Northeast Atlantic from 47 to 59°N along 20°W, *Earth Planet. Sci. Lett.* **115** (1993) 75–87.
- [3] MOORE, W.S., The effect of submarine groundwater discharge on the ocean, *Annu. Rev. Marine Sci.* **2** (2010) 59–88.
- [4] DePAOLO, D.J., MAHER, K., CHRISTENSEN, J.N., McMANUS, J., SEDIMENT transport time measured with U-series isotopes: Results from ODP North Atlantic drift site 984, *Earth Planet. Sci. Lett.* **248** (2006) 394–410.
- [5] FOWLER, S.W., KNAUER, G.A., Role of large particles in the transport of elements and organic compounds through the oceanic water column, *Prog. Oceanogr.* **16** (1986) 147–194.
- [6] MOORE, R.M., SMITH, J.N., Disequilibria between  $^{226}\text{Ra}$ ,  $^{210}\text{Pb}$  and  $^{210}\text{Po}$  in the Arctic Ocean and the implications for chemical modification of the Pacific water inflow, *Earth Planet. Sci. Lett.* **77** (1986) 285–292.
- [7] HALL, I.R., SCHMIDT, S., MCCAVE, I.N., REYSS, J.L., Particulate matter distribution and  $^{234}\text{Th}/^{238}\text{U}$  disequilibrium along the Northern Iberian Margin: Implications for particulate organic carbon export, *Deep-Sea Res.* **I 47** (2000) 557–582.
- [8] VOGLER, S., SCHOLTEN, J., RUTGERS VAN DER LOEFF, M., MANGINI, A.,  $^{230}\text{Th}$  in the eastern North Atlantic: The importance of water mass ventilation in the balance of  $^{230}\text{Th}$ , *Earth Planet. Sci. Lett.* **156** (1998) 61–74.
- [9] LEE, V.E., DePAOLO, D.J., CHRISTENSEN, J.N., Uranium-series comminution ages of continental sediments: Case study of a Pleistocene alluvial fan, *Earth Planet. Sci. Lett.* **296** (2010) 244–254.
- [10] THOMSON, J., WALLACE, H.E., COLLEY, S., TOOLE, J., Authigenic uranium in Atlantic sediments of the last glacial stage — A diagenetic phenomenon, *Earth Planet. Sci. Lett.* **98** (1990) 222–232.
- [11] THOMSON, J., GREEN, D.R.H., VAN CALSTEREN, P., RICHTER, T.O., VAN WEERING, T.C.E., Holocene sediment deposition on a NE Atlantic transect including Feni Drift quantified by radiocarbon and  $^{230}\text{Th}$  excess methods, *Earth Planet. Sci. Lett.* **242** (2006) 170–185.
- [12] COCHRAN, J.K., “The oceanic chemistry of the U- and Th-series nuclides”, *Uranium series Disequilibrium: Applications to Environmental Problems* (IVANOVICH, M., HARMON, R.S., Eds), Clarendon Press, Oxford (1982) 384–430.

- [13] BOJANOWSKI, R., FUKAI, R., BALLESTRA, S., ASARI, H., “Determination of natural radioactive elements in marine environmental materials by ion-exchange and alpha spectrometry”, Proc. 4th Symp. on the Determination of Radionuclides in Environmental and Biological Materials, London, Paper No. 9 (1983).
- [14] CARVALHO F.P., et al., “Radioactivity in public water supplies in the uranium mining regions of Portugal”, Environmental Contamination from Uranium Production Facilities and their Remediation (Proc. Workshop Lisbon, 2004), Proceedings Series, International Atomic Energy Agency, Vienna (2005) 41–51.
- [15] PHAM, M.K., et al., Certified reference material for radionuclides in fish flesh sample IAEA-414 (mixed fish from the Irish Sea and North Sea), Appl. Radiat. Isot. **64** (2006) 1253–1259.
- [16] POVINEC, P.P., et al., Reference material for radionuclides in sediment, IAEA-384 (Fangataufa Lagoon sediment), J. Radioanal. Nucl. Chem. **273** (2007) 383–393.
- [17] CARVALHO, F.P., Distribution, cycling and mean residence time of  $^{226}\text{Ra}$ ,  $^{210}\text{Pb}$  and  $^{210}\text{Po}$  in the Tagus estuary, Sci. Total Environ. **196** (1997) 151–161.
- [18] KU, T.-L., KNAUSS, K.G., MATHIEU, G.G., Uranium in open ocean: Concentration and isotopic composition, Deep-Sea Res. **24** (1977) 1005–1017.
- [19] CHEN, J.H., EDWARDS, R.L., WASSERBURG, G.J.,  $^{238}\text{U}$ ,  $^{234}\text{U}$  and  $^{232}\text{Th}$  in seawater, Earth Planet. Sci. Lett. **80** (1986) 241–251.
- [20] HAMILTON, E.I., The concentration of uranium in air from contrasted natural environments, Health Phys. **19** (1970) 511–520.
- [21] CARVALHO, F.P., Origins and concentrations of  $^{222}\text{Rn}$ ,  $^{210}\text{Pb}$ ,  $^{210}\text{Bi}$  and  $^{210}\text{Po}$  in the surface air at Lisbon, Portugal, at the Atlantic edge of the European continental landmass, Atmos. Environ. **29** 15 (1995) 1809–1819.
- [22] ANDERSON, R.F., Concentration, vertical flux, and remineralization of particulate uranium in seawater, Geochim. Cosmochim. Acta **46** (1982) 1293–1299.
- [23] WALTER, H.J., RUTGERS VAN DER LOEFF, M.M., HÖLTZEN, H., BATHMANN, U., Reduced scavenging of  $^{230}\text{Th}$  in the Weddell Sea: Implications for paleoceanographic reconstructions in the South Atlantic, Deep-Sea Res. **I 47** (2000) 1369–1387.
- [24] SMITH, K.J., LEÓN VINTRÓ, L., MITCHELL, P.I., BALLY DE BOIS, P., BOUST, D., Uranium-thorium disequilibrium in north-east Atlantic waters, J. Environ. Radioact. **74** (2004) 199–210.
- [25] HIROSE, K., SUGIMURA, Y., Thorium isotopes in the surface air of the Western North Pacific Ocean, J. Environ. Radioact. **5** (1987) 459–475.
- [26] NOZAKI, Y.,  $^{226}\text{Ra}$ – $^{222}\text{Rn}$ – $^{210}\text{Pb}$  systematics in seawater near the bottom of the ocean, Earth Planet. Sci. Lett. **80** (1986) 36–40.
- [27] COCHRAN, J.K., et al.,  $^{210}\text{Pb}$  scavenging in the North Atlantic and North Pacific Oceans, Earth Planet. Sci. Lett. **97** (1990) 332–352.
- [28] BACON, M.P., SPENCER, D.W., BREWER, P.G.,  $^{210}\text{Pb}/^{226}\text{Ra}$  and  $^{210}\text{Po}/^{210}\text{Pb}$  disequilibria in seawater and suspended particulate matter, Earth Planet. Sci. Lett. **32** (1976) 277–296.
- [29] BACON, M.P.,  $^{210}\text{Pb}$  and  $^{210}\text{Po}$  results from F.S. ‘Meteor’ cruise 32 in the North Atlantic, Meteor Forsch.-Ergebnisse **A 19** (1977) 24–36.

## INVITED PAPER

- [30] CHUNG, Y., CRAIG, H.,  $^{210}\text{Pb}$  in the Pacific: The GEOSECS measurements of particulate and dissolved concentrations, *Earth Planet. Sci. Lett.* **65** (1983) 406–432.
- [31] TATEDA, Y., CARVALHO F.P., FOWLER, S.W., MIQUEL J.-C., Fractionation of  $^{210}\text{Po}$  and  $^{210}\text{Pb}$  in coastal waters of the NW Mediterranean continental margin, *Cont. Shelf Res.* **23** (2003) 295–316.
- [32] MASQUE, P., SANCHEZ-CABEZA, J.A., BRUACH, J.M., PALACIOS, E., CANALS, M., Balance and residence times of  $^{210}\text{Pb}$  and  $^{210}\text{Po}$  in surface waters of the northwest Mediterranean Sea, *Cont. Shelf Res.* **22** (2002) 2127–2146.
- [33] KUSS, J., WANIEK, J.J., KREMLING, K., SCHULZ-BULL, D.E., Seasonality of particle-associated trace element fluxes in the deep northeast Atlantic Ocean, *Deep-Sea Res.* **I 57** (2010) 785–796.
- [34] MARTIN, P., et al., Export and mesopelagic particle flux during a North Atlantic spring diatom bloom, *Deep-Sea Res.* **I 58** (2011) 338–349.
- [35] CARVALHO, F.P., OLIVEIRA, J.M., SOARES, A.M.M., Sediment accumulation and bioturbation rates in the deep northeast Atlantic determined by radiometric techniques, *ICES J. Mar. Sci.* **68** (2011) 427–435.



# TRADITIONS AND NEW PERSPECTIVES FOR MARINE RADIOECOLOGY IN ROMANIA

V. PĂTRAȘCU, A.S. BOLOGA

Grigore Antipa National Institute for Marine Research and Development,  
Constanta, Romania

## Abstract

The Marine Radioecology Laboratory started its operation in the 1980s, when Romania launched a nuclear programme. Its first activities were developed within a collaboration framework. The beta and gamma global methods have been used for radioactivity measurements in marine samples or in situ. Experimental work was followed by monochannel spectrometry using radiotracers in biota. The IAEA has supported and improved the use of modern methods such as high resolution multichannel spectrometry and liquid scintillation counting. Sustainable monitoring of marine radioactivity has been initiated. Participation in national and international intercomparison tests gave good results. Many research projects and scientific collaborations have been supported. The published results are a reference for further work and impact assessments of contaminants. Nowadays, using European funds, the Laboratory has new perspectives based on modern methods and installations.

## 1. INTRODUCTION

The Romanian Marine Research Institute (RMRI), reorganized as the Grigore Antipa National Institute for Marine Research and Development (NIMRD) in 1989, has developed fundamental and applied research activities in the field of aquatic ecology, since the year of its establishment (1970).

In 1977, the necessity of marine and freshwater primary production assessment lead to building up of the Nuclear Unit (NU) in order to apply the C-14 method in Romanian research. After receiving authorization from the National Commission for Nuclear Activity Control, the NU enlarged its activities and got all institutional support for scientific research. Thus, the holistic approach of the environment has become possible and more efficient for development of complex research at the Black Sea [1]. Due to the international and national requirements in the nuclear power field, marine radioecology became the main objective of this laboratory.

As part of the marine institutional strategy, radioecology covered three main aspects:

- Study of the radionuclides transfer in the environment;
- Knowledge of the effects and radiological impact assessment on environmental and human health;

- Data analysis, modelling and forecasting.

## 2. METHODS

Starting with an experimental device with a low background NE beta counter, VAS-520 proportional counter and RFT counters (20026 and 22024) [2], research activities have been extended [3, 4].

Global beta measurements were carried out by using the NIM standard technique and scintillation detectors (ND304, NE 102A). This method is useful for the first radiometric investigation of beta active samples or for Sr-90 measurements, after radiochemical separation.

Since the improvements of the equipment with IAEA support (1996), beta liquid scintillation measurements have been possible using the TRICARB 1000 analyzer. This method has been used for C-14 field and laboratory experiments [5].

Gamma spectrometric measurements undertaken with a NaI(Tl) scintillation detector and, since 1992, by using semiconductors HPGe (the latter was also enabled by IAEA support, together with a multichannel analyser ORTEC-NORLAND 5500). The method is useful for rapid investigations (as for the NaI detector with higher efficiency) and/or for finer investigations (such as high resolution spectrometry using a HPGe detector).

From time to time, intercalibration exercises took place both at the national (National Institute for Physics and Nuclear Engineering 'Horia Hulubei'-NIPNE, Bucharest: Cs-137, Eu-152) and international (IAEA: Cs-134, Cs-137, Sr-90, Co-60, K-40) level, for water, sediment and biota samples [4, 6].

Several interregional training courses organized by the IAEA (1994 — Istanbul, Turkey; 1997 and 1999 — Karlsruhe, Germany), a summer school organized by IUR-CE (1992 — Budapest, Hungary), an exchange of experience (1993 — Institute of Biology of the Southern Seas Sevastopol, Ukraine, with intercalibration exercise), and further marine research cruises and intercalibration exercises (i.e. 1993 — CoMSBlack; 1998, 2000 — IAEA RER/2/003) were attended.

## 3. RESULTS

The first systematic results on marine environmental radioactivity were obtained after 1976, through collaborative works with NIPNE and later in the framework of a monitoring program initiated by RMRI, with specific laboratories of the Institute for Hygiene and Public Health from Bucharest, the Radiology section of the Clinic Hospital Bucharest-Fundeni, the National Institute for Meteorology and Hydrology, and the Institute for Research and Environment Engineering Bucharest-Afumati,

as well as with the IAEA Laboratory for Marine Radioactivity from Monaco [3] (between 1977 and 1992).

The autonomy which the NU attained after 1992 due to the improvement of equipment with the help of the IAEA within the project “Sources of radioactivity in the marine environment and their relative contribution to overall dose assessment from marine radioactivity” (MARDOS; IAEA-TECDOC-838) and the programme ‘Marine Environmental Assessment of the Black Sea Region’ IAEA TCP RER/2/003/1995–2002), lead to the obtainment of its own results [7–9].

In order to investigate the radioactivity level in the NW Black Sea, a network of stations situated between the Danube River mouths and Vama Veche, was established along the Romanian coast for the sampling of water, sediments and marine organisms (macro algae, molluscs and fish).

This research has shown that Cs-137 still remains present in living organisms after the Chernobyl nuclear accident [7, 10–12] (Table 1).

The bioindicators for radioactivity can be employed as useful tools both in environmental assessment [2, 10–13] as well as for radiological impact assessments on public health (through food chains). Evaluation of the concentration factors (Table 2) was helpful to show a good correlation between Cs isotopes, and to differentiate between acute and chronic contaminations (e.g. fish).

Dose evaluations have shown that the maximum concentrations of Cs-137 in 1986 did not lead to exposures over the maximum admissible level to the critical groups, and even less since they have decreased in the following period [15].

In comparison with other methods of radioactivity analysis, the global beta method can be considered as the first option of analysis. It is rapid, economical, and sufficiently relevant (see the example in Table 3). Beside the spectrometric method, it can include Sr-90 [9, 16].

Initially, experimental work was focused on the determination of the concentration factors of isotopes Fe-59, Co-60, Zn-65, Sr-89, I-131, Cs-134 in marine macroalgae (*Enteromorpha linza*, *Cystoseira barbata*) and molluscs (*Mytilus galloprovincialis*, *Mya arenaria*, *Scapharca inaequivalvis*) [2]. Later, it developed and included studies on the kinetics of concentration and elimination of radionuclides by marine molluscs [8, 13].

Planktonic primary productivity by the C-14 method was also estimated in the Tasaul Lake [5].

Other studies focusing on the assessment of the local correlation between the radionuclide content (K-40) and salinity have shown the following empirical relation [8]:

$$S (\text{‰}) = \Lambda (K-40) \times 3.05 \quad (1)$$

where:

S (‰) is salinity (g ‰)

$\Lambda$  (K-40) is activity of the K-40 (Bq/L)  
 3.05 is a numerical constant.

The objective of a clean sea specified by the Black Sea Convention, as well as by the European Marine Strategy, emphasizes marine radioactivity assessment. Recent initiatives such as that of the International Commission for the Scientific Exploration of the Mediterranean Sea (CIESM) regarding the monitoring network around the Mediterranean and Black Sea that uses the marine bivalve *Mytilus galloprovincialis*, is welcome and involves the NIMRD NU [17–19].

Increasing technical capacity owing to enlarged analytical methodologies is one major target of the NU intended to be fulfilled through the project “RDI development by modernizing of the nuclear technical infrastructure for environment and aquatic resource (TENUME)”, which has European funding. This project will create new perspectives in environmental research by the modernization of tools and techniques for laboratory and field measurements (such as XRF analysis).

TABLE 1. HIGHEST VALUES OF Cs-137 CONCENTRATION IN MARINE COMPONENTS ALONG THE ROMANIAN BLACK SEA SECTOR (Bq/kg FRESH WEIGHT)

Components	'87	'88	'89	'90	'91	'92	'93	'94	'95	'96	'97	'98	'99	'00/01
Macrophytes	4.6	7.1	5.2	3.4	1.9	1.4	2.8	–	81.4 <sup>a</sup>	2.1	1.8	2.9	<1.9	2
Molluscs	3.2	3.3	2.8	1.3	1.5	1.2	2.3	1.2	2.6	1.4	1.9	1.8	1.6	1.5
Fish	11.0	4.3	5.1	4.0	3.9	3.5	4.2	7.2	4.2	–	3.4	3.1	3.7	3.9

<sup>a</sup> After artificial sanding (17 samples / 7 species; *Bryopsis plumosa*: 81.4 ± 2.6; *Ceramium elegans*: 11.0 ± 0.67) .

TABLE 2. CONCENTRATION FACTORS FROM THE ROMANIAN BLACK SEA SECTOR IN THE VICINITY OF THE ACCIDENT SITE<sup>a</sup>

Components	Period	Place	Cs-134	Cs-137
Macrophytes (8 species)	83–91	Constanta–Jupiter	37	40 ± 26
Molluscs / tissue (4 species)	86–91	Constanta–Jupiter	34 ± 18	29 ± 17
Fish (13 species)	83–91 <sup>b</sup>			53 ± 24
<i>Engraulis encrasicolus ponticus</i>	May '86 <sup>c</sup> 3–16 May '86 <sup>d</sup>	Portita–Constanta	38	67 ± 60 226 ± 98

<sup>a</sup> average ± st. dev.

<sup>b</sup> less Cs values from 1986

<sup>c</sup> only Cs values from May 1986, except *Engraulis sp.*

<sup>d</sup> only Cs from May 1986

TABLE 3. COMPARATIVE RANGES OF RADIOACTIVITY FOR MARINE COMPONENTS FROM THE ROMANIAN BLACK SEA SECTOR OF (Bq/kg FRESH WEIGHT) BETWEEN 1992 AND 1997

Components	Gross beta <sup>a</sup>	Sr-90 <sup>b</sup>	Cs-137
Macrophytes	39–683	<0.16–12.3	0.2–81.4
Molluscs	12–192	<0.13–0.7	0.4–2.6
Fish	17–251	<0.15–1.1	1.3–7.2

<sup>a</sup> K-40 standard

<sup>b</sup> Sr-90 standard

#### 4. CONCLUSIONS

- Radioactivity assessment is an important objective for both the European Marine Strategy and the Black Sea Convention, concerning the decrease of artificial isotopes in the environment and its living resources.
- Biota react to radioactive contamination of the marine environment and can be good indicators for environmental quality assessment.
- The above mentioned results have been accepted for the IAEA database (1983–1992), and for publication at national and international level (1983–2005).
- A large variety of nuclear applications can be used in the near future to also consider the marine environment.
- Local and regional cooperation is welcome and necessary for staff training and extended research.
- Maintaining the experience already gained and the proficiency by quality programmes is a real need.

#### REFERENCES

- [1] NICOLAEV, S., et al., Needs for sustainable development of the Romanian Black Sea coast, *Cercetări marine — Recherches marines* **35** (2004) 1–23.
- [2] BOLOGA, A.S., “Experimentally-derived concentration factors of marine biota as radioecological indicators for the Romanian Black Sea shore”, *Frontiers in Radiation Biology (Proc. Mtg Tel Aviv, 1988)* (RIKLLIS, E., Ed.), Weinheim (1990) 595–604.
- [3] BOLOGA, A.S., OSVATH, I., PĂTRAȘCU, V., “Monitoring of marine water, sediment and biota radioactivity in samples from the Romanian sector of the Black Sea by means of gamma spectrometry”, *Sources of Radioactivity in the Marine Environment and their Relative Contribution to Overall Dose Assessment from Marine Radioactivity/MARDOS*, IAEA-MEL-R2/94, INTERNATIONAL ATOMIC ENERGY AGENCY.

- [4] PĂTRAȘCU, V., “Techniques nucleaires et resultats du monitoring roumain de la Mer Noire dans le laboratoire radioecologique de l’Institut Roumain de Recherches Marines”, *Marine Pollution, IAEA-TECDOC-1094*, IAEA, Vienna (1999) 546–547.
- [5] ROSIORU, D.M, et al., The acidification and bubbling radiocarbon method, used in the assessment of phytoplankton production in Romanian coastal lakes, *Cercetări Marine — Recherches Marines* **38** (2008) 73–79.
- [6] PĂTRAȘCU, V., Donnees preliminaires concernant les premiers exercices radiometriques d’intercalibration de l’Institut Roumain de Recherches Marines de Constanta dans la Mer Noire, *Cercetari Marine — Recherches Marines* 27–28 (1994–1995) 357–364.
- [7] BOLOGA, A.S., PĂTRAȘCU, V., Radioactivity in the Romanian Black Sea Sector: One decade after Chernobyl, Vol. 2, *One Decade After Chernobyl: Summing Up the Consequences of the Accident, IAEA-TECDOC-964*, IAEA, Vienna (1997) 469–475.
- [8] PĂTRAȘCU, V., Contributions at Distribution Knowledge of Marine Components Radioactivity and at Evaluation of Some Radioecological Consequences, PhD Thesis, Physical Atomic Institute, Bucharest (1999).
- [9] PĂTRAȘCU, V, BOLOGA, A.S., CUIINGIOGLU, E., “Synthetic results in the radioactivity assessments of the Romanian Black Sea sector after 1992”, *Environmental Changes and Radioactive Tracers (FERNANDEZ, J.M., FICHEZ, R., Eds)*, IRD Editions, Paris (2002) 39–48.
- [10] OSVATH, I., BOLOGA, A.S., DOVLETE, C., Environmental Cs–137 concentration factors for Black Sea biota, Preliminary data, *Rapp. Comm. Int. Mer Medit.* **32** 1 (1990) 320.
- [11] OSVATH, I., DOVLETE, C., BOLOGA, A.S., “Radioactivity in the Romanian sector of the Black Sea”, *Proc. Int. Symp. Post-Chernobyl Environmental Radioactivity Studies in East European Countries, (Kazimierz, 1990)*, (1990) 108–112.
- [12] PĂTRAȘCU V., “Reference data on the relative content of radionuclides in aquatic components at the Romanian Black Sea Littoral”, *Proc. 2nd Int. Conf. on the Mediterranean Coastal Environment (MEDCOAST’95) (Tarragona) (OZHAN, E., Ed.)*, Vol. 3, (1995) 1465–1472.
- [13] PĂTRAȘCU, V., “Transfert des radionucleides  $^{60}\text{Co}$ ,  $^{65}\text{Zn}$ ,  $^{134}\text{Cs}$  aux sediments et aux mollusques marins en conditions de laboratoire”, *Marine Pollution, IAEA-TECDOC-1094*, IAEA, Vienna (1999) 544–545.
- [14] BOLOGA, A.S., et al., “Present level of contaminants in the Romanian Black Sea sector”, *Marine Pollution, IAEA-TECDOC-1094*, IAEA, Vienna (1999) 58–63.
- [15] PĂTRAȘCU, V., “Maximum doses in the Romanian Black sea sector, The Radiological exposure of the European Community to Radioactivity in the Mediterranean sea”, *MARINA MED Project, Proc. Sem. Rome ENEA headquarters, Cigna (A., DELFANTI, R., SERRO, R., Eds)*, *Radiation Protection* **70** (1994) 523–529.
- [16] PĂTRAȘCU, V., BOLOGA, A.S., Considerations on marine gross radioactivity measurements between 1982–1990, *Mediul inconjurător* **3** 2 (1992) 23–28.
- [17] THÉBAULT, H., et al.,  $^{137}\text{Cs}$  baseline levels in the Mediterranean and Black Sea: A cross-basin survey of the CIESM Mediterranean Mussel Watch programme, *Mar. Pollut. Bull.* **57** 6–12 (2008) 801–806.

- [18] PĂTRAȘCU, V., PUSCASU, C., “Radioactivity assessment in Romanian sector of the Black Sea by *Mytilus galloprovincialis*”, *Black Sea Ecosystem 2005 and Beyond* (Proc. Conf. Istanbul, 2006), Vol. 1, Commission on the Protection of the Black Sea Against Pollution (2006) 382–385.
- [19] OSVATH, I., DOVLETE, C., BOLOGA, A.S., Data base for radionuclides in the north-western Black Sea, *Rapp. Comm. Int. Mer Medit.* **33** (1992) 384.



ISOTOPES AND RADIONUCLIDES  
IN THE MARINE ENVIRONMENT



# APPLICATIONS OF RADIUM ISOTOPES TO OCEAN STUDIES

W.S. MOORE

Department of Earth and Ocean Sciences,  
University of South Carolina,  
Columbia, SC, USA

## Abstract

With half-lives ranging from 3.7 days to 1600 a, naturally occurring radium isotopes have been used to study a variety of processes in the ocean. New techniques, which allow rapid analyses of the short lived isotopes,  $^{224}\text{Ra}$  (half-life = 3.7 days) and  $^{223}\text{Ra}$  (half-life = 11 days), have lead to many novel ways to apply radium to oceanography. This paper will focus on how the use of these isotopes has led to breakthroughs in quantifying: (1) the residence time of water in estuaries, (2) coastal ocean mixing rates and (3) submarine groundwater discharge (SGD). With this new understanding of rates and fluxes in the near shore environment, scientists and coastal managers are now able to evaluate sources of nutrients, carbon, and metals and their impact on the coastal ocean. For example, it is now known that SGD rivals rivers as a nutrient source to many coastal environments.

## 1. INTRODUCTION

Uranium is an abundant trace element in the ocean with a concentration averaging about 15 nM. However, thorium produced from U decay is rapidly scavenged and transported to deep-sea sediments. Here,  $^{230}\text{Th}$  decays to produce  $^{226}\text{Ra}$  that may be released from the particles holding the Th. Some of this Ra finds its way back to the ocean, where it mixes through the water column. This picture of U–Th–Ra behaviour was developed early in the study of marine radioactivity [1, 2].

Much of the early interest in  $^{226}\text{Ra}$  in the ocean was based on the hypothesis that concentrations in sea water were almost entirely derived from deep-sea sediments. After entering the water column it was slowly mixed upward to the surface ocean. During this mixing radioactive decay would gradually diminish the concentration. Thus, the rate of vertical mixing could be derived from the  $^{226}\text{Ra}$  distribution [2]. This simple picture became more complicated when it was realized that Ra was being removed from surface waters by biological processes at a rate comparable to its half-life. As these organic rich particles settled through the water column, some dissolved and released Ra; additional release occurred at the seabed. In order to distinguish radioactive decay from the particle cycle, additional tracers were required. Barium was an obvious candidate because of its chemical similarity to Ra.

During the period 1975–1985 there were many papers addressing the marine geochemistry of radium. These were driven largely by the huge GEOSECS dataset of Ra isotopes in all major oceans. During the GEOSECS expedition Ra and Ba were measured in the same water samples and strong correlations were found [3]. It was also noted that  $^{226}\text{Ra}$  was highly correlated with dissolved silica concentrations [4].

After GEOSECS there were several papers that developed models of Ra in the ocean. However, the fraction of the signal due to radioactive decay, and hence the rate of mixing, was difficult to discern. It was obvious that the initial hypothesis required considerable revision. One of the common aspects of the Ra models remained: that Ra was primarily added to deep waters. The fraction added to surface waters was assumed to come primarily from rivers, a source thought to be in the range 1–10% of the deep addition. The realization that inputs to surface waters by submarine groundwater discharge (SGD) were much more important than rivers [5] will require a complete re-evaluation of the global Ra models. Since so much more Ra is being added to surface waters than was expected, the particulate removal and regeneration terms must be increased substantially.

After the GEOSECS data were digested and published, interest in oceanic Ra studies decreased. However, in the past 15 years there has been a revival in interest in Ra isotopes in the marine environment. As Charette and Scholten point out in the introduction to a special issue of Marine Chemistry [6]:

*“Beginning in the mid-1990s, radium underwent a renaissance in the ocean sciences, when it was used to quantify the importance of SGD on the oceanic budget of many trace metals and nutrients ([5, 7] and references therein). Concurrent with this discovery was the production of a commercially available delayed coincidence counter (RaDeCC; [8] which greatly simplified the measurement of the two short-lived Ra isotopes,  $^{224}\text{Ra}$  and  $^{223}\text{Ra}$ . The powerful radioactive ‘clocks’ associated with the short-lived radium isotopes have seen greatly increased application since the advent of RaDeCC”.*

In addition to the Marine Chemistry issue, there have been numerous book chapters and review articles addressing Ra isotope applications [7–14], and three recent additional journal special issues (Biogeochemistry 66, p1–202, 2003; Estuarine Coastal and Shelf Science 76, p455–552, 2008; and Journal of Environmental Radioactivity, 101, 2010) that focus on this topic.

## 2. GEOCHEMICAL PROXIES FOR FLUX ( $^{226}\text{Ra}$ , $^{228}\text{Ra}$ , $^{223}\text{Ra}$ , $^{224}\text{Ra}$ )

The presence of high activities of  $^{226}\text{Ra}$  in coastal waters that could not be explained by river or sediment input led Moore [5] to hypothesize that salty groundwater was responsible for the high activities. This hypothesis has been tested and confirmed in numerous coastal environments (e.g. Refs [15–21]).

The quantification of submarine groundwater discharge (SGD) is facilitated by the differences in half-life (and hence regeneration times) of the Ra isotopes from their thorium (Th) parents. In the marine environment Th is tightly bound to particles, but Ra is more mobile and may desorb into sea water. Salty groundwater contacts more sediment surfaces than do surface waters, therefore groundwaters usually have high activities of Ra. As sediments are flushed, Ra is transferred to estuaries and the coastal ocean. Once lost from the sediments, the Ra isotopes regenerate in the sediment at different rates. The long lived  $^{226}\text{Ra}$  requires 1600 a to regenerate 50% of its activity, but the shorter lived  $^{228}\text{Ra}$  regenerates 50% of its activity in 5.7 years. Because sediments retain Th but not Ra, they serve as a constant source of Ra to marine waters. Surficial coastal aquifers that are continuously flushed with salt water have low activities of  $^{226}\text{Ra}$  because there is not enough time for this isotope to regenerate from its parent. Deeper aquifers that are flushed less efficiently have higher activities of  $^{226}\text{Ra}$ . The presence of water from these distinct sources may be recognized and quantified using  $^{228}\text{Ra}/^{226}\text{Ra}$  activity ratios in surface waters [17, 22, 23].

The two short lived Ra isotopes,  $^{223}\text{Ra}$  and  $^{224}\text{Ra}$ , provide additional evidence of groundwater input. These nuclides regenerate on time scales of days and are therefore especially useful in studies of systems having short residence times. Rama and Moore [15] used the four Ra isotopes to determine that groundwater input to the North Inlet salt marsh occurred where tidal creeks were cut into deeper aquifers rather than through muddy surficial sediments. These short lived isotopes may also provide a means of estimating the residence time of estuarine and coastal waters [24, 25]. The residence time is important because it provides the time scale available for components to accumulate in the water column.

### 3. CASE STUDIES OF THE USE OF RADIUM ISOTOPES OVER DIFFERENT SCALES

To illustrate the applications of radium isotopes to study the ocean on different spatial scales, I offer three examples: In the first we used Ra isotopes to determine the flushing time of a small estuary in South Carolina [25]. The second study used Ra isotopes to determine the coastal mixing rates and inputs of dissolved iron to coastal waters in southern Brazil [26]. The third study used the total inventory of  $^{228}\text{Ra}$  in the upper Atlantic Ocean to estimate the total submarine groundwater discharge to the Atlantic [27].

#### 3.1. Flushing times in estuaries: Impact on biogeochemistry

We define the flushing time of an estuary as the ratio of the total mass or volume of a constituent divided by its rate of renewal. A common way to estimate flushing time is based on the tidal prism, defined here as:

$$P = \int_H^0 A dz \tag{1}$$

where  $A$  (water surface area) is a function of  $z$  (water depth) over  $H$  (tidal range). The volume of the estuary is defined as the product of the average area and depth. The average discharge rate of the estuary is  $Q = P/T$  where  $T$  is the tidal period. Thus, the flushing time ( $T_f$ ) for the estuary is [28]:

$$T_f = \frac{VT}{(1-b)P} \tag{2}$$

Eq. 2 allows for a return of a portion of the water that leaves the estuary during ebb tide. This return flow  $b$  depends on: (1) the tidal period, (2) the initial width of the effluent plume in the receiving channel, (3) the distance from the bank of the receiving channel to the effluent centreline, and (4) a characteristic diffusion length scale. While most variables can be estimated from field data in the source creek,  $b$  cannot since it depends upon the fate of the estuary's effluent after it enters the receiving body. Physical oceanographers estimate  $b$  using an approach based on a simple steady state momentum balance that determines the ratio of the difference between the outflowing ebb velocity and the incoming flood velocity [29]. This approach requires long term measurements of water levels and flow velocities as well as mean volumes of the estuary and the tidal prism [25].

There is another method to determine the return flow factor  $b$ . This is based on a three endmember mixing model developed for Ra isotopes by Moore [22]. This model is used to estimate the fractions of (1) ocean water, (2) river water and (3) groundwater in an estuary. Construct equations for water, salt and  $^{228}\text{Ra}$  balance.

$$f_S + f_R + f_{GW} = 1.00 \tag{3}$$

$$^{228}\text{Ra}_S f_S + ^{228}\text{Ra}_R f_R + ^{228}\text{Ra}_{GW} f_{GW} = ^{228}\text{Ra}_M \tag{4}$$

$$S_S f_S + S_R f_R + S_{GW} f_{GW} = S_M \tag{5}$$

where:

- $f_S$  is the fraction of ocean water,
- $f_R$  is the fraction of river water,
- $f_{GW}$  is the fraction of groundwater endmembers,
- $Ra_S$  is  $^{228}\text{Ra}$  activity,
- $S_S$  is the salinity in the ocean endmember,
- $Ra_R$  is  $^{228}\text{Ra}$  activity,
- $S_R$  is the salinity in the river endmember,
- $Ra_{GW}$  is  $^{228}\text{Ra}$  activity

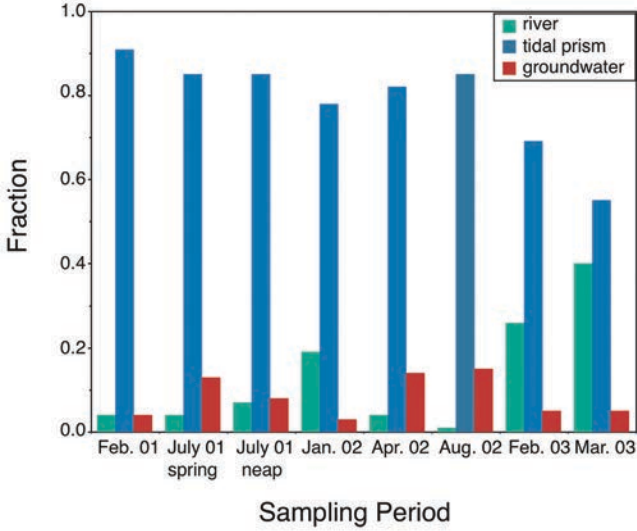


FIG. 1. Fractions of each endmember in estuarine samples collected at different times. Adapted from Ref. [25].

$S_{GW}$  is the salinity in the groundwater endmember,  
 $Ra_M$  is measured  $^{228}\text{Ra}$  activity,  
 $S_M$  is the salinity measured in the sample.

These equations may be solved for the fractions of each endmember present in the estuary sample at any given time [25].

Figure 1 gives the results of this mixing model using estuarine data from various sampling periods and the average composition of groundwater and river water in the Okatee estuary, SC. The return flow  $b$  is implicit in the mixing model. If the incoming sea water is sampled during the 3–4 hours of rising tide, these samples are not a true sea water endmember, but represent a mixture of sea water with the tidal prism exported from the estuary. By using these samples as the sea water endmember, the fraction of this endmember in the estuary is a direct measure of  $b$ , the return flow, i.e.  $f_s = b$ . The values of  $b$  range from 0.55 to 0.91 (average = 0.79) and yield flushing times that range from 1.0 to 4.8 days (average = 2.5 days). This compares well with the physical estimate of  $b = 0.81$ .

The mixing model is sensitive to the assumed values for the average input of salinity and  $^{228}\text{Ra}$  and to measurement errors for individual samples. Because the calculated values for  $b$  approach the limit of 1.0, small positive changes in  $b$  result in large increases in flushing time. For example, increasing  $b$  from 0.85 to 0.91 increases  $T_f$  from 2.9 to 4.8 days. Because of the assumptions and measurement errors,  $T_f$  calculated from the mixing model probably has an error of at least 30%.

3.2. Coastal mixing and SGD flux of iron to the Brazil Current

To quantify SGD fluxes of materials to the coastal ocean, a measure of the residence time of these waters with respect to mixing with the open ocean is required. The short lived radium isotopes provide one means of measuring this mixing rate. These isotopes are contributed to near shore waters by SGD and release from sediments. Once introduced to the water, activities decrease by mixing with lower activity offshore water and by radioactive decay. Moore [24] demonstrated that the distribution of the short lived isotopes over the shelf can be modelled to yield mixing rates. The solution of the mixing equation for the short lived radium isotopes is:

$$\ln A_x = \ln A_{x=0} - (\lambda/K_h)x \tag{6}$$

where

- A is the measured activity at distance x;
- A<sub>x=0</sub> is the activity at the shoreline;
- K<sub>h</sub> is the mixing coefficient;
- λ is the decay constant.

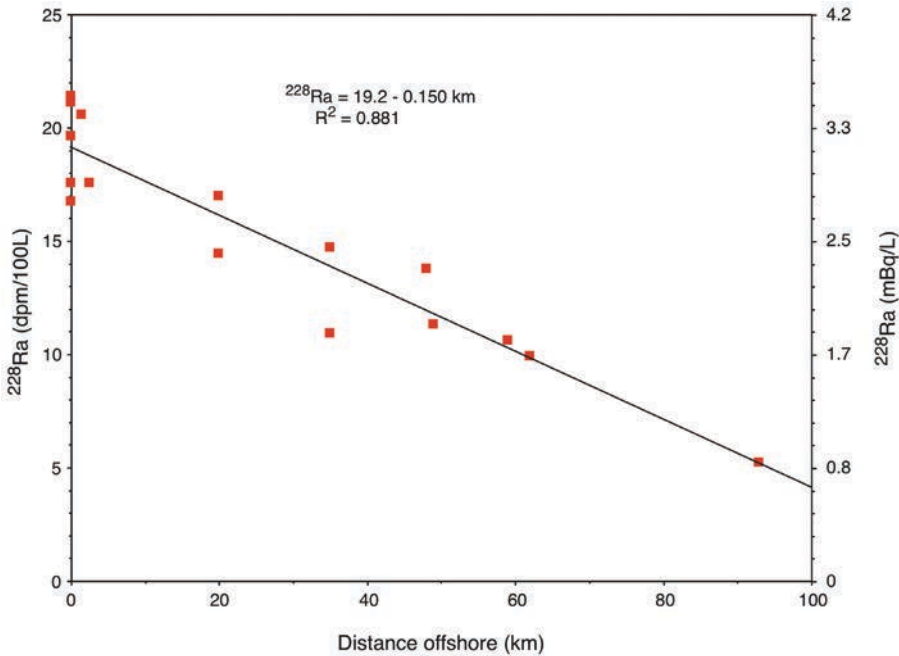


FIG. 2. The distributions of <sup>228</sup>Ra isotopes off the southern coast of Brazil. Note the linear decrease of <sup>228</sup>Ra, indicating conservative mixing across the shelf. Modified from Ref. [26].

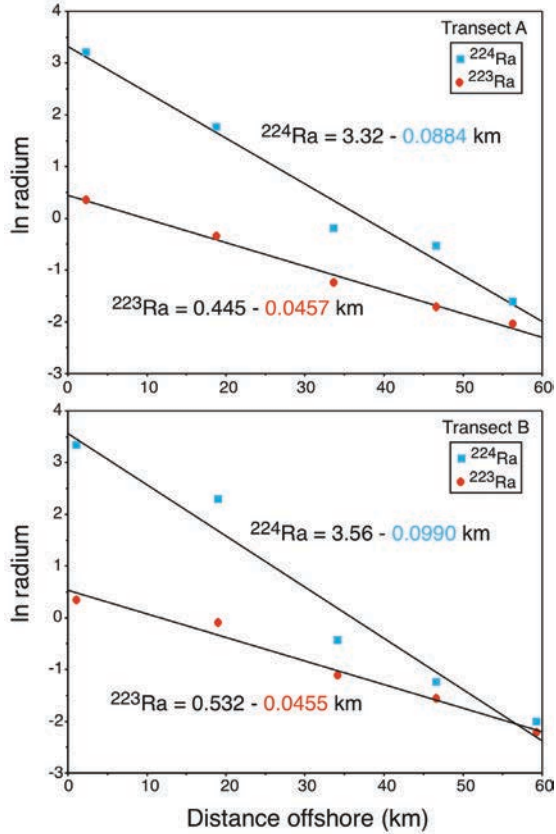


FIG. 3. The distributions of short-lived Ra isotopes off the southern coast of Brazil. Note the exponential decreases of  $^{223}\text{Ra}$  and  $^{224}\text{Ra}$ , indicating mixing and radioactive decay. The  $^{223}\text{Ra}$  data yield a consistent mixing rate of  $338 \text{ m}^2/\text{s}$ . Modified from Ref. [26].

Several assumptions are required to use this model: (1) radium addition to the surface water occurs only in the near shore zone; (2) net cross-shelf advection is zero; (3) cross-shelf mixing is constant; (4) the system is steady state.

During December 2004 we occupied four 60 km offshore transects and one station 90 km off the shore of southern Brazil [26]. There was a strong pycnocline across the shelf on transects A and B except within 10 km of shore. This should prevent radium released into bottom water on the shelf from reaching the surface. The pycnocline was not present on southern transects C and D, meaning that they may be influenced by input from the seabed. We conclude that the first assumption is valid for transects A and B, but not for C and D. Along transects A and B,  $^{228}\text{Ra}$  decreases linearly across the shelf (Fig. 2). This implies that constant mixing, not advection, controls the distribution and supports the second and third assumptions.

Along transects A and B,  $^{223}\text{Ra}$  and  $^{224}\text{Ra}$  decrease exponentially across the shelf (Fig. 3). This also implies that the mixing rate is constant, and supports the third assumption. Due to limited ship time we could not test assumption 4. The slope of the  $\ln\text{Ra}$  vs. distance plot is  $(\lambda/K_h)^{1/2}$ . Solving for  $K_h$  yields mixing rates of  $338\text{ m}^2/\text{s}$  and  $240\text{ m}^2/\text{s}$  for  $^{223}\text{Ra}$  and  $^{224}\text{Ra}$ , respectively.

At steady state the offshore flux of radium must be balanced by new inputs. The offshore flux of  $^{228}\text{Ra}$  is the product of its concentration gradient (Fig. 3) and the mixing rate. Assuming all export is through a minimal 10 m deep mixed layer, the offshore flux is  $5 \times 10^{17}$  atoms/day throughout the 240 km study area. If this flux is sustained by water similar to the beach groundwater samples (average  $^{228}\text{Ra} = 5.2 \times 10^6$  atoms/L), the total SGD flux is  $10^{11}$  L/day.

This SGD flux is important because it transports large concentrations of nutrients [30] and iron [26] to these coastal waters. Just offshore of the study area massive diatom blooms are common. It is likely that these are sustained by the nutrient fluxes

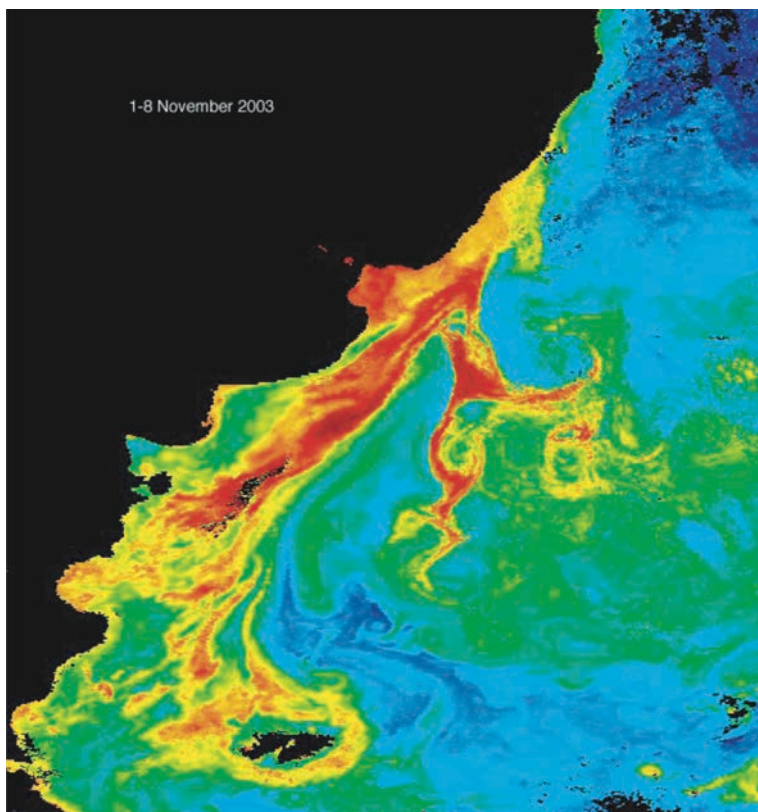


FIG. 4. MODIS ocean colour image of the SE coast of South America showing chlorophyll along the frontal zone of the Brazil–Malvinas Confluence. Image provided by the SeaWiFS Project, NASA's Goddard Space Flight Center and ORBIMAGE. Modified from Ref. [26].

derived from SGD [30]. However, there is a larger issue: the dissolved iron flux. Dissolved iron is a critical micronutrient for ocean productivity. Most open ocean surface waters contain  $<1$  nM of dissolved Fe; this low concentration severely limits productivity even in nutrient rich waters.

The Malvinas Current transports surface water with large concentrations of nutrients from southern Argentina to its convergence with the Brazil Current off southern Brazil. The mixing of these currents can be observed from satellite images because the convergence zones contain high concentrations of chlorophyll (Fig. 4). The Malvinas Current supplies the macronutrients for this productivity. What is the source of the iron?

In this study area dissolved iron maintains very high concentrations in the groundwater. The iron flux associated with SGD can be estimated by multiplying the average iron concentration in the beach groundwaters ( $24 \mu\text{mol/L}$ ) by the SGD flux. This yields an iron flux of  $2 \times 10^6$  mol/day to the coastal ocean.

Some of the iron is removed as the SGD comes into contact with surface waters. However, the average dissolved Fe concentration in the coastal waters was found to be 50 nM, two orders of magnitude higher than typical offshore water. If we consider this 240 km coastline out to 22 km and to a depth of 10 m, this represents an offshore pool of dissolved Fe of  $2.6 \times 10^6$  moles. How much of this Fe can be transported beyond the coast?

For transects 1 and 2 the  $^{223}\text{Ra}$  data indicate a mixing rate of  $338 \text{ m}^2/\text{s}$ . This value can be used to estimate the residence time of water on the shelf, i.e. the time required to remove the water from  $1/e$  of the width of the shelf. If we take the shelf width as 60 km and use the relationship

$$L = (2 K_h t)^{1/2} \quad (7)$$

the residence time for 22 km is 8.3 days. Thus, the offshore flux of dissolved Fe (assuming steady state conditions) is  $3.2 \times 10^5$  moles/day. This flux represents over 10% of the total atmospheric deposition of Fe to the South Atlantic Ocean ( $2.2 \times 10^6$  mol/day). There is no reason that this study area should be unique; similar SGD fluxes of dissolved Fe probably occur all along this coast. Once past the coastal zone the Fe may be entrained in the Brazil Current and transported south to support production in nutrient rich waters of the Brazil/Malvinas Confluence and the upwelling along the continental shelf break. These large inputs of Fe could help fuel the massive plankton blooms evident from satellite chlorophyll images along the coasts of Argentina, Uruguay, and Brazil (Fig. 4).

### 3.3. Radium-228 as a basin scale integrator of submarine groundwater discharge (SGD) to the Atlantic Ocean

During the past decade submarine groundwater discharge (SGD) has become recognized as an important pathway of dissolved materials between the continents and oceans. This process includes any and all flow of water on continental margins from the seabed to the coastal ocean, regardless of fluid composition or driving force [9]. SGD contributes large amounts of nutrients, carbon, and metals to coastal waters [14]. However, measurement of SGD is difficult on regional and larger scales. To evaluate the overall importance of SGD, we would like to know the total flux to each ocean.

Because of their different half-lives, Ra isotopes provide information over a range of temporal and spatial scales.  $^{228}\text{Ra}$ , with its half-life of 5.75 a, enters the upper ocean from the continents and mixes throughout surface waters. Strong gradients occur in both horizontal and vertical dimensions because of radioactive

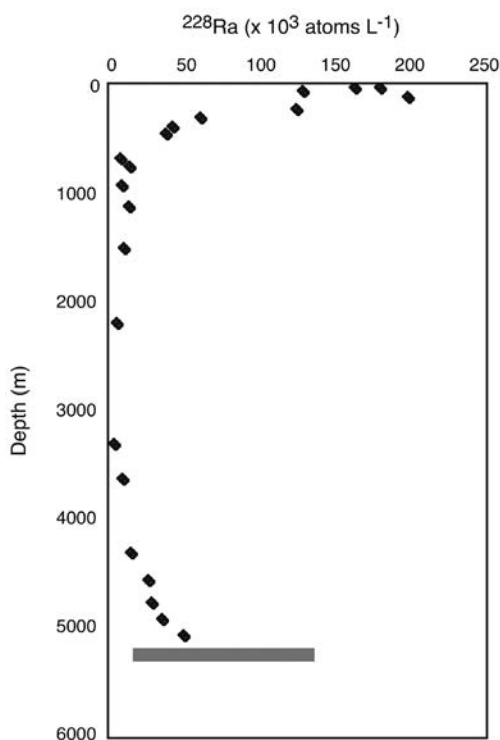


FIG. 5. Typical depth profile of  $^{228}\text{Ra}$  ( $\times 10^3$  atoms/L) in the Atlantic Ocean. The grey bar indicates the seabed. Note that significant concentrations occur in near-surface and near-bottom waters, but not in waters between 1000 and 4000 m depth.

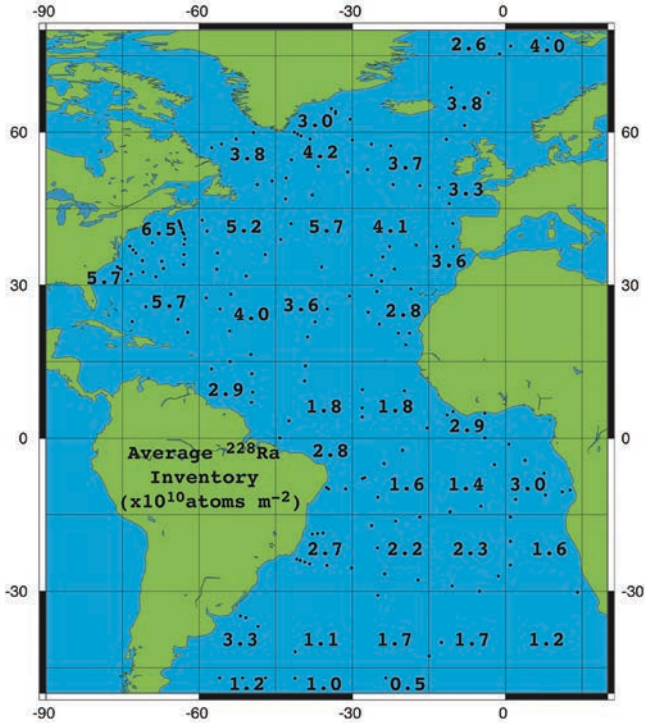


FIG. 6. The inventory of  $^{228}\text{Ra}$  ( $\times 10^{10}$  atoms/m) in the upper 1000 m of the Atlantic Ocean. The points show the stations used to calculate  $^{228}\text{Ra}$  inventories. All stations within each  $15^\circ \times 15^\circ$  box were averaged to yield a bin average, shown as a number in each box. The bin averages were averaged to yield a grand average. The grand average was multiplied by the surface area of the Atlantic to estimate the total  $^{228}\text{Ra}$  inventory in the upper Atlantic. Adapted from Ref. [27].

decay (Fig. 5). Exactly 12% of the total  $^{228}\text{Ra}$  inventory in the ocean disappears each year by this process, i.e.  $\lambda = 0.12/\text{a}$ . To maintain steady state in the upper ocean, there must be an equivalent  $^{228}\text{Ra}$  flux from continental margins, as  $^{228}\text{Ra}$  released from deep-sea sediments (depths 3000–6000 m) does not penetrate into the upper 1000 m. Additionally, we know that SGD is an important conveyer of the  $^{228}\text{Ra}$  flux.

We may use these observations to develop a strategy for determining the total SGD flux to the Atlantic. First, we measure the total  $^{228}\text{Ra}$  inventory in the upper ocean to calculate the decay loss. This provides an estimate of the flux to near surface waters from the continents, assuming the distribution is steady state. Then we evaluate other sources to the upper ocean including release from near shore and continental shelf sediments and river input. If more  $^{228}\text{Ra}$  is decaying than is being supplied, an additional source is required; we assume the missing source is SGD because no other sources are known.

The Transient Tracers in the Ocean project (1981–1989) mapped  $^{228}\text{Ra}$  and  $^{226}\text{Ra}$  distributions in the Atlantic. These data are used to determine the inventory of  $^{228}\text{Ra}$  in the upper Atlantic (Fig. 6).

The  $^{228}\text{Ra}$  inventory (atoms/m) was evaluated by linear interpolation between samples 0–1000 m deep at each station. Between 1000–2000 m  $^{228}\text{Ra}$  was below detection with respect to blank (Fig. 5). To calculate the total inventory, the stations were grouped into  $15^\circ \times 15^\circ$  boxes; all profiles in each box were used to calculate a bin average (Fig. 6). These bin averages were used to calculate a grand average. The grand average inventory of  $^{228}\text{Ra}$  in the upper Atlantic ( $3.0 \times 10^{10}$  atoms/m) was multiplied by the surface area of the Atlantic to calculate the total upper Atlantic inventory of  $2.9 \times 10^{24}$  atoms. Twelve percent of this inventory ( $3.5 \times 10^{23}$  atoms) decay each year ( $1.3 \times 10^{15}$  Bq/a).

To determine the fraction of the required flux that is due to SGD, other sources of  $^{228}\text{Ra}$  to the ocean were evaluated [27]. Release from fine grained sediments contributes 37%, rivers contribute 7%, and atmospheric deposition contributes <1%; the remaining 55% must come from SGD. Measurements of  $^{228}\text{Ra}$  in coastal groundwater (mostly salty groundwater) from the Atlantic coast were used to establish a mean concentration,  $6.2 \times 10^6$  atoms/L. Dividing the SGD  $^{228}\text{Ra}$  flux by this mean concentration revealed that the  $^{228}\text{Ra}$  loss from the upper Atlantic requires a SGD water flux of (2 to 4)  $\times 10^{16}$  L/a.

#### 4. CONCLUSIONS

The SGD flux is probably between 0.8 and 1.6 times the river flux of  $2.4 \times 10^{16}$  L/a to the Atlantic. It must be stressed that SGD is not just fresh water. However, the concentrations of nutrients, metals, and carbon are typically higher in SGD than in river water passing the estuary filter; therefore, we expect SGD to be more important for the input of these materials to the ocean.

The international GEOTRACES project will provide new data on the distribution of  $^{228}\text{Ra}$  in the ocean. These data will be used to test the steady state assumption for the balance of  $^{228}\text{Ra}$  in the Atlantic and to estimate  $^{228}\text{Ra}$  inventories in other oceans.

#### REFERENCES

- [1] EVANS, R. D., et al., The radium and radon content of Pacific Ocean water, life, and sediments, *Am. J. Sci.* **36** (1938) 241–259.
- [2] KOCZY, F.F., “Natural radium as a tracer in the ocean”, *Proc. 2nd UN Int. Conf. Peaceful Uses of Atomic Energy, United Nations, Geneva* (1958) 351–357.

## INVITED PAPER

- [3] LI, Y.-H., et al., Barium in the Antarctic Ocean and implications regarding the marine geochemistry of Ba and <sup>226</sup>Ra, *Earth Planet. Sci. Lett.* **19** (1973) 352–358.
- [4] CHUNG, Y.C., Radium-barium-silica correlations and a two-dimensional radium model for the world ocean, *Earth Planet. Sci. Lett.* **49** (1980) 309–318.
- [5] MOORE, W.S., Large groundwater inputs to coastal waters revealed by <sup>226</sup>Ra enrichments, *Nature* **380** (1996) 612–614.
- [6] CHARETTE, M.A., SCHOLTEN, J.C., Marine Chemistry special issue: The renaissance of radium isotopic tracers in marine processes studies, *Mar. Chem.* **109** (2008) 185–187.
- [7] BURNETT, W.C., et al., Quantifying submarine groundwater discharge in the coastal zone via multiple methods, *Sci. Total Environ.* **367** (2006) 498–543.
- [8] MOORE, W.S., ARNOLD, R., Measurement of <sup>223</sup>Ra and <sup>224</sup>Ra in coastal waters using a delayed coincidence counter, *J. Geophys. Res.* **101** (1996) 1321–1329.
- [9] BURNETT, W.C., et al., Groundwater and pore water inputs to the coastal zone, *Biogeochemistry* **66** (2003) 3–33.
- [10] SWARZENSKI, P.W., U/Th series radionuclides as coastal groundwater tracers, *Chem. Rev.* **107** (2007) 663–674.
- [11] KU, T.-L., LUO, S., “Ocean circulation/mixing studies with decay-series isotopes”, *U–Th Series Nuclides in Aquatic Systems* (KRISHNASWAMI, S., COCHRAN, J.K., Eds), Elsevier, Oxford (2008) 307–344.
- [12] COCHRAN, J.K., KADKO, D.C., “Uranium- and thorium-series radionuclides in marine groundwaters”, *U–Th Series Nuclides in Aquatic Systems* (KRISHNASWAMI, S., COCHRAN, J.K., Eds), Elsevier, Oxford (2008) 345–382.
- [13] CHARETTE, M.A., et al., “Uranium-and thorium-series nuclides as tracers of submarine groundwater discharge”, *U–Th Series Nuclides in Aquatic Systems* (KRISHNASWAMI, S., COCHRAN, J.K., Eds), Elsevier, Oxford (2008) 155–192.
- [14] MOORE, W.S., The effect of submarine groundwater discharge on the ocean, *Annu. Rev. Mar. Sci.* **2** (2010) 59–88.
- [15] RAMA, MOORE, W.S., Using the radium quartet for evaluating groundwater input and water exchange in salt marshes, *Geochim. Cosmochim. Acta* **60** (1996) 4645–4652.
- [16] MOORE, W.S., The effects of groundwater input at the mouth of the Ganges-Brahmaputra Rivers on barium and radium fluxes to the Bay of Bengal, *Earth Planet. Sci. Lett.* **150** (1997) 141–150.
- [17] KREST, J.M., et al., Marsh nutrient export supplied by groundwater discharge: Evidence from radium measurements, *Global Biogeochem. Cycles* **14** (2000) 167–176.
- [18] CHARETTE, M.A., et al., Utility of radium isotopes for evaluating the input and transport of groundwater-derived nitrogen to a Cape Cod estuary, *Limnol. Oceanogr.* **46** (2001) 465–470.
- [19] KELLY, R.P., MORAN, S.B., Seasonal changes in groundwater input to a well-mixed estuary estimated using radium isotopes and implications for coastal nutrient budgets, *Limnol. Oceanogr.* **47** (2002) 1796–1807.
- [20] KIM, G., et al., Large submarine groundwater discharge (SGD) from a volcanic island, *Geophys. Res. Lett.* **30** (2003).

## MOORE

- [21] HWANG, D.-W., et al., Estimating submarine inputs of groundwater and nutrients to a coastal bay using radium isotopes, *Mar. Chem.* **96** (2005) 61–71.
- [22] MOORE, W.S., Sources and fluxes of submarine groundwater discharge delineated by radium isotopes, *Biogeochemistry* **66** (2003) 75–93.
- [23] CROTWELL, A.M., MOORE, W.S., Nutrient and radium fluxes from submarine groundwater discharge to Port Royal Sound, South Carolina, *Aquatic Geochem.* **9** (2003) 191–208.
- [24] MOORE, W.S., Determining coastal mixing rates using radium isotopes, *Cont. Shelf. Res.* **20** (2000) 1993–2007.
- [25] MOORE, W.S., et al., Estimates of flushing times, submarine groundwater discharge, and nutrient fluxes to Okatee Estuary, South Carolina, *J. Geophys. Res.: Oceans* **111** C9 (2006).
- [26] WINDOM, H.L., et al., Submarine groundwater discharge: A large, previously unrecognized source of dissolved iron to the South Atlantic Ocean, *Mar. Chem.* **102** (2006) 252–266.
- [27] MOORE, W.S., et al., Submarine groundwater discharge revealed by <sup>228</sup>Ra distribution in the upper Atlantic Ocean, *Nat. Geosci.* **1** (2008) 309–311.
- [28] SANFORD, L., et al., Model for estimating tidal flushing of small embayments, *J. Waterway, Port, Coastal Ocean Eng.* **118** (1992) 635–654.
- [29] VAN DE KREEKE, J., Residence time: Applications to small boat basins, *J. Waterway, Port, Coastal Ocean Eng.* **109** (1983) 416–428.
- [30] NIENCHESKI, L.F.H., et al., Submarine groundwater discharge of nutrients to the ocean along a coastal lagoon barrier, Southern Brazil, *Mar. Chem.* **106** (2007) 546–561.

# IODINE-129 IN THE EUROPEAN ENVIRONMENT

R. MICHEL, A. DARAOU, M. GORNY, D. JAKOB, R. SACHSE,  
L. TOSCH

Institut für Radioökologie und Strahlenschutz,  
Leibniz Universität Hannover,  
Germany

V. ALFIMOV, H.-A. SYNAL

Labor für Ionenstrahlphysik,  
ETH Hönggerberg,  
Zürich, Switzerland

H. NIES<sup>1</sup>, J. HERRMANN, I. GORONCY

Bundesamt für Seeschifffahrt und Hydrographie,  
Hamburg, Germany

## Abstract

Due to former atmospheric nuclear weapon tests, accidents in nuclear facilities and releases from nuclear reprocessing plants, the natural occurrence of the radionuclide <sup>129</sup>I has been affected on a long term scale by human activities. Particularly in Western Europe, these changes are continuing due to discharges from the nuclear reprocessing plants La Hague and Sellafield. A survey is given on the environmental abundances of <sup>129</sup>I and <sup>127</sup>I in the North Sea, the Northeast Atlantic, as well as on the atmospheric transport of iodine isotopes from the sea to the continent and their pathways to animals and man. Today, the environmental <sup>129</sup>I/<sup>127</sup>I isotope ratios range from 10<sup>-10</sup> to 10<sup>-6</sup> and are far above the pre-nuclear ratio of ~10<sup>-12</sup>. The iodine isotopes are in severe disequilibrium in the different environmental compartments and serve as tracers of the complex environmental chemistry of iodine.

## 1. INTRODUCTION

The natural abundances of the long-lived <sup>129</sup>I ( $T_{1/2} = 15.7$  Ma) have been changed in a sustainable way by fallout from nuclear weapon explosions, nuclear accidents and releases from reprocessing plants. In nature, <sup>129</sup>I is produced by the spontaneous fission of uranium and by interaction of galactic cosmic ray particles with xenon in the Earth's atmosphere. As described elsewhere in detail [1], the total <sup>129</sup>I inventory of the Earth is estimated to be 50 000 kg (326.8 TBq). Most of this

---

<sup>1</sup> Present address: International Atomic Energy Agency, Environment Laboratories, Monaco

inventory is bound in the lithosphere and just 263 kg (1.7 TBq) make up the ‘free’ inventory of the atmosphere, hydrosphere and biosphere. The main natural sources of free  $^{129}\text{I}$  are releases from the lithosphere through volcanic activity and production by cosmic radiation (about 45 % each). In the atmosphere, hydrosphere and biosphere,  $^{129}\text{I}$  mixes with stable  $^{127}\text{I}$ . More than 99 % of the free  $^{129}\text{I}$ , about  $8 \times 10^{14}$  kg, are contained in the oceans and young oceanic sediments. Most authors agree that the  $^{129}\text{I}$  in the atmosphere and biosphere originates mainly from these sources.

The natural equilibrium isotopic ratio  $^{129}\text{I}/^{127}\text{I}$  was estimated to be in the range of  $(0.04\text{--}3.0) \times 10^{-12}$  [2, 3]. Using a detailed equilibrium model, Fabryka-Martin calculated an isotopic ratio of  $5.5 \times 10^{-13}$  for the marine hydrosphere and a slightly higher  $^{129}\text{I}/^{127}\text{I}$ -ratio of  $6.5 \times 10^{-13}$  for soils and the terrestrial biosphere [4]. Measurements of young oceanic sediments yielded a value of  $^{129}\text{I}/^{127}\text{I} = \sim 1.5 \times 10^{-12}$  [5–7]. According to our own analyses of iodine preparations, which had remained sealed since 1918 and 1935 respectively, the equilibrium  $^{129}\text{I}/^{127}\text{I}$  ratio in the terrestrial biosphere appears to be as low as  $2.0 \times 10^{-13}$  with a geometric standard deviation of 1.4.

The anthropogenic production of  $^{129}\text{I}$  started with military and peaceful use of nuclear fission. The atmospheric nuclear explosions added between 43 kg (0.28 TBq) and 150 kg (0.98 TBq) to the free  $^{129}\text{I}$  inventory (see Ref. [1] for references). The uncertainty of these estimates results from a lack of knowledge about the total fission yields of the atmospheric explosions. The main man-made contribution to  $^{129}\text{I}$  in the environment budget, however, originates from the reprocessing of spent nuclear fuel. Comprehensive information on the European nuclear reprocessing plants at La Hague in France and Sellafield in UK is available. Until the year 2005, these plants emitted about 4920 kg (32.2 TBq)  $^{129}\text{I}$ , see Refs [8, 9] for references. About 70% of the total  $^{129}\text{I}$  releases were from La Hague. The majority of these releases, about 85% of the  $^{129}\text{I}$  from Sellafield and about 97% of the  $^{129}\text{I}$  from La Hague, were liquid discharges into the Irish Sea and the English Channel, respectively.

Up to now, there are just very limited reports about the releases from eastern and western military reprocessing plants. The reactor accident of Chernobyl only added a relatively small amount to the free  $^{129}\text{I}$  inventory; 2 kg (13 GBq) and 6 kg (40 GBq) were estimated.

Here, we present results of a long term project aimed at a comprehensive understanding of the abundances of  $^{129}\text{I}$  and  $^{127}\text{I}$  in the European environment and of their pathways through the different environmental compartments to humans; see Refs [1, 8–12] and references therein. The investigations cover analyses of seawater from the English Channel, the Irish Sea, the North Sea and the northeast Atlantic. In addition, they cover analyses of airborne iodine species at the coast of the German island Föhr, time series of precipitation and surface waters from four regions of Lower Saxony, Germany, analyses of soil profiles and topsoils, and various biomaterials including human and animal thyroid glands.

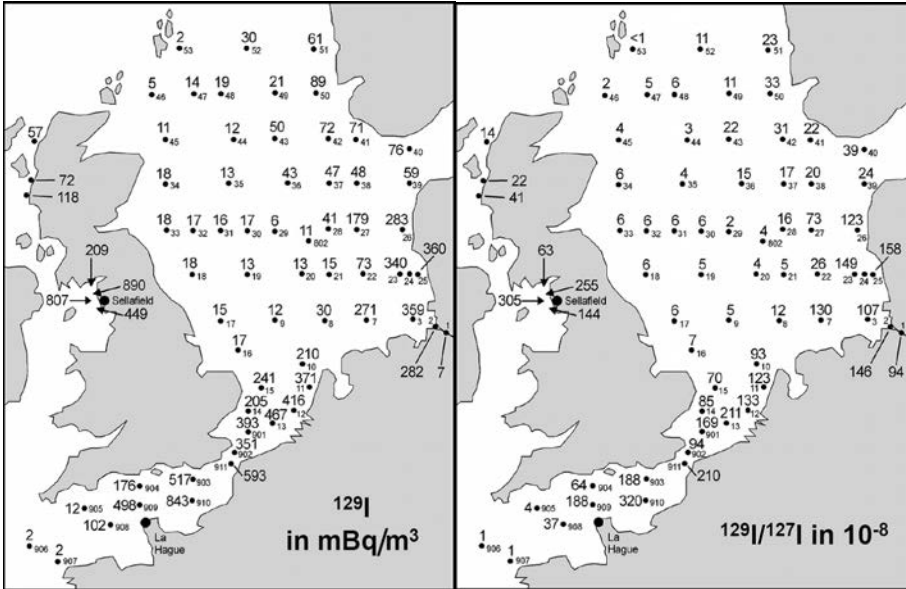


FIG. 1.  $^{129}\text{I}$  activity concentrations (left) and  $^{129}\text{I}/^{127}\text{I}$  isotopic ratios (right) in water from the North Sea sampled during the August 2005 cruise and from the Irish Sea sampled in 2006. The smaller numbers are station numbers, the larger ones the experimental data.

2. IODINE-129 AND IODINE-127 IN SEAWATERS

The activity concentrations<sup>1</sup> in marine surface waters (Fig. 1) show a large range between 2  $\text{mBq/m}^3$  and 890  $\text{mBq/m}^3$ . But even the lowest activity concentrations are more than a factor of 10 higher than those found in seawater from Hawaii (50  $\mu\text{Bq/m}^3$ ) and from the Indian Ocean (90  $\mu\text{Bq/m}^3$ ). The vicinities of the reprocessing plants exhibit the highest activity concentrations: 890  $\text{mBq/m}^3$  off-shore of Sellafield and 843  $\text{mBq/m}^3$  downstream of La Hague at station 910.

The influence of La Hague also extends to the west due to the complicated water currents. Thus, an activity concentration of 100  $\text{mBq/m}^3$  is observed at station 908. The main transport of  $^{129}\text{I}$  from La Hague, however, is through the English Channel in a northeasterly direction to the North Sea. It can be clearly distinguished along the coasts of Belgium, the Netherlands, Germany, and Denmark up to station 26. Along the transport pathway, the  $^{129}\text{I}$  activity concentrations decrease by no more than a factor of three. Behind the eastern mouth of the English Channel, the transport of  $^{129}\text{I}$  from La Hague is confined to a relatively small region along the coastline due to the influence of water masses coming down from the north along the eastern

<sup>1</sup> The following conversion holds: 1 fg  $^{129}\text{I}$  =  $4.67 \times 10^6$  atoms = 6.54 nBq.

British coast. At the German coast, the highest  $^{129}\text{I}$  activity concentrations are seen in the mouth of the Elbe Estuary and along the North Frisian coast.

The transport of  $^{129}\text{I}$  from Sellafield does not have such a clear-cut pattern. The line of four samples from the Irish Sea near Sellafield exhibits some influence of the reprocessing plant in the south and a fast decline of the activity concentrations in the direction of the main current to the north. The coastal samples at Oban, Maror, and Ullapool show further decreasing activity concentrations, so that in the north the activity concentrations are lower by more than a factor of ten than offshore of Sellafield. In the North Sea, the  $^{129}\text{I}$  activity concentrations in the seawater along the north-eastern coast of England, which is dominated by the southbound current along the British coast, do not exceed  $20 \text{ mBq/m}^3$ . The lowest  $^{129}\text{I}$  activity concentration is found with only  $6 \text{ mBq/m}^3$  right in the middle of the North Sea at the Dogger Bank (station 29).

The  $^{129}\text{I}/^{127}\text{I}$  ratios reveal the same pattern as the  $^{129}\text{I}$  activity concentrations (Fig. 1). This is due to the fact that  $^{127}\text{I}$  only shows little variation in the samples analysed. The arithmetic mean and standard deviation across all samples was  $(40 \pm 9) \text{ ng/g}$ ; geometric mean and standard deviation  $44 \times 1.6^{\pm 1} \text{ ng/g}$ . Strong deviations of  $^{127}\text{I}$  concentrations from the mean of our data down to  $10 \text{ ng/g}$  are only seen for samples from the Elbe Estuary. Exceptionally high values up to  $100 \text{ ng/g}$  were observed in summer in samples from the tide-land at the German coast and from the Garonne Estuary. This effect is attributed by us to high biological activity in these areas.

The highest  $^{129}\text{I}/^{127}\text{I}$  isotopic ratios were observed close to Sellafield and closely downstream of La Hague in 2005 with about  $3 \times 10^{-6}$ . At La Hague the ratios are approximately what was reported by Yiou et al. [13] for samples taken between 1984 and 1992. In the vicinity of Sellafield, however, Yiou et al. [13] found isotopic ratios of only  $0.89 \times 10^{-6}$  and  $0.51 \times 10^{-6}$  in samples from 1992. Our data and analyses by Atarashi-Andoh et al. [14] and by Schnabel et al. [15] of samples taken between 2003 and 2005 demonstrate an increase of the isotopic ratios to more than  $10^{-6}$  close to Sellafield.

In the Northeast Atlantic, the  $^{129}\text{I}$  activity concentrations are between  $1.5 \text{ mBq/m}^3$  (Spitsbergen) and  $55 \text{ mBq/m}^3$  at the South Norwegian Coast. Even at the coast of Greenland, south of the Denmark Strait, where the current is directed southwards, about  $2 \text{ mBq/m}^3$  are observed. The  $^{129}\text{I}/^{127}\text{I}$  isotopic ratios near Spitsbergen are with  $10^{-8}$  a factor of ten higher than those reported earlier [13]. Today,  $^{129}\text{I}/^{127}\text{I}$  isotopic ratios below  $1 \times 10^{-8}$  are not found in the North Sea, at the entrance of the English Channel (stations 906 and 907), and in the Northeast Atlantic. Thus, the European  $^{129}\text{I}/^{127}\text{I}$  isotopic ratios are two orders of magnitude higher than the  $10^{-10}$  assumed earlier to present the isotopic ratio in the oceanic mixing zone far away from release points [13, 16]. In our work, the value of  $10^{-10}$  was only observed in samples from the Indian Ocean and from the Pacific at Maui.

## 3. FROM THE SEA TO THE CONTINENT

Iodine from the oceanic mixing layer is likely released to the atmosphere in form of  $\text{CH}_3\text{I}$  as a consequence of the action of marine organisms. In the atmosphere it undergoes photochemical reactions leading to inorganic species. In Germany, a measurement of airborne iodine species was performed at the island of Föhr in April 2002 using a BERNER impactor as well as selective filters to distinguish inorganic and organic iodine species. The distribution density of the particle diameters was bimodal and allowed distinguishing global and local marine aerosols, the latter being the most important part. The distribution of iodine species demonstrates a massive influence of local marine aerosols for the transport of  $^{129}\text{I}$  from the sea to the atmosphere. The  $^{129}\text{I}/^{127}\text{I}$  ratios of iodine species in air ranged from  $12 \times 10^{-8}$  to  $84 \times 10^{-8}$ , significantly lower than in the coastal North Sea water. However, they are sufficiently high to conclude that the iodine in the air originates from a relatively restricted part of the North Sea and the northeast Atlantic; elsewhere the marine isotopic ratios are too low.

Precipitation plays a key role in the transfer of iodine to the continental hydrosphere and pedosphere. In a time series from 1997 to 2005 we investigated open field and throughfalling precipitation at 3 locations in Lower Saxony, Germany and determined the annual deposition rates. The  $^{129}\text{I}/^{127}\text{I}$  ratios in precipitation are between  $10^{-7}$  and  $10^{-6}$ . The  $^{129}\text{I}/^{127}\text{I}$  isotopic ratios are slightly higher at the coast of the North Sea, due to the influence of sea spray, than in regions remote from the sea. In background regions of the northern hemisphere the  $^{129}\text{I}/^{127}\text{I}$  ratios in precipitation increased from the pre-nuclear equilibrium value to  $10^{-9}$  between 1940 and 1950 as revealed by the iodine in an ice core from Switzerland [17]. In 1950, atmospheric  $^{129}\text{I}/^{127}\text{I}$  ratios exceeded  $10^{-9}$ . Ratios continued to increase until the end of the 1980s. Since then, ratios of nearly  $10^{-6}$  were observed in Germany and Switzerland and remained nearly constant until today, though a slight decrease is seen after the year 2000. The fallout of the Chernobyl accident was a short term episode with a highest measured  $^{129}\text{I}/^{127}\text{I}$  ratio of nearly  $10^{-5}$ .

The deposition rates of  $^{127}\text{I}$  and  $^{129}\text{I}$  in Northern Germany are fairly constant with time, but differing for the different regions and for the type of precipitation. The  $^{127}\text{I}$  and  $^{129}\text{I}$  concentrations in precipitation falling through the canopy of trees and the respective deposition data are higher by a factor between 3 and 4 than those in open field precipitation. They show, however, the same  $^{129}\text{I}/^{127}\text{I}$  isotopic ratios of about  $4 \times 10^{-7}$ . The higher concentrations in throughfalling precipitation are interpreted by us as being due to the filtering action of the canopies of the trees and being a proxy of the wet plus dry deposition of iodine isotopes.

The  $^{129}\text{I}$  deposition rates in Western Europe show a steady increase from about  $0.01 \text{ mBq} \cdot \text{m}^{-2} \cdot \text{a}^{-1}$  in the 1950s to more than  $10 \text{ mBq} \cdot \text{m}^{-2} \cdot \text{a}^{-1}$  around the year 2000. During the years 1997–2005, the geometric means of the annual  $^{129}\text{I}$  deposition rates derived from open field precipitation in different regions of Lower Saxony were

$10 \times 1.3^{\pm 1} \text{ mBq} \cdot \text{m}^{-2} \cdot \text{a}^{-1}$ ,  $3.7 \times 1.3^{\pm 1} \text{ mBq} \cdot \text{m}^{-2} \cdot \text{a}^{-1}$  and  $2.5 \times 1.4^{\pm 1} \text{ mBq} \cdot \text{m}^{-2} \cdot \text{a}^{-1}$ , respectively<sup>1</sup>. Through-falling precipitation yielded a geometric mean of annual <sup>129</sup>I deposition rates of  $14 \times 1.3^{\pm 1} \text{ mBq m}^{-2} \text{ a}^{-1}$ . After the year 2000, the annual deposition rates are fairly constant with a slightly falling tendency to the year 2005.

The comparison of the time trend of the annual <sup>129</sup>I deposition rates with the release rates of the European nuclear reprocessing plants in La Hague and Sellafield gives a clear indication that the releases into the sea and the pathway from the sea to the atmosphere is the dominant one; a relevance of the aerial releases cannot be derived from our data. The North Sea appears as the dominant source of airborne iodine in Northern Germany.

The annual fallout of stable <sup>127</sup>I is just a few mg/m<sup>2</sup> in Northern Germany with some slight differences between the regions. From open field precipitation we derived a range from  $1.2 \times 1.4^{\pm 1} \text{ mg} \cdot \text{m}^{-2} \cdot \text{a}^{-1}$  to  $2.7 \times 1.3^{\pm 1} \text{ mg/m}^2$ , while the throughfalling precipitation gave  $5.4 \times 1.2^{\pm 1} \text{ mg} \cdot \text{m}^{-2} \cdot \text{a}^{-1}$ .

The precipitation, and with it the iodine, interact with the topsoil, migrates into deeper soil horizons, charges the surface water and infiltrates the groundwater. The depth dependence of iodine isotopes and their inventories were investigated in seven deep soil profiles from Lower Saxony down to 2 m depth, and demonstrated the complexity of iodine migration [11]. Stable iodine in the soils originates mainly from atmospheric input from the oceans. Considering the annual deposition rates for <sup>127</sup>I of just a few  $\text{mg} \cdot \text{m}^{-2} \cdot \text{a}^{-1}$ , the mean <sup>127</sup>I inventory of the seven soil profiles of  $3.5 \times 1.6^{\pm 1} \text{ g/m}^2$  are the result of an input over thousands of years. Anthropogenic <sup>129</sup>I in the soils was input during the last 50 years only. The <sup>129</sup>I/<sup>127</sup>I ratios in the soil profiles varied by more than two orders of magnitude between  $5 \times 10^{-8}$  and  $10^{-10}$  and showed remarkable differences between the seven locations. However, the lowest <sup>129</sup>I/<sup>127</sup>I ratios at deeper depths still are of the order of  $10^{-10}$ , i.e. about two orders of magnitude higher than the natural equilibrium ratio. Thus, anthropogenic <sup>129</sup>I has already substantially migrated to deeper depths. In a comprehensive set of topsoils from Lower Saxony, the <sup>129</sup>I/<sup>127</sup>I ratios were between  $2 \times 10^{-7}$  and  $2 \times 10^{-9}$ , strongly anti-correlated with the concentration of stable iodine.

The migration of <sup>129</sup>I and <sup>127</sup>I in the soils can only be understood as a time-dependent kinetic process involving unspecific and specific adsorption processes and isotopic exchange depending strongly on the hydrological situation [11]. As a consequence of the long times available for the <sup>127</sup>I to migrate into the ground, <sup>127</sup>I could occupy more stable adsorption places with long characteristic exchange times. The sorption of <sup>129</sup>I in the soil layers mainly occurs by non-specific sorption and the need to exchange with <sup>127</sup>I, which is adsorbed more strongly in deeper layers over long time scales, makes the recent <sup>129</sup>I more mobile and more available than the large amount of <sup>127</sup>I. It turns out that the migration of the iodine isotopes cannot

<sup>1</sup> We use the convenient notation of e.g.  $2.5 \times 1.4^{\pm 1}$  to present geometric means, here 2.5, and geometric standard deviations, here 1.4.

be described by stationary equilibrium models but need time dependent kinetic models which are not available so far.

More than 99% of the  $^{129}\text{I}$  observed in the soils are located in the upper 60 cm of the profiles. This allows the interpretation of the  $^{129}\text{I}$  inventories in the profiles as proxies for the total  $^{129}\text{I}$  inventories. For the seven depth profiles from Lower Saxony, this yields a geometric mean of  $168 \times 1.5^{\pm 1}$  mBq/m<sup>2</sup>. This total inventory in Lower Saxony is more than three orders of magnitude higher than the pre-nuclear value derived for Lutovinovo, Russia, of  $0.084 \pm 0.017$  mBq/m<sup>2</sup> [10].

#### 4. THE IODINE SYSTEM IN DISEQUILIBRIUM AND RADIOLOGICAL RELEVANCE

As a consequence of the different input histories of the two iodine isotopes and the various interactions between the compartments involved,  $^{129}\text{I}$  and  $^{127}\text{I}$  are today in disequilibrium in all the investigated environmental compartments. The measured  $^{129}\text{I}/^{127}\text{I}$  ratios range from  $2.7 \times 10^{-6}$  in coastal seawater from the North Sea to about  $10^{-10}$  in the samples from the Indian Ocean and the Pacific.  $^{129}\text{I}$  concentrations are between  $2 \times 10^{-13}$  g/g and  $10^{-18}$  g/g, i.e. 6.5 mBq/kg and 6.5 nBq/kg, respectively.  $^{127}\text{I}$  concentrations are between  $2 \times 10^{-5}$  g/g and  $10^{-10}$  g/g.

For precipitation and surface waters the ranges of  $^{127}\text{I}$  concentrations are larger than in seawater and the logarithmic means are significantly lower:  $(1.8 \times 1.6^{\pm 1})$  ng/g in open field precipitation,  $(5.9 \times 1.3^{\pm 1})$  ng/g in throughfalling precipitation,  $(7.1 \times 1.7^{\pm 1})$  ng/g in surface water. The  $^{129}\text{I}/^{127}\text{I}$  ratios in these materials cover even broader ranges of about one order of magnitude for open field precipitation and about two orders of magnitude for surface waters. The geometric means are  $4.1 \times 10^{-7}$  for open field precipitation and  $1.3 \times 10^{-8}$  for the surface waters; the geometric standard deviations are 1.8 and 2.5, respectively. Throughfalling precipitation shows a smaller range, exhibited by a geometric standard deviation of 1.4 only. But the mean of  $4.2 \times 10^{-7}$  is indistinguishable from that of the open field precipitation.

The  $^{127}\text{I}$  concentrations in the topsoils in Northern Germany show a strong negative correlation with the  $^{129}\text{I}/^{127}\text{I}$  ratios. This can be understood if one considers that the  $^{129}\text{I}$  concentrations in the topsoils are rather uniform with a geometric mean of  $(84 \times 1.8^{\pm 1})$  fg/g and that the young anthropogenic  $^{129}\text{I}$  is diluted in the soils by the old iodine with lower  $^{129}\text{I}/^{127}\text{I}$  ratios.

The dependence of the  $^{129}\text{I}/^{127}\text{I}$  ratios on the  $^{129}\text{I}$  concentrations looks completely different. In seawater the  $^{129}\text{I}/^{127}\text{I}$  ratios and the  $^{129}\text{I}$  concentrations are highly correlated, the extrapolated correlation line running exactly through the pre-nuclear values. This is to be expected as there are only two sources of  $^{129}\text{I}$ : natural and anthropogenic. The data for open field precipitation, throughfalling precipitation and surface waters plot parallel to the correlation line of the seawater but shifted to lower  $^{129}\text{I}$

concentrations. The samples from the Baltic Sea again show the transition from a seawater regime to a surface water dominated one.

## 5. CONCLUSIONS

The  $^{129}\text{I}/^{127}\text{I}$  ratios in the surface waters cover a broad range with values mostly significantly lower than in precipitation, while the  $^{127}\text{I}$  concentrations in surface water and throughfalling precipitation are indistinguishable. Evidently, the formation of surface waters has to take into account a dilution of fallout iodine with stable  $^{127}\text{I}$  which is only weakly adsorbed in the soils and a considerable runoff of iodine must be taken into account. The ratios in soil profiles demonstrate a high mobility and an accumulation of  $^{129}\text{I}$  in the water unsaturated soil zones, an efficient migration into the water saturated soil layers and an ongoing transfer of anthropogenic  $^{129}\text{I}$  into groundwater.

We will briefly mention results for animal and human thyroid glands. In the thyroid glands of herbivorous animals the  $^{129}\text{I}/^{127}\text{I}$  ratios closely respond to ratios in precipitation; i.e. up to nearly  $10^{-6}$ . Human thyroid glands in Germany show lower  $^{129}\text{I}/^{127}\text{I}$  ratios than animal thyroid glands. The geometric mean of  $^{129}\text{I}/^{127}\text{I}$  ratios in human thyroid glands sampled in Lower Saxony between 1998 and 2002 ranged from  $2 \times 10^{-9}$  to  $3 \times 10^{-8}$  with a geometric mean of  $1.1 \times 10^{-8}$ . This mean value is equivalent to an annual equivalent dose to the thyroid of  $\sim 6$  nSv for adults [9]. Thus, the  $^{129}\text{I}$  abundances in the biosphere in Northern Germany do not give rise to significant radiation exposure. This statement may not hold true for the closest proximities of release points which are not discussed here. In any case, future development should be carefully surveyed since  $^{129}\text{I}$  is an ideal indicator of the long term human impact on the environment. The disequilibria between the iodine isotopes observed in Europe offer a unique chance to use  $^{129}\text{I}$  as a man-made radiotracer for the pathways of iodine through the environment.

## REFERENCES

- [1] MICHEL, R., et al., Iodine-129 and iodine-127 in European seawaters and in precipitation from Northern Germany, *Sci. Total Environ.* **419** (2012) 151–169.
- [2] EDWARDS, R.R., Iodine-129: Its occurrence in nature and its utility as a tracer, *Science* **137** (1962) 851–853.
- [3] KOHMAN, T.P., EDWARDS, R.R.,  $^{129}\text{I}$  as a Geochemical and Ecological Tracer, Report NYO-3624-1, Carnegie Institute of Technology, Pittsburgh, PA (1966).
- [4] FABRYKA-MARTIN, J.T., et al., Natural iodine-129 as an environmental tracer, *Geochim. Cosmochim. Acta* **49** (1985) 337–347.
- [5] FEHN, U., et al., Determination of natural and anthropogenic  $^{129}\text{I}$  in marine sediments, *Geophys. Res. Lett.* **13** (1986) 137–139.

## INVITED PAPER

- [6] SCHINK, D.R., et al.,  $^{129}\text{I}$  in Gulf of Mexico waters, *Earth Planet. Sci. Lett.* **135** (1995) 131–138.
- [7] MORAN, J.E., et al., Variations in  $^{129}\text{I}/^{127}\text{I}$  ratios in recent marine sediments: evidence for a fossil organic component, *Chem. Geol.* **152** (1998) 193–203.
- [8] NIES, H., et al., Kartierung von Tc-99, I-129 und I-127 im Oberflächenwasser der Nordsee, Bundesamt für Strahlenschutz, Salzgitter (2010) (in German), (<http://doris.bfs.de/jspui/handle/urn:nbn:de:0221-201008263031>).
- [9] MICHEL, R., et al., Ableitung von radioökologischen Parametern aus dem langfristigen Eintrag von Iod-129, BMU 2004-650, Bundesministerium für Umwelt, Naturschutz und Reaktorsicherheit (2004), <http://www.bmu.de/strahlenschutz/doc/6872.php> (in German).
- [10] SZIDAT, S., et al., Iodine-129: Sample preparation, quality control and analyses of pre-nuclear materials and of natural waters from Lower Saxony, Germany, *Nucl. Instrum. Methods Phys. Res. B* **172** (2000) 699–710.
- [11] ERNST, T., et al., Migration of iodine-129 and iodine-127 in soils, *Kerntechnik* **68** (2003) 155–168.
- [12] MICHEL, R., et al., Long-lived radionuclides in the environment: on the radio-ecology of iodine-129, *Radioprotection* **40** Suppl. 1 (2005) 269–276.
- [13] YIOU, F., et al.,  $^{129}\text{I}$  from nuclear fuel reprocessing: Potential as an oceanographic tracer, *Nucl. Instrum. Methods Phys. Res. B* **92** (1994) 436–439.
- [14] ATARASHI-ANDOH, M., et al.,  $^{129}\text{I}/^{127}\text{I}$  ratios in surface waters of the English Lake District, *Appl. Geochem.* **22** (2007) 628–636.
- [15] SCHNABEL, C., et al.,  $^{129}\text{I}/^{127}\text{I}$  ratios in Scottish coastal surface sea water: Geographical and temporal responses to changing emissions, *Appl. Geochem.* **22** (2007) 619–627.
- [16] KILIUS, L.R., et al., The dispersal of  $^{129}\text{I}$  from the Columbia River estuary, *Nucl. Instrum. Methods Phys. Res. B* **92** (1994) 393–397.
- [17] WAGNER, M., et al., Increase of  $^{129}\text{I}$  in the environment, *Nucl. Instrum. Methods Phys. Res. B* **113** (1996) 490–494.



# SUPPORTED LEAD IN Pb-210 CHRONOLOGY

D. PITTAUEROVÁ, B. HETTWIG, H.W. FISCHER  
Institute of Environmental Physics,  
University of Bremen,  
Bremen, Germany

## Abstract

A widely applied method of supported lead estimation in sediments using gamma spectrometric  $^{226}\text{Ra}$  determination via  $^{222}\text{Rn}$  short lived daughter products relies on radioactive equilibrium between  $^{226}\text{Ra}$  and  $^{222}\text{Rn}$  being established after sealing the samples. Advantages and disadvantages of methods of  $^{226}\text{Ra}$  estimation in sediments, using either  $^{222}\text{Rn}$  daughter products or direct estimation by 186.2 keV gamma emissions are discussed. An equilibrium experiment was performed using test samples and in one case radioactive equilibrium was not reached. On a theoretical sediment profile it was shown how systematic errors in supported  $^{210}\text{Pb}$  estimation can lead to incorrect interpretations of  $^{210}\text{Pb}_{\text{xs}}$  profiles and therefore affect  $^{210}\text{Pb}$  derived chronologies.

## 1. INTRODUCTION

$^{210}\text{Pb}$  sediment chronology is a frequently used tool for dating recent lacustrine and marine sediment cores or peat bog accumulations [1]. Its range is approximately the last 100–150 a, which is the period of the most significant anthropogenic effects to the environment.  $^{210}\text{Pb}$  (half-life 22.3 a) in sediments consists of two components:

- Supported  $^{210}\text{Pb}$ , which is present due to the authigenic material of the sediment;
- Unsupported (or excess)  $^{210}\text{Pb}$ , which originates from atmospheric deposition.

Excess  $^{210}\text{Pb}$  is then determined by subtracting supported activity from the total activity and used for estimation of accumulation rates and age models. Measurement techniques of the total signal of  $^{210}\text{Pb}$  include either alpha spectroscopy via  $^{210}\text{Po}$  with assumption of radioactive equilibrium between  $^{210}\text{Po}$  and  $^{210}\text{Pb}$  or gamma spectroscopy. Both approaches have certain advantages and disadvantages [2]. In the authors' laboratory, gamma spectroscopy is used. This allows simultaneous estimation of other natural and artificial gamma emitters within a single spectrum and the analysis is non-destructive.

## 2. SUPPORTED $^{210}\text{Pb}$ ESTIMATION

For supported  $^{210}\text{Pb}$ , which is usually assumed to be in radioactive equilibrium with its parent nuclide  $^{226}\text{Ra}$  (half-life 1600 a), analytical options were suggested by Moser [3]. The simplest method, sometimes used in combination with the alpha spectroscopic determination of  $^{210}\text{Pb}$ , is to use the lowest constant activity of a sediment profile (samples with an age greater than 100 a). This method assumes a constant activity of  $^{226}\text{Ra}$  over the entire sediment profile, which is not always the case. It is also possible to measure Ra by alpha counting after radiochemical separation or gamma spectroscopy [3].

### 2.1. Using $^{226}\text{Ra}$ daughter products for supported $^{210}\text{Pb}$ estimation

Gamma spectroscopy using daughter products of  $^{226}\text{Ra}$ , namely short lived  $^{214}\text{Pb}$  and  $^{214}\text{Bi}$  (hence referred to as 'daughter products'), is a widely used method for  $^{226}\text{Ra}$  determination. Here we have to deal mainly with difficulties related to  $^{222}\text{Rn}$  diffusion and recoil emanations from the sample, leading to systematic underestimation of  $^{226}\text{Ra}$  concentration [4]. In the study of Stoulos et al. [5] Rn gas leaking from the sample container, its accumulation in the void upper part of the container and attachment of Rn decay products onto its inner surface, resulting in another geometry, and self-absorption from that of the calibration sample, was resolved by adding active charcoal to the sample. However, this would change properties of the samples, which contradicts one major advantage of gamma spectroscopy for sediment chronology, that it is a non-destructive method. An optional solution is using Rn proof steel containers [5], which would lead to a decline in sensitivity in the detection of low energy gamma radiation of  $^{210}\text{Pb}$ . A common practice in many gamma spectroscopic laboratories is sealing samples using gas tight foil and waiting for at least 21 days to allow ingrowth of daughter products.

### 2.2. Direct estimation

$^{226}\text{Ra}$  can also be directly estimated by its gamma line at 186.2 keV, but interference with the most prominent line of  $^{235}\text{U}$  185.7 keV must be taken into account. A method for correction of the  $^{235}\text{U}$  and  $^{226}\text{Ra}$  interference using the 63.3 keV line of  $^{234}\text{Th}$  as a proxy for  $^{238}\text{U}$  was proposed by Dowdall et al. [6]. In this case a constant natural ratio to  $^{235}\text{U}$  is assumed. When using the 92.6 keV doublet of  $^{234}\text{Th}$ , precautions must be taken due to its potential interference with  $\text{K}_{\alpha 1}$  line from  $^{232}\text{Th}$ . Contribution of  $^{235}\text{U}$  to the 186 keV peak can also be determined using another less intensive  $^{235}\text{U}$  line at 143.8 keV [7], if detectable.

### 3. MOTIVATION

The motivation of this study was the participation of the laboratory in a laboratory intercomparison. It resulted in the recognition of the possibility of underestimating  $^{226}\text{Ra}$  values. It indicated that the existing laboratory practice of estimation of  $^{226}\text{Ra}$  via daughter products using plastic sample dishes sealed in assumed gas proof metallic foil was possibly a weak point. As a countermeasure, the laboratory adopted new thicker metallized plastic foil bags for sealing samples and performed an experiment using soldered steel containers.

### 4. MATERIALS AND METHODS

#### 4.1. Test samples

The test sample, denominated RV VII–2006, was a soil material used for the 7th Intercomparison of environmental samples organized by the German Federal Office for Radiation Protection (BfS) [4]. It was taken from an area in the federal state of Thuringia with naturally increased  $^{226}\text{Ra}$  levels. The test material had been ground into a fine powder, so that 98.8% of the fraction had a particle size of less than 315  $\mu\text{m}$ . A cylindrical plastic dish with a diameter of 70 mm and height of 20 mm was filled with the test sample. It was then sealed in a metallized plastic foil considered to be gas-tight. Another experiment was performed using a steel container with a diameter of 101.5 mm and a height of 31.5 mm in which the test sample was soldered.

#### 4.2. Gamma spectroscopy

The samples were measured by low level low background gamma spectroscopy using a coaxial HPGe detector Canberra Industries (51% rel. efficiency) housed in a 10 cm Pb shielding with Cu, Cd and plastic lining. The spectra were analysed by Canberra Genie 2000 software. Efficiency calibration was performed using the Monte Carlo based LabSOCS calibration tool [8], which takes into account not only sample to detector geometry, but also sample density and composition, as well as measurement container properties.

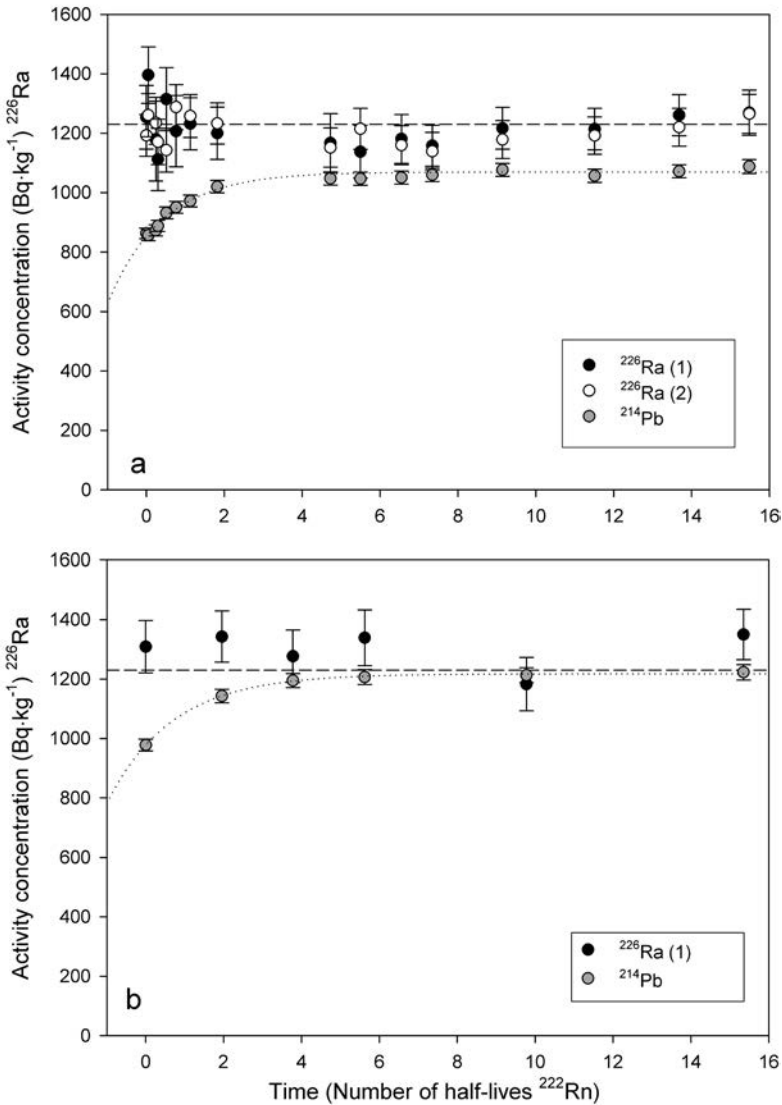


FIG. 1. Establishing of radioactive equilibrium in test sample RV VII-2006 within a time interval of approximately 8 weeks for (a) a plastic dish sealed in a metallized plastic foil and (b) a soldered steel container. In the first case, the  $^{214}\text{Pb}$  values reached only 88% of that of parent  $^{226}\text{Ra}$ , which was determined by the different methods (1) and (2) listed in section 5.1. In the steel container radioactive equilibrium was reached. The dashed line indicates the reference value. The error bars for all data are 1 standard deviation (they include counting statistics and calibration of the measuring device).

## 5. EXPERIMENTAL, RESULTS AND DISCUSSION

### 5.1. Equilibrium test

Gamma spectra of the BfS test samples sealed in the two forms described above (Sec. 4.1) were obtained and recorded repeatedly during approximately 8 weeks (16  $^{222}\text{Rn}$  half-lives) following their sealing in order to observe the process of the establishment of radioactive equilibrium. The daughter product  $^{214}\text{Pb}$  was measured via its 242.0, 295.2 keV and 351.9 keV gamma lines.  $^{226}\text{Ra}$  activities were determined using the gamma line 186.2 keV after subtraction of the  $^{235}\text{U}$  contribution, for which 3 methods were applied:

- (1) Using the  $^{235}\text{U}$  line at 143.8 keV (after interference correction from contributing  $^{223}\text{Ra}$ , determined by the 144.2, 154.2, 269.5, 323.9 and 338.3 keV lines);
- (2) Using 63.3 keV and 92.6 keV line of  $^{234}\text{Th}$  and 1001.0 keV line of  $^{234\text{m}}\text{Pa}$  for estimation of  $^{238}\text{U}$  with activities derived from the natural  $^{238}\text{U}/^{235}\text{U}$  activity ratio of 21.7.

These two methods applied on the metallized plastic foil sealed sample lead to very consistent results with no statistical difference (two sample t-test (34) = 0.46,  $p = 0.65$ ) Fig. 1a).

Finally, a combination of methods (1) and (2) was used, applying all 4 mentioned lines for  $^{235}\text{U}$  contribution estimation, which resulted in the reduction of  $^{226}\text{Ra}$  uncertainty by 43%.

While the mean value of  $^{226}\text{Ra}$  measured by all 3 methods was close to the reported reference value, the equilibrium value of  $^{214}\text{Pb}$  in the metallized plastic foil sealed sample reached only 88% that of  $^{226}\text{Ra}$ . The mechanism of this phenomenon, which has not yet been explained, is speculated to be Rn diffusion through the foil. The very fine material used for the test is prone to show a high emanation rate. Efficiency problem with daughter product estimation can be excluded, because both daughter products  $^{214}\text{Pb}$  and  $^{214}\text{Bi}$  gave consistent results when estimated by lines of wide energy span (between 242 and 1764 keV). In the parallel experiment using a soldered steel container radioactive equilibrium was reached (Fig. 1b).

### 5.2. Possible consequences of supported $^{210}\text{Pb}$ underestimation for chronology

On a theoretical model it is illustrated how systematic underestimation of  $^{210}\text{Pb}_{\text{sup}}$  can affect the resulting sedimentation rate estimation. The simple example (Fig. 2) presents a theoretical non-compacted and non-mixed sediment profile with a constant sedimentation rate of 0.25 cm/a. The sampling interval is 1 cm and the depth of the profile is 20 cm.  $^{210}\text{Pb}_{\text{sup}}$  being constant 25% of the total  $^{210}\text{Pb}$  initial activity (top of the profile) is subjected to underestimation of  $^{210}\text{Pb}_{\text{sup}}$  by 12%. The value of 25% for the ratio between supported lead and total initial  $^{210}\text{Pb}$  was selected as a 'typical value', although based on our experience; it can vary strongly

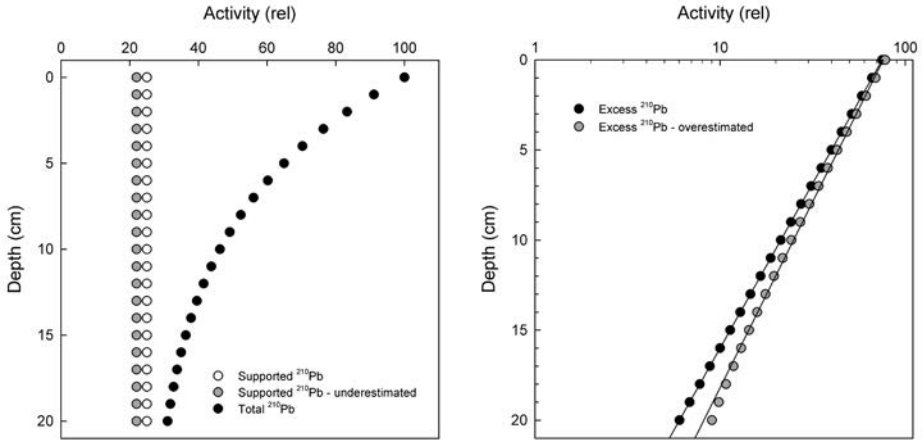


FIG. 2. The effect of systematic  $^{210}\text{Pb}_{\text{sup}}$  underestimation in a  $^{210}\text{Pb}_{\text{xs}}$  model demonstrated on a theoretical depth profile.

according to the local environment, often between 5–50%. Underestimation of supported lead in this example leads to a constant shift of  $^{210}\text{Pb}_{\text{xs}}$  to greater values. After least square fitting the altered dataset by a simple 2 parameter exponential function, the resulting sedimentation rate is 0.282 cm/a, 13% higher than the correct value.

On a real dataset (with scatter caused by counting statistics and other natural causes) excess  $^{210}\text{Pb}$  overestimation can remain unobserved, and could also be attributed to not reaching the ‘dating horizon’. It can possibly be detected by careful examination and finding some regular patterns in the residuals plot (after fitting). The described effect will be strongest in environments with a higher proportion of supported  $^{210}\text{Pb}$ . Systematic error in  $^{210}\text{Pb}_{\text{sup}}$  estimation can therefore have consequences for  $^{210}\text{Pb}_{\text{xs}}$  derived chronologies leading to systematic underestimation of ages.

## 6. CONCLUSIONS

It was shown that although samples for  $^{226}\text{Ra}$  analysis are carefully sealed in presumably gas tight foils, especially in very fine grained samples the radioactive equilibrium required for  $^{226}\text{Ra}$  estimation via daughter products might not be reached.

This can theoretically also have consequences for supported  $^{210}\text{Pb}$  estimation via the  $^{226}\text{Ra}$  daughter products. A systematic underestimation of  $^{210}\text{Pb}_{\text{sup}}$  can result in systematic underestimation in  $^{210}\text{Pb}_{\text{xs}}$  derived ages, as was presented in a theoretical example.

## REFERENCES

- [1] APPLEBY, P.G., “Chronostratigraphic techniques in recent sediments”, Tracking Environmental Change Using Lake Sediments — Volume 1: Basin Analysis, Coring, and Chronological Techniques (LAST, W.M., SMOL, J.P., Eds), Kluwer Academic, Dordrecht, The Netherlands (2001) 171–203.
- [2] ZABORSKA, A., CARROLL, J., PAPUCCI, C., PEMPKOWIAK, J., Intercomparison of alpha and gamma spectrometry techniques used in  $^{210}\text{Pb}$  geochronology, *J. Environ. Radioact.* **93** (2007) 38–50.
- [3] MOSER, R.N., A comparison of methods for the determination of the dating-nuclides  $^{210}\text{Pb}$  and  $^{226}\text{Ra}$ , *J. Radioanal. Nucl. Chem.* **173** (1993) 283–292.
- [4] SCHKADE, U.K., ARNOLD, D., DÖRING, J., HARTMANN, M., WERSHOFEN, H., Gammasspektrometrische Bestimmung der spezifischen Aktivitäten natürlicher Radionuklide in Umweltproben: 7. Vergleichsanalyse “Boden 2006”, BfS-SCHR-41/07, Wirtschaftsverlag NW Verlag für neue Wissenschaft, Berlin (2007) 70 pp (in German).
- [5] STOULOS, S., MANOLOPOULOU, M., PAPASTEFANOU, C., Measurement of radon emanation factor from granular samples: Effects of additives in cement, *Appl. Radiat. Isot.* **60** (2004) 49–54.
- [6] DOWDALL, M., SELNÆS, Ø.G., GWYNN, J.P., DAVIDS, C., Simultaneous determination of  $^{226}\text{Ra}$  and  $^{238}\text{U}$  in soil and environmental materials by gamma spectrometry in the absence of radium progeny equilibrium, *J. Radioanal. Nucl. Ch.* **261** (2004) 513–521.
- [7] JUSTO, J., EVANGELISTA, H., PASCHOA, A.S., Direct determination of  $^{226}\text{Ra}$  in NORM/TENORM matrices by gamma-spectrometry, *J. Radioanal. Nucl. Chem.* **269** (2006) 733–737.
- [8] BRONSON, F.L., Validation of the accuracy of the LabSOCS software for mathematical efficiency calibration of Ge detectors for typical laboratory samples, *J. Radioanal. Nucl. Chem.* **255** 1 (2003) 137–141.



# USE OF STABLE CARBON AND NITROGEN ISOTOPES FOR TROPHIC LEVEL EVALUATION AND FOOD WEBS RECONSTRUCTION IN THE BAY OF BISCAY: CASE STUDY

T. CHOUVELON<sup>a</sup>, J. SPITZ<sup>b</sup>, F. CAURANT<sup>a</sup>, P. MÉNDEZ FERNANDEZ<sup>a</sup>, P. BUSTAMANTE<sup>a</sup>

<sup>a</sup> Littoral Environnement et Sociétés

<sup>b</sup> Centre de Recherche sur les Mammifères Marins

La Rochelle, France

## Abstract

Assessing species' trophic level is one key aspect of ecosystem models, providing an indicator to monitor trophic links and ecosystem changes. The stable isotope ratios (SIR) of carbon and nitrogen provide longer term information on the average diet of consumers than the traditional stomach content method. However, using SIR in predators implies a good knowledge of the factors influencing prey species signature and lower trophic levels themselves, such as spatial and temporal variations. In this study, 129 species belonging to several taxa (i.e. crustaceans, molluscs, fish, marine mammals) from the Bay of Biscay were analysed for their isotopic signatures. Results confirmed the existence of several trophic food webs with probable different baseline signatures in this area, an essential consideration when using the isotopic tool for calculating species trophic level and potential evolution in space and time. Results demonstrated a spatial gradient from the shoreline to the oceanic domain for both carbon and nitrogen.

## 1. INTRODUCTION

The Bay of Biscay is a very large bay opening onto the northeast Atlantic Ocean, located from 1 to 10°W and from 43 to 48°N (Fig. 1). The continental shelf covers over 220 000 km<sup>2</sup>, and extends more than 200 km offshore in the north of the Bay and only 10 km in the south. The hydrological structure of the Bay of Biscay is influenced by two main river plumes (i.e. Loire and Gironde) and a continental slope indented by numerous canyons [1, 2] (Fig. 1). The Bay of Biscay supports both numerous important fisheries and a rich fauna including many protected species (e.g. marine mammals, seabirds, sharks). The management of this ecosystem, which is

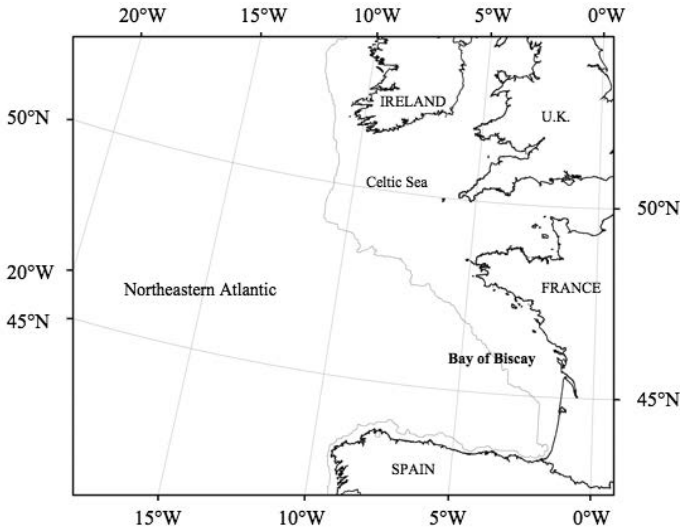


FIG. 1. Map of the study area. The grey line indicates the 200 m isobath.

subjected to numerous anthropogenic impacts, notably depends on the good understanding of its food web structure.

Trophic relationships between species and trophic fluxes govern the ecosystems' structure and functioning. Trophodynamic indicators can be used to reflect the state of marine exploited ecosystems [3]. Such indicators may encompass the measurement of the stable isotope ratios (SIR) of carbon (C) and nitrogen (N) in consumers' tissues. Indeed, SIR constitutes a complementary or alternative approach to traditional methods of dietary studies (e.g. stomach content analysis), as SIR allows the tracing of organic matter in marine food webs [4]. SIR of C are generally used as an indicator of the feeding zone or habitat since the ratios vary little ( $\leq 1\text{‰}$ ) between those of the primary producers or a prey in a local food chain, and those of the consumers [5, 6]. Moreover, in the marine environment, pelagic and/or oceanic primary producers generally present lower  $\delta^{13}\text{C}$  values compared to benthic and/or neritic ones. Therefore, SIR of C allows the distinguishing of the spatial contribution to food intake between pelagic and benthic, and/or between inshore and offshore environments [7, 8]. In contrast, consumers present higher  $\delta^{15}\text{N}$  values relative to their food (between 2.5 and 5‰) [9, 10]. SIR of N are thus generally used as an indicator of the trophic position, and enable the calculation of organisms' trophic level in a given ecosystem [11].

However, using SIR as dietary indicators in a particular ecosystem requires that the general assumptions described above are not violated (that is, good discrimination of the pelagic vs. benthic, or inshore vs. offshore contribution to food intake in consumers which is sufficient and not hidden by other factors). The aim of this study

was therefore to assess spatial variations in SI signatures for the major groups of taxa living in an ecosystem as diverse as the Bay of Biscay.

## 2. MATERIALS AND METHODS

### 2.1. Sampling

We expected that SI ratios of primary consumers and higher trophic levels were more appropriate to reflect spatial variations in the relatively long term, contrary to those of primary producers. Overall, 1520 individuals belonging to 129 species from various taxa (plankton excepted) were therefore analysed for the SI signature in their muscle tissue. Crustaceans, molluscs and fish were collected during the EVHOE groundfish surveys conducted by IFREMER1, from the continental shelf to the shelf edge of the Bay of Biscay in the autumns of 2001 to 2009. Mammalian samples came from stranded animals along the French Atlantic coast, recovered and examined by members of the French Stranding Network between 2001 and 2009. Muscle samples were immediately frozen at  $-20^{\circ}\text{C}$ , then freeze-dried, ground into a fine powder and stored in individual plastic vials for further isotopic analyses.

### 2.2. Stable isotope analysis

Lipids were extracted from muscle sample powders using cyclohexane [12], as they are highly depleted in  $^{13}\text{C}$  relative to other tissue components [13]. Isotopic analyses were then performed with an elemental analyser coupled to an Isoprime (Micromass) continuous flow isotope ratio mass spectrometer (CF IR-MS). The results are presented in the usual  $\delta$  notation relative to the deviation from standards (Pee Dee Belemnite for  $\delta^{13}\text{C}$  and atmospheric nitrogen for  $\delta^{15}\text{N}$ ), in parts per thousand (‰). Based on replicate measurements of internal laboratory standards, the experimental precision is of  $\pm 0.15$  and  $\pm 0.20\text{‰}$  for  $\delta^{13}\text{C}$  and  $\delta^{15}\text{N}$ , respectively.

### 2.3. Data treatment

The major groups of taxa were firstly defined following taxonomic criteria (e.g., Actinopterygian vs. Chondrychtian fish, or bivalve vs. gastropods vs. cephalopod molluscs). The use of such taxonomic groups limited variations due to physiological and metabolic differences that can considerably impact isotopic fractionation between different types of consumers [10]. Moreover, this grouping limited variation linked to excessive morphological differences that directly impact general feeding habits. In this way, Actynopterygians that showed a wide range of individual length were secondly separated into 2 groups, 'large Actynopterygians' ( $56 \pm 20$  cm mean total length), and 'small Actynopterygians' ( $21 \pm 11$  cm mean total length). Then,

the spatial distribution of the studied species both on the vertical axis (i.e. pelagic or demersal/benthic) and on the horizontal axis (i.e. from coastline to oceanic area) was defined following the published literature [e.g. Refs 14, 15]. These classifications were in accordance with the depth and the area organisms were actually trawled in the Bay of Biscay. For cetaceans, affiliation to a spatial group was derived from the monitoring of marine mammal populations in the Bay of Biscay based both on stranding and on shipboard surveys (CRMM, unpublished data), and from published diet in this area [16, 17].

For each taxa, a spatial group of individuals was statistically tested for their difference in  $\delta^{13}\text{C}$  and  $\delta^{15}\text{N}$  values separately. The non-parametric test Kruskal-Wallis (KW), followed by a multiple comparison test with the Holm adjustment method, was used, as data never fulfilled conditions required for parametric statistics.

### 3. RESULTS

Within each major group of taxa, spatial groups displayed significantly different  $\delta^{13}\text{C}$  and  $\delta^{15}\text{N}$  values (KW tests, all  $p < 0.0001$ ). A consistent continuum in stable C and N ratios emerged,  $\delta^{13}\text{C}$  and  $\delta^{15}\text{N}$  values decreasing from nearshore organisms to deep-sea or oceanic ones (Fig. 2). Also, the mean difference in SI signatures between the ‘most depleted group’ in heavier isotopes and the ‘more enriched group’ within each major group of taxa was higher for  $\delta^{15}\text{N}$  values than for  $\delta^{13}\text{C}$  values, in both smaller species (i.e. small Actinopterygians, cephalopods, other taxa, which are expected to have a lower trophic level) and bigger species (i.e. large Actinopterygians, Chondrychians, marine mammals, expected to be their predators) (Fig. 2). It ranged from 1.8 to 2.5‰ and from 1.2 to 2‰ for C, and from 1.7 to 3.9‰ and from 1.3 to 4.3‰ for N in smaller and larger species, respectively.

### 4. DISCUSSION

On the horizontal axis of the spatial distribution, SI signatures in the muscle of Bay of Biscay organisms evidenced a gradient from the coastal to the oceanic habitat for both C and N, consistent for all taxa analysed in this study (Fig. 2). As expected, species inhabiting the offshore waters displayed significantly lower  $\delta^{13}\text{C}$  and  $\delta^{15}\text{N}$  values than those from inshore waters [8]. Moreover, the mean spatial difference in SI signatures was greater for  $\delta^{15}\text{N}$  values than for  $\delta^{13}\text{C}$  values for all taxa. All these results highlight the existence of several food webs with distinct baseline signatures in the Bay of Biscay.

On the vertical axis of the spatial distribution, SI signatures also evidenced a difference between pelagic and demersal/benthic species in lower trophic level organisms (Fig. 2). Pelagic species displayed significantly lower  $\delta^{13}\text{C}$  and  $\delta^{15}\text{N}$

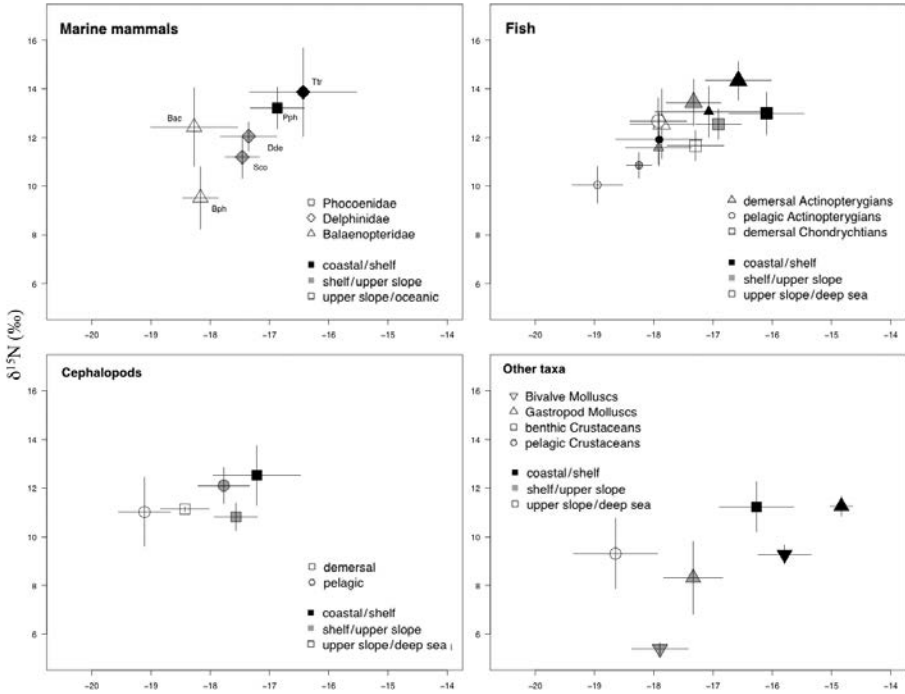


FIG. 2. Muscle  $\delta^{13}\text{C}$  and  $\delta^{15}\text{N}$  values (‰) for various taxa from the Bay of Biscay. Values are means  $\pm$  SD. For fish, the largest triangles correspond to larger species, the smallest triangles to smaller species. For marine mammals, species are not regrouped: Bph — *Balaenoptera physalus*; Bac — *Balaenoptera acutorostrata*; Dde — *Delphinus delphis*; Pph — *Phocoena phocoena*; Ttr — *Tursiops truncatus*. The same scale has been applied for all taxa, to facilitate reading and comparisons between taxa.

values than demersal or benthic species of the same taxonomic group (e.g., small pelagic Actinopterygians vs. small demersal Actinopterygians, pelagic crustaceans vs. benthic crustaceans). Stable C and N ratios linearly co-vary in marine food chains (Fig. 2) [6, 11]. Hence,  $\delta^{13}\text{C}$  values were able to reflect the contribution of pelagic vs. benthic primary producers to food intake [7], as well as  $\delta^{15}\text{N}$  values that may also help to distinguish foraging zones [8]. For instance, in a given environment, benthic invertebrates may present higher  $\delta^{15}\text{N}$  values, likely due to their scavenger behaviour, leading to higher  $\delta^{15}\text{N}$  in their predators in comparison with exclusive zooplankton feeders.

With regard to higher  $\delta^{15}\text{N}$  values in nearshore vs. upper slope and deep-sea organisms in the present study (Fig. 2), the variety of mechanisms that can explain this phenomenon has been discussed in detail in Ref. [8]. Such spatial difference may be more linked to processes occurring at the dissolved inorganic nitrogen level (DIN), rather than variations in trophic structure and feeding habits between different

environments. Then, detailing processes that can enrich  $\delta^{15}\text{N}$  values of the available DIN pool (see [8] and references therein), the following general conclusions can be drawn: (1) when DIN demand is higher than the supply in nutrients, primary producers may use a  $\delta^{15}\text{N}$  enriched N source (e.g. 'recycled' or enriched ammonium, especially if it comes from higher trophic levels), which is then reflected in the local food chain. For instance, during upwelling events in areas subject to this, the physical supply of 'new' nutrients overwhelms the biological uptake rate, favouring  $\delta^{15}\text{N}$  depleted N sources for producers of this environment. Moreover, high primary production during spring on the continental shelf reduces nutrient quantities, thus favouring  $\delta^{15}\text{N}$  enrichment of the available DIN. Even if brief, this effect may be lasting for benthic consumers in particular, due to the sinking of particles to the bottom; (2) rivers may be a vector of  $\delta^{15}\text{N}$  enriched organic matter into coastal waters as well as linked to  $\delta^{15}\text{N}$  enriched anthropogenic inputs derived from human waste, for example.

In the particular case of the Bay of Biscay, it is difficult to assess whether one mechanism or the other is more important. Both processes can be implied and the prevalence of one or the other can change temporally. Indeed, this ecosystem is characterized by contrasting hydrological landscapes, with regions under upwelling influence, regions largely under river plume influence, and intermediate areas. Nevertheless, these landscapes vary greatly in their spatial extent, both seasonally and from one year to another. This is primarily due to the amount of river runoff and river plumes (i.e. Loire and Gironde) that also vary considerably in time [2, 18]. Available nutrients for primary production are thus highly dependent on these temporal variations as well [19, 20], while they can strongly affect  $\delta^{15}\text{N}$  values of primary producers as commented above. This notably raises the question of a hypothetical temporal effect on  $\delta^{13}\text{C}$  and  $\delta^{15}\text{N}$  values in the present work. Nonetheless, 83% of individuals analysed here came from 2008 and 2009 autumn surveys. Also, we only analysed primary consumers and higher trophic levels, which tend to average out short term variations that can impact the  $\delta^{15}\text{N}$  values of primary producers.

## 5. CONCLUSIONS

In conclusion, this study strongly evidences the importance of discriminating the nearshore vs. upper slope and deep-sea environments in the Bay of Biscay, particularly in trophic level calculations derived from  $\delta^{15}\text{N}$  values [21]. Furthermore, such spatial variations and the overall data set of SI signatures made available by this work encourages further study of trophic relationships in the Bay of Biscay's different environments. This is also hopeful for the study of trophic ecology of particularly poorly known species, or those difficult to sample and/or to observe (e.g. deep-sea species, marine mammals).

## ACKNOWLEDGEMENTS

This work was supported through the PhD grant of T. Chauvelon from the Conseil Régional de Poitou-Charentes. The authors are very grateful to J.P. Léauté, R. Bellail and J.C. Mahé from IFREMER for facilitating the sampling during the EVHOE cruises, and to members of the French Stranding Network and the whole staff of CRMM for providing the marine mammal samples. They also thank P. Richard and G. Guillou (LIENSs) for assistance in stable isotope analysis.

## REFERENCES

- [1] KOUTSIKOPOULOS, C., et al., Temporal trends and spatial structures of the sea surface temperature in the Bay of Biscay, *Oceanol. Acta* **21** (1998) 335–344.
- [2] PLANQUE, B., et al., Detecting hydrological landscapes over the Bay of Biscay continental shelf in spring, *Clim. Res.* **28** (2004) 41–52.
- [3] CURY, P.M., et al., Trophodynamic indicators for an ecosystem approach to fisheries, *ICES J. Mar. Sci.* **62** (2005) 430–442.
- [4] MICHENER, R.H., KAUFMAN, L., “Stable isotope ratios as tracers in marine food webs: An update”, *Stable Isotopes in Ecology and Environmental Science*, (MICHENER, R., LAJTHA, K., Eds), Blackwell, Oxford (2007) 238–282.
- [5] DE NIRO, M.J., EPSTEIN, S., Influence of diet on the distribution of carbon isotopes in animals, *Geochim. Cosmochim. Acta* **42** (1978) 495–506.
- [6] KELLY, J.F., Stable isotopes of carbon and nitrogen in the study of avian and mammalian trophic ecology, *Can. J. Zool.* **78** (2000) 1–27.
- [7] FRANCE, R.L., Carbon-13 enrichment in benthic compared to planktonic algae: foodweb implications, *Mar. Ecol. Prog. Ser.* **124** (1995) 307–312.
- [8] SHERWOOD, G.D., ROSE, G.A., Stable isotope analysis of some representative fish and invertebrates of the Newfoundland and Labrador continental shelf food web, *Estuar. Coast. Shelf Sci.* **63** (2005) 537–549.
- [9] DE NIRO, M.J., EPSTEIN, S., Influence of diet on the distribution of nitrogen isotopes in animals, *Geochim. Cosmochim. Acta* **45** (1981) 341–351.
- [10] VANDERKLIFT, A., PONSARD, S., Sources of variation in consumer-diet  $\delta^{15}\text{N}$  enrichment: A meta-analysis, *Oecologia* **136** (2003) 169–182.
- [11] HOBSON, K.A., WELCH, H.E., Determination of trophic relationships within a high Arctic marine food web using  $\delta^{13}\text{C}$  and  $\delta^{15}\text{N}$  analysis, *Mar. Ecol. Prog. Ser.* **84** (1992) 9–18.
- [12] CHOUVELON, T., et al., Species and ontogenic-related differences in  $\delta^{13}\text{C}$  and  $\delta^{15}\text{N}$  values and Hg and Cd concentrations of cephalopods, *Mar. Ecol. Prog. Ser.* **433** (2011) 107–120.
- [13] DE NIRO, M.J., EPSTEIN, S., Mechanism of carbon fractionation associated with lipid synthesis, *Science* **197** (1977) 261–263.
- [14] PALOMARES, M.L.D., PAULY, D. (Eds), *SeaLifeBase*, [www.sealifebase.org](http://www.sealifebase.org), version (12/2010).

- [15] QUERO, J.C., Guide des Poissons de l'Atlantique Européen, Les guides du naturaliste, (DELACHAUX, NIESTLE, Eds), Delachaux et Niestle, Paris (2003) 465.
- [16] SPITZ, J., et al., Diet overlap between harbour porpoise and bottlenose dolphin: An argument in favour of interference competition for food? *Estuar. Coast. Shelf Sci.* **70** (2006) 259–270.
- [17] SPITZ, J., et al., Dietary plasticity of the oceanic striped dolphin, *Stenella coeruleoalba*, in the neritic waters of the Bay of Biscay, *J. Sea Res.* **55** (2006) 309–320.
- [18] PULLAT, I., et al., Hydrographical variability on the French continental shelf in the Bay of Biscay, during the 1990s, *Cont. Shelf Res.* **24** (2004) 1143–1163.
- [19] HERBLAND, A., et al., Phytoplankton spring bloom of the Gironde plume waters in the Bay of Biscay: early phosphorus limitation and food-web consequence, *Oceanol. Acta* **21** (1998) 279–291.
- [20] LUNVEN, M., et al., Nutrient and phytoplankton distribution in the Loire River plume (Bay of Biscay, France) resolved by a new Fine Scale Sampler, *Estuar. Coast. Shelf Sci.* **65** (2005) 94–108.
- [21] VANDER ZANDEN, M.J., RASMUSSEN, J.B., Primary consumer  $\delta^{13}\text{C}$  and  $\delta^{15}\text{N}$  and the trophic position of aquatic consumers, *Ecology* **80** (1999) 1395–1404.

# GLOBAL DISTRIBUTIONS OF $^{137}\text{Cs}$ , $^{239,240}\text{Pu}$ AND THE RATIO OF $^{239,240}\text{Pu}/^{137}\text{Cs}$ IN AN OCEAN GENERAL CIRCULATION MODEL

D. TSUMUNE<sup>a</sup>, M. AOYAMA<sup>b</sup>, K. HIROSE<sup>c</sup>, T. TSUBONO<sup>a</sup>, K. MISUMI<sup>a</sup>, Y. YOSHIDA<sup>a</sup>

<sup>a</sup> Environmental Research Laboratory,  
Central Research Institute of Electric Power Industry,  
Abiko, Japan

<sup>b</sup> Geochemical Research Department,  
Meteorological Research Institute,  
Tsukuba, Japan

<sup>c</sup> Sophia University,  
Tokyo, Japan

## Abstract

The spatial distributions and the temporal variations of  $^{137}\text{Cs}$  and  $^{239,240}\text{Pu}$  concentrations were simulated by using an ocean general circulation model (OGCM). These radionuclides are introduced into the ocean by global fallout originating from atmospheric nuclear weapons tests.  $^{137}\text{Cs}$  derived from global fallout is transported into the ocean interior by advection and diffusion, and the  $^{137}\text{Cs}$  concentration is reduced by radioactive decay. In contrast to  $^{137}\text{Cs}$ ,  $^{239,240}\text{Pu}$ , which is a particle reactive radionuclide, is a biogeochemical tracer. The global distribution of the  $^{239,240}\text{Pu}/^{137}\text{Cs}$  ratio was investigated in an OGCM with a biogeochemical process model. A half regeneration depth (HRD) of  $^{239,240}\text{Pu}$  was estimated from curve fitting of the vertical profile of the  $^{239,240}\text{Pu}/^{137}\text{Cs}$  ratio. Simulated distribution of the HRD is in good agreement with observation, except in the subarctic gyre. The HRD is a good tool to improve the parameters in the biogeochemical process.

## 1. INTRODUCTION

Artificial radionuclides, such as  $^{137}\text{Cs}$  and  $^{239,240}\text{Pu}$ , have been supplied into the ocean by global fallout due to atmospheric weapons tests and nuclear reactor accidents since 1945.  $^{137}\text{Cs}$  is an inertial tracer that advects and diffuses according to oceanic physical processes. Additionally  $^{137}\text{Cs}$  concentration is reduced by radioactive decay with a half-life of 30 a. In contrast to  $^{137}\text{Cs}$ ,  $^{239,240}\text{Pu}$  is a biogeochemical tracer because it is a particle reactive radionuclide.  $^{239,240}\text{Pu}$  behaviour in the ocean is

characterized by scavenging and remineralization processes. The  $^{239,240}\text{Pu}$  concentration is not reduced by radioactive decay on the decadal scale. The half-life of  $^{239}\text{Pu}$  and  $^{240}\text{Pu}$  are 24 100 and 6540 a, respectively.

The  $^{239,240}\text{Pu}/^{137}\text{Cs}$  ratio is a good proxy of biogeochemical processes [1]. The observed  $^{239,240}\text{Pu}/^{137}\text{Cs}$  ratio increased exponentially with increasing depth from 100 to 1500 m. Hirose et al. [1] proposed a half regeneration depth (HRD) of  $^{239,240}\text{Pu}$ , which is estimated from the curve fitting the vertical profile of the ratio. The HRD related to biogeochemical process in the ocean.

$^{239,240}\text{Pu}$  simulations by OGCMs were also conducted with simple scavenging models [2, 3]. Simulated  $^{239,240}\text{Pu}$  concentrations are in good agreement with observation although these models did not explicitly consider biogeochemical processes. A simple one-dimensional biogeochemical model showed the vertical profiles of  $^{239,240}\text{Pu}$  concentrations and their temporal changes [4], however, biogeochemical processes cannot be used to explain a decrease of inventory in the corresponding site without advection processes. We simulate the  $^{137}\text{Cs}$  and  $^{239,240}\text{Pu}$  concentrations simultaneously using an OGCM with biogeochemical process model.

The  $^{239,240}\text{Pu}$  behaviour in the ocean is similar to iron as an important micronutrient, which include biological uptake, the scavenging and remineralization processes. We applied the iron cycle model with different parameters to simulate the  $^{239,240}\text{Pu}$  concentration in the ocean. There are unknown parameters of biogeochemical process in the iron cycle model.  $^{239,240}\text{Pu}$  cycle modelling helps to examine the reasonable parameters in the iron cycle model.

$^{137}\text{Cs}$  behaviour in the ocean is controlled by physical processes.  $^{239,240}\text{Pu}$  behaviour is controlled by both physical and biogeochemical processes. For example, a shallower bias of  $^{137}\text{Cs}$  tracer penetration was shown in the model, especially in the North Pacific [5, 6]. Models have both physical and biogeochemical biases. Physical bias in the model can be reduced by the comparison of the  $^{239,240}\text{Pu}/^{137}\text{Cs}$  ratio and HRD between observation and simulation. It is an advantage to examine the biogeochemical parameters to understand the biogeochemical process.

## 2. METHODS

### 2.1. OGCM and biogeochemical model

We employ an ocean component model of a modified version of NCAR CSM 1.4 consisting of an ocean general circulation model (POP) and biogeochemical model (modified OCMIP-2 BGC model) [7]. The POP's resolution is  $3.6^\circ$  in longitude and  $0.8^\circ$ – $1.8^\circ$  in latitude with 25 levels in the vertical. The modified OCMIP-2 BGC model includes the prognostic computation of new/export production as a function of light, temperature, phosphate and iron concentration, and the dynamical iron cycle. The iron cycle model considers three forms which are dissolved inorganic iron (Fe),

iron content of dissolved organic matter (DOFe) and iron content of the sinking particle (POFe). Fe is injected into the ocean surface by aeolian dust deposition without direct transport to sediment in this model. Fe is converted to DOFe and POFe by biological uptake of Fe. DOFe is remineralized to Fe. Fe is scavenged by POFe. POFe is also remineralized to Fe. The single ligand model [8] is employed for the scavenging processes of Fe. We employed the normal year forcing data [9]. The model simulates 1945 to 2007 after a continuous run of 200 years.

## 2.2. $^{137}\text{Cs}$ and $^{239,240}\text{Pu}$ models

The global distribution of cumulative  $^{137}\text{Cs}$  deposition has been reconstructed from global measurements of  $^{137}\text{Cs}$  in rain, seawater, and soil [10]. The global distribution of  $^{137}\text{Cs}$  deposition was estimated from 1945 to 2007 using these distribution data,  $^{137}\text{Cs}$  deposition data observed at the Meteorological Research Institute (MRI), Tsukuba, Japan, from 1958, and  $^{137}\text{Cs}$  deposition data for 1945–1957 estimated from ice core data [11].  $^{137}\text{Cs}$  advects and diffuses as an inertial tracer and the  $^{137}\text{Cs}$  concentration is reduced only by radioactive decay, with a half-life of 30 a.

$^{239,240}\text{Pu}$  deposition has been observed at MRI from 1958 and was estimated from ice core data [12]. We estimate the global distribution of  $^{239,240}\text{Pu}$  by considering the  $^{239,240}\text{Pu}/^{137}\text{Cs}$  ratio in the sediment deposition for each year. The  $^{239,240}\text{Pu}$  cycle model is similar to the iron cycle model with different parameters. This model considers three forms which are dissolved inorganic  $^{239,240}\text{Pu}$  (Pu),  $^{239,240}\text{Pu}$  content of dissolved organic matter (DOPu) and  $^{239,240}\text{Pu}$  content of the sinking particle (POPu). The unit of  $^{239,240}\text{Pu}$  deposition data is  $\text{Bq}/\text{m}^3$ . The unit of  $^{239,240}\text{Pu}$  is converted from Bq to mole by decay constants of  $^{239}\text{Pu}$  and  $^{240}\text{Pu}$ .  $^{239}\text{Pu}/^{240}\text{Pu}$  of global fallout is estimated to be 0.18 [13]. The biological uptake ratio of Pu to  $\text{PO}_4$  is unknown. We estimated it to be  $4.0 \times 10^{-11}$  (mol/mol) from averaged  $^{239,240}\text{Pu}$  concentration in the ocean. When the  $^{239,240}\text{Pu}/\text{PO}_4$  ratio is smaller than the biological uptake ratio, the biological uptake ratio is set to the  $^{239,240}\text{Pu}/\text{PO}_4$  ratio to prevent minus value of  $^{239,240}\text{Pu}/\text{PO}_4$  concentration. The biological uptake ratio of Pu is much quite smaller than iron. In case of Fe, 60% of scavenged Fe can be remineralized back to dissolved form. In case of  $^{239,240}\text{Pu}$ , 90% of scavenged  $^{239,240}\text{Pu}$  can be remineralized back to dissolved form because the observed  $^{239,240}\text{Pu}$  content of the sinking particle is small compared with Fe.

## 2.3. Database

The observed data of  $^{137}\text{Cs}$  and  $^{239,240}\text{Pu}$  is summarized in the Historical Artificial Radionuclides in the Pacific Ocean and its Marginal Seas database (HAM database) [14]. We pick up 52 vertical profiles of  $^{137}\text{Cs}$  and  $^{239,240}\text{Pu}$  in the North Pacific from the database. There is no correction of radioactive decay of  $^{137}\text{Cs}$  concentration to calculate the  $^{239,240}\text{Pu}/^{137}\text{Cs}$  ratio. The observed  $^{239,240}\text{Pu}/^{137}\text{Cs}$  ratio exponentially increased

with increasing depth from 100m to 1500m. We examined the relationship between  $^{239,240}\text{Pu}/^{137}\text{Cs}$  ratio and depth by fitting the data to an exponential function [1],

$$R_{\text{Pu/Ca}} = R_{\text{Pu/Cs},0} \exp(\lambda Z) \quad (1)$$

where  $R_{\text{Pu/Cs},0}$  and  $\lambda$  are constants and  $Z$  is the water depth, governed by oceanographic conditions. A HRD of  $^{239,240}\text{Pu}$  ( $Z_h$ ) is a HRD(m) related to biogeochemical process in the ocean and is defined as follows:

$$Z_h = 0.693\lambda \quad (2)$$

### 3. RESULTS

Vertical profiles of  $^{137}\text{Cs}$  and  $^{239,240}\text{Pu}$  concentrations showed decadal changes from the 1970s to the 2000s. The simulated vertical distributions of the  $^{137}\text{Cs}$  concentrations and their temporal change are in good agreement with observation (Fig. 1). However, the simulated penetration depth is shallower than observation by known physical bias [5, 6]. The depth of maximum  $^{239,240}\text{Pu}$  concentration deepened and surface  $^{239,240}\text{Pu}$  concentration decreased from the 1970s to the 2000s due to biogeochemical processes (Fig. 2a). Model simulation can represent the vertical profiles and their temporal change (Fig. 2b), however, the simulated depth of maximum  $^{239,240}\text{Pu}$  concentrations are shallower than observation. Causes of the shallower penetration should be examined in both physical and biogeochemical processes of the model. The shallower bias of tracer penetration by an OGCM exists in the physical process of the North Pacific [5, 6]. The reduction of physical bias is necessary to examine the biogeochemical process in comparison with observed data. The simulated  $^{239,240}\text{Pu}$  concentrations in the North Pacific are smaller than those observed. The simulated  $^{239,240}\text{Pu}$  inventory is about 50% smaller than observation in 2000 at the point of Fig. 2. The reason for underestimation may be that close-in fallout from the United States Pacific Proving nuclear testing is not considered in this study. Since mechanisms of close-in fallout from Bikini nuclear explosions are still unknown, we focused on only global fallout  $^{239,240}\text{Pu}$  in this study. In this case, the  $^{239,240}\text{Pu}/^{137}\text{Cs}$  ratio is an effective tool to validate the model including the biogeochemical processes. In fact, the model simulation can produce exponential increase of the  $^{239,240}\text{Pu}/^{137}\text{Cs}$  ratio with increasing depth. This finding suggests that the  $^{239,240}\text{Pu}/^{137}\text{Cs}$  ratio and the HRD calculated from the model simulation are effective for examining the biogeochemical process in the model.

The observed  $^{239,240}\text{Pu}/^{137}\text{Cs}$  ratio exponentially increased with increasing depth from 100 to 1500 m. On the other hand, the simulated ratio exponentially increased from 100 m to 800 m because the penetration depth of  $^{137}\text{Cs}$  is underestimated in the physical model. Simulated HRD is estimated by the ratio from 100 to 800 m

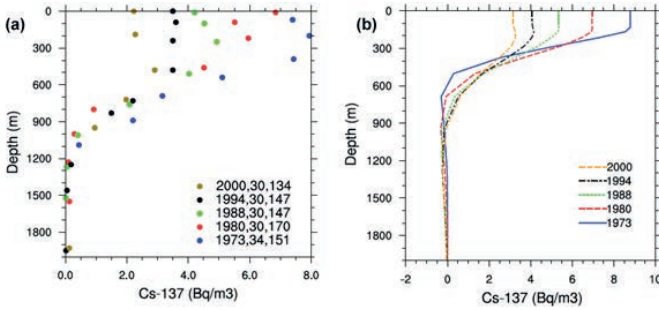


FIG. 1. Vertical profiles of  $^{137}\text{Cs}$  concentration in the North Pacific in 1973, 1980, 1988, 1994 and 2000 (a) Observed data in HAM database ( $30^{\circ}$ – $34^{\circ}\text{N}$ ,  $135^{\circ}$ – $170^{\circ}\text{E}$ ); (b) Simulated results at  $33^{\circ}\text{N}$ ,  $147^{\circ}\text{E}$ .

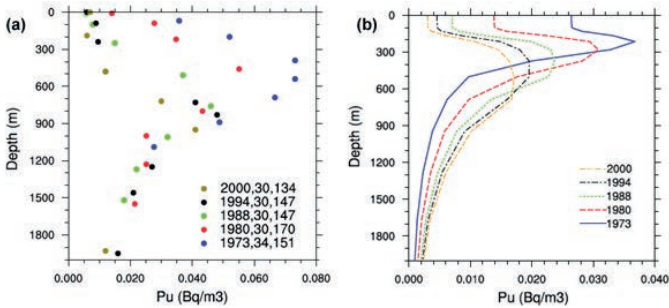


FIG. 2. Vertical profiles of  $^{239,240}\text{Pu}$  concentration in the North Pacific in 1973, 1980, 1988, 1994 and 2000 (a) Observed data in HAM database ( $30^{\circ}$ – $34^{\circ}\text{N}$ ,  $135^{\circ}$ – $170^{\circ}\text{E}$ ); (b) Simulated results at  $33^{\circ}\text{N}$ ,  $147^{\circ}\text{E}$ .

depth. Figure 3 shows the horizontal distribution of the HRD of  $^{239,240}\text{Pu}$  in the North Pacific. The simulated HRD is in good agreement with observation, except in the subarctic gyre. Comparison of the HRD between observation and simulation can reduce the physical bias. Reduction of bias is an advantage to verify biogeochemical process modelling. However, the simulated HRD in the subarctic gyre was shallower than observation. In the subarctic gyre, the simulated  $^{137}\text{Cs}$  concentration by this lower resolution model is markedly higher than observation [5, 6]. This suggests that the physical bias in the subarctic gyre is too large to simulate HRD in this model. Since a higher resolution model could improve the physical bias in the subarctic gyre, it is important to develop a high resolution model including the biogeochemical processes.

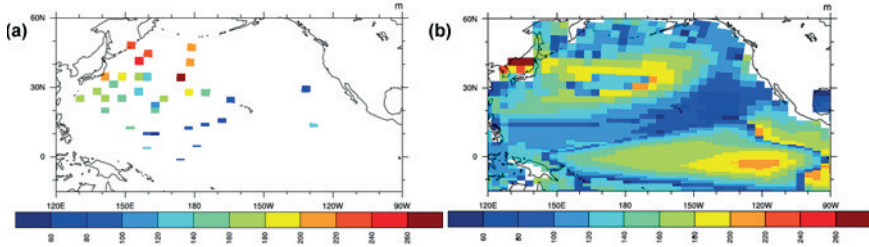


FIG. 3. Horizontal distribution of HRD in the North Pacific (a) Observed data in the HAM database from 1973 to 2005; (b) Simulated results in 2003.

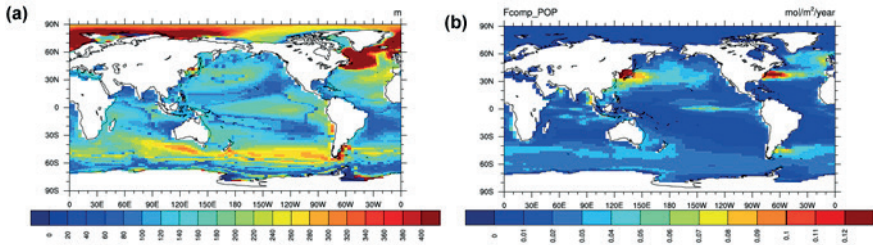


FIG. 4. (a) Global distribution of HRD; (b) export flux of particle organic phosphate at 200m in the model ( $\text{mol}/\text{m}^2/\text{year}$ )

#### 4. DISCUSSION AND SUMMARY

The simulated HRD of plutonium is in good agreement with observation. There is room to improve the parameters of the biogeochemical process in this model. The HRD is a good tool to validate the parameters of the biogeochemical process in the model and to understand the biogeochemical process, because biogeochemical models have a lot of unknown parameters.

Global distribution of the HRD is similar to the export flux of particle organic phosphate in the model (Fig 4). The HRD estimated from  $^{137}\text{Cs}$  and  $^{239,240}\text{Pu}$  is a good proxy of export flux and biogeochemical process. We expect more simultaneous observations of  $^{137}\text{Cs}$  and  $^{239,240}\text{Pu}$  to understand the biogeochemical process in the ocean in the future.

#### ACKNOWLEDGEMENTS

The authors thank F.O. Bryan, S.C. Doney and K. Lindsay for their fruitful comments and for providing the model. The authors also thank T. Motoi, Y. Sasai and T. Kobayashi for their useful comments. The authors also thank M. Yamamoto for his

technical help. This work was supported by a grant from the Ministry of Education, Culture, Sports, Science and Technology (MEXT) of Japan.

## REFERENCES

- [1] HIROSE, K., et al.,  $^{239,240}\text{Pu}/^{137}\text{Cs}$  ratios in the water column of the North Pacific: A proxy of biogeochemical processes, *J. Environ. Radioact.* **100** (2009) 258–262.
- [2] TSUMUNE, D., et al., Numerical simulation of  $^{137}\text{Cs}$  and  $^{239,240}\text{Pu}$  concentrations by an ocean general circulation model, *J. Environ. Radioact.* **69** (2003) 61–84.
- [3] NAKANO, M., POVINEC, P. P., Modelling the distribution of plutonium in the Pacific Ocean, *J. Environ. Radioact.* **69** (2003) 85–106.
- [4] HIROSE, K., “Radionuclides in the Oceans”, RADO 96–97, Proc. Part 1, Radioprotection- Colloq. **32** (1997) C2–225.
- [5] TSUMUNE, D., et al., Behavior of  $^{137}\text{Cs}$  concentrations in the North Pacific in an ocean general circulation model, *J. Geophys. Res.* **108** (2003) 3262.
- [6] AOYAMA, M., et al., Water masses labeled with global fallout  $^{137}\text{Cs}$  formed by subduction in the North Pacific, *Geophys. Res. Lett.* **35** (2008) L01604.
- [7] DONEY, S.C., et al., Natural Variability in a Stable, 1000-Yr Global Coupled Climate- Carbon Cycle Simulation, *J. Climate* **19** (2006) 3033–3054.
- [8] ARCHER, D.E., JOHNSON, K., A model of the iron cycle in the ocean, *Global Biogeochem. Cy.* **14** (2000) 269–279.
- [9] LARGE, W.G., YEAGER, S.G., Diurnal to Decadal Global Forcing for Ocean and Sea-ice Models: The Data Sets and Flux Climatologies, NCAR Technical Note, NCAR/TN 460 (2004) 105.
- [10] AOYAMA, M., HIROSE, K., IGARASHI, Y., Re-construction and updating our understanding on the global weapons tests  $^{137}\text{Cs}$  fallout, *J. Environ. Monitoring* **8** (2006) 431–438.
- [11] TSUMUNE, D., et al., Transport of  $^{137}\text{Cs}$  to the Southern Hemisphere in an ocean general circulation model, *Prog. Oceanogr.* **89** (2011) 38–48.
- [12] HIROSE, K., et al., Annual deposition of  $^{90}\text{Sr}$ ,  $^{137}\text{Cs}$  and  $^{239+240}\text{Pu}$  from the 1961–1980 nuclear explosions: A simple model, *J. Meteor. Soc. Japan* **65** (1987) 259–277.
- [13] HIROSE, K., Plutonium in the ocean environment: its distribution and behavior, *J. Nucl. Radiochem. Sci.* **10** (2009) R7-R16.
- [14] AOYAMA, M., HIROSE, K., Artificial Radionuclides database in the Pacific Ocean: HAM database, *Scientific World Journal* **4** (2004) 200–215.



# ORIGIN OF ORGANIC MATTER IN SEDIMENTS OF THE CAMPOS BASIN (SE BRAZILIAN CONTINENTAL MARGIN) BY MEANS OF STABLE ISOTOPES AND MOLECULAR MARKERS

A.L.R. WAGENER<sup>a</sup>, R.S. CARREIRA<sup>a</sup>, C.O. FARIAS<sup>b</sup>, C.E. REZENDE<sup>c</sup>,  
L.G.M.S. CORDEIRO<sup>b</sup>, D.R. OLIVEIRA<sup>b</sup>, M. ALMEIDA<sup>c</sup>, A. BAETA<sup>a</sup>,  
A.L. SCOFIELD<sup>a</sup>

<sup>a</sup> Departamento de Química,  
Pontifícia Universidade Católica,  
Rio de Janeiro, RJ, Brazil

<sup>b</sup> Faculdade de Oceanografia,  
Universidade do Estado do Rio de Janeiro,  
Rio de Janeiro, RJ, Brazil

<sup>c</sup> Centro de Biociências e Biotecnologia,  
Universidade Estadual do Norte Fluminense,  
Campos dos Goytacazes, RJ, Brazil

## Abstract

Sediment samples were taken from a total of 133 stations in two sampling campaigns (winter 2008/2009 and summer 2009) distributed on the shelf and in transects which extended from 25 m to 3000 m water depth. The region under study is influenced by upwelling, river discharge and beyond the platform by five different water masses. The goal of the work was to examine by means of carbon isotopic composition and lipid biomarkers the provenance of the organic matter pool in the sediments so as to evaluate source strength, degradation and relevance to sustain a benthic community. Isotopic and molecular indicators show the influence of the outflow of the Paraíba do Sul river on the quality and quantity of organic matter (OM) that accumulates on the shelf; however, this influence is dependent on the hydrological regime on the river's basin. In the upwelling region of Cabo Frio, the OM is mainly of autochthonous sources, and evidence of export of labile OM produced on the shelf to the slope was found, which can potentially influence the benthic process at depths between 700 and 1000 m.

## 1. INTRODUCTION

Continental margins are highly productive areas [1], however, the comprehension of their pelagic and benthic ecology is dependent on the quality

rather than the quantity of organic matter (OM) available for primary and secondary producers [2 and references therein]. In addition, continental margins account for a significant fraction of total OM burial in marine sediments [3], and thus may act as a sink for atmospheric CO<sub>2</sub> [4, 5], but this process is primarily controlled by the accumulation of autochthonous (i.e. labile) OM.

The origin of organic matter as well as factors determining that origin can be assessed by means of the stable isotopic composition in the bulk organic matter or in specific compounds. In principle, because land derived material is depleted in <sup>13</sup>C as compared to marine organic matter synthesized by phytoplankton, it is possible to estimate the relative input from both sources to the pool of OM in sediments. However, a number of processes in the water column as well as in the sediments may affect the isotopic record [6–8]. However, they also provide a basis for a wider application of carbon isotope signatures especially if used in combination with molecular markers and elemental composition.

The Campos Basin (20–24 °S and 39–42 °W), located in the SE Brazilian continental margin (SEBCM), is one of the world's major areas of offshore oil exploitation, but also has great ecological significance because the presence, among other aspects, of productive areas associated with the occurrence of upwelling events [9–11], which may extend over hundreds of kilometres in the shelf, e.g. Ref. [12]. Only recently has the geochemistry of OM in recent sediments been studied using isotopic and sedimentological information [13, 14] as well as lipid biomarker distributions [15, 16], but the available information is scarce and of limited space and time resolution.

The present work is part of a larger project entitled Habitats — Environmental Heterogeneity in the Campos Basin by CENPES/PETROBRAS, and aims to use organic carbon stable isotopes and lipid biomarkers to understand the nature and origin of organic matter in the sediments of the Campos Basin, Rio de Janeiro, Brazil, under the influence of an upwelling system (Cabo Frio) and of the Paraíba do Sul River.

## 2. MATERIAL AND METHODS

### 2.1. Sampling

Surficial sediment samples were collected using a VanVeen or a box corer on board the R/Vs Gyre and Miss Emma McCall in the winters of 2008 and 2009 and in the summer of 2009 in three cross-shelf transects (A, B and G) ranging from 50 to 3000 m water depths as well as in a sampling array (approx. 10 to 100 m water depths) in the shelf area potentially influenced by the discharge of Paraíba do Sul River (Fig. 1). A total of 133 stations were defined with samples collected in

triplicate. Samples were stored in clean Al containers at low temperature ( $-20^{\circ}\text{C}$ ) and freeze dried in the laboratory.

$\delta^{13}\text{C}$  (in parts per mil relative to PDB) was determined in all the replicated samples after carbonate removal with acid using a Flash EA coupled to a ThermoFinnigan Delta Plus. Precision was better than 0.3‰. All reported values represent the mean of the replicate samples.

Lipid biomarkers were determined in a composite sample of the three replicates, following the method described by Carreira et al. [16]. In brief, samples were Soxhlet extracted with dichloromethane and methanol (2:1, v:v) for 24 h, bulk extracts were saponified using aqueous 1N KOH to isolate neutral (sterols and alcohols) and acidic lipids (fatty acids). Analyses of sterols and alcohols (as TMS derivatives after reaction with BSTFA at  $85^{\circ}\text{C}$  for 1 h) were performed using gas chromatography coupled to mass spectrometry (Finnigan Focus DSQ GC/MS system) while fatty acids (as methyl esters or FAME after reaction with  $\text{BF}_3/\text{MeOH}$  at  $85^{\circ}\text{C}$  for 2 h) were analysed by gas chromatography with flame ionization detection (Hewlett-Packard 6890).

### 3. RESULTS AND DISCUSSION

The  $\delta^{13}\text{C}$  values found in surface sediments ranged from  $-19.5$  to  $-27.5$ ‰, with an overall mean of  $-23.4 \pm 1.6$ ‰ (Fig. 1). There are large differences between the sampling periods (winter and summer) and among the different regions of the continental margin. Samples collected on the shelf ( $<150$  m water depth) near the Paraíba do Sul River exhibit greater seasonal variation in isotopic composition. Relatively enriched  $\delta^{13}\text{C}$  values ( $-21.9$  to  $-19.6$ ‰; Fig. 1a) are observed at shallow ( $<100$  m) water depths in the winter samples, suggesting a major contribution of autochthonous sources to the total sedimentary OM at these sites [17, 18]. However, summer samples in the same region (i.e. near the Paraíba do Sul River) are generally depleted in  $^{13}\text{C}$  ( $-27.5$  to  $-24.0$ ‰; Fig. 1b), pointing out a shift towards enhanced accumulation of allochthonous OM [17, 18], when compared to winter samples. This change in the nature of OM in the shelf near the Paraíba do Sul River may be explained by the river's hydrologic regime. In the summer, the rainy season in SE Brazil, river flow increases dramatically resulting in the export of continental material further into the shelf. This effect has been observed using radioactive and other tracers in the water column [19] and our data provide additional evidence of such an effect. In winter (the dry season), the decrease in river flow reduces the amount of continental material exported to the shelf as well as the depositional distance from the coast. Additional consideration will be provided by lipid biomarkers (see below). The significant difference in the nature of sedimentary OM near the Paraíba do Sul River also suggests the influence of hydrodynamic factors on the shelf that are responsible for the seasonal resuspension and transport of OM, which, in turn, is favoured by the relatively shallow depths in the shelf.

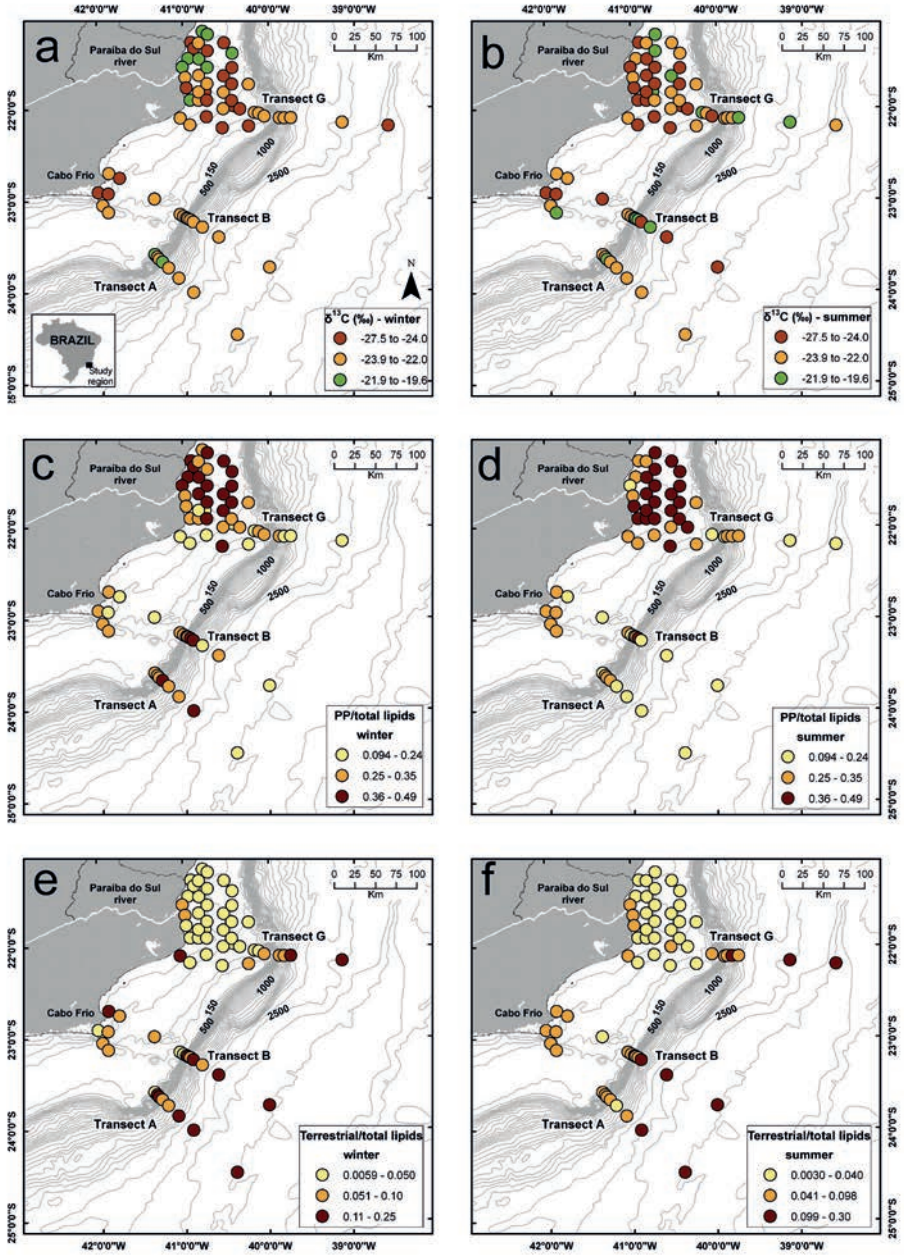


FIG. 1. Isotopic ( $\delta^{13}\text{C}$ ; a, b) and molecular (lipids; c–f) markers of organic matter sources in surface sediments of the Campos Basin in the two samplings campaigns (winter and summer). PP (c, d) represents lipids from autochthonous primary production (PP), ‘terrestrial’ (e, f) are allochthonous lipids. See text for source assignments of lipids.

In the cross-shelf transects A and B, influenced by the upwelling of Cabo Frio, there is little seasonal variation in  $\delta^{13}\text{C}$  (Fig. 1-a, b). Most samples near the coast-line (<100 m water depths) are relatively depleted in  $^{13}\text{C}$  ( $-27.5$  to  $-22.0\%$ ; Fig. 1, a–b), indicating a mixture of OM sources and/or the predominance of an allochthonous source. This result is not consistent with the occurrence of relatively high rates of primary production in the area, induced by the upwelling of cold and nutrient rich deeper waters [9, 10]. Such apparent discrepancy possibly arises from the predominance of sandy sediments in the shallow waters near to Cabo Frio [14], which do not favour the accumulation of sediments of OM produced in the water column. In transects A and B the enrichment in  $^{13}\text{C}$  on the shelf's upper and middle slope (400–1000 m water depths) is noticeable. The accumulation of autochthonous OM in the slope is also indicated by the lipid biomarker distribution (see below). This may be related to the increase of primary production associated with upwelling events, whose influence is known to extend over hundreds of km on the continental margin [20, 21], and suggest export of OM from the shelf to deeper portions of the Campos Basin.

Lipid biomarkers give additional information regarding the sources of OM in the studied region. The assignment of lipids to distinct sources of OM was as follows [15, 22]: (i) primary production: sum of  $\text{C}_{27}$ ,  $\text{C}_{28}$  and  $\text{C}_{29}$  sterols,  $\text{C}_{18}$ ,  $\text{C}_{20}$  and  $\text{C}_{22}$  polyunsaturated fatty acids and phytol; (ii) terrestrial (or allochthonous): sum of long chain ( $>\text{C}_{22}$ ) fatty acids and n-alcohols. The ratio PP/total lipids, i.e. lipids from primary production to total lipids (sum of total fatty acids, sterols and n-alcohols), reveals that adjacent to the estuary of Paraíba do Sul River and the slope stations of transects A and B are the two major areas of accumulation of autochthonous OM in the studied region. The high export of allochthonous materials from the Paraíba do Sul River and the slope stations of transects A and B are the two major areas of accumulation of autochthonous OM in the studied region. The high export of allochthonous materials from the Paraíba do Sul River during summer, as suggested by the  $\delta^{13}\text{C}$  values (Fig. 1b), is not directly inferred from the distribution of lipids, since high values for the ratio PP/total lipids is observed in both seasons (Fig. 1c–d). It is interesting that the concentration of total lipids (data not shown) in the summer samples is almost double that measured in winter at the stations with a high PP/total lipids ratio. Therefore, it seems that in summer (wet season) the increased outflow of the Paraíba do Sul River enhances the primary production in the water column but the terrestrial material exported is depleted in long chain fatty acids and n-alcohols. This could occur if this material is composed predominantly of wood debris instead of leaves from terrestrial plants. However, this hypothesis needs further studies to be confirmed.

The ratio terrestrial/total lipids increases with depth in the transects A, B and G, reaching maxima values between 1000 m and 3000 m water depth (Fig. 1e–f). Therefore, although the concentration of total lipids decreases toward deeper stations in the continental margin (data not shown), the contribution of the less reactive lipid increases, suggesting that the OM in the lower slope and rise becomes more

recalcitrant with a lower nutritional value for the benthic secondary producers. This same trend can also be observed by means of the  $\delta^{13}\text{C}$  (Fig. 1a–b).

#### 4. CONCLUDING REMARKS

The labile OM produced by the upwelling of nutrient rich waters off Cabo Frio is retained to a low degree in the shallow coastal areas due to the predominantly sandy sediments and to complex water circulation but there is evidence of accumulation in the continental slope and therefore of cross-shelf exportation. Both the isotope signature and lipid fingerprint point out such process of labile OM exportation and accumulation in the slope. Nutrients provided by the Paraíba River seem to induce enrichment of labile OM in more restricted areas at lower depths in the shelf.

The low molecular weight biomarkers usually predominant in marine algae and bacteria seem to undergo substantial degradation in the water column at high temperature and show a light incidence in the tropics. As a result, the OM preserved in sediments from deeper areas is principally of allocthonous origin, as concluded from the biomarker and carbon isotope fingerprint. The high turnover rate of marine labile organic matter in tropical seas has impacts on the carbon cycle, since these areas would contribute very little to excess  $\text{CO}_2$  uptake. The predominance of marine OM is restricted to the shelf and to specific areas in the continental slope; nevertheless, the relevance of these areas as a carbon sink must be better evaluated.

#### ACKNOWLEDGEMENTS

We wish to thank PETROBRAS (Brazilian energy company) for providing sampling and financial support for the chemical analyses.

#### REFERENCES

- [1] FASHAM, M.J.R., *Ocean Biogeochemistry: The Role of the Ocean Carbon Cycle in Global Change*, Global Change, The IGBP Series, Springer, Berlin (2003).
- [2] PUSCEDDU, A., et al., Quantity and bioavailability of sediment organic matter as signatures of benthic trophic status, *Mar. Ecol. Prog. Ser.* **375** (2009) 41–52.
- [3] HEDGES, J.I., KEIL, R.G., Sedimentary organic matter preservation: an assessment and speculative synthesis, *Marine Chemistry* **49** (1995) 81–115.
- [4] CHEN, C.-T.A., ., “Exchanges of carbon in the coastal seas”, *The Global Carbon Cycle: Integrating Humans, Climate, and the Natural World* (C.B. FIELD, C.B., RAUPACH, M.R., Eds), Island Press, Washington D.C. (2004) 341–354.

- [5] FRANKIGNOULLE, M. BORGES, A.V., European continental shelf as a significant sink for atmospheric carbon dioxide, *Glob. Biogeochem. Cycles* **15** 3 (2001) 569–576.
- [6] FOGEL, M.L., CIFUENTES, L.A., “Isotope fractionation during primary production”, *Organic Geochemistry: Principles and Application* (ENGEL, M.H., MACKO, S.A., Eds), Plenum Press, New York (1993) 73–98.
- [7] GEARING, P., PLUCKER, E.E., PARKER, P.L., Organic carbon stable isotope ratios of continental margin sediments, *Marine Chem.* **5** (1977) 251–266.
- [8] SACKETT, W.M., Uses of stable carbon isotope compositions of organic carbon in sedimentological studies on tropical marine systems, *Sci. Total Environ.* **58** (1986) 139–149.
- [9] VALENTIN, J.L., ANDRÉ, D.L., JACOB, S.A., Hydrobiology in the Cabo Frio (Brazil) upwelling: two dimensional structure and variability during a wind cycle, *Cont. Shelf Res.* **7** 1 (1987) 77–88.
- [10] GONZALEZ-RODRIGUEZ, E., et al., Upwelling and downwelling at Cabo Frio (Brazil): Comparison of biomass and primary production responses, *J. Plankton Res.* **14** 2 (1992) 289–306.
- [11] GUENTHER, M., et al., Dynamics of bacterial carbon metabolism at the entrance of a tropical eutrophic bay influenced by tidal oscillation, *Aquat. Microbial Ecol.* **50** (2008) 123–133.
- [12] SILVEIRA, I.M.O., et al., A Corrente do Brasil ao largo da costa brasileira, *Rev. Bras. Oceanogr.* **48** 2 (2000) 171–183.
- [13] MAHIQUES, M.M., et al., Modern sedimentation in the Cabo Frio upwelling system, Southeastern Brazilian shelf, *Anais da Academia Brasileira de Ciências* **77** 3 (2005) 535–548.
- [14] MAHIQUES, M.M., et al., Hydrodynamically driven patterns of recent sedimentation in the shelf and upper slope off Southeast Brazil, *Cont. Shelf Res.* **24** 15 (2004) 1685–1697.
- [15] YOSHINAGA, M.Y., SUMIDA, P.Y.G., WAKEHAM, S.G., Lipid biomarkers in surface sediments from an unusual coastal upwelling area from the SW Atlantic Ocean, *Org. Geochem.* **39** 10 (2008) 1385–1399.
- [16] CARREIRA, R.S., et al., Lipid biomarkers in deep sea sediments from the Campos Basin, SE Brazilian continental margin, *Org. Geochem.* **41** (2010) 879–884.
- [17] MACKO, S.A., ENGEL, M.H., PARKER, P.L., “Early diagenesis of organic matter in sediments: assessment of mechanisms and preservation by the use of isotopic molecular approaches”, *Organic Geochemistry* (ENGEL, M.H., MACKO, S.A., Eds), Plenum Press, New York (1993) 211–224.
- [18] MEYERS, P.A., Organic geochemical proxies of paleoceanographic, paleolimnologic, and paleoclimatic processes, *Org. Geochem.* **27** 5/6 (1997) 213–250.
- [19] SOUZA, T.A., et al., Use of multitracers for the study of water mixing in the Paraíba do Sul River estuary, *J. Environ. Radioact.* **101** 7 (2010) 564–570.
- [20] CALADO, L., et al., Eddy-induced upwelling off Cape São Tomé (22°S, Brazil), *Cont. Shelf Res.* **30** 10–11 (2010) 1181–1188.
- [21] CAMPOS, E.J.D., VELHOTE, D., SILVEIRA, I.C.A., Shelf break upwelling driven by Brazil Current cyclonic meanders, *Geophys. Res. Lett.* **27** 6 (2000) 751–754.

- [22] MCCALLISTER, S.L., et al., Sources of estuarine dissolved and particulate organic matter: A multi-tracer approach, *Org. Geochem.* **37** 4 (2006) 454–468.

# APPLICATION OF NATURAL RADIOISOTOPES AS TRACERS OF PARTICULATE ORGANIC CARBON TRANSPORT, EXPORT AND BURIAL PROCESSES IN CHUKCHI SEA, ARCTIC OCEAN

WEN YU, JIANHUA HE

Key Lab of Global Change and Marine-Atmosphere Chemistry,  
State Oceanic Administration,  
Xiamen, China

## Abstract

To evaluate the efficiency of the biological pump and carbon sequestration content on the Arctic shelf, estimations of POC export fluxes derived from  $^{234}\text{Th}/^{238}\text{U}$  disequilibrium and organic carbon burial rate from  $^{210}\text{Pb}$  chronology in sediment core were made during the 3rd Chinese National Arctic Research Expedition (CHINARE-3), Jul 12–Sep 22, 2008. Great deficits of  $^{234}\text{Th}$  to  $^{238}\text{U}$  were observed widely over the Chukchi shelf, with an average  $^{234}\text{Th}/^{238}\text{U}$  of  $0.64 \pm 0.28$ , resulting from intense particle scavenging. The average POC export fluxes in the entire study area, shelf and slope area were  $24.9 \pm 23.3$ ,  $29.5 \pm 23.0$  and  $2.1 \pm 0.5$   $\text{mmol-C}/\text{m}^2\text{d}$ , respectively, i.e. 21% of the primary production on average was exported to the benthos. An organic carbon burial rate of  $517$   $\text{mmol-C}/\text{m}^2\text{a}$  were estimated, accounting for 6% of the average primary production. The efficient biological pump led to  $11.6 \pm 9.0$  T g C exported to benthos and 3.4 T g C buried permanently in the sediment per year, accounting for 0.3% of total POC export amount and 2.1% of total organic carbon burial amount of the global ocean.

## 1. INTRODUCTION

The Chukchi shelf is one of the most productive regions of the world ocean [1] and plays an important role in carbon sequestration. Significant questions are how much of the primary production is exported downward as sinking particles to the benthos and how much of that is finally buried in the sediment.

Thorium-234 ( $^{234}\text{Th}$ ,  $t_{1/2}=24.1$  d), a particle reactive radionuclide produced continuously in the ocean from its soluble parent Uranium-238 ( $^{238}\text{U}$ ,  $t_{1/2}=4.5 \times 10^9$  a), is a useful tracer for quantifying the scavenging and particle export occurring on a timescale of days to months [2] and has been widely used during the last decades.

In this study, we estimated the  $^{234}\text{Th}$  derived export fluxes of particulate organic carbon (POC) from the euphotic zone and the burial rate of organic carbon, and

then the ratios of them to primary production in the Chukchi shelf, to gain a better understanding of the marine carbon cycling processes in the Arctic Ocean.

## 2. SAMPLING AND ANALYTICAL METHODS

12 L seawater samples for  $^{234}\text{Th}$  analysis were collected in Niskin bottles throughout the upper 0–40m water column at 10 stations on the Chukchi shelf and slope, during the 3<sup>rd</sup> Chinese National Arctic Research Expedition (CHINARE 3) (Jul. 12–Sept. 22, 2003). 8 stations out of 10 were on the Chukchi shelf and the other 2 stations (S14 and S22) were on the slope. At stations R05, R09, R13 and R17, samplings were made twice, conducted during Aug. 2–7 and Sept. 6–8 respectively. The second estimate results were marked as R05\*, R09\*, R13\* and R17\*. A map of the study area and sampling sites is shown in Fig. 1.

4 L samples out of 12 L were analysed for total  $^{234}\text{Th}$  (dissolved plus particulate) with the small volume  $\text{MnO}_2$  co-precipitation method including the addition of a  $^{230}\text{Th}$  spike [3, 4]. In order to shorten the filtration time of  $\text{MnO}_2$  suspension onto a 25 mm QMA filter, a modified protocol [5] with a heating step immediately after the addition of  $\text{KMnO}_4$  and  $\text{MnCl}_2$  solutions was applied. The filtered  $\text{MnO}_2$  precipitates were dried, mounted under one layer of Mylar film and two layers of aluminum foil ( $8.0 \text{ mg/cm}^2$ ), and counted onboard with gas flow proportional beta counters (RISØ GM-5-25, Denmark) until the counting uncertainty was below 3%. Each sample was recounted after 5–6 months so as to determine the background of other non- $^{234}\text{Th}/^{234\text{m}}\text{Pa}$  beta emitters. All samples were processed for chemical recovery measurement with an ion exchange method and low background alpha spectrometer

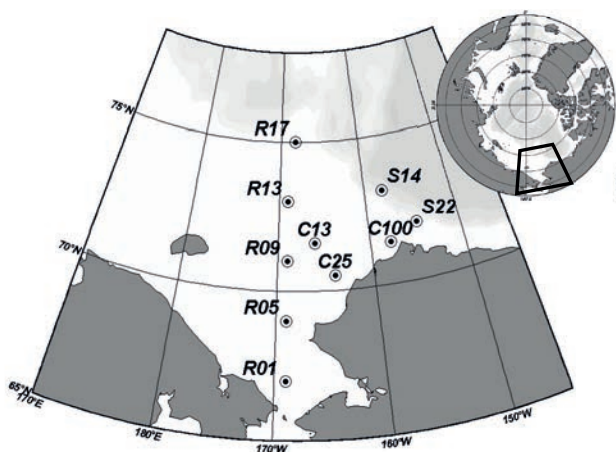


FIG. 1. Study area and sampling stations.

(Canberra 7200-08, US) with an addition of  $^{229}\text{Th}$  internal standard.  $^{234}\text{Th}$  specific activities were decay-corrected to the midpoint time of sampling.

Similarly, 8 L particulate samples filtered onto a QMA membrane were beta counted for initial  $^{234}\text{Th}$  activities and 5–6 months later for final background.  $^{238}\text{U}$  activities were calculated from salinity measurements using the relationship of  $^{238}\text{U}$  (dpm/L) =  $0.0713 \times \text{salinity}$  [6]. The bottom depth of the euphotic zone (1% light layer) was determined by a Secchi disc.

The sediment core was collected at station R17 (168°08.73'W, 75°00.09'N), with a large calibre gravity sampler (SDIOI-DDC2, China), stowed at 4°C on board and sliced into 1 cm thick subsamples in land laboratory. The ground samples were dried at 50°C before Lead-210 ( $^{210}\text{Pb}$ ,  $t_{1/2} = 22.3$  a) analysis [7]. Sediment chronology and organic carbon burial rate was derived from the vertical distribution of excess  $^{210}\text{Pb}$ , which follows the relationship below:

$$\ln A_h = \ln A_0 - \lambda h/s \quad (1),$$

where  $A_h$  and  $A_0$  are respectively the specific activities of excess  $^{210}\text{Pb}$  at depth  $h$  (mm, compaction corrected) and at the water–sediment interface,  $\lambda$  is the decay constant of  $^{210}\text{Pb}$  (0.0311/a), and  $s$  is the sedimentation rate (mm/a).

### 3. RESULTS AND DISCUSSION

#### 3.1. Depth distributions of $^{234}\text{Th}/^{238}\text{U}$ activity ratios

A great variation of  $^{234}\text{Th}$  activity was found within the Chukchi Sea. The activity of total  $^{234}\text{Th}$  ( $T^{234}\text{Th}$ ) ranged from 0.45 to 2.82 dpm/L (on average  $1.53 \pm 0.58$  dpm/L), and the activities of dissolved and particulate  $^{234}\text{Th}$  ( $D^{234}\text{Th}$  and  $P^{234}\text{Th}$ ) ranged from 0.07 to 2.64 dpm/L (on average  $1.09 \pm 0.62$  dpm/L) and from 0.12 to 1.06 dpm/L (on average  $0.43 \pm 0.21$  dpm/L), respectively. The average activities of  $T^{234}\text{Th}$ ,  $D^{234}\text{Th}$  and  $P^{234}\text{Th}$  were  $1.42 \pm 0.58$  dpm/L,  $0.99 \pm 0.61$  dpm/L and  $0.43 \pm 0.18$  dpm/L respectively, while those in the slope were  $2.04 \pm 0.26$  dpm/L,  $1.58 \pm 0.40$  dpm/L and  $0.46 \pm 0.30$  dpm/L respectively. Conversely, at most stations  $^{238}\text{U}$  activity remained relatively constant, ranging from 2.09 to 2.39 dpm/L (on average  $2.25 \pm 0.12$  dpm/L). Exceptions were at 0–10 m depth at the stations R17 and R17\*, located at the marginal ice zone (MIZ), where low  $^{238}\text{U}$  activity of 1.86 dpm/L occurred due to seawater dilution during ice melting.

The vertical distributions of activity ratios of total  $^{234}\text{Th}$  to  $^{238}\text{U}$  ( $^{234}\text{Th}/^{238}\text{U}$ )<sub>A.R.</sub> at all stations were presented in Fig. 2. Deficits of  $^{234}\text{Th}$  were widely found throughout the Chukchi Sea, especially in the shelf region. The average  $^{234}\text{Th}/^{238}\text{U}$ )<sub>A.R.</sub> across the shelf region was  $0.64 \pm 0.28$ , with the lowest ratio 0.20 occurring at 40 m depth at the station C25, indicating an intense particle scavenging effect. Considering the shallow

depth over the Chukchi shelf (~40 m), the large deficit of  $^{234}\text{Th}$  near the seafloor was most likely a result of sediment resuspension [8]. However, intense fluorescence of chlorophyll and high POC concentrations were indeed observed near seabed at station C25 and at some other stations, so the low  $^{234}\text{Th}/^{238}\text{U}$ <sub>A.R.</sub> at the bottom shelf might be a result of  $^{234}\text{Th}$  scavenging by the biogenic particle as well. In the slope region, disequilibrium between  $^{234}\text{Th}$  and  $^{238}\text{U}$  was less apparent, averaging  $0.94 \pm 0.09$ . Note that distinctive  $^{234}\text{Th}$  excesses were observed at the station R17/R17\*, which implied an extra source of  $^{234}\text{Th}$  other than in-situ decay from  $^{238}\text{U}$ . In consideration of the location of the station R17/R17\*, which was at the edge of sea ice, the excess of  $^{234}\text{Th}$  was probably caused by particle release during sea ice melting, and therefore the steady state model of  $^{234}\text{Th}$  scavenging and export in section 3.2 was not valid at these two stations [9].

### 3.2. Scavenging and export rate and residence time of $^{234}\text{Th}$

In the open ocean environment, export fluxes of  $^{234}\text{Th}$  on sinking particles can be determined by solving for the balance of its supply and removal rates with the following steady state mathematical expressions,

$$J_{\text{th}} = (A_{\text{U}} - A_{\text{DTh}})\lambda \quad (2)$$

$$P_{\text{Th}} = J_{\text{Th}} - A_{\text{PTh}}\lambda \quad (3)$$

$$\tau_{\text{D}} = A_{\text{DTh}}/J_{\text{Th}} \quad (4)$$

$$\tau_{\text{P}} = A_{\text{PTh}}/P_{\text{Th}} \quad (5)$$

where  $J_{\text{Th}}$  and  $P_{\text{Th}}$  are the scavenging rate of dissolved  $^{234}\text{Th}$  and the export rate of particulate  $^{234}\text{Th}$ , respectively, and  $\tau_{\text{D}}$  and  $\tau_{\text{P}}$  are the residence times of dissolved and particulate  $^{234}\text{Th}$ .

According to Eqs 2–5, across the study area, the scavenging and export rates of dissolved  $^{234}\text{Th}$  and particulate  $^{234}\text{Th}$  were  $37.2 \pm 15.5 \text{ dpm/m}^3\text{d}$  and  $24.3 \pm 15.1 \text{ dpm/m}^3\text{d}$ , respectively. The residence time of dissolved and particulate  $^{234}\text{Th}$  in water layers ranged from 4–314 d and 4–1038 d with averages of 50 d and 70 d, respectively, which are much shorter than the average residence time of water on the Arctic shelf (5–20 a, [10]), indicating rapid biogeochemical cycling in the study area.

## 4. DISTRIBUTION OF PARTICULATE ORGANIC CARBON CONCENTRATIONS

Concentrations of particulate organic carbon (POC) in the water column are given in Table 1. The POC concentration ranged from  $3.6\text{--}42.2 \mu\text{mol}\cdot\text{C/L}$  over the study area, with an average of  $14.8 \pm 7.5 \mu\text{mol}\cdot\text{C/L}$ . High concentrations of

TABLE 1. EXPORT FLUXES OF  $P^{234}Th$ , POC AND EXPORT RATES OF POC

Stn.	Export depth(m)	$F_{PTh}$ (dpm/m <sup>2</sup> d)	POC/PTh ( $\mu\text{mol}\cdot\text{C}/\text{m}^3\text{d}$ )	$F_{POC}$ (mmol·C/m <sup>3</sup> d)	F/Z (mmol·C/m <sup>3</sup> d)
C100	30	917.6±41.6	14.3±0.6	13.2±0.8	0.44±0.03
C13	30	697.3±40.8	24.6±1.1	17.1±1.2	0.57±0.04
C25	30	1265.2±34.6	62.6±5.7	79.2±7.6	2.64±0.25
R01	30	1298.8±34.7	47.4±2.1	61.6±3.2	2.05±0.11
R05	30	894.9±43.4	29.9±1.6	26.8±1.9	0.89±0.06
R05*	30	1008.3±42.6	26±1.5	26.2±1.9	0.87±0.06
R09	30	648.2±48.4	45±2.3	29.1±2.6	0.97±0.09
R09*	30	529.7±52.9	37.5±2.2	19.9±2.3	0.66±0.08
R13	40	759.7±66.1	10.9±0.3	8.3±0.8	0.21±0.02
R13*	40	533.7±61	25.3±1.2	13.5±1.7	0.34±0.04
S14	60	174.8±93.9	10±0.3	1.8±0.9	0.03±0.02
S22	50	176.6±83.7	14±0.6	2.5±1.2	0.05±0.02

POC (averaged for  $15.8 \pm 7.9 \mu\text{mol}\cdot\text{C}/\text{L}$ ) were found over the shelf area, decreasing in a northerly direction and offshore, consistent with the distribution pattern of chlorophyll a [11].

The POC concentrations observed at stations R05\*, R09\*, R13\* and R17\* (Sept. 6–8) averaged for  $13.9 \pm 7.0 \mu\text{mol}\cdot\text{C}/\text{L}$ , lower than the average concentrations ( $16.1 \pm 7.4 \mu\text{mol}\cdot\text{C}/\text{L}$ ) observed at the same sites a month before (Aug. 2–7), but not as obvious as the variation of chlorophyll a ( $0.80 \pm 0.52 \mu\text{g}/\text{L}$  in August and  $1.72 \pm 1.73 \mu\text{g}/\text{L}$  in September), indicating strong biological activities in the late summer although photosynthesis might be limited by nutrient depletion.

#### 4.1. POC export fluxes from euphotic zone

The export flux of POC ( $F_{POC}$ , in  $\text{mmol}\cdot\text{C}/\text{m}^2\text{d}$ ) from the euphotic zone can be estimated by multiplying  $F_{PTh}$  and the measured POC/ $^{234}Th$  ratio (in  $\text{mmol C dpm}^{-1}$ ) of particulate matter at the export interface, as equation (6) shows.

$$F_{POC} = F_{PTh}(\text{POC}/PTh)_{\text{export depth}} \quad (6)$$

The average POC export flux on the shelf was  $29.5 \pm 23.0 \text{ mmol}\cdot\text{C}/\text{L}$ , much higher than that on the slope (averaged for  $2.1 \pm 0.5 \text{ mmol}\cdot\text{C}/\text{L}$ ). The estimated POC export fluxes at the stations R05, R09, R13 and R17 during Aug. 2–7 and Sept. 6–8

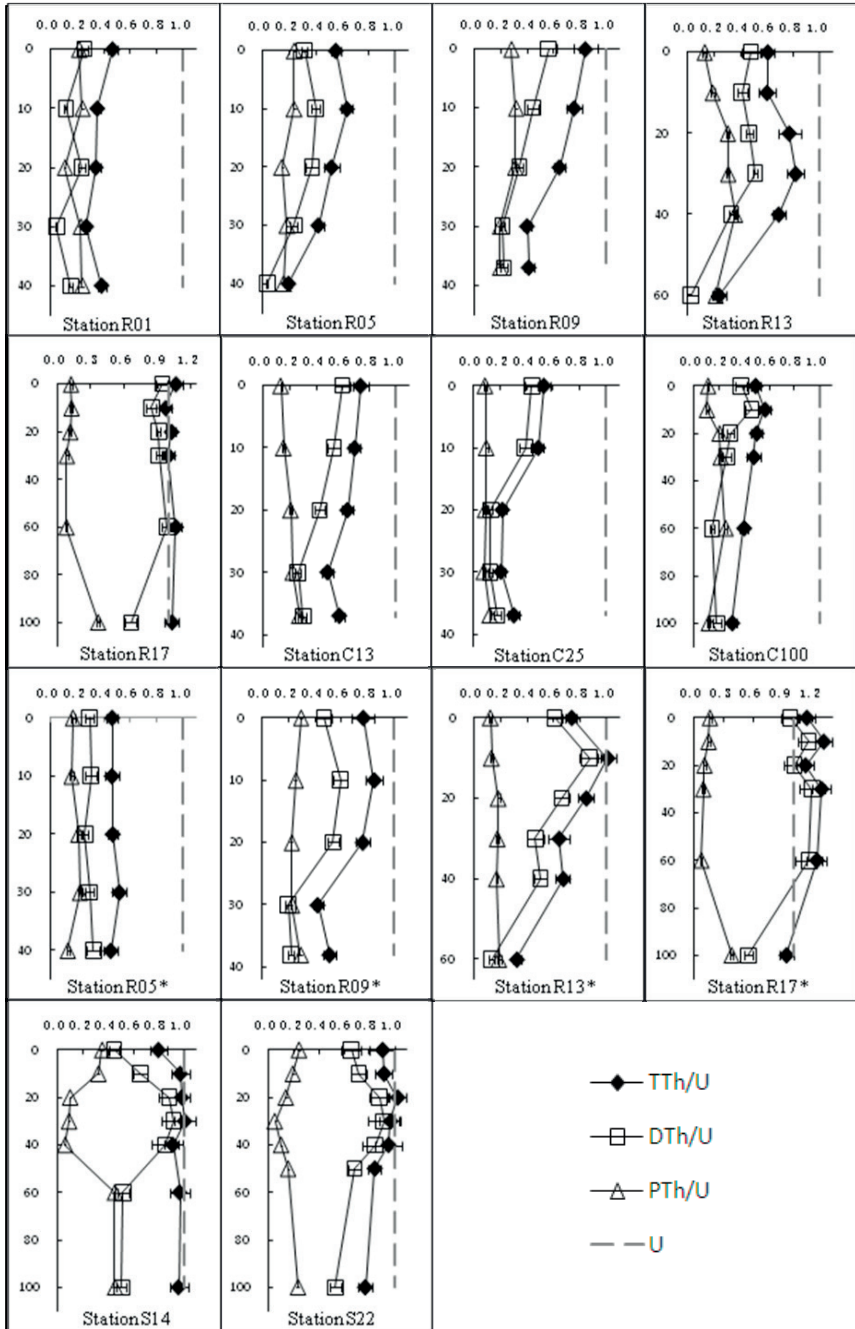


FIG. 2. Vertical distributions of  $^{234}\text{Th}/^{238}\text{U}$  activity ratios (x-axes represent  $^{234}\text{Th}/^{238}\text{U}_{\text{A.R.}}$  and y-axes represent depths, filled diamonds stand for total  $^{234}\text{Th}/^{238}\text{U}_{\text{A.R.}}$ , hollow squares for dissolved  $^{234}\text{Th}/^{238}\text{U}_{\text{A.R.}}$ , and hollow triangles for particulate  $^{234}\text{Th}/^{238}\text{U}_{\text{A.R.}}$ , respectively).

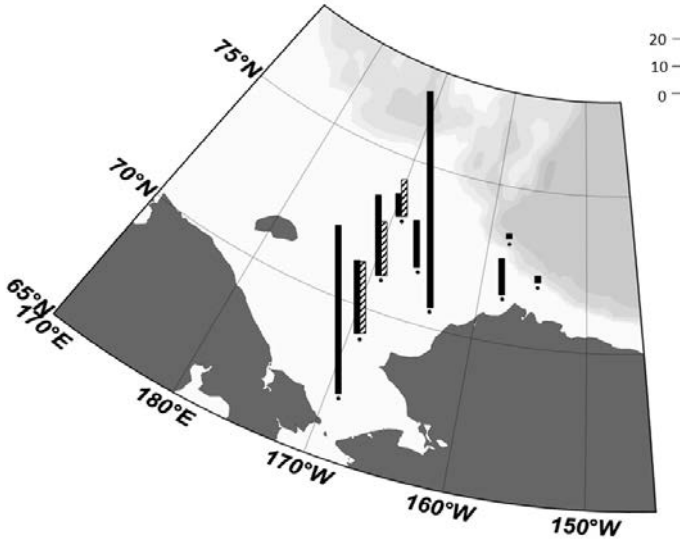


FIG. 3. POC exported fluxes (in  $\text{mmol}\cdot\text{C}/\text{m}^2\text{d}$ ; striped columns represent the results of repeated estimates).

averaged for  $21.4 \pm 11.4 \text{ mmol}\cdot\text{C}/\text{m}^2 \text{ d}$  and  $19.9 \pm 6.4 \text{ mmol}\cdot\text{C}/\text{m}^2 \text{ d}$ , respectively, revealing a still rapid export of POC in the late summertime.

The ratio, defined by Buesseler (1998) [12] as the ratio of  $^{234}\text{Th}$  derived POC export flux to primary production, is used to evaluate the efficiency of the biological pump. The reported primary productions of the Chukchi shelf varied from 11.7 to 197.0  $\text{mmol}\cdot\text{C}/\text{m}^2\text{d}$ , on average 144.2  $\text{mmol}\cdot\text{C}/\text{m}^2\text{d}$  [1, 13–14], and therefore the ThE ratio of Chukchi shelf in this study was 21%. That is, 21% of the particulate organic carbon produced by primary production exported to the benthos as sinking particles. The ThE ratio reported by this study is much higher than that in the mid-latitude ocean (2–11%, [12, 15]), indicating an efficient biological pump in the Arctic shelves.

#### 4.2. Organic carbon burial rate

The sedimentation rate of the north Chukchi Shelf derived with equation (1) was 0.6 mm/a, the apparent mass sediment accumulation rate was 0.72  $\text{kg}/\text{m}^2\text{a}$  and the organic carbon burial rate was 517  $\text{mmol}\cdot\text{C}/\text{m}^2\text{a}$ . Comparing these with the POC

export fluxes and the primary production mentioned above, approximately 35% of the POC export fluxes and 6% of primary production were perennially buried in sediment. With a shelf area of 542 500 km<sup>2</sup> [16], 3.4 T g C organic carbon per year are buried permanently in the Chukchi shelf, accounting for 2.1% of the total buried organic carbon content in seabed sediment (157 T·g·C/a, [17]).

## 5. CONCLUSIONS

Estimations of POC export fluxes and the organic carbon burial rate derived by <sup>234</sup>Th/<sup>238</sup>U disequilibrium and <sup>210</sup>Pb chronology were made during the CHINARE 3 expedition in the Chukchi Sea in summer 2008. Large deficits of <sup>234</sup>Th to <sup>238</sup>U were observed across the Chukchi shelf, resulting from intense particle scavenging. High POC export fluxes of  $24.9 \pm 23.3$  mmol·C/m<sup>2</sup>a and an organic carbon burial rate of 517 mmol·C/m<sup>2</sup> a were estimated, respectively accounting for 21% and 6% of the average primary production. The efficient biological pump led to  $11.6 \pm 9.0$  T·g·C/a being exported to the benthos and 3.4 T·g·C/a being buried permanently in the sediment, accounting for 0.3% of total POC export amount and 2.1% of the total organic carbon burial amount of the global ocean.

## ACKNOWLEDGEMENTS

The authors would like to acknowledge the China Polar Science Strategic Research Fund (20100212), the Youth Fund of State Oceanic Administration (2011531), the Open Fund of the Key Laboratory of Global Change and Marine-Atmospheric Chemistry (GCMAC0902). The sediment sample mentioned in the article was provided by the China Polar Sediment Sample Chamber.

## REFERENCES

- [1] CHEN, M., et al., Biological productivity and carbon cycling in the Arctic Ocean, *Chinese Sci. Bullet.* **47** 12 (2002) 1037–1040.
- [2] COALE, K.H., BRULAND, K.W., <sup>234</sup>Th:<sup>238</sup>U disequilibria within the California Current, *Limnol. Oceanogr.* **30** (1985) 22–33.
- [3] BUESSELER, K.O., et al., An intercomparison of small- and large- volume techniques for thorium-234 in seawater, *Mar. Chem.* **74** (2001) 15–28.
- [4] PIKE, S.M., et al., Quantification of <sup>234</sup>Th recovery in small volume sea water samples by inductively coupled plasma mass spectrometry, *J. Radioanal. Nucl. Chem.* **263** (2005) 355–360.
- [5] CAI, P, et al., An improvement in the small-volume technique for determining thorium-234 in seawater, *Mar. Chem.* **100** (2006) 282–288.

- [6] PATES, J.M., MUIR, G.K.P., U-salinity relationships in the Mediterranean: Implications for  $^{234}\text{Th}$ : $^{238}\text{U}$  particle flux studies, *Mar. Chem.* **106** (2007) 530–545.
- [7] EAKINS, J.D., MORRISON, R.T., A new procedure for the determination of lead-210 in lake and marine sediments, *Int. J. Appl. Radiat. Isot.* **29** 9–10 (1978) 531–536.
- [8] MORAN, S.B., ELLIS, K.M., SMITH, J.N.,  $^{234}\text{Th}$ / $^{238}\text{U}$  disequilibrium in the central Arctic Ocean: Implications for particulate organic carbon export, *Deep-sea Res. II* **44** 8 (1997) 1593–1606.
- [9] RUTGERS VAN DER LOEFF, M.M., MEYER, R., RUDELS, B., et al., Resuspension and particle transport in the benthic nepheloid layer in and near Fram Strait in relation to faunal abundances and  $^{234}\text{Th}$  depletion, *Deep-Sea Res. I* **49** (2002) 1941–1958.
- [10] RUTGERS VAN DER LOEFF, M.M., et al.,  $^{228}\text{Ra}$  as a tracer for shelf water in the arctic ocean, *Deep-Sea Res. II* **42** (1995) 1533–1553.
- [11] LIU, Z.L., CHEN, J.F., et al., Chlorophyll-a concentration and primary productivity in the Chukchi Sea (in preparation).
- [12] BUESSELE, K.O., The decoupling of production and particulate export in the surface ocean, *Glob. Biogeochem. Cycles* **12** (1998) 297–310.
- [13] HAMEEDI, M., Aspects of water column primary productivity in the Chukchi Sea during summer, *Marine Biology* **48** 1 (1978) 37–46.
- [14] LIU, Z.L., CHEN, J.F., ZHANG, T., et al., The Size-fractionated chlorophyll a concentration and primary productivity in the Chukchi Sea and its northern Chukchi Plateau, *Acta Ecological Sinica* **27** 12 (2007) 4953–4962.
- [15] CAI, P., CHEN, W., DAI, M., et al., A high-resolution study of particle export in the southern South China Sea based on  $^{234}\text{Th}$ : $^{238}\text{U}$  disequilibrium, *J. Geophys. Res.* **113** (2008) C04019.
- [16] STEIN, R., MACDONALD, R.W., *The organic carbon cycle in the Arctic Ocean*, New York, Springer (2004) 2–15.
- [17] BERNER, R.A., Burial of organic carbon and pyrite sulphur in the modern ocean: Its geochemical and environmental significance, *Am. J. Sci.* **282** (1982) 451–473.



# **$^{137}\text{Cs}$ DISTRIBUTION IN THE NORTHERN ADRIATIC SEA (2006–2010)**

D. PAVIČIĆ-HAMER  
'Ruđer Bošković' Institute,  
Centre for Marine Research,  
Rovinj, Croatia

D. BARIŠIĆ  
'Ruđer Bošković' Institute,  
Division for Marine and Environmental Research,  
Zagreb, Croatia  
Email: pavivic@cim.irb.hr

## **Abstract**

Artificial radioactivity in the northern Adriatic Sea was assessed by analysis of  $^{137}\text{Cs}$  concentrations in seawater, sediment and marine organisms. A comparison of radioactive contamination was made between different parts of the marine ecosystem including the area of the Po river delta, the protected area of the Lim bay and the Rovinj coastal area in the period from 2006 to 2010. In the area of the Po river delta  $^{137}\text{Cs}$  concentrations in seawater had decreased back to pre-Chernobyl values (2.48 Bq/m), although in sediment they were slightly higher (8.70 Bq/kg). Inside the Lim bay area  $^{137}\text{Cs}$  concentrations in surface water were low (1.93 Bq/m) and, in the mussel *Mytilus galloprovincialis*, even undetectable in this period. In the Rovinj coastal area  $^{137}\text{Cs}$  concentrations in surface water remained constant (2.23 Bq/m), as well as in the surface sediment (1.88 Bq/kg).  $^{137}\text{Cs}$  concentrations were detectable at very low activity levels in *Mugil cephalus* and *Sardina pilchardus*. The data indicate that some species such as the intertidal brown algae *Fucus virsoides* and the benthic fish *Mullus barbatus* are better bio-accumulators of  $^{137}\text{Cs}$  than others. These species should be used as bio-indicators in future monitoring schemes in the Adriatic Sea.

## **1. INTRODUCTION**

The northern Adriatic is a specific Mediterranean environment due to its peculiar climatic and oceanographic characteristics [1]. The northernmost part of the Adriatic is shallow, with depths of around 40 m where the Po river strongly influences the high productivity of the ecosystem with its high nutrient and pollutant input. The dominant source of anthropogenic radionuclides in the Adriatic Sea is global fallout directly from the atmosphere and indirectly from the Po river discharge.  $^{137}\text{Cs}$  is considered to be the most important radionuclide delivered by the fallout for

the assessment of marine pollution by artificial radionuclides [2, 3]. It is transported over long distances by currents and contributes substantially to radioactive contamination of the marine food chain [4, 5].

It is concluded that the general dispersion of  $^{137}\text{Cs}$  results from the different sources of contamination and the water circulation regime in the Adriatic Sea [6]. The Adriatic is connected with the Mediterranean Sea through the Otranto Strait and is characterized by a general cyclonic circulation (inflow along the eastern and outflow along the western coast). The northern Adriatic can be excluded from this general cyclonic circulation. These occasions, when the circulation of the northern Adriatic is 'closed' and under the influence of the Po river are typical of the warm part of the year [7]. During winter, under the influence of cold and dry bora wind, rapid mixing of surface water with deeper water layers occurs and very dense water called Northern Adriatic Dense Water (NADDW) is formed. NADDW flows in the bottom layer of the Adriatic towards the south, passes the Otranto Strait and becomes part of the most dense Mediterranean deep water [1].

The biological behaviour of  $^{137}\text{Cs}$  is similar to potassium. After entering the organism, all caesium is more or less uniformly distributed through the body, with a higher concentration in muscle tissue. The biological half-life of caesium is 70 days. Significant differences in  $^{137}\text{Cs}$  concentration uptake were found among different species growing under similar environmental conditions, suggesting that uptake does not follow physical levels but is influenced by allometric parameters and physiological mechanisms [8]. The brown alga *Fucus vesiculosus* L. has been used as a bio-indicator for the investigation of the impact of the Chernobyl accident on the spatial and temporal distribution of radionuclides in the Baltic Sea [9]. Many aspects favour the selection of the mussel as a bio-indicator: mussels are widespread in coastal environments, sessile, easy to collect, tolerant to changes in environmental conditions and they highly concentrate many contaminants, rendering the measurement of contaminant concentrations technically simple. Clearly the use of the mussel as a biological monitoring indicator has become standard practice in many national and international programmes [2, 10].

The objectives of this study were a radio-ecological assessment of the northern Adriatic by analysis of  $^{137}\text{Cs}$  concentration measurements in seawater, sediments, organisms and by determination of the bio-indicator species. A comparison of radioactive contamination was made between different parts of the marine ecosystem including the area of the Po river delta, the protected area of the Lim bay and the Rovinj coastal area in the period from 2006 to 2010.

## 2. MATERIALS AND METHODS

The methodology used for the sampling, radiochemical analyses and measurements of  $^{137}\text{Cs}$  in sea water samples, sediments and organisms is based on the IAEA

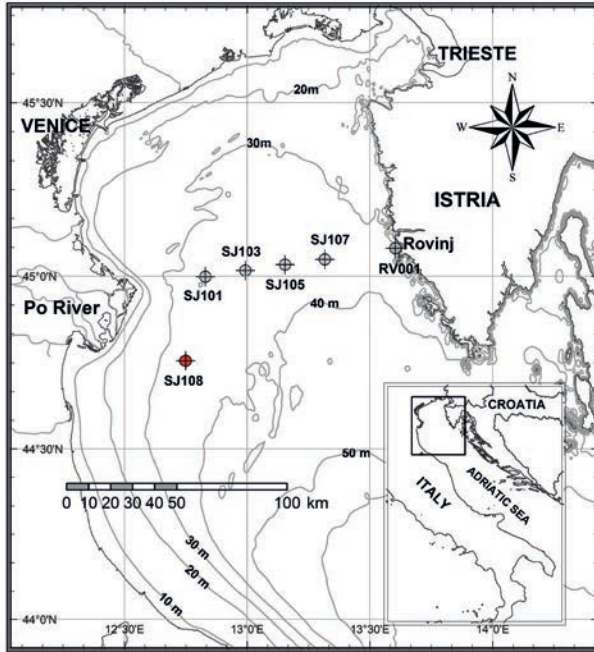


FIG. 1. Station 108 in front of the Po river delta in the northern Adriatic Sea.

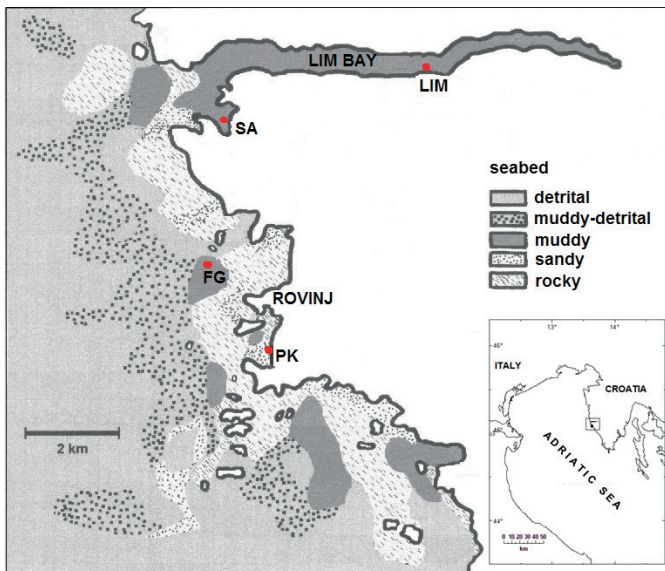


FIG. 2. Location of the sampling sites in the Rovinj coastal area in the northern Adriatic Sea. Stations: FG—Figarola Island, LIM—Lim bay, PK—Punta Corrente and SA—saline lagoon.

TRS No. 118 [10, 11]. Samples were collected from 3 locations in the northern Adriatic Sea within the Croatian national programme during 2006–2010 (Figs 1 and 2). Measuring simple ancillary data such as salinity and temperature could reflect water quality conditions in the sampling sites. At station 108, samples of seawater (0, 15 and 30 m) and sediment with corer (0–10 cm) were collected seasonally. In the Lim bay, samples of seawater and the mussels *Mytilus galloprovincialis* were collected in April and October. As well as in the Rovinj costal area, samples of seawater were collected near the island of Figarola, sediments in the saline lagoon and the brown algae *Fucus virsoides* in Punta Corrente. The locations of the sampling sites are shown on Fig. 2. The pelagic fish *Sardina pilchardus* and the benthic fishes *Mugil cephalus* and *Mullus barbatus* were collected from local fishermen and used for analyses.

A 50 L water volume was co-precipitated using microcrystalline AMP and stable CsCl as carrier for the analysis of  $^{137}\text{Cs}$  content in water. The sediments were frozen at  $-20^{\circ}\text{C}$  after sampling and kept until further use. Sediments were thawed at room temperature and dried at  $105^{\circ}\text{C}$  to constant weight before sample preparation for measurement. All samples of biota were ash at  $360^{\circ}\text{C}$  and refer to wet weight. Samples were counted in cylindrical plastic containers of appropriate volume that were placed directly onto the detector. The efficiency calibration was carried out using sources provided by the IAEA and other sources. The samples were counted for 80 000 seconds on an HPGe detector system (FWHM 1.82 keV at 1.33 MeV, 25% relative efficiency) connected with 8192 channel analyser. Canberra Genie 2000 software was used for the analyses of the spectra recorded.

### 3. RESULTS AND DISCUSSION

Over the past 40 years, the Croatian Ruđer Bošković Institute, Center for Marine Research, Rovinj, has studied the levels and distribution of long lived radionuclides in different marine samples. Today, it continues to monitor radioactive pollution at selected locations in the northern Adriatic Sea. Radioecology assessment was provided with the goal of investigating the distribution and accumulation of radionuclides in the marine ecosystem [4]. The most important environmental problem is to identify the increase of the input rates by periodical reviews of long lived radionuclides in different environmental compartments at appropriate intervals [2, 12]. In the present work the data of  $^{137}\text{Cs}$  activity in the northern Adriatic marine environment are reviewed for seawater, sediments and marine biota in order to deduce the trends for changing levels.  $^{137}\text{Cs}$  was chosen as the most representative anthropogenic radionuclide in the marine environment and has the highest potential contribution to radiation doses to humans via seafood consumption. Due to its solubility it remains for a long period in the water column dispersed widely in the marine environment via water mass circulation [5]. The baseline level of  $^{137}\text{Cs}$  in Adriatic surface water

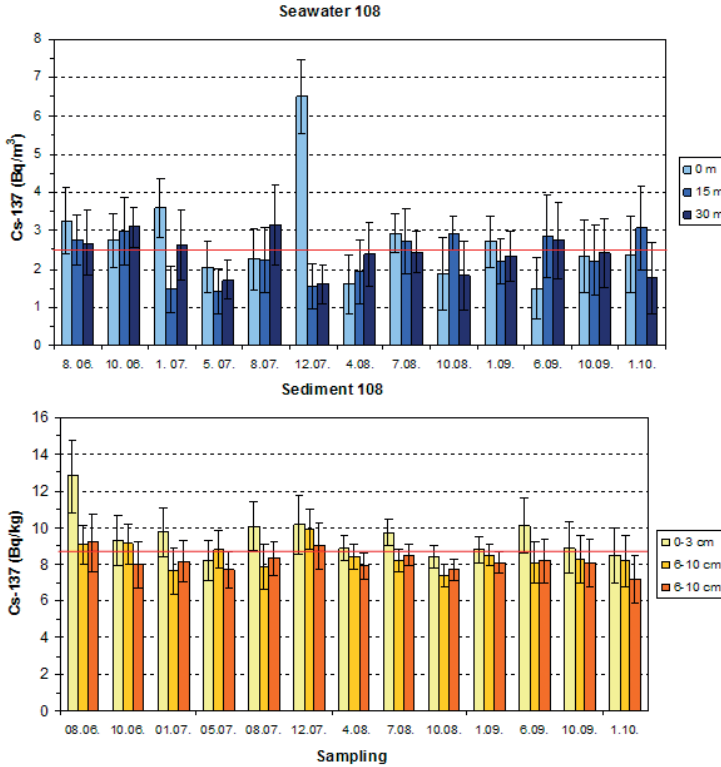


FIG. 3.  $^{137}\text{Cs}$  concentrations in seawater at 3 depths (0, 15 and 30 m) and in sediment layer (0–10 cm) at the station 108 in the northern Adriatic Sea from 2006 to 2010.

in 1985 was around  $4 \text{ Bq/m}^3$ . The Chernobyl accident in 1986 increased  $^{137}\text{Cs}$  concentrations by 2 orders of magnitude; in 1990  $^{137}\text{Cs}$  concentrations had returned to the pre-Chernobyl value [13]. At present, the  $^{137}\text{Cs}$  concentration in the seawater of the northern Adriatic ranges from  $1.5$  to  $3 \text{ Bq/m}^3$ .

The main freshwater source in the Adriatic is the Po river, whose delta is located in the northwestern Adriatic and whose annual mean discharge rate is  $1700 \text{ m}^3/\text{s}$ , carrying 28% of the total runoff into the Adriatic [1]. At the station 108, which was under the direct influence of the Po river discharge,  $^{137}\text{Cs}$  concentrations in the seawater at three depths (0, 15 and 30 m) and in three sediment layers (0–3, 3–6 and 6–10 cm) were investigated seasonally (Fig. 3).  $^{137}\text{Cs}$  concentrations measured in the seawater were mainly in the range between  $1.42$  and  $3.60 \text{ Bq/m}^3$  with the highest value of  $6.51 \text{ Bq/m}^3$  found in surface water in winter 2007. Average  $^{137}\text{Cs}$  concentrations in seawater have decreased back to pre-Chernobyl values ( $2.48 \text{ Bq/m}^3$ ). Vertical profiles of  $^{137}\text{Cs}$  in the water column were characterized by decreasing concentrations from the surface to the bottom [2, 12].  $^{137}\text{Cs}$  concentration decreasing with depth was not found at the station 108, probably due to its low depth and freshwater inflow from the Po

river. Radionuclides deposited from the atmosphere onto surfaces of water bodies are transported into deeper water mainly due to diffusion and convection processes [3]. At the bottom, they contaminate the recent marine sediments. The concentration levels of  $^{137}\text{Cs}$  measured in surface sediments of the Mediterranean Sea are found in the narrow range of 2–10 Bq/kg [2]. At the station 108  $^{137}\text{Cs}$  concentration in recent marine sediment was measured to the depth of 10 cm in 3 sediment layers. We did not find any significant difference between  $^{137}\text{Cs}$  concentration in measured sediment layers, even seasonally. On the other hand, it was found that  $^{137}\text{Cs}$  concentrations were slightly higher (8.70 Bq/kg) in the sediments of the Po river delta area than in the sediments of the Rovinj coastal area (1.86 Bq/kg) indicating radionuclide input by the Po river discharge [6].

Measurements of  $^{137}\text{Cs}$  concentrations in seawater and the mussels *M. galloprovincialis* from the Lim bay were performed from 2006 to 2010 (Fig. 4.). The Lim Bay, located on the western Istrian coast, is 11 km long and less than 600 m wide. The Lim Bay is a protected landscape, with biological importance as a fish spawning site and its inner part is reserved exclusively for mariculture. The water in the bay is brackish, because of its underwater sources of freshwater, and salinity varies seasonally. Therefore, according to data from previous bio-monitoring research, we chose the Lim Bay in this investigation as a reference location [14]. Inside the Lim bay  $^{137}\text{Cs}$  concentrations in seawater were low (1.92 Bq/m<sup>3</sup>) and, as expected in the mussel *M. galloprovincialis*  $^{137}\text{Cs}$  concentrations were undetectable in this period (Fig. 4). In the Rovinj coastal area  $^{137}\text{Cs}$  concentrations in surface seawater remained constant (2.23 Bq/m<sup>3</sup>), as were found within the surface sediment layer (1.89 Bq/kg) (Fig. 4).

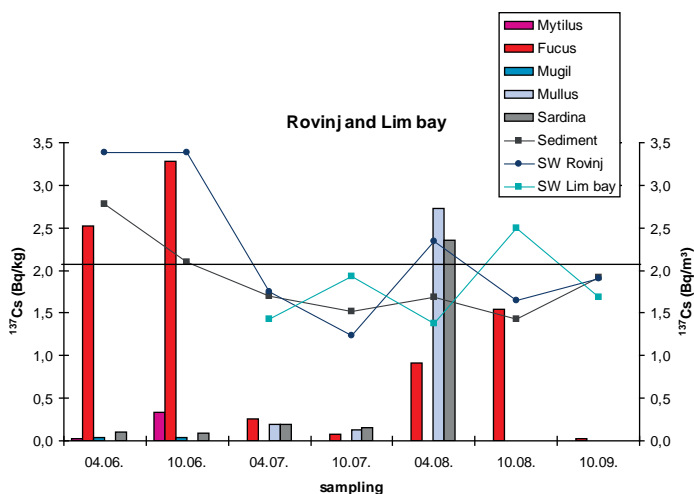


FIG. 4.  $^{137}\text{Cs}$  concentrations in seawater, sediments and biota samples in the Lim bay and the Rovinj coastal area from 2006 to 2010.

$^{137}\text{Cs}$  is known to be incorporated into the muscle tissues of various marine organisms, which may be eaten by humans and the biological uptake of this radionuclide by marine organisms is very important from the radioprotection viewpoint [4, 10]. Results of  $^{137}\text{Cs}$  concentration measurements in selected organisms indicate that some species accumulate radionuclides better than others. In order of concentration of  $^{137}\text{Cs}$ , starting with the lowest, the concentrations were *M. galloprovincialis* (<0.3 Bq/kg w.w.), *M. cephalus* ( $3.5 \times 10^{-2}$  Bq/kg w.w.), *S. pilchardus* (0.58 Bq/kg w.w.), *M. barbatus* (1.02 Bq/kg w.w.), to the highest in *F. virsoides* (1.23 Bq/kg w.w.). The brown alga *Fucus vesiculosus* in north Atlantic is known as a bioindicator for marine radiocontamination [9]. For our investigation we used the endemic Adriatic species *Fucus virsoides*.  $^{137}\text{Cs}$  concentrations were detectable at very low levels in *M. cephalus* and *S. pilchardus* and found only once in *M. galloprovincialis*. Results of investigations indicate that *F. virsoides* and *M. barbatus* can be considered good bio-indicators for monitoring radiocontamination in the Adriatic Sea. Such knowledge of radioactive contamination could be useful in the estimation of the state of the environment and as an input to plans for the protection of the Adriatic Sea.

#### 4. CONCLUSIONS

Artificial radioactivity in the northern Adriatic Sea was assessed by analysis of  $^{137}\text{Cs}$  concentrations in seawater, sediment and marine organisms in different parts of the marine ecosystem, including the area in the Po river delta, the protected area of the Lim bay and the Rovinj coastal area. *Fucus virsoides* and *Mullus barbatus* could be considered as good bio-indicators for monitoring radioactive contamination in the Adriatic Sea.  $^{137}\text{Cs}$  concentration in the seawater of the northern Adriatic ranges from 1.5 to 3 Bq/m<sup>3</sup>. The radiological status of  $^{137}\text{Cs}$  in the northern Adriatic Sea has generally returned to pre-Chernobyl values taking into consideration natural fluctuation due to physicochemical and hydrological parameters in the investigated area.

#### REFERENCES

- [1] CUSHMAN-ROISIN, B., et al., Physical Oceanography of the Adriatic Sea: Past, Present and Future, Kluwer Academic, Dordrecht, Netherlands (2001).
- [2] UNITED NATIONS ENVIRONMENT PROGRAMME, INTERNATIONAL ATOMIC ENERGY AGENCY, Assessment of the State of Pollution of the Mediterranean Sea by Radioactive Substances, MAP Technical Reports Series 62, Athens (1992).
- [3] PAPUCCI, C., DELFANTI, R.,  $^{137}\text{Cs}$  distribution in the eastern Mediterranean Sea: Recent changes and future trends, Sci. Tot. Environ. **237–238** (1999) 67–75.

- [4] FOWLER, S.W., “Biologically mediated removal, transformation and regeneration of dissolved elements and compounds”, *Ocean Margin Processes in Global Change* (MANTOURA, MARTIN, WOLLAST, Eds) (1991) 127–143.
- [5] FLOROU, H., et al., Caesium–137 in the eastern Mediterranean - impact sources and marine pathways, *Fresenius Environmental Bulletin* **12** 1 (2003) 3–9.
- [6] NONNIS MARZANO, F., TRIULZI, C., A radioecological survey of Northern and Middle Adriatic Sea before and after the Chernobyl event (1979–90), *Mar. Pollut. Bull.* **28** 4 (1994) 244–253.
- [7] KRAUS, R., SUPIĆ, N., Impact of circulation on high phytoplankton blooms and fish catch in the northern Adriatic (1990–2004), *Est. Coast. Shelf Sci.* **91** (2010) 198–210.
- [8] SAWIDIS, T., et al., Cesium–137 concentrations in marine macroalgae from different biotopes in the Aegean Sea (Greece), *Ecotox. Environ. Saf.* **54** 3 (2003) 249–254.
- [9] CARLSON, L., HOLM, E., Radioactivity in *Fucus vesiculosus* L. from the Baltic sea following the Chernobyl accident, *J. Environ. Radioactivity* **15** 3 (1992) 231–248
- [10] THE MEDITERRANEAN SCIENCE COMMISSION, Mediterranean Mussel Watch – Designing a Regional Program for Detect-ing Radionuclides and Race-contaminants, CIESM Workshop Series 15, CIESM, Marseilles (2002).
- [11] FOLSOM, T.R., SREEKUMARAN, C., “Some reference methods for determining radioactive and natural caesium for marine studies”, *Reference Methods for Marine Radioactivity Studies*, IAEA Technical Reports Series No. 118, IAEA, Vienna (1970) 129–187.
- [12] INTERNATIONAL ATOMIC ENERGY AGENCY, Worldwide Marine Radioactivity Studies (WOMARS): Radionuclide Levels in Oceans and Seas, IAEA-TECDOC-1429, IAEA, Vienna (2005).
- [13] FRANIĆ, Z., BAUMAN, A., Radioactive contamination of the Adriatic Sea by  $^{90}\text{Sr}$  and  $^{137}\text{Cs}$ , *Health Phys.* **64** 2 (1993) 162–169.
- [14] VUKMIROVIĆ, M., et al., DNA damage in marine mussel *Mytilus galloprovincialis* as a biomarker of environmental contamination, *Mar. Ecol. Prog. Ser.* **109** (1994) 165–171.

# SOURCES OF CO<sub>2</sub> IN THE GULF OF TRIESTE (N. ADRIATIC): STABLE CARBON ISOTOPE EVIDENCE

N. OGRINC<sup>a</sup>, D. TURK<sup>b,c</sup>, S. ZAVADLAV<sup>a</sup>, J. FAGANELI<sup>d</sup>

<sup>a</sup> Department of Environmental Sciences,  
Jožef Stefan Institute,  
Ljubljana, Slovenia

<sup>b</sup> Department of Oceanography,  
Dalhousie University,  
Halifax, Nova Scotia, Canada

<sup>c</sup> Lamont-Doherty Earth Observatory,  
Earth Institute at Columbia University,  
Palisades, New York, USA

<sup>d</sup> Marine Biological Station National Institute of Biology,  
Piran, Slovenia

## Abstract

In the present study the influence of freshwater intrusions on the net carbon dynamics in the Gulf of Trieste (northern Adriatic Sea) were investigated. Carbonate mineral weathering dominates the inorganic carbon geochemical flux of the N Adriatic rivers and thus the origin of dissolved inorganic carbon (DIC) in the gulf seawater. Based on  $\delta^{13}\text{C}_{\text{DIC}}$  values and isotopic mass balance it was estimated that rivers represents about 20% of DIC in spring, while the riverine contribution in autumn is less pronounced probably due to intensive water mixing. The results, therefore, suggest that river inputs play a significant role in the carbon cycling in the Gulf of Trieste due to mixing of higher DIC riverine water with lower seawater DIC. The observed higher summer  $\delta^{13}\text{C}_{\text{DIC}}$  values were due to more pronounced photosynthetic carbon fractionation.

## 1. INTRODUCTION

Despite the coastal ocean being bio-geochemically one of the most active areas in the biosphere due to terrestrial nutrient input the CO<sub>2</sub> system is frequently neglected in global carbon budgets since it covers only about 7% of the total ocean area [1]. The input, production and degradation of organic matter in coastal waters is frequently much higher compared to the open ocean, suggesting that CO<sub>2</sub> fluxes are

very intensive. The coastal waters also comprise, in addition to marginal seas which are CO<sub>2</sub> sinks [2], estuaries which seem to be CO<sub>2</sub> sources [3] due to high organic matter input and consequently high degradation rates, i.e. a heterotrophic system. This origin of CO<sub>2</sub> probably exceeds the CO<sub>2</sub> sink in other coastal areas (shelf). The CO<sub>2</sub> source will probably turn to sink in the future because of increasing atmospheric CO<sub>2</sub> and primary production and parallel decreasing production of biogenic carbonates and their dissolution [3]. Carbonate dissolution and precipitation play an important role in the transformation of terrestrial C [4]. Considering the great reactivity and solubility of carbonates [5], the C flux from carbonate dissolution to surface and groundwaters would increase with increasing water flux and soil zone *p*CO<sub>2</sub> [6]. This, in turn, would increase the flux of riverine inorganic C to the sea. It was found that the calcite saturation indices for waters discharging from major world river systems are nearly all at or below equilibrium with respect to calcite [7]. Investigations of streams draining carbonate bearing watersheds have observed a decrease in alkalinity at low and high discharge conditions [8], but only few studies have characterized the riverine carbonate dynamics on a smaller scale.

The principal aim of this study was to investigate the sources of CO<sub>2</sub> in the Gulf of Trieste, the northernmost part of the semi-enclosed northern Adriatic Sea, using stable C isotopes and ancillary chemical data (alkalinity, Ca). An important challenge is to determine how the terrestrial biogeochemical C cycling in connection with the hydrological system influences the sensitive coastal waters. Because the Gulf of Trieste is a relatively productive area [9] the combination with the above environmental conditions makes this region an interesting study site for the investigation of CO<sub>2</sub> sources affecting C cycling in coastal waters including the CO<sub>2</sub> air–sea interaction.

## 2. STUDY SITE

The Gulf of Trieste is a small (approx. 500 m<sup>2</sup>) and relatively shallow marine basin in the northernmost part of the Adriatic Sea. The gulf exhibits complex hydrodynamics [10] due to freshwater inputs, mainly from the Isonzo/Soča River, the influence of water masses flowing northward along the eastern Adriatic coast, tidal dynamics and atmospheric forcing including Bora wind producing a water outflow from the gulf. The salinity of the surface waters in the gulf ranges between 33 and 38.5 and temperatures from 7°C to 27°C. Vertical temperature and salinity gradients in late summer often result in bottom water hypoxia and occasionally anoxia.

## 3. MATERIAL AND METHODS

The study site, 22 m deep, near the coastal buoy Vida (45°32'55.68"N, 13° 33' 1.89" E; Fig. 1) is located in the southern part of the Gulf of Trieste. Seawater

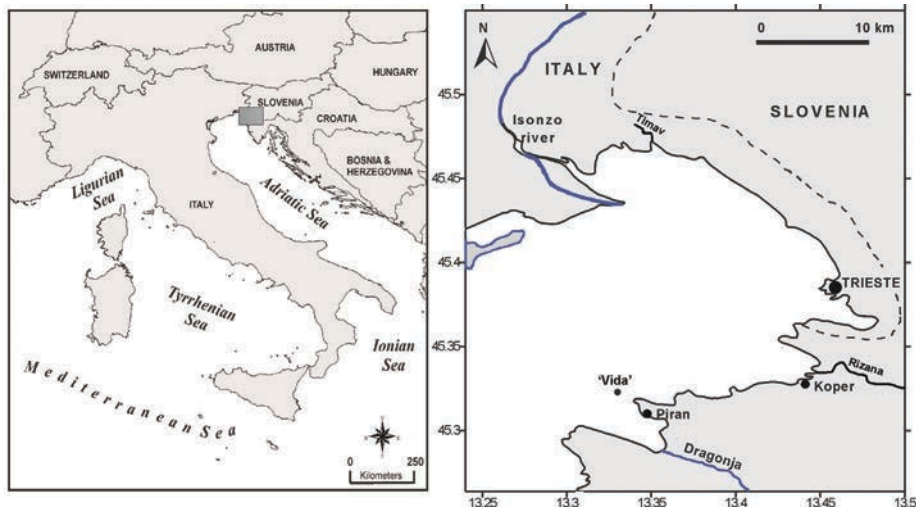


FIG. 1. Location of the study site coastal buoy *Vida* in the Gulf of Trieste (northern Adriatic Sea).

samples were collected from March to November in 2007 approximately weekly at the depth of 3 m, where high frequency measurements of  $p\text{CO}_2$ , were performed [11]. In parallel, continuous measurements of sea salinity (SS), pH, sea temperature (ST) and currents were performed at the depth of 2.7 m [11].

Water samples were filtered through 0.45  $\mu\text{m}$  Millipore HA membrane filters. Total alkalinity (TA) was determined by Gran titration [12]. Ca analysis was performed by ICP-OES. The samples for stable isotope composition of dissolved inorganic carbon ( $\delta^{13}\text{C}_{\text{DIC}}$ ) were prepared by injecting water samples into evacuated septum tubes with phosphoric acid. Released  $\text{CO}_2$  gas was then analysed with continuous flow isotope ratio mass spectrometer (Europa 20–20 with ANCA TG trace gas separation module). Stable isotopic results are reported with  $\delta$ -values as deviations in ‰ from the V-PDB standard. The precisions based on replicate analyses were  $\pm 1\%$  for TA,  $\pm 2\%$  for Ca and  $\pm 0.2\%$  for  $\delta^{13}\text{C}_{\text{DIC}}$ .

The thermodynamic computation was performed with the first and second acidity constant for  $\text{CO}_2$  of Mehrbach et al. [13] using the fitting functions given by Dickson and Millero [14] and the boric acid acidity constant of Lyman [15–17].

#### 4. RESULTS AND DISCUSSION

SS and ST were seasonally dependent ranging from 34.0 to 38.0 and from 11.8 to 26.5°C, respectively. The highest SS and ST were observed in summer. TA,  $\delta^{13}\text{C}_{\text{DIC}}$  values, concentrations of Ca, the saturation state of  $\text{CaCO}_3$  together with the  $p\text{CO}_2$

values during the sampling period from March to November 2007 are presented in Fig. 2. TA ranged from 2.58 to 3.54 mmol/dm<sup>3</sup> and was higher in early spring 2007 when the temperature was the lowest.  $\delta^{13}\text{C}_{\text{DIC}}$  ranged from -2.2 to 1.6‰. These values were generally within the range of -1 to 2.2‰ which is typical for surface sea water all over the world [18]. Lower  $\delta^{13}\text{C}_{\text{DIC}}$  values were observed in parallel with the highest TA concentrations. Concentration of Ca ranged from 7.98 to 13.6 mmol/dm<sup>3</sup>. The calcite and aragonite saturation indexes using the values for calcite and aragonite of Mucci [19] were always >1 indicating that calcite and aragonite precipitation was thermodynamically favoured. The  $p\text{CO}_2$  data show large seasonal variations with higher  $p\text{CO}_2$  values in the summer reaching a maximum of 379  $\mu\text{atm}$  and lower values in the spring and fall reaching a minimum of 220  $\mu\text{atm}$  in November 2007. Unfortunately,  $p\text{CO}_2$  was not measured during the summer in June and July when the highest  $p\text{CO}_2$  could be expected [11].

Lower values of  $p\text{CO}_2$  in spring 2007 were related to the presence of river plumes and coincided with the salinity drop, lower Ca concentrations, higher alkalinity and lower  $\delta^{13}\text{C}_{\text{DIC}}$  values. It was found that at the same period daily discharge for the N Adriatic Rivers (Timavo-Reka, Isonzo/Soča, Dragonja and Rižana) increased. The current simulation data suggested that Timavo River draining karst terrain was primarily responsible for the observed decrease in salinity with possible smaller contribution from Dragonja and Rižana Rivers [11]. During this time, the increase in biomass was also observed. This increase might be connected to an increase in river discharges. TA determined at the mouth of these rivers were higher compared with seawater, with 5.53, 4.48 and 4.96 mmol/dm<sup>3</sup> found in the Timavo, Rižana and Dragonja, respectively. Concentrations of Ca were about ten times lower in rivers than in seawater and ranged from 1.14 to 1.99 mmol/dm<sup>3</sup>.  $\delta^{13}\text{C}_{\text{DIC}}$  values were -12.2‰ in Timavo, -11.0‰ in Rižana and -11.7‰ in Dragonja, respectively.

Based on the observed  $\delta^{13}\text{C}_{\text{DIC}}$  values and isotopic mass balance it was possible to estimate contributions from two different water sources, riverine and marine, using the following relations:

$$\delta^{13}\text{C}_{\text{DIC}} = F_m \delta^{13}\text{C}_{\text{DIC,m}} + F_r \delta^{13}\text{C}_{\text{DIC,r}}$$

$$1 = F_m + F_r$$

where  $F_m$  and  $F_r$  are the respective marine and riverine fractions. For this calculation two different endmembers were required.  $\delta^{13}\text{C}_{\text{DIC,r}}$  values found at the rivers mouth were taken as riverine endmembers, while as marine endmember ( $\delta^{13}\text{C}_{\text{DIC,m}}$ ) the average  $\delta^{13}\text{C}_{\text{DIC}}$  value of 0.6‰ for world surface seawater was used for the calculation [18]. According to our estimates, rivers contributed around 20% to dissolved inorganic carbon (DIC) at the sampling site in spring. This contribution was still present until the end of May accounting for around 8%.

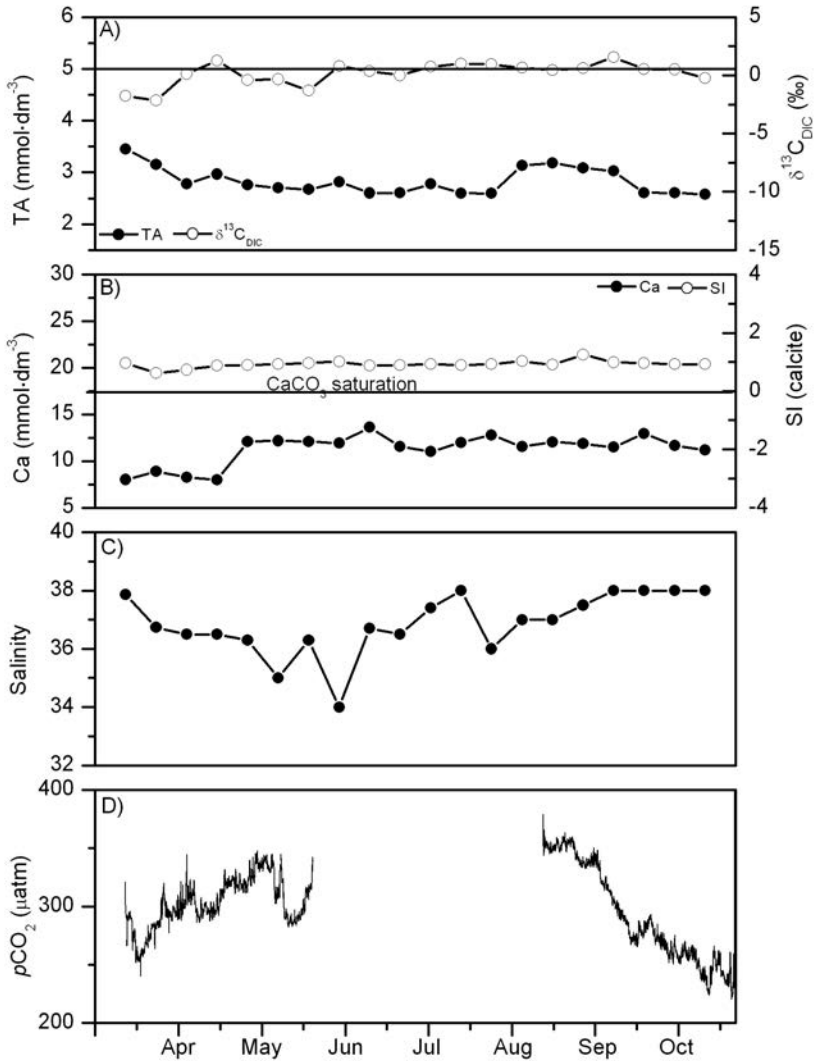


FIG. 2. A) Total alkalinity (TA) and  $\delta^{13}\text{C}_{\text{DIC}}$  together with the line indicating the average value of  $\delta^{13}\text{C}_{\text{DIC}} = 0.6$  for surface sea waters in the world; B) concentrations of Ca and calculated saturation index (SI) for  $\text{CaCO}_3$ . The straight vertical line represents an equilibrium value for  $\text{CaCO}_3$ ; C) sea water salinity (SS); D)  $\text{pCO}_2$  [11], during sampling period March–November 2007.

The freshwater influence was again observed in June when the salinity dropped to 34. During this time, a higher discharge in N Adriatic Rivers was also observed with the higher contribution coming from the Isonzo/Soča River. This river had  $\delta^{13}\text{C}_{\text{DIC}}$  value of  $-7.9\text{‰}$  and was considerably higher compared to other N Adriatic rivers. Based on the data it was estimated that about 23% of DIC was of freshwater origin. The contribution of rivers was again observed at the end of the sampling period in October 2007. At this time another drop in  $p\text{CO}_2$  and elevated Chl *a* data were obtained at the sampling site together with the increase of river discharges. These discharges were an order of magnitude higher than those observed during the spring, but were followed by only a small decrease in salinity and  $p\text{CO}_2$ . It seems that the mixing of the water masses was influenced by the strong Bora wind.

During the summer, higher  $\delta^{13}\text{C}_{\text{DIC}}$  values observed could be related to more intense photosynthetic fractionation of the light carbon isotope.  $^{13}\text{C}$  enrichment in DIC was observed also during the summer 2004 in parallel with an increase in the isotopic composition of particulate organic carbon [20].

## 5. CONCLUSIONS

- (1) We studied the sources of dissolved  $\text{CO}_2$  in the Gulf of Trieste, where the seasonal seawater  $p\text{CO}_2$  dynamic is characterized by a summer maximum and spring and fall minimum, using stable C isotope signatures of DIC. Hence, the Gulf of Trieste is thought to be a net sink of  $\text{CO}_2$  in fall and spring, and occasionally a  $\text{CO}_2$  source in summer.
- (2) Based on  $\delta^{13}\text{C}_{\text{DIC}}$  values and isotopic mass balance it was estimated that rivers represent about 20% of DIC in spring, while the riverine contribution in autumn is less pronounced, probably due to intensive water mixing. Our results suggest that river inputs play a significant role in carbon cycling in the Gulf of Trieste due to mixing of higher DIC river water with lower seawater DIC and biological production associated with high nutrient input.
- (3) The higher summer  $\delta^{13}\text{C}_{\text{DIC}}$  values indicate that photosynthetic carbon fractionation was more pronounced during the summer.
- (4) Further studies are needed to refine the determination of the sources of seawater DIC in the Gulf of Trieste as well as their effect on the ecology of the gulf waters.

## ACKNOWLEDGEMENTS

This research was financially supported by the Slovenian Research Agency under the Research Programmes P1-0143, by EC (Marie Curie FP7-PEOPLE\_IRG

239465), NOAA (NA03OAR4320179) and NSF (OCE-0648275, OCE-0526677). Special thanks are given to W.R. McGillis for  $p\text{CO}_2$  measurements.

## REFERENCES

- [1] WOLLAST, R., "Evaluation and comparison of the global carbon cycle in the coastal zone and in the open ocean", *The Sea: The Global Coastal Ocean: Processes and Methods* (BRINK, K.H., ROBINSON, A.R., Eds.) Vol. 10. Wiley & Sons, N.Y. (1998) 213–252.
- [2] CHEN, C.-T., BORGES, A.V., Reconciling opposite views on carbon cycling in the coastal ocean: Continental shelves as sinks and near-shore ecosystems as sources of atmospheric  $\text{CO}_2$ , *Deep-Sea Res.* II **56** (2009) 578–590.
- [3] BORGES, A.V., et al., Carbon dioxide in European coastal water, *Estuar. Coast. Shelf Sci.* **70** (2006) 375–387.
- [4] BERNER, K.A., BERNER, R.A., *The global water cycle*, Prentice Hall, New Jersey (1996) 397.
- [5] AMIOTTE SUCHET, P., PROBST, J.L., LUDWIG, W., Worldwide distribution of continental rock lithology: Implications for the atmospheric/soil  $\text{CO}_2$  uptake by continental weathering and alkalinity river transport to the oceans, *Glob. Biogeochem. Cycles* **17** (2003) 1038.
- [6] VAN BREENAN, N., PROTZ, R., Rate of calcium carbonate removal from soils, *Can. J. Soil Sci.* **68** (1988) 449–454.
- [7] KEMPE, S., "Long-term records of  $\text{CO}_2$  Pressure fluctuations in fresh waters", *Transport of Carbon and Minerals in Major World Rivers* (DEGENS E.T., et al., Eds), University of Hamburg, (1982) 91–323.
- [8] GROSBOIS, C., et al., Dissolved load of the Loire River: chemical and isotopic characterization, *Chem. Geol.* **170** (2000) 179–201.
- [9] FONDA UMANI, S., et al., Major interannual variations in microbial dynamics in the Gulf of Trieste (northern Adriatic Sea) and their ecosystem implications, *Aquat. Microb. Ecol.* **46** (2007) 163–175.
- [10] MALAČIĆ, V., PETELIN, B., "Gulf of Trieste", *Physical Oceanography of the Adriatic Sea: Past, Present and Future* (CUSHMAN-ROISIN, B., et al., Eds.), Kluwer Academic, Dordrecht, Netherlands (2001) 167–177.
- [11] TURK, D., et al., Carbon dioxide variability and air-sea fluxes in the northern Adriatic Sea, *J. Geophys. Res.* **115** (2010) C10043.
- [12] MILLERO, F.J., et al., Titration alkalinity of seawater, *Mar. Chem.* **44** (1993) 153–165.
- [13] MEHRBACH, C., et al., Measurements of the apparent dissociation constants of carbonic acids in seawater at atmospheric pressure, *Limnol. Oceanogr.* **18** (1973) 897–907.
- [14] DICKSON, A.G., MILLERO, F.J., A comparison of the equilibrium constants for the dissociation of carbonic acids in seawater media, *Deep-Sea Res. A* **34** (1987) 1733–1743.
- [15] LYMAN, J., *Buffer mechanism of seawater*. Ph.D. dissertation, UCLA (1956).

- [16] MILLERO F.J., Thermodynamics of the carbon dioxide system in the oceans, *Geochim. Cosmochim. Acta* **59** (1995) 661–677.
- [17] MILLERO, F.J., et al., Dissociation constants of carbonic acid in seawater as a function of salinity and temperature, *Mar. Chem.* **100** (2006) 80.
- [18] KROPNICK, P.M., The distribution of  $^{13}\text{C}$  of  $\Sigma\text{CO}_2$  in the world oceans, *Deep-Sea Res. A* **32** (1985) 57.
- [19] MUCCI, A., The solubility of calcite and aragonite in seawater at various salinity, temperatures, and one atmospheric total pressure, *Amer. J. Sci.* **283** (1983) 780–799.
- [20] FAGANELI, J., et al., Carbon and nitrogen isotope composition of particulate organic matter in relation to mucilage formation in the northern Adriatic Sea, *Mar. Chem.* **114** (2009) 102–109.

# RADIOTRACERS IN THE BLACK SEA: A TOOL FOR MARINE ENVIRONMENTAL ASSESSMENTS

S.B. GULIN<sup>a</sup>, V.N. EGOROV<sup>a</sup>, G.G. POLIKARPOV<sup>a</sup>, I. OSVATH<sup>b</sup>,  
N.A. STOKOZOV<sup>a</sup>, N.Y. MIRZOEVA<sup>a</sup>, N.N. TERESHENKO<sup>a</sup>,  
L.V. GULINA<sup>a</sup>, V.Y. PROSKURNIN<sup>a</sup>

<sup>a</sup> The A.O. Kovalevskiy Institute of Biology of the Southern Seas (IBSS),  
Sevastopol, Ukraine

<sup>b</sup> International Atomic Energy Agency, Marine Environment Laboratories,  
Monaco

## Abstract

Post-Chernobyl trends of radioactive contamination of the Black Sea showed a relatively high rate of purification of its waters against soluble and particle reactive radionuclides. The apparent half-lives for the decrease of <sup>137</sup>Cs and <sup>90</sup>Sr concentrations in the central Black Sea waters was around 6 and 8 years, respectively, suggesting an additional <sup>90</sup>Sr input by river runoff. These values, particularly for <sup>137</sup>Cs, are considerably lower than in the adjacent Mediterranean basin (~13 years), which is caused by faster dilution of <sup>137</sup>Cs concentration in the upper Black Sea waters due to strong river discharge, and by loss of <sup>137</sup>Cs via the Bosphorus Strait. These factors, together with a higher rate of particle scavenging of plutonium in the mesotrophic Black Sea water, reflect its significant capability for self-cleaning against nuclear and non-nuclear pollutants, which was traced in this study using data on fluxes and time evolution of natural and anthropogenic radioactivity.

## 1. INTRODUCTION

The Black Sea and its drainage basin are located between the European and Asian continents, covering almost 2.5 million km<sup>2</sup> of territory in six Black Sea countries (Bulgaria, Georgia, Romania, Russia, Turkey, and Ukraine). Owing to its geographical location and limited water exchange with the rest of the world's oceans, the Black Sea has been one of the marine basins most contaminated with artificial radioactivity [1–3]. During the pre-Chernobyl period, the main source of radioactive contamination of the Black Sea was global fallout from the atmospheric nuclear weapon tests, which peaked in 1962 before the 1963 Test Ban Treaty was signed between the main nuclear states [1]. As maximum global fallout was observed within the 40–50° N latitude band that runs exactly across the Black Sea, this semienclosed water body received high levels of the fallout radionuclides

derived from the atmospheric weapons testing. The radioactive debris from the Chernobyl NPP accident caused widespread contamination over much of Europe and the surrounding seas [1]. As the closest marine body to the Chernobyl site, the Black Sea and its broad drainage areas have received substantial amounts of the long lived artificial radionuclides, particularly  $^{90}\text{Sr}$ ,  $^{137}\text{Cs}$ , and plutonium isotopes, released into the atmosphere from the damaged nuclear reactor and delivered with the air masses moving south and westward from the accident area [2, 3]. As a result, concentrations of anthropogenic radionuclides in Black Sea surface water increased sharply, exceeding levels measured during the pre-Chernobyl period. Besides direct atmospheric deposition, the Black Sea received (and continues to receive) additional radioactive input by river runoff, particularly to its northwestern area from the Danube and Dnieper Rivers, and from groundwater discharges [2, 3]. Resulting from the contribution of the above mentioned sources of radioactive contamination of the Black Sea, the  $^{90}\text{Sr}$  concentration in its water ranks second after the Irish Sea, and third after the Baltic Sea with respect to  $^{137}\text{Cs}$  concentration in sea water [4].

Extensive radioecological studies performed during the last decades have showed that post-Chernobyl evolution and levels of anthropogenic radioactivity in the Black Sea were governed, except for radioactive decay, by large scale oceanographic, biogeochemical and ecological processes that control the self-cleaning of the Black Sea environments against radioactive contamination: first of all vertical water mixing, which dilutes surface radionuclide concentrations, the loss through the Bosphorus Strait connecting the Black Sea with the Mediterranean and sedimentary scavenging of sorption reactive radionuclides on sinking particles such as phytoplankton fossils and suspended material derived from the land by erosion [3]. Because of the effects of these factors, as well as radioactive decay, the initial inventory of Chernobyl derived radionuclides has decreased abruptly, and will presently reach the pre-accident level, except estuarine zones particularly of the Danube and Dnieper Rivers account for 75% of the total river runoff to the Black Sea and 95% of the runoff entering the NW Black Sea. In turn, study of the post-Chernobyl dynamics of radionuclide concentration in different compartments of the Black Sea ecosystem gave a unique opportunity to evaluate a number of hydrological, geochemical, and ecological processes and to trace their long term changes, achieving eventually an integrated assessment of potential capability of the Black Sea for self-purification against both nuclear and non-nuclear pollutants [1, 3].

This paper summarizes research of the long term changes in concentration and the fate of long lived radionuclides, particularly  $^{137}\text{Cs}$ ,  $^{90}\text{Sr}$  and plutonium, which have been carried out by the IBSS Department of Radiation and Chemical Biology (Sevastopol, Ukraine) in collaboration with the IAEA Marine Environment Laboratories (NAEL, Monaco) during the entire post-Chernobyl period. The applied data were collected in 38 marine cruises implemented under national and international projects, which were supported by the National Academy of Sciences of Ukraine, the IAEA, the EU and the International Union of Radioecology, including

two target expeditions provided by the IAEA in 1998 and 2000 that covered the whole the Black Sea [1, 3]. During these studies, the IBSS has performed standardization and intercomparison of radionuclide measurements organized by IAEA-NAEL. The intercomparison exercises have involved radiometric laboratories of the Black Sea countries, the Ukrainian Research Hydrometeorological Institute, the Joint Institute of Nuclear Research (Dubna, Russia), Woods Hole Oceanographic Institute (USA) and RISØ National Laboratory (Denmark). Overall, more than 4300 results of radiometric measurements obtained within the scope of this study have been integrated in the IAEA database on marine radioactivity GLOMARD [1, 3].

## 2. LEVELS, TRENDS AND TRACER APPLICATIONS OF CHERNOBYL RADIONUCLIDES IN THE BLACK SEA

Temporal evolution of  $^{137}\text{Cs}$  and  $^{90}\text{Sr}$  inventory in the upper Black Sea water was traced in 1986–2004 using time series data on the concentration and vertical distribution of these Chernobyl radionuclides in the central Black Sea basin. It estimated the atmospheric fallout of  $^{137}\text{Cs}$  deposited on the Black Sea surface during the first days after the Chernobyl accident to have been 1700–2400 TBq (Fig. 1), which corresponded to nearly 2% of total  $^{137}\text{Cs}$  release into the environment and exceeded the pre-Chernobyl inventory in the Black Sea water column by a factor of 6–10 [5–7]. This initial post-Chernobyl  $^{137}\text{Cs}$  inventory decreased abruptly to 1600 TBq in 1987 due to fast dilution within the upper mixed water masses because of the high solubility of  $^{90}\text{Sr}$  and  $^{137}\text{Cs}$  in saltwater, and then more gradually to around 500–600 TBq in 1998–2000 and  $350 \pm 60$  TBq in 2001–2004 (Fig. 1). Unlike  $^{137}\text{Cs}$ , the decrease in the  $^{90}\text{Sr}$  inventory was not so monotonic, showing a considerable increase in 2001 [6]. This may be explained by a larger  $^{90}\text{Sr}$  inflow with the river waters due to a stronger runoff occurring in the Dnieper in 1998–1999 and in the Danube River in 1999, as strontium is a highly soluble element in both salt and fresh waters, while caesium is particle reactive and therefore less mobile in riverine environments [8–10].

The decrease of  $^{137}\text{Cs}$  and  $^{90}\text{Sr}$  concentration in surface Black sea water was mainly caused, except for the radioactive decay, by its mixing with the deeper, less contaminated water masses, which has been traced with the use of regionally averaged vertical profiles of  $^{137}\text{Cs}$  and  $^{90}\text{Sr}$  distribution, indicating a three layer structure formed by high concentrations in the upper mixed layer, decreasing concentrations in the gradient layer, and low concentrations in the deep layer underneath [6]. This structure has evolved through the gradual penetration of radionuclides to greater depths and the decrease in surface concentrations [6]. Besides the vertical water mixing, the decrease of the  $^{137}\text{Cs}$  inventory in the surface layer has been controlled by loss through the Bosphorus Strait accounting for 2–2.5% of the  $^{137}\text{Cs}$  inventory [6].

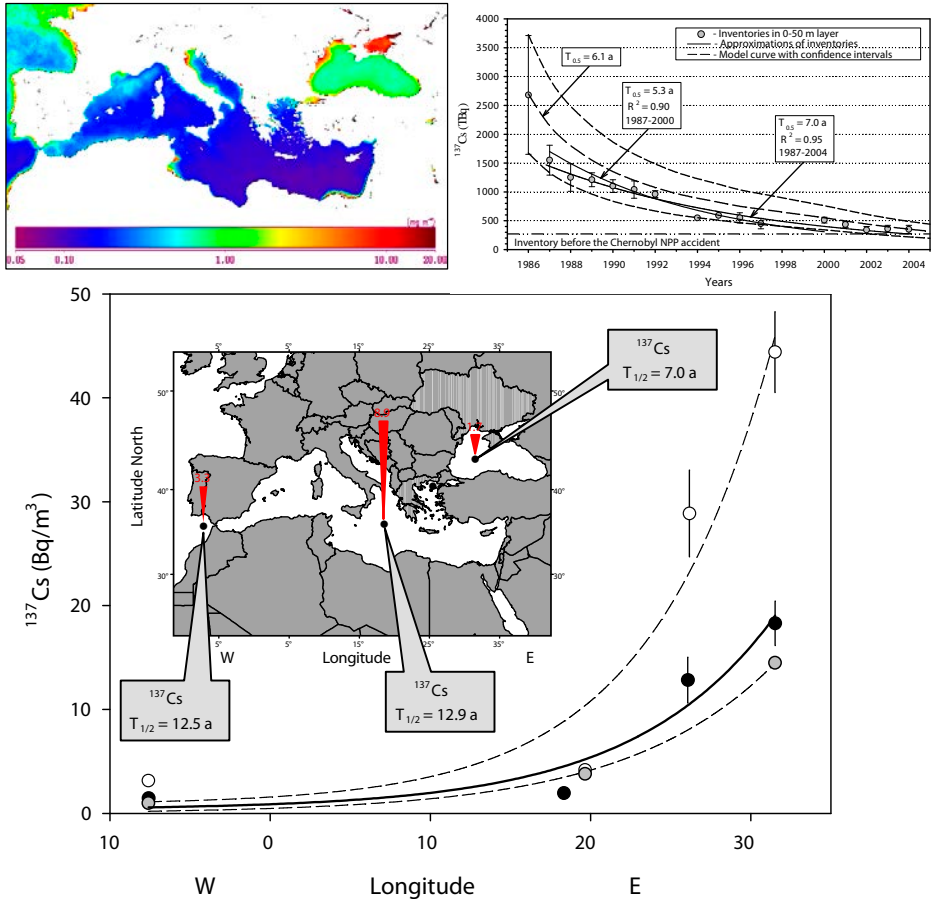


FIG. 1. Longitudinal distribution of  $^{137}\text{Cs}$  and  $^{239+240}\text{Pu}$  (red triangular bars in the map) concentration in the surface water of the western Black Sea, the Aegean Sea (near the Dardanelles), the Ionian Sea and in the Atlantic area adjacent to the Gibraltar Strait, measured in 2002–2003, (●) in comparison with the post- (○) and pre-Chernobyl (●) data obtained in 1988–89 and the early 1980's, respectively [2, 3, 11]. Error bars are shown if greater than symbol size. The position of the sampling sites (black spots on the map) correspond to those shown in Table 1. Numbers above the red bars are related to values of  $^{239+240}\text{Pu}$  concentration,  $\text{mBq}\cdot\text{m}^{-3}$ . The left upper panel shows a satellite map of annual mean surface chlorophyll concentration for 2002 provided by Dr E. Bosc, IAEA-NAEL (the colour coding shows pigment concentration in  $\text{mg}\cdot\text{m}^{-3}$ ). The right upper panel represents temporal evolution of  $^{137}\text{Cs}$  inventory in the 0–50 m layer of the Black Sea after the Chernobyl NPP accident and results of modelling after Refs [5, 6].

Another key factor which influenced the rapid decrease in  $^{137}\text{Cs}$  concentration and inventory in the Black Sea surface water was the dilution with riverine waters coming particularly from the Danube and Dnieper, as the post-Chernobyl  $^{137}\text{Cs}$  input from these rivers was estimated to be in a range of 23–26 TBq for the period 1986–2000, that is negligible (<1.5%) in comparison with the direct atmospheric deposition of this radionuclide on the sea surface [11], while the outflow of  $^{137}\text{Cs}$  through the Bosphorus Strait was 275 TBq over the same period [5, 6]. In comparison, the total amount of  $^{90}\text{Sr}$  delivered to the Black Sea by the Danube and Dnieper in the period 1986–1995 was about 113–115 TBq, reaching  $160 \pm 28$  TBq by 2000, which is comparable with the  $^{90}\text{Sr}$  amount deposited on the Black Sea surface after the Chernobyl accident [11]. As for the  $^{137}\text{Cs}$  and  $^{90}\text{Sr}$  outflow through the Bosphorus Strait, it has been estimated on the basis of time series radionuclide measurements in the Black Sea and Aegean Sea surface waters with the use of data on annual volumes of the Upper Bosphorus Current [6]. As a result, the apparent half-lives of about 6.4 years for  $^{137}\text{Cs}$  and 9.5 years for  $^{90}\text{Sr}$  were calculated from regression exponential functions. Using the model approach developed in Ref. [6], the total outflow of  $^{137}\text{Cs}$  and  $^{90}\text{Sr}$  from the Black Sea to the Sea of Marmara in the period 1986–2000 was assessed as 275 TBq and 126 TBq, respectively. Overall, these data have allowed the conclusion (by exponential extrapolation) that radioactive pollution of the Mediterranean basin with  $^{137}\text{Cs}$  and  $^{90}\text{Sr}$  outflow from the Black Sea will continue over the next 30–40 years and may reach 311 and 168 TBq, respectively [6].

The exponential function approximating the time series measurements of the  $^{137}\text{Cs}$  concentration in the upper Black Sea water resulted in the apparent half-lives for the decrease of the  $^{137}\text{Cs}$  inventory in the 0–50 m layer over 5.3 years in 1987–2000 and 7.0 years in 1987–2004 (Fig. 1). These values were quite comparable with those obtained earlier using a mathematical model [5], which predicted that the  $^{137}\text{Cs}$  inventory in the 0–50 m layer of the Black Sea water column should decrease with a half-life of 6.1 years (Fig. 1). As for the decrease of  $^{90}\text{Sr}$  surface water concentration, its half-life in the 0–50 m layer is longer than that of  $^{137}\text{Cs}$ , varying from 8.3 years in 1986–2000 to 12.6 years in 1986–2005 suggesting the above mentioned additional  $^{90}\text{Sr}$  input by river runoff [6].

Because the processes governing the decline of  $^{137}\text{Cs}$  and  $^{90}\text{Sr}$  concentration in the Black Sea water (i.e. radioactive decay, vertical mixing, dilution with river water and loss via the Bosphorus Strait) are independent of individual chemical and radioactive features of these radionuclides, the obtained half-life values may characterize the self-purification rate of the Black Sea upper waters against soluble contaminants, both nuclear and non-nuclear having similar geochemical behaviour. In order to compare this rate with the capability for self-purification of the nearest marine bodies, the longitudinal distribution of  $^{137}\text{Cs}$  in surface waters of the western Black Sea, the Ionian Sea and the Atlantic Ocean adjacent to the Gibraltar Strait was studied during the 7th Ukrainian Antarctic Expedition in January–May 2002 [12] and near the Dardanelles (Aegean Sea) in 2003. The location of the sampling

sites is mapped in Fig. 1. In this study, the large volume samples of surface water were taken with an in-line filtration/sorption device provided by the IAEA under the RER/2/003 TC Project, which includes a membrane prefilter (Millipore, diameter = 293 mm, nominal pore size = 0.45  $\mu\text{m}$ ) and a pair of filter cartridges (CUNO DPPPZ) impregnated with cupric ferrocyanide, which were connected in series to collect the dissolved  $^{137}\text{Cs}$ . The activity of  $^{137}\text{Cs}$  on pre-filters and cupric ferrocyanide adsorbers was measured by gamma spectrometry using a HPGe detector. The efficiency of sorption of the dissolved  $^{137}\text{Cs}$  was calculated by the comparison of activities on the first and second serial ferrocyanide absorbers. Counting errors were expressed as  $\pm 2\sigma$  (Table 1).

The measurements have shown that  $^{137}\text{Cs}$  concentrations in the surface Atlantic and Mediterranean waters were much lower than those found in the Black Sea (Fig. 1, Table 1), which was more strongly affected by fallout after the Chernobyl accident [7, 11, 13, 14]. Comparison of these data with the results of previous measurements carried out 2–3 years after the Chernobyl accident (in 1988–1989) shows an almost equal reduction of  $^{137}\text{Cs}$  surface concentration in the Mediterranean and Atlantic locations over  $\sim 15$  years by a factor of  $2.24 \pm 0.13$  (Fig. 1). This suggests an apparent half-life of  $^{137}\text{Cs}$  in the surface Mediterranean waters of  $12.9 \pm 1.0$  years and  $12.5 \pm 2.1$  years in the Atlantic area adjacent to the Gibraltar Strait. As this value is much shorter than  $^{137}\text{Cs}$ ' radioactive half-life (30.17 years), it can be concluded that the decrease of  $^{137}\text{Cs}$  surface concentration in these areas is mainly controlled by vertical mixing of the upper water masses with water from deeper layers, which leads to dilution of  $^{137}\text{Cs}$  in the surface water [15]. The lesser half-life value, which was found in the Black Sea, is most likely caused by a faster dilution of the  $^{137}\text{Cs}$  surface water concentration with riverine waters coming mainly from the Danube and Dnieper Rivers, as well as by a loss of  $^{137}\text{Cs}$  via the Bosphorus Strait. This suggestion is supported by the twice lower salinity of the upper Black Sea water ( $\sim 18\%$ ) in comparison with the Mediterranean ( $>37\%$ ) and Atlantic Ocean ( $\sim 36\%$ ) surface waters. Overall,

TABLE 1. LOCATION OF SAMPLING SITES AND CONCENTRATIONS OF  $^{137}\text{Cs}$  AND  $^{239+240}\text{Pu}$  IN SURFACE WATER MEASURED IN THE WESTERN BLACK SEA, AEGEAN SEA (NEAR THE DARDANELLES), THE IONIAN SEA AND IN THE NE ATLANTIC AREA ADJACENT TO THE GIBRALTAR STRAIT IN 2002–2003

Location	Date	Latitude	Longitude	$^{137}\text{Cs}$ ,		$^{239+240}\text{Pu}$ ,	
				(Bq/m <sup>3</sup> )	$\pm 2\sigma$	(mBq/m <sup>3</sup> )	$\pm 2\sigma$
Black Sea	06.05.2002	43°06.95' N	31°31.47' E	18.29	2.14	1.7	0.3
Dardanelles	19.07.2003	40°09.00' N	26°04.01' E	12.83	2.21	-	-
Ionian Sea	02.05.2002	36°20.99' N	18°20.18' E	1.96	0.26	8.8	0.9
Gibraltar Strait	02.01.2002	34°45.56' N	07°35.57' W	1.46	0.28	3.3	0.4

resulting from the diluting and other self-cleaning processes, as well as radioactive decay, the current levels of anthropogenic radionuclides are relatively low and have reached pre-Chernobyl values in most components of the studied marine environments (Fig. 1). At the same time, the relatively high rate of self-purification of the Black Sea waters was revealed not only for soluble radionuclides, such as  $^{137}\text{Cs}$ , but also for particle reactive plutonium isotopes, whose concentration in surface waters was measured during the above mentioned 7th Ukrainian Antarctic Expedition in 2002 [12] in the western Black Sea, the mid-Mediterranean (Ionian Sea) and the Atlantic area adjacent to the Gibraltar Strait (Table 1). The results of these measurements have shown the lowest concentration of  $^{239+240}\text{Pu}$  in the Black Sea ( $1.7 \pm 0.3 \text{ mBq/m}^3$ ), while the highest concentration of this radionuclide,  $8.8 \pm 0.9 \text{ mBq/m}^3$ , was found in the Ionian Sea water (Fig. 1, Table 1) despite its being located much further away from the accident site. These values are quite comparable with those obtained in the early 2000s by other scientists, who found the concentration in the NE Atlantic surface waters to be in the range of  $1.5\text{--}4.1 \text{ mBq/m}^3$ ,  $8\text{--}14 \text{ mBq/m}^3$  in the Mediterranean and  $3\text{--}7.6 \text{ mBq/m}^3$  in the Black Sea [13, 14]. Taking into account that in June 1986 the  $^{239+240}\text{Pu}$  concentration in the surface Black Sea water was in the range of  $6.7\text{--}16.9 \text{ Bq/m}^3$  [2, 7], the apparent half-life of  $^{239+240}\text{Pu}$  in this water is approximately 5–8 years, which is almost half that found in the Mediterranean Sea [13, 14]. Such a rapid decrease in  $^{239+240}\text{Pu}$  concentration in the surface Black Sea water is most likely caused by a higher rate of plutonium scavenging on sinking particles in the mesotrophic Black Sea basin, in contrast to much lower particle concentration, fluxes and scavenging rate in oligotrophic Mediterranean waters (see the respective satellite Chlorophyll a map in Fig. 1). Earlier, the significant role of sedimentation processes in the self-purification of the Black Sea water column against anthropogenic radionuclides and some toxic pollutants (e.g. PCBs, pesticides and mercury), including their deposition in the bottom sediments, has been evaluated, using naturally occurring ( $^{234}\text{Th}/^{238}\text{U}$ ,  $^{210}\text{Pb}/^{226}\text{Ra}$ ) and artificial ( $^{134}\text{Cs}/^{137}\text{Cs}$ ,  $^{238}\text{Pu}/^{239+240}\text{Pu}$ ,  $^{241}\text{Am}$ ) radiotracers [3, 10, 11, 16, 17]. This allowed, for instance, the determination the deposition rate of the main Chernobyl derived radionuclides in the abyssal Black Sea sediments, which was  $3.9\text{--}8.4 \text{ Bq/m}^2\text{a}$  for  $^{137}\text{Cs}$ ,  $0.02 \text{ Bq/m}^2\text{a}$  for  $^{90}\text{Sr}$ ,  $2 \text{ mBq/m}^2\text{a}$   $^{238}\text{Pu}$  and  $11 \text{ mBq/m}^2\text{a}$  for  $^{239+240}\text{Pu}$  [3].

### 3. CONCLUSIONS

The main environmental factors controlling the changes of the highly soluble  $^{90}\text{Sr}$  and  $^{137}\text{Cs}$  concentration in the surface Black Sea water are dilution with the less contaminated deep-sea and riverine waters, as well as outflow through the Bosphorus Strait, while for sorption reactive plutonium isotopes the removal on sinking particles was a key process governing the decrease of their concentration in the Black Sea surface water. These factors led to a gradual decrease of radionuclide concentration

in the Black surface seawater with average effective half-lives for  $^{137}\text{Cs}$  of 7 years, 8–12 years for  $^{90}\text{Sr}$  and 5–8 years for  $^{239+240}\text{Pu}$ . These values are considerably shorter in comparison with those found in the Mediterranean Sea and the NE Atlantic Ocean, where the half-life of  $^{137}\text{Cs}$  in the surface water was  $12.9 \pm 1.0$  and  $12.5 \pm 2.1$  years, respectively. The lesser half-life value, which was found in the Black Sea, is most likely caused by a faster dilution of the  $^{137}\text{Cs}$  surface water concentration with riverine waters coming mainly from the Danube and Dnieper Rivers, as well as by a loss of  $^{137}\text{Cs}$  via the Bosphorus Strait. Resulting from these self-cleaning processes, the current levels of anthropogenic radionuclides are relatively low and have reached the pre-Chernobyl values in most compartments of the studied marine environments.

### ACKNOWLEDGEMENTS

This work was made possible through the logistical support of the National Academy of Sciences of Ukraine and the International Atomic Energy Agency. We are grateful to Dr Emmanuel Bosc, IAEA Environmental Laboratories, who kindly provided us with satellite data on chlorophyll concentration.

### REFERENCES

- [1] INTERNATIONAL ATOMIC ENERGY AGENCY, Inventory of Radioactive Waste Disposals at Sea, IAEA–TECDOC–1105, IAEA, Vienna (1999).
- [2] BUESSELER, K.O., LIVINGSTON, H.D., “Natural and man-made radionuclides in the Black Sea”, Radionuclides in the Oceans: Inputs and Inventories (GUÉGUÉNIAT, P., GERMAIN, P., MÉTIVIER, H., Eds), IPSN, Editions de Physique, Les Ulis, France (1996) 199–217.
- [3] POLIKARPOV, G.G., EGOROV, V.N., (Eds), “Radioecological Response of the Black Sea to the Chernobyl Accident”, ECOSEA-Hydrophysics, Sevastopol (2008).
- [4] NIELSEN, S.P., et al., “Baltic Sea”, Radionuclides in the Environment (Atwood, D.A., Ed.), Chichester (UK), Wiley & Sons (2010) 415–436.
- [5] EGOROV, V.N., et al., Model of large-scale contamination of the Black Sea with the long-lived radionuclides  $^{137}\text{Cs}$  and  $^{90}\text{Sr}$  resulting from the Chernobyl NPP accident, Water Resour. 20 (1993) 326–330 (in Russian).
- [6] EGOROV, V.N., POLIKARPOV, G.G., STOKOZOV, N.A., MIRZOEVA, N.YU., “Balance and dynamics of  $^{137}\text{Cs}$  and  $^{90}\text{Sr}$  concentrations fields in the Black Sea waters”, Radioecological Response of the Black Sea to the Chernobyl Accident, ECOSEA-Hydrophysics (POLIKARPOV, G.G., EGOROV, V.N., Eds), Sevastopol (2008) 217–250 (in Russian).
- [7] POLIKARPOV, G.G., et al.,  $^{90}\text{Sr}$  and  $^{137}\text{Cs}$  in surface waters of the Dnieper River, the Black Sea and the Aegean Sea in 1987 and 1988, J. Environ. Radioact. 13 (1991) 25–28.

- [8] POLIKARPOV, G.G., et al., Inflow of Chernobyl  $^{90}\text{Sr}$  to the Black Sea from the Dnieper River, *Estuar. Coast. Shelf S.* **34** (1992) 315–320.
- [9] MARTIN, J.M., et al., Origin and fate of artificial radionuclides in the Scheldt estuary, *Mar. Chem.* **46** (1994) 189–202.
- [10] GULIN, S.B., et al., Radioactive contamination of the north-western Black Sea sediments, *Estuar. Coast. Shelf S.* **54** (2002) 541–549.
- [11] EGOROV, V.N., et al.,  $^{90}\text{Sr}$  and  $^{137}\text{Cs}$  in the Black Sea after the Chernobyl NPP accident: Inventories, balance and tracer applications, *J. Environ. Radioact.* **43** (1999) 137–155.
- [12] GULIN, S.B., STOKOZOV, N.A.,  $^{137}\text{Cs}$  concentrations in Atlantic and western Antarctic surface waters: Results of the 7th Ukrainian Antarctic Expedition, 2002, *J. Environ. Radioact.* **83** (2005) 1–7.
- [13] FLOROU, H., et al., Dispersion of  $^{137}\text{Cs}$  in the eastern Mediterranean and the Black sea: the time evolution in relation to the sources and pathways, *J. Environ. Protect. Ecol.* **3** (2002) 30.
- [14] DELFANTI, R., et al., Distribution of  $^{137}\text{Cs}$  and other radioactive tracers in the eastern Mediterranean: Relationship to the deepwater transient, *J. Geophys. Res.-Oceans* **108** (2003) 8108.
- [15] BOURLAT, Y., MILLIES-LACROIX, J.-C., PETIT, G.L., BOURGUIGNON, J., “ $^{90}\text{Sr}$ ,  $^{137}\text{Cs}$  and  $^{239+240}\text{Pu}$  in world ocean water samples collected from 1992 to 1994”, *Radionuclides in the Oceans Inputs and Inventories* (GUÉGUÉNIAT, P., GERMAIN, P., MÉTIVIER, H., Eds), Institut de Protection et de Sureté Nucleaire, Cherbourg, France (1996) 75–93.
- [16] GULIN, S.B., POLIKARPOV, G.G., EGOROV, V.N., AARKROG, A., NIELSEN, S.P., “Chronological study of  $^{137}\text{Cs}$  input to the Black Sea deep and shelf sediments”, *Radionuclides in the oceans: Inputs and inventories*, (GERMAIN, P., GUARY, J.C., GUEGUENIAT, P., METIVIER, H., Eds), Proc. Int. Symp., Cherbourg-Octeville, France, 7–11 Oct, 1996, (1997) 257–262.
- [17] GULIN, S.B., Seasonal changes of  $^{234}\text{Th}$  scavenging in surface water across the western Black Sea: an implication of the cyclonic circulation patterns, *J. Environ. Radioact.* **51** (2000) 335–347.



# **Cs-137 IN MARINE SEDIMENTS OF THE EASTERN MEDITERRANEAN FROM THE PRE-CHERNOBYL AGE TO THE PRESENT**

H. FLOROU, N. EVANGELIOU, P. KRITIDIS  
Demokritos National Center for Scientific Research,  
Institute of Nuclear Technology-Radiation Protection,  
Environmental Radioactivity Laboratory (ERL),  
Athens, Greece

## **Abstract**

A survey of the  $^{137}\text{Cs}$  inventory in sediments from the Greek marine environment is presented for the period 1984 to 2007, based on published and unpublished data of ERL. A retrospective summary of the  $^{137}\text{Cs}$  impact assessment is also attempted, based on data covering the period prior to and after Chernobyl up to 2007. Therefore, the sinking time and the ecological half-life of  $^{137}\text{Cs}$  are also estimated in some specific areas of the Eastern Mediterranean and the findings are compared to the deposition data of the first days of the Chernobyl impact. By evaluating all these findings and estimations, a  $^{137}\text{Cs}$  distribution pattern is proposed considering the Chernobyl impact as a case study in this area.

## **1. INTRODUCTION**

Caesium-137 (half-life 30.2 a) was first introduced into the marine environment at the beginning of the atmospheric nuclear weapons testing in 1953 [1] with a peak in 1959 and 1963. The second and largest contamination of many European marine systems with radioactive caesium –  $^{137}\text{Cs}$  and  $^{134}\text{Cs}$  (half-life 2.07 years) was the fallout after the Chernobyl accident in April 1986. Since 1986 the radiological status of the Eastern Mediterranean has been changed. During 1986 the average deposition of  $^{137}\text{Cs}$  from the fallout in the Aegean Sea has been estimated to be approximately 4 kBq/m<sup>2</sup>, whereas the respective value for the Ionian Sea (the area of 24,300 km<sup>2</sup> along the coasts) was considerably lower, 2.5 kBq/m<sup>2</sup> [2]. The total caesium ( $^{137}\text{Cs}$  +  $^{134}\text{Cs}$ , 2/3 of this value was  $^{137}\text{Cs}$ ) input from Chernobyl fallout in the Black Sea and the Eastern Mediterranean has been estimated to be 2400 TBq for the Black Sea, 820 TBq for the Aegean Sea and 600 TBq in the Ionian Sea (60 TBq in the zone of 50 km across the Greek coasts) [3–5]. Besides this, the North Aegean Sea is the area where the Black Sea waters interact with the Aegean Sea waters, through the straits of the Dardanelles, and are diluted, resulting in elevated  $^{137}\text{Cs}$  activity concentrations up to several times higher compared to e.g. the Ionian Sea [2]. Subsequent measurements in this area affirm that the mouth of the Dardanelles in the North Aegean

Sea is the entrance of the radionuclide transfer to the Eastern Mediterranean through the purification process of the Black Sea [6].

In summary, worldwide fallout, Chernobyl fallout (early and late impact from the catchment areas) and transboundary pollution are the sources of the  $^{137}\text{Cs}$  enrichment of the Eastern Mediterranean. Although, the residence time of  $^{137}\text{Cs}$  in the water column is long, it is estimated that  $^{137}\text{Cs}$  from the various sources have reached the bottom sediments, as the remaining period is long enough if compared to the estimated sinking time for the Mediterranean environment.

## 2. BACKGROUND

The Mediterranean Sea is a semi-enclosed marine area, exchanging water, salt, heat and other physicochemical properties through the strait of Gibraltar with the Atlantic Ocean. The basin is characterized by low precipitation and high evaporation, which causes an accumulation of contaminants in seawater and sediment. Because of its lower dilution capacity, the Mediterranean Sea is therefore much more vulnerable to contamination than the coastal regions of oceans [7]. Taking into account the topography, one could note the importance of the eastern

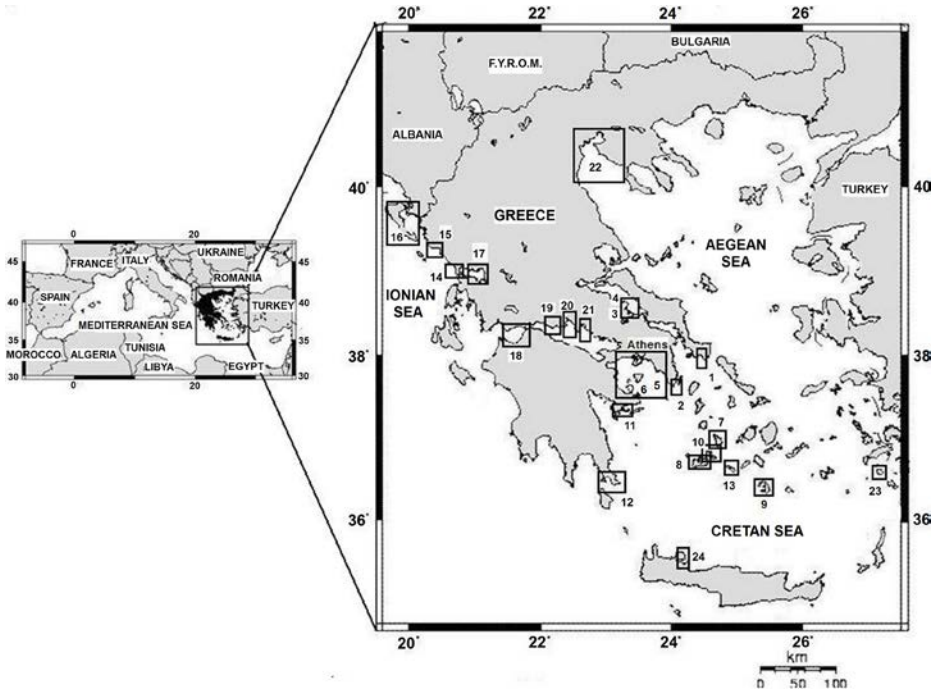


FIG. 1. Sampling sites in Greek territory where sediment samples were collected.

part of the Mediterranean, since it comprises a continuous source of interregional input (Black Sea outfalls to the Northeastern Aegean Sea). However, the motive of determining  $^{137}\text{Cs}$  in Greek marine territory was basic research (pre-Chernobyl age) and monitoring (after Chernobyl accident). Several Greek marine systems have been examined throughout these years (see Fig. 1) and the results are evaluated in the present study.

### 3. EXPERIMENTAL

During the period 1984–2007, sediment samples were collected using several corers in oceanographic vessels, fishing boats and/or diving (coastal). Stones, shells and algae were removed from the samples and the weight of the remaining sediment was recorded. Then the sample was homogenized and dried overnight at 105°C until constant weight. After that, the sample was sieved through a 2 mm sieve, weighed and the weight of the dry sample was recorded. Then the material was homogenized and a subsample was taken to obtain the optimal counting geometry.

The measurements, of 70 000 sec each, were carried out in a high resolution gamma spectrometry system, with an HpGe detector of 20% relative efficiency and computerized multi-channel analyser of 4000 channels in a total spectrum area of 2000 keV and a resolution of 2.0 keV (at 1.33 MeV photopeak of  $^{60}\text{Co}$ ). ORTEC software was used for the analyses of the obtained spectra. The relative statistical error ( $1\sigma$ ) did not exceed 18%.

### 4. RESULTS AND DISCUSSION

#### 4.1. Chernobyl impact

##### 4.1.1. *Distribution to Aegean and Ionian Seas*

Time series data obtained before and just after the Chernobyl accident are illustrated in Fig. 2. The data showed that Chernobyl  $^{137}\text{Cs}$  affected the coastal sediments in some areas one year after the Chernobyl accident by fallout (regions 1–13). Another significant contribution was washout and soil erosion from the land. Particulates submerge rapidly into deeper layers carrying  $^{137}\text{Cs}$  and transporting it to the sediment. However, it seems that a small amount of  $^{137}\text{Cs}$  was transferred to the sediments just after the accident, as  $^{137}\text{Cs}$  remains mostly in ionic form in seawater [8] and is distributed spatially via marine processes (advection, diffusion etc.).

From the time series data it can be noted that the impact to the Ionian Sea (regions 14–16) was inappreciable, as activity concentrations near background levels were found in coastal areas during 1987. An explanation could be that in the Ionian

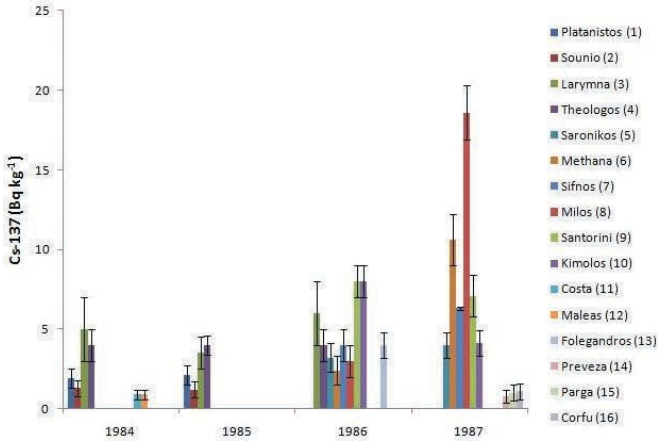


FIG. 2. Time series data of  $^{137}\text{Cs}$  in sediments of several Greek marine areas before and just after Chernobyl.

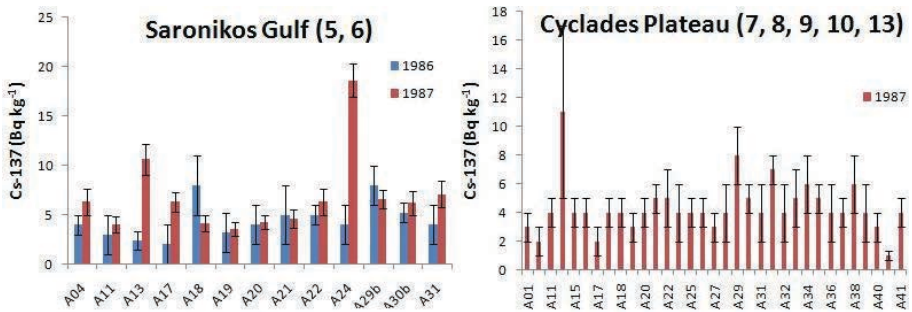


FIG. 3. Spatial distribution of  $^{137}\text{Cs}$  in sediments of the Saronikos Gulf and Cyclades Plateau.

no direct influence (except from fallout) was apparent. In contrast, the Aegean Sea is connected to the Black Sea via the Bosphorus and Dardanelles Straits.

#### 4.1.2. Saronikos Gulf–Cyclades Plateau

The Saronikos Gulf is a marine area that is not affected by intense washout processes, as it accepts low rainfall supplies and inputs from small rivers and ephemeral streams. For that reason, the impact after the accident was limited (Fig. 3). Comparable values were observed in the Cyclades Plateau, although there were no previous measurements of  $^{137}\text{Cs}$  in the area (Fig. 3).

## 4.2. Recent measurements

### 4.2.1. Thermaikos Gulf

Two campaigns were carried out in Thermaikos Gulf during 2005 and 2007. The activities were decay corrected to 25 September 2007. The data showed that activity concentrations of  $^{137}\text{Cs}$  tend to decrease with time, although some extreme values appeared (increased up to 20 times) (Fig. 4). The data are considered to be 2 times higher than those observed before the accident, even though more than 20 years interceded.

### 4.2.2. Gulf of Patras – Nisyros Isl.

Sediment samples from the Gulf of Patras and Nisyros Island were collected during 2004 and 2006, respectively, and the results were corrected for decay to 25 September 2007.  $^{137}\text{Cs}$  ranged from below the detection limit (LD = 0.05 Bq/kg)

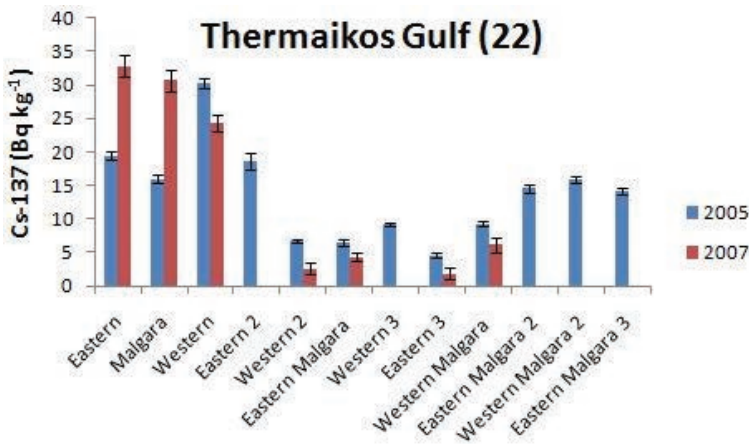


FIG. 4. Spatial distribution of  $^{137}\text{Cs}$  in sediments of the Thermaikos Gulf.

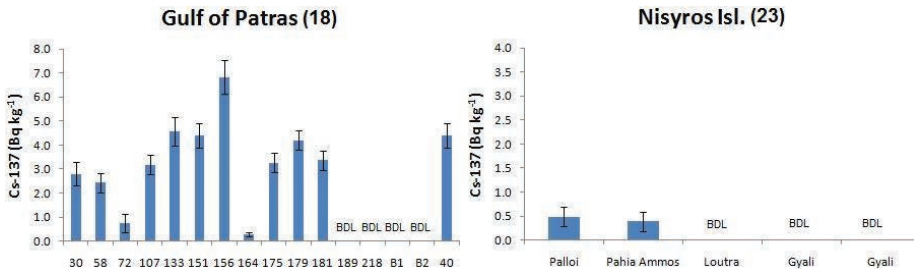


FIG. 5. Spatial distribution of  $^{137}\text{Cs}$  in sediments of the Gulf of Patras and Nisyros Island.

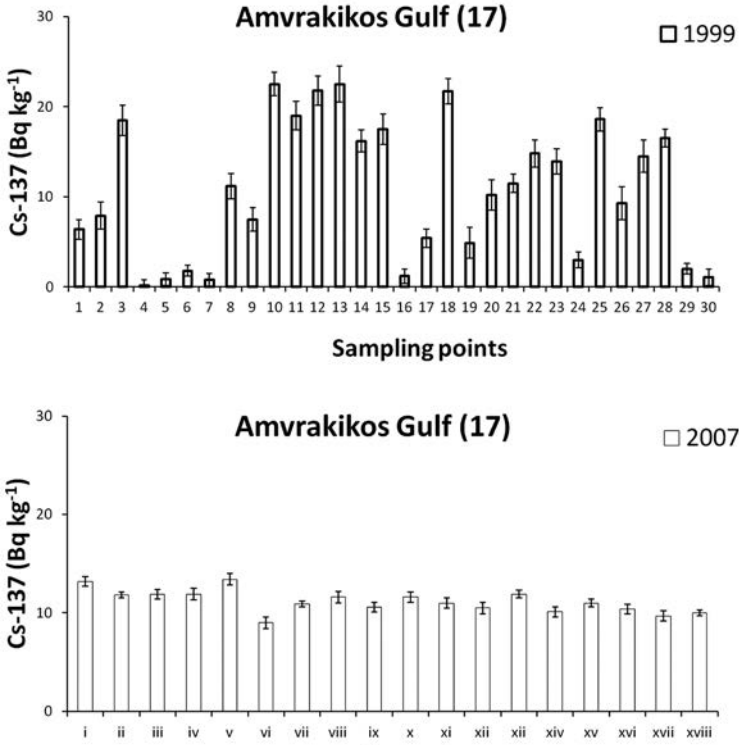


FIG. 6. Spatial distribution of <sup>137</sup>Cs in sediments of the Amvrakikos Gulf.

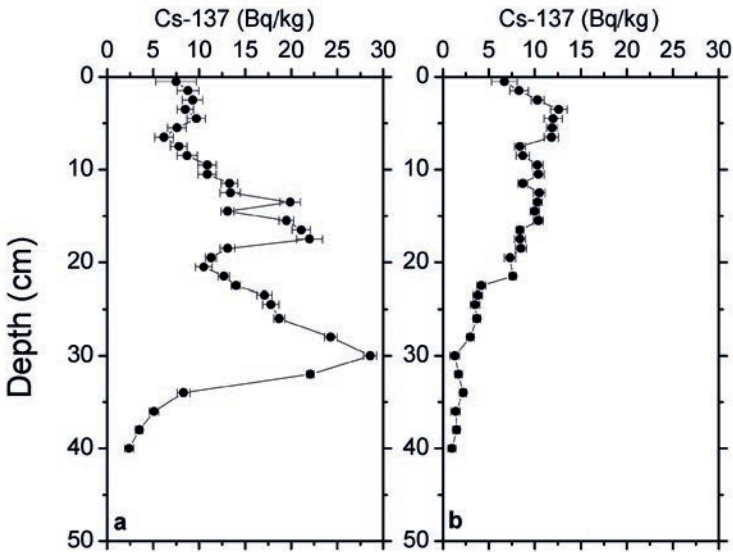


FIG. 7. Vertical profiles of <sup>137</sup>Cs in the Amvrakikos Gulf.

kg) to  $6.9 \pm 0.6$  Bq/kg in the Gulf of Patras (Fig. 5), denoting that  $^{137}\text{Cs}$  tends to background levels. On the other hand, the impact from the accident in Nisyros Island, located in Southeastern Aegean, seems to be negligible, as all values were below 1.0 Bq/kg (Fig. 5).

#### 4.2.3. *Amvrakikos Gulf*

Two campaigns were carried out in the Amvrakikos Gulf in 1999 and 2007, respectively; the latter was organized by the IAEA within the framework of the TC Program RER7.003. All data were corrected for decay to 25 September 2007, which was the last date of sampling.  $^{137}\text{Cs}$  decreased up to 50% in surface sediments of the Amvrakikos Gulf (Fig. 6). In fact, this is prospective, as earlier studies in the area have shown that Amvrakikos Gulf is characterized by intense sedimentation [9, 10].

Moreover, two core samples were collected in the entry (13A) of the Amvrakikos Gulf, as well as in the centre (13B) and the profiles are shown in Fig. 7. From the obtained data, the impact of Chernobyl and nuclear weapon testing processes is apparent in at least one station (13A). Using  $^{137}\text{Cs}$  technique, the sedimentation rate in station 13A was estimated to be 0.54 cm/a. This rate was certified using the  $^{210}\text{Pb}$  method and the respective sedimentation rate was estimated to be  $0.55 \pm 0.02$  cm/a, indicating the application of  $^{137}\text{Cs}$  in sedimentation estimations.

## 5. CONCLUSIONS

- (a) The impact from the Chernobyl accident in surface sediments of the Greek territory was more apparent in 1987 in the coastal sediments as the particulate fraction submerged to the depth.
- (b) The impact was more intense in enclosed marine systems rather than the open sea. This is evidence of the complicated processes that dominate the enclosed gulfs, such as erosion and washout from the land, as well as internal current movements resulting in concentration of pollutants for long time periods inside the gulfs.
- (c) Regarding the recent measurements in several areas of Greece, we conclude that  $^{137}\text{Cs}$  concentrations tend to pre-Chernobyl levels in the open sea. The high concentrations in some enclosed systems are attributed to local phenomena such as the complicated topography and/or the large drainage of freshwater systems, rapid sedimentation rates, etc.
- (d) Finally, the wide applications of  $^{137}\text{Cs}$  as a tracer of marine processes should be noted as it comprises a powerful indicator of current movement, sedimentation, etc.

## ACKNOWLEDGEMENTS

The authors would like to thank the permanent staff of the Environmental Radioactivity Laboratory of the Institute of Nuclear Technology — Radiation Protection for their assistance in sampling and analysis of the samples over all these years. Moreover, acknowledgements are owed to the IAEA for the supervision of the cruise in the Amvrakikos Gulf during 2007 within the framework of the TC Program RER7003.

## REFERENCES

- [1] PUTYRSKAYA, V., et al., Migration of  $^{137}\text{Cs}$  in tributaries, lake water and sediment next term of Lago Maggiore (Italy, Switzerland) – analysis and comparison with Lago di Lugano and other lakes, *J. Environ. Radioact.* **100** 1 (2009) 35–48.
- [2] FLOROU, H., KRITIDIS, P., The dispersion of  $^{137}\text{Cs}$  in the Aegean Sea, *Radiochim. Acta.* **66–67** (1994) 415–417.
- [3] FLOROU, H.,  $^{137}\text{Cs}$  inventory in abiotic component and biota from the Aegean and Ionian Sea – Greece, *Chem. Ecol.* **12** (1996) 253–258.
- [4] KRITIDIS, P., FLOROU, H., Estimation of  $^{137}\text{Cs}$  deposited in Aegean, Cretian Ionian Sea after the Chernobyl accident, *Rapp. Comm. Int. Mer Medit.* **32** 1 (1990) 318.
- [5] KRITIDIS, P., et al., Delayed and late impact of the Chernobyl accident on the Greek environment, *Radiat. Prot. Dosim.* **30** 3 (1990) 187–190.
- [6] EVANGELIOU, N., et al., Temporal and spatial distribution of  $^{137}\text{Cs}$  in Eastern Mediterranean sea: Horizontal and vertical dispersion in two regions, *J. Environ. Radioact.* **100** (2009) 626–636.
- [7] NOUREDDINE, A., et al., Radionuclide tracing of water masses and processes in the water column and sediment next term in the Algerian Basin, *J. Environ. Radioact.* **99** 8 (2008) 1224–1232.
- [8] BUESSELER, K.O., Chernobyl: Oceanographic studies in the Black Sea, *Oceanus* **30** (1987) 23–30.
- [9] POULOS, S.E., et al., Origin and distribution of surface sediments and human impacts on recent sedimentary processes. The case of the Amvrakikos Gulf (NE Ionian Sea), *Cont. Shelf Res.* **28** 20 (2008) 2736–2745.
- [10] KAPSIMALIS, V., et al., Internal structure and evolution of the Late Quaternary sequence in a shallow embayment: The Amvrakikos Gulf, NW Greece, *Mar. Geol.* **222–223** (2005) 399–418.

# CAESIUM AND PLUTONIUM ISOTOPES AS TRACERS OF VARIOUS EVENTS IN SEDIMENT RECORDS IN THE BAY OF TOULON (NORTHWESTERN MEDITERRANEAN SEA)

C. DUFFA, M. ARNAUD, S. CHARMASSON, H. THÉBAULT  
Institut de Radioprotection et de Sureté Nucléaire,  
DEI/SESURE/LERCM,  
La Seyne sur Mer, France

## Abstract

Located along the French Mediterranean coast, the Toulon bay has a specific configuration with two basins. The shallow one is a semi-enclosed basin (Petite Rade) with complex hydrodynamic conditions that contribute to fine sedimentation. The open sea basin, separated from the first one by a long sea wall, receives different anthropogenic inputs. Surface and core sediment sampling cruises took place in 2001 and 2008, in order to study radionuclide spatial dispersion and sediment accumulation.  $^{137}\text{Cs}$  values are statistically higher in the 'Petite Rade' than in the open basin.  $^{239+240}\text{Pu}$  levels range from 0.7 to 2.6 Bq/kg dry weight in surface sediments, up to 6 times higher than elsewhere in Mediterranean coastal areas not influenced by riverine inputs. Plutonium activity ratios ( $^{238}\text{Pu}/^{239+240}\text{Pu}$  and  $^{239}\text{Pu}/^{240}\text{Pu}$ ) labelled atmospheric nuclear weapon testing. Regarding the long cores, the highest plutonium activities, measured by alpha counting and ICP-MS, concern the first ten centimetres with a maximum value of 3.5 Bq/kg dry weight in  $^{239+240}\text{Pu}$ .

## 1. INTRODUCTION

In the Eastern part of the French Mediterranean coast, the Toulon Bay has a unique configuration. It is divided into two basins separated by a long sea wall (1.4 km long) built in the 19th century (Fig. 1). The Little Bay is directly influenced by the anthropogenic impact from the city of Toulon (Pop. 170 000) and military harbour activities. This 7.8 km<sup>2</sup> semi-enclosed and fairly shallow basin (maximum depth of 29 m) receives inputs from a 70 km<sup>2</sup> catchment area, mainly through the Las river. It is linked to the Large Bay by a channel about 30 metres deep. This channel is the main hydrological area of transfer between the Little Bay and the Large Bay. The Large Bay, delimited by the Island of Saint-Mandrier-sur-Mer to the West and the Cap de Carqueiranne to the East, is open to the Mediterranean Sea and subject to the influence of the general water circulation in this region related to the Ligurian Current flowing eastward to westward. The Toulon bay is of significant interest in both economic and ecological terms. Nevertheless, only few studies have been

carried out in this marine area. In recent years a large environmental programme, the ‘Toulon Bay Contract’, has been initiated to carry out an environmental assessment in order to improve the integrated management of this area. As part of this programme, the radio-ecological assessment of the sediment compartment has been carried on, with the aim of both characterizing the contamination levels and the environmental processes.

This article presents the results of two sampling campaigns performed in 2001 and 2008 in this area that permitted the collection and analysis of 26 surface sediment samples and 3 sediment cores. Gamma, alpha and ICP-MS measurements have been done to give the surface and vertical distribution of  $^{137}\text{Cs}$ ,  $^{238}\text{Pu}$ ,  $^{239}\text{Pu}$ ,  $^{240}\text{Pu}$ ,  $^{241}\text{Pu}$  and  $^{241}\text{Am}$ , completed by grain-size measurements. The Pu long lived alpha emitter isotopes ( $^{238}\text{Pu}$  half-life: 87.7 a,  $^{239}\text{Pu}$ : 24.1 ka and  $^{240}\text{Pu}$ : 6.563 ka) formed the subject of several studies as regards their behaviours in the environment. Today, soils and sediments constitute the main plutonium reserves in the environment [1]. The plutonium and americium artificial radionuclides originate from 1960s nuclear weapons testing and the burnup of the US Transit-5-BN-3 nuclear powered satellite during its accidental re-entry into the atmosphere in 1964 (concerns  $^{238}\text{Pu}$  only). The presence of  $^{241}\text{Am}$  is due to the beta decay of its parent nuclide  $^{241}\text{Pu}$  from this global fallout.  $^{137}\text{Cs}$  originates both from nuclear weapons testing and from the Chernobyl accidental release in 1986.

Vertical distributions of the naturally occurring radionuclide  $^{210}\text{Pb}$  have also been determined to estimate the sedimentation regime in this area.  $^{210}\text{Pb}$  is a member

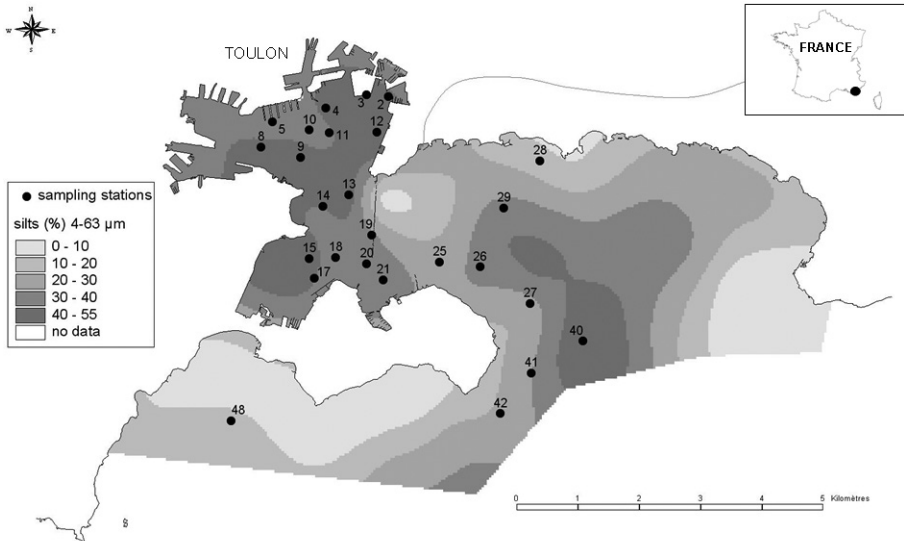


FIG. 1. The Toulon Bay area studied with sampling stations and interpolated silts fraction (the map shows additional and not reported stations).

of the  $^{238}\text{U}$  decay series and is produced in the atmosphere from the decay of  $^{222}\text{Rn}$  emanated from continental rocks and soils.  $^{210}\text{Pb}$  deposited onto the sea surface is rapidly associated to settling particles and accumulates in sediments, where its vertical profile is a function of the sediment accumulation rate and of its physical decay. Because of its 22.3 a half-life,  $^{210}\text{Pb}$  provides an indication of sedimentation occurring over the past 100 a.

Using results from these campaigns, this paper provides an estimation of caesium and plutonium inventories in the Little Bay sediments.

## 2. MATERIALS AND METHODS

### 2.1. Sediment sampling

Twenty surface sediment samples (the top 5 cm) were collected from the Little Bay in the year 2000 by an orange peel grab and Eckman box corer depending on station depths. The location of grab and cores samples are shown in Fig. 1.

Two long cores were obtained during two campaigns in February 2001 and June 2009 in Station 9. They were collected by a multi-corer for a 16 cm section in 2001 and by an interface corer for a 10 cm section. The core was extruded immediately after sampling and sliced every one or two centimetres, in 2001 and 2009 respectively. Freeze dried and dried to 80°C constant weight, the sediment subsamples were crushed, passed through a 2000  $\mu\text{m}$  sieve and put in geometries for gamma direct measurements.

### 2.2. Analyses

- Grain-size analysis of surface samples and core sections were carried out on an aliquot of wet sediment. The analysis was performed on the <2mm fraction by a LS 13320 Beckman Coulter laser grain sizer.
- Direct gamma spectrometry analyses were performed on closed volumes of 60 ml of dried sediment using spectrometers with low background level HPGe Detectors with a 0.5 mm thickness beryllium window IRSN Laboratory [2]. Samples were measured for 24–48 h.  $^{210}\text{Pb}$  (half-life 22.3 a) and  $^{137}\text{Cs}$  activity (30.2 a) were determined based on their respective peaks at 46.5 and 661.7 keV. Self-adsorption corrections were done according to sample type, density and gamma energy using in-house standards. Measurements were done after at least 4 weeks of equilibrium and therefore it was possible to estimate supported  $^{210}\text{Pb}$  using  $^{214}\text{Pb}$  activities.

$^{238}\text{Pu}$ ,  $^{239+240}\text{Pu}$  and  $^{241}\text{Am}$  were determined by alpha counting after radiochemical treatment [3]. Samples are first ashed at 480°C in order to eliminate organic matter and

TABLE 1. <sup>137</sup>Cs, <sup>241</sup>Am, <sup>238</sup>Pu, <sup>239</sup>Pu, <sup>240</sup>Pu AND <sup>241</sup>Pu MASS ACTIVITIES, AND FINE GRAIN-SIZE FRACTION MEASURED IN TOULON BAY SURFACE SEDIMENT SAMPLES

St.	Cs-137 (Bq/kg)	Pu-238 (Bq/kg)	Am-241 (Bq/kg)	Pu-239 (Bq/kg)	Pu-240 (Bq/kg)	Pu-241 (Bq/kg)	Silt < 63µm %
2	10.1 ± 0.6	0.053 ± 0.003	0.55 ± 0.06	1.13 ± 0.01	0.79 ± 0.01	4.34 ± 0.38	40.6
3	3.4 ± 0.3	0.020 ± 0.002	0.25 ± 0.03	0.45 ± 0.04	0.30 ± 0.03	1.65 ± 0.52	35.3
4	6.3 ± 0.3	0.051 ± 0.003	0.56 ± 0.06	1.12 ± 0.05	0.78 ± 0.03	4.33 ± 0.89	35.8
5	4.9 ± 0.3	0.032 ± 0.003	0.33 ± 0.04	0.70 ± 0.03	0.47 ± 0.03	2.56 ± 0.21	37.1
8	9.8 ± 0.7	0.055 ± 0.005	0.52 ± 0.06	1.21 ± 0.03	0.83 ± 0.03	4.20 ± 1.30	36.5
9	8.9 ± 0.7	0.067 ± 0.005	0.88 ± 0.09	1.62 ± 0.07	1.09 ± 0.08	5.87 ± 0.82	37.0
10	3.9 ± 0.3	0.037 ± 0.004	0.40 ± 0.04	0.66 ± 0.04	0.46 ± 0.03	2.88 ± 0.44	51.3
11	7.2 ± 0.6	0.053 ± 0.005	0.53 ± 0.08	1.10 ± 0.06	0.75 ± 0.05	4.63 ± 0.78	46.7
12	12.2 ± 0.9	0.100 ± 0.007	1.14 ± 0.09	2.21 ± 0.06	1.51 ± 0.05	10.82 ± 0.59	37.1
13	9.3 ± 0.7	0.071 ± 0.005	0.84 ± 0.07	1.62 ± 0.03	1.11 ± 0.02	8.43 ± 0.72	50.0
14	4.6 ± 0.4	0.049 ± 0.004	0.65 ± 0.08	1.15 ± 0.12	0.76 ± 0.08	4.20 ± 1.30	39.6
15	7.3 ± 0.5	0.082 ± 0.006	1.07 ± 0.08	1.98 ± 0.05	1.34 ± 0.03	10.10 ± 1.20	41.1
17	6.5 ± 0.5	0.065 ± 0.004	0.77 ± 0.06	1.43 ± 0.02	0.97 ± 0.02	6.90 ± 1.10	34.9
18	5.4 ± 0.4	0.055 ± 0.004	0.71 ± 0.07	1.26 ± 0.06	0.87 ± 0.05	4.16 ± 0.66	35.6
19	6.0 ± 0.5	0.055 ± 0.004	0.68 ± 0.07	1.19 ± 0.07	0.84 ± 0.05	4.39 ± 0.70	36.6
20	8.6 ± 0.6	0.072 ± 0.005	0.78 ± 0.06	1.55 ± 0.02	1.05 ± 0.02	7.80 ± 1.30	10.5
21	6.9 ± 0.6	0.062 ± 0.004	0.72 ± 0.06	1.42 ± 0.04	0.97 ± 0.03	7.03 ± 0.66	20.6
25	3.1 ± 0.3	0.035 ± 0.004	0.41 ± 0.04	0.70 ± 0.02	0.49 ± 0.03	2.98 ± 0.71	24.3
26	4.4 ± 0.3	0.049 ± 0.003	0.57 ± 0.06	1.01 ± 0.05	0.72 ± 0.05	3.74 ± 0.50	41.1
27	1.5 ± 0.2	0.023 ± 0.003	0.25 ± 0.03	0.46 ± 0.04	0.34 ± 0.05	<5.9	35.2
28	5.1 ± 0.4	0.041 ± 0.004	0.54 ± 0.06	0.91 ± 0.04	0.63 ± 0.03	4.30 ± 1.20	20.8
29	2.9 ± 0.2	0.039 ± 0.003	0.49 ± 0.04	0.80 ± 0.08	0.58 ± 0.05	3.15 ± 0.63	12.3
40	6.6 ± 0.5	0.054 ± 0.004	0.73 ± 0.05	1.16 ± 0.07	0.81 ± 0.05	5.00 ± 1.20	22.0
41	3.4 ± 0.3	0.031 ± 0.002	0.42 ± 0.03	0.71 ± 0.04	0.48 ± 0.03	2.84 ± 0.47	3.7
42	3.3 ± 0.3	0.042 ± 0.003	0.50 ± 0.04	0.96 ± 0.05	0.65 ± 0.04	4.10 ± 2.10	19.8
48	1.5 ± 0.2	0.027 ± 0.003	0.40 ± 0.04	0.62 ± 0.02	0.45 ± 0.02	2.88 ± 0.49	4.3

then spiked with  $^{242}\text{Pu}$  and  $^{243}\text{Am}$ , to control the recovery efficiency of the treatment. A double step leaching using concentrated  $\text{HNO}_3$  and  $\text{H}_2\text{O}_2$  makes the radionuclides soluble. Stable elements and natural alpha emitting radioisotopes are then separated from Pu and Am by co-precipitation exchange chromatography and extraction chromatography. Pu and Am are then electro deposited and alpha counted for 7 days.

$^{239}\text{Pu}$ ,  $^{240}\text{Pu}$  and  $^{241}\text{Pu}$  atom determination was performed by ICP-MS. The method is described in Pourcelot et al. [4]. Uncertainties enclosed the measurement stability (5 replicates), the mass bias correction, the activity and the weighting of the tracer and an estimated repeatability of the analysis.

### 3. RESULTS AND DISCUSSION

#### 3.1. Radionuclides in surface sediments

Radionuclide mass activities are reported in Table 1 together with clay and silt fractions.

$^{137}\text{Cs}$  activities were between 1.5 Bq/kg (st. 27 and 48) and 12.2 Bq/kg (st.12). The mean  $^{137}\text{Cs}$  activity in the Little Bay is significantly higher than in the Open Bay, equal to 7 and 3 Bq/kg respectively. While values obtained in the Open Bay are consistent with other results from shelf Mediterranean environment [5, 6], values measured in the Little Bay are higher. The same observation applies to Pu and Am isotopes.  $^{239+240}\text{Pu}$  mean activity in the Little Bay is equal to 2.1 Bq/kg, with a maximum of 3.7 Bq/kg (st.12); in the Open Bay, mean activity is equal to 1.5 Bq/kg. Otherwise,

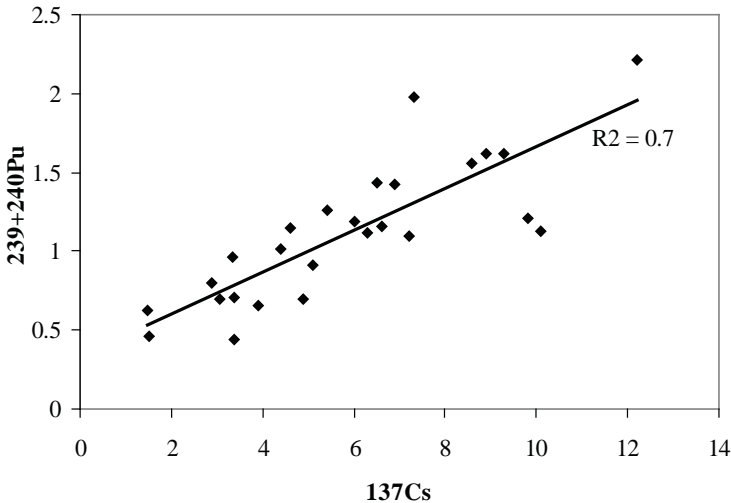


FIG. 2.  $^{137}\text{Cs}$  and  $^{239+240}\text{Pu}$  activity relationship.

$^{137}\text{Cs}$  and  $^{239+240}\text{Pu}$  mass activities are well correlated (Fig. 2) underlying their common origin. The highest values measured in the Little Bay are mainly explained by the sediment grain size. Indeed, fine particle contents are quite important in this area (see Table 1 and Fig. 1). Moreover, the hydrodynamic conditions in this area, with very little sediment suspension, contribute to the accumulation of terrestrial inputs.

$^{238}\text{Pu}/^{239+240}\text{Pu}$  and  $^{239+240}\text{Pu}/^{241}\text{Am}$  mean activity ratios, equal to  $0.027 \pm 0.003$  and  $3.1 \pm 0.6$  respectively (averages  $\pm 2$  sigma errors), correspond to global fallout expected value [7].  $^{239}\text{Pu}/^{240}\text{Pu}$  atom ratios present an isotopic composition tracing this origin ( $0.188 \pm 0.008$ ) and are in agreement both with recent studies' measured values [8–10] and with the reference value reported by Perkins and Thomas [11].

### 3.2. Radionuclide vertical profiles

Results obtained on the core sampled at station 9 in 2001 and 2008 are presented in Fig. 3. Alpha and ICP-MS measurements have only been performed on 2001 core. Gamma spectroscopy was performed both on 2001 and 2008 cores.

$^{210}\text{Pb}_{\text{xs}}$  decreases rapidly between the surface and the 17–18 cm layer.  $^{210}\text{Pb}_{\text{xs}}$  contents in the surface are equal to  $167 \pm 22$  Bq/kg dry weight in 2001 and  $127 \pm 17$  Bq/kg dry weight in 2008. Apparent sediment accumulation rates were estimated from the slope of the linear regression of the  $\ln$   $^{210}\text{Pb}$  excess activity vs. depth assuming a steady state accumulation of sediments and that the excess  $^{210}\text{Pb}$  activity of depositing sediment particles is constant [12]. Sedimentation rates are then estimated to reach  $0.18 \pm 0.02$  cm.a $^{-1}$  from 2001 data (slope calculated between 7 and 16 cm) and  $0.17 \pm 0.06$  cm.a $^{-1}$  using 2009 data (slope calculated between 0 and 10 cm).

The  $^{137}\text{Cs}$  activity presents a maximum mass activity in the layer 5–6 cm ( $11.7 \pm 1$  Bq/kg in 2001 and  $5.7 \pm 0.7$  Bq/kg in 2009). In 2001, it is only measurable until 18 cm. Assuming that the first  $^{137}\text{Cs}$  depositions appeared in 1953, these data suggest a sedimentation rate higher than the ones derived from  $^{210}\text{Pb}_{\text{xs}}$ . This feature has been widely reported and is assumed to be mainly linked to diffusion phenomena (e.g. Ref. [13]).

The concentration of  $^{239+240}\text{Pu}$  in the surface sediment is  $2.7 \pm 0.1$  Bq/kg and a maximum of  $3.5 \pm 0.1$  Bq/kg appears in the layer 5–6 cm, in agreement with that of the  $^{137}\text{Cs}$  profile. Like  $^{137}\text{Cs}$ , it is also measurable until 18 cm deep in 2001, suggesting that these isotopes also undergo diffusion in the sediment pore water. Indeed, Lucey and al. [14] have shown that the plutonium in marine sediment can be associated with relatively mobile geochemical phases.

### 3.3. Inventories and stocks

Assuming that the vertical distribution of artificial radionuclides is homogeneous in the Little Bay, the stock of  $^{239+240}\text{Pu}$  this basin has been calculated. Station 9 total  $^{239+240}\text{Pu}$  and  $^{137}\text{Cs}$  inventories are equal to 279 Bq/m $^2$  and 895 Bq/m $^2$ . Then,

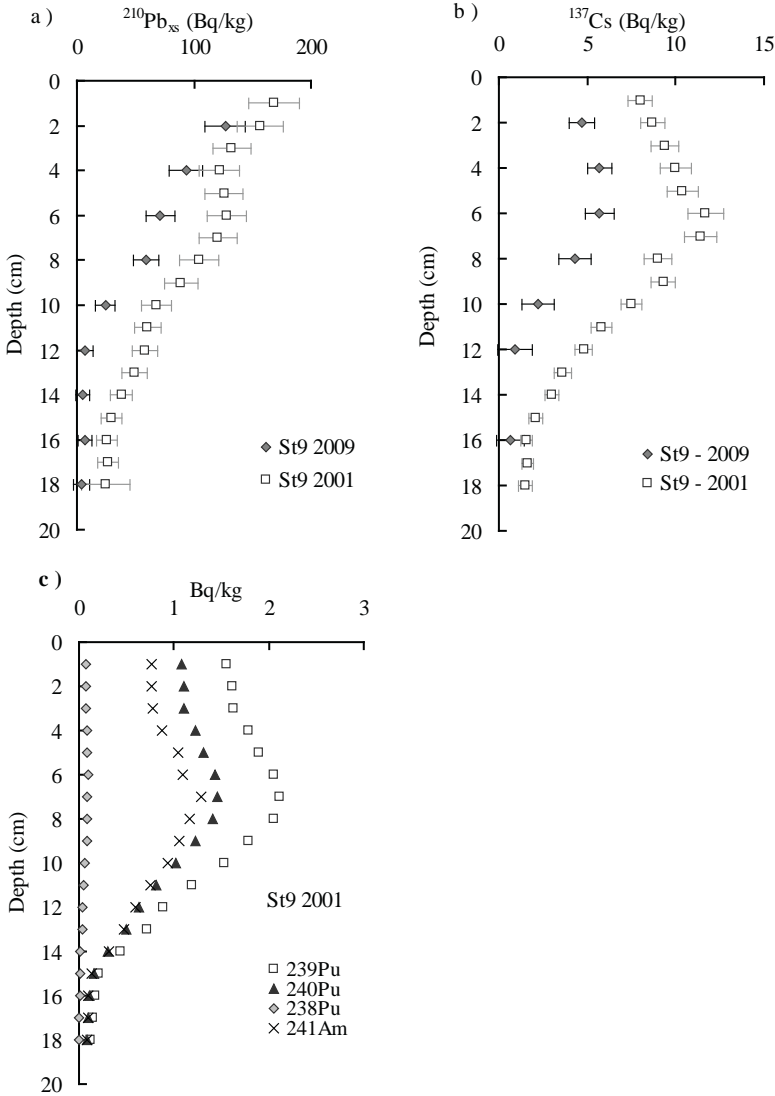


FIG. 3.  $^{210}\text{Pb}_{\text{xs}}$  (a) and  $^{137}\text{Cs}$  (b) vertical distribution in the core sampled at station 9 in 2001 and 2008;  $^{238}\text{Pu}$ ,  $^{239}\text{Pu}$ ,  $^{240}\text{Pu}$  and  $^{241}\text{Am}$  (c), vertical profile in core 9 sampled in 2001.

the stocks of  $^{239+240}\text{Pu}$  and  $^{137}\text{Cs}$  over the 7.8 km<sup>2</sup> Little Bay surface would be about 2.2 GBq and 7 GBq respectively.

Taking into account mean annual precipitation of 700 mm,  $^{239+240}\text{Pu}$  and  $^{137}\text{Cs}$  weapon tests fallout remnant activities in 2001 were estimated respectively to 51 Bq/m<sup>2</sup> (from Ref. [15]) and 1850 Bq/m<sup>2</sup> (from Ref. [16]). Otherwise, Chernobyl

$^{137}\text{Cs}$  fallout in this area was estimated to be about  $2500 \text{ Bq/m}^2$  in 1986 [17]. The total remnant  $^{137}\text{Cs}$  activity in 2001 is then expected to be about  $3600 \text{ Bq/m}^2$ . Based on these estimations, the Little Bay should have received approximately 0.5 GBq of  $^{239+240}\text{Pu}$  and 28 GBq of  $^{137}\text{Cs}$  through direct atmospheric deposits. This direct input represents less than 20% of the estimated stock of  $^{239+240}\text{Pu}$  in the bottom sediment whereas it represents 4 times the estimated stock of  $^{137}\text{Cs}$  in the bottom sediment. These results can be explained by the different physicochemical behaviour of Pu and Cs. We consider that a major part of Pu deposits were accumulated in bottom sediments as this element is mainly associated with particles, whereas Cs is mainly present in the dissolved phase in marine waters ( $K_d = 10^5 \text{ L/kg}$  for and  $4 \times 10^3 \text{ l}\cdot\text{kg}^{-1}$ , [18]). Due to the fact that exchanges with the open sea are very limited, these estimations suggest that at least 80% of the  $^{239+240}\text{Pu}$  measured in the bottom sediments of this part of the Toulon Bay are deriving from catchment basin indirect inputs.

#### 4. CONCLUSION

Caesium and plutonium isotopes appear to have a common origin in the Toulon Bay i.e. the global fallout. In the Little Bay, where exchanges with the open sea are very weak, inputs from the watershed seem to explain the higher levels compared to the other part of the Bay, which is under the influence of the general water circulation. However, in the Little Bay, solid inputs from land to sea appear to be quite low since the sedimentation rate determined via  $^{210}\text{Pb}_{\text{xs}}$  profiles led to values surrounding  $0.2 \text{ cm/a}$ .

Our numbers on inventories are to be considered with caution since they are based on an assumption (extrapolation to the entire Bay from only one core). However, they underline that sediment represents high plutonium storage compared to caesium, which is in agreement with what is known about their behaviour in the marine environment.

#### ACKNOWLEDGEMENTS

This work was supported by the IRSN 'ACCORE programme'. This is the IRSN contribution to the Toulon Bay Contract. The sampling cruise was made possible by the support of the INSU Oceanographic Vessel 'NO Georges Petit' (2001), and the French Navy vessels, 'BSR Chevreuil' (2000) and 'BHO Beutemps-Beau-pré' (2009). The authors are sincerely grateful to the Environmental Radioactivity Measurement Laboratory (IRSN/LMRE, Orsay, France) for gamma and alpha analyses.

## REFERENCES

- [1] LITTLE, C. A., WHICKER, F. W., WINSOR, T.F., Plutonium in a grassland ecosystem at Rocky Flats, *J. Environ. Quality* **9** (1980) 350–354.
- [2] BOUISSET, P., CALMET, D., “Hyper Pure gamma-ray spectrometry applied to low-level environmental sample measurement”, *Proc. Workshop on the Status of Measurement Techniques for the Identification of Nuclear Signatures*, Geel (1997) 73–81.
- [3] GOUTELARD, F., CALMET, D., THOMAS, S., “Determination of Pu isotopes at trace levels in environmental samples: Radioisotopes and stable elements evolution during the radiochemical method, Comparison of three radiochemical protocols”, *Proc. Environmental Radiochemical Analysis (NEWTON, G.W.A., Ed.)*, Blackpool, UK (1998) 97–110.
- [4] POURCELOT, L., et al., Isotopic evidence of natural uranium and spent fuel uranium releases into the environment, *J. Environ. Monit.* **13** (2011) 355–361.
- [5] SANCHEZ-CABEZA, J.A., MOLERO, J., Plutonium, Americium and radiocesium in the marine environment close to the Vandellos I Nuclear power plant before decommissioning, *J. Environ. Radioact.* **51** (2000) 211–228.
- [6] GASCO, C., et al., R., Distributions of Pu, Am and Cs in margin sediments from the western Mediterranean (Spanish coast), *J. Environ. Radioact.* **59** (2002) 75–89.
- [7] UNITED NATIONS, *Ionising Radiation: Sources and Biological Effects (Report to the General Assembly)*, United Nations Scientific Committee on the Effects of Atomic Radiation (UNSCEAR), UN, New York (1982).
- [8] ZHENG, J., YAMADA, M., Vertical distributions of  $^{239+240}\text{Pu}$  activities and  $^{240}\text{Pu}/^{239}\text{Pu}$  atom ratios in sediment cores: Implications for the sources of Pu in the Japan Sea, *Sci. Total Environ.* **340** (2005) 199–211.
- [9] LEE, S.H., et al., Recent inputs and budgets of  $^{90}\text{Sr}$ ,  $^{137}\text{Cs}$ ,  $^{239,240}\text{Pu}$  and  $^{241}\text{Am}$  in the northwest Mediterranean Sea, *Deep Sea Res. II* **50** (2003) 2817–2834.
- [10] KELLEY, J.M., BONDA, L.A., BEASLEY, T.M., Global distribution of Pu isotopes and  $^{237}\text{Np}$ , *Sci. Total Environ.* **237–238** (1999) 483–500.
- [11] PERKINS, R.W., THOMAS, C.W., “Worldwide fallout”, *Transuranic Elements in the Environment (HANSON, W.C., Ed.)*, US DOE/TIC-22800, U.S. Department of Energy, Office of Health and Environmental Research, Springfield, VA (1980) 53–82.
- [12] APPLEBY, P.G., OLDFIELD, F., “Application of  $^{210}\text{Pb}$  to sedimentation studies”, *Uranium-series Disequilibrium: Application to Earth, Marine, and Environmental Sciences (IVANOVICH, M., HARMON, R.S., Eds)*, 2nd edn, Clarendon Press, Oxford (1992) 731–778.
- [13] RADAKOVITCH, O., CHARMASSON, S., ARNAUD, M., BOUISSET, P.,  $^{210}\text{Pb}$  and Caesium accumulation in the Rhone Delta sediments, *Estuarine, Coast. Shelf Sci.* **48** (1999) 77–92.
- [14] LUCEY, J.A., et al., Geochemical fractionation of plutonium in anoxic Irish Sea sediments using an optimised sequential extraction protocol, *Appl. Radiat. Isot.* **60** (2004) 379–385.
- [15] HÖLGYE Z., FILGAS, R., Concentrations of  $^{239+240}\text{Pu}$  and  $^{238}\text{Pu}$  in the surface air of Prague in 1993, 1994 and 1995, *J. Radioanal. Nucl. Chem.* **214** (1996) 303–308.

- [16] MITCHELL, P.I., et al., Preliminary estimates of cumulative caesium and plutonium deposition in the Irish terrestrial environment, *J. Radioanal. Nucl. Chem.* **138** (1990) 241–256.
- [17] RENAUD, P., CHAMPION, D., BRENOT, J., Les retombées radioactives de l'accident de Tchernobyl sur le territoire français – Conséquences environnementales et exposition des personnes, Ed. Tec&Doc, Paris (2007) 190.
- [18] INTERNATIONAL ATOMIC ENERGY AGENCY, Sediment Distribution Coefficients and Concentration Factors for Biota in the Marine Environment, Technical Report Series No. 422, IAEA, Vienna (2004).

# TEMPORAL ASSESSMENT OF NATURAL RADIONUCLIDE BIOACCUMULATION BY THE CUBERA SNAPPER FISH (*LUTJANUS CYANOPTERUS*, CUVIER, 1828) FROM THE BRAZILIAN COAST

W.S. PEREIRA<sup>a,b,1</sup>, A. KELECOM<sup>b,c</sup>, D.A. PY JR<sup>a</sup>

<sup>a</sup> Coordenação de Proteção Radiológica,  
Unidade de Tratamento de Minérios (UTM),  
Indústrias Nucleares do Brasil (INB)  
Poços de Caldas, MG

<sup>b</sup> Curso de Pós-Graduação em Biologia Marinha,  
Instituto de Biologia, Depto. de Biologia Marinha,  
Universidade Federal Fluminense (UFF),  
Niterói, RJ

<sup>c</sup> Programa de Pós-Graduação em Ciência Ambiental,  
Universidade Federal Fluminense (UFF),  
Niterói, RJ

Brasil

## Abstract

The present study aims to assess the seasonal variation in the accumulation of the isotopes  $^{238}\text{U}$ ,  $^{235}\text{U}$ ,  $^{234}\text{U}$ ,  $^{232}\text{Th}$ ,  $^{230}\text{Th}$ ,  $^{228}\text{Th}$ ,  $^{226}\text{Ra}$ ,  $^{228}\text{Ra}$  and  $^{210}\text{Pb}$  in the cubera snapper fish from the coast of the state of Ceará (Brazil). The fish was caught in January (six specimens), June (eight) and September (seven). The uranium and thorium were analysed by electrodeposition, followed by alpha spectrometry. The isotopes of radium and lead were selectively co-precipitated and measured by gross alpha radiometry for  $^{226}\text{Ra}$  and gross beta radiometry for  $^{228}\text{Ra}$  and  $^{210}\text{Pb}$ . No seasonal variations could be observed neither for the uranium and thorium isotopes nor for the  $^{226}\text{Ra}$  isotope. For  $^{228}\text{Ra}$ , the activity concentration in February was equal to that of September, and both were higher than in June. For  $^{210}\text{Pb}$ , the situation was different: the month of February showed a lower activity concentration than in June, which in turn was lower than in September.

---

<sup>1</sup> Present adress. Radioprotection Service, *Unidade de Tratamento de Minérios (UTM)*

## 1. INTRODUCTION

The process of the biological accumulation of radionuclides by marine organisms is widely documented [1–5]. The first reports of the biological accumulation of radionuclides in marine organisms were published in the 1950s, on radionuclides released by a nuclear power reactor in the vicinity of Washington, USA [6, 7]. The first ecological factor to be defined as responsible for the biological accumulation was the trophic chain and this process, which was proportional to the trophic chain, was named biological magnification.

Literature reports three sources of radionuclides to living beings: the food chain [4, 8, 9]; water [10]; and finally sediment and suspended particulates grouped together [5]. These sources are closely related to the accumulation patterns [5].

For the directly proportional pattern, the food chain is the main source of radionuclides [11, 12]. Conversely, the inversely proportional pattern has water as the main source of radionuclides [4]. In this case, when the base of the food chain is phytoplankton, its small size increases the area/volume ratio and this is the factor responsible for the more efficient accumulation at this trophic level. Similarly, when the base of the food chain is the Macrophytes, their flattened geometry also increases the area/volume ratio, thus increasing the efficiency of accumulation here too [12].

Finally, sediment and suspended particulates act indirectly, being either the basis of the food chain — via ingestion of sediment or particles — or releasing radionuclides to the water [2]. In general, most of the radionuclides enter into biological systems through the solid phase [4], and may accumulate differently between the organs [1].

The analysis of radionuclide accumulation by marine organisms is complicated for a number of reasons. Among them, one of the most important is the high dispersion of obtained results, which hinders the establishment of patterns [1, 2].

Seasonality, taxonomic group, trophic level and the size of the organisms are among the most often cited factors known to influence the biological accumulation of radionuclides. Salinity, habitat, latitude, the weight of the organism and the organ examined, are among other factors currently mentioned. Each factor acts differently and can either enhance or decrease the biological accumulation of radionuclides, and sometimes not even affect it at all [4].

Seasonal variations have been detected, which can be caused by a huge range of factors [12]. Such variations generate changes in the ‘fallout’ which, in turn, generate modifications of the concentration of radionuclides in the organisms [13]. This relationship was identified by Pentreath [4] for  $^{65}\text{Zn}$  from organisms near the Columbus River. According to the author, the ‘input’ of  $^{65}\text{Zn}$  into the river suffered the influence of seasonal factors, which in turn had an effect on the organisms in the region. The same relationship was studied by Renfro et al. [14] in the same region and for the same radionuclide, allowing additional conclusions. Thus, according to Renfro et al. [14], in addition to the seasonal variability, the ‘input’ of  $^{65}\text{Zn}$  is subject to other

factors, such as e.g. temperature and feeding. The radionuclide concentration as a factor causing seasonal variation was also identified by Percy and Osterberg [15], in the case of  $^{52}\text{Mn}$ . This variability could only be identified due to the rapid ‘turnover’ of this radionuclide in the chosen bioindicator (liver albacore, *Thunnus albacares*). However, the same authors [15] did not identify seasonal variation for  $^{65}\text{Zn}$  in same bioindicator and attributed the absence of any variation to the longer ‘turnover’ for the latter radionuclide.

The present study aims to assess the seasonal component of biological accumulation of the natural radionuclides  $^{238}\text{U}$ ,  $^{235}\text{U}$ ,  $^{234}\text{U}$ ,  $^{232}\text{Th}$ ,  $^{230}\text{Th}$ ,  $^{228}\text{Th}$ ,  $^{226}\text{Ra}$ ,  $^{228}\text{Ra}$  and  $^{210}\text{Pb}$  in the cubera snapper fish from the coast of the state of Ceará (Brazil).

## 2. MATERIALS AND METHODS

### 2.1. Biological Material: Collection and Preparation

The fish chosen in this work was the cubera snapper (*Lutjanus cyanopterus*, Cuvier, 1828), an aggressive, carnivorous fish that feeds primarily on fish. Its strong canines allow mature cubera to also feed on large crustaceans including lobsters and crabs. Its feeding grounds are typically located near the bottom in rocky reef areas or adjacent to other structures. The cubera snapper is considered a ‘vulnerable’ species by the International Union for the Conservation of Nature and Natural Resources [16]. Six specimens of the cubera snapper were purchased at the fish market close to Praia da Jurema, Fortaleza, Ceará (Brazil) in January, 2007. In addition, eight specimens were collected in June, 2007 and another seven in November, 2007. The fish were stored in plastic bags and transported to the Laboratory of Analytical Chemistry of the Federal University of Ceará (UFC). The whole fish was weighed and dried at constant weight, at  $80^{\circ}\text{C}$ . The biological material was then sent to the Laboratory of Environmental Monitoring of the Ore Treatment Unit (UTM), Brazilian Nuclear Industries (INB). Each whole animal was reduced to ashes at  $450^{\circ}\text{C}$  to yield a pale residue which was homogenized in a mortar and from which aliquots were separated for analysis.

### 2.2. Radionuclides

The radionuclides investigated belong to the U-238, U-235 and Th-232 series:  $^{238}\text{U}$ ,  $^{234}\text{U}$ ,  $^{230}\text{Th}$ ,  $^{226}\text{Ra}$ , and  $^{210}\text{Pb}$  of the U-238 family,  $^{235}\text{U}$  of the  $^{235}\text{U}$  family and  $^{232}\text{Th}$ ,  $^{228}\text{Th}$  and  $^{228}\text{Ra}$ , of the  $^{232}\text{Th}$  family.

The uranium and thorium isotopes were determined by separation on an ion exchange resin column, followed by electro-deposition onto silver disks, and further alpha spectrometry, as described by [16]. Ra-226 activity was determined by

radiochemistry and total alpha radiometry, and that of Ra-228 and Pb-210 by radiochemistry and total beta radiometry [17].

**2.3. Statistical analysis of data**

The data were analysed by mono-factorial variance analysis. The analysis was performed with the statistical package included in Excel, version 2007. Tested hypotheses were:

H0 = averages between sampled months are statistically identical;

H1 = there is at least one average statistically different from the others.

If H0 is refused, the supplementary Student's t-test test was carried out, following Ref. [18], comparing the months two by two. The analysis was also performed with the statistical package included in Excel, version 2007. The tested hypotheses were:

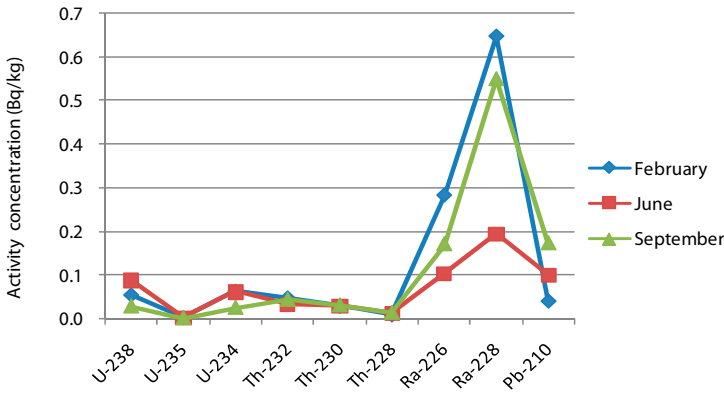


FIG. 1. Monthly average activity concentrations in Bq/kg for analysed radionuclides.

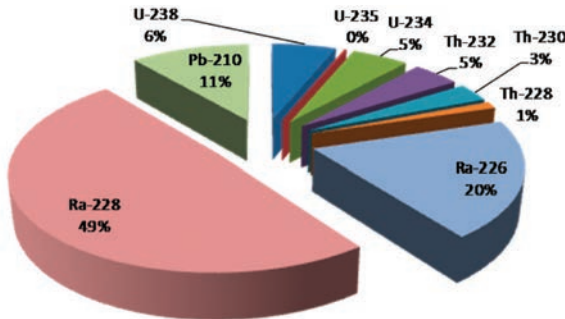


FIG. 2. Percentage distribution of activity concentrations of analysed radionuclides.

TABLE 1. AVERAGE ACTIVITY CONCENTRATIONS OF ANALYSED RADIONUCLIDES, DURING THE MONTHS OF FEBRUARY, JUNE AND SEPTEMBER

Month	Activity concentration averages (in Bq/kg)									N
	<sup>238</sup> U	<sup>235</sup> U	<sup>234</sup> U	<sup>232</sup> Th	<sup>230</sup> Th	<sup>228</sup> Th	<sup>226</sup> Ra	<sup>228</sup> Ra	<sup>210</sup> Pb	
Feb.	0.054	0.002	0.062	0.045	0.028	0.008	0.283	0.646	0.040	6
Jun.	0.088	0.003	0.062	0.026	0.030	0.012	0.103	0.194	0.100	8
Sept.	0.028	0.001	0.025	0.044	0.031	0.013	0.171	0.550	0.173	7
Average	0.057	0.002	0.050	0.041	0.030	0.011	0.186	0.464	0.104	21

H0 = monthly averages are statistically identical

H1 = monthly averages are statistically different.

### 3. RESULTS AND DISCUSSIONS

#### 3.1. Activity concentrations

The average values of the activity concentrations of analysed radionuclide in the cubera snapper fish, collected along the coast of Ceará, Brazil, during the months of February, June and September, are expressed in Table 1, and depicted in Fig. 1.

The percentage distributions of the monthly averages for each radionuclide can be visualized in Fig. 2.

#### 3.2. Statistical analysis of data

The results of ANOVA for temporal assessment are expressed in Table 2. Significant differences were identified between the months for the radionuclides <sup>228</sup>Ra and including <sup>210</sup>Pb. No statistically significant differences were identified between the other radionuclides analysed (<sup>238</sup>U, <sup>235</sup>U, <sup>234</sup>U, <sup>232</sup>Th, <sup>230</sup>Th, <sup>228</sup>Th and <sup>226</sup>Ra) for studied months.

To check the differences of the activity concentrations between the three months for <sup>228</sup>Ra and <sup>210</sup>Pb, Student's t-test was applied. In these additional tests, for the months of February, June and September, activity concentrations of <sup>228</sup>Ra were different. In this case, the values of February and September were greater than the activity concentrations of June. The results of Student's t-test for <sup>228</sup>Ra can be seen in Table 3.

On the contrary, for <sup>210</sup>Pb, all the months showed different activity concentrations; an increase of activity concentration could be observed over the year. Thus,

TABLE 2. RESULTS OF THE ANALYSIS OF VARIANCE FOR TEMPORAL EVALUATION

Radionuclide	F calc	P	F tab	Decision
<sup>238</sup> U	1.79	0.19	3.55	H0 accepted
<sup>235</sup> U	0.95	0.44	3.55	H0 accepted
<sup>234</sup> U	1.40	0.27	3.55	H0 accepted
<sup>232</sup> Th	1.22	0.31	3.55	H0 accepted
<sup>230</sup> Th	0.12	0.88	3.55	H0 accepted
<sup>228</sup> Th	0.54	0.58	3.55	H0 accepted
<sup>226</sup> Ra	1.54	0.25	3.55	H0 accepted
<sup>228</sup> Ra	6.34*	0.008	3.55	H0 rejected
<sup>210</sup> Pb	10.9*	0.0007	3.55	H0 rejected

\* Significant difference at 5%

TABLE 3. STUDENT'S T-TEST TO EVALUATE THE DIFFERENCE BETWEEN THE MONTHS STUDIED FOR <sup>228</sup>Ra

Contrast	t cal	t tab	P	Decision
February and June	3.11*	1.78	0.004	H0 rejected
February and September	0.38	1.79	0.35	H0 accepted
June and September	3.6*	1.77	0.0016	H0 rejected

\* Significant difference at 5%

TABLE 4. STUDENT'S T-TEST TO EVALUATE THE DIFFERENCE BETWEEN THE MONTHS STUDIED FOR <sup>210</sup>Pb

Contrast	t cal	t tab	P	Decision
February and June	2.74*	1.78	0.009	H0 rejected
February and September	3.75*	1.79	0.001	H0 rejected
June and September	2.89*	1.77	0.006	H0 rejected

\* Significant difference at 5%

the lowest activity concentration occurred in February, and the highest in September. The results of Student's t-test for  $^{210}\text{Pb}$  can be seen in Table 4.

The behaviour of the two Ra isotopes was different. Thus, when  $^{228}\text{Ra}$  showed temporal variation,  $^{226}\text{Ra}$  did not. This fact is difficult to explain, since they are isotopes of the same chemical element and should thus behave the same way in the fish. Activity concentrations recorded in this work are similar for both isotopes (magnitude of the order of a tenth of Bq/kg), but reflect differences in mass in the order of thousands (in mass, these activity concentrations for  $^{226}\text{Ra}$  are in the order of  $10^{-10}$  g/kg and for  $^{228}\text{Ra}$  in order of  $10^{-13}$  g/kg). Perhaps this difference in mass can justify the difference in behaviour between the isotopes.

#### 4. CONCLUSION

Temporal variations were not identified in the biological accumulation of the radionuclides  $^{238}\text{U}$ ,  $^{235}\text{U}$ ,  $^{234}\text{U}$ ,  $^{232}\text{Th}$ ,  $^{230}\text{Th}$ ,  $^{228}\text{Th}$  and  $^{226}\text{Ra}$ . For these radionuclides, the time of the year in which the collection occurred did not interfere with biological accumulation. On the contrary,  $^{228}\text{Ra}$  and  $^{210}\text{Pb}$  showed differences of accumulation correlated with the time of collection. For  $^{228}\text{Ra}$ , the month of June showed the lowest activity concentrations and the months of February and September showed equal activity concentrations, such concentrations being higher than in June. Hence, the activity concentrations of  $^{228}\text{Ra}$  displayed the following temporal sequence:

(February = September) > June

For  $^{210}\text{Pb}$ , the situation was different. Activity concentrations increased throughout the year. The activity concentration of February was less than that of June, which in turn was less than that of September. Hence, the activity concentrations of  $^{210}\text{Pb}$  displayed the following temporal sequence:

February < June < September.

Finally, the temporal component proved to have no importance for the radioecology of the radionuclides  $^{238}\text{U}$ ,  $^{235}\text{U}$ ,  $^{234}\text{U}$ ,  $^{232}\text{Th}$ ,  $^{230}\text{Th}$ ,  $^{228}\text{Th}$  and  $^{226}\text{Ra}$  in the cubera snapper fish from the coast of Ceará, Brazil. The isotopes of uranium and thorium displayed a homogeneous accumulation during the year. The same occurred with  $^{226}\text{Ra}$ .

For  $^{228}\text{Ra}$  and  $^{210}\text{Pb}$ , the situation was different, showing temporal variation in biological accumulation. Temporal variations are indications of possible seasonal variations. However, the way the sampling had been carried out did not allow the identification of seasonal variation. For such analysis, collections over a longer period of time should be performed.

## REFERENCES

- [1] PEREIRA, W.S., Distribuição corpórea de polônio-210 em três espécies de peixes da Baía de Sepetiba, Monografia de especialização em biologia marinha, Universidade Federal Fluminense (1995) 62.
- [2] PEREIRA, W.S., Alguns aspectos da bioacumulação de Polônio-210 e Chumbo-210 em *Macrodon ancylodon* (Block & Schenneider, 1864), M.Sc Dissertation, Universidade Federal Fluminense (1999) 124.
- [3] PEREIRA, W.S., Cálculo de dose como ferramenta de radioproteção ambiental, PhD Thesis, Universidade Federal Fluminense (2010) 265.
- [4] PENTREATH, R.J., Radionuclides in marine fish, *Oceanogr. Mar. Biol. A. Rev.* **15** (1977) 365–460.
- [5] ANCELLIN, J., AVARGUÈ, M., BVAR, P., GUYÉGUÉNID, P., VILQUIN, A., “Aspects biologiques et physico-chimiques de la contamination radioactive d’espèces et de sédiments marins”, *Radioactive Contamination of the Marine Environment (Proc. Int. Conf. Seattle, 1972)*, IAEA, Vienna (1973) 225–242.
- [6] ODUM, E.P., *Ecologia*, 1st edn, Guanabara. Rio de Janeiro (1986) 433.
- [7] MARGALEF, R., *Ecologia*, 1st edn, Omega, Barcelona (1982) 951.
- [8] PARFENOV, Y.D., Polonium-210 in the environment and in the human organism, *At. Energy Rev.* **12** 1 (1974) 75–143.
- [9] CHERRY, R.D. & SHANNON, L.V., The alpha radioactivity of marine organisms, *At. Energy Rev.* **12** 1 (1974) 3–45.
- [10] GOUVEA, R.C., SANTOS, P.L., Contribution to the study of radioactivity in marine organism: dosage of  $^{210}\text{Po}$  in *Perna perna*, *L. Sci. Total Environ.* **61** (1987) 117–120.
- [11] SHANNON, L.V., Oceanic circulation deduced from plastic drift cards, *Div. Sea Fish. S. Afr. Inv. Rep.* **100** (1973) 34–45.
- [12] LOVE, R.M., *The chemical biology of fishes*, Academic Press, London (1970) 547.
- [13] DAVIS, J.J., “Cesium and its relationship to potassium in ecology”, *Radioecology (SCHULTZ, V., KLEMENT, A.W., Eds)*, Reinhold, New York (1963) 539–556.
- [14] RENFRO, W.C., FOSTER, W., OSTERBERG, C.L., “Seasonal and aerial distributions of radionuclides in the biota of the Columbia River Estuary”, *The Columbia River Estuary and Adjacent Waters: Bioenvironmental Studies (PRUTER, A.T., ALVERSON, D.L., Eds)*, University of Washington Press, Seattle (1972) 777–798.
- [15] PEARCY, W.G., OSTERBERG, C.L., Zinc-65 and manganese-54 in albacore *Thunnus alalunga* from the west coast of North America, *Limnol. Oceanogr.* **13** (1968) 490–498.
- [16] INTERNATIONAL UNION FOR CONSERVATION OF NATURE AND NATURAL RESOURCES., IUCN Red List of Threatened Species. Version 2010.1., <http://www.iucnredlist.org/apps/redlist/>, accessed on January, 5, 2010.
- [17] GODOY, J.M., LAURIA, D.C., GODOY, M.L.P., CUNHA, R., Development of a sequential method for determination of  $^{238}\text{U}$ ,  $^{234}\text{U}$ ,  $^{232}\text{Th}$ ,  $^{230}\text{Th}$ ,  $^{228}\text{Th}$ ,  $^{228}\text{Ra}$ ,  $^{226}\text{Ra}$  and  $^{210}\text{Pb}$  in environmental samples, *J. Radioanal. Nucl. Chem.* **182** 1 (1994) 165–169.

# INTER AND INTRA BASIN SCALE TRANSPORT OF $^{137}\text{CS}$ IN THE PACIFIC OCEAN

M. AOYAMA<sup>a</sup>, M. FUKASAWA<sup>b</sup>, Y. HAMAJIMA<sup>c</sup>, K. HIROSE<sup>d</sup>,  
T. KAWANO<sup>b</sup>, H. NAKANO<sup>e</sup>, P.P. POVINEC<sup>f</sup>, J.A. SANCHEZ-CABEZA<sup>g</sup>,  
D. TSUMUNE<sup>h</sup>

<sup>a</sup> Geochemical Research Department,  
Meteorological Research Institute,  
Tsukuba, Japan

<sup>b</sup> Research Institute for Global Change,  
Japan Agency for Marine-Earth Science and Technology,  
Yokosuka, Japan

<sup>c</sup> Low-Level Radioactivity Laboratory,  
Institute of Nature and Environmental Technology,  
Kanazawa University,  
Nomi, Japan

<sup>d</sup> Faculty of Science and Technology,  
Sphia University,  
Chiyoda-ku, Japan

<sup>e</sup> Oceanographic Research Department,  
Meteorological Research Institute,  
Tsukuba, Japan

<sup>f</sup> Faculty of Mathematics, Physics and Informatics,  
Comenius University,  
Bratislava, Slovakia

<sup>g</sup> Institut de Ciència i Tecnologia Ambientals,  
and Departament de Física,  
Universitat Autònoma de Barcelona,  
Bellaterra, Spain

<sup>h</sup> Environmental Research Laboratory,  
Central Research Institute of Electric Power Industry,  
Abiko, Japan

## Abstract

The anthropogenic radionuclides, such as  $^{137}\text{Cs}$ ,  $^{90}\text{Sr}$ , and some of the transuranic nuclides, are important tracers of transport and biogeochemical processes in the ocean.  $^{137}\text{Cs}$ , a major fission product present in a dissolved form in seawater, is a good tracer of oceanic circulation on a time scale of several decades. In the Pacific Ocean, 7 cruises were conducted and the 3-D distribution of  $^{137}\text{Cs}$  concentration in the 2000's was observed. Two types of ocean general circulation models were also used to conduct hindcasts of the  $^{137}\text{Cs}$  concentration. Both results allowed the drawing of a detailed picture of the  $^{137}\text{Cs}$  3-D structure. The deposition of  $^{137}\text{Cs}$  mainly occurred in the northern subtropical gyre of the North Pacific Ocean and was later transported into the ocean interior, and a core structure of  $^{137}\text{Cs}$  was found along the Central Mode Water. After crossing the Equator,  $^{137}\text{Cs}$  spreads to the South Pacific through the Ekman transports at the surface.

## 1. INTRODUCTION

The main sources of anthropogenic radionuclides to the world oceans are fall-out from atmospheric nuclear weapon testing, releases from nuclear fuel reprocessing plants and the Chernobyl accident in 1986 [1–4]. The artificial radionuclides,  $^{137}\text{Cs}$ ,  $^{239,240}\text{Pu}$ , other transuranic nuclides and  $^{90}\text{Sr}$  have been studied in the marine environment because (i)  $^{137}\text{Cs}$  and  $^{90}\text{Sr}$ , conservative in sea water, are the most abundant anthropogenic radionuclides and, among these, the main contributors to biological exposure, and (ii) the very long lived  $^{239,240}\text{Pu}$ , non-conservative in sea water, is the most abundant transuranic one. Anthropogenic radionuclides such as  $^3\text{H}$  and  $^{137}\text{Cs}$  have also been used as tracers for oceanographic purposes for a long time [5–12] because they are present in a dissolved form in seawater and they are good tracers of oceanic circulation at a time scale of a few to several decades.

In this paper, we present the 3-D distribution of  $^{137}\text{Cs}$  concentration in 2002–2008 in the Pacific Ocean, based on the results from 7 oceanographic campaigns. We also present results of hindcasts of the  $^{137}\text{Cs}$  concentration by 2 types of ocean general circulation models (OGCM).

## 2. SAMPLING AND METHODS

### 2.1. Sampling

During seven cruises conducted in the Pacific Ocean in the 2000's (Fig. 1) seawater samples were collected [13–17]. Surface and water column samples were collected at 126 stations with sampling spacing of around 300–500 km. Surface water (around 20–80 L) was collected 5 m below the ocean surface by a pumping system.

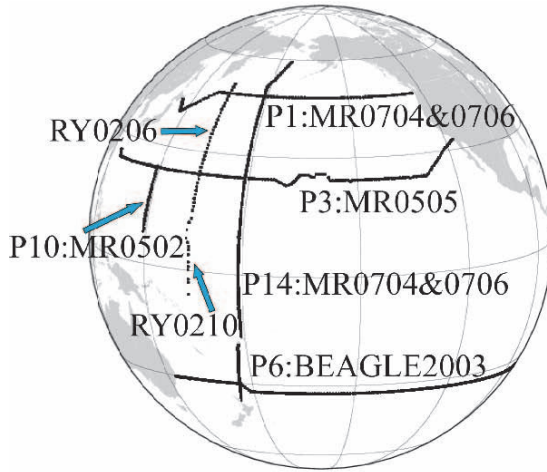


FIG. 1. Cruises in the 2000's in the Pacific Ocean conducted by Japan Meteorological Agency and Japan Agency for Marine-Earth Science and Technology.

Water column samples (from 5 to 20 L) were collected using a Rosette multisampling system and Niskin bottles. All water samples were basically filtered through a membrane filter (Millipore HA, 0.45  $\mu\text{m}$  pore size) immediately after sampling. Filtered water samples were acidified by adding concentrated  $\text{HNO}_3$  (40 mL conc.  $\text{HNO}_3$  for 20L seawater sample, pH  $\sim$  1.6). Then samples were transported to the Meteorological Research Institute (MRI) for sample treatment.

## 2.2. $^{137}\text{Cs}$ extraction and measurement

Recent developments in the analysis of very low  $^{137}\text{Cs}$  levels in underground laboratories have made it possible to determine  $^{137}\text{Cs}$  concentrations even in small seawater samples (5 to 10 L) with high sensitivity and precision [18–20].  $^{137}\text{Cs}$  was concentrated in seawater samples by adsorption onto AMP (ammonium phosphomolybdate) using a method described in detail elsewhere [20–23].  $^{137}\text{Cs}$  activities were determined by low level  $\gamma$ -spectrometry with high efficiency HPGe detectors in MRI and Kanazawa University.

## 3. RESULTS AND DISCUSSION

### 3.1. Three dimensional structures of $^{137}\text{Cs}$ in the Pacific Ocean

Ref. [8] describes a core structure along a pathway of the Central Mode Water at about 400 meters depth at 20°N along 165°E. In this study we found three

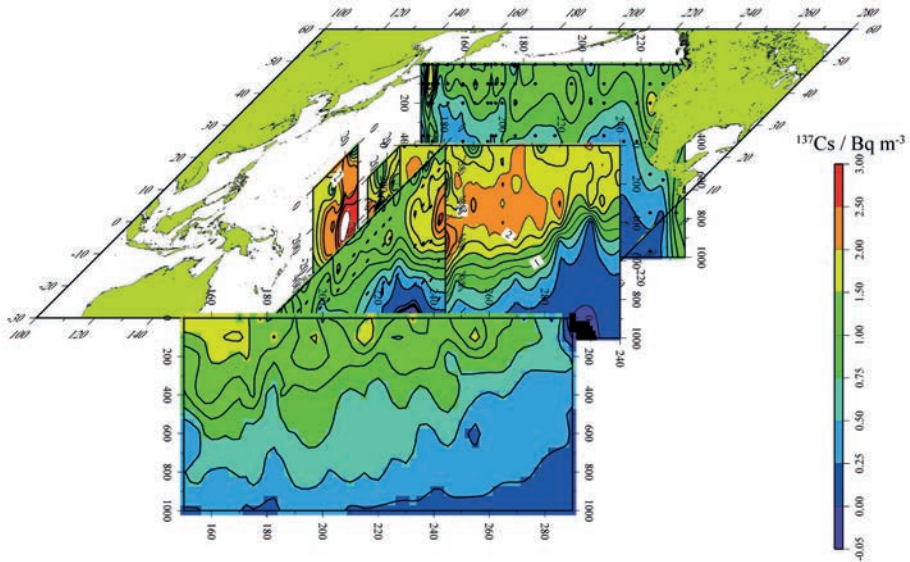


FIG. 2. Three dimensional structure of the  $^{137}\text{Cs}$  concentration in the Pacific Ocean (some portions of sections are omitted to display the main feature).

dimensional structures of  $^{137}\text{Cs}$  in the Pacific Ocean as shown in Fig. 2. A typical feature is that higher  $^{137}\text{Cs}$  levels are found within the subtropical gyre, along a density corresponding to the Central Mode Water in the North Pacific Ocean. The  $^{137}\text{Cs}$  concentrations in the equatorial region and at the subtropical gyre of the South Pacific Ocean, where lower atmospheric deposition of  $^{137}\text{Cs}$  was observed [3], were higher than that in the subpolar region in the North Pacific Ocean.

### 3.2. Meridional distribution of $^{137}\text{Cs}$ inventory along the P14 line

The meridional distribution of the  $^{137}\text{Cs}$  inventory along  $179^\circ\text{E}$ , the P14 line, observed in 2007 is shown in Fig. 3 together with its inventory. The highest  $^{137}\text{Cs}$  inventories are observed between  $20^\circ\text{N}$  and  $40^\circ\text{N}$  and the maximum inventory of  $1420 \pm 100 \text{ Bq/m}^2$  was observed at the station at  $26^\circ\text{N}$  as shown in Fig. 3. In the subpolar region, the inventory ranged from 480 to  $860 \text{ Bq/m}^2$ . In the equatorial region and subtropical gyre in the South Pacific Ocean, the inventory ranged from 490 to  $750 \text{ Bq/m}^2$ . The meridional distribution of the  $^{137}\text{Cs}$  inventory in the 1960s and 1970s showed a maximum at  $30\text{--}40^\circ\text{N}$  [24]. Therefore, the location of the maximum inventory of  $^{137}\text{Cs}$  has been shifted southwards due to the intra-basin transport into the interior of the southern part of the subtropical gyre of the North Pacific [8, 25].

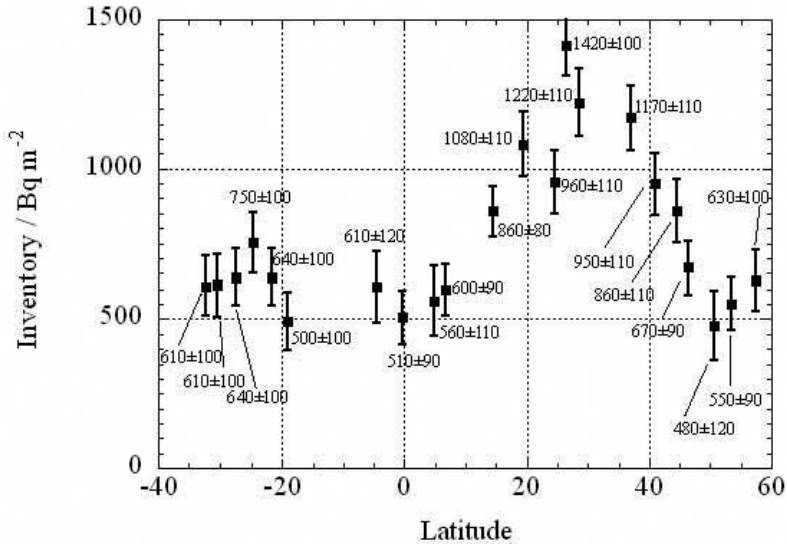


FIG. 3. Meridional distribution of  $^{137}\text{Cs}$  inventory from surface to 1000 m depth along  $179^\circ\text{E}$ , WOCE P14 line, in 2007.

### 3.3. Comparison with model simulations

We used 2 types of OCGMs to conduct hindcasts of the  $^{137}\text{Cs}$  concentrations. Both models allowed the drawing of detailed pictures of the 3-D distribution and intra and inter basin scale transport process in the Pacific Ocean.  $^{137}\text{Cs}$ , which was mainly deposited in the western part of the subtropical gyre, was transported into the ocean interior, where we observed a core structure associated with the Central Mode Water (Fig. 2).

To study intra and inter basin scale transport, a hindcast of the  $^{137}\text{Cs}$  concentration in seawater has been conducted using a  $0.5^\circ \times 1^\circ$  OGCM [25]. A significant amount of  $^{137}\text{Cs}$  concentration appears in the subtropical gyre in the South Pacific, BEAGLE2003 line in Fig. 2 even though the source of  $^{137}\text{Cs}$  was limited to the Northern Hemisphere [26]. In the previous study using the Lagrangian approach [25] we already revealed that the  $^{137}\text{Cs}$  concentration in the South Pacific water is brought by the current that enters the equator through the interior pathway and the Mindanao Current from the subtropical gyre of the North Pacific. The water then flows along the Equatorial Undercurrent, and spreads to the South Pacific through the Ekman transports at the surface. We can also see a weak signal of this pathway, which is represented by relatively high  $^{137}\text{Cs}$  concentrations, at shallower layers just north and south of the equator along the P14 line (Fig. 2).

Another model study [12] focused on global scale transport. The model simulation results suggest that the deposited  $^{137}\text{Cs}$  in the North Pacific advected to the South Pacific and Indian Ocean, and then to the South Atlantic over about four decades. The model estimated the transport rates between each basin and their temporal change. The North Pacific is an important source area of the  $^{137}\text{Cs}$  to other oceans. The inventory of the North Pacific decreased and inventories of other oceans increased.

#### 4. CONCLUSIONS

A three dimensional structure of the  $^{137}\text{Cs}$  concentration during the 2000's in the Pacific Ocean from the surface to 1000 m water depth was depicted based on 7 cruises. The main features obtained in this study are the southward transport of the deposited  $^{137}\text{Cs}$  into the interior of the subtropical gyre in the North Pacific, which forms a basic meridional distribution of the  $^{137}\text{Cs}$  inventory, as well as the cross equator transport which was simulated and analysed by the OGCM model simulations.

#### ACKNOWLEDGEMENTS

The authors thank the Captains and the crew of both the R/V Ryofu-maru and the R/V Mirai. The authors also thank the researchers of the Japan Meteorological Agency, the Japan Agency for Marine-Earth Science and Technology and Marine Works Japan, Ltd., for their help with sample collection during the seven cruises. This work was supported by a grant from the Ministry of Education, Culture, Sports, Science and Technology (MEXT) of Japan. This work was also partly supported by a MEXT Grant-in-Aid for Science Research (KAKENHI 18310017). The authors thank S. Ishikawa and T. Kudo for their help in drawing the figures.

#### REFERENCES

- [1] UNITED NATIONS, "ANNEX C: Exposures to the public from man-made sources of radiation", Sources and Effects of Ionizing Radiation (Report to the General Assembly, with Scientific Annexes I), Vol. 1, United Nations Scientific Committee on the Effects of Atomic Radiation (UNSCEAR), United Nations, Vienna (2000) 158–291.
- [2] AARKROG, A., et al., A comparison of doses from  $^{137}\text{Cs}$  and  $^{210}\text{Po}$  in marine food: A major international study, *J. Environ. Radioact.* **34** 1 (1997) 69–90.
- [3] AOYAMA, M., et al., Re-construction and updating our understanding on the global weapons tests  $^{137}\text{Cs}$  fallout, *J. Environ. Monit.* **8** (2006) 431–438.
- [4] AARKROG, A., Input of anthropogenic radionuclides into the World Ocean, *Deep Sea Res. II* **50** (2003) 2597–2606.

- [5] FINE, R.A., Direct evidence using tritium data for through-flow from the Pacific into the Indian Ocean, *Nature* **315** (1985) 478–480.
- [6] FINE, R.A., et al., The penetration of tritium into the tropical Pacific, *Journal of Phys. Oceanogr.* **17** (1987) 553–564.
- [7] FINE, R.A., et al., The western equatorial Pacific: A water mass crossroads, *J. Geophys. Res.* **99** C12 (1994) 25063–25080.
- [8] AOYAMA, M., et al., Water masses labeled with global fallout  $^{137}\text{Cs}$  formed by subduction in the North Pacific, *Geophys. Res. Lett.* **35** (2008) L01604.
- [9] FOLSOM, T.R., “Some measurements of global fallout suggesting characteristics of the N. Pacific controlling dispersal rates of certain surface pollutants”, *Isotope Marine Chemistry*, (GOLDBERG, E.D., HORIBE, Y., SARUHASHI, K., Eds.), Uchida Rokkakuho, Tokyo (1980) 51–117.
- [10] LIVINGSTON, H.D., POVINEC, P.P., A millennium perspective on the contribution of global fallout radionuclides to ocean science, *Health Phys.* **82** (2002) 656–668.
- [11] TSUMUNE, D., et al., Behavior of  $^{137}\text{Cs}$  concentrations in the North Pacific in an ocean general circulation model, *J. Geophys. Res.* **108** (2003) 3262.
- [12] TSUMUNE, D., et al., Transport of  $^{137}\text{Cs}$  into the Southern Hemisphere in an Ocean General Circulation Model, *Prog. Oceanog.* **89** (2011) 38–48.
- [13] UCHIDA, H., FUKASAWA, M. (Eds), WHP P6, A10, I3/I4 REVISIT DATA BOOK Blue Earth Global Expedition 2003 vols 1, 2, JAMSTEC, Yokosuka (2005).
- [14] KUMAMOTO, Y., WATANABE, S. (Eds), WHP P6, A10, I3/I4 REVISIT DATA BOOK Blue Earth Global Expedition 2003, vol. 3, JAMSTEC, Yokosuka (2007).
- [15] KAWANO, T., UCHIDA, H. (Eds), WHP P10 REVISIT DATA BOOK Field Activity of JAMSTEC towards International Repeat Hydrography and Carbon Program, JAMSTEC, Yokosuka (2007).
- [16] KAWANO, T., UCHIDA, H. (Eds), WHP P03 REVISIT DATA BOOK Field Activity of JAMSTEC towards International Repeat Hydrography and Carbon Program, JAMSTEC, Yokosuka (2007).
- [17] KAWANO, T., UCHIDA, H., DOI, T., (Eds), WHP P01, P14 REVISIT DATA BOOK Field Activity of JAMSTEC towards International Repeat Hydrography and Carbon Program, JAMSTEC, Yokosuka (2009).
- [18] POVINEC, P.P., et al., IAEA-MEL’s underground counting laboratory in Monaco — background characteristics of HPGe detectors with anti-cosmic shielding, *Appl. Radiat. Isot.* **61** (2004) 85–93.
- [19] HIROSE, K., et al., Extremely low background measurements of  $^{137}\text{Cs}$  in seawater samples using an underground facility (Ogoya), *J. Radioanal. Nucl. Chem.* **263** (2005) 349–353.
- [20] AOYAMA, M., HIROSE, K., “Radiometric determination of anthropogenic radionuclides in seawater”, *Analysis of Environmental Radionuclides, Radioactivity in the Environment*, Vol. 2 (POVINEC, P.P., Ed.), Elsevier, Amsterdam (2008) 137–162.
- [21] AOYAMA, M., et al., Low level  $^{137}\text{Cs}$  measurements in deep seawater samples, *Appl. Radiat. Isot.* **53** (2000) 159–162.

- [22] LA ROSA, J.J., et al., Separation of actinides, cesium and strontium from marine samples using extraction chromatography and sorbents, *J. Radioanal. Nucl. Chem.* **248** 3 (2001) 765–770.
- [23] LEVY, I., et al., Marine anthropogenic radiotracers in the Southern Hemisphere: new sampling and analytical strategies, *Prog. Oceanogr.* (2011).
- [24] AOYAMA, M., HIROSE, K., Temporal variation of  $^{137}\text{Cs}$  water column inventory in the North Pacific since the 1960s, *J. Environ. Radioactivity* **69** 1–2 (2003) 107–117.
- [25] NAKANO, H., et al., Analysis of  $^{137}\text{Cs}$  concentration in the Pacific using a Lagrangian approach, *J. Geophys. Res.* **115** (2010) C06015.
- [26] AOYAMA, M., et al., Cross equator transport of  $^{137}\text{Cs}$  from North Pacific Ocean to South Pacific Ocean (BEAGLE2003 cruises), *Prog. Oceanogr.* **89** (2011) 7–16.

## CHAIRPERSONS OF SESSIONS

Session 1	H. GRASSL	Germany
	B. MAYER	Canada
Poster session 1	L. GOURCY	France
	J. LANGMAN	USA
Workshop 1	P.P. POVINEC	Slovakia
	A. WAGENER	Brazil
Session 2	C. BALLENTINE	United Kingdom
	C.G. SKILBECK	Australia
Poster session 2	C. VOSS	USA
	K. BUESSELER	USA
Workshop 2	J.A. SANCHEZ-CABEZA	Spain
	F. CARVALHO	Portugal
Session 3	H. NIES	IAEA
	W. PLASTINO	Italy
Poster Session 3	W. MOORE	USA
	D. PITTAUEROVÁ	Germany
Workshop 3	K. HIROSE	Japan
	R. DELFANTI	Italy
Session 4	P. CARREIRA	Portugal
	D. MARTINEZ	Argentina
Workshop 4	G. DARLING	United Kingdom
	R. PURCHERT	Switzerland
	J. FAMIGLIETTI	USA
	N. STURCHIO	USA
Young scientists poster awards	J. LANGMAN	USA
Session 5	F. LONGSTAFFE	Canada
	R. MICHEL	Germany

## ADVISORY COMMITTEE

H.S.H. PRINCE ALBERT II	Honorary President, Monaco
D. ALLEMAND	Scientific Director, Centre scientifique de Monaco (CSM), Monaco
F. BRIAND	Director General, Mediterranean Science Commission (CIESM), Monaco
W. BURKART	IAEA
R. CALCAGNO	Director, Institut Océanographique, Fondation Albert 1er, Monaco
B. FAUTRIER	Vice-President, Fondation Prince Albert II, Monaco
A. MARATOS	Vice Admiral, President, International Hydrographic Bureau (IHB), Monaco
D. MOHAMAD	Deputy Director General, IAEA
F. QUEVEDO	Director, International Centre for Theoretical Physics (ICTP), Trieste
P. RAMPAL	President, Centre Scientifique de Monaco (CSM), Monaco
A. STEINER	Executive Director, United Nations Environment Programme (UNEP), Nairobi
P. VAN KLAVEREN	Ambassador, Permanent Representative to Scientific, Environmental and Humanitarian International Bodies, Monaco
W. WATSON-WRIGHT	Assistant Director General, Executive Secretary, Intergovernmental Oceanographic Commission of UNESCO (IOC/UNESCO), Paris

## **SECRETARIAT OF SYMPOSIUM**

H. NIES	Scientific Secretary
B. NEWMAN	Scientific Secretary
L. ARAGUÁS ARAGUÁS	Scientific Secretary
M. KHAELSS	Symposium Organizer
M. NEUHOLD	Symposium Organizer
L. BARILARO-HAMONIC	Administrative Support
F. CHAHINE	Administrative Support
J. LE NORMAND	Administrative Support

## **SCIENTIFIC ORGANISING COMMITTEE**

H. NIES	IAEA
B. NEWMAN	IAEA
M. BETTI	IAEA
L. ARAGUÁS ARAGUÁS	IAEA
P.K. AGGARWAL	IAEA



## LIST OF PARTICIPANTS

### ALGERIA

Hocini, N. Centre de Recherche Nucleaire d'Alger  
02, Bd Frantz-Fanon  
P.O. Box: 399  
Alger 16000  
Fax: +213 21 43 42 80  
Email: nadiahocini@yahoo.fr

### ARGENTINA

Bocanegra de Botto, E. Universidad Nacional de Mar del Plata,  
Centro de Geología de Costas y del Cuaternario,  
Calle Funes 3250,  
7600 Mar del Plata,  
Fax: +54 223 475 3150  
Email: emilia.bocanegra@gmail.com

Martinez, D.E. Universidad Nacional del Mar del Plata,  
Instituto de Geología de Costas y del Cuaternario,  
Dean Funes 3350,  
Mar del Plata,  
Provincial de Buenos Aires,  
Email: demarti@mdp.edu.ar

Rodriguez, L. Centro de Estudios Hidro-Ambientales,  
Facultad de Ingeniería y Ciencias Hidricas,  
Ciudad Universitaria CC 217,  
Ruta Nacional 167 km 472.4,  
3000 Santa Fe  
Fax: +54 3424575224  
Email: leticia@fich1.unl.edu.ar

Zabala, M. Instituto de Hidrología de Llanuras,  
República de Italia 780,  
Azul 7300,  
Buenos Aires,  
Email: mzabala@faa.unicen.edu.ar

## AUSTRALIA

Dogramaci, S. Rio Tinto IRON ORE,  
182 St Georges Terrace, Level 9,  
Perth 6000  
Fax: +61 0893665760,  
Email: shawan.dogramaci@riotinto.com

Skilbeck, C. University of Technology Sydney,  
1 Broadway Ultimo,  
P.O. Box: 123,  
Sydney 2007,  
New South Wales  
Fax: +61 295141656  
Email: g.skilbeck@uts.edu.au

Skrzypek, G. The University of Western Australia/John  
de Laeter,  
Centre of Mass Spectrometrypre,  
35 Stirling Highway,  
P.O. Box: MO90,  
Crawley 6009,  
Western Australia  
Fax: +61 8 64887925  
Email: grzegorz.skrzypek@uwa.edu.au

Szymczak, R. Tradewinds (Australia),  
205/4–6 Boorima Place,  
Cronulla 2230,  
NSW  
Email: ron.szymczak@bigpond.com

## AUSTRIA

Kralik, M. Environment Agency Austria,  
Spittelauer Laende 5,  
1090 Vienna  
Email: martin.kralik@umweltbundesamt.at

Leis, A. Joanneum Research Forschungsgesellschaft m.b.H.,  
Institute of Hydrogeology & Geothermics,  
Elisabethstraße 16/11,



- Gastmans, D. Universidade Estadual Paulista,  
Av. 24A, 1515 – Bela Vista,  
Rio Claro (SP) 13506–900  
Fax: +55 19 3532 5119  
Email: gastmans@rc.unesp.br
- Lacerda, L. Instituto de Ciências do Mar – UFC,  
Av. Abolição 3207,  
Fortaleza 60.165–081,  
Ceará  
Fax: +55 8533667014  
Email: ldrude@pq.cnpq.br
- Pereira, W.S. Brazilian Nuclear Industries  
and Federal Fluminense University,  
Pocos Road – Andradas km 20,6,  
PO Box 961,  
CEP 37.701–000 Centro,  
Pocos de Caldas  
Fax: +55 3521073111  
Email: wspereira@inb.gov.br
- Pessenda, L.C.R. Centre for Nuclear Energy in Agriculture,  
Avenida Centenario, 303,  
Piracicaba, Sao Paulo 13416–000  
Fax: +55 19 34294610  
Email: figueira@cena.usp.br
- Sifeddine, A. IRD,  
Rua São João batista. S/N. centro,  
Niteroi 24020–007  
Email: abdel.sifeddine@ird.fr
- Souza, T. Pontifícia Universidade Católica do Rio de Janeiro,  
Marquês de São Vicente, 225 Gávea,  
Rio de Janeiro 22451–900,  
Email: abreu.thaisa@gmail.com
- Wagener, A. Pontifícia Universidade Católica do Rio de Janeiro,  
Rua Marques de São Vicente 225,  
Rio de Janeiro 22453–900

Fax: +55 2135271637  
Email: angela@puc-rio.br

Wanderley, C.

Pontifícia Universidade Católica do Rio de Janeiro,  
Marques de São Vicente, 225 Gávea,  
Rio de Janeiro 22451-900  
Email: cristiana.daw@gmail.com

## **CAMEROON**

Ketchemen-Tandia, B.

University of Douala,  
Faculty of Science, Department of Health Sciences,  
POB 2701  
Email: beatrice\_tandia@yahoo.fr

## **CANADA**

Gunter, B.

G BACH Enterprises Incorporated,  
Edmonton, Alberta  
Email: Bill.Gunter@albertainnovates.ca

Jasechko, S.

University of Waterloo,  
3-4476 Markham St.,  
Alberta Innovates – Technology Futures, VITP,  
Victoria V8Z7X8,  
British Columbia  
Email: sjasechk@uwaterloo.ca

Longstaffe, F.

Department of Earth Sciences,  
The University of Western Ontario,  
London N6A 5B7,  
Ontario  
Fax: +1 5196613198  
Email: flongsta@uwo.ca

Mayer, B.

University of Calgary; Faculty of Science,  
Department of Geology and Geophysics,  
2500 University Drive, NW,  
Calgary, Alberta T2N 1N4  
Fax: +1 403 220 8514  
Email: bmayer@ucalgary.ca

Pourtangestani, K. University of Ontario Institute of Technology,  
2000 Simcoe Street North,  
Oshawa L1H7K4  
Fax: +1 9057643448  
Email: kathy.tangesir@gmail.com

Whiticar, M. School of Earth and Ocean Sciences,  
University of Victoria,  
Centre for Ocean, Earth and Atmospheric Sciences,  
PO Box 3065 STN CSC,  
Victoria, BC V8W 3V6  
Fax: +1 250 721 6200  
Email: whiticar@uvic.ca

## **CHILE**

Aguirre Dueñas, E. Comisión Chilena de Energía Nuclear,  
Centro de Estudios Nucleares La Reina,  
Departamento de Aplicaciones Nucleares,  
Laboratorio de Isótopos Ambientales,  
Amunategui No. 95,  
Casilla 188-D,  
Santiago  
Fax: +56 2 4702570  
Email: eaguirre@cchen.cl

## **CHINA**

Pang, Z. Inst. of Geology and Geophysics,  
19 Beituchengxilu,  
Beijing 100029  
Fax: +86 10 62010846  
Email: z.pang@mail.iggcas.ac.cn

Yu, W. Third Institute of Oceanography, SOA,  
184#, Daxue Road,  
Xiamen City 361005  
Fax: +86 5922195262  
Email: yuwen2001@gmail.com

## **COLOMBIA**

Betancur Vargas, T.

Universidad de Antioquia,  
Carrera 66 N0. 37–18. Apto 101,  
Medellin  
Fax: +57 42195514  
Email: hidrologiasubterranea@gmail.com

## **COSTA RICA**

Agudelo Arango, C.

SENARA – Servicio Nacional de Aguas Subterráneas,  
Riego y Avenamiento,  
Calle Blancos, Goicochea,  
San José 5262–1000  
Fax: +506 22228785  
Email: lagudelo@senara.go.cr

Matamoros Arguedas, R.

SENARA – Servicio Nacional de Aguas Subterráneas,  
Riego y Avenamiento,  
Calle Blancos, Goicochea,  
San José 5262–1000  
Fax: +506 22228785  
Email: raphagmat@gmail.com

## **CROATIA**

Cukrov, N.

Rudjer Boskovic Institute,  
Bijenicka 54,  
Zagreb 10000  
Fax: +385 14680231  
Email: ncukrov@irb.hr

Pavicic-Hamer, D.

Rudjer Boskovic Institute,  
G. Paliaga 5,  
52210 Rovinj  
Fax: +385 52 813496,  
Email: pavicic-hamer@cim.irb.hr

Roller-Lutz, Z.

University of Rijeka, School of Medicine,  
Brace Branchetta 20,  
Rijeka HR 51 000  
Fax: +385 51 651 124  
Email: roller@medri.hr

## **CUBA**

Alonso-Hernandez, C.

Centro de Estudios Ambientales de Cienfuegos,  
AP5,  
Cienfuegos 59350  
Fax: +53 46965146  
Email: carlos@ceac.cu

Diaz Asencio, M.

Center of Environmental Studies,  
Carretera Castillo de Jagua Km 1,5,  
Ciudad Nuclear, Cienfuegos,  
CP 59350, AP5  
Email: misael@ceac.cu

## **DEMOCRATIC REPUBLIC OF THE CONGO**

Ndembo, L.J.

Commissariat General a L'Energie Atomique,  
Centre Regional d'Etudes Nucleaires de Kinshasa,  
Campus de l'Universite de Kinshasa,  
B.P. 868 Kinshasa 11  
Email: jndelongo@yahoo.fr

## **DENMARK**

Hou, X.

Risø National Laboratory for Sustainable Energy,  
Technical University of Denmark,  
P.O. Box 49,  
Roskilde 4000  
Email: xiho@risoe.dtu.dk

## **ECUADOR**

Carrion Mero, P.C.

Escuela Superior Politecnica del Litoral,  
Km. 30.5 Vía Perimetral. Campus Gustavo Galindo,  
Guayaquil 09-01-5863

Fax: +593 42 269412  
Email: pcarrion@espol.edu.ec

## **EGYPT**

Nada, A. Egyptian Atomic Energy Authority,  
National Centre for Nuclear Safety  
and Radiation Control,  
3 Ahmed El-Zomor Street, Nasr City,  
Cairo  
Fax: +20 2 2740238  
Email: nada\_abdelhamid@yahoo.com

## **ETHIOPIA**

Admasu, G. Ministry of Water Resources,  
Haile G/Silassie Avenue,  
PO Box 5744  
Addis Ababa  
Email: nadewgira@yahoo.com

Gebreegziabher, M. Addis Ababa University, Faculty of Sciences,  
Department of Earth Sciences,  
P.O. Box: 124477,  
Addis Ababa  
Fax: +251 111 239 462  
Email: meregebre@gmail.com

## **FINLAND**

Sonninen, E. University of Helsinki,  
Gustaf Hällströmin katu 2,  
P.O. Box: 64,  
Helsinki FI-00014  
Fax: +358 919150741  
Email: eloni.sonninen@helsinki.fi

## **FRANCE**

Barats, A. LRSAE-ICN Univ. de Nice Sophia Antipolis,  
28 avenue de Valrose,  
Bâtiment Fizeau,

Nice CEDEX 2 06108  
Fax: +33 492076367  
Email: aurelie.barats@unice.fr

Barci, V. LRSAE (Laboratoire Radiochimie Sciences,  
Analytiques Environnement),  
28 avenue Valrose,  
Nice 06108  
Fax: +33 492076364  
Email: barci@unice.fr

Barci-Funel, G. LRSAE Universite de Nice-Sophia Antipolis,  
Faculte des Sciences,  
28 avenue Valrose,  
Nice 06108 CEDEX 2  
Fax: +33 492076364  
Email: gbarci@unice.fr

Beriot, M. LRSAE Université de Nice-Sophia Antipolis,  
Faculté des Sciences,  
28 avenue Valrose,  
Nice 06108 CEDEX 2  
Fax: +33 492076364  
Email: gbarci@unice.fr

Bombard, A. Triskem International,  
campus de Ker Lann,  
Parc de Lormandiere Bat C, rue Maryse Bastie,  
Bruz 35170  
Fax: +33 299050727  
Email: abombard@triskem.fr

Brambilla, E. Geosciences Montpellier-Bat 22-CC60,  
Université Montpellier 2  
34095 Montpellier CEDEX 5  
Email: Elena.Brambilla@gm.univ-montp2.fr

Bustamante, P. University of La Rochelle,  
2 rue Olympes de Gouges,  
La Rochelle 17000  
Fax: +33 546458264  
Email: pbustama@univ-lr.fr

- Charmasson, S. Institut de Radioprotection et de Sûreté Nucléaire,  
(IRSN),  
IRSN DEI/SESURE, Centre IFREMER,  
B.P. 330,  
83507 La Seyne Sur Mer CEDEX  
Fax: +33 4 94 30 44 16  
Email: sabine.charmasson@ifremer.fr
- Delattre, H. CEREGE, Aix-Marseille Université, CNRS, IRD,  
Europôle méditerranéen de l'Arbois,  
P.O. Box: 80,  
13545 Aix En Provence  
Email: delattre@cerege.fr
- Duffa, C. Institut de Radioprotection et de Sûreté Nucléaire,  
(IRSN),  
IRSN DEI/SESURE, Centre IFREMER,  
BP 330,  
83507 La Seyne Sur Mer CEDEX  
Fax: +33 4 94 30 44 16  
Email: celine.duffa@irsn.fr
- Gillon, M. Université d'Avignon et de pays de Vaucluse,  
UMR INRA-UAPV EMMAH,  
33 rue Louis Pasteur,  
Avignon 84000  
Email: marina.gillon@univ-avignon.fr
- Giniaux, J. Institut Polytechnique LaSalle Beauvais,  
19 rue Pierre Waguët,  
60000 Beauvais  
Email: jeanne.giniaux@etu.lasalle-beauvais.fr
- Gourcy, L. BRGM,  
3 avenue C. Guillemin,  
P.O. Box: 36060,  
Orleans CEDEX 2 45060  
Fax: +33 238643446  
Email: l.gourcy@brgm.fr
- Hadj Ammar, F. Centre Européen de Recherche et d'Enseignement de  
Géosciences de l'Environnement (CEREGE),

Aix en Provence  
Fax: +216 74 677 425  
Email: friha22@yahoo.fr

Hamelin, B. Centre Européen de Recherche et d'Enseignement de  
Géosciences de l'Environnement,  
Plateau d'Arbois,  
P.O. Box: 80,  
Aix En Provence 13545  
Email: hamelin@cerege.fr

Huneau, F. Université de Bordeaux, UFR des Sciences  
de la Terre et de la Mer,  
avenue des Facultes,  
P.O. Box: B18,  
Talence 33405  
Email: frederic.huneau@u-bordeaux1.fr

Jaunat, J. Institut Egid Université de Bordeaux,  
1 allée Daguin,  
Pessac CEDEX 33607  
Fax: +33 557121001  
Email: jessy.jaunat@egid.u-bordeaux3.fr

Lahr, M. Université de Nice,  
28, avenue Valrose,  
Batiment Fizeau,  
Nice CEDEX 2 06108  
Email: mirandalahr@gmail.com

Michel, H. LRSAE,  
28 avenue Valrose,  
Nice 06108  
Email: hmicHEL@unice.fr

Mounier, L. Thermo Fisher Scientific,  
16 avenue du Québec,  
Villebon sur Yvette,  
P.O. Box: Silic 765,  
91963 Courtaboeuf  
Email: lionnel.mounier@thermofisher.com

- Obrecht, D. CANBERRA,  
1 rue des Hérons,  
Saint Quentin En Yvelines 78182  
Fax: +33139485780  
Email: daniel.obrecht@canberra.com
- Patris, N. IRD-Hydro Sciences Montpellier,  
Maison des Sciences de l'eau-HSM,  
Universite Montpellier 2, Case MSE,  
34095 Montpellier CEDEX 05  
Fax: +33 4 67144774  
Email: npatris@msem.univ-montp2.fr
- Petersen, J. Centre Européen de Recherche et d'Enseignement de  
Géosciences de l'Environnement (CEREGE),  
Avenue Louis Philibert,  
P.O. Box: 80,  
Aix En Provence CEDEX 04 13545  
Email: petersen@cerege.fr
- Philippini, V. Universite de Nice,  
28, avenue Valrose,  
Batiment Fizeau,  
Nice CEDEX 2 06108  
Email: violaine.philippini@unice.fr
- Thébault, H. Institut de Radioprotection et de Surete Nucleaire,  
BP 330,  
La Seyne Sur Mer 83507  
Fax: +33 494304416  
Email: herve.thebault@ifremer.fr
- Travi, Y. University Avignon,  
33 rue Pasteur,  
Avignon 84000  
Fax: +33 4 90144489  
Email: yves.travi@univ-avignon.fr
- Troche, M. Institut Polytechnique LaSalle Beauvais,  
19 rue Pierre Waguët,  
60000 Beauvais  
Email: mylene.troche@etu.lasalle-beauvais.fr

Vallet-Coulomb, C. Centre Européen de Recherche et d'Enseignement de  
Géosciences de l'Environnement,  
Europôle méditerranéen de l'Arbois,  
P.O. Box: 80,  
Aix En Provence 13545  
Email: vallet@cerege.fr

## GERMANY

Aeschbach-Hertig, W. Institute of Environmental Physics, University  
of Heidelberg,  
Im Neuenheimer Feld 229,  
Heidelberg 69120,  
Email: aeschbach@iup.uni-heidelberg.de

Assonov, S. Institut for Geology and Mineralogy,  
University of Köln,  
Zuelpicher Strasse 49a,  
Koeln 50674  
Email: assonov\_sergey@yahoo.com

Eichinger, F. Hydroisotop GmbH,  
Woelkestr. 9,  
Schweitenkirchen 85301  
Email: fe@hydroisotop.de

Emeis, K. ZMAW, University of Hamburg,  
Bundesstr. 55,  
Hamburg 20146  
Fax: +49 40428386347  
Email: kay.emeis@zmaw.de

Frey, S. Albert Ludwigs University of Freiburg,  
Institute of Hydrology,  
Fahnenbergplatz,  
Freiburg 79098  
Fax: +49 761 203 3594  
Email: simon.frey@boku.ac.at

Grassl, H. Max-Planck-Institut für Meteorologie  
Bundesstraße 55, 15 Stock,



- Reichel, Thomas  
Institute of Environmental Physics,  
Im Neuenheimer Feld 229,  
Heidelberg 69120  
Baden Württemberg  
Fax: +49 6221 54-64 05  
Email: Thomas.Reichel@iup.uni-heidelberg.de
- Ritterbusch, F.  
Kirchhoff-Institute for Physics,  
University Heidelberg,  
Im Neuenheimer Feld 227,  
Heidelberg 69120  
Email: florian.ritterbusch@kip.uni-heidelberg.de
- Rosner, M.  
BAM Federal Institute for Materials Research  
and Testing  
Department I. Analytical chemistry;  
reference materials,  
Division I.5 Bioanalytics,  
Unter den Eichen 87,  
12205 Berlin  
Fax: +49 30 8104 3527  
Email: martin.rosner@bam.de
- Sültenfuß, J.  
University of Bremen,  
Otto Hahn-Allee,  
Bremen 28359  
Fax: +49 4212189862152  
Email: suelten@uni-bremen.de
- Theobald, N.  
Federal Maritime and Hydrographie Agency (BSH),  
Bernhard-Nacht-Str. 78,  
20359 Hamburg  
Fax: +49 4031905030  
Email: norbert.theobald@bsh.de
- Voropaev, A.  
Hydroisotop GmbH,  
Woelkestrasse 9,  
85276 Pfaffenhofen  
Fax: +49 8444 928929  
Email: AV@hydroisotop.de

Weigelt-Krenz, S. Federal Maritime and Hydrographic Agency,  
Wuestland 2,  
22589 Hamburg  
Fax: +49 4031905033  
Email: sieglinde.weigelt@bsh.de

Welte, J. Kirchhoff Institute for Physics,  
INF 227,  
Heidelberg 69120  
Fax: +49 6221545179  
Email: welte@kip.uni-heidelberg.de

## **GHANA**

Ganyaglo, S. National Nuclear Research Institute,  
Ghana Atomic Energy Commission,  
Kwabanya,  
P.O. Box: LG 80, Legon-Accra,  
Accra  
Email: sganyaglo@yahoo.co.uk

## **GREECE**

Evangeliou, N. NCSR Demokritos Institute of Nuclear  
Technology-Radiation Protection/Environmental,  
Radioactivity Laboratory,  
Patriarhou Grigoriou Street,  
P.O. Box: 60228,  
Agia Paraskevi, Attiki 15310  
Fax: +30 2106503050  
Email: nevag@ipta.demokritos.gr

Salamalikis, V. University of Patras,  
Department of Physics,  
Laboratory of Atmospheric Physics,  
Patras 26500  
Fax: +30 2610997989  
Email: vsalamalik@upatras.gr

## **GUATEMALA**

Carrillo-Ovalle, H.

Universidad de San Carlos de Guatemala,  
4 calle "A" 1-43 zona 3,  
01003 Guatemala  
Email: leocarri1@yahoo.com

## **HUNGARY**

Babka, B.

Institute of Bio and Environmental Energetics,  
Centre for Agricultural  
and Applied Economic Sciences,  
Egyetem ter 1,  
4032 Debrecen  
Email: babkabea@gmail.com

Janovics, R.

Institute of Nuclear Research  
of the Hungarian Academy of Sciences,  
H-4026 Debrecen, Bem tér 18/c,  
Debrecen  
Email: janovics@atomki.hu

## **INDIA**

Satpathy K.K.

Indira Gandhi Centre for Atomic Research (IGCAR),  
Kalpakkam 603102,  
TamilNadu  
Fax: +91 4427480235  
Email: satpathy@igcar.gov.in

Shive P.R.

National Institute of Hydrology,  
Jal Vigyan Bhawan, IIT Roorkee Campus,  
Roorkee 247 667, Uttarakhand State  
Fax: +91 1332 276414  
Email: spr@nih.ernet.in,  
shive\_prakash@rediffmail.com

## **INDONESIA**

Syahril, S.

Permanent Mission of the Republic  
of Indonesia in Vienna,  
Gustav Tschermakgasse 5-7,



Autamish, J. Ministry of Environment,  
Basra-Al Suneana  
Email: [sadiqjassim05@yahoo.com](mailto:sadiqjassim05@yahoo.com)

## **ISRAEL**

Avrahamov, N. Ben Gurion University of the Negev,  
Beer Sheva 84105  
Email: [katzavn@bgu.ac.il](mailto:katzavn@bgu.ac.il)

Sivan, O. Department of Geological & Environmental Sciences,  
Ben Gurion University of the Negev,  
Beer Sheva 84105  
Email: [oritsi@bgu.ac.il](mailto:oritsi@bgu.ac.il)

## **ITALY**

Adorni-Braccesi, A. Istituto di Geoscienze e Georisorse – CNR,  
Via Moruzzi, 1,  
Pisa 56124  
Email: [a.adorni@igg.cnr.it](mailto:a.adorni@igg.cnr.it)

Allais, E. Laboratorio isotopica ISO4 s.n.c.,  
Via Valperga Caluso 35,  
Torino 10125  
Fax: +39 011655027  
Email: [iso4.dst@unito.it](mailto:iso4.dst@unito.it)

Baneschi, I. Institute of Geosciences and Earth Resources  
(IGG–CNR),  
Moruzzi,1,  
Pisa 56124  
Fax: +39 0503152322  
Email: [i.baneschi@igg.cnr.it](mailto:i.baneschi@igg.cnr.it)

Brattich, E. University of Bologna,  
Environmental Chemistry and Radioactivity Lab,  
Via F. Selmi 2,  
40126 Bologna  
Fax: +39 51 2099456  
Email: [erika.brattich@studio.unibo.it](mailto:erika.brattich@studio.unibo.it)

- Delconte, C.A. National Research Council – Institute of Geosciences  
and Earth Resources,  
Via Ferrata, 1,  
27100 Pavia  
Fax: +39 0382985887  
Email: delconte@crystal.unipv.it
- Delfanti, R. Ente per le Nuove Tecnologie, l’Energia  
e l’Ambiente (ENEA),  
Centro Ricerche Ambiente Marino ‘Santa Teresa’,  
Pozzuolo di Lerici,  
P.O. Box 224,  
19100 La Spezia  
Fax: +39 187 978273  
Email: roberta.delfanti@enea.it
- Gherardi, F. Institute of Geosciences and Earth Resources  
(IGG–CNR),  
Via G.Moruzzi, 1,  
Pisa 56124,  
Email: f.gherardi@igg.cnr.it
- Magro, G. Institute of Geosciences and Earth Resources  
(IGG–CNR),  
Area della Ricerca, via Moruzzi 1,  
Pisa 56100  
Email: g.magro@igg.cnr.it
- Pennisi, M. CNR Istituto di Geoscienze e Georisorse,  
Area della Ricerca, via Moruzzi 1,  
Pisa 56124  
ITALY  
Fax: +39 503152360  
Email: m.pennisi@igg.cnr.it
- Plastino, W. Department of Physics,  
University of Roma Tre,  
Via della Vasca Navale, 84,  
Rome 00146  
Fax: +39 657337102  
Email: plastino@fis.uniroma3.it

Re, V. University Ca' Foscari of Venice,  
Department of Environmental Sciences,  
Dorsoduro-Calle Larga Santa Marta 2137,  
Venice 30123  
Email: re@unive.it

Sacchi, E. Dipartimento di Scienze della Terra,  
Università di Pavia,  
Via Ferrata 1,  
Pavia 27100  
Fax: +39 382985890  
Email: elisa.sacchi@unipv.it

## **JAPAN**

Aoyama, M. Meteorological Research Institute,  
Nagamine 1-1,  
Tsukuba 305-0052  
Fax: +81 29 85 8728  
Email: maoyama@mri-jma.go.jp

Hirose, K. Sophia University,  
Galleria Vert 1115, B57 Gaiku 1,  
Katoridai,  
Tsukuba 300-2655  
Ibaraki  
Email: hirose45037@mail2.accsnet.ne.jp

Ichiyangi, K. Kumamoto University,  
2-39-1 Kurokami,  
Kumamoto 860-8555  
Email: kimpei@sci.kumamoto-u.ac.jp

Tanoue, M. University of Kumamoto,  
5-18-13, Kurokami,  
Kumamoto 860-8555  
Email: masamasa\_tanotano@yahoo.co.jp

## **KENYA**

Kalambuka, H. Applied Nuclear and Radiation Physics Group,  
Department of Physics, University of Nairobi,

Chiromo Lane,  
P.O. Box: 30197,  
Nairobi 00100  
Fax: +254 204449616  
Email: hkalambuka@uonbi.ac.ke

## **KOREA, REPUBLIC OF**

Lee, Sang-Han

Korea Research Institute of Standards and Science,  
1 Doryong-Dong, Yuseoung-Gu,  
Daejeon 305-340,  
Fax: +82 428685671  
Email: s.lee@kriss.re.kr

## **LITHUANIA**

Lujanienė, G.

SRI Center for Physical Sciences and Technology,  
Savanorių 231,  
Vilnius LT-02300,  
Fax: +370 5 2602317  
Email: lujanienė@ar.fi.lt

## **MALAYSIA**

Yii, Mei-Wo

Malaysian Nuclear Agency,  
Block 23,  
43000 Kajang,  
Fax: +603 892 829 77  
Email: yii@nuclearmalaysia.gov.my

## **MEXICO**

Cortés, A.

Instituto de Geofísica, UNAM,  
Circuito Exterior, Ciudad Universitaria,  
Delegación, Coyoacán,  
Mexico, D.F. 04510  
Fax: +52 55 56224198  
Email: tuzacortésilva@gmail.com

Ruiz Fernández, A.

Universidad Nacional Autónoma de México,  
Calz. J. Montes Camarena s/n,  
P.O. Box: 811,

Mazatlan 82000,  
Sinaloa  
Fax: +52 6699826133  
Email: caro@ola.icmyl.unam.mx

## **MONACO**

Tremblay, P. Centre Scientifique de Monaco,  
Avenue Saint-Martin,  
MC-98000,  
Monaco  
Email: ptremblay@centrescientifique.mc

## **MOROCCO**

Bouchaou, L. Universite Ibn Zohr,  
Laboratoire de Geologie Appliquee  
et Geo-Environnement (LAGAGE),  
Faculte de Sciences,  
B.P. 8106,  
Cite Dakhla,  
80000 Agadir  
Fax: +212 528220100  
Email: lbouchaou@yahoo.fr

Fekri, A. Université Hassan II Mohammedia,  
Faculté des Sciences Ben M'Sik,  
Blvd. Commandant Driss Harti,  
B.P.7955,  
20700 Casablanca,  
Fax: +212 522704675  
Email: ahmfekri@menara.ma

Marah, H. Centre Nationale de l'Energie, des Sciences et  
Techniques Nucléaires (CNESTEN),  
Avenue Mohamed V,  
P.O. Box: 1382,  
Rabat 10001  
Fax: +212 537803317  
Email: marah@cnesten.org.ma

Tagma, T.

Ibn Zohr University,  
P.O. Box 8106, Hay Dakhla,  
Agadir 80060  
Fax: +212 5 28 22 01 00  
Email: tariktagma@yahoo.fr

## **NETHERLANDS**

Poelmann, J.W.

Picarro Inc,  
Bezuidenhoutseweg 454,  
Den Haag 2594 BE  
Email: jpoelmann@picarro.com

## **NEW ZEALAND**

Morgenstern, U.G.

GNS Science,  
1 Fairway Drive,  
5010 Lower Hutt,  
Fax: +64 45704600  
Email: u.morgenstern@gns.cri.nz

## **NIGERIA**

Oburo, P.

Nigeria Hydrological Services Agency,  
Federal Ministry of Water Resources,  
Plot 222, Shettima Ali Monguno Crescent Opp.,  
Julius Berger Corporate Head Office,  
Utako District, Abuja,  
Email: poburo@yahoo.com

Shamonda, J.A.

Nigeria Hydrological Services Agency,  
Federal Ministry of Water Resources,  
Plot 222, Shettima Ali Monguno Crescent Opp.,  
Julius Berger Corporate Head Office,  
Utako District, Abuja  
Email: jashamo@hotmail.com

Sikoki, F.D.

University of Port Harcourt,  
Department of Animal and Environmental Biology,  
Fisheries and Hydrobiology Research Unit,  
P.O. Box 5323,

Port Harcourt  
Email: sikokifrancis@yahoo.com

## **NORWAY**

Gwynn, J. Norwegian Radiation Protection Authority,  
Fram Centre,  
Tromsø 9296,  
Email: justin.gwynn@nrpa.no

Holm, E. Norwegian Radiation Protection Authority,  
Grini Næringspark 13,  
P.O. Box: 55,  
Østerås 1332  
Fax: +47 67147407  
Email: elis.holm@nrpa.no

## **PERU**

Gutierrez, D. Instituto del Mar del Perú (IMARPE),  
Esquina Gamarra y General Valle S/N Chucuito,  
Apartado Postal 22,  
El Callao  
Email: dgutierrez@imarpe.gob.pe

Salvatteci, R. Instituto del Mar del Perú (IMARPE),  
Esquina Gamarra y General Valle s/n,  
Callao,  
Email: renato.salvatteci@ird.fr

## **PHILIPPINES**

Castaneda, S. Philippine Nuclear Research Institute (PNRI),  
Commonwealth Avenue, Diliman,  
P.O. Box 213,  
Quezon City 1101,  
Fax: +63 2 9201646  
Email: sscastaneda@pnri.dost.gov.ph

## **PORTUGAL**

- Carreira, P. Instituto Tecnológico e Nuclear,  
Estrada Nacional nº10,  
Sacavém 2686–953 Sacavém  
Fax: +351 219946185  
Email: carreira@int.pt
- Carvalho, F. Nuclear and Technological Institute,  
Fax: +351 219941995  
Email: carvalho@itn.pt
- Eggenkamp, H. Centro de Petrologia e Geoquímica,  
Instituto Superior Técnico,  
Av. Rovisco Pais,  
Lisboa 1049–001  
Fax: +351 21 840 0806  
Email: hermanus.eggenkamp@ist.utl.pt
- Marques, J. Centro de Petrologia e Geoquímica,  
Instituto Superior Técnico,  
Av. Rovisco Pais,  
Lisboa 1049–001  
Fax: +351 218400806  
Email: jose.marques@ist.utl.pt

## **QATAR**

- Al-Qaradawi, I. Qatar University / Qatar Foundation,  
P.O. Box 3304,  
Doha  
Fax: +974 44690779  
Email: ilham@qu.edu.qa

## **ROMANIA**

- Oprea, C.D. Regional Centre for Education,  
11, Mihai Eminescu Street,  
Oradea,  
Bihor  
Fax: +40 259 470222  
Email: coprea2007@yahoo.co.uk

Patrascu, V. Grigore Antipa National Institute for Marine  
Research and Development,  
Blvd Mamaia, No 300,  
900581 Constanta  
Fax: +40 241 831274  
Email: office@alpha.rmri.ro

Varlam, C. Institute of Cryogenics and Isotopic Technologies,  
Uzinei street, no.4, PO Raureni, Box 7,  
Rm. Valcea 240050  
Fax: +40 250732746  
Email: cvarlam@icsi.ro

## **SLOVAKIA**

Povinec, Pavel Comenius University  
Mlynska dolina F1  
Bratislava SK-84248  
Fax: +421 265 425 882  
Email: povinec@fmph.uniba.sk

Rozvadaska, I. Ustav radiacnej ochrany s.r.o.,  
Stanicna 1062/24,  
911 05 Trencin,  
Fax: +421 326401947  
Email: uro@uro.sk

## **SLOVENIA**

Ferjan, T. Geological Survey of Slovenia,  
Dimiceva ulica 14,  
Ljubljana 1109  
Email: tamara.ferjan@geo-zs.si

Kovacic, K. Jozef Stefan Institute,  
Jamova 39,  
Ljubljana 1000  
Email: katarina.kovacic@ijs.si

Kozar-Logar, J. Jozef Stefan Institute,  
Jamova cesta 39,  
1000 Ljubljana

Fax: +386 1 251 93 85  
Email: jasmina.logar@ijs.si

Mali, N. Geological Survey of Slovenia,  
Dimiceva 14,  
1000 Ljubljana  
Fax: +386 1 2809 753  
Email: nina.mali@geo-zs.si

Mezga, K. Geological Survey of Slovenia,  
Dimiceva ulica 14,  
Ljubljana 1000  
Fax: +386 1 2809753  
Email: kim.mezga@geo-zs.si

Torkar, A. Department of Geology,  
University of Ljubljana,  
Privoz 11,  
Ljubljana 1000  
Email: anja.torkar@ntf.uni-lj.si

Urbanc, J. Geological Survey of Slovenia,  
Dimiceva 14,  
Ljubljana 1000  
Fax: +386 1 2809753  
Email: janko.urbanc@geo-zs.si

Zavadlav, S. Jozef Stefan Institute,  
Jamova 39,  
Ljubljana 1000  
Fax: +386 1 5885346  
Email: sasa.zavadlav@ijs.si

## **SOUTH AFRICA**

Bezuidenhout, J. Stellenbosch University,  
Department of Physics (Mil),  
Private Bag X2,  
Saldanha 7395  
Fax: +27 22 702 3060  
Email: Jab@ma2.sun.ac.za

Makgale, L.

National Nuclear Regulator,  
Witch Hazel Avenue, EcoGlades Office Park,  
EcoGlades 2, Block 6,  
Centurion 0169  
Fax: +27 126747103  
Email: lmmakgale@nnr.co.za

## SPAIN

Bolivar Raya, J.P.

Universidad de Huelva,  
Department of Applied Physics,  
Campus El Carmen,  
21071 Huelva  
Fax: +34 959219777  
Email: bolivar@uhu.es

Dueñas Buey, M.C.

University of Málaga.  
Campus Teatinos.  
Málaga 29071  
Fax: +34 952131920  
Email: mcduenas@uma.es

Fernández Jimenez, M.

University of Málaga,  
Campus Teatinos,  
Málaga 29071,  
Fax: +34 952131920  
Email: mafeji@uma.es

Gordo Puertas, Elisa

Universidad de Malaga, Facultad de Ciencias,  
Campus de Teatinos,  
Málaga 29071  
Fax: +34 952131920  
Email: elisagp@uma.es

Hierro, A.

University of Huelva,  
Department of Applied Physics,  
Campus El Carmen,  
21071 Huelva  
Fax: +34 959219777  
Email: almudena.hierro@dfa.uhu.es

Rodriguez-Arevalo, J. Centro de Estudios y Experimentacion de Obras,  
Publicas (CEDEX),  
Alfonso XII, 3 y 5,  
28014 Madrid  
Fax: +34 913 357267  
Email: jra@cedex.es

Sanchez-Cabeza, J.-A. Universitat Autonoma de Barcelona,  
Physics Department,  
Edifici Cc,  
Bellaterra 08193  
Email: joanalbert.sanchez@uab.cat

## **SUDAN**

Elamin, G.M. Ministry of Science and Technology,  
Sudan Atomic Energy Commission (SAEC),  
El Gammaa Street,  
P.O. Box 3001,  
Khartoum 11111  
Fax: +249 183 25 39 42  
Email: Ghadghuda98@hotmail.com

## **SWEDEN**

Aldahan, A. Uppsala University,  
Department of Earth Sciences,  
Villav. 16,  
752 36 Uppsala  
Email: ala.aldahan@geo.uu.se

Chawchai, S. Stockholm University,  
Department of Geological Sciences,  
Stockholm 10691  
Email: sakonvan.chawchai@geo.su.se

## **SWITZERLAND**

Balderer, W. ETH Zurich, Geological Institute,  
Engineering, Geology  
Sonneggstrasse 5,

Zurich 8092  
Email: balderer@erdw.ethz.ch

Bals, A. PICARRO,  
48 ch sous caran,  
1245 collonge Bellerive.  
Geneva  
Email: abals@picarro.com

Corcho Alvarado, J. Institute of Radiation Physics,  
Rue du Grand-Pré 1,  
Lausanne 1007  
Fax: +41 213148299  
Email: Jose-Antonio.Corcho-Alvarado@chuv.ch

Fritz, J. ETH Zurich,  
Geological Institute,  
Engineering Geology,  
Sonneggstrasse 5,  
8092 Zurich  
Email: julia.fritz@erdw.ethz.ch

Gschwend, M. ETH Zurich,  
Geological Institute,  
Engineering Geology,  
Sonneggstrasse 5,  
8092 Zurich  
Email: maurog@ethz.ch

Leuenberger, F. ETH Zurich,  
Geological Institute,  
Engineering Geology,  
Sonneggstrasse 5,  
8092 Zurich  
Email: fanny.leuenberger@erdw.ethz.ch

Purtschert, R. University of Bern,  
Sidlerstrasse 5,  
Bern 3012,  
Email: purtschert@climate.unibe.ch

Schotterer, U.

University of Bern,  
Physics Institute,  
Sidlerstrasse 5,  
Bern 3012  
Email: schotterer@climate.unibe.ch

## **THAILAND**

Laoharajanaphand, S.

Thailand Institute of Nuclear Technology (TINT),  
9/9 Moo7, Tambol Saimoon, Amphur Ongkharak,  
Nakornnayok 26120  
Fax: +66 25620121  
Email: sirinart@tint.or.th

## **THE FORMER YUGOSLAV REPUBLIC OF MACEDONIA**

Anovska-Jovcheva, E.

Ss. Cyril and Methodius University,  
Faculty of Technology and Metallurgy,  
Department of Physics,  
Rudjer Boskovic 16  
91000 Skopje  
Fax: +389 23065389  
Email: anovski@tmf.ukim.edu.mk

Anovski, T.

Ss. Cyril and Methodius University,  
Faculty of Technology and Metallurgy,  
Department of Physics,  
Rudjer Boskovic 16,  
91000 Skopje  
Fax: +389 23065389  
Email: anovski@tmf.ukim.edu.mk

## **TUNISIA**

Ben Hamouda, M.F.

Centre National des Sciences et Technologies  
Nucléaires (CNSTN),  
Technopak,  
Sidi Thabet, 2020  
Fax: +216 71537555  
Email: f\_benhamouda@yahoo.fr

Zouari, K. National School of Engineers,  
Laboratory of Radioanalysis and Environment,  
Route de soukra Km 4 Sfax,  
P.O. Box: 1173  
Sfax 3038  
Fax: +216 74677425  
Email: Kamel.Zouari@enis.rnu.tn

## **TURKEY**

Aközcan, S. Kırklareli University,  
Faculty of Science and Letters,  
Department of Physics,  
Campus of Kavaklı,  
Kırklareli 39160  
Fax: +90 2882461733  
Email: sakozcan35@yahoo.com

Aydin, H. Yuzuncu Yil University,  
Department of Environmental Engineering,  
Van, 65080  
Fax: +90 4322251732  
Email: harun@yyu.edu.tr

Bayari, C. Hacettepe University,  
Dept. of Geological Engineering,  
Hydrogeological Eng. Section,  
Beytepe,  
Ankara 06800  
Email: serdar@hacettepe.edu.tr

Ozyurt, N. Hacettepe University,  
Dept. of Geological Engineering,  
Hydrogeological Eng. Section,  
Beytepe,  
Ankara 06800  
Email: nozyurt@hacettepe.edu.tr

## **UKRAINE**

Gulin, S. Institute of Biology of the Southern Seas,  
2, Nakhimov Av.,

Sevastopol 99011  
Fax: +380 692241581  
Email: s.gulin@ibss.org.ua

Laptev, G.

Ukrainian Hydrometeorological Institute (UHMI),  
37, Prospekt Nauki,  
Kiev 03028  
Fax: +380 44 5255363  
Email: glaptev@uhmi.org.ua

## **UNITED ARAB EMIRATES**

Murad, A.

UAE University,  
PO Box 17551,  
Al-Ain,  
Fax: +971 50 6496162  
Email: ahmed.murad@uaeu.ac.ae

## **UNITED KINGDOM**

Ballentine, C.

University of Manchester,  
School of Earth, Atmospheric  
and Environmental Sciences,  
Williamson Building,  
Oxford Road,  
Manchester M13 9PL  
Fax: +44 161 306 9361  
Email: chris.ballentine@manchester.ac.uk

Darling, W.

British Geological Survey,  
Maclean Building,  
Wallingford,  
Oxfordshire OX10 8 BB  
Fax: +44 1491 692345  
Email: g.darling@bgs.ac.uk

Goody, D.

British Geological Survey,  
Wallingford,  
Oxfordshire OX10 8BB  
Fax: +44 1491 692345  
Email: dcg@bgs.ac.uk

Lindahl, P.J. University of Plymouth,  
School of Geography,  
Earth and Environmental Sciences,  
Drake Circus,  
Plymouth PL4 8AA  
Fax: +44 1752 584110  
Email: patric.lindahl@plymouth.ac.uk

#### **UNITED STATES OF AMERICA**

Baer, D. Los Gatos,  
67 East Evelyn Avenue, Suite 3,  
P.O. Box: Los Gatos Research,  
Mountain View 94041-1529  
Fax: +1 650 9657074  
Email: d.baer@lgrinc.com

Buesseler, K. Woods Hole Oceanographic Institution,  
Mail Stop #25, Clark-447, WHOI,  
Woods Hole 02543  
Email: kbuesseler@whoi.edu

Famiglietti, J. University of California,  
Center for Hydrologic Modelling,  
Irvine, CA 92697-4690  
Fax: +1 949 824 3874  
Email: jfamigli@uci.edu

Fisher, N.S. Stony Brook University,  
School of Marine and Atmospheric Sciences,  
Stony Brook, NY 11794-5000  
Fax: +1 631 632 3072  
Email: nfisher@notes.cc.sunysb.edu

Hsiao, G.S.-J. Picarro Inc.,  
480 Oakmead Parkway, Sunnyvale,  
CA 94089  
Email: ghsiao@picarro.com

Izbicki, J.A. U.S. Geological Survey,  
California Water Science Center,  
4165 Spruance Road, Suite 200,

San Diego, CA 92101  
Fax: +1 619 225-6131  
Email: jaizbick@usgs.gov

Kharaka, Y. US Geological Survey (USGS),  
Water Resources Division,  
345 Middlefield Road  
Menlo Park, CA 94025  
Fax: +1 650 3293538  
Email: ykharaka@usgs.gov

Khare, A. Beta Analytic Inc.  
4985, SW 74 Court.  
Miami 33155  
Florida  
Email: ashroff@betalabservices.com

Koulikov, S. LI-COR, Inc.,  
3671 Enochs Street,  
Santa Clara 95051  
Fax: +14089920725  
Email: sergeui.koulikov@licor.com

Lagrange, K. New York Institute of Technology,  
1855 Broadway,  
New York, NY 10023-7692  
Fax: +1 212 261 1680  
Email: klagranc@nyit.edu

Lai, C.-T. San Diego State University,  
5500 Campanile Drive,  
San Diego, CA 92182-4614  
Fax: +1 619.594.5676  
Email: lai@sciences.sdsu.edu

Lane-Smith, D. Durrige Company, Inc.,  
7 Railroad Avenue, suite D,  
Bedford, MA 01730  
Fax: +1 7816870955  
Email: DLS@durrige.com

Langman, J. American University in Cairo,  
AUC Avenue,  
P.O. Box: 74,  
New Cairo  
Egypt  
Email: jlangman@aucegypt.edu

Michel, R.L. US Geological Survey (USGS),  
Water Resources Division,  
345 Middlefield Road  
Menlo Park, CA 94025  
Fax: +1 650 3295590  
Email: rlmichel@usgs.gov

Moore, W. University of South Carolina,  
701 Sumter Street,  
Columbia 29208, SC  
Fax: +18037776610  
Email: moore@geol.sc.edu

Sericano, J. Texas A&M University,  
833 Graham Rd,  
College Station, TX 77845  
Fax: +1 9798622361  
Email: jsericano@gerg.tamu.edu

Sturchio, N. University of Illinois at Chicago,  
845 West Taylor Street, MC-186,  
Chicago, IL 60607  
Email: sturchio@uic.edu

Voss, C. U.S. Geological Survey,  
431 National Center,  
Reston, VA 20192  
Fax: +1-703-648-5274  
Email: cvoss@usgs.gov

## **VENEZUELA**

Senior Galindo, W. Instituto Oceanográfico de Venezuela (IOV),  
Universidad de Oriente (UDO),  
Av. Universidad, Sector San Luis,

Cerro del Medio. Decanato del Núcleo de Sucre,  
Fax: +582 93 2002343  
Email: wsenior@cantv.net; senior.william@gmail.com

## **VIETNAM**

Vo, H. Institute for Nuclear Science and Technology,  
179 Hoang Quoc Viet, Cau Giay,  
Hanoi 04  
Fax: +84 38363295  
Email: hanhvt@yahoo.com

## **EUROPEAN COMMISSION**

Glatz, Jean-Paul European Commission, Joint Research Centre,  
Institute for Transuranium Elements,  
PO Box 2340,  
76125 Karlsruhe  
Germany  
Fax: +49 7247 951 588  
Email: jean-paul.glatz@ec.europa.eu

Hrnecek, E. European Commission, Joint Research Centre,  
Institute for Transuranium Elements,  
P.O. Box 2340,  
Karlsruhe 76125  
Germany  
Email: Erich.Hrnecek@ec.europa.eu

Hult, M. European Commission, Joint Research Centre,  
Institute for Reference Materials and Measurements,  
Retieseweg 111,  
Geel 2440  
Belgium  
Fax: +32 14584273  
Email: mikael.hult@ec.europa.eu

## **INTERNATIONAL ATOMIC ENERGY AGENCY**

Aggarwal, P.K. IAEA,  
Vienna International Centre,  
PO Box 100,

1400 Vienna  
Austria  
Email: p.aggarwal@iaea.org

Araguas Araguas, L.

IAEA,  
Vienna International Centre,  
PO Box 100,  
1400 Vienna  
Austria  
Fax: +43126007  
Email: L.Araguas@iaea.org

Boisson, F.

IAEA, Marine Environment Laboratory,  
4 Quai Antoine 1er,  
Monaco 98000  
Principality of Monaco  
Fax: +37797977273  
Email: F.Boisson@iaea.org

Bosc, E.

IAEA, Marine Environment Laboratory,  
4 Quai Antoine 1er,  
Monaco 98000  
Principality of Monaco  
Email: e.bosc@iaea.org

Casas-Zamora, J.

IAEA,  
Vienna International Centre,  
P.O. Box: 100,  
1400 Vienna  
Austria  
Email: j.casas@iaea.org

Choudhry, M.A.

IAEA,  
Vienna International Centre  
P.O. Box: 100,  
1400 Vienna  
Austria  
Fax: +43126007  
Email: m.choudhry@iaea.org

Eriksson, M.

IAEA-Marine Environment Laboratory,  
4, Quai Antoine 1er,

98000 Monaco  
Principality of Monaco  
Email: M.Eriksson@iaea.org

Gasser, B. IAEA, Marine Environment Laboratory,  
4, Quai Antoine 1er,  
98000 Monaco  
Principality of Monaco  
Email: B.Gasser@iaea.org

Gerardo-Abaya, J. IAEA,  
Vienna International Centre.  
P.O. Box: 100.  
1400 Vienna  
Austria  
Email: J.Gerardo-Abaya@iaea.org

Kurttas, T. IAEA,  
Vienna International Centre,  
P.O. Box: 100,  
1400 Vienna  
Austria  
Fax: +43126007  
Email: t.kurttas@iaea.org

Lacoue-Labarthe, T. IAEA , Marine Environment Laboratory,  
4 Quai Antoine 1er,  
Monaco 98000  
Principality of Monaco  
Email: tlacouel@gmail.com

Pham, M.K. IAEA, Marine Environment Laboratory,  
4, Quai Antoine 1er,  
98000 Monaco  
Principality of Monaco  
Fax: +37797977273  
Email: m.pham@iaea.org

Matsumoto, T. IAEA,  
Vienna International Centre,  
P.O. Box: 100,  
1400 Vienna

Austria  
Email: t.matsumoto@iaea.org

Miquel, J.-C. IAEA, Marine Environment Laboratory,  
4 Quai Antoine 1er,  
Monaco 98000  
Principality of Monaco  
Fax: +37797977273  
Email: j.c.miquel@iaea.org

Nies, H. IAEA, Marine Environment Laboratory,  
4 Quai Antoine 1er,  
Monaco 98000  
Principality of Monaco  
Fax: +43126007  
Email: H.Nies@iaea.org

Oh, J.R. IAEA, Marine Environment Laboratory,  
4 Quai Antoine 1er,  
Monaco 98000  
Principality of Monaco  
Email: j.oh@iaea.org

Osvath, I. IAEA, Marine Environment Laboratory,  
4 Quai Antoine 1er,  
Monaco 98000  
Principality of Monaco  
Email: i.osvath@iaea.org

Phaneuf, M. IAEA,  
Vienna International Centre,  
P.O. Box: 100,  
1400 Vienna  
Austria  
Email: m.phaneuf@iaea.org

Scholten, J. IAEA, Marine Environment Laboratory,  
4 Quai Antoine 1er,  
Monaco 98000  
Principality of Monaco  
Fax: +37797977273  
Email: j.scholten@iaea.org

Tolosa, I. IAEA, Marine Environment Laboratory,  
4 Quai Antoine 1er,  
Monaco 98000  
Principality of Monaco  
Email: i.tolosa@iaea.org

Vasileva, E. IAEA, Marine Environment Laboratory,  
4 Quai Antoine 1er,  
Monaco 98000  
Principality of Monaco  
Fax: +37797977273  
Email: e.vasileva\_veleva@iaea.org

**INTERGOVERNMENTAL OCEANOGRAPHIC COMMISSION –  
UNITED NATIONS EDUCATIONAL, SCIENTIFIC AND CULTURAL  
ORGANIZATION**

Reguera, B. Instituto Español de Oceanografía,  
Subida a Radiofaro 50,  
P.O. Box: Aptdo. 1552,  
Vigo 36390  
Pontevedra  
Spain  
Fax: +34 986498626  
Email: beatriz.reguera@vi.ieo.es

**UNITED NATIONS EDUCATIONAL, SCIENTIFIC AND CULTURAL  
ORGANIZATION**

Cornet, S. I3M Labo / IUT Cannes Sophia Antipollis,  
Palais Josephine,  
2 avenue General de Gaulle,  
Beausoleil 06240  
France  
Email: decleves@live.fr

**OBSERVER**

Al-Kharusi, L. Ministry of Agriculture and Fisheries Wealth,  
Marine Science and Fisheries Centre,  
PO Box 427 P.C 100,

Sultanate of Oman  
Email: lubnakharusi@hotmail.com

Alonso Rodriguez, R. Instituto de Ciencias del Mar y Limnologia (ICML),  
Universidad Nacional Autonoma de Mexico,  
Unidad Academica de Mazatlan,  
Av. Joel Montes Camarena s/n,  
Apartado Postal 811,  
82000 Mazatlan  
Mexico  
Fax: +52 669 9826133  
Email: rosalba@ola.icmyl.unam.mx

Amaya Monterrosa, O. Universidad de El Salvador; Facultad de Ciencias,  
Naturales y Matemáticas; Escuela de Física,  
Final 25 avenida norte,  
ciudad Universitaria,  
San Salvador  
El Salvador  
Fax: +503 22251500 4406  
Email: oscar.amaya@ues.edu.sv

Arneri, N. Encotech/Los Gatos,  
Via Mola 11 a,  
6900 Lugano  
Switzerland  
Email: nicoletta.arneri@encotech.ch

Bottein, M.-Y. National Ocean Service/NOAA,  
Marine Biotoxins Program  
219 Fort Johnson Road,  
Charleston 29412  
United States of America  
Fax: +1 843 762 8700  
Email: marieyasmine.bottein@noaa.gov

Briceño Guevara, S. Universidad de Costa Rica (UCR),  
Centro de Investigacion en Contaminacion  
Ambiental (CICA),  
Ciudad Universitaria Rodrigo Facio,  
San Pedro de Montes de Oca  
San José 2060

Costa Rica  
Fax: +506 22531363  
Email: subg81@gmail.com

Carrasco, D.

Universidad de Chile,  
Av Independencia 1027,  
Santiago,  
Chile  
Fax: +56 65635244  
Email: dcarrasco@med.uchile.cl

Espinosa-Díaz, L.

Instituto de Investigaciones Marinas y Costeras  
(INVEMAR),  
Carrera 2B No. 26-35, casa 3,  
Portal de Prado,  
Santa Marta  
Colombia  
Fax: +57 5 4328694  
Email: lespinosa@invemar.org.co

Fowler, S.

Villa Bobby, Marine Environment Consultancy,  
8 Allee des oranges,  
Cap d'Ail 06320  
France  
Email: s.fowler@free.fr

Garay Tinoco, J.

Instituto de Investigaciones Marinas y Costeras  
(INVEMAR),  
Cerro Punta Betin,  
Apartado Aereo 1016,  
Santa Marta  
Colombia  
Fax: +57 5 4312986  
Email: jgaray@invemar.org.co

Leclercq, A.

Université de Nice,  
Laboratoire de Radiochimie, Sciences  
et Environnement,  
Parc Valrose  
Email: Amelie.Leclercq@unice.fr

- Lucienna, E. Ministry of Environment,  
181 Haut-Turgeon,  
P.O. Box: 29260  
Port-Au-Prince  
Haiti  
Email: exillucienna@yahoo.fr
- Mayer, A. Centre national de la recherche scientifique (CNRS),  
CEREGE  
B.P. 80  
13545 Aix En Provence CEDEX 04  
France  
Email: adiano.mayer@idpa.cnr.it
- Méndez Calicchio, S. Dirección Nacional de Recursos Acuáticos,  
Constituyente 1497,  
11200 Montevideo  
Uruguay  
Fax: +598 24013216  
Email: smendez@dinara.gub.uy
- Menegon, M. Encotech Sagl,  
Via P.F. Mola 11 A,  
Lugano 9600  
Switzerland  
Email: marco.menegon@encotech.ch
- Morales Ramirez, A. Universidad de Costa Rica (UCR),  
Ciudad Universitaria Rodrigo Facio,  
San Pedro de Montes de Oca,  
San José 2060  
Costa Rica  
Fax: +506 2511 3280  
Email: alvaro.morales@ucr.ac.cr
- Moreira Gonzalez, A.R. Ministerio de Ciencia, Tecnología y Medio Ambiente,  
Centro de Estudios Ambientales de Cienfuegos,  
Carretera Castillo de Jagua Km 1.5,  
5 Cienfuegos 59350  
Fax: +53 43 965146  
Email: angel@gestion.ceac.cu

- Papucci, Carlo
- Ente per le Nuove Tecnologie, l'Energia e l'Ambiente  
(ENEA),  
Centro Ricerche Ambiente Marino  
'Santa Teresa',  
Pozzuolo di Lerici,  
P.O. Box 224,  
19100 La Spezia  
Italy  
Fax: +39 187 978213  
Email: papucci@santateresa.enea.it
- Perdomo Trujillo, L.V.
- Instituto de Investigaciones Marinas y Costeras  
(INVEMAR),  
Cerro Punta Betin,  
Apartado Aereo 1016,  
Santa Marta  
Colombia  
Fax: +57 5 4328682  
Email: laura\_perdomo@invemar.org.co
- Pérez, B.
- Intendencia de Colonia,  
Manuel de Lobo 456,  
P.O. Box: 70000,  
Colonia Del Sacramento  
Uruguay  
Fax: +598 45224709  
Email: sebepe@adinet.com.uy
- Reynaud, S.
- Centre scientifique de Monaco,  
Équipe d'écophysiologie,  
Avenue St. Martin  
Principality of Monaco  
Email: sreynaud@centrescientifique.mc
- Vammen, K.
- Universidad Nacional Autónoma de Nicaragua  
(UNAN),  
Centro de Investigación de los Recursos Acuáticos  
de Nicaragua (CIRA),  
Hosp. Monte España 300 mts al Norte,  
Apartado Postal 4598  
Managua,  
Nicaragua

Fax: +505 2 678169  
Email: kvammen@cira-unan.edu.ni

Vargas, M.

Universidad de Costa Rica (UCR),  
Ciudad Universitaria Rodrigo Facio,  
San Pedro de Montes de Oca,  
San José 2060  
Costa Rica  
Fax: 506 25113182  
Email: mvmontero@gmail.com

Villasol Nunez, A.

United Nations Environmental Programme,  
Carretera del Cristo No. 3,  
Esq. Tiscornia, Casablanca, Regla,  
La Habana  
Cuba  
Fax: +537 8669681  
Email: villasol@cimab.transnet.cu

## AUTHOR INDEX

### A

Adorni-Braccesi, A.: (2) 381  
Aeschbach-Hertig, W.: (1) 7  
Aggarwal, P.K.: (1) 203, 295, 327,  
(2) 271, 281  
Aguirre, E.: (2) 185  
Alcindor, A.: (1) 319  
Aldahan, A.: (1) 463  
Aldave de las Heras, L.: (2) 419  
Alfimov, V.: (2) 467  
Allais, E.: (1) 221, 229, 357  
Almeida, M.: (2) 501  
Alvarez, A.M.: (1) 337  
Amokrane, Y.: (1) 67  
Andreani, D.: (2) 381  
Angeyo, K.H.: (2) 335  
Anovska-Jovcheva, E.: (2) 255  
Anovski, T.: (2) 255  
Antunes da Silva, M.: (2) 63  
Aoyama, M.: (1) 89, 493, (2) 493, 571  
Araguás Araguás, L.: (1) 203, 295, 327,  
(2) 271, 281  
Aravena, R.: (2) 281  
Argiriou, A.A.: (1) 161  
Arnaud, M.: (2) 553  
Arora, M.: (1) 121  
Arvola, L.: (1) 199  
Assonov, S.S.: (1) 377  
Ayenew, T.: (2) 263

### B

Baeta, A.: (2) 501  
Balderer, W.: (1) 273, 279  
Bam, E.: (2) 215  
Barbecot, F.: (1) 67, 83  
Barišić, D.: (2) 519  
Barker, J.A.: (2) 3  
Barros, V.G.: (1) 435  
Bartocci, J.: (2) 395  
Baumann, Z.: (1) 57  
Bendassolli, J.A.: (1) 15

Ben Moussa, A.: (2) 203  
Betancur, T.: (1) 211, (2) 125  
Betti, M.: (2) 395, 419  
Bhatti, J.: (1) 25  
Bielewski, M.: (2) 419  
Bjerre, T.K.: (2) 153  
Bocanegra, E.: (2) 177, 195  
Bogdan, D.: (1) 139  
Boisson, F.: (1) 483  
Bolívar, J.P.: (1) 395  
Bologa, A.s.: (2) 443  
Bombard, A.: (1) 523  
Bombuse, D.L.: (1) 337  
Böttcher, M.E.: (1) 473  
Bouchaou, L.: (1) 303, (2) 169  
Bouchnan, R.: (1) 357  
Boutaleb, S.: (1) 303, (2) 169  
Bramha, S.N.: (1) 501  
Brattich, E.: (1) 387  
Breier, R.: (1) 295  
Brenčić, M.: (1) 153, (2) 19  
Brenninkmeijer, C.A.M.: (1) 377  
Brizmohun, R.: (1) 311  
Buso Jr, A.A.: (1) 15  
Bustamante, P.: (2) 485

### C

Campisi, L.: (1) 473  
Cañete, S.: (1) 409  
Carlos, R.: (2) 419  
Carreira, P.M.: (2) 63  
Carreira, R.S.: (2) 501  
Carrera, J.: (2) 195  
Carrión, P.: (2) 291  
Carvalho, F.P.: (1) 451, (2) 427  
Carvalho, M.R.: (2) 63  
Carvalho, Z.L.: (1) 443, (2) 309  
Castaño, S.: (1) 171  
Caurant, F.: (2) 485  
Celle-Jeanton, H.: (2) 235  
Chamizo, E.: (2) 395

## AUTHOR INDEX

Chang, H.K.: (2) 271, 281  
Charmasson, S.: (2) 553  
Chkir, N.: (2) 225  
Chouvelon, T.: (2) 485  
Cinelli, G.: (1) 387  
Cioni, R.: (2) 35  
Claude, C.: (2) 109  
Cordeiro, L.G.M.S.: (2) 501  
Cukrov, M.: (1) 417  
Cukrov, N.: (1) 417

## D

Dapeña, C.: (1) 263, 349, (2) 125, 177  
Daraoui, A.: (2) 467  
Darius, H.T.: (1) 483  
Darling, W.G.: (2) 3  
Dechraoui Bottein, M.-Y.: (1) 483  
De La Cruz, J.: (1) 337  
Delconte, C.A.: (1) 221, 229  
De Oliveira, P.E.: (1) 15  
Deschamps, P.: (2) 45, 225  
Deshpande, R.D.: (1) 7  
Dias, F.J.S.: (1) 49  
Díaz-Teijeiro, M.F.: (1) 171  
Dindyal, D.: (1) 311  
Dody, A.: (1) 147  
Ducós, E.I.: (1) 349  
Dueñas, C.: (1) 409  
Duffa, C.: (2) 553  
Duliu, O.G.: (1) 139  
Dupuy, A.: (2) 235

## E

Ebonji Seth, C.R.: (1) 113  
Edwards, T.W.D.: (1) 37  
Eggenkamp, H.G.M.: (1) 365  
Egorov, V.N.: (2) 535  
Eichinger, F.: (1) 73, (2) 99  
Eichinger, L.: (1) 237, 273, 279, (2) 73  
Eisenhauer, A.: (1) 473  
Elami, G.M.: (1) 245  
Elfaskaoui, M.: (2) 169  
El Hamouti, N.: (1) 357  
Erbland, J.: (1) 473

Estevez Alvarez, J.R.: (1) 337  
Ettayfi, N.: (1) 303  
Evangelidou, N.: (2) 545

## F

Faganeli, J.: (2) 527  
Fanny, J.O.Y.: (1) 311  
Farias, C.O.: (2) 501  
Faurescu, I.: (1) 139  
Ferjan, T.: (2) 19  
Fernández, M.C.: (1) 409  
Fianko, J.R.: (2) 215  
Fischer, H.W.: (1) 41, 403, (2) 477  
Fisher, N.S.: (1) 57  
Fleitas Estevez, G.: (1) 263  
Florou, H.: (2) 545  
Fórizs, I.: (2) 389  
Franceschi, M.: (2) 235  
Frey, S.: (2) 361  
Fritz, J.: (1) 273  
Fukasawa, M.: (1) 493, (2) 571  
Funk, E.: (2) 73

## G

Ganyaglo, S.Y.: (2) 215  
Gastaud, J.: (1) 89, 493, 513, (2) 395  
Gastmans, D.: (2) 271, 281  
Gebre Egziabher, M.: (2) 263  
Ghaleb, B.: (1) 67  
Gherardi, F.: (2) 27, 35  
Gibert, E.: (1) 67, 83  
Gibrilla, A.: (2) 215  
Gibson, J.J.: (1) 37  
Gil Castillo, R.: (1) 263, 349  
Gillon, M.: (1) 83  
Godoy, J.M.: (1) 49, 443, (2) 309  
Godoy, M.L.D.P.: (1) 49, 443, (2) 309  
Gómez-Guzmán, J.-M.: (2) 395  
Goncalves, J.: (2) 45  
Gonfiantini, R.: (2) 381  
González, I.P.: (1) 337  
González, P.: (1) 337  
Gooddy, D.C.: (2) 3  
Gordo, E.: (1) 409

## AUTHOR INDEX

Gori, L.: (2) 381  
 Gorny, M.: (2) 467  
 Goroncy, I.: (2) 467  
 Gourcy, L.: (2) 117  
 Gouri Sahu: (1) 501  
 Graça, H.: (1) 365  
 Grinenko, V.: (1) 237  
 G.R. Nkoue Ndong: (1) 113  
 Gschwend, M.: (1) 279  
 Guendouz, A.: (2) 45  
 Guidi, M.: (2) 35  
 Gulina, L.V.: (2) 535  
 Gulin, S.B.: (2) 535  
 Gupta, S.K.: (1) 7

### H

Hadj Ammar, F.: (2) 225  
 Hajo, I.: (1) 245  
 Hamajima, Y.: (1) 89, (2) 571  
 Hamelin, B.: (2) 45, 225  
 Happel, S.: (1) 523  
 Harum, T.: (2) 145  
 Hatim, E.: (1) 245  
 Heidinger, M.: (2) 73  
 Herrmann, J.: (2) 467  
 Hettwig, B.: (1) 403, (2) 477  
 Hierro, A.: (1) 395  
 Hinsby, K.: (2) 153  
 Hirata, R.: (2) 281  
 Hirose, K.: (1) 89, 493, (2) 493, 571  
 Hocini, N.: (2) 343  
 Hong, Gi-Hoon: (1) 513  
 Hou, X.L.: (1) 463  
 Hoyos, D.Á.: (1) 211  
 Hrneckek, E.: (2) 419  
 Hsissou, Y.: (2) 169  
 Huang, T.: (2) 91  
 Huitu, E.: (1) 199  
 Huneau, F.: (2) 235  
 Hunjak, T.: (1) 99  
 Hussein, S.: (1) 463

### I

Ichiyanagi, K.: (1) 107, 131

### J

Jakob, D.: (2) 467  
 Janovics, R.: (2) 369  
 Jasechko, S.: (1) 37  
 Jaunat, J.: (2) 235  
 Jeřkovský, M.: (1) 89  
 Jianhua He: (2) 509  
 Jiménez, S.: (2) 291  
 Jofré, E.: (2) 185  
 Jovchev, Z.: (2) 255

### K

Kacem, A.: (2) 161  
 Kaiser, J.: (1) 473  
 Kattaa, B.: (1) 179  
 Kattan, Z.: (1) 179  
 Kawano, T.: (2) 571  
 Kebede, S.: (2) 263  
 Kelecom, A.: (2) 563  
 Ketchemen-Tandia, B.: (1) 113  
 Khalaj Amirhosseini, Y.: (2) 351  
 Kim, Chul-Soo: (1) 513  
 Kim, C.-S.: (1) 493  
 Kong, Y.: (2) 91  
 Korun, M.: (1) 255  
 Kovačič, K.: (1) 255  
 Kožar-Logar, J.: (1) 255, (2) 11  
 Kretschmer, N.: (2) 185  
 Kritidis, P.: (2) 545  
 Külls, C.: (2) 361  
 Kumar, B.: (1) 121  
 Kurttas, T.: (1) 203, (2) 203

### L

Lacerda, L.D.: (1) 49  
 Lai, Chun-Ta: (1) 189  
 La Rosa, J.: (1) 513  
 Le Coustumer, P.: (2) 235  
 Lee, Sang-Han: (1) 513  
 Leis, A.: (1) 473, (2) 11, 145  
 Leuenberger, F.: (1) 273, 279  
 Levy, I.: (1) 89, 493  
 Leyva Bombuse, D.: (1) 349

## AUTHOR INDEX

Lgourna, Z.: (1) 303  
Linderberg, J.: (2) 153  
Lojen, S.: (1) 417, (2) 53  
Lorenz, G.D.: (2) 73  
Luaces, C.A.: (1) 337  
Lujanienė, G.: (2) 411  
Lutz, H.O.: (1) 99  
Lykoudis, S.P.: (1) 161

## M

Machrafi, R.: (2) 403  
Macias, F.: (1) 15  
Magro, G.: (2) 35  
Major, I.: (2) 369  
Malek, M.A.: (1) 425  
Mali, N.: (2) 11  
Mami, M.: (2) 343  
Mance, D.: (1) 99  
Manzano, M.: (1) 287, 327, (2) 281  
Marah, H.: (2) 319  
Marbán, L.: (1) 349  
Marca, A.: (1) 473  
Marín, S.: (2) 185  
Marins, R.V.: (1) 49  
Marques, J.M.: (1) 365, (2) 63  
Martínez, D.E.: (2) 177, 195  
Massault, M.: (1) 67, 83, (2) 169  
Massone, H.E.: (2) 177  
Matamoros-Arguedas, R.: (2) 245  
Maturana, H.: (2) 185  
Mayer, A.: (2) 109  
Méndez Fernandez, P.: (2) 485  
Mezga, K.: (2) 83  
Michelot, J.-L.: (2) 45  
Michelot, J.L.: (2) 169  
Michel, R.L.: (1) 203  
Michel, R.: (2) 467  
Mirzoeva, N.Y.: (2) 535  
Misumi, K.: (2) 493  
Mohanty, A.K.: (1) 501  
Moleiro León, L.: (1) 263  
Molnár, M.: (2) 369  
Moore, W.S.: (2) 453  
Moreira, I.: (2) 309  
Mulitza, S.: (1) 41

Muñoz, J.F.: (2) 185  
Murad, A.: (1) 463

## N

Nada, A.A.: (2) 137  
Nakahara, M.: (1) 425  
Nakano, H.: (2) 571  
Nathaniel, W.: (2) 169  
Ndembo, L.J.: (2) 299  
Newman, B.: (1) 203  
Ngo Boum, S.: (1) 113  
Nies, H.: (2) 395, 467  
Noret, A.: (1) 67  
Nunes, D.: (2) 63

## O

Ogrinc, N.: (2) 527  
Ogwari, P.O.: (2) 335  
Oliveira, D.R.: (2) 501  
Oliveira, J.M.: (1) 451  
Oliveira, T.M.N.: (1) 435  
Olivera Acosta, J.: (1) 263, 349  
Ortiz, C.: (2) 185  
Osae, S.: (2) 215  
Osvath, I.: (2) 535  
Ouda, B.: (2) 319  
Oyarzún, J.: (2) 185  
Oyarzún, R.: (2) 185

## P

Palacio, C.: (1) 211  
Palacio, P.: (1) 211, (2) 125  
Panarello, H.O.: (1) 349  
Pang, Z.: (2) 91  
Passarini Jr, J.: (1) 15  
Pătrașcu, V.: (2) 443  
Paul, D.: (2) 389  
Pavičić-Hamer, D.: (2) 519  
Pennisi, M.: (1) 221, (2) 381  
Peralta Vital, J.L.: (1) 263, 349  
Pereira, W.S.: (2) 563  
Pérez, M.: (1) 409  
Pessenda, L.C.R.: (1) 15  
Petelet-Giraud, E.: (2) 117

## AUTHOR INDEX

Petersen, J.O.: (2) 45  
 Pham Mai Khanh: (2) 395  
 Pietroniro, A.: (1) 37  
 Pittauerová, D.: (1) 41, 403, (2) 477  
 Plieschnegger, M.: (2) 145  
 Plummer, N.: (2) 299  
 Polikarpov, G.G.: (2) 535  
 Poo, M.: (2) 195  
 Popov, V.: (2) 255  
 Possnert, G.: (1) 463  
 Pourtangestani, K.: (2) 403  
 Povinec, P.P.: (1) 89, 295, 493, 513,  
 (2) 571  
 Prasad, M.V.R.: (1) 501  
 Proskurnin, V.Y.: (2) 535  
 Purtschert, R.: (2) 109, 153  
 Py Jr, D.A.: (2) 563

### Q

Quejido, A.J.: (1) 337  
 Quiroz Londoño, O.M.: (2) 177  
 Qurtobi, M.: (2) 319

### R

Racchetti, E.: (1) 229  
 Raibi, F.: (2) 319  
 Rai, S.P.: (1) 121  
 Ravi, Y.: (2) 299  
 Reguera, B.: (1) 483  
 Re, V.: (1) 357  
 Rezende, C.E.: (1) 49, 443, (2) 501  
 Ricardi-Branco, F.: (1) 15  
 Richtáriková, M.: (1) 295  
 Rizzo, F.: (1) 357  
 Robinson, M.: (2) 3  
 Rodríguez-Arévalo, J.: (1) 171  
 Rodríguez, L.: (1) 327, (2) 281  
 Rodríguez, M.: (1) 337  
 Roller-Lutz, Z.: (1) 99  
 Romero, P.: (2) 291  
 Roos, P.: (1) 493  
 Rosner, M.: (2) 377  
 Rucandio, I.: (1) 337

### S

Sacchi, E.: (1) 221, 229, 311, 319, 357  
 Saccon, P.: (1) 473  
 Sachse, R.: (2) 467  
 Sadler, R.: (2) 389  
 Salamalikis, V.: (1) 161  
 Sam, A.K.: (1) 245  
 Samantara, M.K.: (1) 501  
 Sanchez-Cabeza, J.A.: (1) 89, 493,  
 (2) 571  
 Sánchez, M.: (1) 337  
 Santa, D.: (1) 211  
 Satpathy, K.K.: (1) 501  
 Savarino, J.: (1) 473  
 Schlosser, C.: (2) 361  
 Schmitt, R.: (2) 145  
 Schneider, J.: (2) 73  
 Schneider, T.: (1) 7  
 Schuck, T.J.: (1) 377  
 Sciuto, P.F.: (2) 381  
 Scofield, A.L.: (2) 501  
 Selvanayagam, M.: (1) 501  
 Shimada, J.: (1) 131  
 Siddeeg, S.E.M.B.: (1) 245  
 Singh, R.D.: (1) 121  
 Šivo, A.: (1) 295  
 Skrzypek, G.: (2) 389  
 Smellie, J.A.T.: (1) 73, (2) 99  
 Smita Achary, M.: (1) 501  
 Soare, A.: (1) 139  
 Soares, A.M.: (1) 451  
 Sonninen, E.: (1) 199  
 Souza, T.A.: (1) 49, (2) 309  
 Spitz, J.: (2) 485  
 Stadler, H.: (2) 145  
 Startsev, N.: (1) 25  
 Stefanescu, I.: (1) 139  
 Stokozov, N.A.: (2) 535  
 Streng, R.: (1) 523  
 Sturchio, N.: (2) 271  
 Sudepta Biswas: (1) 501  
 Suk, Moon-Sik: (1) 513  
 Sültenfuß, J.: (1) 473, (2) 109  
 Suwarman, R.: (1) 107

## AUTHOR INDEX

Světlík, I.: (2) 369

Sýkora, I.: (1) 89

Synal, H.-A.: (2) 467

### T

Tagma, T.: (1) 303, (2) 169

Taigbenu, A.E.: (1) 319

Tanoue, M.: (1) 131

Taous, F.: (2) 319

Taylor, P.: (1) 377

Tereshenko, N.N.: (2) 535

Thébault, H.: (2) 553

Torkar, A.: (1) 153

Tosch, L.: (2) 467

Tositti, L.: (1) 387

Trabelsi, R.: (2) 161

Trav, Y.: (2) 109

Tsubono, T.: (2) 493

Tsumune, D.: (2) 493, 571

Turk, D.: (2) 527

### U

Ulbrich, S.: (1) 403

Urbanc, J.: (2) 83

### V

Vaca, F.: (1) 395

Valdez, L.: (1) 349

Valladares, A.: (1) 327

Van Pelt, A.: (2) 145

Varlam, C.: (1) 139

Varni, M.: (1) 287

Vasileva, E.: (2) 395

Vaz, C.: (1) 435

Vengosh, A.: (1) 303, (2) 169

Vidotto, E.: (1) 15

Vitvar, T.: (2) 299

Vives, L.: (1) 327, (2) 281

Voerkelius, S.: (1) 237

Vogl, J.: (2) 377

Voropaev, A.: (1) 237

Vo Thi Tuong Hanh: (2) 327

Vreča, P.: (1) 153, (2) 19

### W

Waber, H.N.: (1) 73, (2) 99

Wacker, L.: (2) 369

Wagener, A.L.R.: (2) 501

Wanderley, C.V.A.: (1) 443

Warner, N.: (1) 303

Weinzettel, P.: (1) 287

Wen Yu: (2) 509

Whiticar, M.J.: (1) 25

Wieser, M.: (1) 7

Wills, B.: (1) 211

Wonkam, C.: (1) 113

Wyse, E.: (1) 513

### Y

Yagob, T.I.: (1) 245

Yamanaka, M.D.: (1) 107

Yim, S.A.: (1) 493

Yoshida, Y.: (2) 493

### Z

Zabala, M.E.: (1) 287

Zavadlav, S.: (2) 53, 527

Ženišová, Z.: (1) 295

Zerobin, W.: (2) 145

Zine, N.: (2) 319

Zouari, K.: (2) 45, 161, 203, 225

Zulauf, A.: (1) 523

Zuppi, G.M.: (1) 357, 435



# Where to order IAEA publications

In the following countries IAEA publications may be purchased from the sources listed below, or from major local booksellers. Payment may be made in local currency or with UNESCO coupons.

## AUSTRALIA

DA Information Services, 648 Whitehorse Road, MITCHAM 3132  
Telephone: +61 3 9210 7777 • Fax: +61 3 9210 7788  
Email: service@dadirect.com.au • Web site: <http://www.dadirect.com.au>

## BELGIUM

Jean de Lannoy, avenue du Roi 202, B-1190 Brussels  
Telephone: +32 2 538 43 08 • Fax: +32 2 538 08 41  
Email: jean.de.lannoy@infoboard.be • Web site: <http://www.jean-de-lannoy.be>

## CANADA

Bernan Associates, 4501 Forbes Blvd, Suite 200, Lanham, MD 20706-4346, USA  
Telephone: 1-800-865-3457 • Fax: 1-800-865-3450  
Email: customercare@bernan.com • Web site: <http://www.bernan.com>

Renouf Publishing Company Ltd., 1-5369 Canotek Rd., Ottawa, Ontario, K1J 9J3  
Telephone: +613 745 2665 • Fax: +613 745 7660  
Email: order.dept@renoufbooks.com • Web site: <http://www.renoufbooks.com>

## CHINA

IAEA Publications in Chinese: China Nuclear Energy Industry Corporation, Translation Section, P.O. Box 2103, Beijing

## CZECH REPUBLIC

Suweco CZ, S.R.O., Klecakova 347, 180 21 Praha 9  
Telephone: +420 26603 5364 • Fax: +420 28482 1646  
Email: nakup@suweco.cz • Web site: <http://www.suweco.cz>

## FINLAND

Akateeminen Kirjakauppa, PO BOX 128 (Keskuskatu 1), FIN-00101 Helsinki  
Telephone: +358 9 121 41 • Fax: +358 9 121 4450  
Email: akatilaus@akateeminen.com • Web site: <http://www.akateeminen.com>

## FRANCE

Form-Edit, 5, rue Janssen, P.O. Box 25, F-75921 Paris Cedex 19  
Telephone: +33 1 42 01 49 49 • Fax: +33 1 42 01 90 90  
Email: formedit@formedit.fr • Web site: <http://www.formedit.fr>

Lavoisier SAS, 145 rue de Provigny, 94236 Cachan Cedex  
Telephone: + 33 1 47 40 67 02 • Fax +33 1 47 40 67 02  
Email: romuald.verrier@lavoisier.fr • Web site: <http://www.lavoisier.fr>

## GERMANY

UNO-Verlag, Vertriebs- und Verlags GmbH, Am Hofgarten 10, D-53113 Bonn  
Telephone: + 49 228 94 90 20 • Fax: +49 228 94 90 20 or +49 228 94 90 222  
Email: bestellung@uno-verlag.de • Web site: <http://www.uno-verlag.de>

## HUNGARY

Librotrade Ltd., Book Import, P.O. Box 126, H-1656 Budapest  
Telephone: +36 1 257 7777 • Fax: +36 1 257 7472 • Email: books@librotrade.hu

## INDIA

Allied Publishers Group, 1st Floor, Dubash House, 15, J. N. Heredia Marg, Ballard Estate, Mumbai 400 001,  
Telephone: +91 22 22617926/27 • Fax: +91 22 22617928  
Email: alliedpl@vsnl.com • Web site: <http://www.alliedpublishers.com>

Bookwell, 2/72, Nirankari Colony, Delhi 110009  
Telephone: +91 11 23268786, +91 11 23257264 • Fax: +91 11 23281315  
Email: bookwell@vsnl.net

## ITALY

Libreria Scientifica Dott. Lucio di Biasio "AEIOU", Via Coronelli 6, I-20146 Milan  
Telephone: +39 02 48 95 45 52 or 48 95 45 62 • Fax: +39 02 48 95 45 48  
Email: info@libreriaaeiou.eu • Website: [www.libreriaaeiou.eu](http://www.libreriaaeiou.eu)

## **JAPAN**

Maruzen Company Ltd, 1-9-18, Kaigan, Minato-ku, Tokyo, 105-0022  
Telephone: +81 3 6367 6079 • Fax: +81 3 6367 6207  
Email: journal@maruzen.co.jp • Web site: <http://www.maruzen.co.jp>

## **REPUBLIC OF KOREA**

KINS Inc., Information Business Dept. Samho Bldg. 2nd Floor, 275-1 Yang Jae-dong SeoCho-G, Seoul 137-130  
Telephone: +02 589 1740 • Fax: +02 589 1746 • Web site: <http://www.kins.re.kr>

## **NETHERLANDS**

De Lindeboom Internationale Publicaties B.V., M.A. de Ruyterstraat 20A, NL-7482 BZ Haaksbergen  
Telephone: +31 (0) 53 5740004 • Fax: +31 (0) 53 5729296  
Email: books@delindeboom.com • Web site: <http://www.delindeboom.com>

Martinus Nijhoff International, Koraalrood 50, P.O. Box 1853, 2700 CZ Zoetermeer  
Telephone: +31 793 684 400 • Fax: +31 793 615 698  
Email: info@nijhoff.nl • Web site: <http://www.nijhoff.nl>

Swets and Zeitlinger b.v., P.O. Box 830, 2160 SZ Lisse  
Telephone: +31 252 435 111 • Fax: +31 252 415 888  
Email: infoho@swets.nl • Web site: <http://www.swets.nl>

## **NEW ZEALAND**

DA Information Services, 648 Whitehorse Road, MITCHAM 3132, Australia  
Telephone: +61 3 9210 7777 • Fax: +61 3 9210 7788  
Email: service@dadirect.com.au • Web site: <http://www.dadirect.com.au>

## **SLOVENIA**

Cankarjeva Zalozba d.d., Kopitarjeva 2, SI-1512 Ljubljana  
Telephone: +386 1 432 31 44 • Fax: +386 1 230 14 35  
Email: import.books@cankarjeva-z.si • Web site: <http://www.cankarjeva-z.si/uvoz>

## **SPAIN**

Díaz de Santos, S.A., c/ Juan Bravo, 3A, E-28006 Madrid  
Telephone: +34 91 781 94 80 • Fax: +34 91 575 55 63  
Email: compras@diazdesantos.es, carmela@diazdesantos.es, barcelona@diazdesantos.es, julio@diazdesantos.es  
Web site: <http://www.diazdesantos.es>

## **UNITED KINGDOM**

The Stationery Office Ltd, International Sales Agency, PO Box 29, Norwich, NR3 1 GN  
Telephone (orders): +44 870 600 5552 • (enquiries): +44 207 873 8372 • Fax: +44 207 873 8203  
Email (orders): book.orders@tso.co.uk • (enquiries): book.enquiries@tso.co.uk • Web site: <http://www.tso.co.uk>

### **On-line orders**

DELTA Int. Book Wholesalers Ltd., 39 Alexandra Road, Addlestone, Surrey, KT15 2PQ  
Email: info@profbooks.com • Web site: <http://www.profbooks.com>

### **Books on the Environment**

Earthprint Ltd., P.O. Box 119, Stevenage SG1 4TP  
Telephone: +44 1438748111 • Fax: +44 1438748844  
Email: orders@earthprint.com • Web site: <http://www.earthprint.com>

## **UNITED NATIONS**

Dept. I004, Room DC2-0853, First Avenue at 46th Street, New York, N.Y. 10017, USA  
(UN) Telephone: +800 253-9646 or +212 963-8302 • Fax: +212 963-3489  
Email: publications@un.org • Web site: <http://www.un.org>

## **UNITED STATES OF AMERICA**

Bernan Associates, 4501 Forbes Blvd., Suite 200, Lanham, MD 20706-4346  
Telephone: 1-800-865-3457 • Fax: 1-800-865-3450  
Email: customercare@bernan.com • Web site: <http://www.bernan.com>

Renouf Publishing Company Ltd., 812 Proctor Ave., Ogdensburg, NY, 13669  
Telephone: +888 551 7470 (toll-free) • Fax: +888 568 8546 (toll-free)  
Email: order.dept@renoufbooks.com • Web site: <http://www.renoufbooks.com>

**Orders and requests for information may also be addressed directly to:**

### **Marketing and Sales Unit, International Atomic Energy Agency**

Vienna International Centre, PO Box 100, 1400 Vienna, Austria  
Telephone: +43 1 2600 22529 (or 22530) • Fax: +43 1 2600 29302  
Email: sales.publications@iaea.org • Web site: <http://www.iaea.org/books>

The International Symposium on Isotope Hydrology, Marine Ecosystems and Climate Change Studies was held from 27 March to 1 April 2011 in Monaco, to commemorate the fiftieth anniversary of the establishment of the IAEA laboratory in the Principality of Monaco. The symposium was jointly organized by the IAEA Water Resources Programme and the IAEA Environment Laboratories. The event also represented the thirteenth edition of the quadrennial Symposium on isotope hydrology and water resources management, which has been regularly organized by the IAEA since 1963. The technical sessions covered aspects related to the use and application of isotope tools in a broad spectrum of scientific disciplines through invited talks, oral and poster presentations and workshops. The five technical sessions covered the following topics: (a) the role of isotopes in understanding and modelling climate change, marine ecosystems and water cycles (b) carbon dioxide sequestration and related aspects of the carbon cycle (c) isotopes and radionuclides in the marine environment, (d) groundwater assessments of large aquifers and (e) analytical methods and instrumentation. These proceedings contain the presentations made at the symposium.



Water  
Resources  
Programme



Environment  
Programme

**INTERNATIONAL ATOMIC ENERGY AGENCY  
VIENNA**

ISBN 978-92-0-135610-9  
ISSN 0074-1884